ASTROPHYSICS AND SPACE SCIENCE PROCEEDINGS

B.S. Koribalski
H. Jerjen
Editors

Galaxies in the Local Volume

Springer

Galaxies in the Local Volume

ASTROPHYSICS AND SPACE SCIENCE PROCEEDINGS

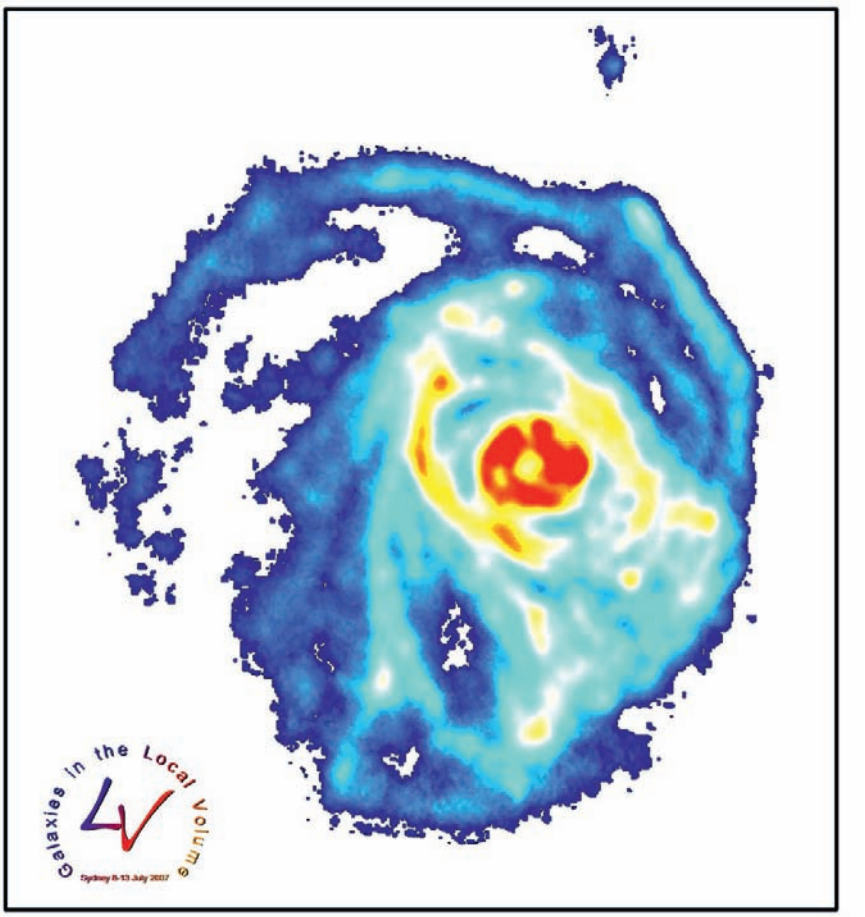

ATCA HI mosaic of the giant spiral galaxy M83 and its dwarf companion UGCA 365 (B. Koribalski and LVHIS Team)

Galaxies in the Local Volume

B.S. Koribalski
Editor

CSIRO Australia Telescope National Facility, Sydney, Australia

H. Jerjen
Editor

Australian National University, Mount Stromo Observatory, Australia

Springer

Editors
Bärbel Silvia Koribalski
CSIRO
Austalia Telescope
National Facility
76 P.O. Box
NSW, Epping 1710
Australia

Helmut Jerjen
Australian National University
Research School of Astronomy
& Astrophysics
Canberra ACT 2611
Private Bag
Weston Creek PO
Australia

ISBN: 978-1-4020-6932-1 e-ISBN: 978-1-4020-6933-8

Library of Congress Control Number: 2007942782

Printed on acid-free paper.

9 8 7 6 5 4 3 2 1

springer.com

to our friends

Preface

The Local Volume is a treasure trough. Not only does it harbour the most exciting objects in the Universe, but the most wonderful people studying its content. It was with great delight that we welcomed students, postdocs, and senior researchers to gather in Sydney, Australia, to present their latest results, marvel at the new findings of other researchers and discuss possible interpretations, future projects and new ideas.

It is our great pleasure to present the proceedings of the *Galaxies in the Local Volume* symposium, held at the Australian National Maritime Museum (ANMM) in Darling Harbour, Sydney, from July 8 to 13, 2007.

The *Local Volume* — the sphere of radius 10 Mpc centered on the Local Group — is the home for over 500 galaxies, many of which congregate in well-known groups such as Sculptor, Centaurus, and M 81. Decades of painstaking research bring us to this point in time where observations across a wide range of wavelengths and high resolution computer simulations are available for the

majority of these nearby galaxies. Given the many recent advances in our understanding of the star formation and ISM composition of nearby galaxies and, more generally, in the field of *Near-Field Cosmology* it was timely to hold a conference on the subject and to review the Local Volume by bringing together researchers from the community. The conference provided a vibrant forum for presentations and discussions across a broad range of astrophysical topics, including the challenges we might be able to tackle with future facilities such as the Atacama Large Millimeter Array (ALMA) and the international Square Kilometre Array (SKA).

Over the five days of the conference, we had 68 contributed and invited talks as well as a large number of very short (1min., 1 slide) poster presentations. More than 50 posters were displayed in the Tasman Light deck of the Maritime Museum and eagerly discussed during the breaks. All contributions (talks & posters) that we received are included in this book reflecting the great diversity of the scientific programme and offering an exquisite display of the cutting-edge research in the field. — Some of the questions we focussed on during the symposium were:

- What is the 3D distribution, kinematics and SF density of galaxies in the Local Volume ?
- What drives star formation in galaxies - nature or nurture ? What is the star formation history of galaxies in the Local Volume ?
- How does the Local Volume provide/constrain cosmological parameters ?
- How big are galaxies and what lies between them ? What determines the size of a galaxy ?
- What are the global properties of galaxy environments ?

A big **Thank You !** to all participants of the Sydney symposium on *Galaxies in the Local Volume*. You were great; you made this a wonderful conference full of exciting results, lively discussions and new ideas.

We would like to extend our sincere gratitude to the following people:

- the Scientific Organising Committee (SOC) for their excellent advice on the scientific programme,
- the Local Organising Committee (LOC) for their commitment in the organisation of the event; in particular, Erik Muller for his truly outstanding dedication to the organisation of the *Galaxies in the Local Volume* symposium as well as the *Elizabeth and Frederick White Conference on the Magellanic System* (July 16/17, 2007); Vicky Fraser for her excellent and continuing administrative support; Naomi McClure-Griffiths for her help and for creating a catching symposium logo; and Ángel López-Sánchez for his help in finalising the abstract booklet and designing the poster for the symposium,

- the session chairs who agreed, often on very short notice, to introduce the speakers and co-ordinate the questions,
- the PhD students who, often with even shorter notice, helped with one or two sessions throughout the week; these are Emma Kirby, Ivy Wong, Nic Bonne, Shane Walsh, Janine van Eymeren, Deanna Matthews, Patrick Tisserand, and Annie Hughes. It was marvellous to be able to rely on so many capable and friendly colleagues !
- Evan Skillman for his entertaining after-dinner speech,
- Ayesha Begum and Jayaram Chengalur (FIGGS poster), Fabian Walter and Frank Bigiel (THINGS poster), David Thilker (GALEX poster), Daniel Dale (SINGS poster), Tony Wong (BIMA SONG poster), Janice Lee (11HUGS poster), and Ángel López-Sánchez (LVHIS poster),
- Joss Bland-Hawthorn for his comprehensive summary, addressing the questions we raised, and concluding the symposium,
- all contributors to this volume. Thank You !

We also like to thank the following institutions and organisations for their financial support:

- DEST Australia-India Strategic Research Fund (AISRF)
- CSIRO Australia Telescope National Facility (ATNF)
- Australian Academy of Science
- ANU Research School of Astronomy & Astrophysics (RSAA)
- Anglo-Australian Observatory (AAO)
- School of Physics, University of Sydney
- Sydney Observatory

We hope you very much enjoy reading this book.

Sydney,
September, 2007

Bärbel Koribalski
Helmut Jerjen

Scientific Organising Committee:

Bärbel Koribalski (Chair, Australia Telescope National Facility, Australia)
Joss Bland-Hawthorn (Anglo Australian Observatory, Australia)
Erwin de Blok (University of Capetown, South Africa)
Jayaram Chengalur (National Centre for Radio Astrophysics, India)
Yasuo Fukui (Nagoya University, Japan)
Deidre Hunter (Lowell Observatory, USA)
Judith Irwin (Queen's University, Canada)
Helmut Jerjen (Australian National University, Australia)
Rob Kennicutt (Cambridge University, United Kingdom)
Ofer Lahav (University College London, United Kingdom)
Geraint Lewis (University of Sydney, Australia)
Jürgen Ott (National Radio Astronomy Observatory, USA)
Eline Tolstoy (Kapteyn Astronomical Institute, The Netherlands)

Local Organising Committee:

Bärbel Koribalski (Chair, ATNF)
Erik Muller (ATNF)
Vicki Fraser (ATNF)
Ángel López-Sánchez (ATNF)
Naomi McClure-Griffiths (ATNF)
Helen Sim (ATNF)
Geraint Lewis (University of Sydney)

Contents

Part I Invited and Contributed Talks

The Local Velocity Anomaly
R. Brent Tully 3

Outlining the Local Void with the Parkes H I ZOA and Galactic Bulge Surveys
Renée C. Kraan-Korteweg, N. Shafi, B. S. Koribalski, L. Staveley-Smith, P. Buckland, P. A. Henning, and A. P. Fairall 13

The Context of the Local Volume: Structures and Motions in the Nearby Universe
Matthew Colless 17

Mining the Local Volume
Igor D. Karachentsev, Valentina Karachentseva, Walter Huchtmeier, Dmitry Makarov, Serafim Kaisin, Margarita Sharina, and Lidia Makarova 21

Properties of Voids in the Local Volume
Anton Tikhonov and Anatoly Klypin 31

Using Local Volume Data to Constrain Dark Matter Dynamics
Guilhem Lavaux, R. Mohayaee, S. Colombi, and R. B. Tully 37

The Local Volume HI Survey (LVHIS)
Bärbel S. Koribalski and the LVHIS team 41

Investigating Dark Matter and MOND in Local Volume Galaxies
Nicolas J. Bonne 45

Deepest Near-IR Surface Photometry of Galaxies in the Local Sphere of Influence
Emma Kirby, Helmut Jerjen, Stuart Ryder, and Simon Driver 49

Ionized and Neutral Gas in the Starburst Galaxy NGC 5253
Ángel R. López-Sánchez, Bärbel Koribalski, César Esteban, and Jorge García-Rojas 53

The Smallest H I Galaxies
Tom Oosterloo, Katarina Kovač, Thijs van der Hulst, Marc Verheijen, and Emma Ryan-Weber 57

FIGGS: Faint Irregular Galaxies GMRT Survey
Ayesha Begum, Jayaram N. Chengalur, Igor D. Karachentsev, Margrita Sharina, and Serafim Kaisin 61

Gas Rich Galaxies from the FIGGS Survey
Jayaram N. Chengalur, Ayesha Begum, Igor D. Karachentsev, Margrita Sharina, and Serafim Kaisin 65

The Evolution of the ISM in Star Forming Galaxies
Eric M. Wilcots 69

Magnetic Fields in Irregular Galaxies
Amanda A. Kepley, Stefanie Mühle, Eric M. Wilcots, John Everett, Ellen Zweibel, Timothy Robishaw, and Carl Heiles 73

Future ASKAP Studies of the Local Volume
Lister Staveley-Smith 77

An Ultraviolet-to-Radio Broadband Spectral Atlas of Nearby Galaxies
Daniel A. Dale 81

Diagnostic Value of Mid-Infrared Fine Structure Lines in Galaxies
Caroline Bot and the SINGS team 85

Warm Molecular Hydrogen in Nearby Galaxies: Results from the SINGS Sample
Hélène Roussel and the SINGS team 89

Molecular Gas, Cloud Properties, and Star Formation in Dwarf Galaxies
Alberto D. Bolatto, Adam K. Leroy, Fabian Walter, Leo Blitz, and Erik Rosolowsky 93

THINGS: The H I Nearby Galaxy Survey
Fabian Walter, Elias Brinks, Erwin de Blok, and Frank Bigiel 97

The Star Formation Law at Sub-Kiloparsec Resolution
Frank Bigiel, Adam Leroy, and Fabian Walter 105

The GALEX View of Ongoing Disk Formation in the Local Volume
David A. Thilker 109

The ACS Nearby Galaxy Survey Treasury: 9 Months of ANGST
Julianne Dalcanton, Beth Williams, and the ANGST collaboration 115

ESO540-032: a Transition-Type Dwarf in the Sculptor Group
Gary S. Da Costa, Helmut Jerjen, and Antoine Bouchard 123

Resolving the Outer Disks and Halos of Nearby Galaxies
Anil Seth, Roelof de Jong, David Radburn-Smith, and Harry Ferguson . . 127

Recent Star Formation Histories of Nearby Galaxies
Evan D. Skillman 131

HST/ACS Observations of Extremely Metal-Poor Blue Compact Dwarf Galaxies
Alessandra Aloisi 139

Matching the Local and Cosmic Star Formation Histories
Igor Drozdovsky, Andrew Hopkins, Antonio Aparicio, Carme Gallart, and the LCID team 143

Dense Molecular Gas in Nearby Southern Starburst Galaxies
Jürgen Ott, Christian Henkel, Axel Weiß, and Fabian Walter 147

NANTEN2 Project: CO and C I Survey of the Local Group
Toshikazu Onishi, Norikazu Mizuno, Akira Mizuno, Yasuo Fukui, and the NANTEN2 Consortium 151

The Mass-to-Light Ratios of Spiral Disks
Robin Ciardullo and Kimberly A. Herrmann 155

The Surprisingly Abnormal Halo of the "Normal" Elliptical Galaxy, NGC 3379
Elizabeth Wehner, William Harris, Gretchen Harris, and Andrew Layden 159

Infrared Study of the SNR Evolution in NGC 6946
Tom H. Jarrett, J. Rho, W. Reach, and P. Appleton 163

Modeling Non-Circular Motions in Disk Galaxies: A Bar in NGC 2976
Kristine Spekkens and J.A. Sellwood 167

Gravitational Stability in the Disk of M 51
Marc Hitschfeld, C. Kramer, K.F. Schuster, S. Garcia-Burillo, and J. Stutzki 171

The Kinematics and Ages of the Nearby Elliptical NGC 5128
Kristin A. Woodley, W. E. Harris, M. A. Beasley, E. Peng, T. Bridges, D. Forbes, Gretchen L. H. Harris, and G. Mackie 175

Integral-Field Spectroscopy of the Centaurus A Nucleus
Davor Krajnović, Rob Sharp, and Niranjan Thatte 179

Visualising the Local Volume
David G. Barnes and Christopher J. Fluke 183

The Stromlo Missing Satellites Survey
Helmut Jerjen 187

Boötes II: A Retrospective
Shane Walsh, Helmut Jerjen, and Beth Willman 191

Observational Constraints on the "Missing Satellite" Problem from SDSS
Sergey Koposov and Vasily Belokurov 195

Space Motions of the Draco, Fornax, and Sagittarius Dwarf Spheroidal Galaxies
Slawomir Piatek, Carlton Pryor, and Edward Olszewski 199

Extragalactic Stellar Astronomy
Miguel A. Urbaneja, Rolf-Peter Kudritzki, and Fabio Bresolin 203

First Results From the Large Binocular Telescope: Deep Photometry of New dSphs
Matthew G. Coleman, and Jelte de Jong 207

Proper Motions in the Andromeda Subgroup
Andreas Brunthaler, Mark J. Reid, Heino Falcke, Christian Henkel, and Karl M. Menten 211

Contrasting the Milky Way and M 31 Satellite Galaxies
Alan W. McConnachie 215

Strangers in the Night: Is AndXII Just Passing Through the Local Group?
Geraint F. Lewis, S. C. Chapman, J. Penarrubia, R. Ibata, A. McConnachie, N. Martin, M. Irwin, A. Blain, B. Letarte, K. Lo, A. Ludlow, and K. O'Neil 219

Substructure Along M 31's Southeast Minor Axis: The Forward Continuation of the Giant Southern Stream
Karoline M. Gilbert, M. Fardal, J. S. Kalirai, P. Guhathakurta, M. C. Geha, J. Isler, S. R. Majewski, J. C. Ostheimer, R. J. Patterson, D. B. Reitzel, E. Kirby, and M. C. Cooper 223

Young Star Clusters in M 31
Heather Morrison, Nelson Caldwell, Paul Harding, Jeff Kriessler, James A. Rose, and Ricardo Schiavon 227

A Spectroscopic Survey of M 31 Dwarf Spheroidal Galaxies
Jasonjot S. Kalirai, Puragra Guhathakurta, Marla C. Geha, Karoline M. Gilbert, Steven R. Majewski, and Rachael L. Beaton 231

The Relics of Structure Formation: High-Velocity Clouds Around M 31
Tobias Westmeier, R. Braun, C. Brüns, J. Kerp, and D. A. Thilker 235

High-Velocity Clouds Merging with the Milky Way
Felix J. Lockman 239

The Origin of the Magellanic Stream and its Leading Arm
David L. Nidever, Steven R. Majewski, and W. Butler Burton 243

Evolution of the Small Magellanic Cloud
Kenji Bekki 247

Spitzer Survey of the Large Magellanic Cloud: Surveying the Agents of a Galaxy's Evolution (SAGE): Initial Results
Margaret Meixner, K. Gordon, R. Indebetouw, B. Whitney, M. Meade, B. Babler, J. Hora, U. Vijh, S. Srinivasan, C. Leitherer, M. Sewilo, C. Engelbracht, M. Block, B. For, R. Blum, W. Reach, J-P. Bernard, and the SAGE Team 251

Metallicity and Mean Age Across M 33
Maria-Rosa L. Cioni, M. Irwin, A. M. N Ferguson, A. McConnachie, B. C. Conn, A. Huxor, R. Ibata, G. Lewis, and N. Tanvir 255

How does Gas Get into Galaxies?
Joss Bland-Hawthorn 259

Part II Poster Contributions

New HST/ACS Data of the Starburst Irregular Galaxy NGC 4449
Francesca Annibali, A. Aloisi, J. Mack, M. Tosi, R. P. van der Marel, L. Angeretti, C. Leitherer, and M. Sirianni 269

H I Deficiency in X-ray Bright Groups
Ramesh Balasubramanyam, Chandreyee Sengupta, and K.S. Dwarakanath 271

Ca II and Na I Absorption Signatures from the Circumgalactic Gas of the Milky Way
Nadya Ben Bekhti, M. Murphy, P. Richter, and T. Westmeier 273

The Orbital History of the LMC
Gurtina Besla, Nitya Kallivayalil, Lars Hernquist, Brant Robertson, T. J. Cox, Roeland P. van der Marel, and Charles Alcock 275

Star Formation in the SMC Young Cluster NGC 602: Spatial and Temporal Distribution
Lynn Redding Carlson, E. Sabbi, M. Sirianni, J. L. Hora, A. Nota, M. Meixner, J. S. Gallagher III, M. S. Oey, A. Pasquali, L. J. Smith, M. Tosi, and R. Walterbos 277

Supernova Remnant Populations in Nearby Star-Forming Galaxies
Laura Chomiuk and Eric Wilcots 279

Simulations of Dynamical Evolution of Galaxy Groups
Yaroslav Chumak and Oleg Chumak 281

Surveying the Monoceros Ring: Locations, Velocities and a Contentious Dwarf
Blair Conn, G. Lewis, R. Lane, R. Ibata, N. Martin, and M. Irwin 283

The Stellar Structures Around Disk Galaxies
Igor Drozdovsky, N. Tikhonov, A. Aparicio, C. Gallart, M. Monelli, S. Hidalgo, E. J. Bernard, O. Galazutdinova, G. Bono, N. Sanna, and the LCID team 285

A Long Overdue Synthesis Image of Centaurus A
Ilana J. Feain, T. J. Cornwell, R. D. Ekers, R. Norris, B. M. Gaensler, J. Ott, M. Johnston-Hollitt, T. Murphy, E. Middelberg, and J. Bland-Hawthorn 287

The SAGE View of Star Formation in the Large Magellanic Cloud
Jason Harris, B. Whitney, K. Gordon, M. Meixner, M. Meade, B. Babler, R. Indebetouw, J. Hora, C. Engelbracht, B.-Q. For, M. Block, K. Misselt, U. Vijh, C. Leitherer, and T. Robitaille 289

CO 4–3 and [C I] 1–0 in Circinus and NGC 4945
Carsten Kramer, Marc Hitschfeld, Manuel Aravena, Frank Bertoldi, Jürgen Stutzki, Yasuo Fukui, and the NANTEN2 team 291

Atomic Gas Associated with GMCs in the LMC
Annie Hughes, T. Wong, J. Ott, E. Muller, J. L. Pineda, and Y. Mizuno 293

Molecular Clouds and Star Formation in the Magellanic System by NANTEN
Akiko Kawamura, Y. Mizuno, T. Minamidani, N. Mizuno, T. Onishi, A. Mizuno, and Y. Fukui 295

Wide-Field Imaging Survey of Leo II Dwarf Spheroidal Galaxy: Stellar Content and Distribution
Yutaka Komiyama 297

Interactions and Star Formation Activity in Wolf-Rayet Galaxies
Ángel R. López-Sánchez and César Esteban 299

Interactions and Starburst Activity in Galaxy Groups: The Case of Tol 9 in Klemola 13 Group
Ángel López-Sánchez, B. S. Koribalski, C. Esteban, and J. Hibbard 301

The Complex H I Structure of IC 10
Eva Manthey and Tom Oosterloo 303

Constrained Simulations of the Local Universe
Luis A. Martinez-Vaquero, Gustavo Yepes, Yaniv Dover, Yehuda Hoffman, Anatoly Klypin, and Stefan Gottlöber 305

The Outer Stellar Populations in the LMC
Ingrid Meschin, C. Gallart, A. Aparicio, R. Carrera, M. Monelli, and P. B. Stetson 307

Characterising Magellanic Stream Turbulent H I
Deanna Matthews, Lister Staveley-Smith, Peter Dyson, Naomi McClure-Griffiths, and Erik Muller 309

An Observational Study of the GMCs in the Magellanic Clouds in Millimeter and Submillimeter Wavelengths
T. Minamidani, N. Mizuno, Y. Mizuno, A. Kawamura, T. Onishi, T. Hasegawa, K. Tatematsu, M. Ikeda, Y. Moriguchi, N. Yamaguchi, J. Ott, T. Wong, E. Muller, J. L. Pineda, A. Hughes, L. Staveley-Smith, U. Klein A. Mizuno, S. Nikolić, R. S. Booth, A. Heikkilä, L.-Å. Nyman, M. Lerner, G. Garay, S. Kim, M. Rubio, and Y. Fukui 311

The Results of Sub-mm Observations in the Large Magellanic Cloud with the NANTEN2 Telescope
Yoji Mizuno, N. Mizuno, A. Kawamura, T. Onishi, Y. Fukui, H. Ogawa, J. Stutzki, F. Bertoldi, B. C. Koo, M. Rubio, M. Burton, A. Benz, and the NANTEN2 Team 313

Kiso Outer Galaxy Survey: Stellar Radial Distribution of the Galaxy
Hiroyuki Nakanishi, H. Mito, F. Egusa, S. Komugi, Y. Nakada, N. Kobayashi, S. Onodera, T. Aoki, Y. Sofue, R. Kandori, and T. Miyata 315

Large Magellanic Cloud Distance from Cepheid Variables using Least Squares Solutions
Choong Ngeow and S. M. Kanbur 317

High-Resolution Dark Matter Density Profiles of Two THINGS Dwarf Galaxies
Se-Heon Oh, W. J. G. de Blok, Fabian Walter, and Elias Brinks 319

VLA-ANGST: Star Formation History and ISM Feedback in Nearby Galaxies
Jürgen Ott, Evan Skillman, Julianne Dalcanton, Fabian Walter, Andrew West, Bärbel S. Koribalski, and Dan Weisz 321

Lessons from the Space Velocities of the Satellite Galaxies of the Milky Way
Carlton Pryor, Slawomir Piatek, Edward Olszewski 323

Spectral Diagnostics, Kinematics and Abundances Based on a New Population of Planetary Nebulae Discovered in the LMC
Warren Reid and Quentin Parker 325

Magellanic Clouds in Interaction: Evolutionary Search for Good Models
Adam Ruzicka, Jan Palous, and Christian Theis 327

Compact and Isolated Groups of Galaxies in the Local Universe
Julio Saucedo-Morales, P. Loera-González, and A. Santillán-González . . 329

Structure and Kinematics of CO ($J = 2 - 1$) Emission in the Central Region of NGC 4258
Satoko Sawada-Satoh, P. T. P. Ho, S. Muller, S. Matsushita, J. Lim . . . 331

Infrared Excess Emission From Asymptotic Giant Branch Stars in the Large Magellanic Cloud
Sundar Srinivasan, M. Meixner, U. Vijh, C. Leitherer, K. Volk, F. Markwick-Kemper, R. D. Blum, J. R. Mould, K. A. Olsen, S. Points, B. A. Whitney, M. Meade, R. Indebetouw, J. L. Hora, K. Gordon, C. Engelbracht, B. For, M. Block, and C. Misselt 333

The Origin of the Giant Stellar Stream of M 31
Mikito Tanaka, M. Chiba, Y. Komiyama, M. Iye, and P. Guhathakurta . 335

SkyMapper and the Southern Sky Survey
Patrick Tisserand, S. Keller, B. Schmidt, and M. Bessell 337

NIBLES: an HI Census of Local SDSS Galaxies
Wim van Driel, S. Schneider, M. Lehnert, and the NIBLES Consortium 339

Fabry-Pérot Interferometry of Nearby Irregular Dwarf Galaxies
Janine van Eymeren, Michel Marcelin, Dominik J. Bomans 341

Astronomers! Do You Know Where Your Galaxies are?
Matthew T. Whiting 343

The Effelsberg–Bonn H I Survey (EBHIS)
Benjamin Winkel, J. Kerp, P. Kalberla, and R. Keller 345

Near-Infrared Properties of NOIRCAT
O. Ivy Wong, Rachel L. Webster, Meryl Waugh, Virginia A. Kilborn, and Lister Staveley-Smith 347

Galaxy Transformation in Action! The Spiral Galaxy WKK 6176
Patrick A. Woudt, Renée C. Kraan-Korteweg, Uta Fritze-von Alvensleben, and John Lucey 349

Early-Type Galaxies at z < 0.2 Seen with GALEX
Suk-Jin Yoon, Hyun-Jin Bae, Kiyun Yun, Yumi Choi, Seok-Joo Joo, Hong-Gyun Woo, and Mihwa Han 351

List of Participants 353

Index 357

Part I

Invited and Contributed Talks

The Local Velocity Anomaly

R. Brent Tully

Institute for Astronomy, University of Hawaii, Honolulu, USA
tully@ifa.hawaii.edu

1 Historical Notes

1.1 What is the Local Velocity Anomaly?

The Local Velocity Anomaly was first discussed at the Vatican Conference in 1988 [3, 19] and was given attention for a few years [5, 6, 24]. Subsequently, there has been little notice of the phenomenon. The observation is the following: our Galaxy lies in a structure that has very low internal motions in a cosmic expansion reference frame but there is a discontinuity of velocities as we step to the nearest adjacent structures. A modern view of peculiar velocities is provided by Figure 1 [12]. In earlier discussions, we referred to our home structure as the Coma–Sculptor Cloud. Here we refer to the co-moving part of it as the 'Local Sheet'. The nearest adjacent structure is the Leo Spur, found to have large negative peculiar velocities.

There is a relationship to the historic Hubble Constant controversy. There was a point of view [2, 10] that what was seen as the Local Velocity Anomaly was just a manifestation of Malmquist bias. The normal consequence of Malmquist bias is underestimation of distances that gets worse as one goes farther away, resulting in increasing estimates of the Hubble parameter with distance [17]. An upturn in the Hubble parameter is seen at ~ 1000 km s^{-1}. Is it due to Malmquist bias (and low H_0) or is it something that, at least in part, requires a physical explanation? Malmquist bias can be mitigated [22]. In any event, modern data shows unambiguously that the Local Velocity Anomaly is a real phenomenon.

1.2 The Great Attractor Problem

Since that same Vatican Conference there has been an appreciation that what we see in the distribution of galaxies does not adequately explain the motion inferred by the Cosmic Microwave Background (CMB) dipole [12]. Our motion with respect to the CMB reference frame is close to the plane of our Galaxy

B.S. Koribalski, H. Jerjen (eds.), *Galaxies in the Local Volume*,
doi: 10.1007/978-1-4020-6933-8_1,

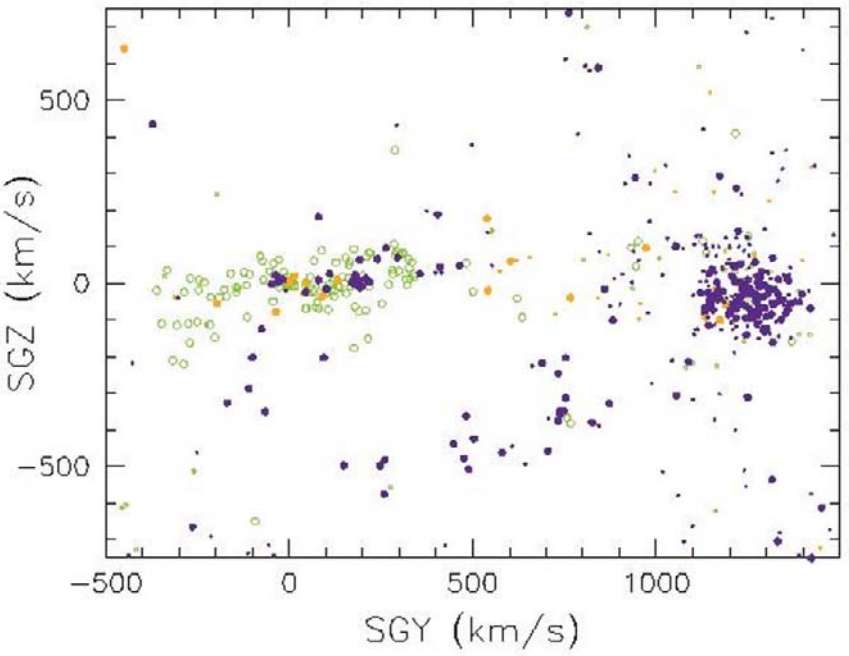

Fig. 1. Peculiar velocities < -100 km/s are coded solid purple (black), peculiar velocities $> +100$ km/s are coded solid orange (grey), and peculiar velocities within 100 km/s of zero are coded green (grey) with open symbols. Our Galaxy lies at SGY=SGZ=0 within the "Local Sheet". The Leo Spur lies at negative SGZ and the Virgo Cluster is the dense clump of galaxies at the right.

(even after subtraction of our Galactic orbital motion). The dipole in the distribution of galaxies, as determined back in 1988 from the distribution of galaxies seen in Figure 2 [7] was near but not precisely aligned with the CMB dipole direction. It was reasonable to suspect that there were many galaxies hidden in the zone of avoidance and a considerable industry developed to look for them [9, 7]. Objects were found but not in the quantity required to explain the offset of the CMB dipole direction away from the supergalactic equator (defined by the ridgeline of the pronounced vertical band to the right of center in the plot) toward the supergalactic south (to the right of that ridgeline). Already in 1988 [12], the prescient but unsubstantiated suggestion was made that this offset might be the consequence of a push from the Local Void.

1.3 Dynamical Models

There have been attempts to reconstruct the development of local structure [15, 18]. Numerical Action models involve the reconstruction of orbits to match

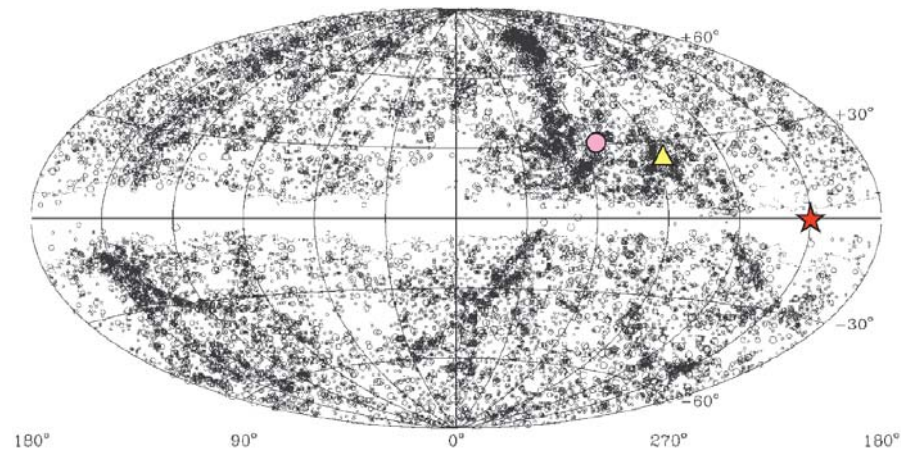

Fig. 2. Distribution of galaxies in Galactic coordinates, adapted from reference [7]. The CMB dipole apex is indicated by the yellow triangle. The dipole in the distribution of observed galaxies is indicated by the pink circle. The offset could be due to sources in the plane of the Milky Way, say centered in the vicinity of the red star. Alternatively, the offset might be attributed to a *lack* of galaxies 180° removed in longitude.

the observed distribution of galaxies. Masses are assigned to galaxies in proportion to light. Resultant models are evaluated through a comparison of predicted and observed peculiar velocity fields. The greatest deficiency of the models has been an inability to explain the *amplitude* of the motions seen in the Local Velocity Anomaly. Model velocities were only large enough with unreasonably large masses assigned to nearby galaxies. More on the resolution of this problem in the ensuing discussion.

1.4 The Local Void

The Local Void was identified in the *Nearby Galaxies Atlas* [11]. It begins at the edge of the Local Group. It is poorly understood because much of it lies behind the plane of the Milky Way. It is hard to see nothing, especially when it is obscured. The H I Parkes All Sky Survey [9] penetrates the zone of avoidance and clearly shows that the Local Void is to be taken seriously. The Local Void occupies much of the foreground in the underdense region in the left half of Fig. 2.

2 What's New?

We now have a database of almost 1800 distances to galaxies within 3000 km/s. Over 600 of these have accuracies better than 10%, derived from either the

Cepheid Period–Luminosity [4], Tip of the Red Giant Branch (TRGB) [16], or Surface Brightness Fluctuation [2] methods. The rest are based on luminosity–linewidth measures [8, 20, 22]. With distances, d, it is possible to separate the radial component of peculiar velocities, V_{pec}, from observed velocities, V_{obs}: $V_{pec} = V_{obs} - H_0 d$. In this analysis we take $H_0 = 74$ km/s/Mpc.

A map of peculiar velocities is shown in the aitoff projection in supergalactic coordinates of Figure 3. It is seen that motions in the lower right quadrant are overwhelmingly toward us while motions in the upper left quadrant are predominantly away from us. This pattern can be explained if we have a velocity toward the lower right quadrant. The inferred apex of our motion is identified on the figure by the cross labeled 'LSC'. The relationship with the CMB dipole should be noted.

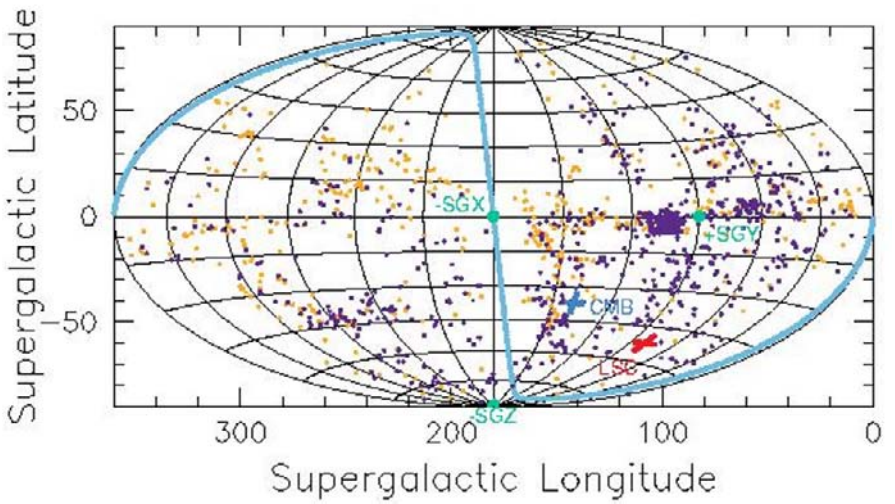

Fig. 3. Peculiar velocities of galaxies within 3000 km/s projected in supergalactic coordinates. Peculiar velocities $> +100$ km/s are indicated by orange (grey) circles and peculiar velocities < -100 km/s are in purple (black). The Virgo Cluster is seen as the dense knot of objects near the +SGY axis. The motion of the Local Sheet with respect to these galaxies is toward the red cross labeled 'LSC' (Local Supercluster). The direction of the CMB vector in the same rest frame is indicated by the blue cross labeled 'CMB'. The blue (grey) band indicates the plane of our Galaxy. The directions of the supergalactic –SGX, +SGY, and –SGZ axes are labeled.

Figure 4 uses the same data but steps from our location at the center of the scene to a vantage point looking in from a large distance. From the viewing position that is chosen, once again galaxies in the lower right tend to have negative peculiar velocities and galaxies in the upper left tend to have positive peculiar velocities. *The pattern is explained if we are moving with respect to*

the ensemble of observed objects toward the lower right, in the direction of the bar emanating from the origin.

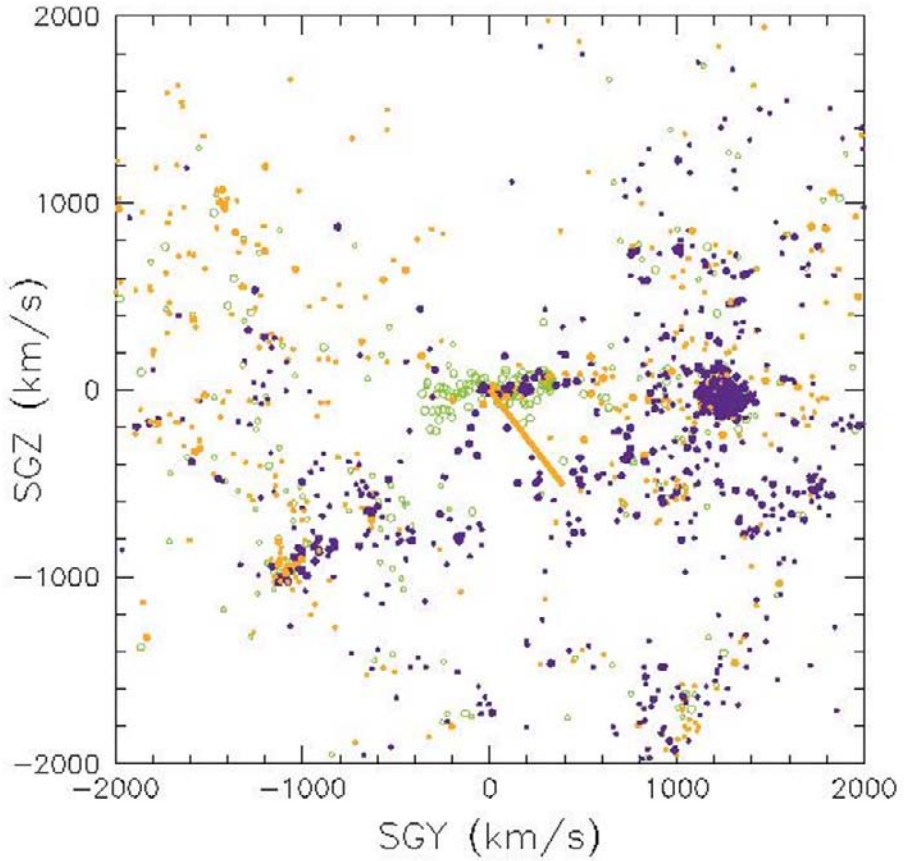

Fig. 4. Peculiar velocities seen by an observer on the +SGX axis in supergalactic coordinates. Large negative and positive peculiar velocities are shown in orange (grey) and purple (black) as in the previous figure. As in Fig. 1, galaxies with peculiar velocities within 100 km/s of zero are shown by open green (grey) circles. The Local Sheet, the horizontal structure around the origin, is moving in the direction of the orange (grey) bar toward the lower right. The Virgo Cluster is at SGY = 1200 km/s, SGZ = 0 km/s; the Fornax Cluster is at SGY = –1000 km/s, SGZ = –1000 km/s.

We zoom in on this scene with Figure 5. It is seen that the pattern of peculiar velocities (negative to lower right, positive to upper left) only begins beyond $\sim$ 7 Mpc, outside our immediate structure. Within 7 Mpc, almost 200 galaxies now have well observed TRGB distances and are found to be expanding with roughly the Hubble law with very low peculiar velocities [7].

This entire local region is moving together in the direction toward the lower right. We are calling our co-moving flattened structure the *Local Sheet*.

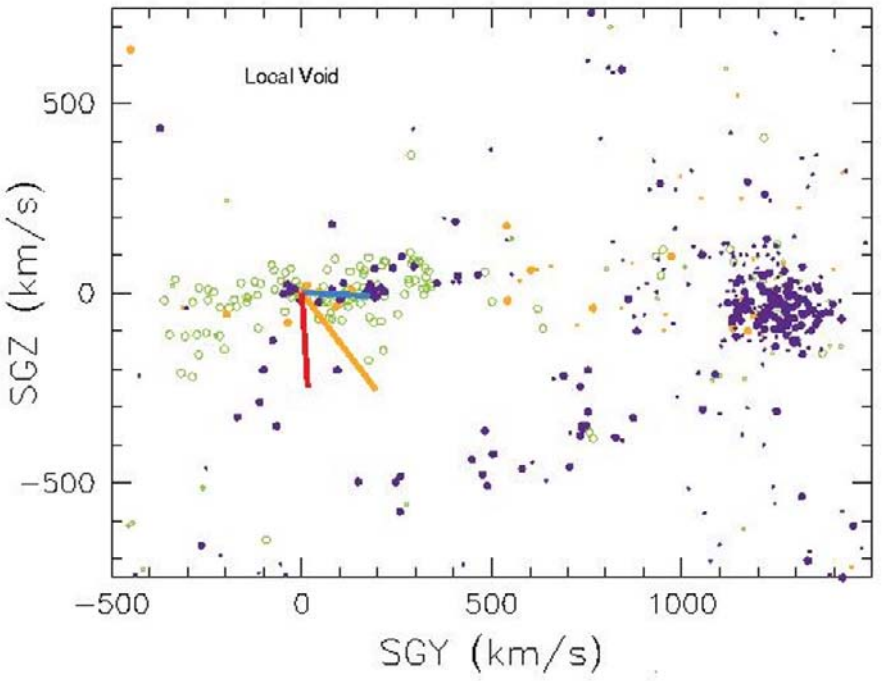

Fig. 5. Blow up of the central region of Fig. 4. The vector of the motion of the Local Sheet with respect to galaxies with measured distances less than 3000 km/s is indicated by the orange (grey) bar pointing toward the lower right. The horizontal blue (black) bar is the component of the Local Sheet motion directed toward the Virgo Cluster, the clump at the right edge of the figure. The residual, after subtraction of the component toward the Virgo Cluster from the observed Local Sheet motion, is the red (black) bar directed almost straight down. Motion in this direction is suspected to be due to expansion away from the Local Void at positive SGZ.

The Virgo Cluster is the prominent knot of objects with net negative velocities at the right edge of Fig. 5. It has long been appreciated that this structure influences our motion [1] and dynamical models provide an estimate of the amplitude [14]. The velocity of the Local Sheet with respect to galaxies beyond 7 Mpc and within 3000 km/s is 323 km/s. A component is directed toward the Virgo Cluster with an amplitude of 185 km/s, which is in reasonable accord with expectations given $\sim 1 \times 10^{15}\ M_\odot$ in the cluster at 17 Mpc. If this component is subtracted from the observed vector, the result is a vector

of amplitude 259 km/s in a direction close to the supergalactic south pole. This direction is orthogonal to the disk of the Local Sheet. It is not toward anything substantial, but it is directly *away* from the Local Void.

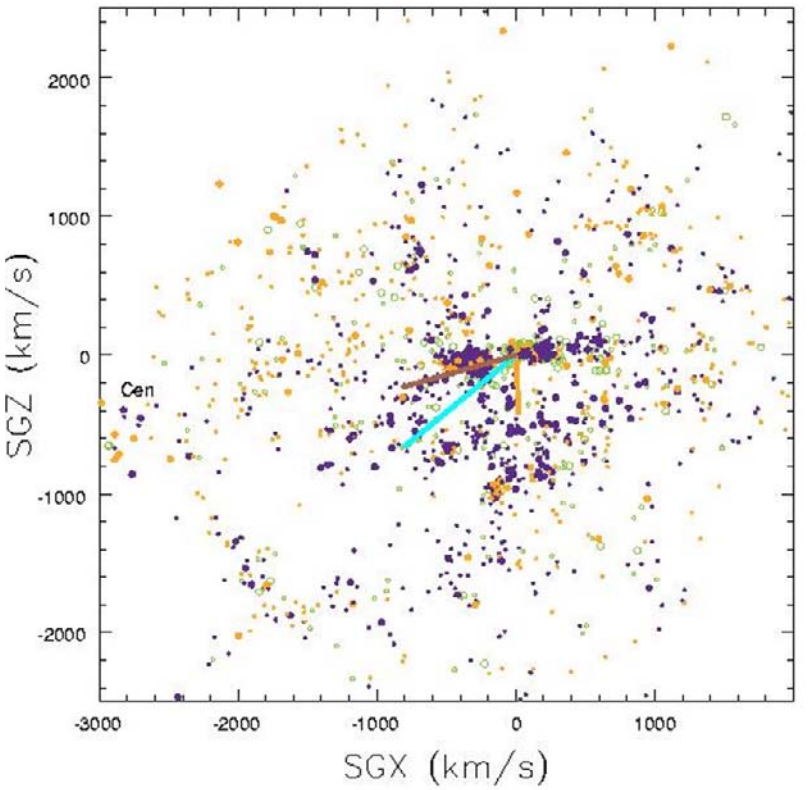

Fig. 6. Peculiar velocities seen by an observer looking in along the –SGY axis. From this angle, rotated 90 degrees from Fig. 4, the orange (grey) vector of the motion of the Local Sheet with respect to galaxies within 3000 km/s is pointed almost straight down. The CMB vector in the same frame of rest is indicated by the cyan (grey) bar pointing down and to the left. The difference, if the orange vector is subtracted from the cyan vector, gives the brown (black) bar pointing almost horizontal to the left. This is a vector attributed to influences on scales greater than 3000 km/s. It is directed quite close to the position of the Centaurus Cluster at SGX = –2700 km/s, SGZ = –500 km/s.

We will return to a consideration of the motion away from the Local Void in the next section, but let us first look at the importance of this component in the inventory that makes up the motion reflected in the CMB dipole. With Fig. 6 we have rotated 90° in the supergalactic equatorial plane and see that

the orange vector displayed in Fig. 4 is directed almost straight down in this new view. The cyan vector directed toward the lower left is the projection of the CMB dipole vector of 631 km/s. The difference between these two is the brown vector of 455 km/s, pointing almost horizontal (ie, close to the supergalactic equator) to the left. This component was not picked up by our sample of distances, so is attributed to structure at velocities greater than 3000 km/s.

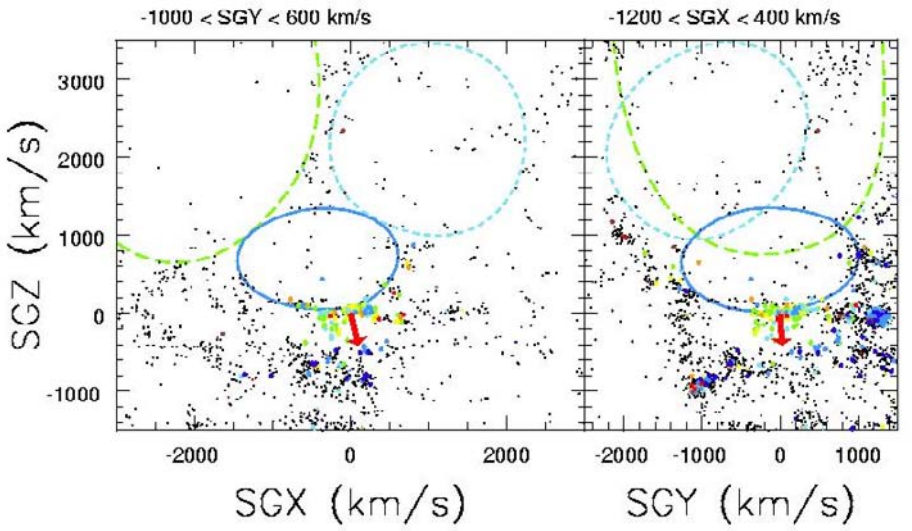

Fig. 7. Two projections of the region of the Local Void. The ellipses outline three apparent sectors of the Local Void. The solid dark blue ellipse shows the projection of the nearest part of the Local Void, bounded at our location by the Local Sheet. North and South extensions of the Local Void are identified by the light blue short–dashed ellipse and the green long–dashed ellipse, respectively. These sectors are separated by bridges of wispy filaments. The red vector indicates the direction and amplitude of our motion away from the void.

3 Voids Push

In a more complete description of this research [12] it is shown that a completely empty hole in an otherwise uniform medium in a ΛCDM cosmology with matter density $\Omega_m = 0.3$ expands at 16 km/s/Mpc. In the present situation, we want to interpret 260 km/s as expansion away from the Local Void. It is required that the Local Void have a diameter of at least 45 Mpc. To the degree that it is not empty, it must be larger.

There is an attempt to illustrate the region of the Local Void with Figure 7. It is difficult to give a fair representation, first because much of it is concealed behind the center of our Galaxy, and second because it is so very large. The region is not entirely empty of galaxies. Several minor filaments lace through the volume and motivate us to separate the nearest part of the Local Void from more distant North and South extensions. On observational grounds, an ensemble void region of greater than 45 Mpc cannot be excluded.

A probem mentioned earlier with dynamic models is now illuminated. Those models require some assumption about the distribution of matter in the zone of avoidance. A priori, it would be unreasonable to assume that this region is empty, and modelers use a variety of recipes that usually result in assigning the mean density to unseen places. Future models should consider what happens if the sector of the Local Void is left empty.

Perhaps the most interesting issue raised in this study is the following. There are debates about whether voids are really empty of matter or whether they are just low density regions where star formation is inefficient. Researchers have studied voids at large distances in attempts to answer this question but have given little attention to the void that starts only 1 Mpc away. We are in a unique position to study the peculiar motion of the shell bounding our own void. The observed motion away from the Local Void, the Local Velocity Anomaly, might represent the best available evidence that voids are really empty.

This report summarizes research undertaken with Ed Shaya, Igor Karachentsev, Hélène Courtois, Dale Kocevski, Luca Rizzi, and Alan Peel and published as reference [12]. Videos in support of the discussion are found at `http://www.ifa.hawaii.edu/~tully/`. Financial support has been provided by the US National Science Foundation and Space Telescope Science Institute.

References

1. M. Aaronson, J.P. Huchra, J.R. Mould, P.L. Schechter, R.B. Tully: 1982, ApJ, 258, 64
2. L. Bottinelli, L. Gouguenheim, G. Paturel, P. Teerikorpi: 1986, A&A, 156, 157
3. S.M. Faber, D. Burstein: Motions of Galaxies in the Neighborhood of the Local Group. In: *Large-Scale Motions in the Universe: Vatican Study Week*, ed by V.C. Rubin, G.V. Coyne (Princeton University Press 1988) p116
4. W.L. Freedman et al.: 2001, ApJ, 553, 47
5. E. Giraud: 1990, A&A, 231, 1
6. M. Han, J.R. Mould: 1990, ApJ, 360, 448
7. I.D. Karachentsev et al.: 2003, A&A, 398, 479
8. I.D. Karachentsev, S.N. Mitronova, V.E. Karachentseva, Y.N. Kudrya, T.H. Jarrett: 2002, A&A, 396, 431
9. D.D. Kocevski, H. Ebeling, C.R. Mullis, R.B. Tully: 2007, ApJ, 662, 224

10. R.C. Kraan-Korteweg, L. Cameron, G.A. Tammann: 21cm Line Widths and Distances of Spiral Galaxies. In *Galaxy Distances and Deviations from Universal Expansion*, ed by BF Madore and R.B. Tully (Reidel Publishing Co 1986) p65
11. R.C. Kraan-Korteweg, O. Lahav: 2000, A&AR, 10, 211
12. D. Lynden-Bell, O. Lahav: Whence Arises the Local Flow of Galaxies? In: *Large-Scale Motions in the Universe: Vatican Study Week*, ed by V.C. Rubin, G.V. Coyne (Princeton University Press 1988) p199
13. M.J. Meyer et al. (HIPASS collaboration): 2004, MNRAS, 350, 1195
14. R. Mohayaee, R.B. Tully: 2005, ApJ, 635, L113
15. S.D. Phelps, P.J.E. Peebles, E.J. Shaya, R.B. Tully: 2001, ApJ, 554, 104
16. S. Sakai, B.F. Madore, W.L. Freedman: 1996, ApJ, 461, 713
17. A. Sandage: 1999, AJ, 117, 157
18. E.J. Shaya, P.J.E. Peebles, R.B. Tully: 1995, ApJ, 454, 15
19. R.B. Tully: Distances to Galaxies in the Field. In: *Large-Scale Motions in the Universe: Vatican Study Week*, ed by V.C. Rubin, G.V. Coyne (Princeton University Press 1988) p169
20. R.B. Tully, J.R. Fisher: 1977, A&A, 54, 661
21. R.B. Tully, J.R. Fisher: 1987, *Nearby Galaxies Atlas*, Cambridge University Press
22. R.B. Tully, M.J. Pierce: 2000, ApJ, 533, 744
23. R.B. Tully, E.J. Shaya, I.D. Karachentsev, H. Courtois, D.D. Kocevski, L. Rizzi, A. Peel: 2007, ApJ, submitted (astro-ph/0705.4139)
24. R.B. Tully, E.J. Shaya, M.J. Pierce: 1992, ApJS, 80, 479
25. J.L. Tonry et al.: 2001, ApJ, 546, 681

Helmut Jerjen, Brent Tully, Emma Kirby and Patrick Woudt

Outlining the Local Void with the Parkes H I ZOA and Galactic Bulge Surveys

Renée C. Kraan-Korteweg[1], N. Shafi[1], B. S. Koribalski[2], L. Staveley-Smith[3], P. Buckland[3], P. A. Henning[4], and A. P. Fairall[1]

[1] Astronomy Department, University of Cape Town, South Africa
kraan@circinus.ast.uct.ac.za
[2] Australia Telescope National Facility, CSIRO, Epping, NSW 1710, Australia
[3] School of Physics, University of Western Australia, Australia
[4] Institute for Astrophysics, University of New Mexico, Albuquerque, USA

1 The Local Void

The *Local Void* was first identified by Tully [11] as a very local region ($cz \lesssim 3000$ km s^{-1}) devoid of galaxies located next to the Galactic Bulge $0° \lesssim \ell \lesssim 90°$ within Galactic latitudes of $|b| \lesssim 30°$. The lack of galaxies in that area must partly be influenced by the high foreground extinction and star density. Nevertheless, the reality of the void was never doubted as it extends beyond the optical and near-infrared Zone of Avoidance (ZOA) and can be traced to relatively high latitudes (see Figs. 1 and 2). The continuity of low galaxy density across the opaque part of the ZOA was recently corroborated by HIPASS [5, 9, 14], which is unaffected by extinction or star density.

The actual size, extent and so-called "emptiness" of the Local Void has remained a matter of much debate. Some suggest the *Local Void* to be larger and extend to the more distant Microscopium (or Sagittarius) Void at $cz \sim 4500$ km s^{-1} (e.g. [2]), while others identified filamentary structures at larger longitudes ($l \sim 60°$) that separate off two distinct smaller voids (Delphinus and Cygnus [10, 2, 1]), hence reducing the size of the *Local Void*. Independently, careful scrutiny of sky survey plates in Hercules/Aquila did reveal various dwarf galaxies [4] suggesting that the *Local Void* might not be quite as galaxy-free as previously thought.

The interest in this nearest of voids recently escalated again with the claims on dynamical grounds, that the *Local Void* must be much larger (of the order of 50 Mpc) and extremely empty – if not filled with Dark Energy – to explain the repulsive peculiar motion of the *Local Void* on the Milky Way of $\sim$260 km s^{-1} with respect to the Local Supercluster restframe [12, 13], as well as the large peculiar motion recentley found for the dwarf galaxy ESO461-36 in the *Local Void* that seems to suggest that it is being catapulted out of the Local Void with $\sim$230 km s^{-1} [12].

B.S. Koribalski, H. Jerjen (eds.), *Galaxies in the Local Volume*,
doi: 10.1007/978-1-4020-6933-8_2,

2 The Parkes ZOA H I Surveys

Better and tighter observational constraints on the size and census of the Local Void can only be achieved through deep H I surveys. Three systematic deep H I surveys performed with the Multibeam Receiver of the 64 m Parkes radio telescope cover a large fraction of the *Local Void*. Their integration time is a factor $4-5$ longer than HIPASS [9, 14] and reach sensitivities of $rms \sim 6$ mJy [1, 6, 8]. The instantaneous velocity range is -1200 to 12 700 km s^{-1} as in HIPASS. These are the deep southern ZOA survey (ZOA) [6, 3] plus northern extension (NE) [1] which encompass the Galactic longitude range $196^\circ \leq \ell \leq 52^\circ$ for latitudes of $|b| \leq \pm 5^\circ$, plus a recent extension towards higher latitudes in the Galactic Bulge region, made because of the interest in large-scale structures such as the Local Void, the Great Attractor and the Ophiuchus (super)cluster.

The Galactic Bulge extension (GB) has an average of 20 scans, hence slightly lower compared to the 25 scans of the ZOA and NE surveys. It extends to Galactic latitudes of $\pm 10^\circ$ for the longitude range $332^\circ \leq \ell \leq 36^\circ$, reaching up to higher positive latitudes ($+15^\circ$) for $348^\circ \leq \ell \leq 20^\circ$. The combined survey area is outlined in Fig. 2.

3 Outlining the Local Void

The distribution of the galaxies detected in the deep H I surveys are displayed in Fig. 1 in a redshift cone out to 6000 km s^{-1} (ZOA+NE with dark (blue) large dots; GB with ligter (red) large dots for $5^\circ < |b| < 10^\circ$ resp. $+15^\circ$ including galaxies from the shallower HIPASS for $-10^\circ < b < 15^\circ$ (smaller dots; cyan). The redshift cones on the right-hand side reflect the galaxy distribution above (top) and below (bottom) the ZOA, for $5^\circ < |b| < 30^\circ$ respectively, based on published redshifts as in LEDA.

When discussing the various features of the *Local Void*, the reader is also referred to Fig. 2 which illustrates sky projections (in gal. coordinates) of redshift intervals of widths $\Delta v = 1000$ km s^{-1}. Note that the data outside the outlined H I survey region depends on availability of redshift data in the literature (LEDA) and constitutes an uncontrolled data set.

While the galaxy density in the longitude range of the *Local Void* (about $330^\circ - 45^\circ$) is clearly lower than the rest of the sky (Fig. 1), it is by no means as devoid of galaxies as previously thought. It is in fact quite striking that the *Local Void* area based purely on the deep H I data set (left) – which is sensitive to low-mass (gas-rich) dwarf galaxies – is much more populous compared to the *Local Void* region at higher latitudes (right panels) for which no deep H I survey is available.

The overall under-dense region seems to extend to about 6000 km s^{-1} (see both Figs. 1 & 2), hence supportive of Tully's larger void. However, a filament is visible around 3000 km s^{-1} which clearly seems to divide this larger under-dense region into a nearer and distant void (previous *Local Void* and

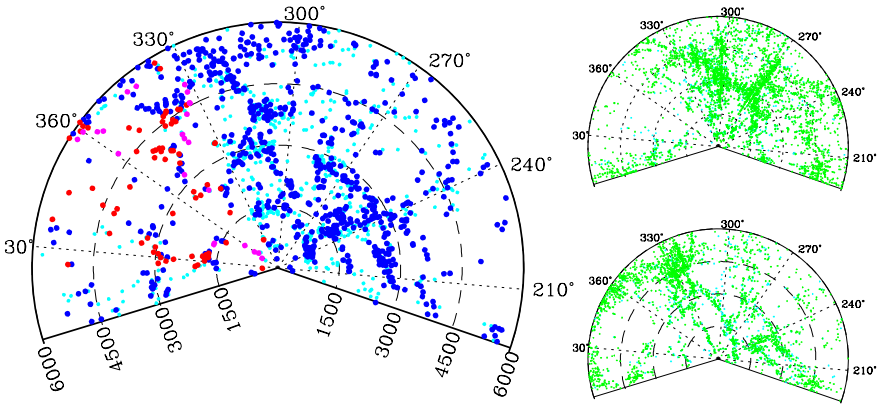

Fig. 1. Distribution of H I galaxies along the ZOA out to 6000 km s^{-1} detected in the deep Parkes H I ZOA and NE surveys ($|b| \leq 5°$; blue), the GB extension ($\pm 10°$ resp. $+15°$ for $332° \leq \ell \leq 36°$, and $348° \leq \ell \leq 20°$) as well as galaxies from HIPASS (shallower) for $-10° \leq b \leq 15°$ (small lighter dots). The boundaries of the *Local Void* lie somewhere within $330° \lesssim \ell \lesssim 60°$. For visualisation of continuation of large-scale structure, pie diagrams above *(top)* and below *(bottom)* the GP ($5° < |b| < 30°$) based on redshift data in the literature (LEDA) are shown on the *right*.

Microscopium Void). But neither of these two voids appear well defined nor really empty. Within the nearer *Local Void* there seems to exist a protrusion into that void at about 1500 km s^{-1} (prominent in both Fig. 1 & 2), while an extension that crosses the Great Attractor Wall at the location of the Norma cluster seems to cut into the more distant Microscopium void at $\ell \sim 350°, v \sim 4500$ km s^{-1} and $340°, 5000$ km s^{-1}.

It can be argued that the larger *Local Void* consists of a huge under-dense region out to $cz \lesssim 6000$ km s^{-1} from about $345° - 45°$ in longitude and $-30°$ to about $+45°$ in latitude, which possibly is connected to the Cygnus and Delphinus voids at slightly higher longitudes (see e.g. [1]). However, various filamentary features criss-cross and divide this larger *Local Void* into smaller voids. And these smaller voids are not empty either. Even within the nearest part of the *Local Void* ($cz \lesssim 1500$ km s^{-1}) some – very low mass – galaxies have been detected with the H I surveys.

A project has begun to systematically study the global properties of the galaxies in and around these voids based on their H I-masses and near-infrared morphology and luminosity. The latter is being obtained with the InfraRed Survey Facility (IRSF) at the SAAO (instantaneous JHK_s bands). Preliminary inspection of some of the *Local Void* galaxies seem to suggest that the galaxies in the voids are extreme low-mass, faint galaxies while the ones making up the borders of the smaller voids seem more consistent with normal luminous spiral galaxies.

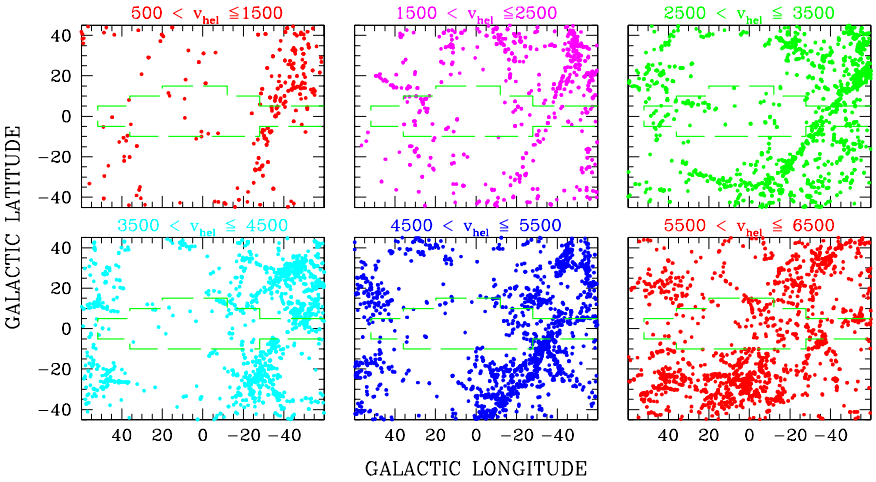

Fig. 2. Six redshift slices of widths $\Delta v = 1000$ km s^{-1} ranging from $500 - 1500$ km s^{-1} to $5500 - 6500$ km s^{-1} centered on the GB, respectively the *Local Void* based on the deep Parkes H I surveys (ZOA+NE+GB; the combined H I survey area is marked) as well as published redshifts in the literature (LEDA).

Acknowledgements. Financial support from the National Research Foundation as well as the University of Cape Town is kindly acknowledged (RKK, NS, AF). This research used the Lyon-Meudon Extragalactic Database (LEDA), supplied by the LEDA team, CRAL, Obs. de Lyon.

References

1. Donley J.L., Staveley-Smith L., Kraan-Korteweg, R.C. et al.: AJ **129**, 220 (2005)
2. Fairall A.P.: *Large-Scale Structures in the Universe*, (Wiley, Chichester 1998)
3. Henning, P.A. et al.: in prep.
4. Karachentseva V.E., Karachentsev I.D., Richter, G.M.: A&AS **135**, 221 (1999)
5. Koribalski B.S., Staveley-Smith L., Kilborn V.A. et al.: AJ **128**, 16 (2004)
6. Kraan-Korteweg, R.C.: in *From Cosmological Structures to the Milky Way*, RvMA 18, ed. S. Röser, (Wiley, New York 2005), 48
7. Kraan-Korteweg R.C., Lahav, O.: A&AR **10**, 211 (2000)
8. Kraan-Korteweg R.C., Staveley-Smith L., Donley J., Koribalski B., Henning, P.A.: in *Maps of the Cosmos*, IAU Symp. 216, eds. M. Colless, L. Staveley-Smith, & R. Stathakis, (ASP, San Francisco 2005), 203
9. Meyer M.J., Zwaan M., Webster R.L. et al.: MNRAS **350**, 1195 (2004)
10. Nakanishi K., Takata T., Yamada T. et al.: ApJS **112**, 245 (1997)
11. Tully R.B., Fisher J.R.: *Nearby Galaxies Atlas*, (Cambridge Univ. Press 1987)
12. Tully, R.B., Shaya, E.J., Karachentsev I.D. et al.: (astro-ph/0705.4139)
13. Tully, R.B.: these proceedings (astro-ph/0705.2449)
14. Wong O.I., Ryan-Weber E.V., Garcia-Appadoo D.A. et al.: MNRAS **371**, 1855 (2006)

The Context of the Local Volume: Structures and Motions in the Nearby Universe

Matthew Colless

Anglo-Australian Observatory, PO Box 296, Epping, NSW 1710, Australia
colless@aao.gov.au

1 The 6dFGS and 2MRS redshift surveys

The 6dF Galaxy Survey (6dFGS; www.aao.gov.au/local/www/6df; [6, 7]) is a redshift and peculiar velocity survey of the local universe. The observations were obtained during 2001–2006 using the AAO's UK Schmidt Telescope and the 6dF spectrograph [8]. The 6dFGS covers 92% of the southern sky with $|b|>10°$. Its primary sample is from the 2MASS Extended Source Catalog (XSC; [5]) and consists of galaxies with $K_{\rm tot} < 12.65$. For this sample the redshift completeness is 88% and the median redshift is $z \approx 0.05$. The 6dFGS also includes secondary samples to comparable limits of $H < 12.95$, $J < 13.75$ (from the 2MASS XSC) and $r_F < 15.60$, $b_J < 16.75$ (from the SuperCosmos Sky Survey [4]). The 6dFGS peculiar velocity survey is using the Fundamental Plane to derive distances and velocities for about 15,000 bright early-type galaxies. The 6dFGS database comprises approximately 137,000 spectra and 124,000 galaxy redshifts, plus photometry and images. The final data release will be made public in August 2007 (Jones et al., in prep.; see www-wfau.roe.ac.uk/6dfgs). Figure 1 shows the fine detail of the large-scale structure that is revealed by two slices through the local volume surveyed by the 6dFGS.

The 2MASS Redshift Survey (2MRS; [1, 2]) is an all-sky survey that so far has obtained redshifts for 23,150 of the 24,773 2MASS galaxies with extinction-corrected magnitudes brighter than $K_S = 11.25$ (i.e. 1.4 mag brighter than 6dFGS). Almost all of the 1600 galaxies without redshifts are at low Galactic latitudes ($|b| < 5°$) or are obscured/confused by the dust and high stellar density towards the Galactic Centre. Northern galaxies are being observed by the Whipple Observatory 1.5m telescope, the Arecibo 305m telescope and the Green Bank 100m telescope; in the south, most galaxies at high Galactic latitude (about 6000 galaxies with $|b| > 10°$) were observed as a part of the 6dFGS, while those at low Galactic latitudes are being observed at CTIO. The 2MRS has a median redshift of $z \approx 0.02$ (6000 km s^{-1}) and is the densest all-sky redshift survey to date.

B.S. Koribalski, H. Jerjen (eds.), *Galaxies in the Local Volume*,
doi: 10.1007/978-1-4020-6933-8_3,

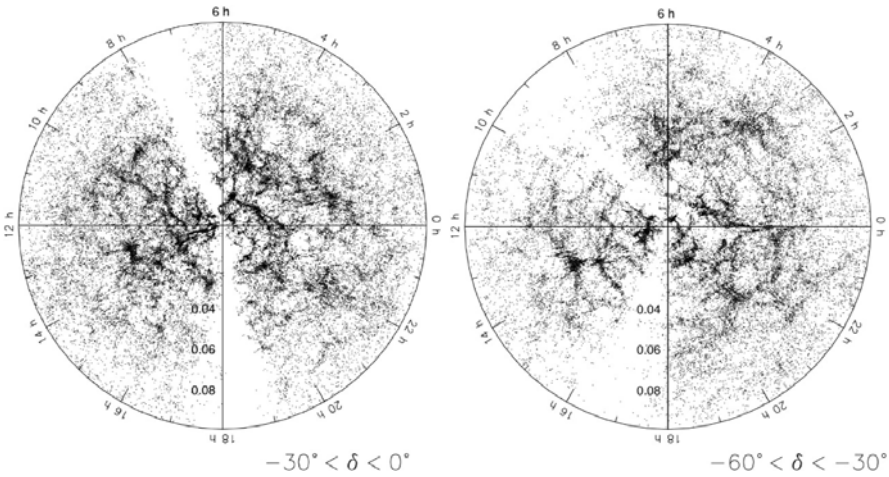

Fig. 1. Two slices through the 6dFGS volume showing the structures out to $z = 0.1$ in the declinations ranges $-30°$ to $0°$ and $-60°$ to $-30°$. The empty sectors are the projection of the $|b| < 10°$ Zone of Avoidance around the Galactic Plane.

2 The density field in the local universe

Erdoğdu et al. [1, 2] have used the 2MRS to reconstruct the density field in the local volume and to predict the corresponding velocity field and the dipole of the Local Group motion. The reconstruction is based on the linear theory of structure formation using a technique following that of Fisher et al. [3]. The 3D density field in redshift space is decomposed into spherical harmonics and Bessel functions, and then the real-space density field is constructed using a Wiener filter. This combination of spherical harmonics and Wiener filtering smooths the noisy data and gives an optimal reconstruction in the sense of minimising the variance between the true and reconstructed fields. It also allows the treatment of linear redshift distortions and greatly reduces the statistical uncertainties and errors introduced by non-linear effects. The 2MRS is well-suited to this approach due to its near all-sky coverage; the unsurveyed regions close to the Galactic Plane are masked by interpolating the distribution of neighbouring galaxies. The galaxy power spectrum assumed for the reconstruction has a CDM shape with $\Gamma = 0.2$, $\sigma_8 = 0.7$ and $\beta = 0.5$; comparison of the reconstruction to the data gives a reduced χ^2 of 1.3.

Figure 2 shows the reconstructed real-space density field in redshift shells of thickness 1000 $\mathrm{km\,s^{-1}}$ over the range $cz = 2000 - 7000$ $\mathrm{km\,s^{-1}}$. The main structures in this volume are labelled in Figure 2, and include the nearby Virgo, Hydra and Centaurus clusters, the Great Attractor region around the Norma cluster, the Perseus-Pisces and Pavo-Indus-Telescopium superclusters, and, in the outermost shell, the Coma cluster and the Great Wall. Also of interest are the large low-density void regions, in particular the network of

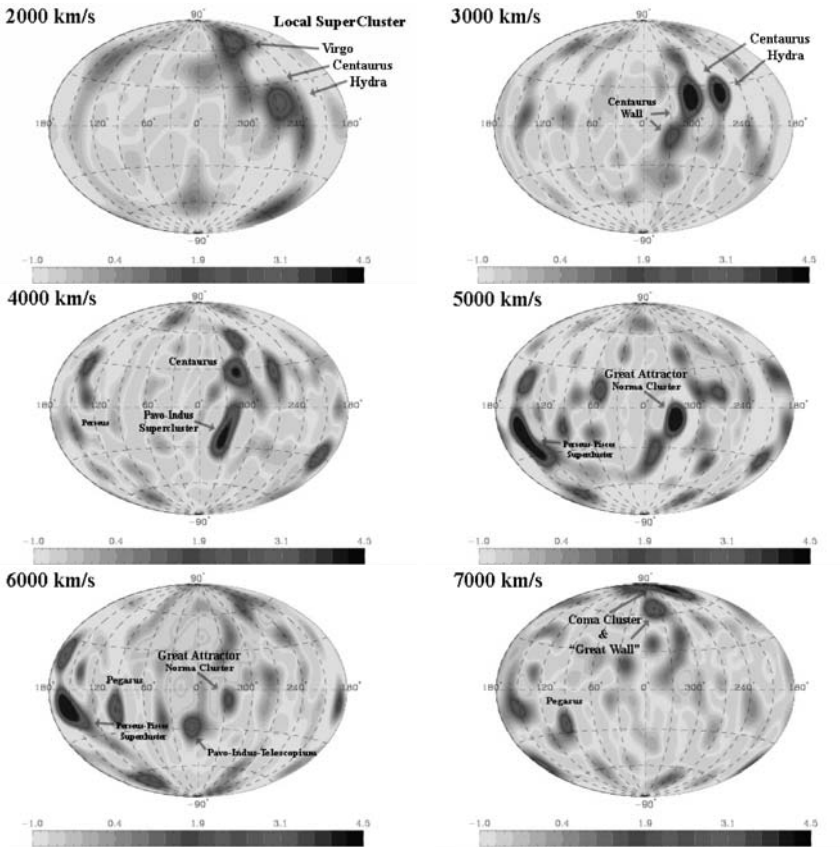

Fig. 2. The Wiener-filtered density field of the local volume in 1000 km s^{-1} thick redshift shells over the range $cz = 2000 - 7000$ km s^{-1}, from the Virgo cluster out to the Coma cluster [2].

voids including the Local Void that dominates the lowest-redshift shell. Detailed discussion of these structures can be found in [2].

3 The peculiar velocity field

The peculiar velocity field emerges simply and naturally from the Fisher et al. [3] method, since the harmonic expansion of the radial velocity field can be derived from that of the gravity field, which in turn, under linear theory assumptions, is proportional to the harmonic expansion of the density field.

Figure 3 shows the predicted velocity field obtained from the 2MRS in the Supergalactic Plane out to $cz = 20,000$ km s^{-1}; velocities are shown in both

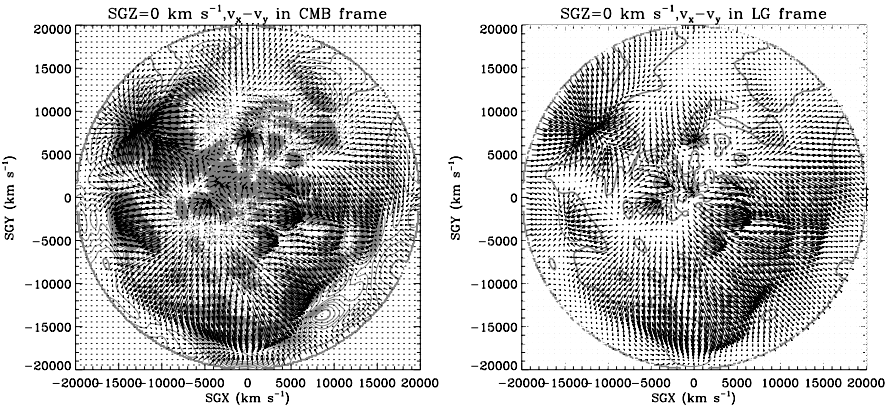

Fig. 3. The predicted velocity field in the Supergalactic Plane out to a distance of 20,000 km s^{-1}, shown in the restframes of (at *left*) the CMB and (at right) the Local Group [2].

CMB and Local Group (LG) frames. The choice of reference frame is significant: at smaller distances it is easier to see the real nature of the structures in the CMB frame than in the LG frame, as the LG velocity dominates; at larger distances, galaxies have positive CMB radial velocities, so it is easier to compare the velocities in the LG frame than in the CMB frame. There is a clear prediction for backside infall into the Great Attractor region (this is most clearly visible in the LG frame).

Together, the 2MRS and 6dFGS provide the best and most detailed information on the structures in the local universe to date. Future work will focus on comparing the predicted velocity field from the 2MRS with the observed velocity field from the 6dFGS.

Acknowledgements. I thank the 6dFGS and 2MRS teams for allowing me to present results from both projects.

References

1. P. Erdoğdu, J.P. Huchra, O. Lahav, M. Colless et al.: MNRAS **368**, 1515 (2006a), see `cfa-www.harvard.edu/∼huchra/2mass/team.php`
2. P. Erdoğdu, O. Lahav, J.P. Huchra, M. Colless et al.: MNRAS **373**, 45 (2006b)
3. K.B. Fisher, O. Lahav, Y. Hoffman, D. Lynden-Bell, S. Zaroubi: MNRAS **272**, 885 (1995)
4. N.C. Hambly, H.T. MacGillivray, M.A. Read et al.: MNRAS **326**, 1295 (2001)
5. T.H. Jarrett, T. Chester, R. Cutri et al.: AJ **119**, 2498 (2000)
6. D.H. Jones, W. Saunders, M. Colless et al.: MNRAS **355**, 747 (2004)
7. D.H. Jones, W. Saunders, M.A. Read, M. Colless: PASA **22**, 277 (2005)
8. F.G. Watson, Q.A. Parker, S. Miziarski: SPIE **3355**, 834 (1998)

Mining the Local Volume

Igor D. Karachentsev[1], Valentina Karachentseva[2], Walter Huchtmeier[3], Dmitry Makarov[1], Serafim Kaisin[1], Margarita Sharina[1], and Lidia Makarova[1]

[1] Special Astrophysical Observatory, Russian Academy of Sciences, N. Arkhyz, 369167, Russia
ikar@sao.ru,dim@sao.ru,skai@sao.ru,sme@sao.ru,lidia@sao.ru
[2] Astronomical Observatory, Kiev National University, Kiev, 04053 Ukraine
vkarach@observ.univ.kiev.ua
[3] Max-Planck-Institut für Radioastronomie, Auf dem Hügel 69, D-53121 Bonn, Germany p083huc@mpifr-bonn.de

1 The Local Volume census

The first step towards compiling a Local Volume (LV) sample of galaxies situated within 10 Mpc was made by Kraan-Korteweg & Tammann [1] who published a list of 179 nearby galaxies with radial velocities $V_{\rm LG} < 500\,{\rm km\,s^{-1}}$. Then Karachentsev [2] updated their list to 226 objects. Later, fast increasing the LV sample was proceeding by different ways: a) via Z-surveys of the known (UGC, MCG, CGCG) catalogues; b) based on special searches for dwarf members of nearby groups around M 31, M 81, IC 342, Cen A, NGC 253, M 94, M 101, NGC 6946; c) from searches for LSB galaxies in wide sky regions; d) via special H I and NIR surveys in the Zone of Avoidance; e) from blind H I sky surveys (Staveley-Smith et al. [3], Koribalski et al. [3]).

During the last decade, a comprehensive study of the LV galaxies was undertaken by Karachentseva & Karachentsev and their co-workers. The basic steps of this long-term project are listed in Table 1.

General observational data on 451 galaxies were summarized in the *Catalog of Neighboring Galaxies* by Karachentsev et al. [6]. The present version of the LV sample contains 550 objects.

As it is known, the simpler selection criterion taken for any sample, the easier interpretation of the sample properties. This Heisenberg's principle of (un)certainty gives a great advantage to the LV sample because of its simplest selection criterion, $D < 10$ Mpc.

However, an improving census of the Local Volume has a two-way traffic. Modern automated redshift surveys, like SDSS, 2dF, DEEP2, 6dF, produce a lot of spurious objects with radial velocities around zero. For instance, the DEEP2 survey generated about 700 false members of the LV fixed in LEDA

B.S. Koribalski, H. Jerjen (eds.), *Galaxies in the Local Volume*,
doi: 10.1007/978-1-4020-6933-8_4,

Table 1. Basic stages of the project.

Item	Means	Status	Results
All-sky search for new Local Volume members.	POSS-II, ESO/SERC.	100%	350 new LSB dwarf galaxies were found.
H I line survey of 600 dwarfs from KK-lists.	Effelsberg, Nancey, ATCA.	100%	100 new LV dwarfs with $V_{\rm LG} < 550$ km s^{-1}.
CCD (B,V,R)-imaging of the LV galaxies.	6m SAO, 2.5m Nordic.	50%	150 LV members resolved into stars for the first time.
Distance measurements to the LV galaxies.	HST.	50%	accurate TRGB distances to 200 galaxies.
Hα imaging all the LV galaxies.	6m SAO, 2.2m ESO.	60%	H II-pattern and SFR for 300 galaxies.
H I velocity field for 90 tiny dIrrs [5].	GMRT	80%	Dark Matter properties on scales of $\sim$1 kpc.

and NED. There are also some cases in these databases, like "dIrr galaxy" AM 0912-241 with $V_h = +614$ km s^{-1} which turns out to be a photographic emulsion defect.

2 Mapping galaxy distribution and peculiar velocities in the LV

The sky distribution of the LV galaxies looks extremely inhomogeneous owing to the presence of galaxy groups [7] and voids [8]. The spatial distribution of the nearest galaxies inside and around the Local group (LG) is presented in Fig. 1 in Supergalactic coordinates. Galaxies of different linear diameters are shown by different size balls. The circle indicates the radius of zero-velocity surface ($R_o = 0.9$ Mpc) separating the LG against the cosmic Hubble expansion. The edge-on view of the LG and its suburbs (lower panel) demonstrates larger scatter of dwarf galaxies with respect to the SG plane.

While having accurate velocities and distances for $\sim$200 LV galaxies, one can study the distribution of peculiar velocities within the LV. Fig. 2 presents a peculiar velocity map for the LV galaxies in equatorial coordinates given in the LG reference frame and smoothed with a window of 15°. The distribution shows the local Hubble flow to be generally quiet ($\pm$30 km s^{-1}) with a small area of negative peculiar velocities about –250 km s^{-1} in the direction towards the Leo constellation. This phenomena can be caused by the apparent motion of the Local Sheet as a whole from the large Local void towards the neighboring Leo cloud [9]. Note that the local peculiar velocity field observed on a scale of 10 Mpc has not any relation to the so-called Virgo-centric infall often used by different authors to "improve" distances to nearby galaxies via their velocities.

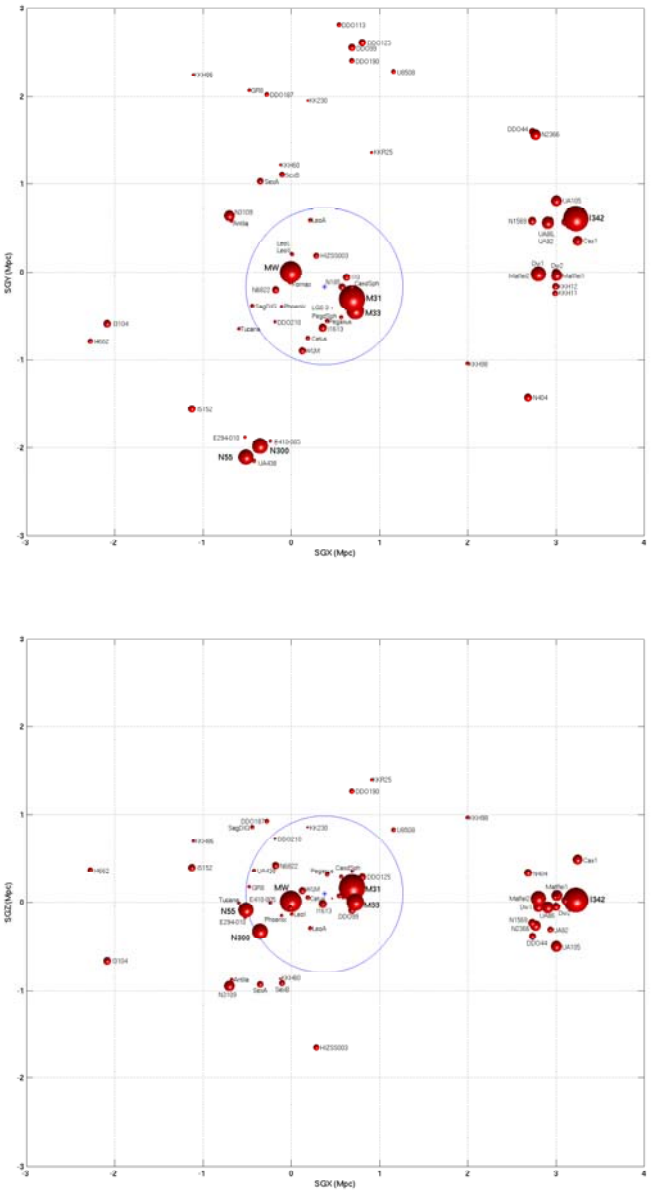

Fig. 1. Spatial distribution of the nearest galaxies inside and around the Local group in Supergalactic coordinates.

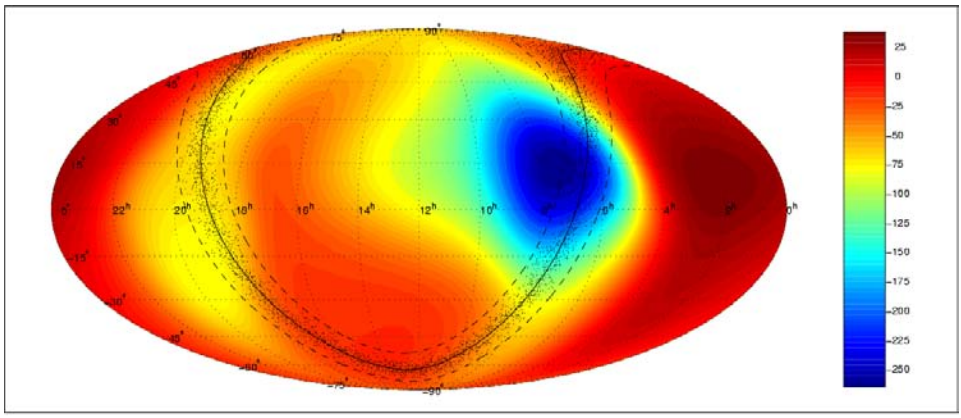

Fig. 2. Peculiar velocity map for the LV galaxies.

3 Some basic relations for the LV galaxies

Besides the global (external) Hubble law, galaxies follow another internal "Hubble law-2", the linear relation between their rotation velocity and standard radius:

$V = h \cdot R$,

where $h = 137H_0$, or $1/h = 100$ Myr. This leads to the known empirical relations between total mass M_t, luminosity L, total angular momentum J, and surface brightness SB of a galaxy:

$M_t \propto L \propto R \cdot V^2 \propto R^3$,

meaning that the average spatial densities of giant, normal, and dwarf galaxies are almost the same;

$L \propto V^3$,

corresponding on a logarithmic scale to the Tully-Fisher relation;

$J \propto M \cdot V \cdot R \propto M^{5/3}$,

which is known as Muradyan law valid for a much wider range of cellestial bodies from asteroids to galaxy superclusters [10];

$SB \propto L/R^2 \propto R$,

Binggeli-Grebel relation (valid also for E and dSph galaxies), which makes one search for extremely faint dwarf galaxies among the objects of the lowest surface brightness. These empirical scaling relations probably mean that the stellar populations of dwarf and giant galaxies reside in dark matter "corsets" of a standard profile.

As it was shown by Roberts [11], hydrogen masses of disk-like galaxies follow the empirical relation:

$M_g \propto R^2$,

i.e. the mean HI surface brightness of giant and dwarf disks is almost the same. This Roberts law leads to the following scaling relations:

$M_g/M_t \propto R^2/R^3 \propto 1/R \propto M_t^{-1/3}$,
meaning that dwarf galaxies are relatively more gas-rich systems, being capable of longer star formation activity than giant ones;

$M_g \propto R \cdot V \propto j$,
this Zasov relation between total hydrogen mass and specific angular momentum of galaxies, shown in Fig. 3, means that galaxy disks are situated in the state of equilibrium just above the threshold of gravitational instability driving their star formation processes [12].

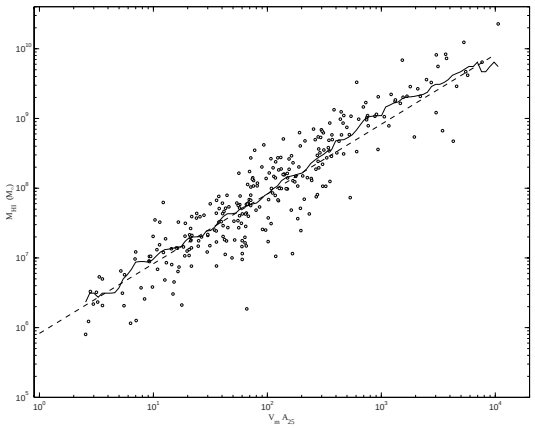

Fig. 3. The total hydrogen mass vs. specific angular momentum of galaxies.

4 Hα flux and SFR for the LV galaxies

Systematic Hα imaging of the LV galaxies allows us to measure their star formation rate (SFR) for them in an unprecedented wide range. As distinct from other samples, the LV sample offers a unique opportunity to study the SFR for galaxies of different types and in different environments without significant selection biases.

The left and right panels of Fig. 4 present the SFR of nearby galaxies versus their blue absolute magnitude and hydrogen mass, respectively. The dashed lines correspond to a constant SFR per unit luminosity or unit hydrogen mass. As can be seen from the left diagram, most of the galaxies brighter than -13^m follow a linear regression with the constant specific SFR. However, SFRs and hydrogen masses demonstrate a steeper relationship [SFR] $\propto \mathcal{M}_{HI}^{3/2}$, shown on the right panel by the solid line. This feature seems to be in harmony with the following considerations noted by Tutukov [13]. According to the Schmidt law for local SF sites, their rate of transformation of gas into stars is proportional to the square of the gas density:

$d(n_g)/dt \propto (n_g)^2$.
Taking into account the above mentioned relations between the galaxy disk parameters, we find that

$SFR \propto d(n_g)/dt \cdot R^3 \propto (n_g)^2 \cdot R^3 \propto (M_g)^2/R \propto M_g^{3/2}$,

i.e. obtain the known Kennicutt law, but for the galaxies themselves, not for individual H II regions only. Therefore, evolutionary history of disks of galaxies looks to be driven mainly by SF processes.

To characterize the past and the future evolution status of a galaxy, we introduce two dimensionless parameters:

$p_* = \log [SFR] \cdot T_0/L_B$ and $f_* = \log M_{HI}/[SFR] \cdot T_0$.

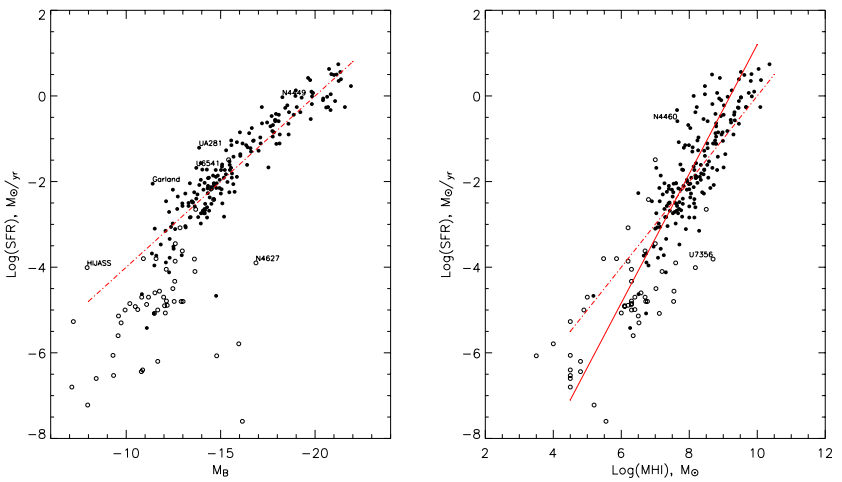

Fig. 4. The SFR of nearby galaxies vs. their blue absolute magnitude *(left)* and hydrogen mass *(right)*.

The former parameter describes the galaxy formation timescale, the latter shows the gas depletion timescale, both expressed in the Hubble time units, T_0. The distribution of the LV galaxies on the p_*, f_*-plane is displayed in Fig. 5. As a whole, the LV population concentrates around the origin ($p_* = 0, f_* = 0$) of this diagnostic diagram. It means that the observed luminosity of a typical LV galaxy may be reproduced with its observed SFR, and a typical LV galaxy has enough gas to continue its observed SFR during the next Hubble time. However, galaxies of different morphological types occupy different regions on the p_*, f_*- diagram that must be a subject of elaborate analysis.

It is generally accepted that the enhanced star formation in galaxies is triggered by their interaction. But we did not find clear evidence for such a suggestion. Curiously, the strongly disturbed tidal dwarf "Garland" near

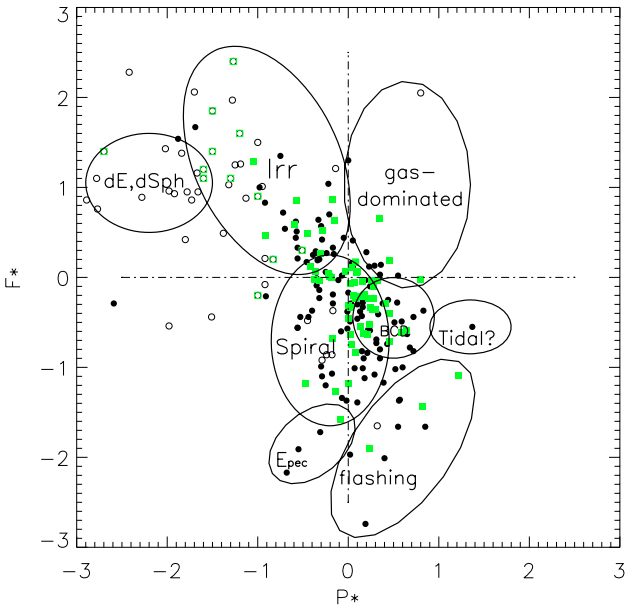

Fig. 5. Distribution of the LV galaxies on the p_*, f_*-plane.

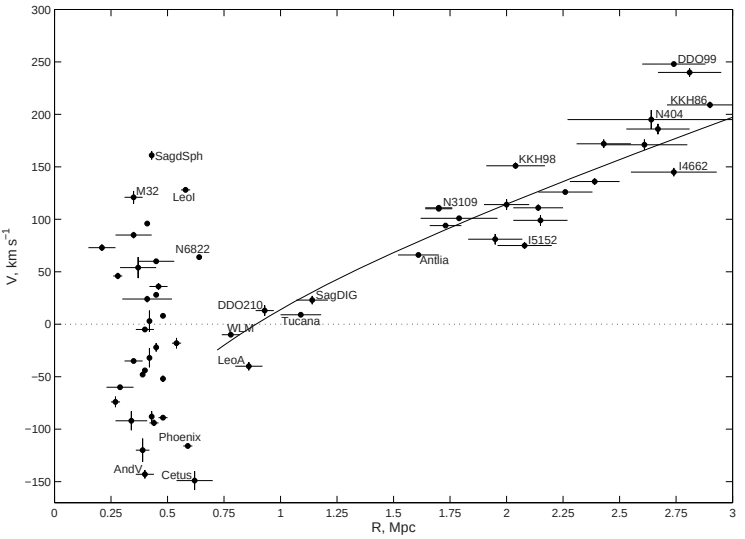

Fig. 6. The local Hubble flow in the immediate surroundings of the Local group.

NGC 3077 and the very isolated blue galaxy UGCA 281 have almost the same extremely high specific SFR (see left panel in Fig. 4).

5 Basic properties of the nearest groups

Over the last few years, searches for new nearby dwarf galaxies and accurate distance measurements for them lead to a significant increase of the population of known neighboring groups. Table 2 presents basic parameters of the seven nearest groups situated within 5 Mpc from us: distance to the group centroid, number of the group members with known radial velocities, 1D velocity dispersion, projected radius, crossing time, virial mass, total blue luminosity and virial mass-to-luminosity ratio.

Table 2. Basic parameters of the nearest groups.

Parameter	Milky Way	M 31	M 81	Cen A	M 83	IC 342	Maffei
D, Mpc	0.01	0.78	3.63	3.66	4.56	3.28	3.01
Nv	18	18	24	29	13	8	8
σ_v,km/s	76	77	91	136	61	54	59
R_p, Mpc	.16	.25	.21	.29	.16	.32	.10
T_{cross}, Gyr	2.1	3.3	2.3	2.2	2.7	5.9	1.8
M_{vir}, 10^{10}	95	84	157	725	86	76	100
L_B, 10^{10}	3.3	6.8	6.1	6.0	2.5	3.2	2.7
M/L, solar	29	12	26	121	34	24	37

Remarkably, the centroids of the groups have a radial velocity dispersion around the local Hubble flow of only 25 $\mathrm{km\,s^{-1}}$.

Precise measurements of distances and radial velocities for galaxies surrounding a group permits us to determine the radius of zero-velocity surface, R_o, which separates the group from the global cosmic expansion, and then the total mass of the group defined by Lynden-Bell [14] as

$M_t = (\pi^2/8G) \cdot R_o^3 \cdot T_o^{-2}$.

Fig. 6 exhibits the local Hubble flow in the immediate surroundings of the Local group. Distances and velocities are given with respect to the LG centroid. Similar "cold" velocity patterns are also seen around other nearby groups, yielding R_o values within $0.7 - 1.4$ Mpc.

6 Some LV parameters important for cosmology

In spite of the presence of local voids, the average density of luminosity within the radius of 8 Mpc around us exceeds $1.5 - 2.0$ times the global luminosity

density [6]. Almost the same excess is also seen in the local H I mass density [15]. About 2/3 of the LV galaxies belong to known virialized groups like the LG. Because the average virial mass-to-luminosity ratio for them is 40 $M_\odot/L_\odot$, the mean local mass density within 8 Mpc turns out to be 0.10 in units of the global critical density. This quantity is $2-3$ times as low as the global density of matter, $\Omega_m = 0.27$. To remove the discrepancy between the global and local quantities of Ω_m, we assume that the essential amount of dark matter ($\sim$70%) exists outside the virial radius of the groups.

It should be stressed that the number density of test particles (dwarf galaxies) in the LV is much higher than in any other distant volume. Therefore, systematically investigating the LV has a great advantage in probing the dark matter distribution on scales of $0.3-3$ Mpc. In this respect we note that the sum of virial mass for seven nearest groups (around the Milky Way, M 31, M 81, Cen A, M 83, IC 342, and Maffei) consists of 1.3×10^{13} $M_\odot$. But the sum of their total masses estimated via R_o from external galaxy motions is 0.86×10^{13} $M_\odot$ for the classical case of $\Lambda = 0$, and 1.25×10^{13} $M_\odot$ for $\Omega_\lambda = 0.73$. Because the mean radius R_o for the groups exceeds 5 times their mean virial radius, the agreement of independent internal and external mass estimates may be interpreted as the absence of a dark matter outside the R_{vir}. This unexpected result should be proven by new observational data.

Acknowledgements: This work was supported by DFG–RFBR grant 06–02–04017 and RFBR grant 07-02-00005.

References

1. Kraan-Korteweg, R.C. & Tammann, G.A. 1979, AN, **300**, 181
2. Karachentsev, I.D. 1994, Astron. Astrophys. Trans., **6**, 1
3. Staveley-Smith, L., Juraszek, S., Koribalski, B.S., et al. 1998, AJ, **116**, 2717
4. Koribalski, B.S., et al. 2004, AJ, **128**, 16
5. Begum, A., Chengalur, J., Karachentsev, I.D., et al. 2006, MNRAS, **365**, 1220
6. Karachentsev, I.D., Karachentseva, V.E., Huchtmeier, W.K., Makarov, D.I. 2004, AJ, **127**, 2031
7. Karachentsev, I.D. 2005, AJ, **129**, 178
8. Tikhonov, A.V. & Karachentsev, I.D. 2006, ApJ, **653**, 969
9. Tully, R.B., Shaya, E.J., Karachentsev, I.D., et al. 2007, (astro-ph/0705.4139)
10. Carrasco, L., Roth, M., Serrano, A. 1982, A&A, **106**, 89
11. Roberts, M.S. 1969, AJ, **74**, 859
12. Zasov, A.V. 1974, Astron. Zh., **51**, 1225
13. Tutukov, A.V. 2006, Astron. Rep., **50**, 526
14. Lynden-Bell, D. 1981, Observatory, **101**, 111
15. Zwaan, M.A., Staveley-Smith, L., Koribalski, B.S., et al. 2003, AJ, **125**, 2842

Brent Tully and Igor Karachentsev

Properties of Voids in the Local Volume

Anton Tikhonov[1] and Anatoly Klypin[2]

[1] Department of Mathematics and Mechanics, St. Petersburg State University, Russia avt@gtn.ru
[2] Astronomy Department, NMSU, USA aklypin@nmsu.edu

Summary. Current explanation of the overabundance of dark matter subhalos in the Local Group (LG) indicates that there may be a limit on the mass of a halo, which can host a galaxy. This idea can be tested using voids in the distribution of galaxies: at some level small voids should not contain any (even dwarf) galaxies. We use observational samples complete to $M_B = -12$ with distances less than 8 Mpc to construct the void function (VF): the distribution of sizes of voids empty of any galaxies. There are ∼30 voids with sizes ranging from 1 to 5 Mpc. We also study the distribution of dark matter halos in very high resolution simulations of the LCDM model. The theoretical VF matches the observations remarkably well only if we use halos with circular velocities larger than 45 ± 10 km/s. This agrees with the Local Group predictions. Small voids look quite similar to their giant cousins: the density has a minimum at the center of a void and it increases as we get closer to the border. Thus, both the Local Group data and the nearby voids indicate that isolated halos below 45 ± 10 km/s must not host galaxies and that small (few Mpc) voids are truly dark.

1 Introduction

The observational discovery of giant voids was soon followed by the theoretical understanding that voids constitute a natural outcome of structure formation via gravitational instability. Emptiness of voids – the number of small galaxies in the voids – is an interesting question for both the observations and the theory to tackle [1]. Cosmological simulations predict (e.g., [2]) that many small DM halos should reside in voids. There seems to be no disagreement between the LCDM theory and the observations regarding the giant voids defined by M_* galaxies or by 10^{12} $M_\odot$ halos [3]. The situation is less clear on smaller scales. In the region of ~ 10 Mpc around the Milky Way, where observations go to remarkably low luminosities, small voids look very empty: dwarf galaxies do not show a tendency to fill the voids and voids are still relatively large. The theory predicts that many dwarf dark matter halos should be in the voids, which puts it in the collision course with observations. Yet, below some mass

B.S. Koribalski, H. Jerjen (eds.), *Galaxies in the Local Volume*,
doi: 10.1007/978-1-4020-6933-8_5,

the halos are expected to stop producing galaxies inside them. There are different arguments for that: stellar feedback [4] or photoionization may play a significant role in quenching star formation in too small halos. Still, it is difficult to get a definite answer because the physics of dwarfs at high redshifts is quite complicated.

Satellites of the Local Group give a more definite answer. Current explanation of the overabundance of the dark matter subhalos [5] assumes that dwarf halos above $V_c \approx 50$ km/s were forming stars before they fall into the Milky Way or M 31. Once they fall in, they get severely striped and may substantially reduce their circular velocity producing galaxies such as Draco or Fornax with the rms line-of-sight velocities only few km/s. The largest subhalos retain their gas and continue form stars, while smaller ones may lose the gas and become dwarf spheroidals. Halos below the limit never had substantial star formation. They are truly dark. This scenario implies that $V_c \approx 50$ km/s is the limit for star formation in halos. If this picture is correct, it can be tested with small-size voids: they must be empty of any galaxies and are filled with gas and dark matter halos.

Tully [6] noted that the Local Supercluster contains a number of filaments and that those outline the so-called Local Void, which begins just outside the Local Group and extends in the direction of the North Pole of the LSC. The Local Void looks practically free from galaxies. Over the past few years special searches for new nearby dwarf galaxies have been undertaken using numerous observational data. At present, the sample of galaxies with distances less than 10 Mpc lists about 500 galaxies. For half of them the distances have been measured to an accuracy as high as 8–10% [7]. Over the last 5 years snapshot surveys with Hubble Space Telescope (HST) have provided us with the TRGB distances for many nearby galaxies. The absence of the "finger of God" effect in the Local Volume simplifies the analysis of the shape and orientation of nearby voids. Observations of the Local Volume have detected dwarf systems down to extremely low luminosity. This gives us unique possibility to detect voids which may be empty of any galaxies. Tikhonov & Karachentsev [8] analyzed nearby voids. Here we continue the analysis using an updated list of galaxies (Karachentsev, private communication). The volume limited sample is complete for galaxies with abs. magnitudes $M_B = -12$ within 8 Mpc radius.

We use N-body simulations done with the Adaptive Refinement Tree code [9]. The simulations are for spatially flat cosmological LCDM model with following parameters: $\Omega_0 = 0.7, \Omega_\Lambda = 0.3; \sigma_8 = 0.9; H_0 = 70$ km/s/Mpc. As a measure of how large is a halo we typically use the maximum circular velocity V_c, which is easier to relate to observations as compared with the virial mass. For reference, halos with $V_c = 50$ km/s have virial mass about 10^{10} $M_\odot$ and halos with $V_c = 20$ km/s have virial mass about 10^9 $M_\odot$. We use two simulations: (1) Box 80 Mpc/h (Box80); mass per particle $3 \times 10^8 h^{-1}$ $M_\odot$; simulations cover the whole volume and (2) Box 80 Mpc/h (Box80S); spherical region of 10 Mpc inside 80 Mpc/h box resolved with $5 \times 10^6 h^{-1}$ $M_\odot$ particles.

In order to detect voids, we place a 3d mesh on the observational or simulation volume. We then find initial centers of voids as the mesh centers having the largest distances to nearest objects. In the next iteration, an initial spherical void may be increased by adding additional off-center empty spheres with smaller radius. The radius of the spheres is limited to be larger than 0.9 of the initial sphere and their centers must stay inside the volume of the first sphere. The process is repeated few times. It produces voids which are slightly aspherical, but voids never become more flattened than 1:2 axial ratio. Artificial objects are placed on the boundaries of the sample to prevent voids getting out of the boundaries of the sample. We define the cumulative void function (CVF) as the fraction of the total volume occupied by voids with effective radius larger than $R_{\rm eff} = (3V_{\rm void}/4\pi)^{-1/3}$.

2 Results

We use two samples to construct the CVF of the Local Volume: (1) Galaxies brighter than $M_B = -12$ mag inside a sphere of radius 8 Mpc and (2) all galaxies inside 7.5 Mpc. Results are presented in Fig. 1 (bottom right). There are ∼30 voids in the observational sample. We limit the radius of voids to be more than 1 Mpc. The two subsamples indicate some degree of stability: the inclusion of a few low-luminosity galaxies does not change the void function.

We use the Box80 simulation (full volume) to construct a sample of 40 "Local Volumes". The selection criteria are: (1) no halos with $M > 10^{14}$ $M_\odot$ inside a 8 Mpc sphere (thus, no clusters in a sample); (2) the sphere must be centered on a halo with $150 < V_c < 200$ km/s (Milky Way analog); (3) the number of halos found inside 8 Mpc sphere with $V_c > 180$ km/s within 10% is the average number expected for a sphere of this radius. The halo catalogs are complete down to halos with circular velocity $V_c = 40$ km/s. The second simulation (Box80S) provides one sample and it is complete down to 20 km/s. Fig. 1 (bottom left) shows the CVF for different samples of halos and the observed CVF. Results indicate that voids in the distribution of halos with $V_c > 45$ km/s give the best fit to the observed CVF. The theoretical CVF goes above the observational data if we use circular velocities larger than 60 km/s. If we use significantly lower limits, than the theory predicts too few large voids. The theoretical results match the observations if we use $V_{circ} = 45 \pm 10$ km/s. In this case, the match is remarkably good: the whole spectrum of voids is reproduced by the theory.

According to LCDM simulations a totally empty front part of the Local Void is probable. In a sample of ten 8 Mpc "Local Volumes" half of the cases have voids comparable to the largest voids in the LV if we consider the entire LV sample.

The top panel in Fig. 1 shows the luminosity function of galaxies. We also show the Schechter approximation with parameters: $\alpha = -1.21$, $M_* = -19.9 + 5\log h$, $\Phi_* = 1.9\times10^{-2}h^3$ Mpc^{-3}. The approximation is the average luminosity

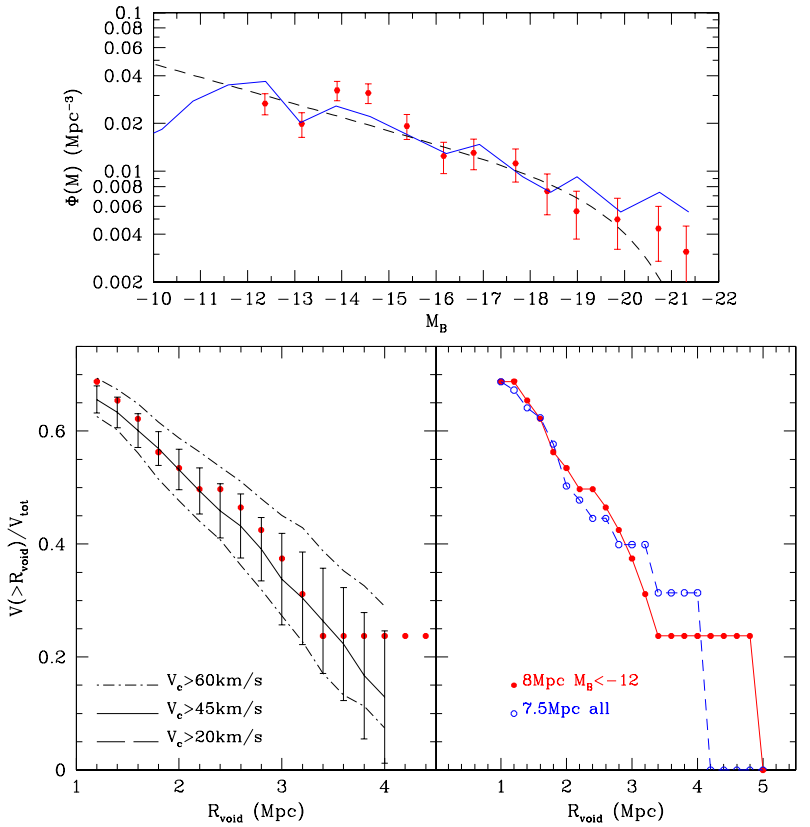

Fig. 1. *(Bottom right:)* The void function for two observational samples. The solid curve and filled circles are for a complete volume limited sample with $M_B < -12$ mag and $R < 8$ Mpc. The open circles are for all observed galaxies inside 7.5 Mpc. Comparison of the samples shows reasonable stability of the void function. *(Bottom left:)* Observational data (the complete sample) are compared with the distribution of voids in samples of halos with different limits on halo circular velocity. CVF for $V_c = 45$ km/s provides a remarkably good fit to observations. Note that the LCDM model predicts very large empty regions. *(Top:)* Luminosity function of galaxies. Circles with errors show results for 8 Mpc sample. The solid curve is for the 4 Mpc sample scaled down by factor 2.7. The dashed curve is for the Schechter approximation.

function of galaxies in the B-band in the Universe (not in our sample). It provides a very good fit to our data. This means that the sphere of radius 8 Mpc contains the average number of galaxies: $N_{8\mathrm{Mpc-sample}}/N_{\mathrm{average}} = 1$. We also show the luminosity function for another complete sample: $R < 4$ Mpc. In this case, the *shape* of the luminosity function is the same, but its normalization is different: $N_{4\mathrm{Mpc-sample}}/N_{\mathrm{average}} = 2.7$.

3 Conclusions

- The LCDM model is consistent with the cumulative volume functions of voids in the distribution of galaxies for a large luminosity range. According to LCDM, large empty voids in the Local Volume such as the Local Void are probable.
- There are significant (up to few Mpc) holes in the distribution of halos predicted by LCDM that are free from halos with $V_c > 20$ km/s: any halos of astronomical interest.
- Voids in the distribution of halos with $V_c > 45 \pm 10$ km/s reproduce the Cumulative Void Function of Local Volume galaxy sample. We can treat this value as a limit of appearance of a galaxy in a DM halo.
- The luminosity function in the Local Volume (8 Mpc) has the shape and the normalization of the average LF in the Universe. There is a substantial overdensity of galaxies inside a sphere of radius 4 Mpc. It has 2.7 times more galaxies than the average expected for a sphere of this size.

Acknowledgements

We thank I.D. Karachentsev for providing us an updated list of his 'Catalog of Neighboring Galaxies'. A. Klypin acknowledges support of NSF grants to NMSU. Computer simulations used in this research were conducted on the Columbia supercomputer at the NASA Advanced Supercomputing Division and at the Leibniz-Rechenzentrum, München, Germany. A. Tikhonov acknowledges support of grant no. MK-6899.2006.2 from the President of Russia.

References

1. P. J. E. Peebles: ApJ, **557**, 495 (2001)
2. S. Gottlöber, E. L. Łokas, A. Klypin, & Y. Hoffman: MNRAS, **344**, 715 (2003)
3. S. G. Patiri et al: MNRAS, **372**, 1710 (2006)
4. A. Dekel, & J. Silk: ApJ, **303**, 39 (1986)
5. A. V. Kravtsov, O. Y. Gnedin, & A. Klypin: ApJ, **609**, 482 (2004)
6. R. B. Tully, & J. R. Fisher: *Atlas of Nearby Galaxies* (Cambridge University Press 1987)
7. I. D. Karachentsev, V. E. Karachentseva, W. K. Huchtmeier, & D. I. Makarov: AJ, **127**, 2031 (2004)
8. A. V. Tikhonov, & I. D. Karachentsev: ApJ, **653**, 969 (2006)
9. A. V. Kravtsov, A. Klypin, & A. M. Khokhlov: ApJ Suppl., **111**, 73 (1997)

Henry Lee, Bärbel Koribalski, and Janine van Eymeren

Using Local Volume Data to Constrain Dark Matter Dynamics

Guilhem Lavaux[1], R. Mohayaee[1], S. Colombi[1], and R. B. Tully[2]

[1] Université Paris 6/Institut d'Astrophysique de Paris, 98bis Boulevard Arago, 75014 Paris, France lavaux@iap.fr
[2] Institute for Astronomy, University of Hawaii, Honolulu, USA

1 Introduction

The peculiar velocities of galaxies hold a lot of information on the current dynamical state of the mass tracers such as galaxies or groups of galaxies in the Universe. This information can be used to constrain the relationship between the mass tracers and the underlying dark matter mass distribution responsible for the observed dynamic. This gives a measurement of β, the linear growth factor of density fluctuations, which yields either a measure of $\Omega_{\rm m}$, the mean matter density in the Universe, or of the shape of the function $M/L(L)$. We propose here to show that Lagrangian reconstructions of peculiar velocities permit this kind of comparison and may serve to constrain the above two quantities. However these constraints can only be tight if observational biases are taken into account correctly, which is in most cases possible. Galaxies in the Local Volume, with good peculiar velocity measurements, may thus help constraining the dark matter dynamics.

Lagrangian reconstruction predicts peculiar velocities of individual mass tracers from only their redshift position and their mass. We will illustrate the reconstruction procedure by means of the Monge-Ampère-Kantorovitch (MAK) reconstruction, which has already been extensively tested on simulations [1, 2]. The impact of observational biases such as redshift distortion, mass-to-light assignment (diffuse mass, M/L relation), incompleteness effect, finite volume effects, statistical measurement of β has only been studied thoroughly in [3]. Here we propose to look more precisely at the consequence of choosing a specific mass-to-light assignment on detected tracers.

To study the aforementioned effects, we use a 128^3 N-body collisionless sample in a $200^3\ h^{-3}$ Mpc^3 volume [2], with $\Omega_{\rm m} = 0.30$, $\Omega_\Lambda = 0.70$. From a halo catalogue, *FullMock*, built from the sample, we have produced mock catalogues. *FullMock* is obtained using a standard Friend-of-friend algorithm, whose linking parameter is chosen to be a fifth of the mean particle separation of the original sample. Halos of less than 5 particles were left unbound and

B.S. Koribalski, H. Jerjen (eds.), *Galaxies in the Local Volume*,
doi: 10.1007/978-1-4020-6933-8_6,

the corresponding particles put in a set called the "background field". This set represents 63% of the total mass of the simulation.

2 Correctable observational biases

The result of including all the observational effects mentioned in the introduction, except the mass-to-light assignment problem, in mock catalogues are given in Fig. 1. As one can see for a standard mock catalogue, built to have approximately the same features as observed redshift catalogues (such as 2MASS Redshift Survey, 2MRS hereafter), there is no significant bias introduced on reconstructed velocities. However the scatter may be significant, all the more that the number of measurements is low, which means a good statistical description of the error is needed to achieve an unbiased Bayesian estimator of $\Omega_{\rm m}$ from measurements. A problem that is not highlighted in this figure, is that incompleteness correction, if done unwisely, *e.g.* by assuming a wrong $\Omega_{\rm m}$, may yield an offset in the relation shown in the right panel of Fig. 1. Unfortunately, a similar offset is introduced by a wrong choice of the Hubble constant H and thus its measurement may be hindered by incompleteness effects though hopefully without strongly affecting the $\Omega_{\rm m}$ measurement.

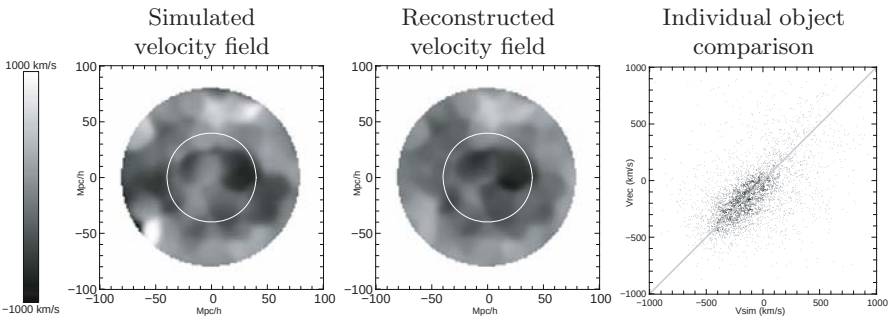

Fig. 1. Result of a reconstruction including finite volume effects (selection and boundary effects), redshift distortion, incompleteness. *(Left:)* simulated velocity field smoothed with a 5 h^{-1} Mpc Gaussian filter. The white circle shows the 40 h^{-1} Mpc region inside the 80 h^{-1} Mpc deep mock catalogue. *(Middle:)* reconstructed velocity field smoothed equally. *(Right:)* individual comparison between reconstructed and simulated velocities for halos of the mock catalogue inside the white circle.

3 Mass-to-light assignment

Diffuse mass – The first problem comes from the intrinsic limitation of redshift catalogues: they have a lower luminosity cut-off which translates to a minimum lower mass. In fact, in 2MRS, with $L_{\rm min,K} \simeq 10^9 {\rm L}_\odot$, and using [4],

we find that $\simeq 50\%$ of the mass distribution may be missing in real data. We have tried to reproduce that problem in *FullMock* by not using the background field to build the reconstruction mesh. It has lead to an overestimation of the reconstructed peculiar velocities because the gravitational field of the halos is in reality screened by the background field. On the contrary, if one predicts the amount of missing mass and introduces it homogeneously in the reconstruction mesh, reconstructed peculiar velocities are underestimated because of a too important screening effect. This two extreme cases lead, for mock catalogues, to low constraints on $\Omega_{\rm m}$: $0.15 \leq \Omega_{\rm m} \leq 0.74$. However we showed there is an optimal compromise between those two situations that give an unbiased reconstruction, with nearly no extra scatter on reconstructed velocities, when compared to a reconstruction on *FullMock*.

M/L relation – Another fundamental problem of mass-to-light assignment is the use of a unique M/L relation to transform detected galactic luminosities to dynamical masses. We have built a luminosity catalogue from *FullMock* using the M/L relation given by [5]. A mass tracer catalogue is then recovered by assuming either a constant M/L or a M/L as given by [6] which is obtained by mapping a Press-Schechter mass function to a Schechter luminosity function. The reconstructed velocities are then compared to the simulated ones. We tried also to introduce a significant uniform scatter on the logarithm of the mass M of halos in the original mock catalogue. The width of the distribution was chosen with $\Delta \log_{10} M = 1$ to be consistent with observations. The result of these three tests is that a random uncertainty on the M/L relation does not produce bias and leads only to a relatively small increase of the scatter between reconstructed and simulated velocities, whereas changing the relation (even a little) quickly introduces a significant systematic when comparing these same velocities.

4 Application to an Extended Nearby Galaxies Catalog

While these results are still preliminary (Lavaux et al., in preparation), we present here a MAK reconstruction for which we have tried to account for redshift distortion, zone of avoidance, finite volume effect and incompleteness. We chose $M/L = 300$ for elliptical galaxies and $M/L = 100$ for spiral galaxies. This choice is motivated by observations of velocity dispersion of groups. As we have neglected the influence of the diffuse mass, we are most likely going to overestimate reconstructed peculiar velocities and thus to underestimate $\Omega_{\rm m}$, as shown in § 3. Fig. 2 summarises the result obtained using this reconstruction. The reconstructed line-of-sight peculiar velocities look in agreement with measurements, at least in the central region. Of course, in the outer part of the catalogue measured velocities are both intrinsically noisy and incorrectly reconstructed because of boundary effects. The right panel shows that reconstructed velocities are well correlated to measurements but that there

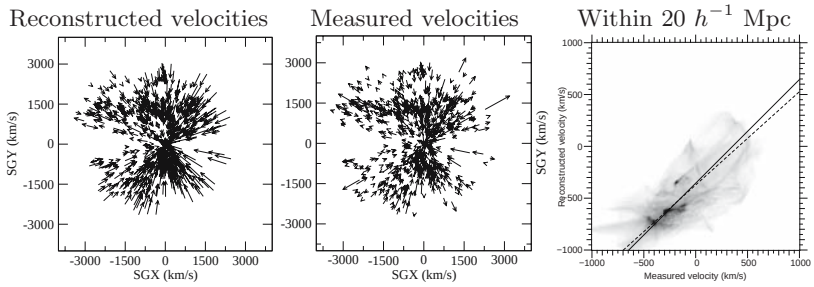

Fig. 2. *(Left:)* line-of-sight component of reconstructed velocities for objects with a measured velocity. *(Middle:)* same as left panel but for the measured velocities. *(Right:)* Comparison between reconstructed and measured velocity field, obtained after adaptive smoothing of the corresponding individual velocities on a uniform grid. The solid line corresponds to $\Omega_{\rm m} = 0.30$ and the dashed-line to $\Omega_{\rm m} = 0.38$ (result given by the Bayesian estimator).

is an offset most probably coming from an incompleteness correction defect, mentioned in § 2, that needs be corrected in future reconstructions.

5 Conclusion and perspective

So far we have checked the influence of each observational bias and shown what must be included to extract useful informations on dark matter dynamics. The first applications of our method to real galaxy catalogues look successful though are still probably affected by some of the biases. More checking must be conducted as has been done on mock catalogues to establish the amount of systematics. We are now going to apply the method to a bigger catalogue like 2MRS or 6dF to decrease finite volume effects. Other information may be extracted from Lagrangian reconstruction of the Local Volume such as local initial conditions for constrained simulations and statistical quantities (power spectrum, cosmological parameters) that may be compared to those obtained by CMB experiments.

References

1. Y. Brenier, U. Frisch, M. Hénon, G. Loeper, S. Matarrese, R. Mohayaee, and A. Sobolevskiĭ: MNRAS, **346**, 501 (2003)
2. R. Mohayaee, H. Mathis, S. Colombi, and J. Silk: MNRAS, **365**, 939 (2006)
3. G. Lavaux, R. Mohayaee, S. Colombi, R. B. Tully, F. Bernardeau, and J. Silk: MNRAS, submitted, astroph/0707.3483 (2007)
4. R. K. Sheth and G. Tormen: MNRAS, **329**, 61 (2002)
5. R. B. Tully: ApJ, **618**, 214 (2005)
6. C. Marinoni & M. J. Hudson: ApJ, **569**, 101 (2002)

The Local Volume HI Survey (LVHIS)

Bärbel S. Koribalski[1] and the LVHIS team

[1]Australia Telecope National Facility, CSIRO, PO Box 76, Epping, NSW 1710, Australia Baerbel.Koribalski@csiro.au

1 Introduction

The 'Local Volume' — the sphere of radius ∼10 Mpc centered on the Local Group — includes at least 500 known galaxies. What makes this volume special is the fact that we can obtain (a) accurate velocities and independent distances for all its member galaxies, (b) the most detailed and sensitive multi-frequency observations, and (c), as a result, a complete census of the Local Volume (LV) galaxies and their properties. This allows us to create a dynamic 3D view of the Local Universe, leading to a thorough understanding of the local flow field, ie. the Hubble flow and its dispersion. Interferometric H I measurements in particular provide a greater understanding of the overall matter distribution (baryonic and non-baryonic) in the Local Volume and are crucial to accurately define the low-mass end of the H I mass function.

Reliable, independent distance estimates for LV galaxies are being gathered either from the luminosity of Cepheids, the tip of the red giant branch (TRGB), or surface brightness fluctuations. These are listed in *'A Catalog of Neighboring Galaxies'* by Karachentsev et al. [2] together with the optical and H I properties of 451 LV galaxies. To expand and deepen our knowledge of the nearby Universe several teams are currently targeting LV galaxies, among them the *"Local Volume HI Survey"* (LVHIS; Koribalski et al.), the *"Faint Irregular Galaxies GMRT Survey"* (FIGGS; Begum et al.), *"The HI Nearby Galaxy Survey"* (THINGS; Walter et al.), and the *"VLA-ANGST HI Survey"* (Ott et al.).

2 LVHIS Observations and Results

Using the Australia Telescope Compact Array (ATCA), the LVHIS team is producing detailed H I distributions, mean H I velocity fields and 20-cm radio continuum maps for a complete sample of more than 70 southern galaxies selected from HIPASS (see, eg., Koribalski et al. 2004[3]). Each galaxy is typically observed for 3×12 hours total, using different array configurations, to

B.S. Koribalski, H. Jerjen (eds.), *Galaxies in the Local Volume*,
doi: 10.1007/978-1-4020-6933-8_7,

achieve good *uv*-coverage (out to 1.5 km baselines), medium resolution ($\sim$40″, 4 km s^{-1}) and high sensitivity (1 mJy beam^{-1}). In some cases we will be able to make very high-resolution ($\sim$10″) images using all ATCA baselines to 6 km. The low-resolution ATCA observations are now complete and the results, in particular the H I moment maps of all observed galaxies, are displayed on the web at `www.atnf.csiro.au/research/LVHIS`. — The LVHIS project goals are:

(1) Investigation of **local galaxy environments**: using H I synthesis observations we trace the faint outer envelopes of the known LV galaxies as well as detect their low-mass companions down to H I mass limits of $\sim 10^4 \times D^2$ M$_\odot$ (see, e.g., Fig. 1). We are also searching for neutral gas that is not taking part in the regular galaxy rotation, e.g. high velocity clouds and tidal streams. So far, only a few previously uncatalogued galaxies have been found while asymmetric gas envelopes are common. Several results have been shown in Koribalski 2006 [4].

(2) Determination and analysis of H I **rotation curves** (see, e.g. Bonne, this volume): these will allow us to estimate the total mass and therefore the dark matter content of individual LV galaxies and trace virtually all of the galactic dark matter in the Local Volume. We will take into account the influence of non-circular motions on the shape of rotation curves and explore a variety of models that optimally fit the best-determined curves.

(3) Determination of the true **Tully-Fisher** (TF) relation (incl. the baryonic TF): this will be achieved using independent distances, well-determined H I rotational velocities and a homogeneous set of optical & infrared magnitudes. The analysis of deep AAT *H*-band images, so far obtained for 56 LV galaxies is presented by Kirby et al. (this volume).

(4) Determination of the H I **mass function** for the Local Volume: by obtaining accurate H I masses for a complete sample of nearby galaxies with well established distances, we can significantly improve our knowledge of the faint end of the H I mass function (see also Oosterloo, this volume).

(5) Estimate of accurate **star formation rates** (or upper limits) for the sample from the 20-cm radio continuum flux density to equally faint limits ($\sim 2 \times 10^{-5} D^2$ M$_\odot$ yr^{-1}). These will be compared to SFR estimates obtained from SINGS [6] and enable us to investigate on which scales the radio-infrared correlation breaks down. We will be able to estimate the overall SFR density at $z = 0$ and compare with values measured at other wavelengths.

ATCA observations for the *"Local Volume H*I *Survey"* (LVHIS) will be finalised in 2008, but further observations with the GMRT, WSRT and the eVLA are needed to complete the census of Local Volume galaxies. All-sky and deep H I surveys planned with the Australian SKA Pathfinder (ASKAP), a large interferometer to be located in Western Australia (see Johnston et al. [1], and Staveley-Smith, this volume) will provide the next step in our understanding of the Universe.

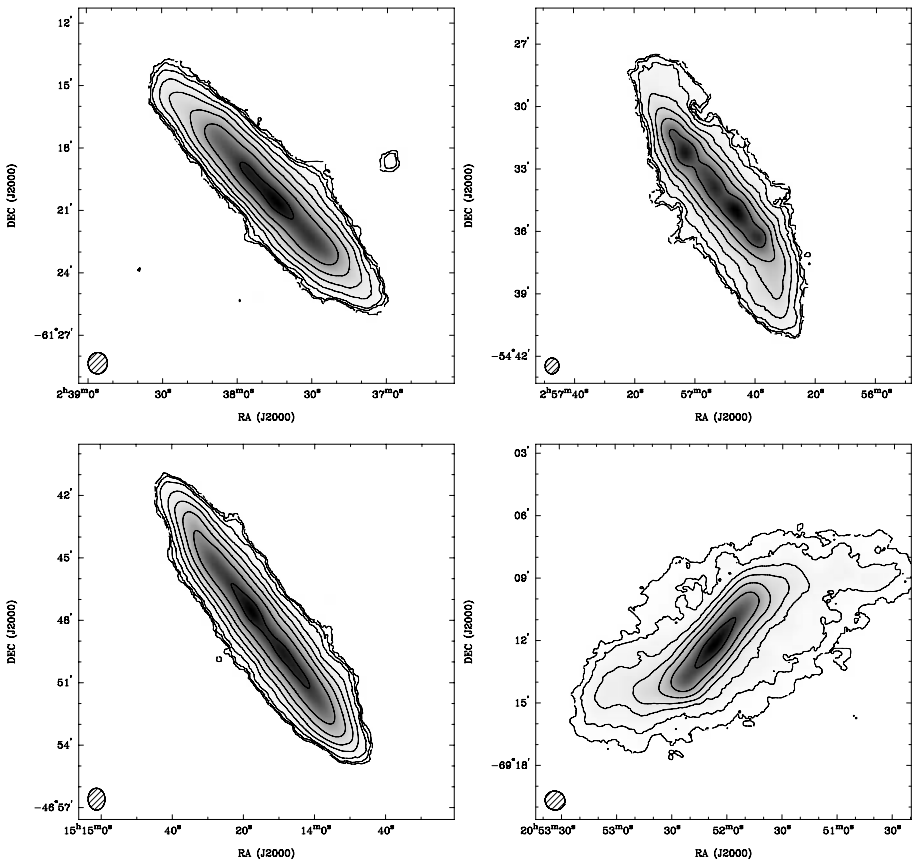

Fig. 1. ATCA H I distributions of four nearby, edge-on galaxies galaxies obtained as part of the LVHIS project: ESO115-G021 *(top left)*, ESO154-G023 *(top right)*, ESO274-G001 *(bottom left*, and IC 5052 *(bottom right)*.

In Fig. 1 we show the H I distributions of four edge-on galaxies in the Local Volume, observed with the Australia Telescope Compact Array (ATCA) as part of the LVHIS project. A detailed analysis of these galaxies will be published shortly by Koribalski and collaborators.

ESO115-G021 (HIPASS J0237–61, $D = 4.66$ Mpc) is a beautiful edge-on galaxy. with significant star-formation along the thin disk. We note that the main concentration of stars is offset (to the NE) from the galaxy centre. In the deep ATCA H I images we detect a dwarf companion ($v_{\rm sys} = 508$ km s^{-1}; $M_{\rm HI} = 4.5 \times 10^5$ M$_\odot$) at a projected distance of 6.′0 or ∼8 kpc. Some disturbance of the ESO115-G021 disk can be seen in the vicinity of the companion, possibly indicating tidal interaction.

ESO154-G023 (HIPASS J0256–54, $D = 5.55$ Mpc) is another remarkable galaxy. It shows a double-sided warp which commences outside the optical disk. The SINGG Hα image shows numerous H II regions in the inner disk.

ESO274-G001 (HIPASS J1514–46, $D = 3.02$ Mpc) is a large edge-on galaxy, slightly obscured by Galactic dust and foreground stars ($A_B = 1.1$ mag at $b = 9.^\circ3$). The H I distribution and velocity field of this galaxy are remarkably symmetric.

IC 5052 (HIPASS J2052–69, $D = 6.03$ Mpc) is the most surprising galaxy in this sample of nearby edge-on galaxies. While optical and infrared images show a rather flat, edge-on disk, the observed H I distribution indicates an extended and highly warped gaseous disk.

Given the similarity and relative isolation of all four galaxies, it will be interesting to investigate what determines, e.g., the extent and shape of their gaseous disks and the location of star forming regions. — **In summary**, we have briefly outlined the goals and status of the "Local Volume H I Survey" (LVHIS) project, and shown a few examples of the gaseous disks of nearby edge-on galaxies. The main characteristic of the LVHIS project is the delivery of homogeneous H I and radio continuum datasets for a *complete* sample of Local Volume galaxies ($D < 10$ Mpc). These datasets have high sensitivity, moderate to high angular resolution, and excellent velocity resolution. We will investigate the environments the LV galaxies, their H I rotation curves and overall mass distribution, their star formation rates, as well as the (baryonic) Tull-Fisher relation and the H I mass function.

Acknowledgements.

The author would like to thank all her collaborators in the LVHIS project who significantly contributed to the observations, analysis, and results as well as to the success of this conference: Emma Kirby, Nic Bonne, Janine van Eymeren, Ángel López-Sánchez, Igor Karachentsev, Jürgen Ott, Lister Staveley-Smith, Erwin de Blok, and Helmut Jerjen.

References

1. S. Johnston, et al.: PASA, submitted (2007)
2. I.D. Karachentsev, et al.:, AJ **127**, 2031 (2004)
3. B.S. Koribalski et al.: AJ **128**, 16 (2004)
4. B.S. Koribalski: ESO Astrophysics Symposium on *"Groups of Galaxies in the Nearby Universe"*, eds. I. Saviane, V.D. Ivanov, and J. Borissova, Springer, p. 27 (2006)
5. B.S. Koribalski et al.: MNRAS, submitted (2008)
6. R.C. Kennicutt et al.: PASP **115**, 928 (2003)

Investigating Dark Matter and MOND in Local Volume Galaxies

Nicolas J. Bonne

Research School of Astronomy and Astrophysics, Australian National University, Mt Stromlo Observatory, Cotter Rd, Weston, ACT 2611, Australia
nic42@mso.anu.edu.au

Summary. Employing the most recent Local Volume H I Survey (LVHIS) [5] data we are going to derive high-resolution H I rotation curves for ∼28 gas-rich nearby galaxies. Combining these kinematical results with stellar-mass tracing near-IR *H*-band photometry [5] and accurate TRGB distances [3, 4], we study the dark matter mass profiles of the sample galaxies and test the ability of Modified Newtonian Dynamics (MOND) to explain the observed rotation curves and to investigate the Mass Discrepancy-Acceleration Relation.

1 Flat Rotation Curves and the Missing Mass Problem

In the last three decades, observations made of the rotation curves of galaxies indicate clearly the presence of unseen or "missing" mass beyond their optical radii. The H I component of a spiral galaxy generally extends far beyond the luminous stellar disk of such systems. Thus, an effective means of tracing the potential and determining the distribution and quantity of this non-luminous mass is through observations of the motions of its H I component.

The shape of rotation curves and problem of missing mass is traditionally explained by invoking dark matter (generally in the form of a spherical or oblate halo surrounding the galaxy). However, an empirically equally good, though less favored solution to this problem is provided by Modified Newtonian Dynamics (MOND) [10, 9], a theory that suggests the gravitational acceleration of a particle is not linearly proportional to the force, at low values of acceleration. The flat outer portions of rotation curves observed for many late type galaxies can be well fitted by a combination of either of these two models along with disk, bulge and gas component rotation curves derived from the stellar and H I distributions.

1.1 MOND, An Alternative to Dark Matter

The theory of Modified Newtonian Dynamics or MOND, first postulated by [10, 9] implies that, rather than invoking dark matter to explain the dynamics

B.S. Koribalski, H. Jerjen (eds.), *Galaxies in the Local Volume*,
doi: 10.1007/978-1-4020-6933-8_8,

of galaxies and galaxy systems, Newton's laws of gravity can be modified to yield similar results.

Though disregarded by much of the astronomical community, MOND must be given some credit as it has been shown to be at least as empirically accurate as most DM halo models when used, in conjunction with the observed distribution of stars and gas, to predict the flattened outer rotation curves of disk galaxies [1, 12, 7]. Even if MOND is eventually shown to be invalid, it is still a very efficient "recipe" to describe galaxy systematics. In most cases, fits are made with reasonable mass-to-light (M/L) values for the stellar component. In fact, one of the arguments in favor of MOND is that M/L values generally conform with those predicted by stellar population synthesis models.

The concept of MOND is as follows. The true gravitational acceleration $\mathbf{g}$ is related to the Newtonian acceleration $\mathbf{g_N}$ as follows:

$$\mu(g/a_0)\ \mathbf{g} = \mathbf{g_N} \tag{1}$$

where a_0 is the MOND acceleration parameter and $\mu(x)$ is an unspecified function which behaves as follows:

$$\mu(x) = 1, \quad x \gg 1 \qquad \mu(x) = x, \quad x \ll 1 \tag{2}$$

and $\mu(x)$ is taken to be

$$\mu(x) = x(1 + x^2)^{-1/2} \tag{3}$$

The asymptotic behavior of this function allows for Newtonian dynamics at higher acceleration limits and MOND at low acceleration limits. This consequently explains the observed behavior of rotation curves very well. The rotation law for MOND is given by

$$\frac{V^2}{r} = g \tag{4}$$

and as r becomes large,

$$V^4 = GMa_0 \tag{5}$$

This relation is consistent with the empirical Tully-Fisher relation [13] ($V^4 \propto L$) for spiral galaxies.

The parameter a_0 has been set to a standardized value of 3734 $\mathrm{km\,s^{-2}\,kpc}$ which was initially determined in a number of independent ways. Most notably, Milgrom used the theoretical stellar population M/L and velocities of a large sample of galaxies in conjunction with equation 5 to obtain a mean value for a_0. His reasoning was such that if equation 5 was true, then v^4/L should be proportional to M/L. The standardized a_0 has uncertainties of roughly 20% associated with it and is the parameter that seems to produce the best fit for the majority of observed rotation curves. However, because MOND is an

acceleration dependent modification, the adopted value of a_0 depends upon an assumed distance scale (in this case, $H_0 = 75\ \mathrm{km\,s^{-1}\,Mpc^{-1}}$). That is, a_0 is seen to scale inversely with the distance to a galaxy [1]. The quality of a fit made using MOND is thus dependent on the assumed distance to a galaxy. For this reason, one of the major problems associated with MOND is caused by the rigidity with which the value of a_0 has been fixed. As a MOND fit effectively has no free parameters except for the M/L of the galaxy's stellar component, any galaxy whose observed rotation curve differs considerably from that predicted by MOND can effectively falsify the theory, provided that the distance to said galaxy is well known and M/L values are reasonable. At present, only a surprisingly small number of galaxies, notably NGC 2841, are not well fitted by MOND at their assumed distances. However, within the uncertainties of the galaxy distances, MOND has remained valid.

1.2 The Mass Discrepancy-Acceleration Relation

With newly available data it will also be possible to thoroughly explore the Mass Discrepancy-Acceleration relation [8]. This is a "rephrasing" of MOND as a purely empirical relation. That is, the mass discrepancy in disk galaxies has been shown to correlate with acceleration, increasing systematically with decreasing acceleration below some critical value.

1.3 Testing and Comparing MOND to Dark Matter Halos

As a comparison, both the NFW [11] and pseudo-isothermal dark halo models will also be tested for each of the derived rotation curves. For many galaxies the resolution of the data will not be significantly high to discern the central dark matter distribution in any great detail (i.e. investigation of the cusp/core problem). Regardless, comparing DM and MOND fits will be a good check for the reliability of fits. For example, if MOND fails to accurately describe a derived rotation curve, it will be interesting to see whether DM fares any better. Likewise, it may also be possible that MOND will explain several of the rotation curves to a better degree than DM can.

More significant studies of the DM content of the LVHIS galaxies with extended H I envelopes will also be possible. Using derived H I rotation curves and moments maps for these galaxies, it will be possible to gain insight into the structure and dispersion of the non visible component in the far outer parts, in other words, the shape (degree of oblateness) of the dark halos associated with the galaxies.

2 The Advantages of LVHIS for Testing MOND and Dark Matter

In order to test MOND and DM systematics, the first aim of this project will be to derive H I rotation curves for an initial sample of 28 LVHIS galaxies.

This will be achieved primarily by constructing tilted ring models of available velocity fields. Though this method assumes circular motion in the H I disk, it is the best method of modeling any variations in inclination and position angle which may be present. Near IR H-band photometry will be used to derive the stellar component's contribution to the rotation curve and the LVHIS H I data will be used to determine the gas component.

The LVHIS sample is ideal for this task as it offers high resolution, detailed observations of a large number of galaxies, many with accurate TRGB distance estimates. With these accurate distances, and using the MOND acceleration parameter, fixed to its accepted value of $a_0 = 3734\ \mathrm{km\,s^{-2}\,kpc}$, a thorough test of MOND will be possible, where the only free parameter in fits will be the M/L of the stellar component. Fits will be further constrained by the fact that the range of M/L in H-band is small [2]. Due to the nature of MOND theory, any single galaxy whose observed rotation curve is seen to differ considerably from that predicted by MOND can effectively falsify the theory, provided that its distance is accurately known and its M/L is reasonable. Alternatively, if MOND is able to predict the observed rotation curves for every galaxy for which it is tested, this will serve to further strengthen the case for MOND. Either outcome will be a significant result.

References

1. K. G. Begeman, A. H. Broelis, R. H. Sanders: MNRAS **249**, 523 (1991)
2. R. S. de Jong, E. F. Bell: Stellar M/L Ratios and Spiral Galaxy Dynamics. In: *The Mass of Galaxies in Low and High Redshifts*. ed by R. Bender, A. MacKay (2003), pp 213
3. I. D. Karachentsev, V. E. Karachentseva, W. K. Huchtmeier, D. I. Makarov: AJ **127**, 2031 (2004)
4. I. D. Karachentsev, A. Dolphin, R. B. Tully, M. Sharina, L. Makarov, D. Makarov, V. Karachentseva, S. Sakai, E. J. Shaya: AJ **131**, 1361 (2006)
5. E. Kirby, H. Jerjen, S. Ryder and S. Driver: in prep. (2007)
6. B. Koribalski: this volume
7. S. S. McGaugh, W. J. G de Blok: ApJ **499**, 66 (1998)
8. S. S. McGaugh: ApJ **609**, 652 (2004)
9. M. Milgrom: ApJ **270**, 365 (1983)
10. M. Milgrom: ApJ **270**, 371 (1983)
11. J. F. Navarro, C. S. Frenk, S. D. M. White: ApJ **462**, 563 (1996)
12. R. S. Sanders: ApJ **473**, 117 (1996)
13. R. B. Tully, J. R. Fisher: A&A **54**, 661 (1977)

Deepest Near-IR Surface Photometry of Galaxies in the Local Sphere of Influence

Emma Kirby[1], Helmut Jerjen[1], Stuart Ryder[2], and Simon Driver[3]

[1] Research School of Astronomy and Astrophysics, Australian National University, Australia emma@mso.anu.edu.au, jerjen@mso.anu.edu.au
[2] Anglo-Australian Observatory, Australia sdr@aao.gov.au
[3] School of Physics and Astronomy, University of St. Andrews , U.K. spd3@st-and.ac.uk

Summary. We present near-IR, deep (4 mag deeper than 2MASS) imaging of 56 Local Volume galaxies. Global parameters such as total magnitudes and stellar masses have been derived and the new near-IR data combined with existing 21-cm and optical B-band data. We present multiwavelength relations such as the H I mass-to-light ratio and investigate the maximum total baryonic mass a galaxy can have.

1 Photometry Beyond the 2MASS Limit

H-band (1.6μm) images of 56 local galaxies ($D < 10$ Mpc) were obtained with the Infrared Imager and Spectrograph 2 (IRIS2) at the 3.9m Anglo-Australian Telescope (AAT) between October 2004 and September 2006. IRIS2 has a Rockwell HAWAII–1 HgCdTe array with a pixel scale of $0\farcs45$ pixel^{-1} and a $7\farcm7 \times 7\farcm7$ field-of-view. The total on-source integration time was 30 min with a mean seeing of $1\farcs3$.

The data reduction was carried out using the ORAC-DR pipeline within the STARLINK package. Instrumental magnitudes for field stars were obtained employing standard IRAF routines and were cross-correlated with the 2MASS Point Source Catalog to provide photometric calibration. The measured total H-band luminosity of each galaxy was converted into a stellar mass by adopting a mass-to-light ratio of $\Upsilon_*^H = 1.0$ M$_\odot$/L$_\odot$. A detailed description the observations and analysis can be found in Kirby et al [1].

2 Sharing the Baryons

The relationship between the stellar mass (from optical or near-IR measurements) and the gas (from 21-cm line observations) in a galaxy provides insight

B.S. Koribalski, H. Jerjen (eds.), *Galaxies in the Local Volume*,
doi: 10.1007/978-1-4020-6933-8_9,

into galaxy evolution. We use our data combined with data from the literature to examine the H I mass-to-light ratio as well as the relationship between the H I mass and the stellar mass. The literature data that we include is coming from Virgo Cluster galaxies listed in the Goldmine database [2]. We also include the B-band data of Warren et al. [3] and Bouchard et al. [4] which have been transformed to the H-band employing the optical - near infrared magnitude transformation discussed in Kirby et al. [1]. This allows us to investigate this relationship for a wide range of galaxy morphologies.

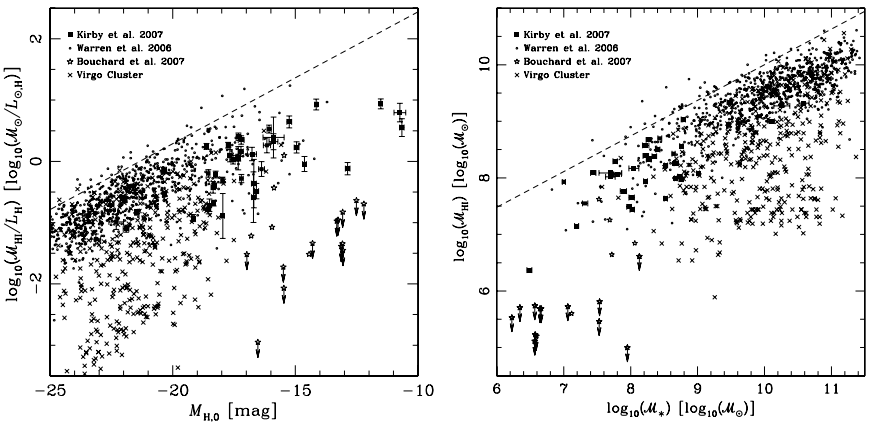

Fig. 1. *(Left:)* H I mass-to-light ratio versus absolute H-band magnitude. *(Right:)* H I mass versus stellar mass. In both plots the dashed line represents the upper envelope to a galaxy's potential mass-to-light ratio.

2.1 The H I mass-to-light ratio

The H I mass-to-light ratio measures the relative amounts of gas and stars in a galaxy. In Fig. 1 (left panel) we show the H I mass-to-light ratio for the selected galaxies. Warren et al. [3] proposed that there is an upper envelope to a galaxy's mass-to-light ratio at a given luminosity (dashed line). This suggests that the minimum amount of stars that a galaxy will form is related to the initial baryonic mass, a hypothesis supported by the theoretical work of Taylor & Webster [5]. For a galaxy to lie above this upper envelope, it would have to be very massive yet also have low surface brightness (to remain optically undetected) and low H I column density. However, HIDEEP [6] found no giant LSB galaxies and no galaxies with H I column density less than $10^{20}\,\mathrm{cm}^{-2}$ despite a sensitivity limit 1.5 dex lower than this.

2.2 H I mass versus stellar mass

Although the H I mass-to-light ratio is frequently used to describe the relationship between the gas and the stars in a galaxy, when examining Fig. 1 (left panel), it is important to note that the two parameters plotted are dependent on each other. A better way to look at this is presented in the right hand panel of Fig. 1 where we show how the H I mass relates directly to the stellar mass.

Our sample, containing late-type dwarfs, is closer to the upper envelope than the early-type dwarf sample of Bouchard et al. [4]. Similarly, the sample of field galaxies of Warren et al. [3] is much closer to the upper envelope than the Virgo Cluster data that is dominated by Es and dEs. This highlights that the relationship between the stellar and gas masses is dependent on the environment and hence implicitly on the morphological type.

In the H I mass versus stellar mass plot, the upper envelope clearly does not have a gradient of unity. A 45° line represents galaxies with exactly half their baryonic mass in stars and half in gas. High mass galaxies lie systematically below a 45° line whereas low mass galaxies can fall either above or below a 45° line. This means that the fraction of baryonic mass in stars is dependent on the total baryonic mass.

2.3 Stellar mass fraction versus total baryonic mass

In Fig. 2, a direct comparison between the stellar fraction of the baryonic content and the total baryonic mass in a galaxy is given. The empirically determined dashed line represents the minimum mass fraction required for the galactic disk to remain stable against star formation. It seems that at lower masses, galaxies can stabilise with less of their gas converted into stars. This is again supported by the theoretical work of Taylor and Webster [5].

Fig. 2 shows that the minimum stellar fraction of the baryonic mass goes to 1 as the total baryonic mass approaches 10^{12} $M_{\odot}$ suggesting that there is an upper limit to the total baryonic mass a galaxy can have. This upper limit is in good agreement with the observed upper limit of high redshift galaxies ($0.01 < z < 4$) found by Rocca-Volmerange et al. [7] and the theoretical value discussed by Rees and Ostriker [8].

3 Conclusion

Comparisons of the gas mass and the stellar mass provides insight into galaxy evolution. Galaxies with high baryonic mass-to-light ratios are often cited as solutions to ongoing cosmological problems, in particular reconciling the faint-end of the galaxy luminosity function with the predicted CDM Halo Mass Function.

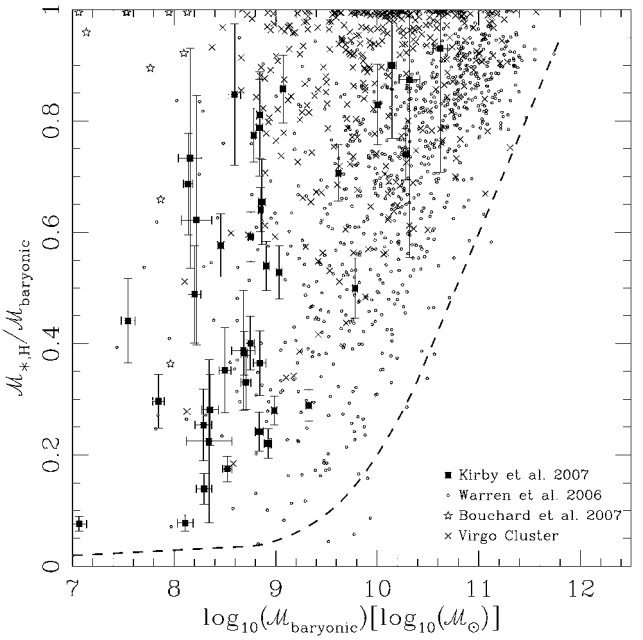

Fig. 2. Relation between the stellar mass fraction and the total baryonic mass in local galaxies. The dashed line is the empirical minimum mass fraction possible for a galaxy with a given total baryonic mass.

The maximum total baryonic mass of a galaxy (both observational and theoretical) corresponds to the mass of a galaxy which has converted all of its gas into stars. Our empirical results strongly suggest an upper baryonic mass limit of 10^{12} $M_{\odot}$.

Acknowledgements

The authors acknowledge financial support from the Australian Research Council via the grant DP0451426.

References

1. E. Kirby, H. Jerjen, S. Ryder & S. Driver: in prep (2007)
2. G. Gavazzi et al.: A&A **400**, 451 (2003)
3. B. Warren, H. Jerjen & B. Koribalski: AJ **131**, 2056 (2006)
4. A. Bouchard, H. Jerjen, G. Da Costa & J. Ott: AJ **133**, 261 (2007)
5. E. Taylor & R. Webster: ApJ **634**, 1067 (2005)
6. R. Minchin, M. Disney, P. Boyce et al.: MNRAS **346**, 787 (2003)
7. B. Rocca-Volmerange et al.: A&A **415**, 931 (2004)
8. M. Rees & J. Ostriker: MNRAS **179**, 541 (2007)

Ionized and Neutral Gas in the Starburst Galaxy NGC 5253

Ángel R. López-Sánchez[1], Bärbel Koribalski[1], César Esteban[2], and Jorge García-Rojas[2]

[1] Australia Telescope National Facility, CSIRO, PO Box 76, Epping, NSW 1710, Australia Angel.Lopez-Sanchez@csiro.au
[2] Instituto de Astrofísica de Canarias, Spain

We present the main results of our analysis of the ionized and the neutral gas in the blue compact dwarf galaxy NGC 5253. The ionized gas of its nucleus was studied using VLT UVES data, leading to the detection of the weak O and C recombination lines and the confirmation of a localized N (possibly also He) enrichment resulting from chemical pollution by Wolf-Rayet stars. The neutral gas was analyzed using new ATCA data from the LVHIS project and shows intriguing kinematics that could suggest that NGC 5253 has interacted with a gas-rich dwarf companion or the nearby, giant spiral M 83.

1 The starburst galaxy NGC 5253

The dwarf galaxy NGC 5253 lies at a distance of 4.0 Mpc [4] (i.e., $1'' \sim 19$ pc) and has an optical size of $\sim 5' \times 2'$, giving the appearance of a dwarf elliptical galaxy. Its starbursting nature is revealed using Hα filters [1, 12]: the galaxy shows a lot of ionized gas, including a filamentary structure that is extending perpendicular to its optical major axis. It is therefore classified as a blue compact dwarf (BCD) galaxy, being one of the closest starbursts. NGC 5253 belongs to the M 83 subgroup within the Centaurus Group.

We are performing a detailed study of both the ionized and the neutral gas of NGC 5253. The ionized gas is studied via deep echelle spectrophotometry data taken with the Very Large Telescope UVES spectrograph. The neutral gas is analyzed using new Australia Telescope Compact Array (ATCA) data provided by the 'Local Volume H I Survey' (LVHIS) project [7].

2 The ionized gas in the center of NGC 5253

A detailed description of our high spatial and spectral resolution analysis of the ionized gas in NGC 5253 is presented in [9]. We have measured the

B.S. Koribalski, H. Jerjen (eds.), *Galaxies in the Local Volume*,
doi: 10.1007/978-1-4020-6933-8_10,

intensities of a large number of permitted and forbidden emission lines in four zones of the central part of the galaxy, obtaining two main results. Firstly, we confirm a localized nitrogen enrichment, as well as a possible slight helium pollution, in two of the central starbursts of the galaxy. The enrichment pattern completely agrees with that expected by the pollution of the winds of massive stars in the Wolf-Rayet phase. Furthermore, the amount of enriched material needed to produce the observed overabundance is consistent with the mass lost by the number of Wolf-Rayet stars estimated in the starbursts. Secondly, we have detected faint C II and O II recombination lines, the first time that these lines are unambiguously detected in a dwarf starburst galaxy. The ionic abundances derived from the recombination lines are from 0.20 to 0.40 dex higher than those calculated from collision excited lines (CELs), in agreement with the result found in other Galactic and extragalactic H II regions [3]. This abundance discrepancy could be due to the presence of temperature fluctuations in the ionized gas of NGC 5253. The abundances derived from CELs are underestimated when such temperature variations are not considered [14]. If they are also present in extragalactic H II regions, important galaxy properties such metallicity could be biased when only CELs are used [15].

3 The analysis of the neutral gas of NGC 5253

New radio data of NGC 5253 have been obtained from the LVHIS project [7] using three different ATCA configurations: 1.5A, 750A and EW367. The data were reduced and analyzed using the MIRIAD software. Low resolution H I datacubes were obtained, excluding the longest baselines (i.e., those to antenna 6). The H I datacube is composed by 32 channels; the channel width is 6 km/s. The beam size is $86'' \times 47''$, and the rms noise is $\sim$2 mJy/beam.

3.1 H I distribution

Figure 1 (left) shows the H I distribution overlaid onto the DSS R-band image of NGC 5253. Our H I map is deeper than the previous VLA map obtained by [5]. The neutral gas is now seen more extended than the optical size of the galaxy ($\sim 9' \times 5'$), although its northern area presents a peculiar morphology. The H I maximum coincides with the optical center of the galaxy. We derive a total H I flux density of 31.1 ± 1.5 Jy km/s, similar to that given by [13], $F_{\rm HI} = 33.4 \pm 9.9$ Jy km/s. The total H I mass is $M_{\rm HI} = (1.17 \pm 0.06) \times 10^8\ M_\odot$.

3.2 H I velocity field

The H I velocity field of NGC 5253 (Figure 1, right) is intriguing. We confirm the previous result found by [5] which indicates that the neutral gas *is not* rotating about the optical minor axis of the galaxy but seems to *rotate about its*

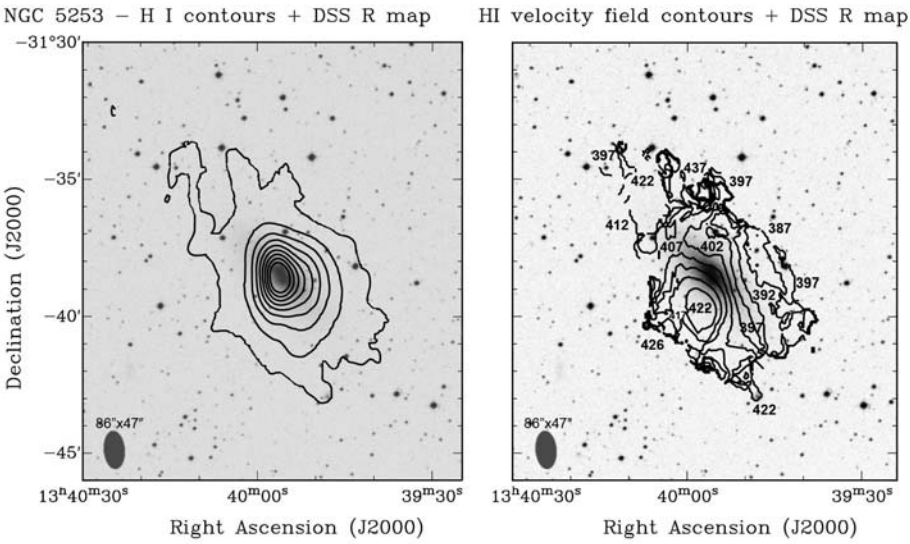

Fig. 1. *(Left:)* Contours of the H I distribution in NGC 5253 overlaid onto a DSS *R*-band image. *(Right:)* H I velocity field of NGC 5253. Notice that the velocities increase along the optical minor axis of the galaxy.

optical major axis. Some authors have suggested that this behavior could be consequence of some kind of outflow or that we are seeing the first stages of the formation of a polar ring. However, CO observations suggest that molecular clouds are infalling into NGC 5253 [16, 10]. Another possibility is the disruption and/or accretion of a dwarf gas-rich companion, or perhaps NGC 5253 suffered an interaction with the neighboring galaxy M 83, which lies at a radial distance of only 500 kpc, being the projected separation between them 130 kpc. Van den Bergh [17] and [2] suggested that the nuclear starburst observed in NGC 5253 was triggered as a result of an interaction with M 83 around 1 Gyr ago. Indeed, the properties found in NGC 5253, such its star formation activity, the presence of super-star clusters and the extended and filamentary Hα structure, resemble those observed in the famous starburst M 82, that very probably suffered an interaction with its massive neighbor M 81 around 1 Gyr ago [11], being evident in the prominent H I tidal tails seen in the M 81/M 82 group [18]. The new ATCA data of M 83 provided by the LVHIS project [6, 7] reveal a peculiar H I morphology in its outskirts, remarking an asymmetric tidal arm bending towards the east that suggests that M 83 has interacted or merged with another, smaller galaxy. Did NGC 5253 interact with M 83 in the past and the consequences are nowadays still observed? If this hypothesis is correct, this result would reinforce the main conclusion obtained by [3], that interactions trigger the star formation activity in dwarf Wolf-Rayet galaxies.

4 Radio-continuum emission in NGC 5253

We have also obtained a 1.4 GHz radio-continuum map of NGC 5253 using our new ATCA data. We derive a total flux of $S_{1.4\,\mathrm{GHz}} = 87.1 \pm 3.5$ mJy, in agreement with the previous value of $S_{1.4\,\mathrm{GHz}} = 85.8 \pm 3.4$ mJy given by [19]. The star-formation rate (SFR) derived using our data is $\mathrm{SFR}_{1.4\,\mathrm{GHz}} \sim 0.03$ $\mathrm{M}_{\odot}$ yr^{-1}. This value is considerably smaller than the SFR estimation derived from FIR flux densities, $\mathrm{SFR}_{FIR} \sim 0.12$ $\mathrm{M}_{\odot}$ yr^{-1} and an order of magnitude smaller that the SFR obtained using the Hα flux, $\mathrm{SFR}_{\mathrm{H}\alpha} \sim 0.27$ $\mathrm{M}_{\odot}$ yr^{-1} [1].

5 Conclusions

NGC 5253 is still a puzzling BCD galaxy. The analysis of the ionized gas reveals chemical pollution by massive stars and suggests the existence of temperature fluctuations. The kinematics of the neutral gas is intriguing and could be the consequence of interaction with a companion, perhaps with M 83.

References

1. Calzetti, D., Harris, J., Gallagher III, J.S., Smith, D.A., Conselice, C.J., Homeier, N. & Kewley, L. 2004, AJ, 127, 1405
2. Cardwell, N. & Phillips, M.M. 1989, ApJ, 338, 789
3. García-Rojas, J. & Esteban, C. 2007, ApJ, accepted (arXiv:0707.3518)
4. Karachentsev, I., Karachentseva, V.E., Huchtmeier, W. & Makarov, D.I. 2004, AJ, 127, 2031
5. Kobulnicky, H.A, & Skillman, E.D. 1995, ApJ, 454, L121
6. Koribalski, B. 2005, PASP, 22, 331
7. Koribalski, B. et al., in preparation, see also these proceedings.
8. López-Sánchez, Á.R. 2006, *Massive star formation in dwarf Wolf-Rayet galaxies*. PhD Thesis, La Laguna University, Tenerife, Spain, *see astro-ph/0704.2846 for a 16 pages English summary with figures.*
9. López-Sánchez, Á.R., Esteban, C., García-Rojas, J., Peimbert, M. & Rodríguez, M. 2007, ApJ, 656, 168
10. Meier, D.S., Turner, J.L., & Beck, S.C. 2002, AJ, 124, 877
11. Mayya, Y.D., Bressan, A., Carrasco, L. & Hernández-Martínez, L. 2006, ApJ, 649, 172
12. Meurer, G.R. et al. 2006, ApJS, 165, 307
13. Paturel, G., Theureau, G., Bottinelli, L., Gouguenheim, L., Coudreau-Durand, N., Hallet, N. & Petit, C. 2003, A&A, 412, 57
14. Peimbert, M. 1967, ApJ, 150, 825
15. Peimbert, M., Peimbert, A., Esteban, C., García-Rojas, J., Bresolin, F., Carigi, L., Ruiz, M.T. & López-Sánchez, Á.R. 2007, RevMexAA (Serie de Conferencias), 29, 72
16. Turner, J.L., Beck, S.C., & Hurt, R.L. 1997, ApJ, 474, L11
17. van den Bergh, S. 1980, PASP, 92, 122
18. Yun, M., Ho, P., Lo, K. 1994, Nature, 372, 530
19. Yun, M.S., Reddy, N.A. & Condon, J.J. 2001, ApJ 554, 803

The Smallest H I Galaxies

Tom Oosterloo[1,2], Katarina Kovač[2], Thijs van der Hulst[2], Marc Verheijen[2], and Emma Ryan-Weber[3]

[1] ASTRON, Postbus 2, 7990 AA, Dwingeloo, The Netherlands
oosterloo@astron.nl
[2] Kapteyn Astronomical Institute, University of Groningen, Postbus 800, 9700 AV, Groningen, The Netherlands
[3] Institute of Astronomy, Madingley Road, Cambridge, CB3 0HA, UK

The study of the smallest dwarf galaxies provides insight into how the least massive dark matter halos retain cool gas and may manage to form stars. Various processes are thought to suppress star formation in low-mass halos, including the effects of global reionisation (e.g., Benson et al. [1], Cooray & Cen [3]), the heating and removal of gas via supernovae and stellar wind feedback (e.g., Dekel & Woo [4], Ricotti & Gnedin [8]), ram pressure and tidal stripping (e.g., Blitz & Robishaw [2]), or simply a temperature floor in the interstellar medium (Kaufman, Wheeler & Bullock [6]). Depending on which effect dominates, the smallest galaxies could be dark, be gas free or be detectable only in H I. Here we report on two projects to study the gas properties of the smallest galaxies.

1 A survey for small H I galaxies

To study galaxies with H I masses below a few times 10^7 $M_\odot$, we conducted a blind H I survey, using the WSRT, of a nearby volume (of about 90 deg^2 on the sky) in the constellation Canes Venatici (CVn). This region is known to host a population of nearby, small galaxies (the CVn I and CVn II groups). Together with the Local Group and the Sculptor Group, these groups extend along the line of sight up to a redshift of 1200 km s^{-1}. One main reason for choosing this region is that here the velocity flow closely follows a cold Hubble flow. The possibility of using the Hubble flow to estimate distances for nearby objects makes this region an excellent target for a blind H I survey.

The WSRT was used in mosaic mode to cover this large region on the sky. In total, almost 1400 pointings were observed over 60 × 12 hr. The effective integration time per position is about 80 minutes. This gives a noise level of 0.8 mJy beam^{-1} for a spatial resolution of 30 arcsec and velocity resolution of 33 km s^{-1}, making it substantially deeper than e.g. HIPASS. The 5-σ detection

B.S. Koribalski, H. Jerjen (eds.), *Galaxies in the Local Volume*,
doi: 10.1007/978-1-4020-6933-8_11,

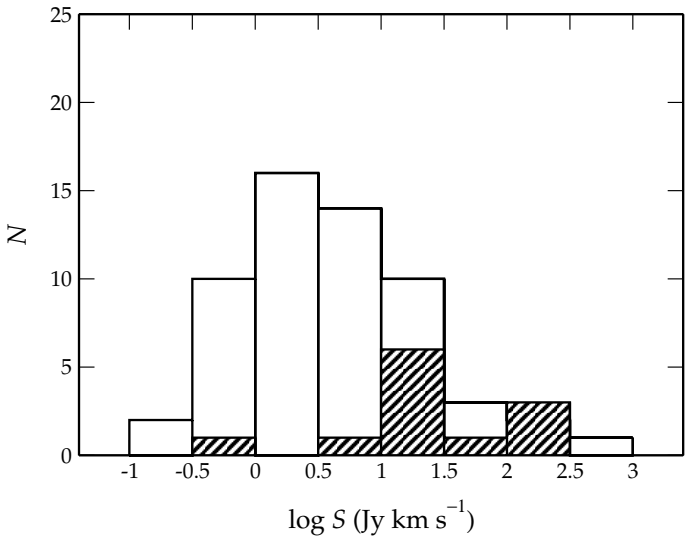

Fig. 1. Distributions of the observed integrated H I flux (S) of the galaxies detected in our blind H I survey. The shaded histogram is for galaxies belonging to the CVn I group (i.e. redshift > 400 km s^{-1}) while the open histogram is for galaxies with recession velocity above that limit.

limit over one resolution element is about $5\times10^4 D^2$ M$_\odot$. In redshift, the survey volume goes out to about 20 Mpc. We detected 70 galaxies, all detections have an optical counterpart. The smallest detection has an H I mass of 5×10^6 M$_\odot$ while half the sample has a mass below 10^8 M$_\odot$. Deeper and higher resolution follow-up observations were done on the 20 smallest galaxies, allowing us to study the internal kinematics of these galaxies. A full description of this work, including discussions of the H I-mass functions and (Baryonic) Tully-Fisher relations, can be found in Kovač [7].

What we discuss here is that there is a hint that there is a lower limit to the H I mass of galaxies in the volume we have surveyed. In Fig. 1 we give the histogram of the integrated flux S of the galaxies detected in our survey where we have separated the CVn I group, i.e. we have split the sample at a recession velocity of 400 km s^{-1} (corresponding to 5.5 Mpc, being the back of the CVn I group; there are 12 galaxies below this cutoff). For a purely flux-limited sample, the distribution of the integrated flux should not depend on distance. However, Fig. 1 suggests that there is a lack of nearby, faint galaxies. Following a Kolmogorov-Smirnov test, the distributions of S for the two subsamples are different at the 99% level of confidence. Closer than 5.5 Mpc, only one galaxy has an H I mass below 10^7 M$_\odot$ while the detection limit at 5.5 Mpc is about 10^6 M$_\odot$. Simulations of our detection procedure show that there is no observational bias against faint, nearby galaxies. This suggests that the difference could imply a physical absence of these galaxies

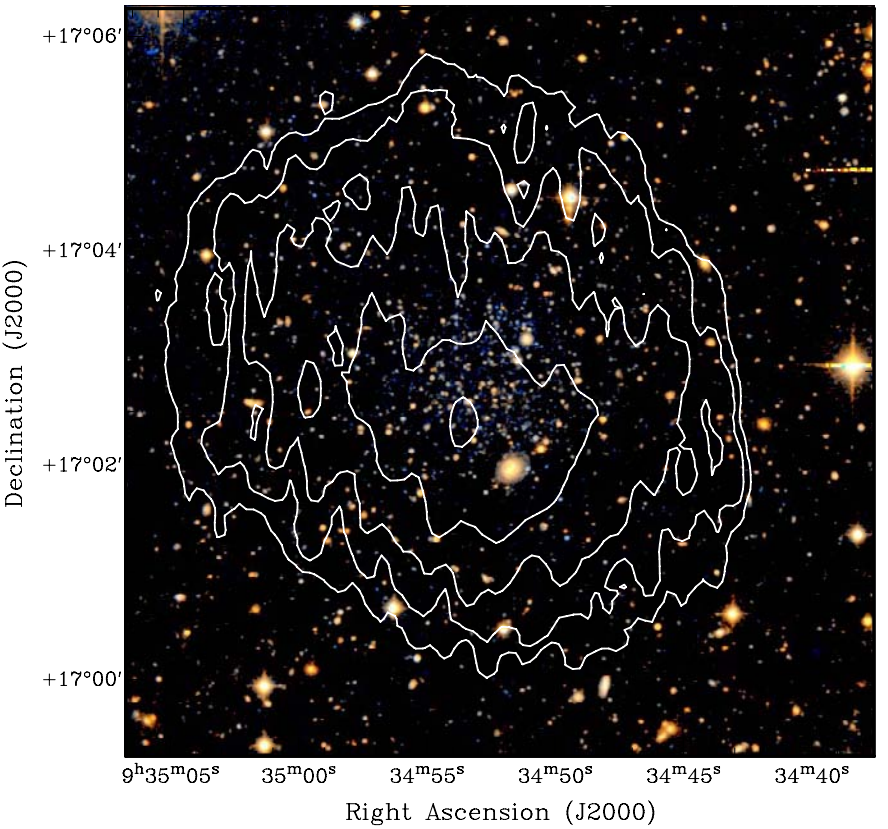

Fig. 2. Total H I contours of Leo T on top of the optical image published by Irwin et al. [2]. The spatial resolution is 12×50 arcsec (25×100 pc). Contour levels are $2, 5, 10, 20$ and 50×10^{19} cm^{-2}.

in the CVn I group. The volume surveyed is relatively small and the CVn I group is probably not representative, but this result could suggest that the effects discussed in the introduction may cause a lower limit to the gas mass of galaxies.

2 The H I in Leo T

Another strategy to study the smallest galaxies is to investigate the dwarf galaxies in our Local Group (LG). In the last few years, the number of known LG dwarfs has increased significantly. One recent addition is Leo T (Irwin et al. [2]), a dwarf "transition" galaxy at a distance of 420 pc. Leo T is particularly interesting as it is the faintest dwarf known to date where star formation has occurred recently.

As noted by [2], the HIPASS data suggest that Leo T may contain H I. Recent observations of Leo T with the WSRT (performed by TO and ERW) indeed show that this galaxy is indeed very gas rich. Figure 2 shows the total H I contours on top of the optical image. Contrary to many other LG dwarfs, the H I in Leo T appears to be quite symmetric and is centred on the optical galaxy. This is surprising given the recent star formation. In e.g. Phoenix, the H I is displaced from the optical galaxy which is likely due to the gas being blown out by the star formation (St-Germain et al. [11]). In Leo T, the kinematics of the H I gives no indications for gas outflows.

The total H I mass of Leo T is 2.8×10^5 $M_\odot$ while the stellar mass is estimated to be 1.2×10^5 $M_\odot$, hence the gas content is among the highest observed in any galaxy ($M_{\rm HI}/L_V = 5$). Eighty percent of the baryons in Leo T are in atomic gas. The kinematics of the H I shows no obvious systematic pattern like rotation, although a small gradient of a few km s^{-1}, exists over the very inner region. The overall gas dispersion is 6.9 km s^{-1} which is the same as the observed stellar dispersion (Simon & Geha [8]). This implies that the dynamical mass in the region where H I is observed is at least (depending on assumed geometry) 3.3×10^6 $M_\odot$ ($M_{\rm dyn}/L_V > 50$). Leo T is, like all LG dwarfs, completely dark-matter dominated.

The observed peak column density is 7×10^{20} cm^{-2}. This is near the threshold where a cold interstellar medium can form and where star formation may occur (Shaye [9]). Interestingly, the shape of the H I spectra shows that Leo T appears to have a cold (few 100 K) and a warm (600 K) neutral medium. It therefore appears that the conditions in the ISM are such that star formation could occur, consistent with the recent star formation in Leo T.

References

1. Benson A. J., Frenk C. S., Lacey C. G., Baugh C. M., Cole S. 2002, MNRAS, 333, 177
2. Blitz L., Robishaw T. 2000, ApJ, 541, 675
3. Cooray A., Cen R. 2005, ApJ, 633, L69
4. Dekel A., Woo J. 2003, MNRAS, 344, 1131
5. Irwin et al. 2007, ApJ, 656, L13
6. Kaufmann T., Wheeler C., Bullock J. S., 2007, MNRAS, submitted, arXiv:0706.0201
7. Kovač, K. 2007, PhD Thesis, University of Groningen, `http://dissertations.ub.rug.nl/faculties/science/2007/k.kovac/`
8. Ricotti M., Gnedin N. Y. 2005, ApJ, 629, 259
9. Shaye, J. 2004, ApJ, 609, 667
10. Simon, J. D., Geha, M. 2007, ApJ, in press, arXiv:0706.0516
11. St-Germain, J., Carignan, C., Côte, S., Oosterloo, T. 1999, AJ, 118, 1235
12. Taylor, E. N., Webster, R. L. 2005, ApJ, 634, 1067

FIGGS: Faint Irregular Galaxies GMRT Survey

Ayesha Begum[1], Jayaram N. Chengalur[2], Igor D. Karachentsev[3], Margrita Sharina[3], and Serafim Kaisin[3]

[1] Institute of Astronomy, University of Cambridge, Madingley Road, Cambridge, U.K. ayesha@ast.cam.ac.uk
[2] National Centre for Radio Astrophysics, TIFR, Pune University Campus, Ganeshkhind, Pune, India
[3] Special Astrophysical Observatory, Nizhnii Arkhys 369167, Russia

1 Introduction

H I 21cm aperture synthesis observations of spiral galaxies is a mature field with over two decades of history – probably something of the order of a thousand galaxies have already been imaged. However, the observations have tended to focus on bright ($\sim$ L$_*$) galaxies with H I masses $\sim 10^9$ M$_\odot$. Dwarf galaxies (M$_B \gtrsim -17$) require substantial investments of telescope time, and have hence not been studied in similar numbers.

To start addressing this imbalance, we have been conducting an H I imaging study of faint dwarf galaxies – the Faint Irregular Galaxies GMRT Survey (FIGGS). The immediate goal of FIGGS is to obtain high quality observations of the atomic ISM in a large, volume limited sample of faint, gas rich, dwarf irregular galaxies. Here we briefly describe the survey and discuss some of the science that we anticipate can be done with this data set.

2 FIGGS Sample

The FIGGS galaxies form an H I flux limited subsample of the Karachentsev et al. (2004) catalog of galaxies within 10 Mpc. Specifically, the FIGGS sample consists of 65 faint dwarf irregular (dIrr) galaxies with M$_B \gtrsim -14.5$, H I flux integral $\gtrsim 1$ Jy km s^{-1} and optical sizes $\gtrsim$ 1 arcmin. The FIGGS galaxies represent the extreme low-mass end of the dIrr population, with a median M$_\mathrm{B} \sim -13$ and a median H I mass $\sim 3 \times 10^7$ M$_\odot$. Figure 1 compares the distributions of gas fraction, luminosity and dynamical mass of the FIGGS galaxies with that of existing samples of galaxies with H I aperture synthesis observations. As can be seen, the FIGGS survey substantially extends the

B.S. Koribalski, H. Jerjen (eds.), *Galaxies in the Local Volume*,
doi: 10.1007/978-1-4020-6933-8_12,

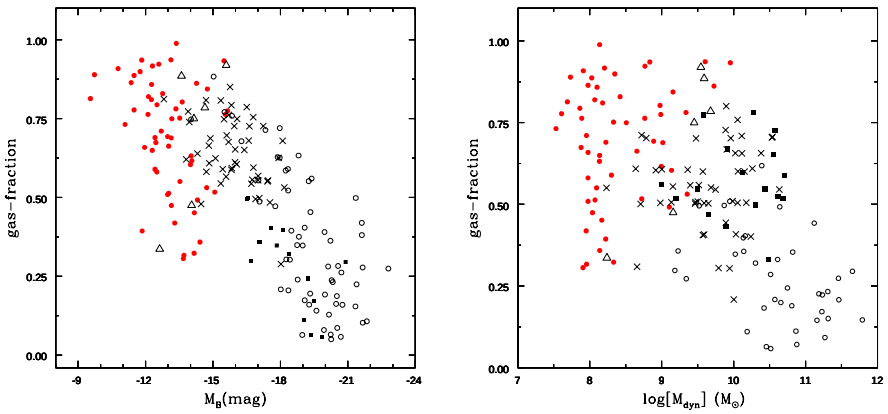

Fig. 1. The gas fraction of FIGGS galaxies (filled black/red circles) and previously studied galaxies (other black symbols) plotted as functions of absolute blue magnitude *(left)* and dynamical mass *(right)*. Note how the GMRT FIGGS sample extends the coverage of all three galaxy properties.

region of parameter space which has largely gone untouched by previous H I imaging studies.

The typical GMRT integration time per source for most galaxies is ∼5–6 hours, which gives a typical rms of ∼2–3 mJy/beam per channel. It is worth emphasising that our observations used a relatively high velocity resolution (∼1.6 $\mathrm{km\,s^{-1}}$, i.e. ∼4 times better than most earlier interferometric studies of such faint dwarf galaxies). This high velocity resolution is crucial to detect large scale velocity gradients in the faintest dwarf galaxies. Our observations show that, (unlike what one is lead to believe from coarser velocity resolution observations, e.g. Lo et al. 1993), most faint dwarf irregular galaxies in fact have large scale systematic patterns in their velocity fields (Fig. 2, see also Begum et al. 2006). Galaxies from the FIGGS sample are the faintest known galaxies to show such regular kinematics.

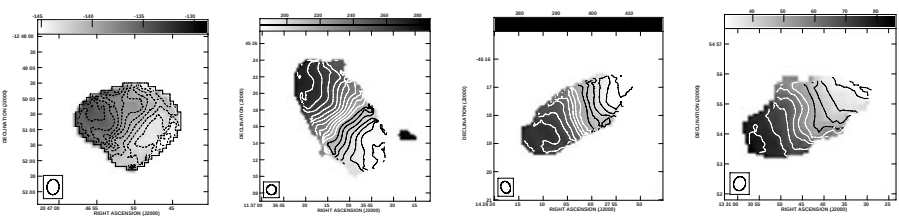

Fig. 2. The regular velocity fields of some of the faintest FIGGS galaxies.

The GMRT H I images are supplemented by single dish H I observations, HST V and I band imaging of the resolved stars and ground based Hα imaging using the 6-m BTA telescope. Distances accurate to $\sim$10% are available for most of the galaxies in our sample − the FIGGS sample is the first large sample of faint dIrr for which interferometric data is available and distances are accurately known. Additionally, the H II region abundances and Hα rotation curves are being obtained on the WHT, INT telescopes on La Palma and 6-m BTA telescope respectively.

3 Science Drivers for FIGGS

One of the main goals of FIGGS is to use the H I images in conjugation with the optical data to study the interplay between the neutral ISM and star formation in the faintest, lowest mass, gas rich dIrr galaxies. The FIGGS data will enable us to study the ISM of most of our sample galaxies at a linear resolution of $\sim$15–150 pc – i.e. comparable to the scales at which energy is injected into the ISM through supernova and stellar winds. FIGGS thus provide a unique opportunity to study the feedback of star formation in low mass, gas rich galaxies, which in turn will allow us to understand the processes driving star formation in these galaxies. Examples of GMRT H I maps at 3″ resolution (corresponding to linear scale of $\sim$30–90 pc) are shown in Fig. 3.

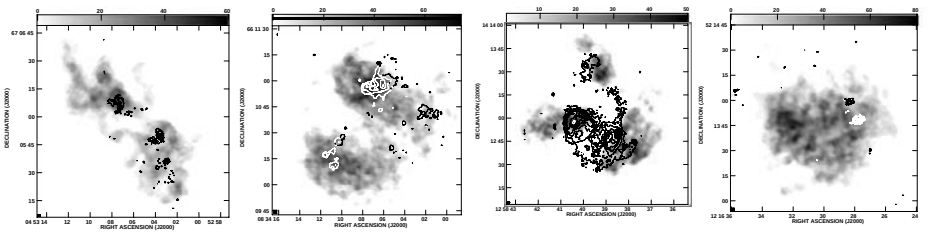

Fig. 3. GMRT integrated H I images of some of the FIGGS galaxies (greyscales) at 3″ resolution (corresponding to a linear scale of $\sim$30–90 pc) overlaid on Hα images (contours).

The second major aim of this survey is to extend the Baryonic Tully Fisher relation (McGaugh et al. 2000) to a regime of very low mass/luminosity that has not yet been well explored. While for the brighter galaxies W_{50} (the velocity width at 50% emission), once corrected for random motions and instrumental broadening, is a good measure of the rotational velocity of the galaxy (Verheijen 1999), this is not true in the case of faint dwarf galaxies where random motions could be comparable to the peak rotational velocities (e.g.,

Begum et al. 2003). For such galaxies, it is important to accurately correct for the pressure support ("asymmetric drift" correction) for which one needs to know both the rotation curve as well as the distribution of the H I gas, both of which can only be obtained by interferometric observations such as in FIGGS.

Our final objective is to use the H I kinematics of FIGGS galaxies, in conjunction with the Hα rotation curves to accurately determine the density distribution of the dark matter halos of faint galaxies. Serendipitous discoveries are an added bonus – for example, FIGGS has discovered some very extended H I disks around dwarf galaxies e.g. GMRT H I images of NGC 3741 ($M_B \sim -13.0$) showed it to have an H I extent of $\sim$8.3 times R_{Ho} (Holmberg radius) (follow-up WSRT+DRAO+GMRT observations found $\sim$8.8 R_{Ho}) – NGC 3741 has the most extended H I disks and we could derive a rotation curve up to a record of 38 times the disk scale length. NGC 3741 has $M_D/L_B \sim 107$ – which makes it one of the "darkest" irregular galaxies known (Begum et al. 2005).

As a service to the community, calibrated (u,v) data, data cubes, MOMNT maps, rotation curves etc. from the FIGGS survey will be publicly released at the end of our survey.

References

1. Begum, A., Chengalur, J. N., Karachentsev I. D., Kaisin, S. S. & Sharina, M. E. 2006, MNRAS, 365, 1220
2. Begum, A., Chengalur, J. N. & Karachentsev I. D., 2005, A&A, 433, L1
3. Begum, A., Chengalur, J. N. & Hopp, U., 2003, NewA, 8, 267
4. Karachentsev, I. D., Karachentseva, V. E., Huchtmeier, W. K. & Makarov, D. I., 2004, AJ, 127, 2031
5. Lo, K. Y., Sargent, W. L. & Young, K., 1993, AJ, 106, 507
6. McGaugh, S. S., Schombert, J., Bothun, G. D. & de Blok, W. J., 2000, ApJ, 533, 99
7. Verheijen, M., 1999, Ap&SS, 269, 671

Gas Rich Galaxies from the FIGGS Survey

Jayaram N. Chengalur[1], Ayesha Begum[2], Igor D. Karachentsev[3], Margrita Sharina[3], and Serafim Kaisin[3]

[1] National Centre for Radio Astrophysics, TIFR, Pune University Campus, Ganeshkhind, Pune, India chengalur@ncra.tifr.res.in
[2] Institute of Astronomy, University of Cambridge, Madingley Road, Cambridge, U.K.
[3] Special Astrophysical Observatory, Nizhnii Arkhys 369167, Russia

1 Introduction

The FIGGS (Faint Irregular Galaxy GMRT Survey) is aimed at creating a multi-wavelength observational data base for a volume limited sample of the faintest gas rich galaxies. As described in more detail in the contribution by Begum et al. in these proceedings, the galaxies form an H I flux and optical diameter limited subsample of the Karachentsev et al. (2004) catalog of galaxies within 10 Mpc. The sample consists of 65 galaxies with $M_B \gtrsim -14.5$ with median $M_B \sim -13$ and a median H I mass $\sim 3 \times 10^7$ $M_\odot$. H I aperture synthesis data (from the Giant Meterwave Radio Telescope – GMRT) has been obtained for all galaxies in the sample. Because the GMRT has a hybrid configuration (see Swarup et al. 1991) images at a variety of spatial resolutions (ranging from $\sim 40''$ to $\sim 3''$) can be made from a single GMRT observation run. Galaxies in the FIGGS survey have substantially lower M_{HI} and L_B that typical of galaxies in earlier aperture synthesis surveys. The GMRT observations also used a velocity resolution ($\sim$1.6 kms^{-1}), that is ~ 4 times better than most earlier interferometric studies of such faint dwarf galaxies. This high velocity resolution is crucial to detect large scale velocity gradients, which cannot be clearly distinguished in lower velocity resolution observations (see e.g. Begum et al. 2003a, 2003b, 2004a, 2004b, and for contrast Lo et al. 1993). In this paper we discuss two very gas rich galaxies that were observed as part of the FIGGS survey, viz. NGC 3741 and And IV.

2 Two extremely gas rich galaxies

NGC 3741 ($M_B \sim -13.13$) has $M_{HI}/L_B \sim 5.8$. GMRT observations of this galaxy have been presented in Begum et al. (2005). And IV, was originally thought to be a satellite of the Andromeda (M 31) galaxy. However, based on

B.S. Koribalski, H. Jerjen (eds.), *Galaxies in the Local Volume*,
doi: 10.1007/978-1-4020-6933-8_13,

HST imaging Ferguson et al. (2000) argue that it is likely to be a background galaxy that happens to lie in projection close to the disk of M 31. Consistent with this interpretation, they derive a distance of 6.11 Mpc for it (using the Tip of the Red Giant Branch technique) – this places And IV beyond the confines of the local group. The H I velocity measured for this galaxy (i.e. 234 km/s; Braun et al. 2003) is also substantially different from that of the nearest portion of the disk of M 31. The galaxy has a blue magnitude of ~ -12.37, which implies that $M_{HI}/L_B \sim 13$.

3 H I in NGC 3741 and And IV

The GMRT observations (Begum et a. 2005) showed that NGC 3741 had an H I disk that extends to ~ 8.3 times its Holmberg radius. This makes it probably the most extended gas disk known. Our observations allowed us to derive the rotation curve (which is flat in the outer regions) out to ∼38 optical scale lengths. NGC 3741 has a dynamical mass to light ratio of ∼107 and is one of the "darkest" irregular galaxies known. Follow up WSRT observations are presented in Gentile et al. (2007).

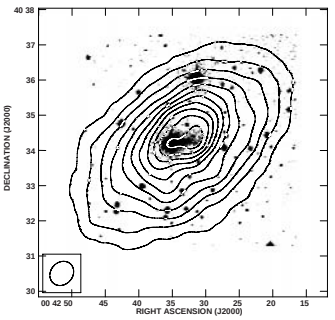

Fig. 1. The GMRT moment 0 image of And IV (at $\sim 44''$ resolution), overlaid on the DSS image.

For And IV, the GMRT observations show that its gas disk extends out to ~ 6 Holmberg radii. Figure 1 shows the integrated H I emission from And IV at $44'' \times 38''$ resolution, overlaid on the Digitised Sky Survey (DSS) image. Figure 2 shows the velocity field of And IV at $26'' \times 23''$ resolution. The velocity field is regular and a large scale velocity gradient, consistent with systematic rotation, is seen across the galaxy. From the rotation curve (Fig. 3) the ratio of the dynamical mass to the blue luminosity is $M_{\rm dyn}/L_B \sim 237$!.

These very large dynamical mass to blue luminosity ratios naturally lead one to ask whether extremely gas rich dwarf galaxies have abnormally small

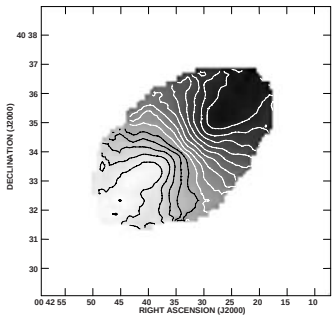

Fig. 2. The GMRT moment 1 image (velocity field) of And IV (at $\sim 26''$ resolution).

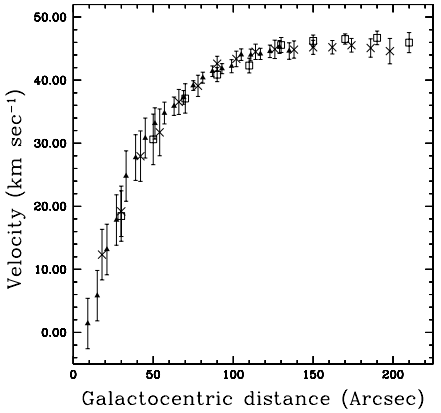

Fig. 3. Rotation curve of And IV as derived from the GMRT data.

baryon fractions, i.e. have they just been inefficient at forming stars, or did they end up with less than the typical baryon fraction? The ratio of baryonic to dark matter is expected to systematically vary with halo mass, since small halos are both inefficient at capturing hot baryons (e.g. during the epoch of reionization) and also because small halos are less able to prevent energy input from star bursts from leading to escape of baryons (see e.g. Gnedin et al. 2002). In Figure 4 we show the baryon fraction (as determined at the last measured point of the rotation curve) for a sample of galaxies with well measured rotation curves. The average cosmic baryon fraction is shown as a horizontal line. As can be seen, there is a large scatter in baryon fraction, and there is no systematic trend for a lower baryon fraction in smaller galaxies. In particular, although gas rich galaxies (shown as solid points in the figure), have somewhat extreme baryon fractions, they lie within the range of that

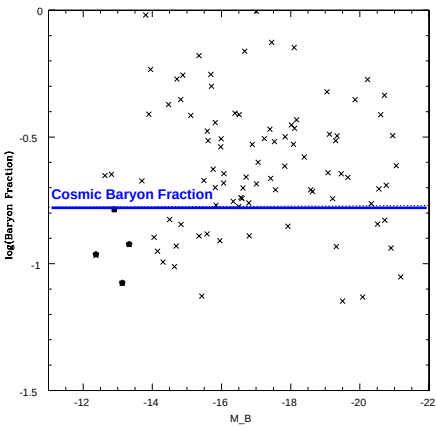

Fig. 4. Baryon fraction (within the last measured point of the rotation curve) as a function of blue luminosity for a sample of galaxies with well measured rotation curves. The cosmic baryon fraction is shown as a horizontal line. Four gas rich galaxies, viz. DDO 154, NGC 3741, ESO215-G?009 (Warren et al. 2004) and And IV are shown as solid points.

observed for galaxies in general. As such these galaxies have got their "fair share" of baryons, but for some reason have been unable to convert them into stars.

References

1. A. Begum, J. N. Chengalur, I. D. Karachentsev, S. S. Kaisin, M. E. Sharina: MNRAS, **365**, 1220 (2006)
2. A. Begum, J. N. Chengalur, I. D. Karachentsev: A&A, **433**, L1 (2005)
3. A. Begum, J. N. Chengalur: A&A, **424**, 509 (2004)
4. A. Begum, J. N. Chengalur: A&A, **413**, 525 (2004)
5. A. Begum, J. N. Chengalur: A&A, **409**, 879 (2003)
6. A. Begum, J. N. Chengalur, U. Hopp: NewA, **8**, 267 (2003)
7. R. Braun, D. Thilker, R. A. M. Walterbos: A&A, **406**, 829 (2003)
8. A. M. N. Ferguson, J. S. Gallagher, R. F. G. Wyse: AJ, **120**, 821 (2000)
9. O. Y. Gnedin, H. Zhao: MNRAS, **333**, 299 (2002)
10. G. Gentile, P. Salucci, U. Klein, G. L. Granato: MNRAS, **375**, 199 (2007)
11. I. D. Karachentsev, V. E. Karachentseva, W. K. Huchtmeier, D. I Makarov: AJ, **127**, 2031 (2004)
12. K. Y. Lo, W. L. Sargent, K. Young: AJ, **106**, 507 (1993)
13. G. Swarup, S. Ananthakrishnan, V. K. Kapahi, A. P. Rao, C. R. Subrahmanya, V. K. Kulkarni: Current Science **60**, 95 (1991)
14. B. E. Warren, H. Jerjen, B. S. Koribalski: AJ, **128**, 1152 (2004)

The Evolution of the ISM in Star Forming Galaxies

Eric M. Wilcots

University of Wisconsin-Madison, 475 N. Charter St. Madison, WI 53706, USA
ewilcots@astro.wisc.edu

1 Introduction

With the exception of galaxy-galaxy interactions feedback from massive stars is the single most important driver of the evolution of the ISM in star-forming galaxies. The strong stellar winds and subsequent supernovae explosions (SNe) associated with massive stars deposit a tremendous amount of energy into the ambient medium, affecting the distribution and kinematics of the ISM and generating both hot gas and cosmic rays.

Our group has undertaken a systematic study of feedback in a sample of nearby star-forming galaxies. While the galaxies in our sample are all actively forming stars, they are typically not considered starburst systems. We are primarily interested in measuring the efficiency and effect of feedback in normal, star-forming galaxies in the local Universe. Our sample includes the irregular galaxies IC 10, IC 1613, WLM, NGC 2537, NGC 4214, and NGC 1569, as well as the spiral galaxies NGC 3184, NGC 3631, NGC 628, IC 5332, NGC 4618, and NGC 4395.

2 Dwarf Galaxies: IC 10

Thurow & Wilcots (2005) observed the main star-forming disk of IC 10 using the Densepak integral field unit (IFU) on the WIYN 3.5m telescope. The observations yielded measurements of the Hα velocity and line widths across the disk of IC 10. On average the Hα velocity was consistent the H I velocity throughout the disk. The Hα linewidths, however, were considerably higher. Thurow & Wilcots (2005) identified two major components to the Hα linewidth, a relatively narrow component with FWHM$_{H\alpha}$ of 40–50 km s^{-1} and a broader component with FWHM$_{H\alpha}$ of 80–100 km s^{-1}. With the exception of single region in the northern part of the disk there was no kinematic evidence of expanding shells and bubbles.

B.S. Koribalski, H. Jerjen (eds.), *Galaxies in the Local Volume*,
doi: 10.1007/978-1-4020-6933-8_14,

We also observed H I in IC 10 using the A configuration of the Very Large Array (VLA). When combined with our earlier VLA observations (Wilcots & Miller 1998), these new data yielded a spatial resolution of 8.2 pc ×7.8 pc at the distance of IC 10 (Saha et al. 1996). To quantify the impact of massive stars on the neutral ISM we corrlated the high resolution H I map with the locations of 11 massive star clusters identified by Hunter (2001). The H I in the vicinity of the clusters was nearly featureless; we do not detect any expanding shells or any enhancement in the H I velocity dispersion in the environment of most of the star clusters. The H I velocity dispersion map is shown in Fig. 1. We see that the maximum velocity dispersions are only $\sim$20 km s^{-1} and more typically $\sim$12 km s^{-1} even in regions coincident with the massive young clusters. The only outflows we detect in IC 10 are associated with steep gradients in the density of the ambient ISM.

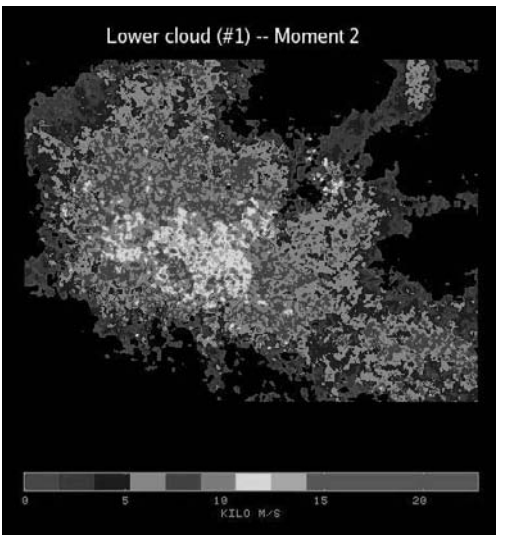

Fig. 1. The H I velocity dispersion for the central star-forming cloud in IC 10.

Taking the derived ages of the clusters (4–20 Myr; Hunter 2001), the mechanical energy deposited by a single massive star in terms of its stellar wind and SNR, and the initial mass function, we calculated the total energy deposited into the ISM of IC 10 by the massive stellar population being $3 - 11 \times 10^{53}$ erg. By comparison, the *observed* kinetic energy of the neutral and ionzed gas is only $\sim 10^{53}$ erg. The conclusion we draw is that there is significantly more energy deposited than can directly accounted for in the kinematics of the neutral and ionized gas. This energy is likely going into the hot phase of the ISM, but we see that feedback is not likely to significantly alter the distribution of the cool or warm phases of the ISM in these galaxies.

3 Summary: Feedback in Dwarf Galaxies

While we have only highlighted IC 10 in this discussion, the results are comparable to what we find in other similar irregular galaxies (e.g., Wilcots & Thurow 2001). Our survey of feedback in nearby star-forming dwarf galaxies shows that:

- The ionized gas is "stirred up", with typical Hα velocity dispersions of 80–100 km s^{-1};
- High velocity ($v \geq 100$ km s^{-1}) outflows are restricted to nuclear starbursts and/or steep gradients in the density of the ambient ISM;
- There is no observed loss of the cool ISM;
- H I holes are not necessarily correlated with H II regions or OB associations;
- and, the kinematics of the cool and ionized gas cannot account for the energy deposited from stellar winds and SNe.

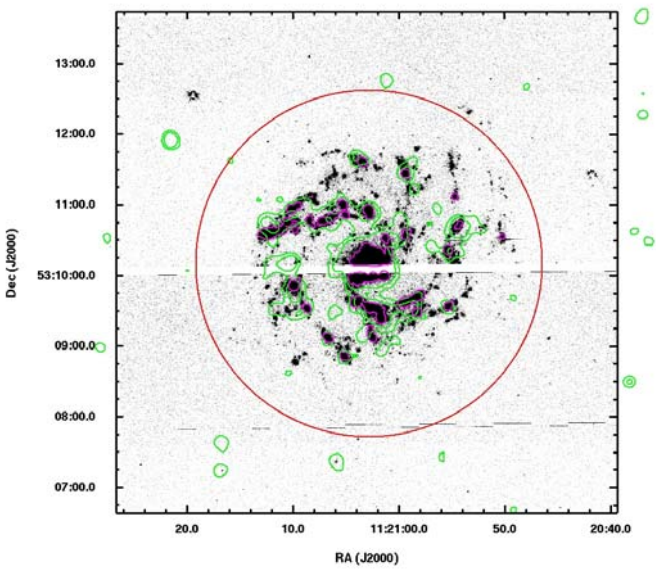

Fig. 2. We show the X-ray contours overlaid on an Hα image of NGC 3631.

4 Diffuse X-ray Emission in Spiral Galaxies

A key component of the feedback phenomenon is the origin and evolution of the diffuse hot gas produced by SNe. We have used the Chandra X-ray

Observatory to study the diffuse hot gas in a sample of nearby, face-on spiral galaxies. The results discussed below are described in more detail in Doane et al. (2004) and Doane et al. (2007). An example of the distribution of the diffuse hot gas in a spiral galaxy is shown in Fig. 2. The large circle represents the optical extent of NGC 3631, while the greyscale is a continuum-subtracted Hα image. The contours are the diffuse X-ray emission. It is very clear that the X-ray emission is well correlated with the spiral arms and H II regions.

Assuming solar metallicity, we fit the X-ray spectra for each galaxy with a two-temperature thermal model. Our fits yielded low temperatures of $1 - 2 \times 10^6$ K with a high temperature component of $5 - 8 \times 10^6$ K. For comparison, the high temperatures are hotter than any known Galactic superbubbles, but are consistent with observations of regions in the Large Magellanic Cloud (e.g. Dunne, Points, & Chu 2001). The cooling times for the gas are typically $10^6 - 10^7$ years. We used the observed emission measure with estimates of the scale heights of the disks to calculate the pressure, P/k, of the hot superbubbles. In each case the derived pressures of the hot gas coincident with the H II regions were factors of 3–4 higher than the ambient pressure of the Galactic ISM. In the extreme, the hot gas in the bulge of NGC 3631 is overpressured by factors of 10–20. We do not yet know if this overpressure is driving a galactic outflow.

4.1 Summary: Diffuse X-ray Emission in Spiral Galaxies

We find that the diffuse X-ray emission is highly correlated with both the spiral arms and H II regions, and, in many cases, it is spatially coincident with the neutral gas. The bulk of the diffuse X-ray emission arises from less than 25% of the area of the disk. Our fits to the X-ray spectrum indicate that the X-ray "bubbles" are generally over-pressured with respect to the average ambient pressure and, therefore, could be feeding a galactic fountain. While we have used the standard two temperature fit to the diffuse X-ray emission, the X-ray spectra can be equally well fit with a model with a continuum of temperatures. While this is a more physical model we do not have the necessary S/N ratio in the *CXO* spectra in order to adequately discern between the competing models.

References

1. J.E. Coppock, E.M. Wilcots: BAAS **38**, 1137 (2006)
2. N.E. Doane, W.T. Sanders, E.M. Wilcots, M. Juda: AJ **128**, 2712 (2004)
3. N.E. Doane, E.M. Wilcots, R. Benjamin, W.T. Sanders: AJ, submitted (2007)
4. B.C. Dunne, S.D. Points, Y-H Chu: ApJS **136**, 119 (2001)
5. D.A. Hunter: ApJ **559**, 225 (2001)
6. A. Saha, J.G. Hoessel, J. Krist, G.E. Danielson: AJ **111**, 197 (1996)
7. J.C. Thurow, E.M. Wilcots: AJ **129**, 745 (2005)
8. E.M. Wilcots, B.W. Miller: AJ **116**, 2363 (1998)
9. E.M. Wilcots, J.C. Thurow: ApJ **555**, 758 (2001)

Magnetic Fields in Irregular Galaxies

Amanda A. Kepley[1], Stefanie Mühle[2], Eric M. Wilcots[1], John Everett[1,3,4], Ellen Zweibel[1,3], Timothy Robishaw[5], and Carl Heiles[5]

[1] Department of Astronomy, University of Wisconsin-Madison, 475 N. Charter St., Madison, WI 53706, USA kepley@astro.wisc.edu, ewilcots@astro.wisc.edu, everett@physics.wisc.edu, zweibel@astro.wisc.edu
[2] Department of Astronomy and Astrophysics, University of Toronto, 50 St. George St., Toronto, Ontario M5S 3H4, Canada muehle@astro.utoronto.ca
[3] Center for Magnetic Self-Organization in Laboratory and Astrophysical Plasmas
[4] Department of Physics, University of Wisconsin–Madison, 1150 University Ave., Madison, WI 53706-1390, USA
[5] 601 Campbell Hall, Department of Astronomy, University of California at Berkeley, Berkeley, CA 94720-3411, USA robishaw@astro.berkeley.edu, heiles@astro.berkeley.edu

Magnetic fields are an important component of the interstellar medium. They channel gas flows, accelerate and distribute energy from cosmic rays, and may be a significant component of the galactic pressure, especially in low-mass galaxies [1]. A priori, one wouldn't expect irregular galaxies to have large scale magnetic fields. The most common dynamo mechanism, the $\alpha - \omega$ dynamo, relies on differential rotation to stretch small scale fields into large scale fields [2]. Most irregular galaxies, however, are either solid-body rotators or show little rotation [3]. Despite this, observations of NGC 4449 [4] and the Large Magellanic Cloud (LMC) [5] have revealed the presence of large-scale magnetic fields in these galaxies.

Previous observations of a small number of irregular galaxies reveal a range of magnetic field properties. See Table 1 for a summary. Observations of the irregular galaxy NGC 4449 [4] show a strong large-scale field. Theoretical work has suggested that a bar and a fast dynamo are needed to reproduce the observed field structure [6]. The LMC has a weak large-scale field possibly generated by a cosmic-ray driven dynamo [5]. The magnetic field structures of NGC 6822 and IC 10 [7] are weak and almost completely random. The lack of a large-scale magnetic field in these galaxies may be caused by a combination of their intense star-formation and their lower rotation velocities [7].

The goal of this project is to significantly increase the number of irregular galaxies with observed magnetic field structures to better answer the following questions: (1) what generates and sustains large-scale magnetic fields in

B.S. Koribalski, H. Jerjen (eds.), *Galaxies in the Local Volume*,
doi: 10.1007/978-1-4020-6933-8_15,

irregular galaxies? and (2) what causes the range of observed magnetic field structure?

1 Measuring Magnetic Fields in Galaxies

There are many techniques for measuring magnetic fields [8]. We use diffuse synchrotron emission at centimeter wavelengths as a tracer of the magnetic field. High-resolution observations are crucial for minimizing the effects of beam depolarization. In general, the optimal observing frequency for these observations is 6 cm because there is low Faraday depolarization [9] at this frequency, but the synchrotron emission is still quite strong. The increasing strength of synchrotron emission at long wavelengths is neutralized by an increase in the amount of Faraday depolarization (which goes as roughly as wavelength squared) at these wavelengths.

We use the Very Large Array (VLA) and single dish radio observations from either the Green Bank Telescope (GBT) or the Effelsberg 100-m telescope to obtain radio continuum polarization measurements of several irregular galaxies at three frequencies: 20 cm, 6 cm, and 3 cm. The VLA observations have the high resolution necessary for us to detect small-scale magnetic field structure, while the single dish observations allow us to correct the VLA observations for unresolved large-scale structure. Observing at 3 different wavelengths allows us to separate the free-free emission from the synchrotron emission and determine rotation measures.

We have selected galaxies that have a range of sizes, rotation rates, and star formation rates and that complement previous observations [4, 5, 7]. See Table 1 for a summary of galaxy properties.

2 Preliminary Results: NGC 4214 and NGC 1569

NGC 4214 has a slower rotation rate and weaker bar than NGC 4449 and a higher star formation rate per unit area. From the 6 cm VLA image of the continuum emission from this galaxy, we determined the amount of synchrotron emission using Hα images supplied by Deidre Hunter to estimate the thermal contribution to the 6 cm emission. There is very little polarized emission associated with this galaxy. The total field in this galaxy is about $4\mu G$ and it is mostly random.

NGC 1569 has the highest star formation rate per unit area in our sample, and one of the highest star formation rates out of all galaxies in the local universe. It is possibly ejecting much its interstellar medium [10, 11] either through a pressure-drive, accelerating wind or a detonation.

Figure 1 shows a 6 cm VLA image of the synchrotron emission from NGC 1569 with vectors showing the orientation of the magnetic field and the

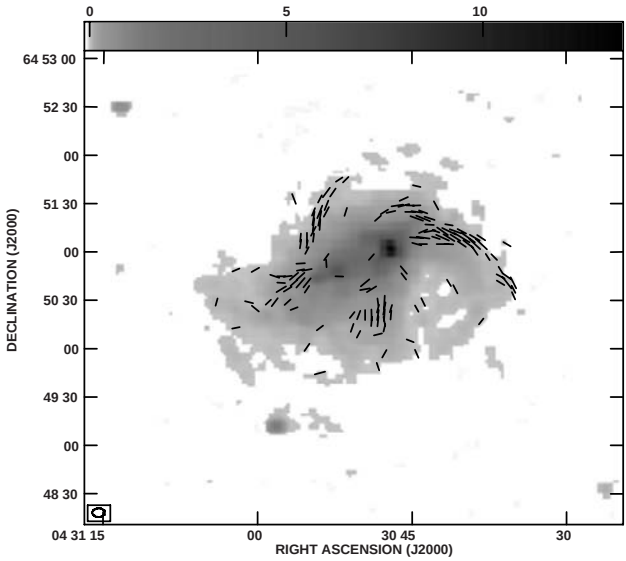

Fig. 1. Synchrotron emission from NGC 1569 at 6 cm overlaid with polarization vectors. The length of the vector indicates the strength of the polarized intensity ($1''$ is 5 μJy beam^{-1}) and the angle indicates the direction of the magnetic field.

intensity of the polarized emission. Again, we have used Hα images provided by Deidre Hunter to estimate the thermal contribution to the 6 cm emission.

X-ray observations [12] suggest that the northern half of the galaxy is tilted away from the line of sight, so it is not surprising that we do not see synchrotron emission from this half of the galaxy. The southern half of the galaxy, however, shows a wealth of features. An arm of synchrotron emission is seen on the western edge of the galaxy. Inside this arm, there is an Hα arm and inside the Hα arm, there is an X-ray arm [12]. The large scale magnetic field seen on the western arm is likely the result of a compression of gas or a shock. As gas is compressed, it drags the magnetic field along with it and amplifies the field. Most of the field lines in this galaxy are roughly perpendicular to the disk, except at the ends of the disk.

When we compare the 6 cm image to a 3 cm image, we see that the polarization vectors in the southern portion of the galaxy and along the western arm rotate very little between the two wavelengths. Based on the observed orientation of the fields between the two wavelengths, the rotation measure is constrained to be less than 32 rad m^{-2}. This result suggests that the line integral of the magnetic field along the line of sight times the thermal electron distribution is small.

The mostly random magnetic field structure of NGC 4214 closely resembles the magnetic field structure of NGC 6822 and IC 10. This galaxy probably does not have a strong enough rotation rate or bar to sustain a large-scale

field. NGC 1569 has a large-scale magnetic field that appears to be shaped primarily by gas outflowing from the disk of the galaxy. The extent to which the magnetic field shapes or drives the outflow is the subject of further investigation. We are also reducing observations of NGC 1313 and NGC 1156 to add their magnetic field structures to the overall picture of magnetic field structures in irregular galaxies.

Table 1. Properties of Galaxies in Sample

Galaxy	Optical Extent kpc	$\log(SFR_D)$ $M_\odot\,yr^{-1}\,kpc^{-2}$	$V_{max}/\sin(i)$ $km\,s^{-1}$	Bar?	$B_{uniform}$ μG	B_{total} μG
Previous Observations [4, 7, 5]						
NGC 4449	7×5	–2	110	strong bar	6 – 8	14
LMC	9.4×8	–2.9	50	yes	1	4.3
NGC 6822	2.3×2.0	–1.96	52	yes	< 3	< 5
IC 10	2.0×1.7	–1.3	30	no	< 3	5–15
Our Sample						
NGC 4214	10×8	–1.10	30	weak bar	~ 0	4
NGC 1569	2.1×1.0	0.11	40	yes	3–5	6
NGC 1156	7.5×6	–0.87	75	yes	?	?
NGC 1313	10.6×8.0	–0.78	89	strongest bar	?	?

References

1. R. Beck: Magnetic Fields in the Milky Way and Other Spiral Galaxies. In: *How Does the Galaxy Work?*, ASSL Vol. 315, ed by E. J. Alfaro, E. Pérez, and J. Franco (Kluwer Academic Publishers, Dordrecht The Netherlands 2004) pp 277–286
2. R. M. Kulsrud: ARAA **37**, 37 (1999)
3. E. K. Grebel: Dwarf Galaxies in the Local Group and in the Local Volume. In *Dwarf galaxies and their environment*, ed by K. S. de Boer, R.-J. Dettmar, and U. Klein (Shaker Verlag, Aachen Germany 2001) pp 45–52
4. K. T. Chyży, R. Beck, S. Kohle, et al: A&A **355**, 128 (2000)
5. B. M. Gaensler, M. Haverkorn, L. Staveley-Smith, et al: Science **307**, 1610 (2005)
6. K. Otmianowska-Mazur, K. T. Chyży, M. Soida, and S. von Linden: A&A **359**, 29 (2000)
7. K. T. Chyży, J. Knapik, D. J. Bomans, et al: A&A **405**, 513 (2003)
8. E. G. Zweibel and C. Heiles: Nature **385**, 131 (1997)
9. B. J. Burn: MNRAS **133**, 67 (1966)
10. C. L. Martin: ApJ **506**, 222 (1998)
11. U. Lisenfeld, T. W. Wilding, G. G. Pooley, and P. Alexander: MNRAS **349**, 1335 (2004)
12. C. L. Martin, H. A. Kobulnicky, and T. M. Heckman: ApJ **574**, 663 (2002)

Future ASKAP Studies of the Local Volume

Lister Staveley-Smith

School of Physics, University of Western Australia, Crawley, WA 6009, Australia
Lister.Staveley-Smith@uwa.edu.au

Summary. The Australian SKA Pathfinder (ASKAP) will be a powerful instrument for performing large-scale surveys of galaxies. Its frequency range and large field of view makes it especially useful for an all-sky survey of Local Volume galaxies, and will probably increase the number of known galaxies closer than 10 Mpc by a factor of two and increase, by at least an order of magnitude, the number detected in H I. Implications for our knowledge of the H I mass function for the very faintest galaxies and for the structure and dynamics of the Local Volume are discussed.

1 Introduction

The Local Volume is a key region for the study of the properties of galaxies, including: (1) their internal structure and dynamics; (2) their spatial distribution and dynamics in an environment which lies in the outskirts of a supercluster; and (3) their complete evolutionary history, by virtue of our ability to resolve individual stars. The Local Volume is particularly useful for studying the faintest galaxies and is well-served by having a wealth of accurate redshift-independent TRGB distances through recent surveys by the HST [4].

As shown elsewhere in these proceedings, detailed studies of Local Volume galaxies in the 21cm line of neutral hydrogen have been particularly fruitful. These have recently been rejuvenated by surveys at other wavebands including those of *Spitzer* and *GALEX*. Due to the sensitivity and resolution, such surveys have often been drawn towards the luminous galaxy population. However, the Local Volume also offers a unique opportunity to study the faintest galaxies observable and many studies (e.g. *SINGG, LVHIS, THINGS*) have also been careful to select their samples across a range of intrinsic luminosity.

The Square Kilometre Array (SKA) will be a radio telescope of unprecedented power to observe galaxies in the radio continuum and in the 21cm line. Its sensitivity will easily surpass existing telescopes and allow Local Volume galaxies to be studied at the highest spatial resolution. However, it's not due to come on-line for at least a decade. Nevertheless, the next generation of so-called 'SKA pathfinders' are around the corner. Their purpose is to test

B.S. Koribalski, H. Jerjen (eds.), *Galaxies in the Local Volume*,
doi: 10.1007/978-1-4020-6933-8_16,

Table 1. The planned specifications of the Australian SKA Pathfinder (ASKAP), as listed in the expansion option of [1].

Specification	Value	Units
Frequency range	700–1800	MHz
Number of antennas	45	
Antenna diameter	12	m
Total area	5089	m^2
System Temperature T_{sys}	35	K
Field of view	30	deg^2
Maximum baseline	0.4 – 8	km
Instantaneous bandwidth	300	MHz

SKA technologies, yet provide sufficient sensitivity to obtain useful science and provide a valuable source of survey material for the SKA itself. Examples of proposed pathfinders are the Allen Telescope Array (ATA) and the Apertif upgrade to WSRT in the northern hemisphere, and MeerKAT and the Australian SKA Pathfinder (ASKAP) in the southern hemisphere. In this brief paper, I will look at the implications for our knowledge of the Local Volume in the proposed ASKAP surveys.

2 The Australian SKA Pathfinder (ASKAP)

ASKAP (formerly xNTD/MIRANdA) is a so-called '1% SKA pathfinder' although, in reality, it will likely have a collecting area A, of only 0.5% of a square kilometre [1]. However, due to its enormous field-of-view Ω, its speed ($\propto \Omega A^2 T_{sys}^{-2}$) will greatly exceed that of the existing 64 to 300-m class of single-dish radio telescopes and even the large synthesis arrays such as ATCA, GMRT, WSRT, and the VLA. The properties of ASKAP as listed in [1] are summarized in Table 1. ASKAP is due to be located at Boolardy Station in Western Australia in an extremely radio-quiet environment. It will therefore be able to combine an uncluttered view of the redshifted 21-cm Universe with powerful widefield technology, to produce fast, deep surveys which, apart from the enormous data volumes, will be relatively straightforward to deal with in data reduction pipelines.

3 A Local Volume Survey

A natural survey to contemplate with ASKAP, and one discussed in [1] is an all-sky 21cm survey. Given the specifications listed in Table 1, and given a year of survey time, a survey covering 2π sr will reach an rms sensitivity of $\sim$0.26 mJy beam^{-1} in a resolution element of 100 kHz (corresponding to 21

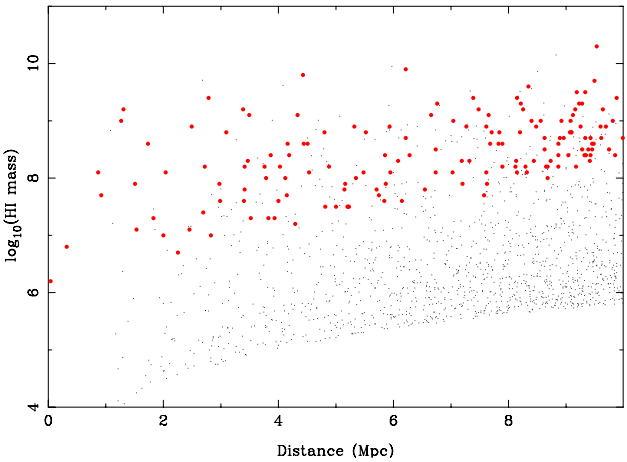

Fig. 1. The H I masses of 1280 putative Local Volume galaxies detected in a simulated 1-yr ASKAP survey covering 2π sr are shown as small dots. Known galaxies, detected in the HIPASS survey [3] are shown as solid circles. Local Group galaxies within 1 Mpc are not simulated. This simulation assumes a compact ASKAP configuration, thus represents the maximum number of detections expected.

$\mathrm{km\,s^{-1}}$)[1]. Such a survey will not only be able to detect high-mass galaxies out to slightly beyond $z = 0.2$, but will also detect significant numbers of low-mass galaxies in the Local Volume.

Figure 1 shows a detailed simulation of the H I masses of galaxies expected to be detected at distances within 10 Mpc by an all-sky ASKAP survey. The simulation assumes the HIPASS H I mass function [5], a HIPASS mass-velocity width relationship, and a compact ASKAP configuration. At the edge of the Local Group ($\sim$1 Mpc), a few galaxies of H I masses below 10^5 $M_\odot$ are expected and, at all points within the Local Volume, galaxies down to 10^6 $M_\odot$ are expected to be detected.

The numbers of galaxies detectable in such an ASKAP survey is enormous – around 2×10^6 out to the survey redshift limit. Within 10 Mpc, around 1280 are predicted, or 2560 over the whole sky if an equivalent northern survey was feasible. This is over four times greater than the number of galaxies ($\sim$550) presently known to reside in the Local Volume [10], and indicates the impact a future ASKAP survey is likely to make on our knowledge of the region. However, this prediction is heavily dependent on extrapolating the HIPASS mass function by two orders of magnitude down the mass function! Any deviation from this has significant implications for the prediction. This is demonstrated in Figure 2 which is a mass function recovered from the above simulation. Above 10^7 $M_\odot$ it reproduces, as it should, the HIPASS mass function. Below

[1] The actual frequency resolution of ASKAP will be better ($\sim$20 kHz), but 100 kHz is appropriate for galaxy *detection*.

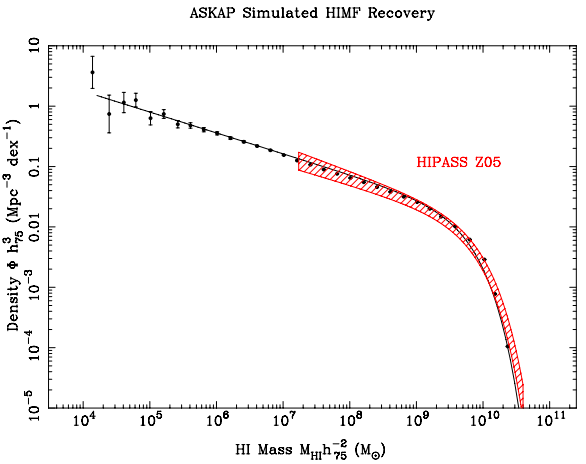

Fig. 2. An H I mass function derived from a simulated 1-yr ASKAP survey covering 2π sr, again assuming a compact ASKAP configuration. For comparison, the known H I mass function from HIPASS [5] is plotted in the hatched area.

that, the recovered mass function has a slope of -1.35 ± 0.01, very close to the simulated slope of -1.37. A steeper faint-end slope (a natural prediction for CDM halos) will result in much greater numbers of low-mass objects.

4 Discussion

The high number of galaxies that, in all likelihood, remain to be discovered in the Local Volume will allow a remarkably dense sampling of the extragalactic environment of the Local Group. This will allow an accurate mapping of the large-scale filamentary features joining the Local Group with Sculptor and other groups. Combined with the redshift-independent distances that are possible for such nearby objects, it will also allow a study of the Hubble flow, infall towards filaments, and tidal stretching owing to nearby overdense regions such as the Local Supercluster and underdense regions such as the Local Void.

References

1. Johnston, S. et al. 2007, PASA (submitted)
2. Karachentsev, I. 2007, these proceedings
3. Koribalski, B.S. et al. 2004, AJ 128, 16
4. Rizzi, L., Tully, R.B., Makarov, D., Makarova, L., Dolphin, A.E., Sakai, S., Shaya, E.J. 2007, ApJ, 661, 815
5. Zwaan, M.A. et al. 2005, MNRAS, 359, L30

An Ultraviolet-to-Radio Broadband Spectral Atlas of Nearby Galaxies

Daniel A. Dale

University of Wyoming, USA ddale@uwyo.edu

The ultraviolet-to-radio continuum spectral energy distributions are studied for all 75 galaxies in the Spitzer Infrared Nearby Galaxies Survey (SINGS), with a particular focus on the infrared and ultraviolet data. The 24 μm morphology can be a useful tool for parametrizing the global dust temperature and ultraviolet extinction in nearby galaxies. The dust emission in dwarf/irregular galaxies is clumpy and warm accompanied by low ultraviolet extinction, while in spiral galaxies there is typically a much larger diffuse component of cooler dust and average ultraviolet extinction. For galaxies with nuclear 24 μm emission, the dust temperature and ultraviolet extinction are relatively high compared to disk galaxies.

1 The Sample

The complete imaging data set for all 75 SINGS galaxies is presented in [1]. The dataset combines deep GALEX ultraviolet and Spitzer infrared imaging with a wealth of ancillary data at optical, near-infrared, submillimeter and radio wavelengths. This contribution focuses on the ultraviolet and infrared data, but all the fluxes presented in [1] are 'global' in the sense that they are spatially-integrated over the entirety of each galaxy.

2 Far-Infrared Color

Figure 1 plots the infrared-to-ultraviolet ratio versus far-infrared color for the entire SINGS sample. An interesting feature to this plot is the apparent wedge-shaped distribution, with a progressively smaller range in the infrared-to-ultraviolet ratio for cooler far-infrared colors. The small data points without error bars come from the (*IRAS*-based) *GALEX Atlas of Nearby Galaxies* [2] and follow the same general distribution as the SINGS data, suggesting that

B.S. Koribalski, H. Jerjen (eds.), *Galaxies in the Local Volume*,
doi: 10.1007/978-1-4020-6933-8_17,

this wedge-shaped distribution is unlikely a sample selection effect. Presumably the upper left-hand portion of this figure, for example, is empty since a large infrared-to-ultraviolet ratio requires lots of dust opacity, but higher opacity implies a larger density of interstellar dust closer to heating sources, therefore leading to warm dust and high values of $f_\nu(70\ \mu\mathrm{m})/f_\nu(160\ \mu\mathrm{m})$.

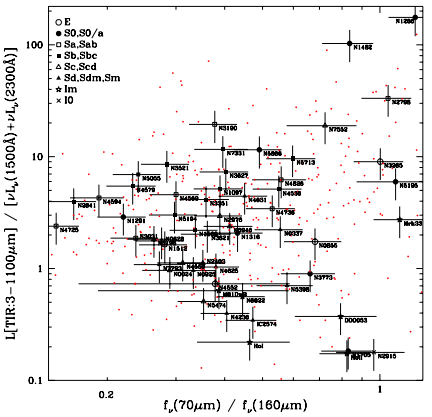

Fig. 1. The infrared-to-ultraviolet ratio as a function of far-infrared color for the SINGS sample. Data from the *GALEX Atlas of Nearby Galaxies* [2] are also shown as small data points without error bars.

The relative distribution of dust grains and their heating sources may, in fact, play a key role in creating this overall wedge-shaped distribution. As argued above, it is reasonable to assume that galaxies with relatively high $f_\nu(70\ \mu\mathrm{m})/f_\nu(160\ \mu\mathrm{m})$ ratios have hotter dust since the dust in such systems is near sites of active star formation or active nuclei. Moreover, galaxies that appear as several bright clumps in the infrared provide a large number of low optical depth lines-of-sight from which ultraviolet photons may escape. Such clumpy galaxies would hence show comparatively low infrared-to-ultraviolet ratios. On the other hand, ultraviolet photons from galaxies that appear in the infrared as a single point-like blob of nuclear emission would encounter significant extinction, and hence such galaxies would exhibit high infrared-to-ultraviolet ratios and high dust temperatures. In contrast to hot dust systems, galaxies with relatively low $f_\nu(70\ \mu\mathrm{m})/f_\nu(160\ \mu\mathrm{m})$ ratios have cooler dust because the dust is not in spatial proximity of the hot stars [7]. The heating of dust via the weaker ambient interstellar radiation field would be fractionally higher in these galaxies. Therefore, their morphological appearance in the infrared should be comparatively smooth.

Since the relative distribution of interstellar grains and their heating sources is central to the scenario outlined above, we turn to the 24 μm

morphology of SINGS galaxies to provide a test of the above scenario. MIPS 24 μm data may be uniquely suited for such a test, as the data have significantly higher spatial resolution than either 70 or 160 μm imaging, and effectively trace both interstellar grains and active sites of star formation [5, 3]. In fact, the 24 μm emission can be spatially closely associated with H II regions, and in such cases is probably dominated by dust from *within* these regions [4, 6]. To facilitate our analysis, we have decomposed the 24 μm images into unresolved (point sources) and resolved emission.

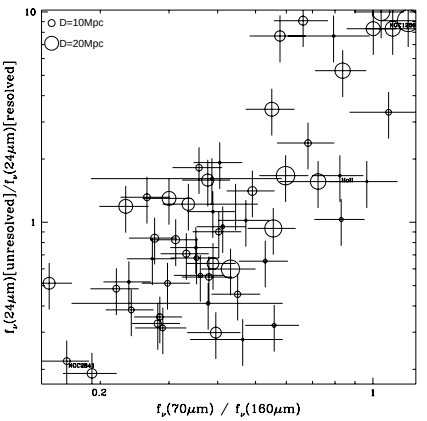

Fig. 2. The ratio of unresolved-to-resolved 24 μm emission as a function of far-infrared color (see Section 2). A 25% uncertainty is used for the error bars in the unresolved-to-resolved ratio. Symbol sizes are scaled according to galaxy distance.

An image of all the detected point sources is created along with a difference image made by subtracting the point source image from the observed image. The fluxes are measured in the point source ("unresolved") and difference ("resolved") images in the same aperture used for the total galaxy measurement. In addition, nuclear fluxes are measured in a 12″ radius circular aperture on the observed image. The results from this analysis are displayed in Figures 3 and 2. In Figure 3 the symbol size linearly scales with the ratio of unresolved-to-resolved 24 μm emission, with the largest symbols corresponding to ratios $\sim$10. In addition, each data symbol reflects the ratio of nuclear-to-total 24 μm emission, as indicated in the figure legend. Galaxies dominated by a single point source of nuclear emission at 24 μm appear preferentially in the upper righthand portion of the diagram. These galaxies contain hot dust and show relatively high infrared-to-ultraviolet ratios since the dust is centrally concentrated near the heating sources in the nuclei. Note that nuclear activity is not the main factor in determining the 24 μm morphology — only two of the point-like systems have active nuclei (NGC 1266

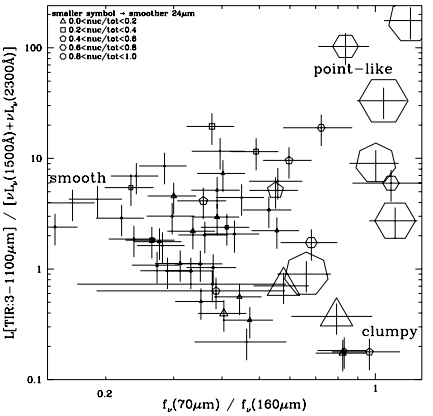

Fig. 3. Similar to Figure 1, but with symbol size scaled according to the ratio of unresolved-to-resolved 24 μm emission; the largest symbols have this ratio equal to $\sim$10. Each data point is also symbolized according to the ratio of nuclear-to-total 24 μm emission (see Section 2).

and NGC 5195). Systems with clumpy 24 μm morphologies appearing in the lower righthand corner still contain hot dust; the dust is concentrated around several heating sources, not just the nuclear ones. Moreover, the clumpy distribution provides a larger number of low τ or 'clean' lines-of-sight for ultraviolet photons to escape the galaxies, decreasing their infrared-to-ultraviolet ratios (see, for example, [8]). Finally, galaxies with smoother 24 μm morphologies exhibit cooler far-infrared colors. To see this latter effect more clearly, we show in Figure 2 the ratio of unresolved-to-resolved 24 μm emission as a function of far-infrared color. Clearly there is a trend, indicating that the 24 μm morphology can, for nearby galaxies, indicate the relative separation between interstellar grains and their heating sources.

References

1. D. Dale et al: ApJ, **655**, 863 (2007)
2. A. Gil de Paz et al: ApJ, in press (2007)
3. K. Gordon et al: ApJS, **154**, 215 (2004)
4. G. Helou et al: ApJS, **154**, 253 (2004)
5. J. Hinz et al: ApJS, **154**, 259 (2004)
6. E. Murphy et al: ApJ, **638**, 157 (2006)
7. N. Panagia: AJ, **78**, 9 (1973)
8. H. Roussel: ApJ, **632**, 227 (2005)

Diagnostic Value of Mid-Infrared Fine Structure Lines in Galaxies

Caroline Bot[1] and the SINGS team

[1]California Institute of Technology, Pasadena CA 91125, USA
bot@caltech.edu

Infrared fine structure lines are commonly observed in H II regions, where they are primarily excited by collisions between electrons and ions. Widely used empirical methods combine the emission from these with hydrogen recombination lines or radio continuum measurements to deduce heavy element abundances. However, these abundance studies could have issues. In particular, they rely on the assumption that ionized hydrogen and the different ionized heavy elements are co-spatial. We present an analysis of fine structure line emission from Ar, Ne and S in the nuclei of nearby galaxies from the Spitzer Infrared Nearby Galaxies Survey (SINGS) observed with the Infrared Spectrograph (IRS) onboard the Spitzer Space Telescope, and in a sample of Galactic H II regions observed with the Short Wavelength Spectrometer (SWS) (Giveon et al. [3]). The goal is to compare the emission measure weighted filling factors deduced from each element (H, Ar, Ne and S) in order to test for consistency and improve the diagnostic value of these lines.

1 The method

The method is to relate the observed intensities of fine-structure lines from various ionization stages to the emission measure weighted filling factor P_X, describing the region where the element X is ionized and where emission originates. This parameter is defined as:

$$P_X = \frac{\int\int n_e^2 \mathrm{d}l\mathrm{d}\Omega}{\Omega_{obs}} \tag{1}$$

where n_e is the electron density, l is the size of the ionized region along the line of sight, Ω is the solid angle of the ionized region and Ω_{obs} is the solid angle observed. This quantity drives the fine structure line intensities of each ionized element, together with metallicity. By assuming that Ar, Ne and S abundances

B.S. Koribalski, H. Jerjen (eds.), *Galaxies in the Local Volume*,
doi: 10.1007/978-1-4020-6933-8_18,

are well estimated by oxygen abundances and constant Ar/O, Ne/O and S/O ratio (because all these elements originate from the same massive stars), the P parameters are computed by combining the flux of the different ionization states observed for each element. For comparison, P parameters can also be computed from hydrogen recombination lines and in that case, no abundance estimate is necessary.

This method is applied to Ar, Ne and S fine structure lines observed in spectroscopy with IRS in the 36" $\times$ 18" central regions of 45 SINGS galaxies. Hydrogen line emission in the SINGS galaxies was more difficult to obtain: Hα line emission from optical images (Calzetti et al. [2]) are considered as lower limits due to sensitivity issues. Paα intensities corrected from extinction were also estimated using the 24μm intensities and the 24μm-Paα^{corr} correlation [2] but are considered as upper limits due to the possible contamination by diffuse 24μm emission. In each galaxy, we used oxygen abundances estimated using two different strong optical emission line diagnostics[6]: one relying on photoionization models [5] and one deduced from empirical methods (Pilyugin & Thuan [7]). These O/H estimates are used with constant Ar/O, Ne/O and S/O [4] with large uncertainties representing the dispersion between samples and methods from the literature.

In addition, we applied our analysis to a sample of Galactic H II regions taken from the literature [3]. This SWS set of observations is of particular interest since the fine structure lines and the hydrogen recombination line Brα were observed with the same instrument, therefore avoiding sensitivity biases. Furthermore, it enables us to compare our analysis in a sample of large nuclear regions of nearby galaxies to a sample of resolved H II regions in a single galaxy (the Milky Way). In order to be consistent with the analysis of the SINGS sample, we took two different O/H gradients: one obtained with the Pilyugin & Thuan method [8] and a more "standard" gradient [9].

2 Results

We compared P for Ar, Ne and S both in the SINGS and the Galactic sample (Fig. 1). We observe a global correlation between the P parameters of each element, but systematic deviations from the agreement are clearly seen with the following trend: $P_{Ar} \geq P_{Ne} \geq P_S$. Our interpretation of these offsets is that the region where Ar, Ne and S are ionized are characterized by distinct values of P. In particular, the regions are not cospatial.

An alternative interpretation would be to attribute these offsets to abundance variations of these elements. In particular, this could be interpreted in terms of depletion of elements onto grains (in particular for sulfur) or different enrichment of the insterstellar medium by stars (large production of neon by Wolf-Rayet stars for example). If this is the case, then the abundances of S have been generally underestimated with respect to Ne, which have been underestimated with respect to those of Ar.

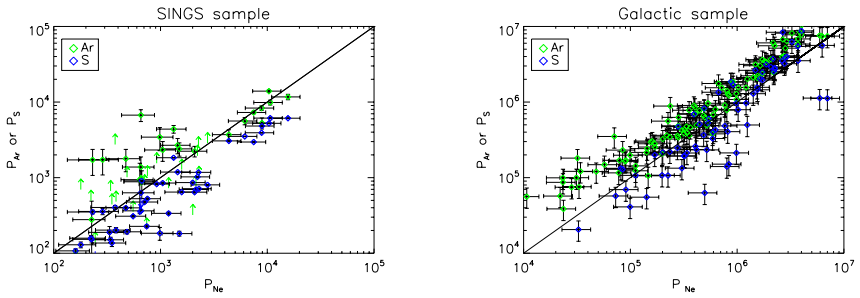

Fig. 1. Comparison of the P parameter for argon, neon and sulfur in the SINGS sample *(left panel)* and in the Galactic sample *(right panel)*. A 1:1 line is displayed to represent where points should fall if the ionized argon, ionized neon and ionized sulfur emitting regions had the same physical properties (electron densities and spatial extent). Regions where only one of the ionization states of an element have been detected are labeled as lower limits.

Since early photoionization models [1] were published, it has been recognized that the volumes occupied by the different ionized elements are not the same. This difference in radius will be linked to the ionizing potentials of the different species and the shape of the ionizing spectrum. If this effect is dominant, we expect the P parameter to display a systematic bias depending on the ionizing potential of the element considered and the importance of the bias will depend on the hardness of the ionization spectrum. Figure 2 shows the progression of the mean P parameter for each element as a function of the lowest ionization potential of the traced states for the two samples and the different [O/H] calibrations. We observe a definite trend of P deviations decreasing with ionization potential from Ar to S in the SINGS sample and from Ar to Ne in the Galactic sample. Whether this trend extends to hydrogen is difficult to say in both samples with present uncertainties on oxygen abundance calculations.

3 Conclusion

The differences in P parameters we are observing may come from differences in the effective areas covered by the different heavy elements that are ionized. The non co-spatiality of the ionized regions has strong implications on the uses of mid-infrared fine structure lines. One of them is on the estimate of abundances from mid-IR fine structure lines. Not taking into account the P variations between elements would lead to systematic bias in abundance estimates from the infrared.

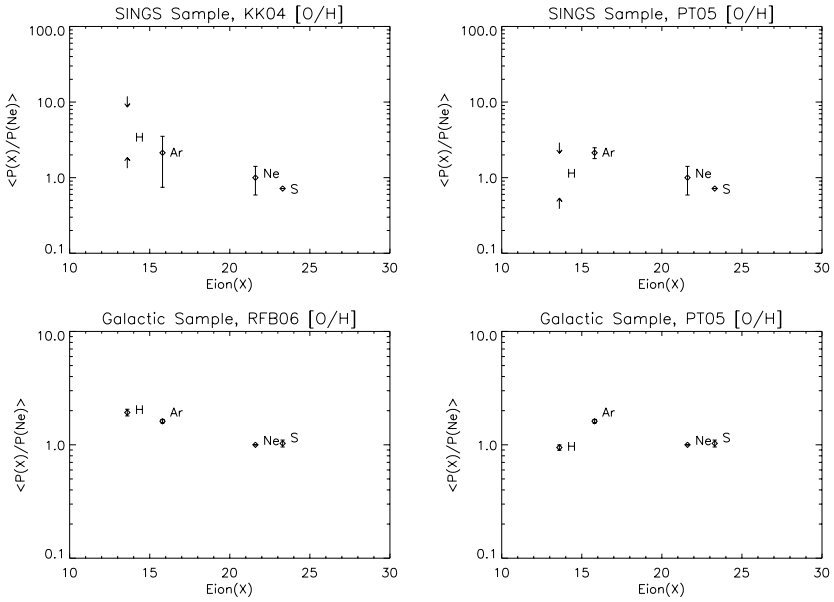

Fig. 2. Progression of the mean P parameter for each element (X=H, Ar or S) normalized to its value for Neon, as a function of the lowest ionization potential of the observed states of the element. The error bars correspond to the error on the mean. The *upper panel* displays the results for the SINGS sample, with the [5] calibration on the *left* and the Pilyugin & Thuan [7] calibration on the *right*. The *lower panel* shows similar plots for the Galactic sample, with the Rudolph et al. [9] calibration on the *left* and the Pilyugin & Thuan [7] on the *right*.

References

1. Balick, B. & Sneden, C.: ApJ, **208**, 336 (1976)
2. Calzetti, D., Kennicutt, Jr., R. C., Engelbracht, C. W., et al.: ApJ, in press, astro-ph/0705.3377 (2007)
3. Giveon, U., Sternberg, A., Lutz, D., Feuchtgruber, H., & Pauldrach, A. W. A.: ApJ, **566**, 880 (2002)
4. Henry, R. B. C. & Worthey, G.: PASP, **111**, 919 (1999)
5. Kobulnicky, H. A. & Kewley, L. J.: ApJ, **617**, 240 (2004)
6. Moustakas, J.: in prep. (2007)
7. Pilyugin, L. S. & Thuan, T. X.: ApJ, **631**, 231 (2005)
8. Pilyugin, L. S., Thuan, T. X., & Vílchez, J. M.: MNRAS, **367**, 1139 (2006)
9. Rudolph, A. L., Fich, M., Bell, G. R., et al.: ApJS, **162**, 346 (2006)

Warm Molecular Hydrogen in Nearby Galaxies: Results from the SINGS Sample

Hélène Roussel[1] and the SINGS team

[1]Max-Planck-Institut für Astronomie, Heidelberg, 69117 Germany
roussel@mpia-hd.mpg.de

Molecular hydrogen is the most abundant molecule, and constitutes the material from which stars condense (with trace amounts of other molecules). Since the neutral interstellar medium (ISM) is mostly molecular in the inner regions of massive galaxies, H_2 dominates there the total interstellar mass. Emission lines of H_2 are found in the ultraviolet (fluorescence), in the near-infrared (vibration-rotation lines) and in the mid-infrared (pure rotation lines). Even the latter require substantial excitation temperatures in order to be observed, at least $T_{\rm exc} \approx 70$ K, which implies that the cold phase cannot be observed directly. The total H_2 mass is most commonly estimated from observations of the J=1–0 rotation line of CO, requiring only $T_{\rm exc} \approx 5\,$K, easily attained, the gas being heated at minimum by cosmic ray ionization in the general ISM.

Even though H_2 emission cannot be used as tracer of the total H_2 mass, it provides important information on the multifarious excitation of the molecular medium, that can be related to galaxy activity in terms of star formation, AGN processes and dynamical perturbations. In normal galaxies, a major energy input to the ISM is provided by stellar radiation; this is thus expected to be a dominant contributor to H_2 excitation. In photodissociation regions (PDRs), H_2 is pumped by FUV photons, followed by fluorescence and radiative cascade through the vibration-rotation levels, and is also heated by collisions with warm gas, itself heated by photoelectrons ejected from dust grains by FUV photons. Other potentially important sources of H_2 heating are shocks, X-rays from AGNs, and formation of H_2 into excited states.

The SINGS program (Kennicutt et al. 2003, http://sings.stsci.edu/) allows the study of rotational H_2 emission in a large sample of normal galaxies, of all morphological and nuclear types. Their infrared luminosities ($L_{\rm FIR} = 10^7$ to $6 \times 10^{10}\,{\rm L}_\odot$) are representative of the general galaxy population. Recent studies of rotational H_2 emission in (ultra)luminous galaxies have been offered by Rigopoulou et al. (2002) and Higdon et al. (2006). For more details on SINGS results than is practical to give here, the reader is referred to Roussel et al. (2007).

B.S. Koribalski, H. Jerjen (eds.), *Galaxies in the Local Volume*,
doi: 10.1007/978-1-4020-6933-8_19,

We measured the S(0) (i.e J=2–0) to S(3) (J=5–3) pure rotational lines in 66 targets within 57 galaxies, mostly nuclear regions, with an aperture solid angle of ≈300 or ≈800 arcsec^2, corresponding to a median diameter of 900 pc. Since the critical densities of these lines are low, they will almost always be thermalized, and the temperatures and column densities can be derived in the LTE assumption, in the temperature range effectively constrained by the data ($100 < T(\mathrm{K}) < 1000$). The column densities of warm gas in many targets appear to be commensurate with those observed in resolved PDRs, which suggests that the beam is filled with these regions, in case they are the dominant energy providers. Figure 3 also shows that, for the star-forming regions, there is a well defined dependence of (local) column densities of warm gas on the host galaxy total stellar mass (or similarly the total infrared luminosity). This kind of behavior is exhibited by the surface brightness of cold molecular gas and star formation rate tracers, pointing to massive star formation as the dominant source of H_2 rotational emission in normal galaxies. Figure 3 also clearly shows that low-luminosity AGNs do not follow any such relation. The derived lower temperatures are on average $T_1 = 144 \pm 24$ K for the 31 star-forming nuclei and $T_1 = 180 \pm 45$ K for the 25 LINER/Sy nuclei. The median of the mass ratio of warm H_2 to total H_2 is 10% for star-forming regions (up to 30–40%) and 4% for AGNs.

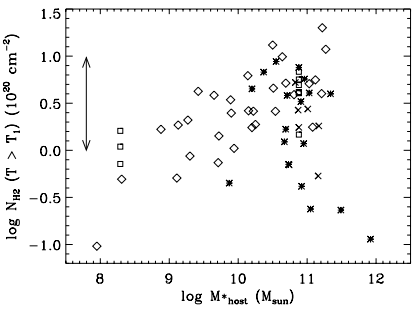

Fig. 1. Relation between the host total stellar mass and the column density of warm H_2 within our ∼kpc apertures. Diamond symbols stand for star-forming nuclei, squares for extranuclear H II complexes, and stars and crosses for LINER and Sy nuclei, respectively. The arrow to the left shows the range of column densities observed in resolved PDRs such as the Orion Bar and NGC 7023.

Other arguments incite to favor a dominant excitation in PDRs:
(1) The power ratios of H_2 to the total dust emission are consistent with PDR model predictions, indicating ratios of radiation field intensity G_0 to gas density n spanning the narrow range $0.1 < G_0/n < 1$. The observed temperatures also suggest, for the component dominating the integrated emission within the beam, $100 < G_0/(1.6 \times 10^{-6}\ \mathrm{W\,m^{-2}}) < 5000$ and $500 < n/\mathrm{cm^{-3}} < 10^4$, conditions typical of the surface of molecular clouds illuminated by OB stars.
(2) The association of H_2 emission with several simultaneously observed dust and gas tracers is tightest with the broad bands emitted by PAHs. Even though the radiation field intensity felt by the dust varies by a factor 10 in our targets, the H_2/PAH ratio is insensitive to it (Fig. 2). Owing to the shape

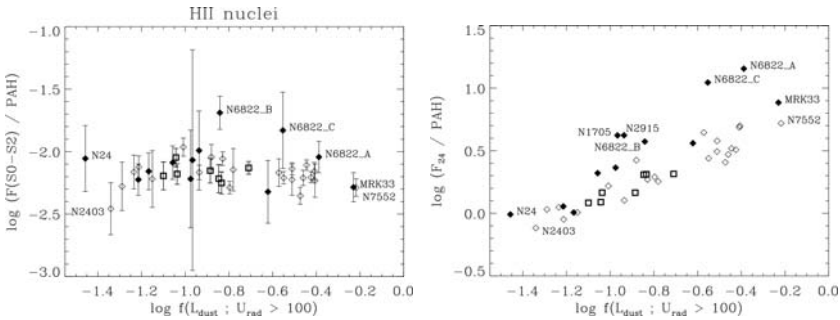

Fig. 2. The warm H_2 to PAH power ratio is invariant as a function of radiation field intensity, that is quantified here both by the parameter in the abscissa and by the 24 μm to PAH power ratio. Dwarf galaxies are shown by filled diamonds.

of the photon absorption cross-section of PAHs, this strongly suggests that both PAHs and H_2 are excited predominantly in PDRs with relatively elevated radiation fields (but not necessarily high densities).
Star formation activity necessarily generates shocks and turbulence, but their contribution to the excitation of the lowest rotational levels must be small (otherwise, the correlation with PAHs and the total dust emission would not be so tight, and the temperatures would be higher than observed).

A surprise was, in half the star-forming targets, the detection of non-equilibrium ortho to para ratios (ortho levels are those with odd rotational number J; para levels, even J). Ortho-para conversion does not occur radiatively, nor through collisions with H_2, but through reactions with H and H^+, or dissociation and reformation. The fact that ortho to para ratios are weakly correlated with the total H_2 brightness, which depends strongly on n (but also on G_0), is consistent with the hypothesis that non-equilibrium ortho to para ratios are caused by relatively low densities. This is one of several indications of a possibly high fraction of diffuse molecular gas in normal galaxies.

LINER and Seyfert nuclei distinguish themselves from star-forming targets not only by lower column densities of warm H_2 and lower mass fractions of total H_2 in the warm phase, but also by higher temperatures (column densities and temperatures are anticorrelated in a natural way), and a clear excess of H_2 emission with respect to dust emission. Given the constancy of H_2 to PAH power ratios R in star-forming targets, we quantify H_2 excesses by $R > \bar{R} + 2.6\sigma_R$ (at 99% confidence). In practice, this definition selects H_2 emission that cannot arise from PDRs.

X-rays from AGNs, able to pass through large column densities, are thought to have a profound influence on the heating and chemistry of molecular gas. By comparing our data and nuclear X-ray fluxes (from Chandra observations) with models of X-ray irradiation, we find however that X-ray heating is not efficient enough to account for the observed H_2 excesses. Shocks in supernova remnants are in principle able to produce moderate H_2 excesses,

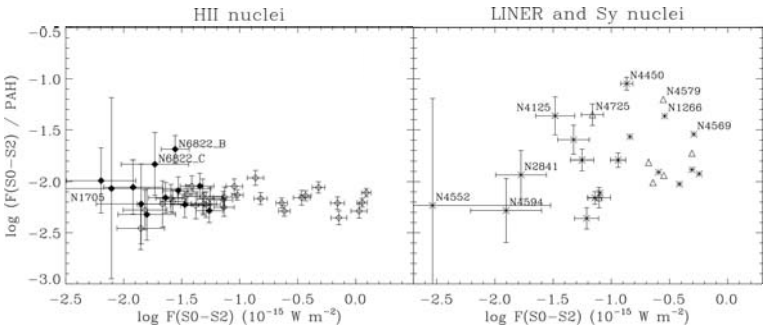

Fig. 3. Warm H_2 to PAH power ratios as a function of H_2 flux, for star-forming targets *(left)* and low-luminosity AGNs *(right)*.

i.e. only in a fraction of the targets. We noticed that some of the galaxies with the brightest H_2 emission display signs of morphological and kinematical distortions, and at least one has a starburst outflow. We thus propose that the strongest H_2 excesses are caused by large-scale shocks induced by dynamical perturbations or by starburst winds.

Is heating by cosmic rays significant ?
It was pointed out that radio galaxies such as NGC 1316 (= Fornax A) should have a high abundance of cosmic rays, that might provide a non-negligible fraction of the total H_2 heating. Quantifying this is arduous, chiefly because the energy spectrum of cosmic ray nuclei is unconstrained at the low energies where ionization losses to the neutral gas occur. We assumed a magnetic field strength satisfying the minimum-energy condition, a relativistic proton to electron abundance ratio of 40 at 1 GeV, and a proton energy density $dn(E)/dE \propto E^{-1.55}$ above 10 MeV (such as produced by non-linear shock acceleration models). Combining these assumptions with the observed synchrotron radiation of electrons (within the inner $\approx$5 kpc of NGC 1316), we find that cosmic ray heating falls short by about two orders of magnitude. Although a more satisfactory model is needed, we thus consider cosmic rays an unlikely source of heating for the warm H_2.

Prospects: Extensive surveys of rotational H_2 will become possible, both with a large instantaneous field of view and a high spectral resolution, with the proposed H2EX satellite (P.I. F. Boulanger), provided it is approved. In the limited context of our study, these prospects seem particularly engaging: the direct characterization of molecular gas content and physical conditions and their regulation by star formation, including in objects where a constant CO/H_2 ratio is no longer a valid approximation; the exploitation of bright H_2 emission as a signpost of extensive shocks in tidal interactions, for which the evidence is mounting (see e.g. Ogle et al., 2007 and Appleton et al., 2006).

Molecular Gas, Cloud Properties, and Star Formation in Dwarf Galaxies

Alberto D. Bolatto[1], Adam K. Leroy[2], Fabian Walter[2], Leo Blitz[3], and Erik Rosolowsky[4]

[1] Department of Astronomy, University of Maryland, College Park, MD 20742, USA bolatto@astro.umd.edu
[2] Max-Planck Institute for Astronomy, Heidelberg, Germany
[3] Department of Astronomy, University of California, Berkeley, CA 94720, USA
[4] Harvard-Smithsonian Center for Astrophysics, Cambridge, MA 02138, USA

A key issue in galaxy evolution is understanding the link between gas and star formation. A clear, quantitative picture of how atomic gas turns into molecular clouds, which in turn lead to stars, is a requirement to properly model structure formation in the universe. Our most widespread (and most successful) recipe for the relation between gas and star formation in galaxies, Kennicutt's formulation of the Schmidt law [12], relates the total surface density of gas, Σ_H, to that of star formation rate, Σ_{SFR}, in an almost linear function: $\Sigma_{SFR} \propto \Sigma_H^{1.3}$. Strong hints exist, however, that the process that turns gas into stars is regulated by the formation of molecules and self gravitating molecular clouds — indeed we know that star formation, with the possible exception of the first generation of stars, is a process that occurs only in molecular clouds. Recent studies, for example, show that the Schmidt law overpredicts by factors of 10 to 30 the star formation observed in Damped Lyman Alpha systems (DLAs) under general assumptions about their geometry [2]. We will argue that part of the solution to this conundrum is that star formation is a molecular process, while atomic gas dominates the column density in DLAs. Gaining quantitative understanding about the relative importance of the different processes that regulate the transformation of gas into stars requires studying the formation, properties, and distribution of molecular gas in objects other than the Milky Way, and that is best done in galaxies in the local volume.

Most of these galaxies are dwarf galaxies, which we will arbitrarily define as galaxies with inclination-corrected maximum rotational velocities $v_{\rm rot} < 100\,{\rm km\,s^{-1}}$. These tend to be low metallicity objects, which is actually a bonus at probing conditions relevant to structure formation in the universe and at testing the limitations of star formation recipes. Molecular gas is considerably less prevalent in these objects than in Milky Way-class galaxies, for reasons

B.S. Koribalski, H. Jerjen (eds.), *Galaxies in the Local Volume*,
doi: 10.1007/978-1-4020-6933-8_20,

that are discussed elsewhere [3]. Indeed CO emission, our main tracer of cold H_2, is faint in dwarf galaxies [4], which makes its study challenging.

1 Resolved Molecular Cloud Properties

In order to study the properties of individual giant molecular clouds (GMCs) in nearby galaxies we imaged a sample of these objects at high angular resolution using millimeter-wave interferometers (the Berkeley-Illinois-Maryland Array, BIMA, and the Owens Valley Radio Observatory array, OVRO), and added to this sample observations at similar linear resolution of regions in the Magellanic Clouds obtained using the Swedish-ESO Submillimeter Telescope (SEST). These observations were analyzed employing an algorithm developed specially for this type of problems, which attempts to remove the biases introduced by differences in sensitivity and linear resolution among the data sets [5].

The results for the size-line width relation in the sample of extragalactic GMCs are shown in Figure 1a, compared with the canonical sample of Milky Way GMCs [7]. The striking fact is that the differences are minimal, and most extragalactic GMCs follow the Galactic $\sigma = 0.72\ R^{0.5}$ law within the errors. Under the assumption of turbulence-supported molecular clouds in approximate virial equilibrium, this means that the mean molecular surface density of GMCs is approximately the same in the Galaxy as everywhere else, $\Sigma_{H_2} \sim 170\ M_\odot\ pc^{-2}$ [6].

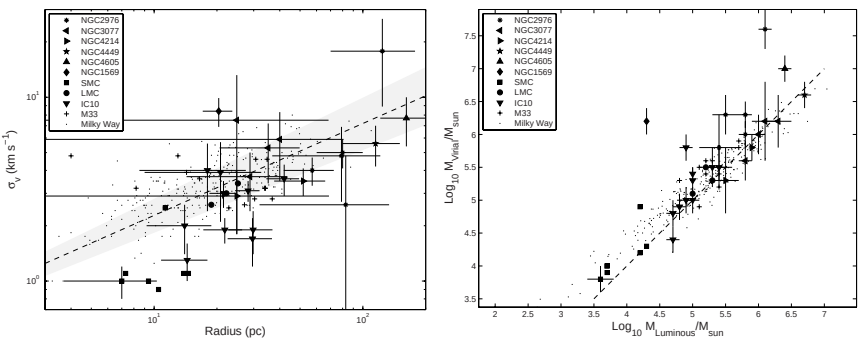

Fig. 1. Resolved properties of extragalactic GMCs, compared to Galactic GMCs. *(a, left)* Velocity dispersion versus linear size, or size-line width relation. *(b, right)* Luminous mass versus virial mass, or luminosity-virial mass relation. In every case the small dots and the lines illustrate the results of the sample of Galactic GMCs [7].

The results for the luminosity-virial mass relation (Fig. 1b) are also remarkably compatible with those in the Galaxy. This suggests that in

extragalactic GMCs the CO intensity traces their virial mass with approximately the same factor as in the Milky Way. The outliers in these relations deserve discussion that is beyond the scope of this short contribution. However, the overall picture is that GMCs in other galaxies, even in those with metallicities as low as 0.2 solar, are very similar to those in the Galaxy. And in these structures, the proportionality between the CO intensity and the H_2 column density is approximately Galactic.

2 The Star Formation Law at Low Metallicity

Despite these similarities between large and small galaxies, it is clear that something drastic happens at low masses and metallicities. Figure 2 shows that both the ratio of molecular to stellar mass and the star formation rate per molecular mass are different for the lowest mass systems that are detected in CO, which for sensitivity reasons are very local galaxies. This fact points either to an accounting problem, where not all the H_2 is accounted for by the CO emission with a Galactic proportionality, or to a change in the star formation efficiency in the lowest mass systems. Figure 2b is the molecular version of the Schmidt law, where we use only the gas directly related to star formation. The most discrepant point is the Small Magellanic Cloud (SMC), the lowest metallicity system detected in CO.

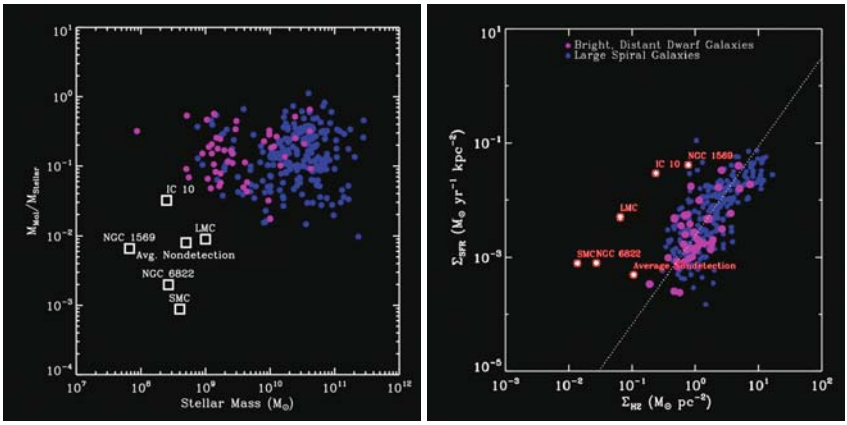

Fig. 2. *(a, left)* Ratio of molecular mass to stellar mass, plotted against stellar mass. Most galaxies exhibit an approximately constant molecular to stellar mass ratio, with the exception of the lowest mass systems detected in CO. *(b, right)* The molecular version of the Schmidt law, relating the molecular gas reservoir to the star formation activity. The same low mass systems show an excess of SFR for their surface density of H_2 inferred from CO.

Which of these possibilities is the answer? Some of the previous work on the SMC strongly suggested a change in the proportionality between CO emission and H_2 column density on the basis of a virial mass analysis of the CO data [8, 9]. The difference with our results could be methodological (both these studies neglected to correct for the finite size beam of the telescope), or a selection effect (our sample in these sources consist of only a few clouds). Fortunately there is an alternative way to answer this question, and it consists of modeling the far infrared emission of the source to obtain a dust opacity, and from this a total gas mass [10].

We recently used this method to establish the molecular mass of the SMC, and found it to be larger than our virial analysis may indicate, $M_{H_2} \approx 3 \times 10^7$ $M_\odot$ [11]. This is about 15% of the atomic mass contained in the same region studied. It appears that the reason why this molecular mass was not detected in our virial mass analysis has to do, in part, with its location: we measure H_2 halos around each CO-bright GMC, that are on average 30% more extended than the CO regions. Another reason is the presence of extended regions of low level H_2 column density ($\Sigma_{H_2} \sim 30$ $M_\odot$ pc^{-2}) without CO counterparts. The proportionality factor between the global CO emission and the total H_2 mass yielded by this analysis is approximately 50 times the Galactic value [11].

The amount of molecular gas found in this analysis brings the SFR in the SMC into agreement with the general relation in galaxies (c.f., Fig. 2b). This shows that the validity of the molecular Schmidt law extends to very low masses and metallicities, and suggests that problems with overpredictions in systems dominated by atomic gas, such as DLAs, stem from relating their H I content to their star formation. Indeed, in the SMC, using the total mass of gas would also overpredict the observed SFR by about an order of magnitude.

References

1. Kennicutt, R. C. 1998, ApJ, 498, 541
2. Wolfe, A. M., & Chen, H.-W. 2006, ApJ, 652, 981
3. Bolatto, A. D., Jackson, J. M., & Ingalls, J. G. 1999, ApJ, 513, 275
4. Taylor, C. L., Kobulnicky, H. A., & Skillman, E. D. 1998, AJ, 116, 2746
5. Rosolowsky, E., & Leroy, A. 2006, PASP, 118, 590
6. McKee, C. F. 1999, NATO ASIC Proc. 540: The Origin of Stars and Planetary Systems, 29
7. Solomon, P. M., Rivolo, A. R., Barrett, J., & Yahil, A. 1987, ApJ, 319, 730
8. Rubio, M., Lequeux, J., Boulanger, G. 1993, A&A, 271, 9
9. Mizuno, N., Rubio, M., Mizuno, A., Yamaguchi, R., Onishi, T., & Fukui, Y. 2001, PASJ, 53, L45
10. Israel, F. P. 1997, A&A, 328, 471
11. Leroy, A. K., Bolatto, A. D., Stanimirović, S., Mizuno, N., Israel, F. P., & Bot, C. 2007, ApJ, 663, 990

THINGS: The H I Nearby Galaxy Survey

Fabian Walter[1], Elias Brinks[2], Erwin de Blok[3], and Frank Bigiel[1]

[1] Max-Planck-Institut für Astronomie Heidelberg, Germany walter@mpia.de, bigiel@mpia.de
[2] Centre for Astrophysics Research, University of Hertfordshire, Hatfield AL10 9AB, UK E.Brinks@herts.ac.uk
[3] Department of Astronomy, University of Cape Town, Private Bag X3, Rondebosch 7701, South Africa edeblok@circinus.ast.uct.ac.za

1 Introduction

For decades, studies of the atomic interstellar medium (ISM), through observations of the 21-cm line of atomic hydrogen (H I), have proven to be fundamental for our understanding of the processes leading to star formation, the dynamics and structure of the ISM, and the (dark) matter distribution, thereby touching on major issues related to galaxy evolution. Since the discovery of the H I line, this line has been used as a 'workhorse' line for the studies of the ISM in our own and other galaxies. In fact, H I observations opened up a whole new field of studies of the ISM as H I was abundantly detected in galaxies and is not attenuated by interstellar dust. In addition, its Doppler shift provides information about the velocity of the emitting gas. This obviously provides important information on the physical properties of the interstellar gas and the associated kinematics of the ISM.

Early studies, using single dish telescopes (yielding resolutions of $\sim 10'$), naturally concentrated on performing detailed studies of the Galaxy and obtaining some global measurements of other nearby systems. Only after radio interferometers became available did it become feasible to obtain detailed, spatially resolved H I images of external galaxies. However, given the intrinsically low surface brightness of the H I emission, large collecting areas were needed, in particular if high-resolution ($< 1'$) imaging was desired. Thus, with the advent of more and more powerful radio interferometers, H I emission could eventually be mapped at high resolution ($10''$) and sensitivity: To date, numerous high-resolution H I studies of galaxies have been performed, including M 31 [2], M 101 [4], Holmberg II [7], IC 2574 [9], NGC 6822 [3], the Magellanic Clouds [8], [6] and a first high-resolution survey by [1], to name but a few. Although remarkable progress has been achieved in these studies, the lack of high-resolution H I observations in a statistically significant sample of nearby galaxies precludes a systematic study of the physical characteristics

B.S. Koribalski, H. Jerjen (eds.), *Galaxies in the Local Volume*,
doi: 10.1007/978-1-4020-6933-8_21,

of the atomic ISM – this lack of observations was the main motivation for the survey presented here.

2 THINGS Survey Design

2.1 Sample Selection

THINGS is targeting a subset of the Spitzer Infrared Nearby Galaxy Survey (SINGS) Legacy Project, a multi-wavelength project designed to study the properties of the ISM in nearby galaxies [5]. Galaxies were chosen to cover the full range of physical properties, from low-mass, metal-poor, quiescent dwarf galaxies to massive spiral galaxies: The THINGS galaxies and their properties cover a wide range of star formation rates ($\sim 10^{-3}$ to 6 $M_\odot\,yr^{-1}$), total H I masses M_{HI} (0.01 to 14×10^9 $M_\odot$), absolute luminosities M_B (–11.5 to –21.7 mag), metallicities (7.5–9.2 in units of 12+log(O/H)) and evolutionary stages. Early type (E/S0) galaxies were excluded from the THINGS target list, as the characteristics of their ISM is quite distinct from that of spiral and irregular galaxies. Edge-on systems (e.g., M 82) were also excluded as the radial structure of the ISM can not be disentangled from projection effects in these systems. The sample was furthermore limited to galaxies at distances $D < 15$ Mpc to ensure that structures smaller than 500 pc can be resolved (this is limited by the maximum H I resolution of $6''$ that can be achieved at the VLA, as discussed below). Local Group galaxies were also excluded because of their large angular size (which is not covered by most SINGS products).

2.2 Spatial Resolution

The main scientific goals for THINGS (see below) require an angular resolution of order a few 100 parsecs in order to resolve neutral atomic gas complexes, to trace the fine structure of the H I and to resolve spiral arms in our target galaxies. This resolution is also required to accurately derive the central shape and slope of the rotation curve of each galaxy. Given the distances to our sample galaxies, this corresponds to an angular resolution of $6''$, which can be achieved using the Very Large Array (VLA) in its D, C and B array configurations. Objects at declinations lower than about -20 degrees are observed with the extended north arm to ensure a homogeneous *uv*-coverage. We note that this resolution is also well matched to that typically obtained for the other data products from Spitzer (e.g., resolution at 24μm: $\sim6''$) and GALEX (resolution in NUV: $\sim5''$).

2.3 Velocity Resolution

Many of our science goals require high *velocity* resolution: The $1\,\sigma$ velocity dispersion of the warm neutral medium hovers near $6-7$ km s^{-1} (full width

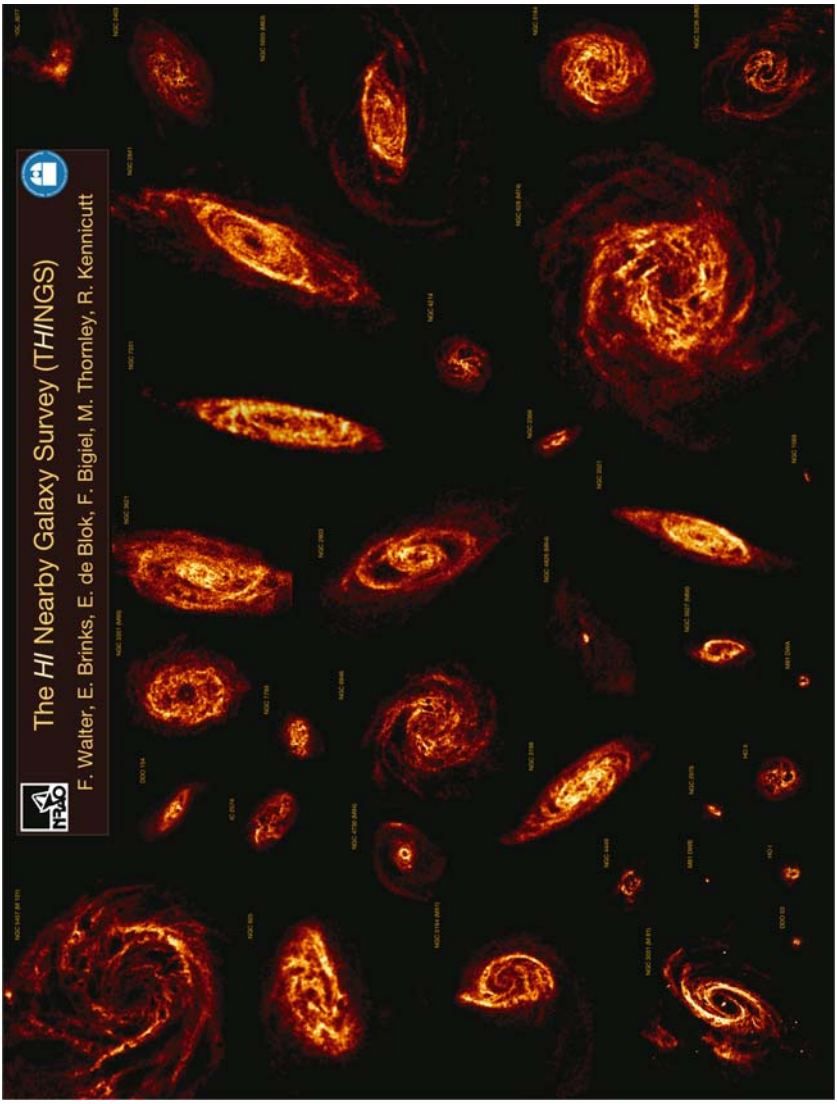

Fig. 1. Integrated H I maps of all galaxies in THINGS. Galaxies are shown on the same physical scale. Note the different galactic environments sampled by THINGS, from the low-mass dwarf galaxies in the M 81 group (bottom left) to massive spiral galaxies. These maps show an enormous amount of structure (such as spiral arms and H I holes and shells).

half maximum, FWHM: $\sim 16\,\mathrm{km\,s^{-1}}$); therefore all observations are done with at least $5\,\mathrm{km\,s^{-1}}$ velocity resolution in order to Nyquist sample the FWHM of the H I line. The latter constraint implied that many observations in the VLA archive could not be incorporated in our analysis (as typical velocity resolutions chosen for those observations were poorer) – these galaxies were reobserved as part of THINGS.

2.4 Sensitivity Considerations

To investigate the threshold for star formation (at a canonical H I column density level of about $10^{21}\,\mathrm{cm^{-2}}$) a sensitivity (expressed in column density) at least a factor of three better is required. In B-array, the gain is of order 15 K per mJy for a $6''$ beam. Observations of on average 7 hours on source, observing 2 polarizations, reach a 1σ rms noise of typically $0.4\,\mathrm{mJy\,beam^{-1}}$ (or 6 K) which corresponds to a column density limit of better than $3.2 \times 10^{20}\,\mathrm{cm^{-2}}$ (a detection in 2 channels of $5\,\mathrm{km\,s^{-1}}$ width at the $3\,\sigma$ level). Higher surface brightness sensitivities are reached by convolving the data. THINGS observations have typical column density thresholds of $4 \times 10^{19}\,\mathrm{cm^{-2}}$ at $30''$ resolution which is adequate to trace the outer regions of the galaxies and to detect the presence of potential tidal features.

3 Main Science Drivers of THINGS

There are a number of science drivers that capitalize on the unique properties of the THINGS data products. The interested reader is referred to the respective papers for a detailed description of the various projects (all the papers cited in this section are in preparation). In summary, de Blok et al. (2008) present a detailed analysis of high-resolution rotation curves and mass models (including new constraints for the stellar mass-to-light ratio) for the majority of THINGS galaxies. In Fig. 2 we show the results for one galaxy of our sample (NGC 2403) – see the figure caption and de Blok et al. (2008) for details. Trachternacht et al. (2008) present kinematically derived centres of the THINGS targets and perform a harmonic decomposition to constrain the non-circular motions in the galaxies. This study shows that non-circular motions in THINGS are not negligible, but they are not strong enough to turn 'cuspy' dark matter halos into 'isothermal' ones. Oh et al. (2008) present a new method to remove these non-circular motions from the velocity fields to derive accurate rotation curves unaffected by these motions (they also present models to derive the stellar mass-to-light ratio based in infrared data). This is of particular importance for the dwarf galaxies in THINGS. The star formation properties are addressed in the work by Leroy et al. (2008) and Bigiel et al. (2008). Leroy et al. test the various star formation and threshold recipes that have been proposed to explain the observed star formation in galaxies – they also describe a new method how to calculate star formation rate *maps*

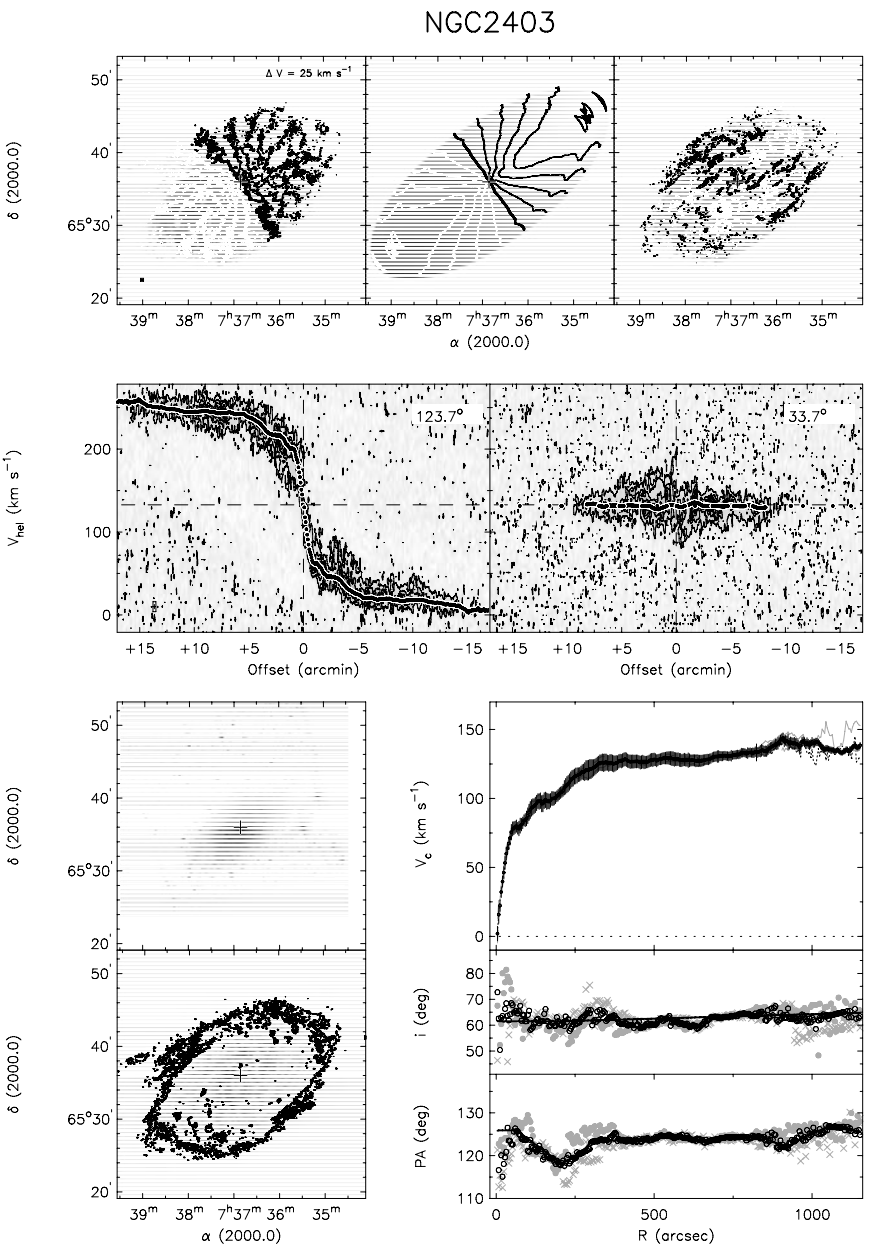

Fig. 2. NGC 2403 is shown as an example for the dynamical analysis. — See next page for a full description of this figure.

Fig. 2. — continued: NGC 2403 is shown as an example for the dynamical analysis (de Blok et al. 2008). The *top panels* show the observed velocity field *(left)*, the model velocity field *(centre)* and the residual map *(right)*. *Below*, the position velocity diagrams along the major and minor axes are shown. *(Bottom left:)* Comparison of the extent of the H I to the stellar disk (here: the 3.6μm map taken from SINGS). *(Bottom right:)* Rotation curves, and change of inclination and position angle as a function of galactocentric radius (for details see de Blok et al. 2008).

for individual galaxies. They find that the recipes based on pressure being the driver to turn atomic gas into molecular gas work best to explain the observed star formation activity in THINGS galaxies. Bigiel et al. perform a pixel-by-pixel comparison of the SFR and measured gas densities for a sample of THINGS galaxies to constrain the Schmidt-Kennicutt law on small scales (for further information see the contribution by Bigiel et al., this volume). Tamburro et al. (2008) uses the offset seen between the H I and 24 micron emission to derive an average timescale for star formation to commence in spiral arm environments. The many holes seen in the THINGS H I data products (and their statistical properties) are discussed in Bagetakos et al. (2008). The fine scale structure of the ISM is also addressed by Usero et al. (2008) who study the peak surface brightness distribution in THINGS. Portas et al. (2008) present a study of the H I edges seen in the THINGS data products. Finally, Zwaan et al. (2008) use the THINGS data to compare the H I properties in nearby galaxies to the H I absorption properties found in Damped Lyman Alpha (DLA) systems at high redshift. They find that the line-widths in the $z \sim 2-3$ DLAs (as measured through Δv_{90}) is significantly higher than what is seen at $z = 0$ (based on the THINGS data).

4 Summary

In this paper we have briefly summarized the present status of the THINGS project – The H I Nearby Galaxy Survey. THINGS is a large observational project executed at the NRAO Very Large Array (VLA) to obtain 21-cm H I observations of the highest quality (spatial resolution $\sim 7''$, velocity resolution ≤ 5.2 km s^{-1}) of nearby galaxies. A key characteristic of the THINGS database is the homogeneous sensitivity as well as spatial and velocity resolution of the H I data that is at the limit of what can be achieved with the VLA for a significant sample of galaxies. A sample of 34 objects at distances $\sim 2 < D < 15$ Mpc (resulting in linear resolutions of ∼100–500 pc) are targeted in THINGS, covering a wide range of star formation rates ($\sim 10^{-3}$ to 6 M$_\odot$ yr^{-1}), total H I masses M$_{\rm HI}$ (0.01 to 14×10^9 M$_\odot$), absolute luminosities M$_{\rm B}$ (–11.5 to –21.7 mag), metallicities (7.5–9.2 in units of 12+log(O/H)) and evolutionary stages. We have presented a description of the sample selection and the observational requirements. The scientific goals of THINGS

are to investigate key characteristics of the interstellar medium related to galaxy morphology, star formation and mass distribution across the Hubble sequence. The first THINGS papers address issues such as the small-scale structure of the ISM, the (dark) matter distribution in THINGS galaxies, and the processes leading to star formation.

References

1. Braun, R. 1995, A&AS, 114, 409
2. Brinks, E. & Bajaja, E. 1986, A&A, 169, 14
3. de Blok, W. J. G. & Walter, F. 2000, ApJ, 537, L95
4. Kamphuis, J., Sancisi, R., & van der Hulst, T. 1991, A&A, 244, L29
5. Kennicutt, R. C., et al. 2003, PASP, 115, 928
6. Kim, S., Dopita, M. A., Staveley-Smith, L., Bessell, M. S. 1999, AJ, 118, 2797
7. Puche, D., Westpfahl, D., Brinks, E., & Roy, J. 1992, AJ, 103, 1841
8. Staveley-Smith, L., Sault, R. J., Hatzidimitriou, D., Kesteven, M. J., & McConnell, D. 1997, MNRAS, 289, 225
9. Walter, F., & Brinks, E. 1999, AJ, 118, 273

Fabian Walter and Jürgen Ott

Bärbel Koribalski

The Star Formation Law at Sub-Kiloparsec Resolution

Frank Bigiel, Adam Leroy, and Fabian Walter

Max-Planck-Institut für Astronomie, Königstuhl 17, D-69117, Heidelberg, Germany; bigiel@mpia.de, walter@mpia.de, leroy@mpia.de

In a sample of 9 spiral galaxies, we show that inside ~ 0.4 r_{25}, where the gas in spirals is mostly molecular, a single power law with a slope $N = 1.0 \pm 0.2$ relates the star formation rate surface density, $\Sigma_{\rm SFR}$, to the gas surface density, $\Sigma_{\rm gas}$, pixel-by-pixel at 500 pc resolution. This implies that gas forms stars with constant efficiency in this regime. The data in this regime match up well with disk-averaged measurements of $\Sigma_{\rm SFR}$ and $\Sigma_{\rm gas}$. We find a clear saturation in $\Sigma_{\rm HI}$ at ~ 12.5 $M_\odot$ pc^{-2}. All gas in excess of this surface density is molecular.

1 Introduction

A robust, quantitative measurement of the relationship between star formation rate (SFR) and gas density constrains theoretical models of star formation and serves as input to simulations and models of galaxy evolution [1, 2, 3, 4, 5]. Here we present results investigating this relationship pixel-by-pixel at 500 pc resolution across the whole optical disk of 9 spiral galaxies.

This work uses high resolution H I data from 'The H I Nearby Galaxy Survey' (THINGS) [6], CO data from the BIMA 'Survey of Nearby Galaxies' (BIMA-SONG) [7], 24 μm data from the '*Spitzer* Infrared Nearby Galaxy Survey' (SINGS) [8] and UV data from the GALEX 'Nearby Galaxy Survey' (NGS) [9].

2 Distributions of $\Sigma_{\rm SFR}$ versus $\Sigma_{\rm HI,H2,HI+H2}$

The GALEX FUV traces predominantly O and early B stars. It therefore offers a picture of recent ($\sim$100 Myr) unobscured star formation. Where star formation is obscured by dust, we use 24 μm emission from hot dust to assess obscured star formation. We combine FUV and 24 μm emission to obtain a complete census of unobscured and obscured star formation following [13] and derive maps of star formation surface density, $\Sigma_{\rm SFR}$.

B.S. Koribalski, H. Jerjen (eds.), *Galaxies in the Local Volume*,
doi: 10.1007/978-1-4020-6933-8_22,

Figure 1 shows the distribution of $\Sigma_{\rm SFR}$ vs. $\Sigma_{\rm HI}$ (top left), $\Sigma_{\rm H2}$ (top right), and $\Sigma_{\rm gas} = \Sigma_{\rm HI+H2}$ (lower right) for all sampling points in all spirals in our sample.

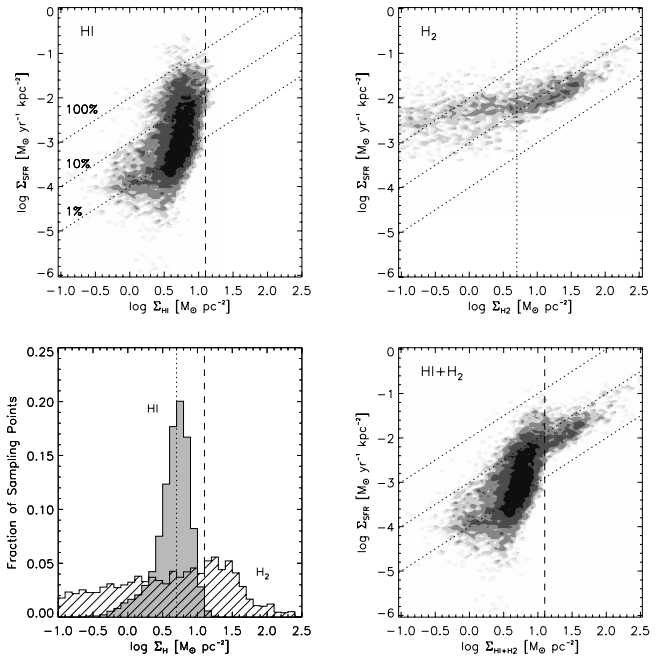

Fig. 1. $\Sigma_{\rm SFR}$ as a function of three kinds of neutral gas surface density: $\Sigma_{\rm HI}$ *(top left)*, $\Sigma_{\rm H2}$ *(top right)*, and $\Sigma_{\rm gas} = \Sigma_{\rm HI+H2}$ *(bottom right)*. Sampling results for all spiral galaxies are plotted together. The data are gridded into cells with bin size 0.05 dex. From light grey to dark grey, the contours represent 1, 2, 5, and 15 data points per cell. Each data point represents an independent sampling point of the galaxy disk at 500 pc resolution. Dashed vertical lines in the H I (upper left) and total gas (bottom right) plots show the surface density where H I saturates. The dotted vertical line in the H_2 plot (upper right) shows the approximate sensitivity of BIMA-SONG. Diagonal lines show constant star forming efficiencies of 1%, 10% and 100% per 10^8 yrs. This corresponds to gas depletion times from top to bottom: 10^8, 10^9, and 10^{10} yrs, respectively. The *bottom left panel* shows the normalized distribution of H I and H_2 surface densities in the sample.

2.1 H I Saturation

The top left panel of Figure 1 shows $\Sigma_{\rm SFR}$ vs. $\Sigma_{\rm HI}$ and demonstrates that a saturation effect is a general feature of our data. Near the saturation surface density, the distribution becomes nearly vertical with a sharp right edge near

the saturation value itself. The bottom left plot shows normalized histograms of $\log \Sigma_{\rm HI}$ and $\log \Sigma_{\rm H2}$. The H I shows a clear truncation near the threshold. Indeed, the bulk of H I mass lies in a surprisingly small regime of $\Sigma_{\rm HI}$, mostly between $\Sigma_{\rm HI} \sim 0.3$ $\rm M_\odot\,pc^{-2}$ and the saturation limit. By contrast, $\log \Sigma_{\rm H2}$ shows no such pile-up and cutoff. Our data agree with those of [10] and [11] that the saturation coincides with a phase transition in the ISM. This is evident from Figure 1. Only $\Sigma_{\rm H2}$ extends to high surface densities and the highest star formation efficiency (SFE) points in the top left (H I-only) panel can be seen from the other two panels to be associated with CO emission detected by BIMA-SONG.

2.2 H I, H_2, Total Gas, and the Star Formation Law

The narrow range of H I surface densities span a very large range of $\Sigma_{\rm SFR}$ and SFEs. Within one order of magnitude in $\Sigma_{\rm HI}$, $\Sigma_{\rm SFR}$ covers 4 orders of magnitude and the SFE spans two orders of magnitude. Figure 1 clearly shows that neither $\Sigma_{\rm SFR}$ nor the SFE can be predicted by $\Sigma_{\rm HI}$; i.e. the H I surface density does not appear to play a critical role in setting the star formation rate. Unlike $\Sigma_{\rm HI}$, $\Sigma_{\rm H2}$ shows a relatively clear, monotic relationship with $\Sigma_{\rm SFR}$ down to the sensitivity of BIMA-SONG. It is obvious from Figure 1 that a single power law can describe the relationship between $\Sigma_{\rm SFR}$ and $\Sigma_{\rm H2}$ but not between $\Sigma_{\rm SFR}$ and Σ_{gas} a clear knee marks the transition from an atomic to molecular ISM in Figure 1.

2.3 Comparison with measurements integrated over galaxy disks

Kennicutt [12] measured $\Sigma_{\rm SFR}$, $\Sigma_{\rm HI}$, and $\Sigma_{\rm H2}$ integrated over the disks of 61 normal spiral galaxies and 36 starburst galaxies. He found a strong relationship between $\Sigma_{\rm SFR}$ and $\Sigma_{\rm gas}$ and that a single power law describes all of his data. To investigate how our results compare to his, we plot his datapoints along with our combined distribution in the left panel of Figure 2. We use the plotting symbols from Figure 6 of [12] and show $\Sigma_{\rm SFR}$ vs. $\Sigma_{\rm gas}$ for all of our spirals as contours (the contours representing our data are identical to the lower right panel in Figure 1). We adjust the SFRs from [12] to account for the difference in assumed IMFs. The plot shows that there is no real contradiction between our finding and the data of [12]. Particularly, the 61 normal spirals occupy the same regime in $\Sigma_{\rm SFR}$ and $\Sigma_{\rm gas}$ like our spirals.

3 The Molecular Star Formation Law

In the central parts of spirals, the gas is almost exclusively molecular and both $\Sigma_{\rm SFR}$ and $\Sigma_{\rm gas}$ tend to be fairly high. The right panel in Figure 2 shows the results of a power law fit to $\Sigma_{\rm SFR}$ and $\Sigma_{\rm gas}$ for data within 0.4 r_{25} in all

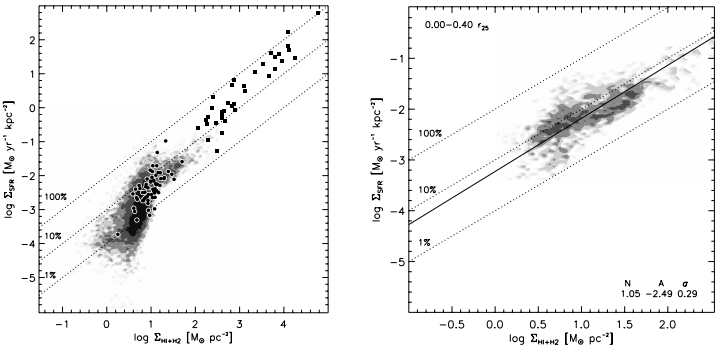

Fig. 2. *(Left panel:)* $\Sigma_{\rm SFR}$ versus $\Sigma_{\rm gas}$ in greyscale contours for all spiral galaxies in our sample; these are the same data and contour levels as the bottom right panel in Figure 1. Overplotted are data from [12]. These are $\Sigma_{\rm SFR}$ and $\Sigma_{\rm gas}$ integrated across the optical disk for 61 normal spiral galaxies (filled circles) and 36 starburst galaxies (filled squares). We normalize his values to use our adopted IMF. *(Right panel:)* $\Sigma_{\rm SFR}$ versus $\Sigma_{\rm gas}$ within 0.4 r_{25} in all our spirals galaxies. From light grey to dark grey, the cells show contours of 1, 2 and 5 data points per cell. The black solid line shows the best fit power law, which has a power-law index $N = 1.05$ and a power-law coefficient $A = -2.19$.

our spiral galaxies. The power-law fit is shown as a solid black line. The best fit parameters are $N = 1.05$ for the power-law index and $A = -2.49$ for the power-law coefficient; the RMS scatter of $\Sigma_{\rm SFR}$ about the fit is 0.29 dex, a factor of ≈ 2. In this regime, our data suggest a direct proportionality between $\Sigma_{\rm SFR}$ and $\Sigma_{\rm gas} \approx \Sigma_{\rm H2}$ with a constant gas depletion time of $\sim 10^9$ yr.

References

1. Springel, V., & Hernquist, L. 2003, MNRAS, 339, 289
2. Boissier, S., & Prantzos, N. 1999, MNRAS, 307, 857
3. Tan, J. C., Silk, J., & Balland, C. 1999, ApJ, 522, 579
4. Krumholz, M. R., & McKee, C. F. 2005, ApJ, 630, 250
5. Matteucci, F., Panagia, N., Pipino, A., Mannucci, F., Recchi, S., & Della Valle, M. 2006, MNRAS, 372, 265
6. Walter, F., this volume
7. Helfer, T. T., Thornley, M. D., Regan, M. W., Wong, T., Sheth, K., Vogel, S. N., Blitz, L., & Bock, D. C.-J. 2003, ApJS, 145, 259
8. Kennicutt, R. C., Jr., et al. 2003, PASP, 115, 928
9. Gil de Paz, A., et al. 2007, ApJS, accepted, astro-ph/0606440
10. Wong, T. & Blitz, L. 2002, ApJ, 569, 157
11. Martin, C. L. & Kennicutt, R. C. 2001, ApJ, 555, 301
12. Kennicutt, R. C. 1998, ApJ, 498, 541
13. Leroy, A., et al. 2008, in prep.

The GALEX View of Ongoing Disk Formation in the Local Volume

David A. Thilker

Center for Astrophysical Sciences, The Johns Hopkins University, 3400 N. Charles Street, Baltimore, MD 21218, USA dthilker@pha.jhu.edu

We summarize the results of a search for extended ultraviolet disk (XUV-disk) galaxies in a sample of 189 nearby S0-Sm targets observed by GALEX, following the discovery of outer disk star formation in Local Volume members M 83 and NGC 4625. We find that XUV-disk galaxies are surprisingly common but have varied morphology. Type 1 objects (>20% incidence) have structured, UV-bright/optically-faint emission features in the outer disk, beyond the traditional star formation threshold. Type 2 XUV-disk galaxies (∼10% incidence) exhibit an exceptionally large, UV-bright/optically-low-surface-brightness (LSB) zone having blue $UV - K_s$ outside the effective extent of the inner, older stellar population, but not reaching extreme galactocentric distance. Type 1 disks are associated with spirals of all types, whereas Type 2 XUV-disks are predominantly found in late-type spirals. XUV-disk galaxies of both types are systematically more gas-rich than the general galaxy population. Minor external perturbation may stimulate XUV-disk incidence, at least for Type 1 objects. XUV-disks are the most actively evolving galaxies growing via inside-out disk formation in the current epoch.

1 Motivation & Sample

It has been known from deep Hα imaging that some galaxies possess very extended star-forming disks (e.g. Ferguson et al. 1998). However, the incidence and underlying cause of this behavior are still unknown. The new ultraviolet imaging surveys from NASA's GALEX (*Galaxy Evolution Explorer*) mission greatly facilitate the study of low-intensity, outer disk star formation in a statistically significant number of galaxies (Gil de Paz et al. 2007). GALEX imaging benefits from a very low sky background, high sensitivity, and a large field-of-view. By observing in the UV, GALEX probes a population of OB stars (rather than only the higher temperature O stars predominantly ionizing H II regions traced by Hα emission), and thus can catch galaxy evolution processes occurring at very low SFR surface densities (Σ_{SFR}).

B.S. Koribalski, H. Jerjen (eds.), *Galaxies in the Local Volume*,
doi: 10.1007/978-1-4020-6933-8_23,

Our survey sample was comprised of 189 disk galaxies ($-0.5 \leq T \leq 9.5$, consequently S0–Sm) within 40 Mpc included in the GALEX Atlas of Nearby Galaxies (Gil de Paz et al. 2007) and having $i \leq 80°$, $D_{25} > 90$", in addition to modest Galactic extinction, $A_V \leq 0.5$. By selecting only objects from the Atlas, we ensured that all galaxies were observed with homogeneous (deep) sensitivity. Further details of the survey and observations are given in Thilker et al. (2007, TBM07).

2 Galaxy classification method

The UV/optical morphology of XUV-disk galaxies is highly varied. A complete description of observed XUV-disk types is given in TBM07. Here, we briefly summarize the fundamentals of our classification procedure which leads to Type 1, Type 2, and Mixed-type objects.

- We define Type 1 XUV-disks as those galaxies having more than one structured complex of UV-bright emission at positions outside of a centralized, contiguous region contained by a [Galactic extinction-corrected] threshold contour at $\Sigma_{SFR} = 3{\times}10^{-4}$ $M_\odot$ yr^{-1} kpc^{-2} (evaluated at 1 kpc resolution). Boissier et al. (2007) demonstrated that for the galaxies of Martin & Kennicutt (2001) showing a sharp azimuthally drop (in Hα) attributed to a SF threshold mechanism, typical Σ_{SFR} are near this fiducial level when evaluated at the Hα "edge" – even if the edge is merely a consequence of "missing" the outer, short-lived, infrequently-formed H II regions.
- To quantitatively identify Type 2 XUV-disk structures, we defined a "low surface brightness (LSB) zone" as the region contained *within* the anticipated SF threshold [Σ_{SFR}] contour yet *outside* a K_s-band contour enclosing 80% of the total K_s luminosity of the galaxy. If the average $UV(AB) - K_s(AB)$ of the LSB zone is ≤ 4, indicating the relative importance of recent star formation with respect to the underlying disk, *and* the area of the zone, $S(LSB)$, is at least 7 times the enclosed area of the K_s contour, $S(K_{s0})$, then we classify the galaxy as a Type 2 XUV-disk (or Mixed-type, if the Type 1 definition is also met).

Figures 1 and 2 show Local Volume galaxies NGC 5055 and NGC 2090, which typify the Type 1 and Type 2 XUV-disk classes, respectively.

3 Results

3.1 XUV-disk galaxy incidence

We have identified a set of 54 XUV-disk galaxies selected from our sample of 189 nearby S0-Sm targets. This shows that XUV-disk SF is a common evolutionary process in the spiral galaxy population.

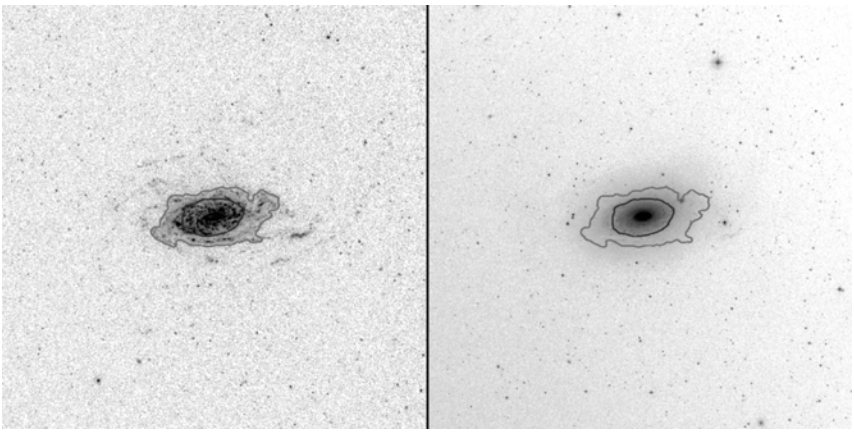

Fig. 1. NGC 5055 (M 63), a Type 1 XUV-disk galaxy, in FUV *(left)* and optical *(right)* bands. Two contours are shown (identical in each panel). The inner contour represents the [80%] effective extent of the galaxy in 2MASS K_s imaging, whereas the outer contour indicates the anticipated position of the star formation threshold estimated as described in the text. Numerous UV-bright stellar complexes can be seen beyond the outer [threshold] contour, extending to a few times the D25 galaxy size such as originally found in M 83 (Thilker et al. 2005, Gil de Paz et al. 2007b).

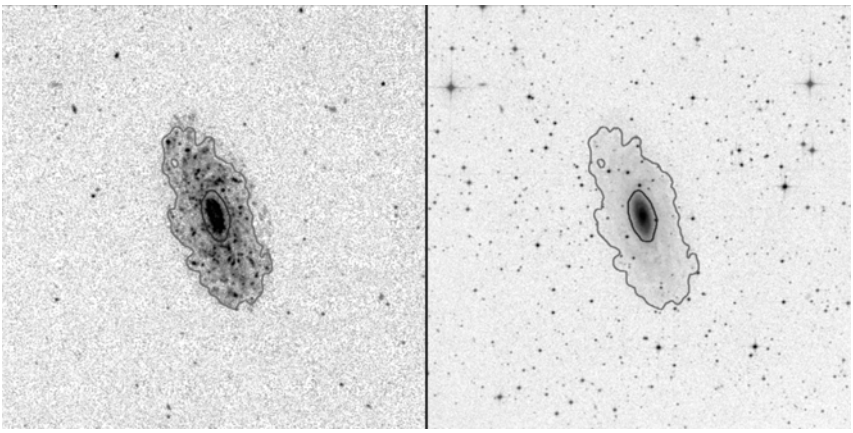

Fig. 2. NGC 2090, a Type 2 XUV-disk galaxy, in FUV *(left)* and optical *(right)* bands. Contours are as described for Fig. 1. For classification purposes, we define the LSB zone to be the area between the contours. The LSB zone of this XUV-disk galaxy is exceptionally large and blue ($FUV - K_s < 4$) giving it the Type 2 designation.

We found 30 objects satisfying only the Type 1 XUV-disk definition, 17 objects satisfying only the Type 2 definition, and 7 galaxies matching both definitions (mixed-type). Considering the union of the first and last groups, we find that *approximately >20% [37/189] of the nearby spiral galaxy population is supporting massive star formation in outer disk locales beyond the classically expected star formation threshold. We emphasize this estimate of incidence for Type 1 XUV-disk structure in our sample is a lower limit.* Some outer, low mass stellar complexes probably remain undetected in galaxies near our 40 Mpc distance limit. Indeed, cataloged Type 1 XUV-disks are not distributed evenly throughout our survey volume. *Regarding the objects having an exceptionally large, blue LSB zone (Type 2 and mixed-type XUV-disk galaxies), we find that they comprise about 13% [24/189] of our sample.* In our sample, distance does not seem to inhibit the identification of Type 2 structures, given that 8 of 71 galaxies at $D < 16$ Mpc satisfy the Type 2 definition, compared to 10 of 70 beyond 20 Mpc. As noted above, *the overall incidence of XUV-disk star formation is >29% [54/189] in the local Universe.*

3.2 Global and environmental properties of XUV-disks

In Figure 3a we show a histogram of Hubble type (T) for the entire sample and both groups of XUV disks. Our survey sample is clearly weighted toward intermediate type spirals. *Type 1 XUV-disks are distributed over a very broad range in T*, with galaxies occupying nearly every bin with the exception of the extrema in T (for which there are very few objects in our sample). K-S testing indicates that the T distribution of Type 1 XUV-disks matches that of the entire sample at the 82% confidence level. *The distribution of Type 2 XUV-disk galaxies is more skewed toward late-type spirals, with the vast majority of detections having $T > 5$.* With K-S testing, we can exclude ($> 99\%$ confidence) the possibility that Type 2 XUV-disks are drawn randomly from the survey sample. The nearly ubiquitous distribution in T for Type 1 objects suggests the presence of a Type 1 XUV-disk has more to do with the environment or interaction/accretion history of a galaxy than the host galaxy itself.

Figure 3b shows the distribution of our entire sample and that of XUV-disks, symbols coded according to type, in the T-L_K plane. L_K is a reliable, nearly extinction-free tracer for the stellar mass of a galaxy (Bell & de Jong 2001). There is no apparent offset between the XUV-disk galaxies and the overall population, leaving open the possibility of episodic XUV-disk star formation (with XUV active objects drawn from the same parent sample).

The gaseous content of the galaxies in our sample is well characterized. In Figure 3c we show the distribution of M_{HI}/L_B vs. L_K for XUV-disks in comparison to ordinary galaxies. M_{HI}/L_B is commonly utilized to classify gas-rich and gas-poor systems. *XUV-disks of all type (but especially Type 1) are systematically displaced from the overall distribution in the sense that they are gas-rich (by about a factor two from the survey median at constant L_K).* Though not shown here, XUV-disk galaxies have enhanced H I content

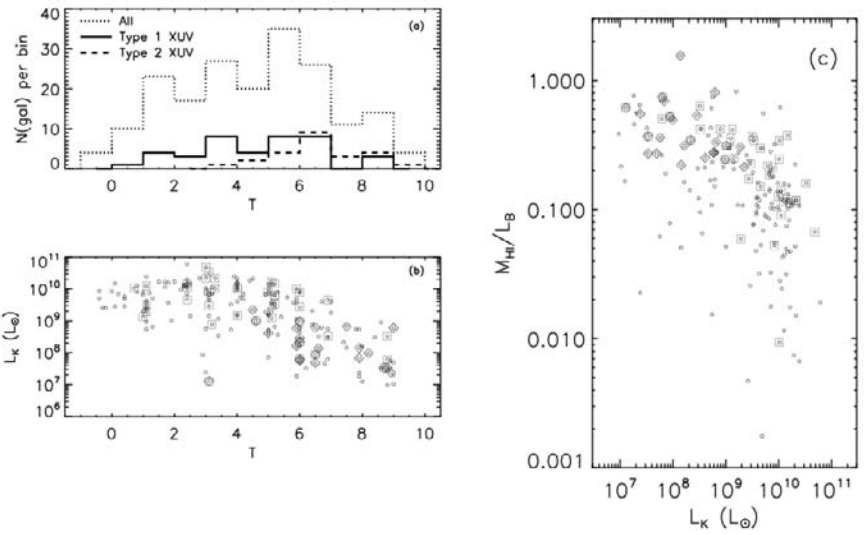

Fig. 3. Distribution of XUV-disks in (a) Hubble type, (b) L_K versus Hubble type, and (c) gas richness (M_{HI}/L_B) versus L_K. In panels (b) and (c), circles are plotted for all objects in the survey sample, squares are shown for Type 1 XUV disks, and diamonds indicate Type 2 XUV-disks.

relative to spirals of matching global SFR. This is what one would expect for the Type 1 XUV-disks – if the outer disk gas is not present, we would not see UV evidence for star formation unless the H I was very recently stripped (as might happen in a cluster environment). Although the increased gas-richness in XUV-disks is not surprising, our knowledge is limited concerning the origin of the outer disk gas and the mechanisms promoting SF therein.

Some XUV-disk galaxies (e.g. NGC 4625, Gil de Paz et al. 2005) are clearly interacting galaxies, have obvious nearby companions, or show morphological clues suggestive of external perturbation (optically, or in the UV). In order to quantify the potential effectiveness of interaction-induced gas motions as a driver of outer disk SF, we computed the tidal perturbation parameter, f (Varela et al. 2004). This measure specifies the ratio of the tidal force imposed on a galaxy (G) of size R by a possible perturber (P) and the internal force per unit mass in the outer part of galaxy G. K-S testing shows the Type 1 f distribution agrees with the entire sample at 91% confidence. If Type 1 structures are linked to external perturbation, it is of a level commonly encountered in the spiral galaxy population, and not of the strength formally defined as perturbed by Varela et al. (2004). The *Type 2 XUV-disks are slightly more isolated than not (only 29% chance agreement with entire sample)*, though a wide range in f is still seen for these galaxies. We note that the f-distribution of Type 2 disks matches that of late-type spirals (91% confidence), so the isolation may

simply be a reflection of the progenitor galaxy population. XUV-disks could also be perturbed by undetected low mass / low surface brightness objects in their vicinity, or even high velocity clouds with gas but no stellar component. Although based on heterogenous data and analyses available in the literature, *more than 75% of the Type 1 XUV-disk objects show morphological or* H I *evidence for interaction/merger or minor external perturbation of some sort* (e.g. HVCs). *About half of the Type 2 XUV-disks appear to be recently disturbed.* In at least some of these cases, the tidal perturbation parameter falsely indicates that they are isolated.

3.3 Local Volume XUV-disk galaxies

Our initial survey shows the Local Volume is home to at least 18 XUV-disk galaxies. They are: NGC 300 (1), NGC 628 (1), NGC 1512 (1), NGC 2090 (2), NGC 2403 (M), NGC 2541 (2), NGC 3031 (1), IC 2574 (2), NGC 3344 (1), NGC 3621 (1), NGC 4236 (2), NGC 4258 (1), NGC 4625 (1), NGC 5055 (1), NGC 5236 (1), NGC 5457 (1), NGC 5474 (M), and NGC 5832 (M), where the code in brackets indicates the XUV-disk type (1, Mixed, or 2). Although many more XUV-disk galaxies will be found at larger distance, these nearby objects provide a rare opportunity to study the resolved stellar content of the XUV-disk clusters using HST. Such work is already underway for M 83, NGC 5055, and NGC 2090. We specifically hope to obtain an understanding for the actualized stellar IMF, cluster mass function, and eventually the long term star formation history in this environment – enabling a crucial link between the often-surprising UV and LSB optical properties of the outer disk.

References

1. Bell, E. F., & de Jong, R. S. 2001, ApJ, 550, 212
2. Boissier, S. et al. 2007, ApJS, in press
3. Ferguson, A. M. N., Wyse, R. F. G., Gallagher, J. S., & Hunter, D. A. 1998, ApJ, 506, L19
4. Gil de Paz, A., et al. 2005, ApJ, 627, L29
5. Gil de Paz, A., et al. 2007, ApJ, 661, 115
6. Gil de Paz, A., et al. 2007b, ApJS, in press
7. Martin, C. L., & Kennicutt, R. C., Jr. 2001, ApJ, 555, 301
8. Thilker, D. A., et al. 2005, ApJ, 619, L79
9. Thilker, D. A., et al. 2007, ApJS, submitted
10. Varela, J., Moles, M., Márquez, I., Galletta, G., Masegosa, J., & Bettoni, D. 2004, A&A, 420, 873

The ACS Nearby Galaxy Survey Treasury: 9 Months of ANGST

Julianne Dalcanton, Beth Williams, and the ANGST collaboration

University of Washington jd@astro.washington.edu

The study of nearby galaxies has been revolutionized by the Hubble Space Telescope (HST). The high spatial resolutions of WFPC2 and ACS reveal individual stars and parsec-scale structures, permitting studies of stellar populations, star formation histories, stellar clusters, and detailed galaxy morphologies. However, despite the large number of HST projects on these topics, past observations have been piecemeal, averaging fewer than 5 orbits per program and lacking any coherent plan in spite of the considerable overlap in the core scientific goals of many of the proposals. Within a single galaxy, or from galaxy to galaxy, the location of the HST exposures is chaotic (having been chosen independently and for different purposes), and the filters and depths of the exposures are highly variable. The resulting archive defies any uniform comparative study of galaxies in the Local Universe and dramatically reduces HST's scientific legacy.

The ACS Nearby Galaxy Survey Treasury program (ANGST) aims to rectify this situation by creating a uniform, multiwavelength archive of observations of a volume-limited sample of nearby galaxies. This volume-limited survey will provide complete and unbiased sampling of the local Universe, thereby maximizing the legacy impact of the resulting dataset, and enabling meaningful comparisons among galaxies in the sample and with cosmological simulations. The chosen volume encompasses 69 galaxies in diverse environments, including close pairs, small & large groups, filaments, and truly isolated regions.

1 Sample Selection

The galaxies in ANGST were chosen to provide a volume-limited sample spanning a range of environments to allow for: (1) ready comparison to N-body simulations; (2) measurement of correlations between star formation history (SFH) and local density; (3) statistically significant measures of rare quantities (e.g., disk & globular cluster specific frequency in low luminosity galaxies,

B.S. Koribalski, H. Jerjen (eds.), *Galaxies in the Local Volume*,
doi: 10.1007/978-1-4020-6933-8_24,

the rate of star bursts, etc.); and (4) creation of an unbiased legacy sample. We selected the sample from Karachentsev's Catalog of Neighboring Galaxies, updated with revised distances. We restricted the catalog to galaxies outside the zero velocity surface of the Local Group, due to the efficacy of ground-based observations within 2 Mpc, and to $|b| > 20$ deg, to avoid sample incompleteness. We imposed an outer distance limit of 3.5 Mpc, except in the directions of the M 81 group and the NGC 253 clump of the Sculptor filament, where we extended our distance limit to 4 Mpc to include a greater range of galaxy environments and luminosities. The resulting sample is plotted in Figure 1 as a function of distance and absolute magnitude.

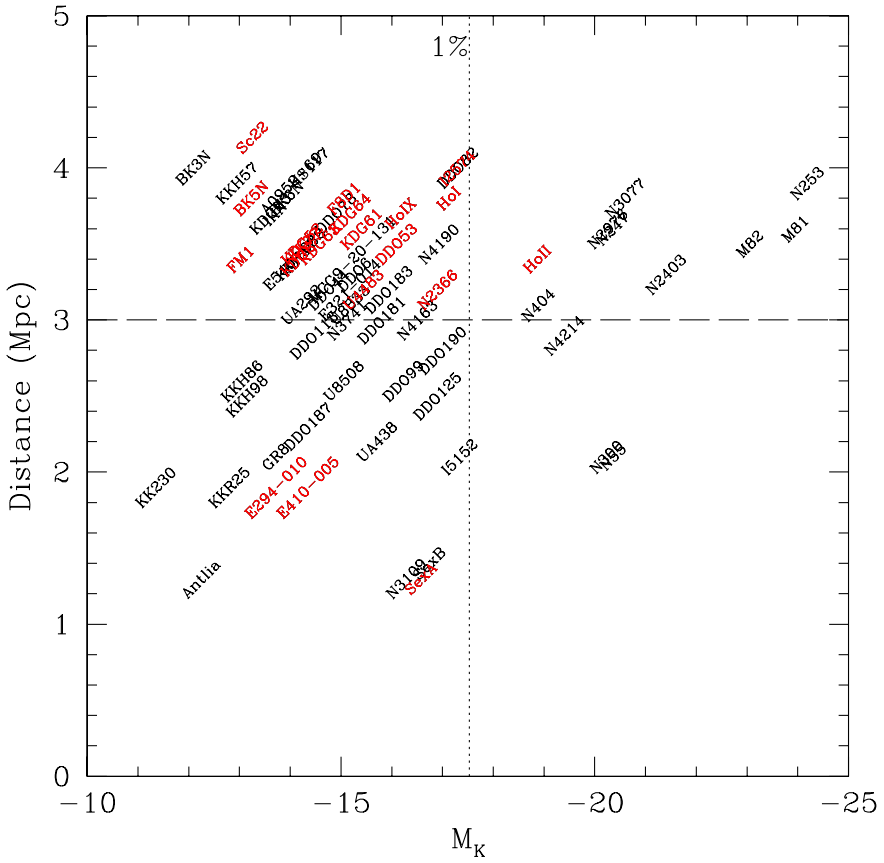

Fig. 1. The ANGST sample as a function of absolute K-band magnitude and distance. The galaxies to the right of the vertical line contain 99% of the K-band luminosity of the ANGST survey volume, and were targeted with deep fields. Galaxies in grey had sufficient archival data that new observations were not required.

2 Survey Design

The primary goal of ANGST is to derive both the recent and ancient star formation histories for a volume limited sample of galaxies. Reaching this goal requires the two-tiered strategy of single deep fields plus a wide-field radial tiling. For each galaxy, the deep field is optimized for high completeness and photometric accuracy in the red clump, whose position and internal structure, in combination with the red giant branch stars, provide strong constraints on the ancient star formation history. However, this deep field must be placed in low surface brightness regions to prevent crowding from compromising the depth of the observations. When needed, each deep field is therefore complemented by a wide-field tiling consisting of shallower imaging of a single radial strip across each galaxy's major axis (Figure 2; top). These wide-field tiles allow us to recover the recent star formation history as a function of position within the galaxy, and to connect the older SFH determined from the deep fields to the galaxy as a whole.

The deep fields and wide field radial tilings are deployed as follows. First, all galaxies in the volume are imaged with the wide field tiling, which consists of a single pointing for dwarf galaxies, and a strip of up to 5 overlapping ACS pointings extending from the center of the galaxy outwards for larger galaxies. An example of the tiling strategy and the resulting color-magnitude diagrams (CMDs) derived from an inner and outer radial tile is shown in Figure 2 for NGC 247. Second, only the galaxies which dominate the stars in the local volume ($M_K < -17.5$, to the right of the dashed vertical line in Figure 1) are imaged with the additional single deep field. Figure 3 shows the field placement and resulting CMD for the deep field in M 81. Exposure times for the deep field ranged from 2 orbits for the nearest galaxies (i.e. no additional observing time was needed beyond the standard 2-orbit radial tiling for galaxies within $D < 2.5$ Mpc), to 20 orbits in more distant galaxies with larger than average foreground extinction. A total of 295 orbits was granted for the entire program, which was distributed among 45 galaxies. The remaining 24 galaxies had sufficient archival ACS data that additional observations were not needed.

The ANGST observations were carried out with either a $F475W + F606W + F814W$ filter combination for the brightest galaxies, or a $F475W + F814W$ combination for the fainter galaxies. For the bright galaxies, the three-filter combination will allow extinction corrections, particularly when combined with future UV and/or NIR imaging. For the faint galaxies ($M_B > -14$), the two filter combination is sufficient for recovering an accurate CMD, since these systems are largely dust-free. The choice of the $F475W$ filter over the more commonly used $F606W$ filter provides better color separation of key CMD features, increasing the accuracy of the recovered star formation history. Typical CMDs for two faint galaxies are shown in Figure 4, demonstrating the diversity of the stellar populations seen in the Local Volume.

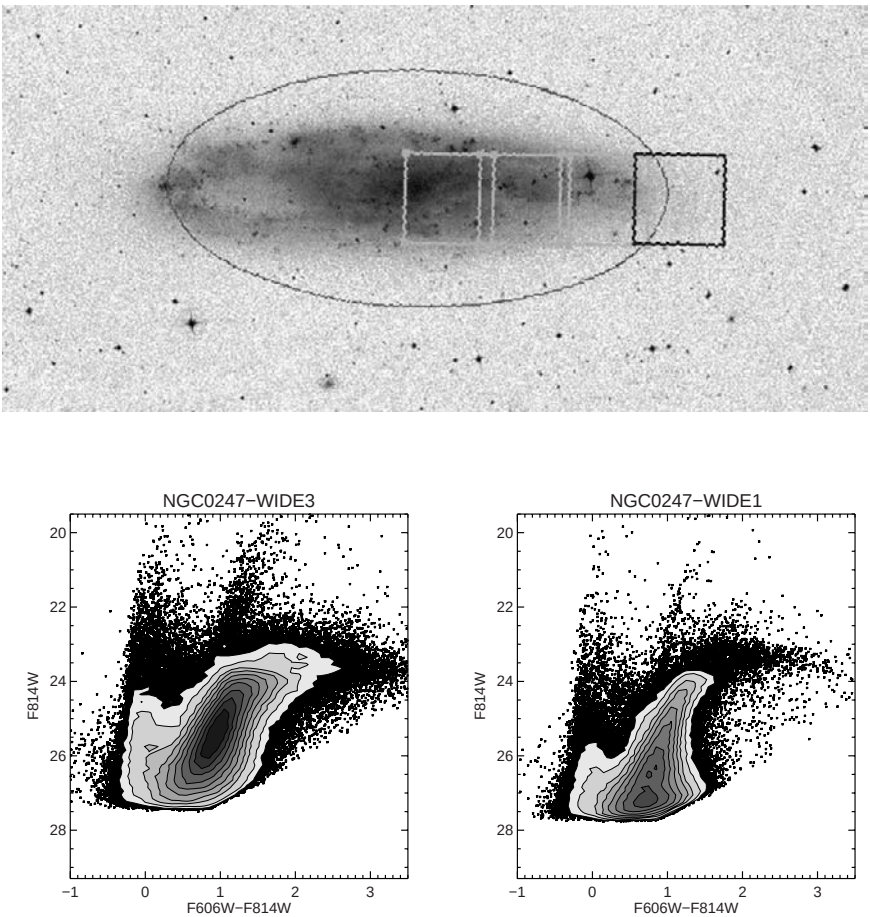

Fig. 2. The *upper panel* shows the positions of three 2-orbit radial tiles and one outer deep field pointing for NGC 247. The *lower panels* show $F606W - F814W$ CMDs for the innermost *(left)* and outermost *(right)* field in the radial tiling for NGC 247; the deep field was not observed before the ACS failure. Note the significant differences in the populations of bright recently formed stars, and the width of the CMD. The CMD of the inner region has increased width and decreased depth due to higher extinction and crowding. NGC 247 is one of the three most distant bright galaxies in the sample, and thus these CMDs represent somewhat worse than average data quality. In spite of this, the CMDs each contain several hundred thousand stars.

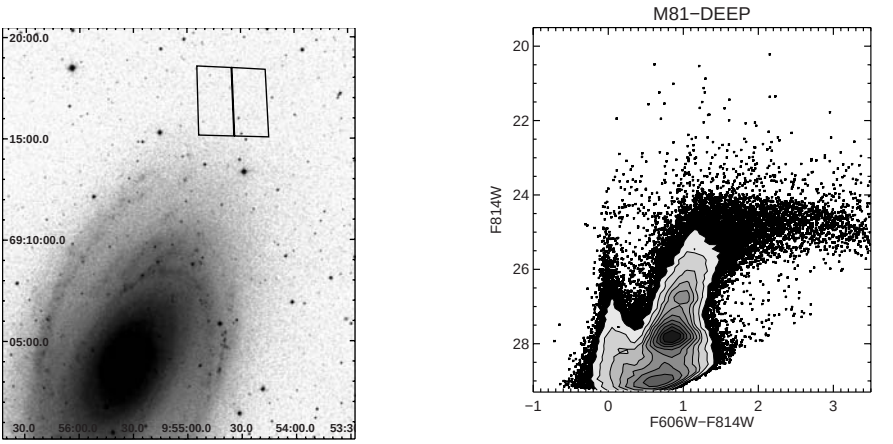

Fig. 3. The location of the M 81 deep field *(left)* and the resulting CMD *(right)*. Note the presence of young main sequence and helium burning stars, due to the extension of the spiral arm. Both the red clump and the AGB bump are well resolved.

The resulting CMDs have typical depths of $27 - 28^m$ in $F814W$ for the 2-orbit tilings (depending on the level of crowding) and 29^m for the deep fields in distant galaxies. These depths allow us to see *at least* 3.5 magnitudes below the tip of the red giant branch ($M_{F814W} > -0.5$) for the radial tilings of the most distant galaxies.

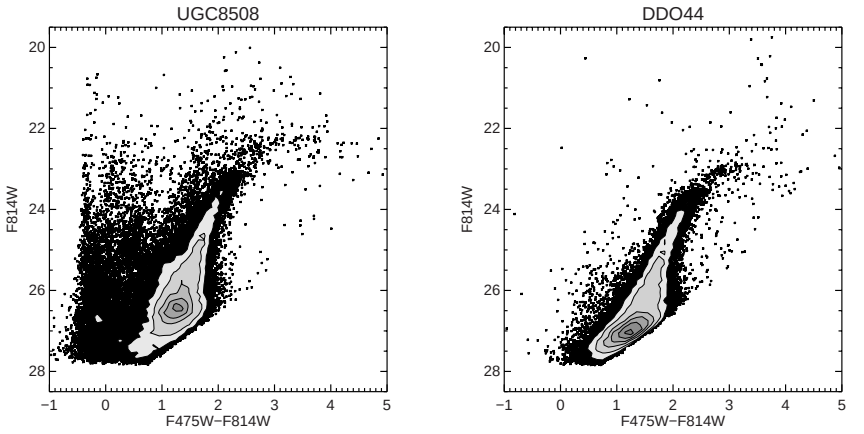

Fig. 4. $F475W - F814W$ CMDs for a dwarf irregular at 2.6 Mpc (UGC 8508; *left*) and a dwarf elliptical at 3.2 Mpc (DDO 44; *right*) from the ANGST survey.

3 The Aftermath of the ACS Failure

Tragically, ACS failed during the execution of the ANGST program. Of the 295 orbits granted to the program, only 104 were executed. We lost roughly half of the orbits allocated to fainter galaxies, and ∼70% of the orbits allocated to massive galaxies. The majority of these latter were lost from the planned deep field observations, which were completed for only 2 galaxies (not including galaxies close enough that no additional deep pointing was required).

After conducting a thorough review of the status of the ACS observations and the current and future capabilities of HST, we decided to pursue continuing a modified version of the ANGST program with WFPC2. While continuing the program with WFC3 or a restored ACS would certainly be preferable, given the uncertainties in the shuttle program and the real possibility that no imager would be successfully installed during the servicing mission, we judged that it was more important to continue establishing a legacy archive than to hold out for better data that might never arrive. We chose instead to: (1) reduce our outer distance limit to 3.5 Mpc; (2) reduce our depth requirement for our deep fields; (3) concentrate on high-efficiency $F606W + F814W$ imaging only; (4) adjust the depth of the wide field tilings to a constant absolute magnitude limit, rather than a constant exposure time; and (5) include less homogeneous archival data. An initial appeal to STScI allowed us to convert 116 of the lost orbits to WFPC2, to obtain deep fields for NGC 55, NGC 4214, NGC 404, NGC 2403, NGC 3109, Sextans B, and IC 5152. A follow-up Director's Discretionary proposal restored the needed radial tilings for NGC 55 and NGC 3109 (25 orbits total). These observations are currently underway.

4 Multiwavelength Follow-up

The rich database of stellar photometry produced by ANGST makes the sample galaxies ideal targets for multi-wavelength followup. By combining the star formation histories recoverable from ANGST with H I, IR, and UV observations, we can trace the rich interplay between star formation and the ISM with exquisite precision. For example, as shown in Figure 5, the ACS imaging allows us to construct CMDs for individual UV bright regions revealed in GALEX imaging. These CMDs in turn allow us to age date the star formation event that lead to the UV emission. We are currently using these techniques to trace the temporal evolution of UV and Hα emission. In addition to the GALEX observations underway, the ANGST galaxies are also a subset of the Spitzer Local Volume Legacy Survey (PIs: Kennicutt & Lee), which will allow us to extend this analysis to the IRAC and MIPS wavebands.

Members of the ANGST team are also involved in studying the impact that feedback from star formation has on the ISM. We have recently begun a Large VLA program (PI: Ott) to extend the observational strategy of the

THINGS survey (PI: Walter) to all ANGST galaxies with signs of any on-going or recent star formation. The resulting dataset will be used not only to identify the ISM properties that lead to star formation, but the reciprocal impact that past star formation (as revealed by the ANGST CMDs) has had on the structure and kinematics of the surrounding cold ISM.

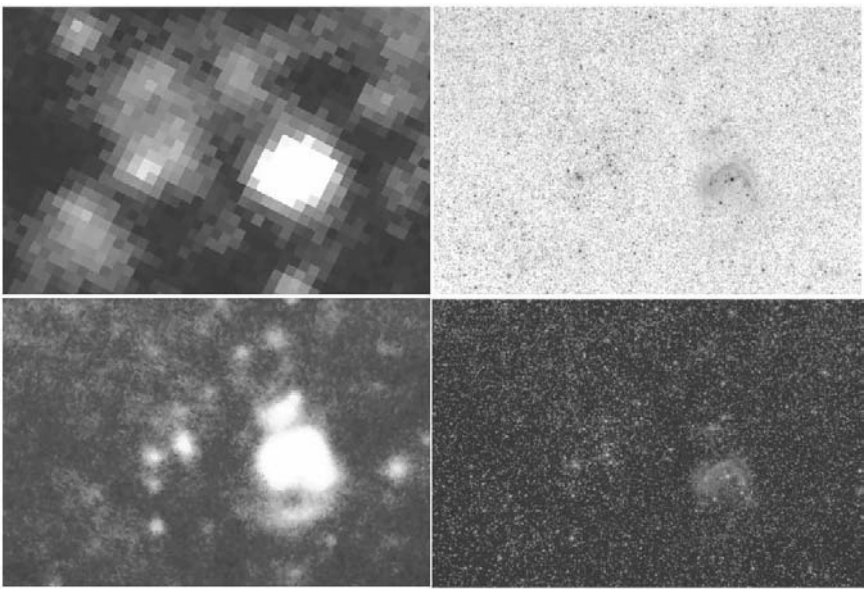

Fig. 5. A comparison between GALEX *(upper left)*, Hα *(lower left)*, and ACS ($F606W$: *top right*, and 3-color: *lower right*) imaging in a small section of NGC 300. The density of stars in the HST image is high enough to produce well-populated CMDs for individual UV-bright regions, allowing us to age-date individual regions with varying Hα/UV fluxes. For example, the brightest UV clump has a main sequence age of 4.5 Myr, while the clump on the lower left (which lacks Hα emission), has a 9 Myr burst superimposed on an older ∼100 Myr burst

5 On-going Work

The principal science projects on which the ANGST collaboration is currently working are: the recent and ancient star formation histories of M 81 (PI: Williams); the spatially resolved recent star formation histories of dwarfs (PI: Weisz); variable stars and the distance to M 81 (PI: McCommas); the structure and stellar content of dwarf halos (PI: Dalcanton); calibration of UV and Hα flux as a function of star formation history (PI: Gogarten); spatially resolved star formation histories in spirals (PI: Gogarten); the cluster

populations of the Local Volume (PIs: Seth & Olsen); improved isochrones and extinction modeling in the ACS filter set (PI: Girardi). We have full working pipelines for both ACS and WFPC2, and all data have been reduced. A companion Archival Legacy program ("Archival Nearby Galaxies: Reuse, Reduce, Recycle: ANGRRR") to produce stellar photometry for the entire HST archive of non-Local Group galaxies within 5 Mpc is underway. All of the data and photometric catalogs for both ANGST and ANGRRR will be publicly released, allowing the community to use this resource for years to come.

Julianne Dalcanton

ESO540-032: a Transition-Type Dwarf in the Sculptor Group

Gary S. Da Costa[1], Helmut Jerjen[1], and Antoine Bouchard[2]

[1] Research School of Astronomy & Astrophysics, ANU, Mt Stromlo Observatory, via Cotter Rd, Weston, ACT 2611, Australia. gdc,jerjen@mso.anu.edu.au
[2] Universite de Lyon 1, Centre de Recherche Astronomique de Lyon, Observatoire de Lyon, Saint-Genis Laval; and CNRS, École Normale Supérieure de Lyon, Lyon, France. bouchard@obs.univ-lyon1.fr

1 Introduction

The *dwarf Irregular* galaxies (dIrr) are gas-rich systems, with hydrogen mass to blue luminosity ratio (M_{HI}/L_B) values exceeding one in solar units, and active star formation. The *dwarf Elliptical* galaxies (dE), on the other hand, are usually gas-free, with (M_{HI}/L_B) values substantially less than one. In most instances they are not actively forming stars, although their star formation histories are complex and varied. These dwarf galaxy types exhibit a morphology-density relation, in the sense that dE galaxies tend to be found in denser environments. For example, within the Local Group, the vast majority of the dE systems are found as companions to the Milky Way or M31, while the dIrr members are mostly relatively isolated.

In the Local Group there are also dwarf galaxies that are *transition-types*, systems that possess moderate amounts of gas ($M_{HI}/L_B \approx 0.1$–0.5) and a low-level of current or recent star formation within a dominant older population. We note in passing that the recently discovered distant Milky Way companion Leo T [5] is more likely a low luminosity dwarf irregular, than a genuine transition-type galaxy, as it appears M_{HI}/L_B for this dwarf exceeds one [5]. The relationship between these classes of dwarf galaxies remains controversial: e.g., [4] argue that the existence of an offset in the luminosity-metallicity relation between dEs and dIrrs indicates different evolutionary paths. They suggest that transition-type dwarfs are the progenitors of dE (dSph) systems, in the sense that in low density environments where ram-pressure stripping mechanisms are ineffective, transition-type dwarfs should be common [4].

One obvious way to test this suggestion is to investigate the properties of dwarf galaxies in environments beyond the Local Group. The Sculptor Group is a low density aggregation of galaxies ranging in distance from ∼1.5 to ∼4 Mpc. It contains at least five low-luminosity early-type dwarf galaxies. Their neutral gas content has been studied by [1], who found that four are likely

B.S. Koribalski, H. Jerjen (eds.), *Galaxies in the Local Volume*,
doi: 10.1007/978-1-4020-6933-8_25,

to be transition-type objects: the M_{HI}/L_B values are in the range 0.1–0.2 [1]. The fifth system, Scl-dE1, was not detected in H I and has $M_{HI}/L_B < 0.04$ [1] as expected for a dE system. The transition-type nature of ESO410-005 and ESO540-032 is further supported by stellar population studies: both dwarfs show evidence for modest amounts of relatively recent star formation [7, 6]. We present here new data for ESO540-032: the optical observations reach considerably fainter than the ground-based study of [6], and the new H I observations have higher spatial resolution and signal-to-noise compared to [1]. The transition-type nature of this dwarf galaxy is confirmed.

2 Hubble Space Telescope Observations

HST/ACS observations of ESO540-032 were obtained in August 2006 with total integration times of 8960sec in the $F606W$ (wide-V) filter and 6708sec in the $F814W$ (wide-I) filter. The exposures used a standard dither pattern and were combined and corrected using the standard ACS data-processing pipeline. The DAOPHOT - ALLSTAR package [9] was used to determine photometry from the combined images. The calibration procedures outlined in [8] were then used to convert the photometry to the ACS VEGAMAG system and then to Johnson-Cousins V and I magnitudes.

The resulting colour-magnitude diagram is shown in Fig. 1, where the data have been separated into three radial bins based on distance from the galaxy centre. All three bins are clearly dominated by an old red giant branch (RGB) population, though as noted originally by [6] there is a small population of blue stars confined to the central regions of the galaxy. Application of a Sobel edge-detection filter to the RGB I-band luminosity function constructed from Fig. 1 places the RGB-tip at $I = 23.82 \pm 0.12$ mag. Using a reddening of $E(V-I)$ of 0.03 mag and assuming $M_I(\mathrm{TRGB}) = -4.05$ (e.g. [2]), this yields a distance of 3.7 ± 0.2 Mpc, consistent with previous estimates. The luminosity of the dwarf is then $M_V = -12.3$, using the total apparent magnitude from [6]. Given the distance estimate, a comparison of the colour of the RGB with those of globular clusters provides an estimate of the mean metallicity of the dwarf. This value, $[\mathrm{Fe/H}] = -1.7 \pm 0.2$, is strictly a lower limit, as at fixed abundance younger RGB stars are bluer. However, since the number of intermediate-age upper-AGB stars above the RGB tip in Fig. 1 is not substantial, the effect of any age difference on the mean metallicity value is likely to be small. With this metallicity and the absolute magnitude derived above, the location of ESO540-032 in the metallicity-luminosity diagram is reasonably consistent with the Local Group relation.

Knowledge of the distance also allows isochrones to be fitted to the stars to the blue of the RGB, the bluest of which undoubtedly represent a main sequence population. Using isochrones from [3] the age of the blue star population is potentially as young as 100 Myr, perhaps less. Similar conclusions were reached by [6]. The isochrones also show that many of the stars that

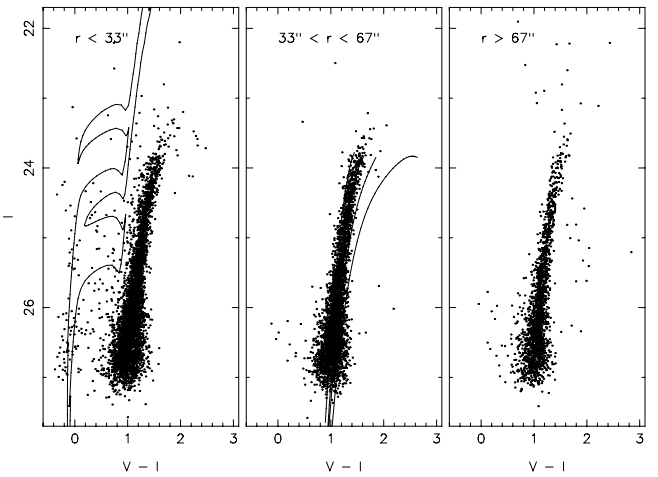

Fig. 1. Colour-magnitude diagrams for the Sculptor group transition-type dwarf galaxy ESO540-032. Note that the blue stars are found only in the central region. The isochrones shown in the *left panel* are for ages of 100 and 200 Myr and Z = 0.001. The globular cluster giant branches shown in the *middle panel* are M 15 ([Fe/H] = –2.17), NGC 6752 (–1.54), NGC 1851 (–1.36), and 47 Tuc (–0.71). Both the isochrones and the giant branches are plotted using an apparent I-band modulus of 27.87 and a reddening E($V - I$) = 0.03.

lie between the main sequence and the RGB, as well as the stars brighter and bluer than the RGB tip, can be understood as young stars in post main sequence phases of evolution. Clearly there has been an episode of star formation in ESO540-032 in the relatively recent past. Unfortunately, the small number of main sequence stars makes any attempt to measure the recent star formation history difficult – deeper observations are required.

3 Australia Telescope Compact Array Observations

Using the Parkes telescope [1] detected H I in the field of ESO540-032 at a velocity expected for objects in the Sculptor group. Using this velocity they were then able to use archival ATCA observations to demonstrate the detected H I was spatially coincident with the dwarf galaxy. The signal-to-noise of the archival observations, however, was low and the detection marginal. To confirm the detection, and particularly to establish the relative location of the peak of the H I with respect to the optical image, the galaxy was re-observed using longer integration times. Fig. 2 shows the results: H I is clearly detected and equally clearly, the H I distribution is centered on the optical centre of the galaxy. Further, given the beam size (cf. Fig. 2), there is no compelling evidence to suggest that the H I gas is more extended than the optical light distribution, which extends at least as far the edge of the ACS field. The total

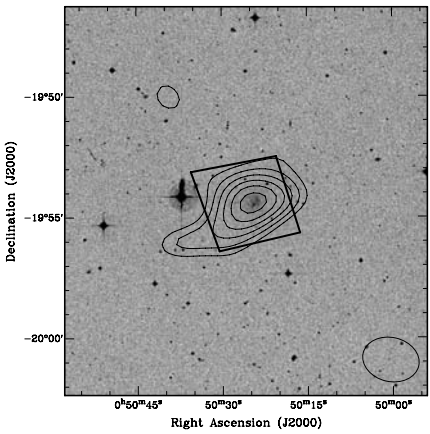

Fig. 2. H I density contours superposed on a Digital Sky Survey image of ESO540-032. The lowest contour represents 4×10^{18}cm^{-2} (2.5σ above background) and the contour interval is 2×10^{18} cm^{-2}. The beam size of $109'' \times 142''$ is shown in the bottom right corner. The quadrilateral outlined by the solid lines is the ACS field.

H I mass is $9.1 \pm 1.7 \times 10^5$ solar masses, the peak density is 15.2×10^{18}cm^{-2} and the M_{HI}/L_B ratio is 0.15±0.04, comparable to Phoenix [10].

4 Conclusions

The presence of a modest amount of recent star formation in a dominant old stellar population (age at least 6–8 Gyr given the comparative lack of upper-AGB stars), and the presence of a modest amount of gas, clearly confirm ESO540-032 as a transition-type dwarf galaxy in the Sculptor group (cf. [6, 1]). We have similar data for the other low-luminosity early-type dwarfs in this group – it will be interesting to see whether the analysis of these additional data supports the hypothesis of [4] that transition-type galaxies will be common compared to dE/dSph galaxies in low density environments.

References

1. A. Bouchard, H. Jerjen, G. S. Da Costa & J. Ott: AJ, **130**, 2058 (2005)
2. G. S. Da Costa & T. E. Armandroff: AJ, **100**, 162 (1990)
3. L. Girardi, G. Bertelli, A. Bressan, C. Choisi et al: A&A, **391**, 195 (2002)
4. E. K. Grebel, J. S. Gallagher & D. Harbeck: AJ, **125**, 1926 (2003)
5. M. J. Irwin, V. Belokurov, N. W. Evans et al: ApJ, **656**, L13 (2007)
6. H. Jerjen & M. Rejkuba: A&A, **371**, 487 (2001)
7. I. D. Karachenstev, M. E. Sharina, E. K. Grebel et al: ApJ, **542**, 128 (2000)
8. M. Sirianni, M. J. Lee, N. Benítez, J. P. Blakeslee et al: PASP, **117**, 1049 (2005)
9. P. B. Stetson: PASP, **106**, 250 (1994)
10. J. St-Germain, C. Carignan, S. Côté, & T. Oosterloo: AJ, **118**, 1235 (1999)

Resolving the Outer Disks and Halos of Nearby Galaxies

Anil Seth[1], Roelof de Jong[2], David Radburn-Smith[2], and Harry Ferguson[2]

[1] Harvard-Smithsonian Center for Astrophysics, USA aseth@cfa.harvard.edu
[2] Space Telescope Science Institute, USA

In a hierarchical merging scenario, the outer parts of a galaxy are a fossil record of the galaxy's early history (e.g. [1]). Observations of the outer disks and halos of galaxies thus provide a tool to study individual galaxy histories and test formation theories. Locally, an impressive effort has been made to understand the halo of the Milky Way, Andromeda, and M 33 (e.g. [9, 4, 6] and contributions in this volume). However, due to the stochastic nature of halo formation, a better understanding of this process requires a large sample of galaxies with known halo properties. The GHOSTS[3] project (PI: R. de Jong) aims to characterize the halos and outer portions of 14 nearby ($D = 4$–14 Mpc) spiral galaxies using the Hubble Space Telescope. Figure 1 shows the type, rotation velocity and inclination of all 14 galaxies. Detection of individual stars in the outer parts of these galaxies enables us to study both the morphological properties of the galaxies, and determine the stars' metallicity and age.

1 Disk and Halo Profiles

The GHOSTS data consists of ∼6 ACS or WFPC2 fields in each galaxy, primarily distributed along the major and minor axes (see Fig. 2). This areal coverage allows us to characterize the shape of the outer disk and halo components, especially in the eight edge-on galaxies in our sample where disk and halo components can be easily separated. Using individual stars, we can trace out the number density profile down to equivalent $i_{\rm AB}$-band surface brightnesses of ∼31 mag/arcsec^2. We discuss here two initial results on the disk and halo profile of NGC 4244.

The edge-on galaxy NGC 4244 is a low mass ($V_{\rm rot} \sim 100$ km/s), SAcd galaxy, similar to local group spiral M 33. The GHOSTS data is shown in Figure 2, with a CMD of one of the outer disk fields showing the richness of the stellar populations detected in our data. In addition to the prominent red

[3] GHOSTS = Galaxy Halos, Outer disks, Streams, Thick disks, and Star clusters

B.S. Koribalski, H. Jerjen (eds.), *Galaxies in the Local Volume*,
doi: 10.1007/978-1-4020-6933-8_26,

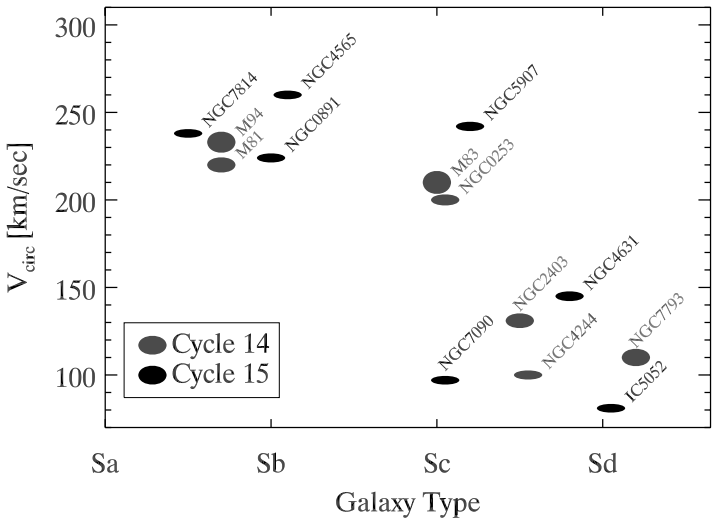

Fig. 1. The galaxy type vs. the circular velocity for the GHOSTS sample of galaxies. Shape of the circle indicates the inclination of the galaxy. Grey points were part of the Cycle 14 snapshot project, black points are part of the Cycle 15 large project.

giant branch (RGB), smaller numbers of young main sequence and helium burning stars (MS) and asymptotic giant branch stars (AGB) are seen. These populations cover the entire history of the galaxy (see [11]).

Along the major axis, we find that the disk exhibits a strong truncation at a radius of $\sim 420''$ (see [2] for details). Such truncations or breaks in the surface density profile are commonly observed in disk galaxies, but we are able to resolve the stellar populations across a truncation for the first time. Interestingly, the break occurs in the same location for all of the stellar populations from young to old. Also, the break occurs at the same radius for populations located above the midplane of the galaxy as well. These results show that the break radius in this galaxy has been roughly constant over time, thus favoring dynamical mechanisms for producing the break (e.g. [3]) versus star formation threshold mechanisms (e.g. [7]).

The minor axis of NGC 4244 is also very interesting. As noted in [11], the scale height of the old RGB population is higher than the younger stellar populations. With the GHOSTS data, we are able to trace this RGB profile out to $\sim$10 kpc ($\sim$30 scale heights) above the plane (see [12] for details). The exponential profile seen in our original data gives way to a slower decline above $\sim$2.5 kpc. If fit to an exponential, this more diffuse component has a scale height similar to the scale length of the main NGC 4244 disk, suggesting that we are detecting a spheroidal halo. Despite being very tenuous, this halo appears to be more massive than the halo expected for such a low-mass galaxy [10].

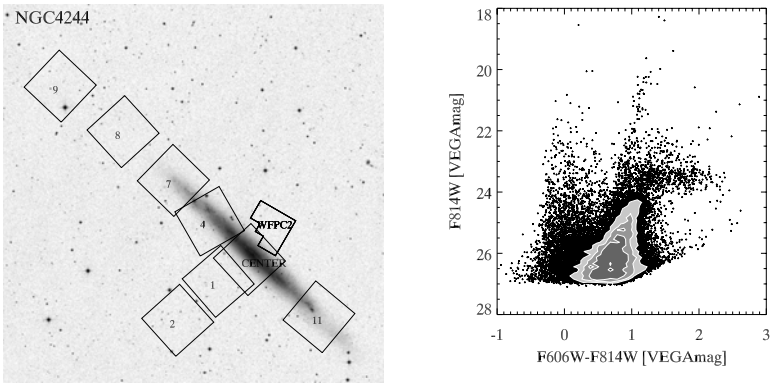

Fig. 2. *(Left:)* Numbered fields show the GHOSTS data for NGC 4244. Other archival HST data is also shown. *(Right:)* The color-magnitude diagram of field number 7 containing more than 20,000 stars. The contours outline the RGB component, with the younger MS and AGB components creating the other features.

2 Metallicity and Age information

The metallicity distribution of stars in the halos of galaxies provides information on the mass of the galaxies which were shredded to make the halo. The color of individual RGB stars depends primarily on their metallicity, and therefore is commonly used to derive the metallicity distribution.

We have considered two different methods for constructing metallicity distribution functions (MDFs). First, we interpolate each individual star in our CMD onto a grid of isochrones assuming an age of 10 Gyr. From this, we have found that a majority of the GHOSTS fields have MDFs that peak at [Z] ~ -0.7. This occurs in both fields which are apparently dominated by stars in the outer disk and others which appear to be halo-dominated.

While the interpolation method is roughly correct, the photometric errors translate into asymmetric errors in the metallicity and the contribution of AGB stars below the tip of the RGB is ignored. These uncertainties particularly affect the metal-poor end, preventing us from determining if these stars are present.

To try improving on this method we are using CMD fitting techniques in which model CMDs of a given age (including both RGB and AGB stars) are convolved with realistic errors. As an example of this method, we present results from our observations of a prominent stellar stream in M 83 at a projected distance of ∼25 kpc from the galaxy center. Using the Starfish code [5] and Padova models with updated AGB tracks [8], we fit the CMD of this field to a series of models at different ages. The CMD of the stream and the best-fitting model is shown in Figure 3. This model has a peak metallicity of [Z] = –0.5, suggesting the stream is quite metal-rich. Furthermore, the AGB

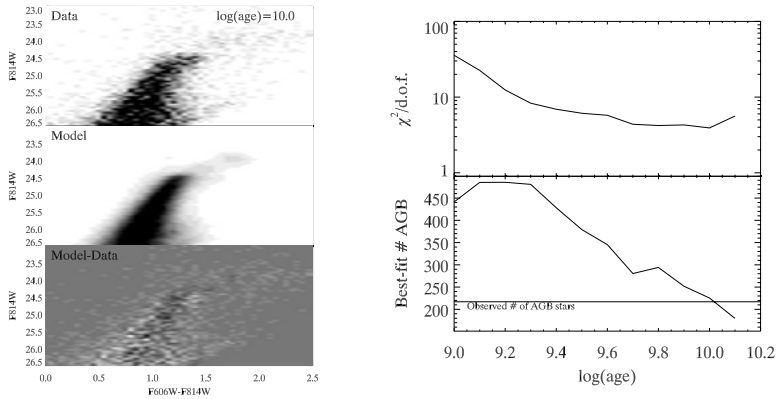

Fig. 3. *(Left:)* Hess diagrams of the M 83 stream data, the best-fitting 10 Gyr model, and residuals. *(Right:)* The best-fitting models' reduced χ^2 and number of AGB stars versus age. The AGB stars are significantly overproduced at ages younger than 5 Gyr.

stars provide us with the possibility of constraining the age of the stream. The right side of Figure 3 shows the reduced χ^2 of the best-fitting model vs. age. Clearly models with ages larger than 5 Gyr are favored, primarily because models with younger stars significantly overproduce AGB stars.

Conclusions: The GHOSTS survey is providing information on the shape and metallicity of the halos and outer disks of 14 nearby galaxies. We have presented initial results on the major- and minor-axis profiles of NGC 4244 and the metallicity and age of the stream in M 83. Analysis of the full sample of galaxies will provide strong constraints on models of galaxy formation.

References

1. Bullock, J. S., & Johnston, K. V. 2005, ApJ, 635, 931
2. de Jong, R. S. et al. 2007, astro-ph/0708.0826
3. Debattista, V. P., et al. 2006, ApJ, 645, 209
4. Gilbert, K. M. et al. 2006, ApJ, 652, 1188
5. Harris, J. & Zaritsky, D. 2001, ApJS, 136, 25
6. Ibata, R. et al. 2007, astro-ph/0704.1318
7. Kennicutt, R. C. 1989, ApJ, 344, 685
8. Marigo, P., & Girardi, L. 2007, A&A, 469, 239
9. Morrison, H. L. et al. 2000, AJ, 119, 2254
10. Purcell, C. W., Bullock, J. S., & Zentner, A. R. 2007, astro-ph/0703004
11. Seth, A. C., Dalcanton, J. J., & de Jong, R. S. 2005, AJ, 130, 1574
12. Seth, A. et al. 2007, astro-ph/0701704

Recent Star Formation Histories of Nearby Galaxies

Evan D. Skillman

University of Minnesota, Minneapolis, MN 55455, USA skillman@astro.umn.edu

1 Using HST to Map Recent Star Formation in Nearby Dwarf Galaxies: Testing Our Knowledge of the Star Formation Process

The first HST color magnitude diagram of the stars in the nearby dwarf irregular galaxy Sextans A [4] (see Figure 1) revealed for the first time a clear separation between the brightest main sequence stars and the blue helium burning (BHeB) stars - intermediate and high mass stars that have evolved beyond the main sequence, ignited helium burning in their cores, and have migrated back to the blue side of the color magnitude diagram. The separation of the main sequence stars and the BHeB was made possible by the high angular resolution of the HST (reducing photometric errors due to blends) and the low metallicity of Sextans A which leads to low differential reddening.

These BHeB stars afford a special opportunity to study the recent star formation histories of nearby galaxies. Because the position of a BHeB star in the CMD represents a unique age (as opposed to, for example, the main sequence or the red giant branch where a single position can correspond to a large range of ages), one can convert the BHeB luminosity function directly into a star formation history (SFH) (with the assumption of a universal initial mass function). The main limiting factor of this technique is that the position of the BHeB stars blends into the red clump at an age between 0.5 and 1 Gyr. Because one knows the positions of the BHeB stars in the galaxy, then one can produce a spatially resolved SFH (i.e., it is possible to produce "movies" of the recent star formation).

Translating the BHeB star luminosity function into a SFH depends on the accuracy of the stellar evolution models. We have different lines of evidence that the stellar evolution models provide an excellent guide to this stage of evolution. The first line came from the early HST observations themselves. Although the position of the blueward extension of the stellar evolution tracks is a strong function of both metallicity and stellar mass, excellent agreement

B.S. Koribalski, H. Jerjen (eds.), *Galaxies in the Local Volume*,
doi: 10.1007/978-1-4020-6933-8_27,

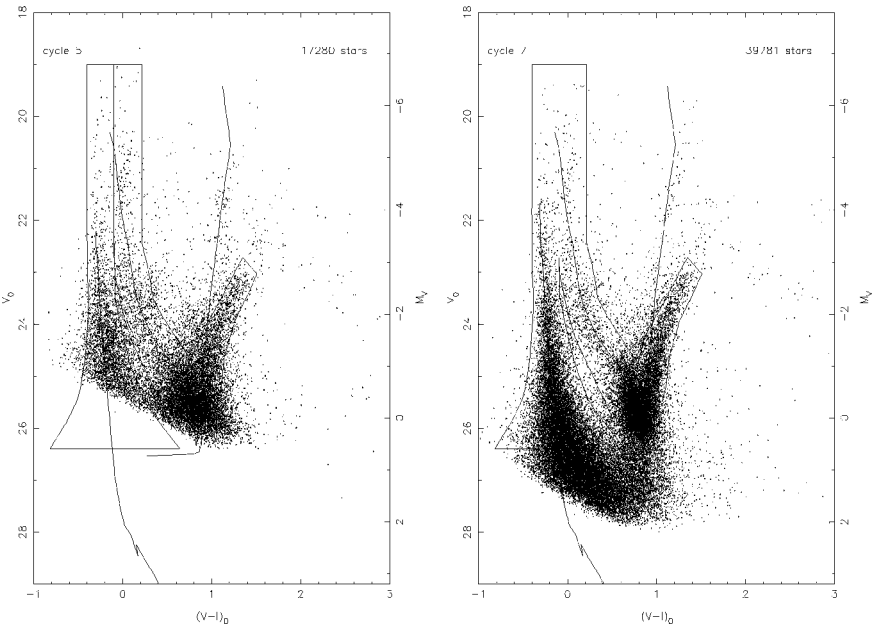

Fig. 1. HST WFPC2 color-magnitude diagrams for Sextans A. The *left panel* shows shallow (2 orbits) Cycle 5 data [4], and the *right panel* shows deeper (24 orbits) Cycle 7 data. The right axis shows the absolute magnitude for the adopted distance modulus of $(M - m) = 25.8$. The data have been corrected for Galactic extinction. The most obvious difference between the two data sets is the increased photometric sensitivity of the Cycle 7 data. The curves come from the stellar evolution models of [1], and indicate the main sequence, the blue edge of the He-burning loop, and the red edge of the He-burning loop. The polygonal regions indicate the selection regions for the MS, BHeB, and RGB. Brighter than $V = 22$ the color index of the blue and red supergiants differ from the models. However, for fainter stars the agreement between the model curves and the data is excellent, particularly for the faint BHeB sequence. (From [6].)

between observations and models was found by choosing the stellar evolution tracks for the metallicity determined from the H II region abundances for Sextans A. This is a very important point. There are no low metallicity, young stellar clusters in the Milky Way galaxy or the Magellanic Clouds which allow the stellar evolution modelers to calibrate their codes in this regime (the oxygen abundance in Sextans A is a factor 3 lower than in the Small Magellanic Cloud). When these stars were first observed in the extragalactic context, the agreement with models can be taken as confirmation of a prediction.

In a more recent study, Dohm-Palmer et al. [6] used deeper HST photometry of Sextans A to compare recent star formation histories recovered from

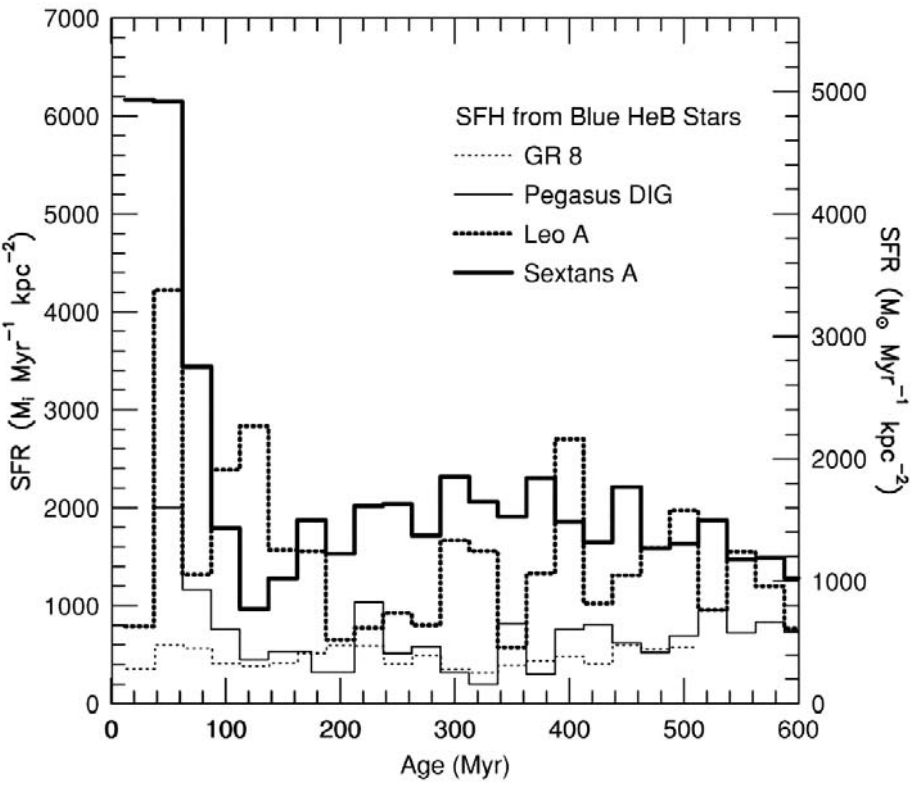

Fig. 2. The recent star formation histories of four nearby dI galaxies derived from the blue HeB luminosity function. The age bins are 25 Myr. Sextans A consistently has the highest SFR/area, followed by Leo A. Pegasus and GR 8 have a very similar SFR/area, which is consistently lower than in the other two galaxies. Despite the relatively high time resolution which increases the sensitivity to variations, none of the galaxies show evidence for strong bursts of star formation, and there is little evidence for periods of no star formation. The left axis is labeled in units of M_i, the average initial mass of the assumed IMF (= 0.81 $M_\odot$ for a Salpeter IMF and 0.53 $M_\odot$ for a Scalo IMF). The right axis has been labeled assuming M_i = 0.8 $M_\odot$. (From [5]).

both the main-sequence stars and the BHeB stars for the last 300 Myr. The excellent agreement between these independent star formation rate (SFR) calculations is a resounding confirmation for the legitimacy of using the BHeB stars to calculate the recent SFR. Dolphin et al. [7] derived the recent SFH of Sextans A from the entire CMD and found good agreement with that derived from the BHeB stars alone.

Many researchers are concerned about how the rotation of the galaxies is dealt with, whether stars disperse from their formation sites (via inter-cluster

disruption), and how this will affect the inferred patterns of star-formation regions in the galaxies. Because the dwarf galaxies that we observe are dominated by solid-body rotation, the spatial relationships between features are preserved over time. This also means that there is no differential shear to stretch out and destroy features. The question of time scale for dissipation of star forming regions is an interesting one, and is discussed extensively in the appendix of [4]. The theoretical results [2, 14, 12] favor time scales for the dissolution of star clusters of order several hundred million years. Empirically, we see the BHeB stars highly clustered at old ages ($\sim$500 Myr), so it appears the stars do not move very far from each other in this amount of time.

Additionally, Dohm-Palmer et al. [3] used all of the HST observations of Sextans A in order to compare the ratio of blue to red supergiants. This ratio provides an observational constraint on the relative lifetimes of these two phases that is a sensitive test for convection, mass-loss, and rotation parameters. Analyzing the ratio as a function of age, or, equivalently, mass eliminates the confusion of unknown star formation histories (as in previous studies of this ratio). The functional form of the observed ratio matches the model extremely well with an offset of roughly a factor of 2 (and the offset is seen as support of the latest models which include rotation). Given these tests of reliability of the stellar models, we feel confident that using the BHeB stars to construct recent star formation histories is well justified.

Dohm-Palmer et al. [5] employed HST photometry of four nearby dwarf irregular galaxies (Sextans A, Leo A, Pegasus, and GR 8) and derived recent star formation histories for these galaxies (see Figure 2). At the time, the surprising result was the lack of bursts or episodes of enhanced star formation. With time bins of only 25 Myr for the last 500 Myr, with the possible exception of enhanced star formation rates in the last 50 Myr for Sextans A and Leo A, all four galaxies are best described as nearly constant star formation rates. In retrospect, perhaps the lack of truly zero star formation rates is as surprising as the lack of periods of enhanced star formation. These nearly constant, low level star formation rates confirm the picture for low surface brightness dwarf irregular galaxies as "down but not out," [9] and the conclusion of Monica Tosi and Laura Greggio and their collaborators that the duration of truly quiescent phases must be very short compared to the active phase (e.g., [15]).

The detailed, spatially resolved, star formation history of Sextans A, when compared to the present day H I distribution reveals three zones which experience repeated episodes of star formation [6]. Two of these zones are associated with high column density neutral gas, while the third, and oldest, is not. Our interpretation of this pattern of star formation is that it is an orderly yet stochastic process. Star formation begins on the edge of a gas structure and progressively eats away at the cloud, breaking it up and inducing further star formation. A more quantitative analysis of the star formation process must await a larger sample of galaxies with spatially resolved star formation histories to allow correlation studies with the physical properties of the galaxy (see next section).

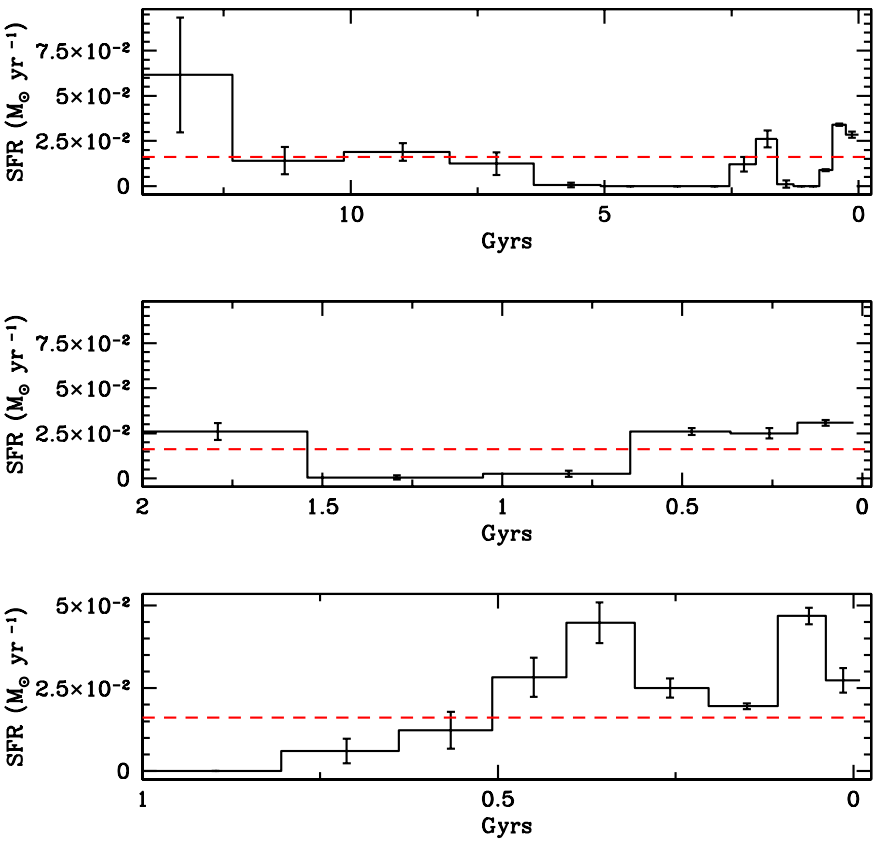

Fig. 3. The derived SFH for the M 81 dwarf galaxy DDO 165 from our HST ACS photometry (Weisz et al., in prep.). The SFH history is presented in three different time frames with appropriate time resolution, the total global SFH at low time resolution, the last 2 Gyr at intermediate resolution, and the last 1 Gyr at relatively high time resolution. The horizontal line represents the average star formation rate over the Hubble time. Here we see an intense burst of star formation that lasted for roughly 500 Myr. In her Ph.D. thesis work, Janice Lee identified DDO 165 as a post-starburst galaxy based on its very low equivalent width of Hα emission. The H I observations of DDO 165 show very disrupted kinematics, indicative of a recent interaction.

Putting all of this together gives a picture of quasi-continuous star formation in present day dwarf galaxies, where bursts are the exception and not the rule. The low effective yields seen in some of these galaxies are then more likely due to a more complex picture (as opposed to large gas outflows caused by central starbursts). This implies that "leaky box" models of evolution are most likely to provide a good guide to the evolution of these systems (see also [16]).

2 HST ACS Observations of M 81 Dwarfs

Studies of the impact of star formation ('feedback') on the properties of a galaxy are of fundamental importance to understanding galaxy evolution. One crucial aspect in these studies is a precise census of the recent star formation in a galaxy. I am leading a collaborative effort (team members: John Cannon, Andy Dolphin, Rob Kennicutt, Janice Lee, Fabian Walter, Dan Weisz) to analyze HST ACS observations of a sample of nine M 81 dwarfs with the aim of deriving spatially resolved star formation histories with a time resolution of roughly 30 Myr over the last 500 Myr. The M 81 group contains a large number of dwarf galaxies with a wide variety of current star formation rates [10]. Our sample comprises nine dwarf galaxies in the M 81 group spanning a wide diversity of SFHs. The sample spans ranges of 6 magnitudes in luminosity, 1000 in current star formation rate, and 0.5 dex in metallicity. The ACS observations allow us to directly observe the strength and spatial relationships of all of the star formation in these galaxies in the last 500 Myr. We can then quantify the star formation and measure (1) the fraction of star formation that is triggered by feedback, (2) the fraction of star formation that occurs in clusters and associations, and (3) to what degree star formation is governed by the feedback from star formation. Because most of our sample are SINGS galaxies [11], the ACS observations will be complemented with high–quality ancillary data collected by our team for all galaxies (e.g., Spitzer, UV/optical/NIR, VLA H I). This will enable us to construct prescriptions of how star formation and feedback depend on metallicity, size, gas content, and current star formation rates in galaxies.

As an example of what one can expect from this study, Figure 3 shows the recent SFH of DDO 165, revealing a rather dramatic burst of star formation in the recent past. At the conference I showed a movie of this, demonstrating that the burst was spread throughout the galaxy, and likely triggered by an interaction. Note also, the heightened star formation rate at about 2 Gyr ago. This is far too old to be detected by BHeB stars, and is an indication of structure within the AGB stars. Figure 4 shows synthetic CMD from the derived SFH for the M 81 dwarf galaxy DDO 165 shown in Figure 3. The stripe of AGB stars at $V \sim 24.5$ mag. corresponds to the burst of star formation 2 Gyr ago. This is also seen in the data, but more clearly so in the synthetic CMD.

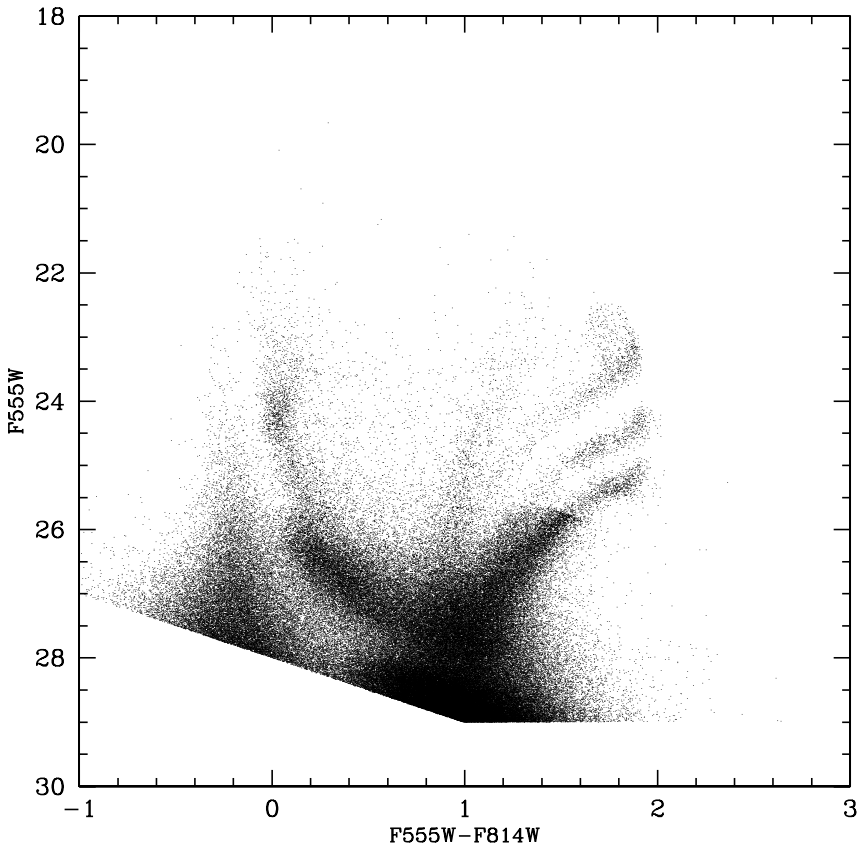

Fig. 4. A synthetic CMD from the derived SFH for the M 81 dwarf galaxy DDO 165 shown in Fig. 3. Note the structure in the AGB. This figure demonstrates the power of using the AGB star distributions in the CMD to constrain the SFHs on timescales of $1 - 3$ Gyr. This is the timescale for interaction of galaxies within groups, and, thus, will provide a very valuable tool for investigating the relationship between SFR and interactions within nearby groups of galaxies.

Historically, the AGB has been a very uncertain part of the CMD for SFH modeling [8]. However, there has been significant recent progress in the models of AGB stars [13]. As the models and data come into better agreement, we can expect better constraints on the SFHs back to $\sim$3 Gyr ago. This will probe the relevant timescales for interactions in the nearby groups of galaxies. Although the M 81 dwarfs project was designed to focus on ages back to 0.5 Gyr ago, we hope to provide interesting results for even older ages.

I would like to thank the conference organizers for inviting me to this most excellent conference.

References

1. Bertelli, G., Bressan, A., Chiosi, C., Fagotto, F., & Nasi, E.: A&AS **106**, 275 (1994)
2. Binney, J., & Tremaine, S.: Galactic Dynamics, Princeton University Press, p. 442 (1987)
3. Dohm-Palmer, R.C., & Skillman, E.D.: AJ **123**, 1433 (2002)
4. Dohm-Palmer, R.C., Skillman, E.D., Saha, A., Tolstoy, E., Mateo, M., Gallagher, J.S., Hoessel, J., Chiosi, C., & Dufour, R.J.: AJ **114**, 2514 (1997)
5. Dohm-Palmer, R.C., Skillman, E.D., Gallagher, J.S., Tolstoy, E., Mateo, M., Dufour, R.J., Saha, A., Hoessel, J., & Chiosi, C.: AJ **116**, 1227 (1998)
6. Dohm-Palmer, R.C., Skillman, E.D., Mateo, M., Saha, A., Dolphin, A., Tolstoy, E., Gallagher, J.S. & Cole, A.A.: AJ **123**, 813 (2002)
7. Dolphin, A.E., et al.: AJ, **126**, 187 (2003)
8. Gallart, C., Zoccali, M., & Aparicio, A.: ARA&A **43**, 387 (2005)
9. Hunter, D.A., & Gallagher, J.S.: ApJS **58**, 533 (1985)
10. Karachentsev, I.D., & Kaisin, S.S.: AJ **133**, 1883 (2007)
11. Kennicutt, R.C., Jr., et al.: PASP **115**, 928 (2003)
12. Kroupa, P.: MNRAS **277**, 1522 (1995)
13. Marigo, P., & Girardi, L.: A&A **469**, 239 (2007)
14. Terlevich, E.: MNRAS **224**, 193 (1987)
15. Tosi, M., Greggio, L., Marconi, G., & Focardi, P.: AJ **102**, 951 (1991)
16. Tolstoy, E., Venn, K., Shetrone, M., Primas, F., Hill, V., Kaufer, A., Szeifert, T.: Ap&SS **281**, 217 (2002)

HST/ACS Observations of Extremely Metal-Poor Blue Compact Dwarf Galaxies

Alessandra Aloisi[1,2]

[1] Space Telescope Science Institute, 3700 San Martin Drive, Baltimore, MD 21218, USA aloisi@stsci.edu
[2] on assignment from the Space Telescope Division of the European Space Agency

New deep HST/ACS photometry of the extremely metal-poor star-forming dwarf galaxy I Zw 18 is presented and compared to a similar study of its twin sister SBS 1415+437. Chemically-unevolved systems like I Zw 18 or SBS 1415+437 represent the closest analog to primordial galaxies in the early universe. It has also been argued that some of these objects (e.g., I Zw 18) may be genuine nearby 'young' galaxies. However, by revealing the existence of an evolved red stellar population in both I Zw 18 and SBS 1415+437, our HST/ACS observations do not support such an interpretation.

1 Introduction

In hierarchical formation scenarios, dwarf ($M < 10^9$ $M_\odot$) galaxies are the first systems to collapse and start forming stars, supplying the building blocks for the formation of more massive systems. As remnants of this process, present-day dwarfs may have been sites of the earliest star-formation (SF) activity in the universe. However, the most metal-poor ($12 + \log(O/H) < 7.6$, i.e. $Z < 1/20$ $Z_\odot$) dwarf irregular (dIrr) and blue compact dwarf (BCD) galaxies have been repeatedly pointed out as candidate "primeval" galaxies in the nearby universe, with ages $< 100 - 500$ Myr (e.g., Izotov & Thuan 1999).

The only direct way to unambiguously infer the evolutionary status of a metal-poor dIrr/BCD is to resolve it into stars with deep HST observations, and study stellar features in the color-magnitude diagram (CMD). The brightest of these features that contains stars of significant age is the Red Giant Branch (RGB), formed by low-mass stars with ages $\sim 1 - 13$ Gyr. In the last 15 years all metal-poor dIrrs in the Local Group and BCDs with $D < 15$ Mpc have been imaged with HST. An RGB has been detected in all those galaxies for which photometric data exist that go deep enough to reach the RGB tip (TRGB, brightest phase of the RGB) in the CMD.

The only possible exception so far is the BCD I Zw 18. With $12 + \log(O/H) = 7.2$, i.e. $Z = 1/50$ $Z_\odot$, I Zw 18 is the most metal-poor galaxy

B.S. Koribalski, H. Jerjen (eds.), *Galaxies in the Local Volume*,
doi: 10.1007/978-1-4020-6933-8_28,

in the nearby universe. After other groups had already resolved its brightest individual stars, our group was the first to go deep enough to detect asymptotic giant branch (AGB) stars in HST/WFPC2 images with ages of at least several hundreds Myr and possibly up to a few Gyrs (Aloisi et al. 1999; see also Östlin 2000). More recently, Izotov & Thuan (2004) presented new deep HST/ACS observations. Their I vs. $V-I$ CMD shows no sign of an RGB, from which they concluded that the most evolved (AGB) stars are not older than 500 Myr. This result was subsequently challenged by Momany et al. (2005) and our group (Tosi et al. 2007) based on a better photometric analysis of the same data. This showed that many red sources do exist at the expected position of an RGB, and that their density drops exactly where a TRGB would be expected. However, small number statistics, large photometric errors, and incompleteness at the TRGB, did not allow a conclusive statement.

2 New HST/ACS Observations of I Zw 18

We were awarded 24 additional orbits with ACS over a three-month period starting in October 2005 (GO program 10586, PI Aloisi) to better understand the evolutionary status of I Zw 18. The observations were obtained in 12 different epochs in F606W and F814W to: (1) build a deeper CMD to search for RGB stars; (2) detect and characterize Cepheids at the lowest metallicity available in the local universe; and (3) use both Cepheids and a possible TRGB detection to determine an accurate distance to I Zw 18 (see Aloisi et al. 2007).

PSF-fitting photometry was performed on deep images that were obtained by combining the exposures in each filter with MultiDrizzle. After application of aperture corrections, the count rates were transformed to Johnson-Cousins V and I magnitudes. Values shown and discussed hereafter are corrected for $E(B-V) = 0.032$ mag of Galactic foreground extinction, but not for any extinction intrinsic to I Zw 18. The archival ACS data in F555W and F814W (GO program 9400, PI Thuan) were also re-processed in a similar manner. The two ACS datasets were then combined by demanding that stars should be detected in all the four deep images (V and I for both datasets).

3 Results and Interpretation

Figure 1a shows the resulting I vs. $V-I$ CMD of I Zw 18. The CMD shows faint red stars exactly at the position where an RGB would be expected. Figure 2 shows the luminosity function (LF) of the red stars. It shows a sharp drop towards brighter magnitudes, exactly as would be expected from a TRGB. The magnitude of the discontinuity, $I = 27.27 \pm 0.14$, implies a distance modulus $m - M = 31.30 \pm 0.17$, i.e., $D = 18.2 \pm 1.5$ Mpc. The TRGB distance is consistent with the distance as inferred from the analysis of the Cepheid variables identified by our program (Aloisi et al. 2007). This

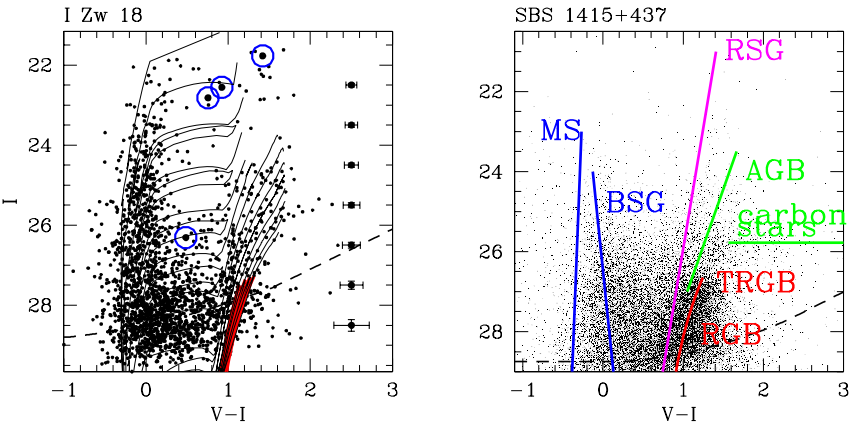

Fig. 1. *(Left:)* HST/ACS CMD for I Zw 18 (Aloisi et al. 2007). Median photometric errors at $V-I=1$ (determined by comparison of measurements from GO-9400 and GO-10586) are shown as function of I on the right side of the panel. Padua isochrones from 5.5 Myr to 10 Gyr are overlaid, with the RGB phase for isochrones from 1.7 to 10 Gyr colored red. The isochrones have metallicity $Z=0.0004$ (as inferred from the H II regions of I Zw 18) and are shown for the distance $D=18.2$ Mpc ($m-M=31.30$). The CMD includes stars in both the main and secondary bodies of I Zw 18. Open circles highlight the four confirmed variables, which are plotted according to their intensity-averaged magnitudes. *(Right:)* HST/ACS CMD for SBS 1415+437 (Aloisi et al. 2005). The main evolutionary sequences seen in the data are indicated in approximate sense as colored straight lines: main sequence (MS), blue supergiants (BSG), red supergiants (RSG), the red giant branch (RGB) with its tip (TRGB), the asymptotic giant branch (AGB), and carbon stars. Both CMDs are corrected for Galactic foreground extinction. Dashed lines are estimates of the 50% completeness level. The vertical axes of the panels are offset from each other by 0.61 mag, i.e. the difference in distance modulus between the galaxies (see Fig. 2). Some ~ 10 times more stars were detected in SBS 1415+437, owing to its smaller distance.

agreement further supports our interpretation of the LF drop in Fig. 2 as a TRGB feature.

The evidence for an RGB in I Zw 18 is further strengthened by comparison to another BCD, SBS 1415+437, observed by us with a similar HST/ACS set-up (Aloisi et al. 2005). This galaxy is not quite as metal poor as I Zw 18 ($12+\log(O/H)=7.6$) and is somewhat nearer at $D\approx 13.6$ Mpc. But taking into account the differences in distance and completeness, the CMDs of these galaxies look very similar. Since SBS 1415+437 has an unmistakable RGB sequence, this suggests that such an RGB sequence exists in I Zw 18.

4 Conclusions

Our HST/ACS observations of I Zw 18 and SBS 1415+437 provide improved insight into the evolutionary status of metal-poor BCDs by indicating that

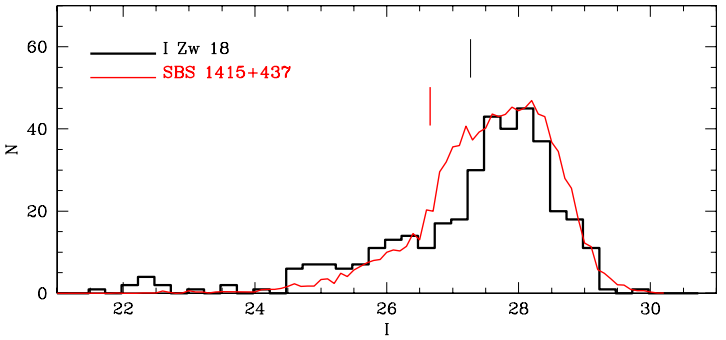

Fig. 2. I-band LFs for stars with red colors in the range $V - I = 0.75 - 1.5$ mag, inferred from the CMDs in Fig. 1. Normalizations are arbitrary. Vertical marks indicate the positions of the TRGB, as determined using a Savitzky-Golay filtering technique developed by one of us (see Cioni et al. 2000). At these magnitudes there is a steep LF drop towards brighter magnitudes, due to the end of the RGB sequence. By contrast, the LF drop towards fainter magnitudes at $I > 28$ mag is due to incompleteness in both cases. Apart from a shift $\Delta(m - M) \approx 0.61$, these metal-poor BCD galaxies have very similar LFs.

underlying old (> 1 Gyr) populations are present in even the most metal-poor systems. The coherent picture that emerges is that these galaxies did not form recently ($z < 0.1$) and may well be as old as the first systems that collapsed in the early universe. Deeper studies (well below the TRGB) will be needed to pinpoint the exact onset of the star formation in these extreme objects.

The author would like to thank all her collaborators that made these projects possible, in particular F. Annibali, G. Clementini, R. Contreras, G. Fiorentino, C. Leitherer, J. Mack, M. Marconi, I. Musella, A. Saha, M. Sirianni, M. Tosi, and R. van der Marel.

References

1. Aloisi, A., et al. 2007, ApJ, in press, arXiv:0707.2371
2. Aloisi, A., Tosi, M., & Greggio, L. 1999, AJ **118**, 302
3. Aloisi, A., van der Marel, R. P., Mack, J., Leitherer, C., Sirianni, M., & Tosi, M. 2005, ApJ **631**, L45
4. Cioni, M.-R. L., van der Marel, R. P., Loup, C., & Habing, H. J. 2000, A&A **359**, 601
5. Izotov, Y. I., & Thuan, T. X. 1999, ApJ **511**, 639
6. Izotov, Y. I., & Thuan, T. X. 2004, ApJ **616**, 768
7. Momany, Y., et al. 2005, A&A **439**, 111
8. Östlin, G. 2000, ApJ **535**, L99
9. Tosi, M., Aloisi, A., Mack, J., & Maio, M. 2007, in IAU Symp. 235, "Galaxy Evolution Across the Hubble Time", ed. F. Combes & J. Palous, (Cambridge: Cambridge University Press), 65

Matching the Local and Cosmic Star Formation Histories

Igor Drozdovsky[1,2], Andrew Hopkins[3], Antonio Aparicio[1], Carme Gallart[1], and the LCID team[4]

[1] Instituto de Astrofísica de Canarias, C/Vía Lactea s/n, 38200, La Laguna, Tenerife, Spain dio@iac.es
[2] Astronomical Institute of St.Petersburg State University, Russia
[3] University of Sydney, School of Physics, Bldg A28, NSW 2006, Australia ahopkins@physics.usyd.edu.au
[4] http://www.iac.es/project/LCID

Summary. Given the many recent advances in our understanding of the star formation history (SFH) of the Local Group and other nearby galaxies, and in the evolution of star formation with redshift, we present a new comparison of the comoving space density of the star formation rate as a function of look-back time for the Local and Distant Universe. We update the Local SFH derived from the analysis of resolved stellar populations ("fossil records") in individual nearby galaxies, based on our own estimates as well as available in the literature. While the preliminary comparison of SFHs is found to be broadly consistent, the detailed discrepancies still remain, including excess of the Local SFR density in the most recent epoch.

The goal of this project is to establish whether the star formation history (SFH) of galaxies in the local Universe is consistent with the cosmic (global) SFH inferred from surveys of distant, 'high-redshift', galaxies. A common approach based on the redshift surveys aims to measure indicators of recent star formation in galaxies at different distances, which due to the finite speed of light, give us a view of different cosmic epochs. One of the drawbacks of this approach is that it is not directly possible to connect different galaxies, measured at different redshifts, into a coherent evolutionary sequence, to provide a consistent picture of *observed* galaxy evolution. Moreover, the detail in which these galaxies can be studied is limited since they are mostly unresolved, and their faintness limits the wavelength resolution of any spectroscopic measurements. An alternative, and complementary, approach focuses on galaxies nearby enough to be resolved into their component stars. For these systems we can use well established stellar evolution theory, together with photometry and spectroscopy of individual stars of various ages, to interpret the "fossil record" of their star formation, and to trace the evolution of each from its formation to the present time. Despite a limited volume and sample sizes, the

B.S. Koribalski, H. Jerjen (eds.), *Galaxies in the Local Volume*,
doi: 10.1007/978-1-4020-6933-8_29,

high quality SFH one can obtain with this method is valuable information in a general cosmological context. In particular, it provides important clues to the earliest stages of star formation that are progressively harder to probe with galaxy redshift surveys targeting the most distant systems, as well as to probe issues that are not accessible through large-scale galaxy surveys (e.g., uncertainties in conversion factors from luminosity to SFR, dust attenuation, shape of the stellar and galaxy mass functions, etc). Initial comparisons suggest these different approaches do not yield the same results [8, 6], but the errors are large, paradoxically, due to the lack of complete normalized SFHs of nearby galaxies.

New observational data, better understanding of stellar structure and evolution, and recent developments, coupled with greater computing power, of automated techniques that measure the star formation histories by statistical comparison of models and observations (e.g., [1]) have radically modified our view of star formation in the Milky Way (MW) and Andromeda (M 31), the two gravitationally dominant galaxies of the Local Group (e.g., [9, 2]). Our knowledge of the star formation history in other nearby galaxies has also been significantly improved, thanks to the possibility of analyzing their faint and ancient resolved stellar populations (e.g., [3, 4]). These low mass stars have extremely long lifetimes, comparable to the age of the Universe, and retain in their atmospheres the gas, with the elemental abundances intact, from the time of their birth. Thus, they provide critical information on the early (initial) star formation rate and heavy element abundance. The total number of galaxies where these old (> 10 Gyr) stars are measurable has doubled since the 2001 publication of Hopkins et al. [6].

In the past few years the measurement of the evolution of the star formation rate (SFR) in various types of galaxies at a broad range of redshifts has also tremendously progressed. An example of an extensive compilation drawn from the literature of SFR density measurements over redshifts $0 < z < 6$ has been done by Hopkins & Beacom [5], following an investigation that carefully addressed issues associated with corrections for obscuration by dust within galaxies, internally consistent calibrations for the various star-formation rate indicators, and constraints on the initial distribution of stellar masses in a burst of star formation, among others. Taken together, the most recent and robust data indicate a compellingly consistent picture of the cosmic SFH constrained to within factors of about $\sim$3. There is now growing evidence that the evolution is essentially flat beyond $z \sim 1$, however it is still unclear whether at $z > 3$ the evolution flattens, or declines or continues to increase.

In Fig. 1, we present an updated comparison of the comoving space density of the star formation rate as a function of look-back time for the Local Group and the distant Universe. To measure the comoving space density for the Local Group, we integrated the best currently known SFHs for the galaxies

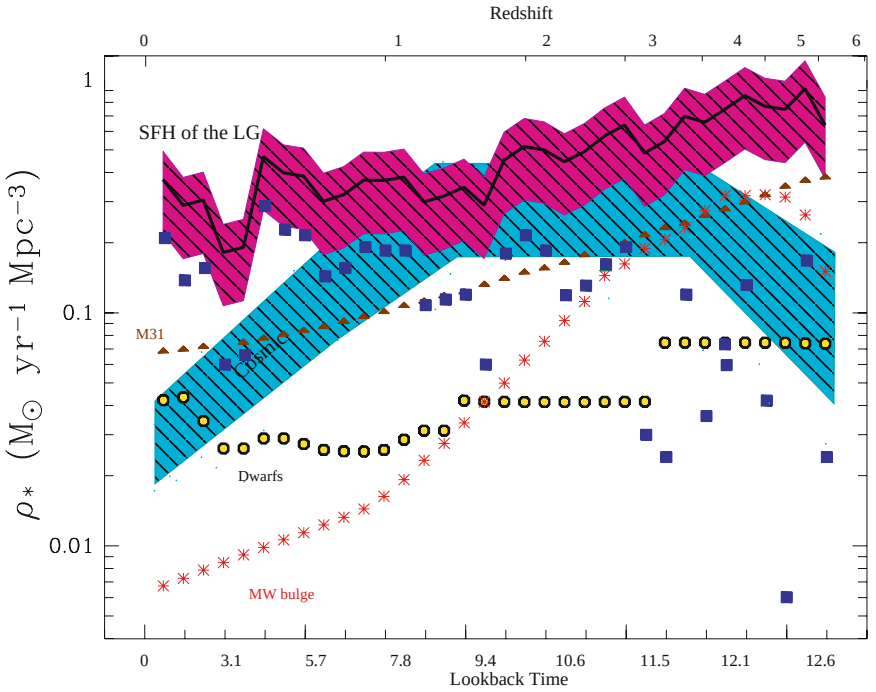

Fig. 1. Comparison of the Local Group SFH (solid line and hatched region) with that from a compilation of redshift surveys (grey shaded area) for a $(H_0, \Omega_M, \Omega_\Lambda) = (70, 0.3, 0.7)$ cosmology. The squares, stars, triangles and circles show the contributions from the MW disk, MW bulge, M 31 and dwarf galaxies, respectively.

within a volume defined by a 1.5 Mpc radius sphere, each normalized by its current total star formation rate, similar to the Hopkins et al. [6] approach. The cosmic SFH is taken from the compilation of Hopkins & Beacom [5], and scaled to ensure consistency with the Salpeter initial mass function. The shaded area indicates the uncertainty in the star formation rate densities for the Local Group (dominated by a factor of 3 uncertainties in the total star formation histories of the MW and M 31, and in the cosmic star formation rate). The results of this comparison are:

- An excess of the local star formation density in the recent ∼5 Gyr is mainly due to the fluctuations of the star formation of the MW disk.
- Between ∼8 and ∼12 Gyr, the SFH of the LG is broadly consistent with the Cosmic one.
- The early/initial evolution of the LG was dominated by the spheroidal component of the MW and M 31.
- The overall trend of ρ_* from the LG supports a fairly flat evolution of the SFR, suggesting factors ∼10 extinction correction to high-redshift UV-based SFR measures.

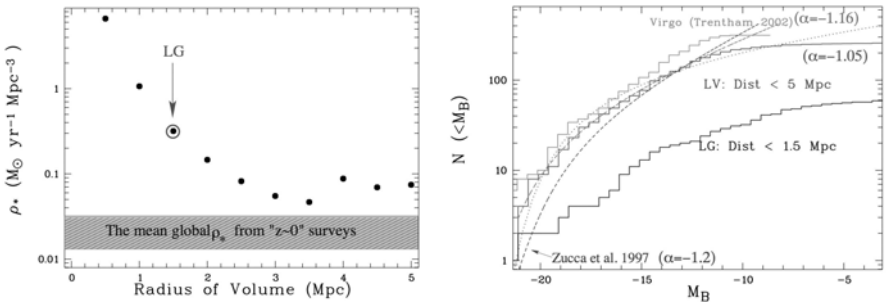

Fig. 2. *(Left:)* Current (Hα) star formation density as a function of volume size (radius sphere). *(Right:)* Integral blue luminosity function (cumulative histogram) for the different samples of nearby Galaxies and fitted Schechter function (dashed lines).

The important question is whether the star formation in the Local Group was representative of the cosmic mean. Following an extension of the Copernican principle, one can assume that the Local Group has no special location in the Universe and hence its SFHs should be explained rather naturally, without appeal to special conditions. Certainly there are some peculiarities of the LG environment (Fig. 2), such as a dominance by two large spirals, an excess of the local current SFR density, and a deficiency of dwarf galaxies in comparison with denser environments. At the same time, about 85% of all galaxies are situated outside the dense environments of rich clusters, with roughly half of them belonging to groups, like the Local Group, while the remaining half are scattered in the 'field' [7]. An extension of the "fossil record" studies to a larger volume will provide the more robust comparison of the Local and Cosmic SFHs.

References

1. A. Aparicio, C. Gallart, C. Chiosi, and G. Bertelli: ApJ, **469**, L97 (1996)
2. T. M. Brown, E. Smith, H. C. Ferguson, et al.: ApJ, **652**, 323 (2006)
3. A. E. Dolphin, D. R. Weisz, E. D. Skillman, & J. A. Holtzman: astro-ph/0506430 (2005)
4. C. Gallart and the LCID team: Rev. Mex. A&A, **29**, 158 (2007)
5. A. M. Hopkins and J. F. Beacom: ApJ, **651**, 142 (2006)
6. A. M. Hopkins, M. J. Irwin, and A. J. Connolly: ApJ, **558**, L31 (2001)
7. I. D. Karachentsev: AJ, **129**, 178 (2005)
8. E. Tolstoy: astro-ph/9807154 (1998)
9. B. F. Williams: AJ, **126**, 1312 (2003)

Dense Molecular Gas in Nearby Southern Starburst Galaxies

Jürgen Ott[1], Christian Henkel[2], Axel Weiß[2], and Fabian Walter[3]

[1] National Radio Astronomy Observatory, 520 Edgemont Road, Charlottesville, VA 22903, USA; jott@nrao.edu
[2] Max-Planck-Institut für Radioastronomie, Auf dem Hügel 69, D-53121 Bonn, Germany; chenkel@astro.umn.edu, aweiss@mpifr-bonn.mpg.de
[3] Max-Planck-Institut für Astronomie, Königstuhl 17, D-69117 Heidelberg, Germany; walter@mpia-hd.mpg.de

Summary. With the Australia Telescope Compact Array, a sample of 8 galaxies have been searched for lines of ammonia, HCN, and HNC. Those molecules are known to trace high-density molecular gas, a gas phase that is closely related to associated star formation. For gas with densities $\gtrsim 10^4$ cm^{-3} we find that the temperature is around $\sim 30 - -50$ K, independent of the surrounding starburst activity. The HCN/HNC ratio, however, becomes $\sim$1.5 where the starburst activity is strongest and increases by factors of a few within a few hundreds of pc. This line ratio gradient likely indicates a gradient of gas density, increasing toward starburst centers with values $\sim 10^6$ cm^{-3} at the peaks. At a stable temperature this translates into higher pressures and pressure support may therefore play a larger role in the stability and formation of molecular clouds in starburst centers. We do not find that an AGN significantly influences the state of the dense molecular gas phase.

1 Introduction

Stars form out of the raw material of molecular clouds. In forming a star, the parent molecular cloud undergoes various stages of gravitational collapse, each time altering its size, dynamics, density, and its chemical and physical state. The physical properties are mainly characterized by density and temperature of the molecular gas and the determination of these properties are key to understand the triggering mechanisms and efficiency of star formation on galactic scales. As pointed out by, e.g., [2], the amount of molecular gas with densities of $\sim 10^2$ cm^{-3}, as traced by CO, and the current star formation rate are described by a power-law distribution which is related to the Kennicutt-Schmidt law [4, 8]. Denser gas masses, however, traced by molecules with larger electric dipole moment such as HCN (H_2 densities $\gtrsim 10^4$ cm^{-3}) correspond linearly to the current rate of star formation and thus is a direct measure of it (see also [5, 2, 11] for a discussion). The study of this dense gas

B.S. Koribalski, H. Jerjen (eds.), *Galaxies in the Local Volume*,
doi: 10.1007/978-1-4020-6933-8_30,

phase is therefore indispensable to understand the state of the molecular gas just before its conversion into stars.

In starburst galaxies, the star formation rate within a certain, mostly nuclear region is much higher than in normal spiral galaxies. This phenomenon leads to the following questions: Under which conditions is a starburst phase initiated? How is a starburst sustained? What causes a starburst phase to stop? And what is the influence of a starburst on its surroundings and the gas and metal contamination of the intergalactic medium? The availability and properties of the dense molecular gas phase play a key role in all the different starburst phases. In turn, the gas is also largely under the influence of stellar feedback, mainly in the form of strong stellar winds and supernova explosions, that may change its ability to collapse, form stars and thus to maintain the starburst phase. — In this contribution, we like to concentrate on high density tracers that share a chemical network. To do so, we chose to observe the nitrogen-bearing molecules ammonia (NH_3), HCN, and HNC that are connected by standard chemistry [7]. Ammonia is known to be an excellent thermometer for dense gas (e.g., [10, 9]). With this parameter known, the low density/high temperature – high density/low temperature degeneracy obtained from solutions of radiative transfer models of purely rotational transitions of linear molecules can be broken, and the density derived. Models for the HCN/HNC ratio are shown in [7].

2 Sample, Observations, and Results

Our sample consists of eight galaxies, listed in Table 1. In addition to nearby starburst galaxies we also included galaxies with active galactic nuclei (AGN) to investigate its influence on the molecular gas. All observations were performed interferometrically with the Australia Telescope Compact Array (ATCA), mainly in its most compact hybrid configurations. The targeted lines were NH_3 (1,1), (2,2), (3,3), and (6,6) at 1.2 cm wavelength, and HCN(1-0) and HNC(1-0) at 3 mm.

Name	Distance [Mpc]	SFR [$M_\odot$ year^{-1}]	AGN present?
NGC 253	2.6	3	no
NGC 4945	3.6	5	yes
Circinus	4.2	2	yes
M 83	4.5	3	no
NGC 1808	14	10	yes
NGC 1365	18	16	yes
NGC 3256	37	63	no
Arp 220	78	286	no

Table 1. Sample of galaxies, their distance and star formation rates. The last column displays the presence of an observed AGN.

The brightest regions of dense molecular gas are found close to the nuclei of their respective hosts, usually at the inner Lindblad resonances. These are

the locations where spiral features connect and which exhibit large optical extinction (for the example of NGC 1365, see Fig. 1).

The ammonia measurements typically reveal two different temperatures (for the methods used to determine the temperatures, see[6]); dense material with ammonia emission shows kinetic temperatures around 30–50 K, absorption spectra against strong radio continuum sources, however, reveal much warmer, less dense components in excess of ∼100 K. Those temperatures are largely independent of whether the molecular cloud is very close to current starburst activity or somewhat further away.

The HCN/HNC ratio varies with a clear trend toward lower ratios at locations toward the strongest starburst activity. Typical values are ∼1.5 at the very center of the starburst in galaxies such as NGC 253, NGC 1365, or M 83. The HNC lines weaken considerably with respect to HCN further away from a starburst and we measure HCN/HNC ratios of ∼4 at distances of a few hundred pc. Galaxies with an AGN but no strong starbursts, e.g., Circinus have larger HCN/HNC ratios of ∼5–9 at any location, similar to normal, non-starburst spirals.

3 Discussion and Conclusions

The gradient of lower HCN/HNC ratios closer to the most active starburst regions and higher values further away might be interpreted in different ways: (a) [7] show that the abundance ratio between the two molecules is close to unity when the gas approaches temperatures of 20 K or less. This effect seems not to be the dominant one in the starburst galaxies as our ammonia-derived kinetic temperatures are closer to 30–50 K. (b) [7, 1] suggest that HNC is produced in even larger quantities than HCN or, in the case of highly ionized molecular gas, in the same quantities via $HCNH^+ + e^-$. At high temperatures, HNC can be converted to HCN via HNC + H → HCN + H [7]. Close to a starburst, much of the atomic gas phase is converted either into molecular gas [3] or ionized by stellar feedback into H^+. Due to the lack of atomic hydrogen, the reaction rate could therefore decelerate, leaving much of the HNC preserved with a resulting lower HCN/HNC ratio. This reaction, however, requires a relatively high activation energy of ∼200 K which seems to be larger than the kinetic temperatures that we find in the dense molecular cores. Nevertheless, this temperature is present in the more tenuous molecular material observed in ammonia absorption. (c) At a given temperature, [7] shows that the HCN/HNC abundance ratio is a function of volume density. At ∼40 K, measured via ammonia, the HCN/HNC ratio becomes unity at densities of $\sim 10^6$ cm^{-3} and HCN/HNC ≈ 10 at 10^5 cm^{-3}. The measured HCN/HNC gradient would therefore correspond to a volume density gradient with high densities close to the starburst center. In addition, if the column densities increase, both, the HCN and HNC lines may become optically thick and produce an HCN/HNC ratio closer to unity. If the HCN/HNC ratio, under

the condition of a relatively stable temperature (see above) can indeed be interpreted as a density gradient, this also implies that the pressure $P/k = nT$ increases toward the starburst centers. Molecular clouds may therefore have a somewhat stronger pressure support component in starburst than in more normal regions of galaxies. For galaxies with an AGN, we do not observe any difference to those without an AGN. We therefore conclude that an AGN has only little influence on the state of the densest phases of molecular gas.

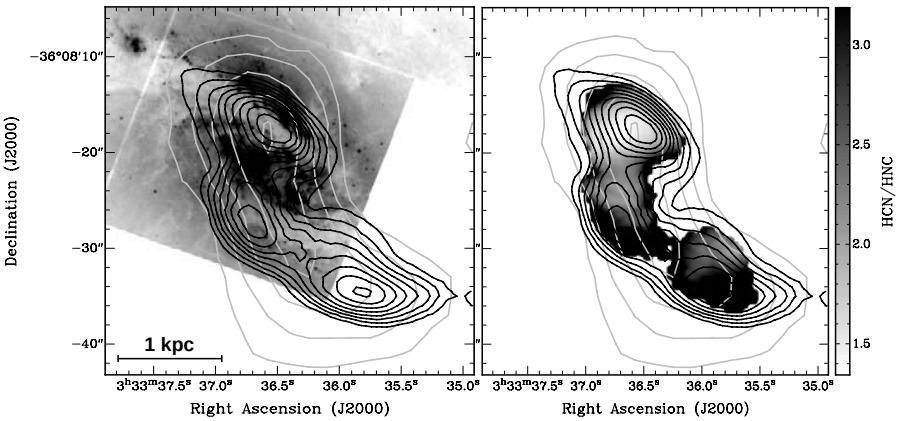

Fig. 1. NGC 1365. *(Left:)* Logarithmic-scaled Hubble Space Telescope F606W image with contours of HCN (*black*) and ammonia (3,3) (*grey*). Ammonia kinetic temperatures are 31 K and 38 K toward the very northern and very southern molecular peaks, respectively. *(Right:)* The same HCN contours overlaid on a map of the HCN (1-0)/HNC (1-0) line ratio. A gradient is visible with the lowest HCN/HNC values closest to the main starburst core.

References

1. Aalto, S., Polatidis, A. G., Hüttemeister, S., & Curran, S. J.: A&A **381**, 783 (2002)
2. Gao, Y., & Solomon, P. M.: ApJ **606**, 271 (2004)
3. Helfer, T. T., Thornley, M. D., Regan, M. W., Wong, T., Sheth, K., Vogel, S. N., Blitz, L., & Bock, D. C.-J.: ApJS **145**, 259 (2003)
4. Kennicutt, R. C., Jr.: ApJ **498**, 541 (1998)
5. Krumholz, M. R., & Thompson, T. A.: ArXiv e-prints, arXiv:0704.0792 (2007)
6. Ott, J., Weiß, A., Henkel, C., & Walter, F.: ApJ **629**, 767 (2005)
7. Schilke, P., Walmsley, C. M., Pineau Des Forets, G., Roueff, E., Flower, D. R., & Guilloteau, S.: A&A **256**, 595 (1992)
8. Schmidt, M.: ApJ **129**, 243 (1959)
9. Ungerechts, H., Winnewisser, G., & Walmsley, C. M.: A&A **157**, 207 (1986)
10. Walmsley, C. M., & Ungerechts, H.: A&A **122**, 164 (1983)
11. Wu, J., Evans, N. J., II, Gao, Y., Solomon, P. M., Shirley, Y. L., & Vanden Bout, P. A.: ApJL **635**, L173 (2005)

NANTEN2 Project: CO and C I Survey of the Local Group

Toshikazu Onishi, Norikazu Mizuno, Akira Mizuno, Yasuo Fukui, and the NANTEN2 Consortium

Nagoya University, Chikusa-ku, Nagoya 464-8602, Japan
ohnishi@a.phys.nagoya-u.ac.jp

1 Introduction

Star formation is a fundamental process that dominates the cycling of various matters in galaxies. Stars are formed in molecular clouds, and the formed stars often affect the parent body of the molecular gas strongly via their UV photons, stellar winds, and supernova explosions. It is therefore of vital importance to reveal the distribution of molecular gas in an entire galaxy in order to investigate the star formation history. Recent progress in developing (sub-)millimeter wave receiver systems has enabled us to rapidly increase our knowledge on molecular clouds, which are the site of star formation. The "NANTEN" telescope has an angular resolution of 2.′6 at 115 GHz and rapidly revealed the molecular view of the Galaxy, LMC, and SMC with its relatively high spatial resolution. The spatial coverage of NANTEN is comparable to or larger than that by CfA 1.2m telescopes in the southern sky [1]. In this paper, I shall introduce some of the results obtained from the NANTEN CO surveys. I shall also present here a project overview and the first observational results of NANTEN2, which is an upgrade of NANTEN to Atacama at an altitude of 4,800m, aiming at realizing large-scale surveys in the Local Group in molecular lines and atomic carbon lines at sub-mm.

2 NANTEN project

The 4-m radio telescope of Nagoya University equipped with the highest sensitivity SIS receiver at 115 GHz allowed us to cover a large area within a reasonable time at an angular resolution high enough to resolve dense cores in nearby (within 1 kpc) dark clouds and also to resolve distant (up to 30 kpc from the sun) giant molecular clouds. In 1996, the 4-m telescope "NANTEN" was installed at Las Campanas observatory in Chile under mutual collaboration with the Carnegie institution of Washington, and we started a CO

B.S. Koribalski, H. Jerjen (eds.), *Galaxies in the Local Volume*,
doi: 10.1007/978-1-4020-6933-8_31,

survey toward the southern sky. Two major works with the NANTEN telescope were a Galactic plane CO survey and the Magellanic Clouds molecular cloud survey. The other projects are to observe various objects including high-mass star forming regions (Carina, Centaurus, Orion, Bright-Rimmed Clouds), SNRs/Supershells (Vela SNR, Gum Nebula, Carina Flare), Galactic center, low-mass star forming regions (Ophuichus, Lupus, Chamaeleon, Pipe nebula), Galactic high-latitude molecular clouds (Aquila, infrared-excess clouds), and so on. Many of the results are presented in two special issues of PASJ 1999 vol. 51 No. 6 and 2001 vol. 53 No. 6.

The Galactic plane survey includes more than 1,100,000 spectra. The observing grid spacings are $4'$ between 5 degrees from the Galactic plane and $8'$ for the area above 5 degrees in the galactic latitude with a $2\farcm6$ beam. In the longitudinal direction almost 200 degrees, i.e., $l = 220^\circ$ to 60° have been covered. The velocity resolution and coverage are 0.65 $\mathrm{km\,s^{-1}}$ and $\sim$500 $\mathrm{km\,s^{-1}}$, respectively. Typical rms noise fluctuations are $\sim$0.4 K at a velocity resolution of 0.65 $\mathrm{km\,s^{-1}}$. One of the notable features seen especially in this survey is the existence of a number of vertical features perpendicular to the galactic plane. This survey leads to a detection of new objects, such as CO supershells created by multiple supernovae (e.g., [2, 7]), molecular floatation loops around the Galactic center [5], and molecular jets which are considered to be formed by jets from high energy sources in the Galactic plane (Yamamoto et al. submitted to ApJ).

The survey in the LMC gave us a complete sample of about 300 molecular clouds with an angular resolution as high as about 40 pc ([3, 4], Fukui et al. submitted). The GMC dataset includes those with different star formation activities throughout the galaxy. We found that about 76% of the GMCs are actively forming stars or clusters, while 24% show no signs of massive star or cluster formation. The number and surface mass densities of the GMCs are higher by a factor of 1.5–2 at the edge of the Super Giant Shells (SGSs) than elsewhere (e.g., [8]). It is also found that young stellar clusters are more actively formed in the GMCs facing to the center of the SGSs. These results suggest the formation of the GMCs and the cluster is triggered by dynamical effects of the SGSs. This LMC survey also resulted in collaboration studies in optical, infrared, H I, and radio continuum wavelengths. Recent infrared observations, Spitzer and AKARI, revealed the distribution and properties of the YSOs and they show that the CO distribution is spatially very well correlated with that of young stars detected in the infrared surveys.

3 NANTEN2 project

The "NANTEN2" is an upgrade of the 4-m mm telescope, NANTEN. The upgrade started by moving NANTEN from Las Campanas to Atacama in Northern Chile at an altitude of 4,800m in 2004 to realize a large-scale survey at sub-mm wavelengths. In this new project, we will make large-scale surveys

toward the Galaxy and nearby galaxies including the Magellanic Clouds mainly in submillimeter wavelength. We will reveal the physical and chemical states of the interstellar gas in various density regions with the highly excited CO (carbon-monoxide) and CI (neutral carbon) spectra at sub-millimeter wavelength (100–800 GHz). With thorough extensive surveys, we will make studies of star formation process in the Local Group and investigate the dynamical effects of energetic explosive events like supernovae and supershells on the interstellar matter.

We installed a new main dish to achieve the sub-mm observations for NANTEN2. It consists of 33 aluminum panels that are adjustable with actuators (3 for each panel), and a light-weight carbon fiber back structure. After adjustment of the main reflector using photogrammetry and holography, the expected surface accuracy is 15 micron rms. The new telescope is enclosed in a dome with a shiftable GoreTex membrane to prevent perturbations such as strong wind and sunlight. The installation started at the beginning of 2004. We successfully started sub-mm observations in September 2006, with a 490/810 GHz single-channel receiver. The beam sizes and main beam efficiencies at 460 GHz and 810 GHz are measured to be $\sim 38''/50\%$ and $\sim 23''/45\%$, respectively. The pointing accuracy is less than $10''$ if we observe pointing sources frequently. The observed targets include high-mass star forming regions, the Galactic center, LMC/SMC, nearby galaxies and so on. Some of the results were submitted to the Astronomy and Astrophysics (Kramer et al. for Carina cloud and Hitschfeld et al. for NGC 4945/Circinus).

The highest observing frequencies will be covered by KOSMA SMART (Sub-Millimeter Array Receivers for Two frequencies) receiver [6], a new multibeam receiver capable of observing both 490 GHz and 810 GHz radiation simultaneously and effectively. The lower frequencies, 230 GHz and 345 GHz, will be covered by single pixel receivers developed by Nagoya University, which will be used for the Galactic plane and LMC molecular cloud survey with a spatial resolution of $\sim 1'$. These two receiver systems can be easily switched according to the sky opacity.

NANTEN2 will be equipped with such low-noise superconducting receivers and the field of view of NANTEN2 is larger than those of ASTE, APEX, and ALMA. NANTEN2 will be suitable to cover a large sky area within a short observation time while the resolution is coarser than those of these other telescopes. In this sense, NANTEN2 and other telescopes in Atacama are complementary relationship. The NANTEN2 observations provide a large database of interstellar matter in the Galaxy and the Magellanic Clouds. This database must be a useful guide for the future science with ALMA.

This project is in collaboration between universities in Japan (Nagoya Univ. and Osaka Prefecture Univ.), in Germany (Univ. of Cologne and Univ. of Bonn), in South Korea (Seoul National Univ.), in Chile (Univ. of Chile), in Australia (Univ. of New South Wales, Sydney Univ. and Macquarie Univ.), and Switzerland (ETH Zurich).

Acknowledgements
The NANTEN project is based on the mutual agreement between Nagoya University and the Carnegie Institution of Washington. We acknowledge that this project was able to be realized by contributions from many Japanese public donators and companies. This work is financially supported in part by a Grant-in-Aid for Scientific Research from the Ministry of Education, Culture, Sports, Science and Technology of Japan (No. 15071203) and from JSPS (No. 14102003, core-to-core program 17004 and No. 18684003).

Fig. 1. NANTEN2 telescope

References

1. T. M. Dame, D. Hartmann, P. Thaddeus: ApJ **547**, 792 (2001)
2. Y. Fukui, T. Onishi, R. Abe, A. Kawamura, K. Tachihara, R. Yamaguchi, A. Mizuno, H. Ogawa: PASJ **51**, 751 (1999)
3. Y. Fukui et al.: PASJ **51**, 745 (1999)
4. Y. Fukui, N. Mizuno, R. Yamaguchi, A. Mizuno, T. Onishi: PASJ **53**, 41 (2001)
5. Y. Fukui et al.: Science **314**, 106 (2006)
6. U. U. Graf, et al.: Millimeter and Submillimeter Detectors for Astronomy. Edited by Phillips, Thomas G.; Zmuidzinas, Jonas. Proceedings of the SPIE **4855**, 322 (2003)
7. K. Matsunaga, N. Mizuno, Y. Moriguchi, T. Onishi, A. Mizuno, Y. Fukui: PASJ **53**, 1003 (2001)
8. R. Yamaguchi, N. Mizuno, A. Mizuno, M. Rubio, R. Abe, H. Saito, Y. Moriguchi, K. Matsunaga, T. Onishi, Y. Yonekura, Y. Fukui: PASJ **53**, 985 (2001)

The Mass-to-Light Ratios of Spiral Disks

Robin Ciardullo and Kimberly A. Herrmann

Department of Astronomy & Astrophysics, Penn State University, 525 Davey Lab, University Park, PA USA 16802 rbc@astro.psu.edu, herrmann@astro.psu.edu

1 The Experiment

Our understanding of galaxy formation is severely limited by our lack of knowledge about galactic mass profiles. We know that disk galaxies are surrounded by dark matter halos, but from the rotation curve alone, it is impossible to decouple the gravitational contribution of the halo from that of the disk. While it is possible to glean some information about disk baryons from population synthesis models, what is really needed are dynamical measurements of disk mass surface density.

In principal, this is straightforward. In a rotating disk, the velocity dispersion of stars in the direction perpendicular to the disk is directly proportional to disk surface mass, Σ. For an isothermal disk

$$\sigma_z^2(R) = \pi G \Sigma(R) z_0, \tag{1}$$

where z_0 is the scale height of the stars. Since studies of edge-on spirals yield measurements of z_0 that are constant with radius, velocity dispersion measurements in face-on galaxies can provide a direct measure of disk mass.

Stellar velocity dispersions for a few face-on galaxies have been obtained via integrated-light absorption-line spectroscopy [1, 2, 3]. Unfortunately, these data only extend one to two disk scale lengths. To go out further, to radii where the dark matter begins to dominate, one needs to observe individual stars of the old disk. Planetary nebulae (PNe) are ideal for this purpose. In a large spiral galaxy, one can easily detect $\sim$200 of these objects with a 4-m class telescope, and each PN can be measured with $\sim$5 $\mathrm{km\,s^{-1}}$ precision. Moreover, since all populations with ages between $\sim$1 and $\sim$10 Gyr make planetary nebulae, there is no doubt that PNe sample the old disk of the galaxy, and not a younger, non-equilibrium component.

We have been conducting a kinematic survey of planetary nebulae in the 6 face-on spiral galaxies given in Table 1. Listed are our survey radius, the number of PNe measured photometrically and spectroscopically, and the galaxy's

B.S. Koribalski, H. Jerjen (eds.), *Galaxies in the Local Volume*,
doi: 10.1007/978-1-4020-6933-8_32,

inclination, R-band disk scale length, foreground reddening, and distance, as determined from the PN luminosity function [4, 5]. Note that none of the galaxies are precisely face-on: in addition to σ_z, the PN velocities also reflect galactic rotation and the other two components of the disk's velocity ellipsoid.

Table 1. Program Galaxies

Galaxy	$r_{\rm survey}$	N(phot)	N(spec)	i	r_0	$E(B-V)$	D(Mpc)
M 33	$33'$	152	140	56°	$8'.2$	0.041	0.94 ± 0.04
M 74	$5'$	192	83	6.5°	$1'.3$	0.070	8.2 ± 0.2
M 83	$10'$	235	127	24°	$1'.5$	0.066	4.8 ± 0.1
M 94	$5'$	149	123	35°	$0'.7$	0.018	4.5 ± 0.2
M 101	$8'$	65	60	17°	$2'.3$	0.009	7.4 ± 0.5
IC 342	$7'$	167	90	25°	$4'.2$	0.558	3.5 ± 0.3

Removing rotation is straightforward: we can simply use H I rotation curves from the literature and later apply a small correction for asymmetric drift. Separating out σ_z from the radial (σ_R) and azimuthal (σ_φ) components of the velocity ellipsoid is a bit harder, and requires measurements of the line-of-sight velocity dispersion at different position angles around the galaxy. We can eliminate σ_φ from consideration since the disk orbits are close to circular and obey the epicyclic approximation

$$\sigma_\varphi^2 = \sigma_R^2 \left(\frac{1}{2} + \frac{1}{2} \frac{\partial \ln V_{\rm circ}}{\partial \ln R} \right) \tag{2}$$

However to remove σ_R, we need to invoke stability arguments. To be stable against disk buckling, $\sigma_z > 0.25\,\sigma_R$ [6]. Moreover, if we combine the Toomre criterion against axisymmetric perturbations [7] with the isothermal disk equation, then

$$Q \equiv \frac{\sigma_R \kappa}{3.36 G \Sigma(R)} > 1 \quad + \quad \sigma_z^2 = \pi G z_0 \Sigma(R) \quad \Longrightarrow \quad \sigma_z^2 < \left(\frac{\kappa \pi z_0}{3.36} \right) \sigma_R \tag{3}$$

where κ, the epicyclic frequency of the orbits, is known from the rotation curve.

$$\kappa = \frac{V_{\rm circ}}{R} \left(2 + 2\,\frac{\partial \ln V_{\rm circ}}{\partial \ln R} \right)^{1/2} \tag{4}$$

This places a severe constraint on the possible combinations of σ_R and σ_z which can generate the line-of-sight velocity dispersion.

2 Results

Plotted in Fig. 1 are our derived values of σ_z, along with the behavior expected from constant mass-to-light ratio disks. The figure demonstrates that in the

inner disks, the constant mass-to-light assumption is valid. This agrees with integrated-light absorption-line measurements [1, 2, 3]. However in the outer disks, there is evidence for excess mass. This is particularly true for M 33 and M 101, which have kinematic scale lengths that are larger than their optical scale lengths. M 94's disk appears to have a constant mass-to-light ratio over its inner $\sim$ 4 scale lengths ($\sim$ 5 kpc), but then the disk mass surface density flattens. The most remarkable object is M 83, whose z-direction velocity dispersion appears almost constant over 5 disk scale lengths.

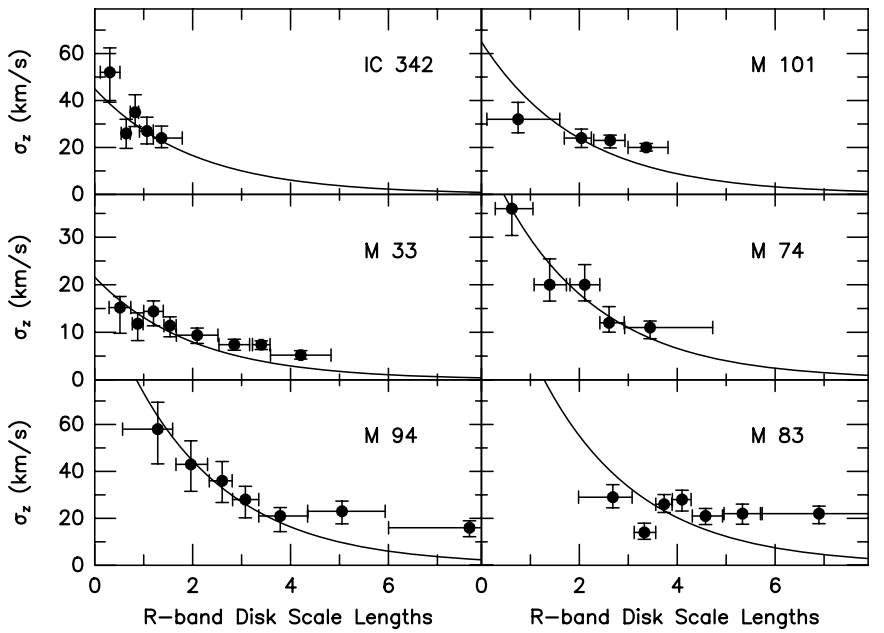

Fig. 1. The z-direction velocity dispersion for planetary nebulae in the disks of six face-on spirals. The curves give the trend expected for constant mass-to-light ratio disks. Note the relatively large velocity dispersions present at large radii.

In the *left panel* of Fig. 2, we adopt scale lengths and central surface brightnesses from the literature and translate our values of disk mass into mass-to-light ratios. At first glance, the data appear to suggest the presence of large amounts of dark matter in the galaxies' outer disks. However, this is likely due to the uncertain extrapolation of the galaxies' surface brightness, rather than a physical effect. As the right hand panel of Fig. 2 demonstrates, when we use PN number counts to estimate population luminosity (assuming the disk produces $2 \times 10^{-9}\,\mathrm{PN}\,L_{\odot}^{-1}$ in the top half magnitude of luminosity function [8]), the high mass-to-light ratios disappear. Bright PNe are not ideal tracers of surface brightness, since their numbers can be affected by extinction

and their production rate is population dependent. But the data do point out the need to acquire better surface photometry in the outer parts of galaxies.

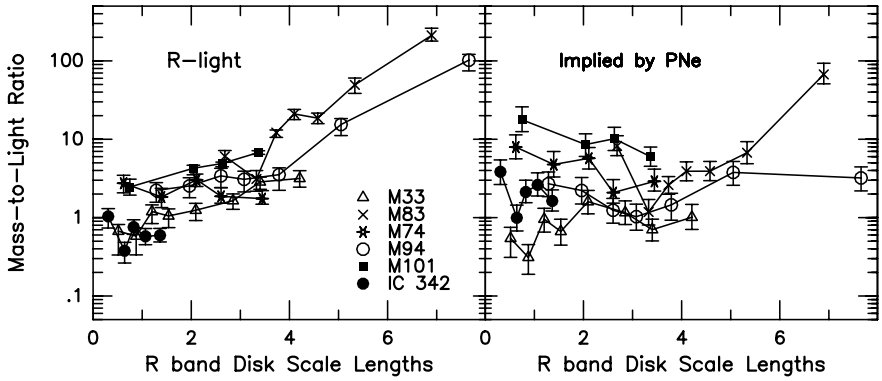

Fig. 2. Disk mass-to-light ratio as a function of radius for the six face-on spirals. The *left panel* uses (and extrapolates) disk surface brightnesses from the literature; the *right panel* uses our PN number counts to infer disk brightness.

The preliminary results presented above are somewhat sensitive to the chosen value of z_0, since the derived values for surface mass are inversely proportional to this scale height. This effect is somewhat mitigated by the presence of z_0 in the stability equations, but if spiral disks flare in their outer regions, then our dynamical masses will be overestimates.

We are in the process of completing our PN surveys in these six large spirals. In particular, more velocities will shortly be available in M 74, M 83, and IC 342. When combined with improved optical and infrared surface photometry, our data will produce the first kinematically-measured mass-to-light ratios for the outer disks of a large set of spiral galaxies.

References

1. R. Bottema: A&A **275**, 15 (1993)
2. J. Gerssen, K. Kuijken, M.R. Merrifield: MNRAS **288**, 618 (1997)
3. J. Gerssen, K. Kuijken, M.R. Merrifield: MNRAS **317**, 545 (2000)
4. R. Ciardullo, J.J. Feldmeier, G.H. Jacoby, R.K. de Naray, M.B. Laychak, P.R. Durrell: ApJ **577**, 31 (2002)
5. R. Ciardullo: Extragalactic Distances from Planetary Nebulae. In: *Lecture Notes in Physics: Stellar Candles for the Extragalactic Distance Scale*, vol 635, ed by W. Gieren, D. Alloin (Springer-Verlag, Heidelberg) pp 243–263
6. D. Merritt, J.A. Sellwood: ApJ **425**, 567 (1994)
7. A. Toomre: ApJ **139**, 1217 (1964)
8. R. Ciardullo, S. Sigurdsson, J.J. Feldmeier, G.H. Jacoby: ApJ **629**, 499 (2005)

The Surprisingly Abnormal Halo of the "Normal" Elliptical Galaxy, NGC 3379

Elizabeth Wehner[1], William Harris[1], Gretchen Harris[2], and Andrew Layden[3]

[1] McMaster University, Hamilton, ON, Canada wehnere@physics.mcmaster.ca, harris@physics.mcmaster.ca
[2] University of Waterloo, Waterloo, ON, Canada glharris@astro.uwaterloo.ca
[3] Bowling Green State University, Bowling Green, OH, USA layden@baade.bgsu.edu

1 Introduction

NGC 3379, an E1 giant in the nearby Leo I group, is often considered (quite literally) to be a textbook example of a normal elliptical galaxy. Typical elliptical galaxies are expected to contain a substantial metal-rich stellar component in their outer halos. A previous study by [1], which used HST WFPC2 to examine halo stars, finds red stellar colors out to $6'$ from NGC 3379's center. More recently, [2] find almost solar values of metallicity in their near-IR study of the NGC 3379 red giant branch stars at distances out to the same $6'$ location (17 kpc) from the galaxy's center. In order to probe this trend at higher radii, we obtained deep ACS V and I-band data on a field extending out to 27–38 kpc.

2 Results and Discussion

Our field of view was chosen to probe "true" halo stars, and as such, is located twice as far from the center as the most far reaching previous study of NGC 3379. Our ACS field was placed at a distance of $10\farcm9$ or 33 kpc projected radius from the galaxy's center (see Figure 1). In total, we measured $\sim$5300 giant stars in our field of view. The color-magnitude diagram is shown in Figure 2. These data reveal a surprisingly flat metallicity distribution, quite atypical for an elliptical galaxy – NGC 3379 contains an unusually high number of blue, metal-poor stars.

Upon closer inspection, the blue and red stars are also distributed differently across the frame. As can be seen in Figure 3, these data reveal a surprising and unique metallicity distribution: the stars more metal-rich than $[m/H] = -0.7$ fall off rapidly in number with galactocentric distance, whereas

B.S. Koribalski, H. Jerjen (eds.), *Galaxies in the Local Volume*,
doi: 10.1007/978-1-4020-6933-8_33,

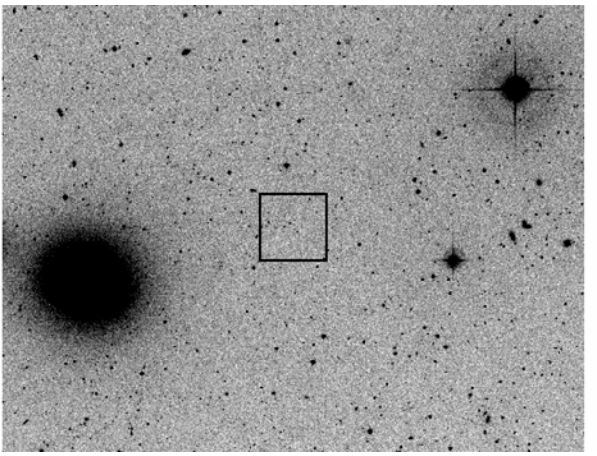

Fig. 1. NGC 3379 and the location of our ACS field.

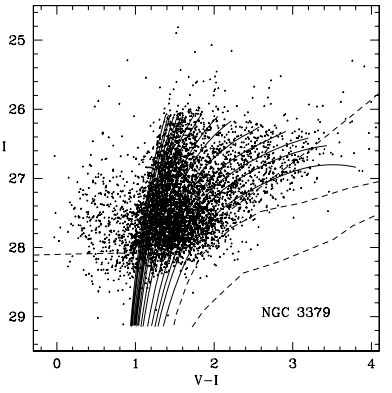

Fig. 2. Color-magnitude diagram for the NGC 3379 red giants, with model red-giant tracks superimposed on the data points. All tracks are for ages of 12 Gyr, but differ in metallicity roughly in steps of $\Delta[Fe/H] \simeq 0.1$. Tracks are from [3].

the bluer, more metal-poor stars are more smoothly distributed across the field (see Figure 4).

To better understand this unusual metallicity distribution, we fit a simple, accreting-box accreting model (see [4] for more details) shown in Figure 5. Unlike all other E galaxies for which we know about their stellar metallicity distribution, NGC 3379 requires at least two distinct chemical evolution components to fit its combined MDF. These results suggest we may be seeing an extended disk or bulge component in this galaxy, such as that seen in M 31, that reaches its "edge" near 35 kpc, while at still larger radii the more

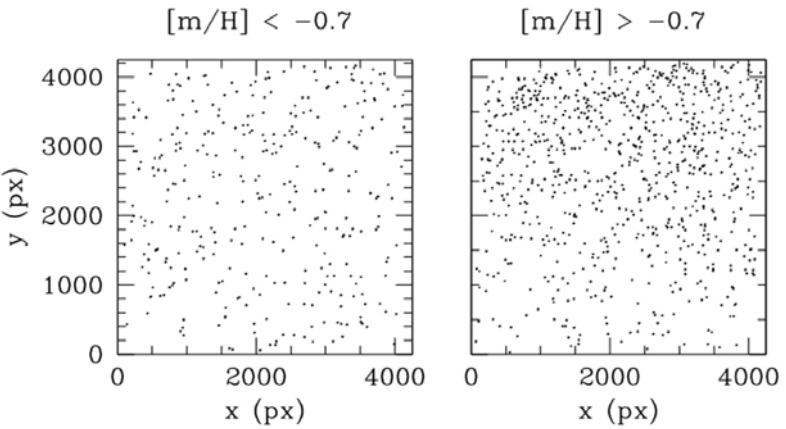

Fig. 3. Positions of the bright stars on the ACS image, in the magnitude range $26.0 < I < 27.3$. The center of NGC 3379 is off the diagram at the top. The *left panel* shows the blue, metal-poor RGB stars ([m/H] < 0.7, equivalent to Z < 0.2 $Z_\odot$) while the *right panel* shows the red, metal-richer giants ([m/H] > 0.7). The red population exhibits a much stronger gradient in number density across the frame.

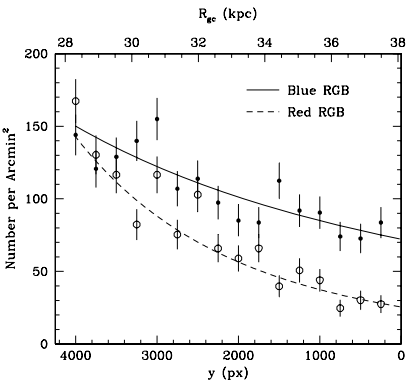

Fig. 4. Number density σ (number of stars per arcmin^2) as a function of position on the image. The solid symbols and solid line show the data for the blue, metal-poor stars with [m/H] < 0.7 plotted in the previous figure. The open symbols and dashed line show the same data for the red, metal-rich group with [m/H] > 0.7. The numbers along the top border of the plot give the projected distance R_{gc} (in kpc) from the center of NGC 3379. The blue population density falls off with radius as $\sigma \sim R^{-1.2}$ (solid curve) while the red population falls off as $\sigma \sim R^{-6.0}$ (dashed curve).

metal-poor component – perhaps a Milky-way like classical halo – continues outward. Our fortunate choice of field location maps the transition point between these two populations.

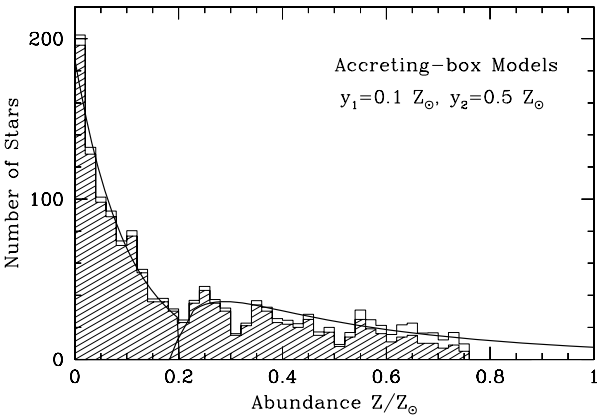

Fig. 5. Histogram of heavy-element abundance distribution, plotted in linear form as number of stars per unit $Z/Z_{\odot}$. The predicted N(Z) distributions for each stage of a two-stage chemical evolution model are shown as solid lines. The low metallicity component has an effective yield $y_{eff} = 0.1\ Z_{\odot}$, and the higher-metallicity component starts with pre-enriched gas and has an effective yield 5 times higher

We suggest that one important difference between our work and other halo studies conducted at similar physical distances from their respective galaxy centers (such as [5, 6]), is that our field is at a larger radius in units of the galaxy's effective radius than any other previous work. We suggest that more studies at $R \geq 10\ R_{eff}$ are required to detect the emergence of a "classical", metal-poor halo in other galaxies.

References

1. Sakai, S., Madore, B.F., Freedman, W.L., Lauer, T.R., Ajhar, E.A., & Baum, W.A. 1997: ApJ, 478, 49
2. Gregg, M.D., Ferguson, H.C., Minniti, D., Tanvir, N., & Catchpole, R. 2004: AJ, 127, 1441
3. VandenBerg, D.A., Swenson, F.J., Rogers, F.J., Iglesias, C.A., & Alexander, D.R. 2000: ApJ, 532, 430
4. Harris, W.E., Harris, G.L.H., Layden, A. C., & Wehner, E.M.H. 2007: ApJ, 666, 903
5. Harris, W.E., & Harris, G.L.H. 2002: AJ, 123, 3108
6. Rejkuba, M., Greggio, L., Harris, W.E., Harris, G.L.H., & Peng, E.W. 2005: ApJ, 631, 262

Infrared Study of the SNR Evolution in NGC 6946

Tom H. Jarrett[1], J. Rho[1], W. Reach[2], and P. Appleton[3]

[1] Spitzer Science Center, USA jarrett@ipac.caltech.edu
[2] Planck Science Center, USA reach@ipac.caltech.edu
[3] Herschel Science Center, USA apple@ipac.caltech.edu

We present ground-based near-infrared imaging and Spitzer Space Telescope mid-infrared imaging of the nearby ($D \sim 6$ Mpc) starburst galaxy NGC 6946, focusing on the extensive population of supernova remnants (SNRs). Selected from deep NIR imaging of the shock-sensitive emission lines [Fe II] 1.644μm and H_2 2.121μm, the SNRs are predominately located in the spiral arms where core-collapse supernovae trace the ongoing massive star formation. The SNR sample represents a set of evolutionary 'snapshots', following the earliest stages of a remnants life through the adiabatic expansion phase and into the radiative 'snow-plow' phase. In combination with an extensive body of radio-to-Xray data we use our 'snapshot' sample to study how the interaction between supernovae and their birth clouds evolve from the earliest stages to the relatively mature phase in which the remnant settles back into the ISM.

1 Introduction

Supernovae (SNe), though rare, are one of the most important sources of energy input to the interstellar medium (ISM). When a massive star ends its life in a supernova explosion, it often does so in the molecular cloud complex in which it was born. SNe compress, heat, ionize and chemically alter the surrounding atomic and molecular gas, as well as accelerate particles associated with the ISM. The direct impact of the blast wave on clumps, the thermal radiation from the hot interior of the SN, and the cosmic rays should visibly perturb the excitation, chemistry, and dynamics of the ISM. Strong shocks alter or destroy dust grains in molecular clouds, thereby liberating iron back into the gas phase on time scales $\sim 10^2 - 10^4$ years [1]. In the extended post-shock region photo-ionization produces a cooling zone of strong [Fe II] emission arising from medium density gas ($n \sim 10^2 - 10^3$ cm^{-2}) of iron-rich ejecta and dust-liberated iron, while fluorescent and collisionally-excited H_2 lines of the 1-0 vibrational state arise at higher densities, $n > 10^3$ cm^{-2} [2, 3, 4]. In the

B.S. Koribalski, H. Jerjen (eds.), *Galaxies in the Local Volume*,
doi: 10.1007/978-1-4020-6933-8_34,

near-infrared, [Fe II] at 1.644μm is exceptionally bright for SNRs, typically 10 times brighter than Br-γ [5], and yet is only weakly detected in H II regions [6].

2 Searching for Embedded Supernova Remnants in NGC 6946

We have made a substantial effort to search for and study Galactic SNRs interacting with clouds using the near-infrared [Fe II] 1.64μm and H_2 (1-0) 2.12μm lines [7, 8, 9, 10]. These lines are just bright enough to be detected in nearby galaxies using large ground-based telescopes, thus permitting simultaneous study of multiple SNRs under diverse conditions and evolutionary stage [11]. For this reason we have recently undertaken a detailed NIR study of the prodigious SN-producing galaxy NGC 6946. Through our very deep emission-line images we have identified dozens of SNR candidates, predominately located in the spiral arms where core-collapse SNe trace the ongoing massive star formation (Fig. 1). Our SNR sample represents a set of evolutionary snapshots, following the earliest stages of a remnants life, t $\sim$ few years, through the adiabatic expansion phase and into the radiative snow-plow phase, t $\sim 10^5$ years. In the mid-infrared, lower-excitation transitions arise from the warm gas component, representing the bulk of the ISM that is modified by the blastwave and post-shock radiation. With [Fe II] selecting SNRs ranging through this evolutionary span, Spitzer imaging and spectroscopy may be used to uniquely study how the interaction between SNe and their birth clouds evolve from the earliest stages to the relatively mature state in which the remnant settles back into the ISM.

There are several factors that make NGC 6946 an ideal laboratory to study SNRs. It is relatively nearby, $\sim$5.9 Mpc [12], allowing for detailed study on size scales smaller than molecular clouds ($1'' = 29$ pc). The face-on spiral arms are free from confusing projection effects, allowing study of its vigorous star-formation in the nucleus and spiral arms, which possess a wide diversity in density, temperature and metallicity ISM conditions [13, 14]. It is also one of the most studied galaxies in the local Universe, it holds the distinction of being the first extragalactic source in which the H_2 molecule was detected in its MIR rotational transitions [15] and is part of the Spitzer Infrared Nearby Galaxy Survey (SINGS; [4]), featuring comprehensive Spitzer imaging and spectroscopy of the nucleus and a select set of H II regions in the disk. Lastly, NGC 6946 is a veritable supernova factory, with eight SNe observed in the last 50 years, the latest being SN2004et [17], and dozens of radio and X-ray remnants identified throughout the disk and nucleus.

3 Narrow-band Imaging Results

We have identified more than 25 [Fe II] 1.64μm SNR candidates using our deep NIR line imaging obtained with the Hale 200" telescope of the Palomar

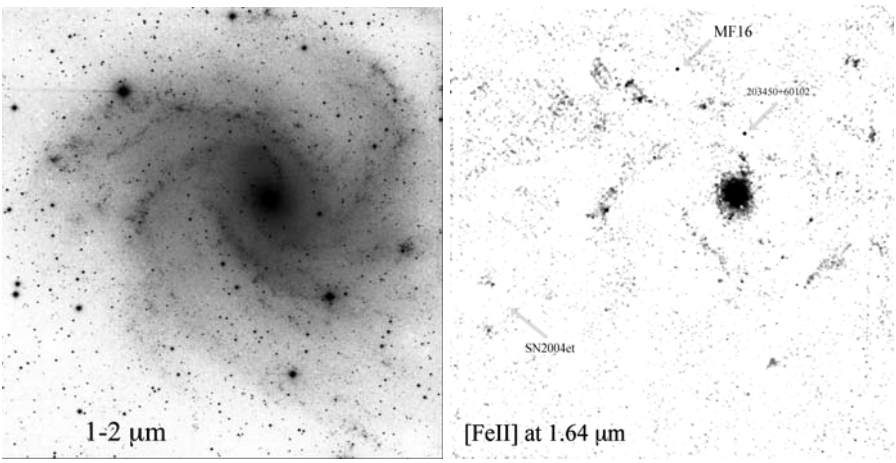

Fig. 1. The galaxy NGC 6946 as seen in the near-infrared. The *left panel* shows a combined 1–2.2μm mosaic of a $\sim 12'$ field. The *right panel* shows the 1.64μm [Fe II] emission map of the same field. The most prominent detections are indicated with arrows: 203500+60113 (MF16) and 203450+60102, both located north of the nucleus. Also indicated, the recent supernova, SN2004et, does not have [Fe II] or H_2 in emission.

Observatory; Fig. 1a shows the combined near-infrared continuum mosaic of NGC 6946, and Fig. 1b shows the resulting [Fe II] line emission. The brightest [Fe II] sources are denoted with arrows. Most of the [Fe II] sources are spatially correlated with non-thermal radio sources [18] and X-ray sources [19], signifying young remnant ages ($t < 10^4$ years; [20]). Comparing the [Fe II] with radio continuum, Fig. 2a, a linear trend likely arises from mutually density-dependent synchrotron and [Fe II] emission mechanisms. The one notable outlier in the radio-NIR trend, 203450+60102, is deeply embedded in an H II complex; consequently, the [Fe II] may also arise from photodissociation regions (PDRs).

The brightest [Fe II] source, 203500+60113 ("MF16"), see Fig. 2b, is also extremely bright in optical Hα and [S II] [21], and is the most luminous X-ray SNR known [19] with $L_x \sim 10^{40}$ ergs s^{-1}. The true nature of the source remains quite uncertain; possible scenarios include multiple SN explosions, blast-waves interacting with multiple pulsars, jet-beaming or a micro-blazar activity, and intermediate blackhole accretion. Strong [Fe II] and H_2 emission, confined to a point-like source (beam $\sim 1'' - 2''$), see Fig. 2b, must arise from strong shocks that are modifying the gas. The 1.64μm and mid-infrared emission is consistent with a SN blast-wave in a clumpy medium, but may also be associated with a pre-collapse jet that is now impacting the dense gas, similar to what is seen for W49B [10] in the Milky Way.

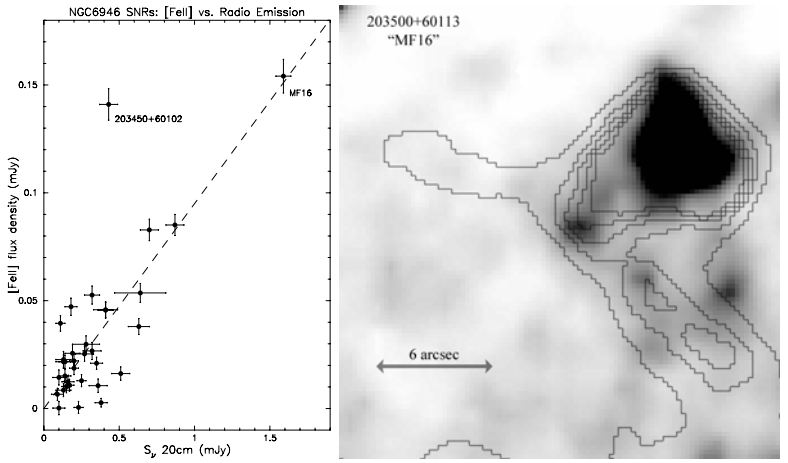

Fig. 2. The *left panel* shows the comparison between the 1.64μm [Fe II] emission and the 20cm radio continuum for the SNR candidates. The radio data comes from [22] and [18]. The *right panel* shows the mid-infrared view of the ultra-luminous X-ray source MF16 (203500+60113). The Spitzer IRAC 4.5μm grey-scale is overlaid with contours from the Spitzer IRAC 8.0μm mosaic. The remnant is clearly seen in the 4.5μm window, bolstered by H_2 and [Fe II] lines, while the morphology at 8.0μm hints at the presence of the emission, also indicative of H_2 ro-vibrational emission.

References

1. Tielens, A, et al., 1994, ApJ, 431, 321
2. Hollenbach, D. J., & McKee, C. F. 1989, ApJ, 342, 306
3. Oliva, E., Moorwood, A., Danziger, I. 1989, A&A, 214, 307
4. Mouri, H., Nishida, M., Taniguchi, Y., & Kawara, K. 1990, ApJ, 360, 55
5. Alonso-Herrero, A., Rieke, M. J., Rieke, G. H., & Ruiz, M. 1997, ApJ, 482, 747
6. Graham, J. R., Wright, G. S., & Longmore, A. J. 1987, ApJ, 313, 847
7. Reach, W., & Rho, J, 2000, ApJ, 544, 843
8. Rho, J., et al., 2003, ApJ, 529, 299
9. Reach, W., Rho, J, & Jarrett, T. 2005, ApJ, 618, 297
10. Keohane, J.W., Reach, W., Rho, J. & Jarrett, T.H., 2007, ApJ, 654, 938
11. Morel, T., Doyon, R., & St.-Louis, N. 2002, MNRAS, 329, 398.
12. Karachentsev, I., Sharina, M., & Huchtmeier, W. 2000, A&A, 362, 544
13. Ball, R., Sargent, A., Scoville, N., Lo, K., & Scott, S. 1985, ApJ, 298, L21
14. Elmegreen, D., Chromey, F., & Santos, M. 1998, 116, 1221
15. Valentijn, E. A., et al., 1996, A&A, 315, 145
16. Kennicutt, R. et al., 2003, PASP, 115, 928
17. Rho, J., Jarrett, T., Chugai, N, Chevalier, R. 2007, ApJ, in press
18. Lacey, C., & Duric, N. 2001, ApJ, 560, 719
19. Holt, S., Schlegel, E., Hwang, U., Petre, R. 2003, ApJ, 588, 792
20. Hirashita, H. & Hunt, L. 2006, A&A, 460, 67
21. Matonick, D., & Fesen, R. 1997, ApJS, 112, 49
22. Lacey, C., Duric, N., & Goss, W. M. 1997, ApJS, 109, 417

Modeling Non-Circular Motions in Disk Galaxies: A Bar in NGC 2976

Kristine Spekkens[1,2] and J.A. Sellwood[2]

[1] National Radio Astronomy Observatory (NRAO)[†], USA
[2] Department of Physics and Astronomy, Rutgers, the State University of New Jersey, 136 Frelinghuysen Road, Piscataway, NJ, USA 08854
spekkens@physics.rutgers.edu, sellwood@physics.rutgers.edu

Summary. We give a brief description of a new model for non-circular motions in disk galaxy velocity fields, that does not invoke epicycles. We assume non-circular motions to stem from a bar-like or oval distortion to the potential, as could arise from a triaxial halo or a bar in the mass distribution of the baryons. We apply our model to the high-quality CO and Hα kinematics of NGC 2976 presented by [5]; it fits the data as well as their model with unrealistic radial flows, but yields a steeper rotation curve. Our analysis and other evidence suggests that NGC 2976 hosts a bar, implying a large baryonic contribution to the potential and thus limiting the allowed dark matter halo density.

1 Introduction

A robust determination of the mass distribution in a spiral galaxy from its kinematics requires an estimate of the contribution from non-circular motions to the observed flow pattern. With the availability of high-quality velocity fields for many galaxies in the local volume (e.g. Koribalski, Walter, this volume), detailed studies of the importance of non-circular motions in spirals are now feasible.

The flow pattern of an observed velocity field is typically analysed by performing an harmonic analysis in each of a series of concentric rings (e.g., [1, 3]). Standard practice is then to invoke perturbed epicycle theory to interpret the resulting kinematic components in terms of physical processes or structures in the disk (e.g., [3]). However, some nearby systems exhibit non-circular flows whose amplitudes rival that of the inferred mean orbital speed $\bar{V}_t(r)$ (e.g., [5]): the epicyclic approximation breaks down in this case, and the mass distribution derived by assuming that $\bar{V}_t(r)$ reflects circular orbital balance in the system (ie. adopting $\bar{V}_t(r)$ as the "rotation curve") is suspect.

[†] NRAO is a facility of the National Science Foundation operated under cooperative agreement by Associated Universities, Inc.

B.S. Koribalski, H. Jerjen (eds.), *Galaxies in the Local Volume*,
doi: 10.1007/978-1-4020-6933-8_35,

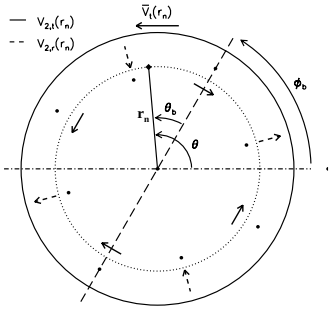

Fig. 1. Bisymmetric model flow pattern in the disk plane. The horizontal dash-dotted line is the major axis. The diamond denotes a point at (r_n, θ), and the arrows show the extrema of $V_{2,r}(r_n)$ and $V_{2,t}(r_n)$. Adapted from Fig. 1 of [6].

We recently presented a new technique for fitting generalized non-axisymmetric flow patterns to velocity fields without making the epicyclic approximation [6]. We summarize this work here, and focus on a model in which flows stem from a bisymmetric distortion to an axisymmetric potential (Sect. 2). The model describes the kinematics of NGC 2976 presented by [5] as well as that from their harmonic analysis. We find a steeper rotation curve in NGC 2976 than estimated by these authors, which we attribute to a large baryonic contribution from a bar (Sect. 3).

2 The Bisymmetric Model

We attempt to fit the non-circular motions in observed velocity fields by making the following assumptions: (1) The non-circular flow stems from a bar-like or oval distortion to the potential. (2) Since the dominant kinematic signature of a bisymmetric distortion to the potential is also bisymmetric (e.g. [4]), harmonics of order $m > 2$ are neglected. (3) The non-circular motions are oriented about a fixed axis ϕ_b, with the radial and tangential components of the flow exactly out of phase with each other as required in a steady bar-like flow (e.g. [4]). (4) The disk is flat, and thus has the same inclination i at all radii r.

The bisymmetric model $V_{\rm model}(r, \theta)$ at some general point in the deprojected velocity field is therefore described by:

$$\frac{V_{\rm model} - V_{\rm sys}}{\sin i} = \bar{V}_t \cos\theta - V_{2,t} \cos(2\theta_b) \cos\theta \; - \; V_{2,r} \sin(2\theta_b) \sin\theta \; , \qquad (1)$$

and the geometry in the disk plane is shown in Fig. 1. The phases θ and θ_b are the angles relative to the major axis and bisymmetric flow axis (or bar axis), respectively, and $V_{\rm sys}$ is the disk systemic velocity. The non-parametric profiles $V_{2,r}(r)$ and $V_{2,t}(r)$ are the radial and tangential components of the bisymmetric flow.

For comparison with the work of [5] we also consider a radial flow model, that is equivalent to a harmonic analysis including only $m = 0$ terms:

$$\frac{V_{\rm model} - V_{\rm sys}}{\sin i} = \bar{V}_t \cos\theta + \bar{V}_r \sin\theta \; . \qquad (2)$$

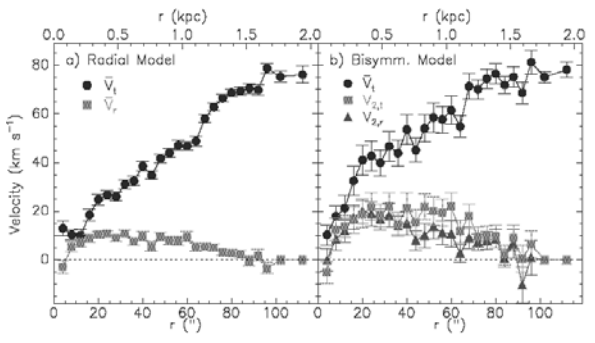

Fig. 2. Fitted velocity field components for NGC 2976 for (a) the radial and (b) the bisymmetric models. Adapted from Fig. 3 of [6].

When the non-circular motions are small, $\bar{V}_t(r)$ derived from equations (1) and (2) will be comparable and will reflect circular orbital balance in the system: this is the essence of the epicyclic approximation (e.g. [3]). Since we do not require weak perturbations here, the different physical interpretations invoked by the bisymmetric and radial models for the resulting flows may yield different $\bar{V}_t(r)$ as well.

3 A Bar in NGC 2976

We apply the models to the high-quality CO and Hα velocity field for the nearby, low-mass spiral NGC 2976 presented by [5]. For each model we simultaneously fit for the velocity profiles and the disk properties, allowing each parameter to vary independently. Our final radial and bisymmetric models of NGC 2976 have similar goodness-of-fit statistics, disk geometries and flow patterns: both are therefore adequate parametrizations of the data (see Table 1 and Fig. 2 of [6]). Figure 2 shows the velocity field components obtained for both models. The radial model reproduces the results obtained by [5]. While both models provide reasonable fits to the NGC 2976 kinematics, Fig. 2 illustrates that $\bar{V}_t(r)$ from the bisymmetric model rises more steeply than $\bar{V}_t(r)$ in the radial model. The reason for this difference is illustrated in Fig. 3, that shows sky-plane projections of the angular variations of the separate velocity profiles at $r = 20''$ in both models. By definition, the non-circular motions in the radial model must project to zero along the major axis [$\theta = 0$]. This is not the case in the bisymmetric model, where the contribution from non-circular motions depends on the phase of the bar. The bisymmetric model for NGC 2976 favors $\phi_b \sim 17°$, and in projection its bar and major axes are nearly aligned (see top horizontal axis of Fig. 3). There is therefore a large negative contribution from $V_{2,t}$ that offsets $\bar{V}_t$ at $\theta = 0$, resulting in a $V_{\rm model}$ similar to that in the radial model.

The amplitude of the radial flows required by the radial model of NGC 2976 is prohibitively large (see [6]). We therefore conclude that the bisymmetric

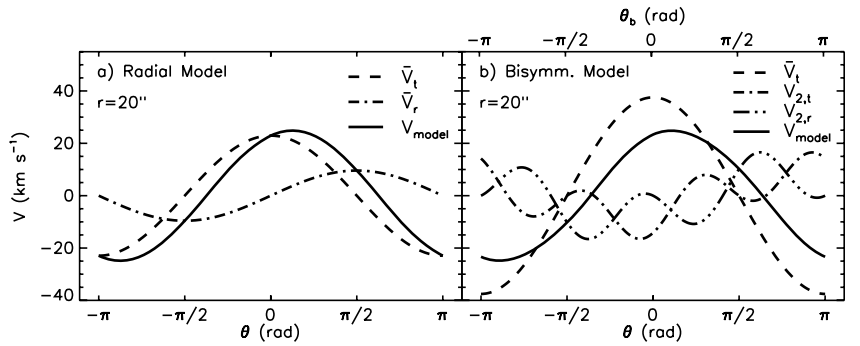

Fig. 3. Projected contributions from different kinematic components at $r = 20''$ in (a) the radial and (b) the bisymmetric models. Adapted from Fig. 6 of [6].

model better reflects the physical structure of this system. When non-circular motions are large $\bar{V}_t(r)$ is not a precise indicator of circular orbital balance, and we are developing self-consistent fluid-dynamical models of NGC 2976 to better measure this quantity. Nonetheless, the bisymmetric model implies that the rotation curve of NGC 2976 rises more steeply than estimated by [5]. There is evidence that the non-circular flows in NGC 2976 are caused by a bar rather than a triaxial halo: our kinematic bar axis and extent are identical to the photometric ones proposed by [2], and ϕ_b is roughly coincident with the major axis of the CO distribution from [5]. Since this in turn implies a large baryonic contribution to the potential, it is unlikely that the steeper rotation curve in NGC 2976 implies a high dark matter halo density.

Even if the large non-circular motions found in other nearby spirals can be attributed to bar-like distortions, Fig. 3 shows that the bisymmetric model will not always yield a steeper rotation curve than estimated previously. The change in $\bar{V}_t(r)$ relative to the radial model result depends on the phase of the bar axis, and would be shallower than the latter if, for example, ϕ_b is aligned with the disk minor axis.

We thank Josh Simon for providing the data for NGC 2976. KS is a Jansky Fellow of NRAO, and JAS is supported by grants AST-0507323 and NNG05GC29G.

References

1. K. G. Begeman: Ph.D. Thesis, Univ. of Groningen, the Netherlands (1987)
2. K. Ménendez-Delmestre et al: ApJ, **657**, 790 (2007)
3. R. H. M. Schoenmakers, M. Franx, P. T. de Zeeuw: MNRAS, **292**, 349 (1997)
4. J. A. Sellwood, A. Wilkinson: Rep. Prog. Phys., **56**, 173 (1993)
5. J. D. Simon, A. D. Bolatto, A. Leroy, L. Blitz: ApJ, **596**, 957 (2003)
6. K. Spekkens, J. A. Sellwood: ApJ, **664**, 204 (2007)

Gravitational Stability in the Disk of M 51

Marc Hitschfeld[1], C. Kramer[1], K.F. Schuster[2], S. Garcia-Burillo[3], and J. Stutzki[1]

[1] KOSMA, I. Physikalisches Institut, Universität zu Köln, Zülpicher Straße 77, 50937 Köln, Germany hitschfeld@ph1.uni-koeln.de, kramer@ph1.uni-koeln.de, stutzki@ph1.uni-koeln.de
[2] IRAM, 300 Rue de la Piscine, F-38406 S^t Martin d'Hères, France schuster@iram.fr
[3] Observatorio de Madrid, Alfonso XII, 3, 28014 Madrid, Spain s.gburillo@oan.es

1 Abstract

Star formation laws, like i.e. the Schmidt law relating star formation rate and total gas density, have been studied in several spiral galaxies but the underlying physics are not yet well understood.

M 51, as a nearby face-on galaxy grand design spiral studied in many line transitions, is an ideal target to study the connection between physical conditions of the gas and star formation activity. In this contribution we combine molecular, atomic, total gas and stellar surface densities and study the gravitational stability of the gas (Schuster et al. [5], Hitschfeld et al. [3]).

From our IRAM-30m ^{12}CO 2–1 map and complementary H I-, radio continuum- and ACS B-band data we derive maps of the total gas density and the stellar surface density to study the gravitational stability of the gas via the Toomre Q-parameter. As an important factor in this analysis we also present a map indicating the velocity dispersion of the molecular gas estimated from the equivalent widths $\Delta v_{\rm eq}$ of the ^{12}CO 2–1 data.

2 The velocity dispersion of the molecular gas

The velocity dispersion is important for the calculation of the Toomre Q-parameter as it is hindering gravitational collapse. The map of the equivalent widths of ^{12}CO 2–1 $\Delta v_{\rm eq} = \int T dv / T_{\rm pk}$ is shown in Fig. 1. It is related to the velocity dispersion via $\sigma_{\rm CO} = \Delta v_{\rm eq}/(2\sqrt{2\ln 2})$.

The equivalent widths drop from the center to the outskirts by up to a factor of 5 from less than $\sim$20 km s^{-1} to 102 km s^{-1}. The inner spiral arm structure of M 51 in the northern part is much less prominent than in the integrated intensity map (Schuster et al. [5]).

B.S. Koribalski, H. Jerjen (eds.), *Galaxies in the Local Volume*,
doi: 10.1007/978-1-4020-6933-8_36,

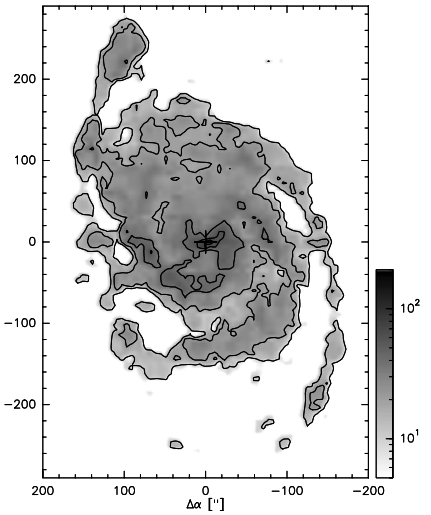

Fig. 1. The map of the equivalent widths of ^{12}CO 2–1 $\Delta v_{\rm eq}$. Contours show 10, 20, 40, 60 to 80 km s^{-1}.

3 The Toomre *Q*-parameter

The Toomre Q-parameter [7] describes the instability of a differentially rotating, homogeneous thin gas disk against axial symmetric disturbances. It is related to the epicyclic frequency κ, the velocity dispersion of the gas $\sigma_{\rm gas}$ and the total gas surface density $\Sigma_{\rm gas}$ via:

$$Q_{gas} = \frac{\kappa \sigma_{\rm gas}}{\pi G \Sigma_{\rm gas}}. \tag{1}$$

The epicyclic frequency is determined from the rotation curve of M 51, we assume that $\sigma_{\rm gas}$ can be estimated from $\sigma_{\rm CO}$. The surface density $\Sigma_{\rm gas}$ is constructed from complementary VLA-H I data and the ^{12}CO 2–1 data as described in Schuster et al. [5].

As a next step of the stability analysis the stellar component is taken into account (Hitschfeld et al. [3]). The Q-parameter for a pure stellar disk takes the equivalent form as Q_{gas}. The epicyclic frequency determined from the rotation curve is identical. A good approximation for an combined Q-parameter (Wang & Silk [8]) is:

$$Q_{total}^{-1} = Q_{gas}^{-1} + Q_{*}^{-1}. \tag{2}$$

To calculate Q_* we obtained the HST-ACS B-band image of Mutchler et al. [4] and converted it to a stellar mass surface density assuming a constant mass-to-luminosity ratio $M_*/L_B = 1.54$ (Shetty et al. [6]). The stellar velocity dispersion is significantly larger than the gas velocity dispersion and can be estimated using an exponential fall-off (Bottema et al. [2]) depending on the stellar scale height of the disk.

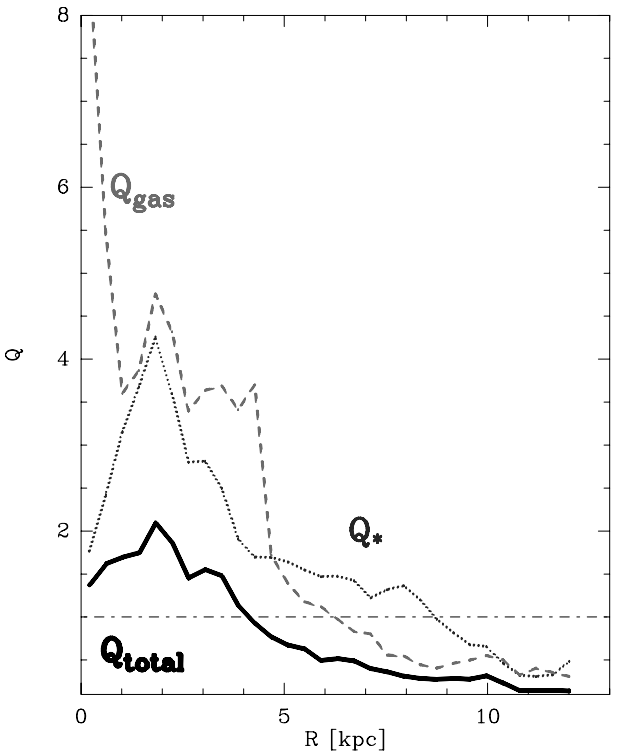

Fig. 2. Radial averages of the Toomre Q-parameter for the total gas Q_{gas}, stellar component Q_* and the total Q_{total}. All parameters have been calculated from inclination corrected quantities. A horizontal line delineates $Q = 1$ for critically stable conditions.

3.1 Results

The radial averages of Q_*, Q_{gas} and Q_{total} summed in elliptical annulli of 10" are presented in Fig. 2. The importance of the stellar contribution is evident and lowers the Q-parameter by up to 50%. Due to the stars the inner part is significantly closer to gravitational collapse than estimations from the gas-only analysis would predict. The gravitational collapse and formation of Giant Molecular Clouds is thus possible and predicted over large regions of the disk. This agrees with previous studies by Boissier et al. [1] of radial averages of the Toomre Q-parameter in their sample of galaxies comparing the gas-only Q_{gas} and Q_{total}.

The map of the combined Q-parameter is shown in Fig. 3. The total Q exceeds 1 in the inner interarm regions and drops to being critical to collapse ($Q \leq 1$) in the spiral arms indicated by the two black logarithmic spirals. From galactocentric radii of around 4 kpc and beyond Q drops below 1 indicating gravitational instability. Note that the Q-parameter in the neighbour

galaxy NGC 5195 is significantly underestimated due to the exponential decline assumed for the velocity dispersion of the stars.

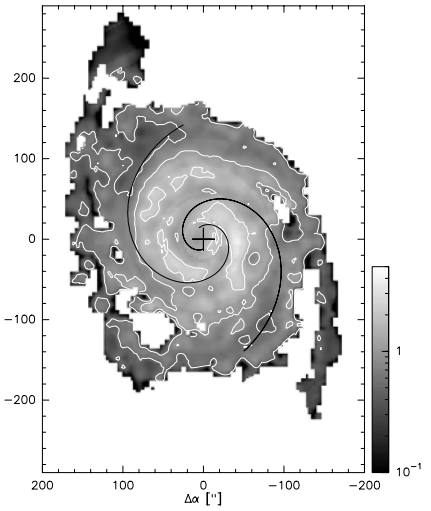

Fig. 3. Map of the combined Toomre Q-parameter of the stellar and gaseous component Q_{total}. In black, two logarithmic spirals indicate the position of the inner spiral arms.

Star formation is observed over large scales in the disk of M 51 and in particular massive, young stars are found in the inner part and especially in the spiral arms. Since not only gravitational stability governs star formation but also mechanism like i.e. spiral density waves and more locally turbulence and supernovae explosions, the Toomre criterion naturally fails to explain the exact location of stars. It is important as a threshold and necessary precondition for star formation.

References

1. Boissier, S., et al.: MNRAS, 346, 1215 (2003)
2. Bottema, R.: A&A, 275, 16 (1993)
3. Hitschfeld, M., Kramer, C., et al.: in prep. (2007)
4. Mutchler, M., et al.: AAS, 206, 1307 (2005)
5. Schuster, K. F. , Kramer, C. , Hitschfeld, M., et al.: A&A, 461, 143 (2007)
6. Shetty, R., Vogel, S.N., Ostriker, E.C., et al.: ApJ, 665, 1138 (2007)
7. Toomre, A.: ApJ, 139, 1217 (1964)
8. Wang, B., Silk, J.: ApJ, 427, 759 (1994)

The Kinematics and Ages of the Nearby Elliptical NGC 5128

Kristin A. Woodley[1], W. E. Harris[1], M. A. Beasley[2], E. Peng[3], T. Bridges[4], D. Forbes[5], Gretchen L. H. Harris[6], and G. Mackie[5]

[1] Department of Physics and Astronomy, McMaster University, Hamilton, ON L8S 4M1, Canada woodleka@physics.mcmaster.ca, harris@physics.mcmaster.ca
[2] Instituto de Astrofisica de Canarias, Calle Vía Láctea s/n, E-38200 La Laguna, Tenerife, Spain beasley@iac.es
[3] Herzberg Institute of Astrophysics, 5071 West Saanich Road, Victoria, BC V8V 2X6, Canada eric.peng@nrc-cnrc.gc.ca
[4] Department of Physics, Queen's University, Kingston, ON K7L 3N6, Canada tjb@astro.queensu.ca
[5] Centre for Astrophysics and Supercomputing, Swinburne University, Hawthorn, VIC 3122, Australia dforbes@astro.swin.edu.au, gmackie@astro.swin.edu.au
[6] Department of Physics and Astronomy, University of Waterloo, Waterloo, ON N2L 3G1, Canada glharris@astro.uwaterloo.ca

1 Introduction

NGC 5128 (Centaurus A) is a giant elliptical galaxy less than 4 Mpc away. Its globular cluster (GC) system has a specific frequency on the low end for giant elliptical galaxies of $S_N \simeq 2.2 \pm 0.6$ [1], however, this is twice as high as in typical disk galaxies. It also has optical features suggestive of a merger and accretion history: faint isophotal shells [2], a prominent dust lane, gas, and star formation. GCs, as single-aged, single-metallicity objects, are excellent tracers of the formation history of their host galaxy, and NGC 5128 is a prime candidate for both kinematic and age studies.

2 Age Study of NGC 5128 Globular Clusters

A recent spectroscopic study [3] obtained high quality signal-to-noise spectra of ∼200 GCs in NGC 5128, using the 2dF facility at the Anglo-Australian telescope. Their findings indicate a bimodal spectroscopic metallicity distribution function at high statistical significance, with a possible intermediate metallicity population, shown in Figure 1 (left panel).

Ages and metallicities for the GCs in NGC 5128 obtained [3] are shown in Figure 1 (right panel). Their findings indicate that ∼90% of the NGC 5128

B.S. Koribalski, H. Jerjen (eds.), *Galaxies in the Local Volume*,
doi: 10.1007/978-1-4020-6933-8_37,

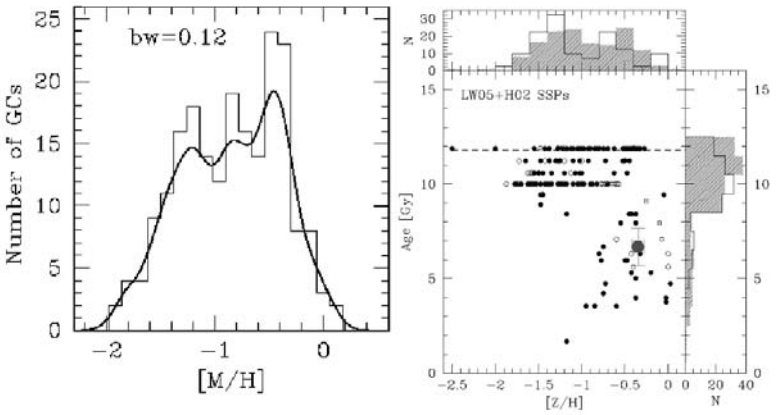

Fig. 1. *(Left:)* Metallicity distribution function for 207 globular clusters with signal-to-noise >20 in NGC 5128 derived from an empirical relation based on Milky Way GCs. The histogram and Gaussian density kernel estimate with bin/kernel bandwidth of 0.12 are shown. *(Right:)* The ages and metallicities for 147 GCs with signal-to-noise >30 (solid circles) and for ∼50 Milky Way GCs (open circles) using models from [4] with near solar abundance corrections [5]. The horizontal dashed line shows the old age limit of the model. The large open hexagon represents the spheroid of NGC 5128 ($r_e/2$ aperture along the major axis). The collapsed distributions for age and metallicity are shown for NGC 5128 (shaded) and Milky Way (open) GCs.

GC sample have old ages comparable to the Milky Way GCs. It is also evident from the study that $\leq 15\%$ are between $\sim 4-8$ Gyr and are more metal-rich on average than the old GCs in the sample. Only one GC with an age < 2 Gyr was identified.

3 Kinematic Study of NGC 5128 Globular Clusters

Recent studies [6, 7] have examined the kinematics of the GC and planetary nebula (PN) populations within NGC 5128. The kinematics were fit with the equation

$$v_r(\Theta) = v_{sys} + \Omega\ R\ sin(\Theta - \Theta_o) \tag{1}$$

where v_r is the object's observed radial velocity, v_{sys} is the galaxy's systemic velocity, R is the projected radial distance from the center of NGC 5128 (assuming a distance of 3.9 Mpc), and Θ is the projected azimuthal angle of the object measured in degrees east of north. The systemic velocity is held constant at 541 km s^{-1} [8], and the rotation amplitude, ΩR, and rotation axis, Θ_o, were obtained.

By comparing the metal-rich and metal-poor populations separately, it is shown in Figure 2 that the rotation amplitude is identical, within the uncertainties, for the two populations, as is the rotation axis.

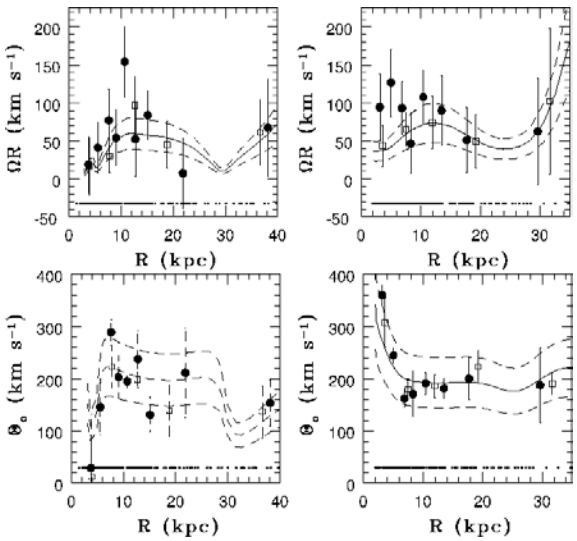

Fig. 2. The rotation amplitude *(top panels)* and the rotation axis *(bottom panels)* as a function of projected galactocentric radius from the centre of NGC 5128 of the metal-poor *(left)* and metal-rich *(right)* GCs. Open squares are radial bins of 0–5, 5–10, 10–15, 15–25, and 25–50 kpc, solid circles are equal numbered bins of 20 GCs, and solid lines are exponentially weighted points with varying bin width and dashed lines are the 35% and 25% uncertainties of the weighted data for the rotation amplitude and rotation axis. The open circles are the radial distribution of the populations at the bottom.

Figure 3 shows the velocity dispersion, as an example of the kinematic study presented in [7] of the entire GC system and PNe population. Spatial biases along the photometric major axis exist for both tracer populations of objects (see [7, 9] for more discussion). There appear to be dissimilar velocity dispersions between the two populations beyond a galactrocentric distance of 12–15 kpc. A declining velocity dispersion of the PNe population could indicate a difference in the orbital anisotropy compared with the GC population.

The kinematic study has also been extended out into the satellite group environment [6] of which NGC 5128 is the brightest member. Applying the same kinematic technique shows that the rotation amplitude and rotation axis of the satellite galaxies is the same as the halo of NGC 5128 traced by its GCs, within the uncertainties of this study.

4 Conclusions

Armed with radial velocities of 340 GCs and 780 PNe, we have performed a complete kinematic analysis within the halo of NGC 5128. Our kinematic

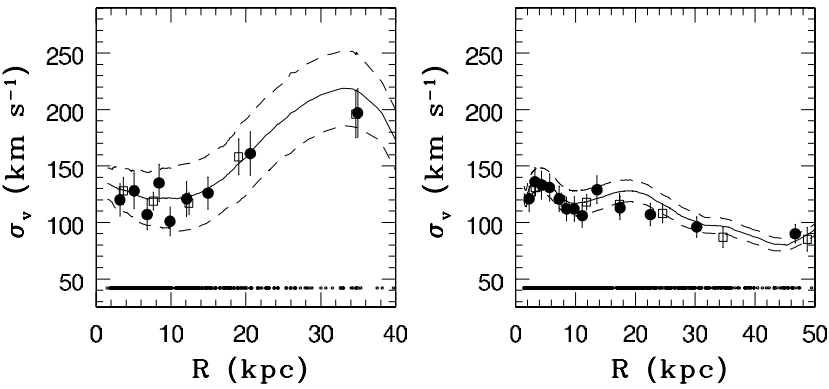

Fig. 3. *(Left:)* The velocity dispersion of the GC system of 340. *(Right:)* the PNe population of 780. The symbols are the same as in Figure 2.

results indicate that the metal-poor and metal-rich GCs share identical kinematics within the uncertainties. A comparison of the GC kinematics with the PNe indicate similar results as well, however the velocity dispersions between the two populations are quite different beyond a 15 kpc distance from the centre of NGC 5128. Comparing the kinematics of the halo of NGC 5128 to that of the satellite group environment also shows a continous link between the halo and the group. To these we have now been able to add a recent age study, performed with high quality spectral data of ∼150 GCs in NGC 5128 [3], that clearly indicates both metal-rich and metal-poor GCs are predominately old. Our smooth kinematic results, along with our age study of GCs, indicate that NGC 5128 could have formed early on as the giant galaxy that was already centrally dominant in the Centaurus group. The more recent activity visible in its inner halo indicates that NGC 5128 continues to build up by a series of minor mergers and accretions from within its group environment.

References

1. W.E. Harris, G.L.H. Harris, P. Barmby, D.E. McLaughlin, D. Forbes: AJ **132**, 2187 (2006)
2. E.W. Peng, H.C. Ford, K.C. Freeman, R.L. White: AJ **124**, 3144 (2002)
3. M.A. Beasley, T. Bridges, E. Peng, W.E. Harris, G.L.H. Harris, D.A. Forbes, G. Mackie: submitted to MNRAS (2007)
4. H.-c. Lee, G. Worthey: ApJS **160**, 176 (2005)
5. M.L. Houdashelt, S.C. Trager, G. Worthey, R.A. Bell: BAAS **34**, 1118 (2002)
6. K.A. Woodley: AJ **124**, 2424 (2006)
7. K.A. Woodley, W.E. Harris, M.A. Beasley, E.W. Peng, T.J. Bridges, D.A. Forbes, G.L.H. Harris: AJ **134**, 494 (2007)
8. X. Hui, H.C. Ford, K.C. Freeman, M.A. Dopita: ApJ **449**, 592 (1995)
9. E.W. Peng, H.C. Ford, K.C. Freeman: ApJ **602**, 685 (2004)

Integral-Field Spectroscopy of the Centaurus A Nucleus

Davor Krajnović[1], Rob Sharp[2], and Niranjan Thatte[1]

[1] Denys Wilkinson Building, University of Oxford, Keble Road, OX1 3RH, U.K.
dxk@astro.ox.ac.uk, thatte@astro.ox.ac.uk
[2] Anglo-Australian Observatory, Epping NSW 1710, Australia
rgs@aaoepp.aao.gov.au

Summary. We report integral-field spectroscopic observations with the Cambridge Infra-Red Panoramic Survey Spectrograph (CIRPASS) mounted on the GEMINI South telescope of the nucleus of the nearby elliptical NGC 5128 (Centaurus A). We detect 2-dimensional distributions of the following emission-lines: [P II], [Fe II] and Paschen β and extract spatially resolved 2D kinematics of Paβ and [Fe II] emission-lines only. The kinematics of the two emission-lines are similar, but the Paβ velocity gradient is steeper in the centre while the velocity dispersion is low everywhere. Assuming simple disk geometry we estimate the mass of the central black hole. We obtain $\mathrm{M}_\bullet = 8.25^{+2.25}_{-4.25} \times 10^7$ $\mathrm{M}_\odot$, for $PA = -3^\circ$ and $i = 25^\circ$, excluding the $\mathrm{M}_\bullet - \sigma$ relation prediction at a 3σ confidence level, which is in good agreement with previous studies.

1 Introduction

A thick dust lane that crosses the Centaurus A galaxy (Cen A), making it a show case for astronomical public relations, hides the centre of the galaxy and its constituents. Deep in the center, at the bottom of the potential well, there lies a supermassive black hole (SMBH), a powerful monster responsible for AGN activity, radio and X-ray jets emanating from the nucleus and spectacular large scale radio-lobes which surround the optical galaxy. The conspicuous shape of the galaxy and the central activity are likely related and have the origin in a recent major merger with a disk galaxy. However, what makes Cen A a truly exceptional galaxy is its proximity. At a distance of ~ 3.5 Mpc [1], Cen A is both the closest AGN and recent merger, a great case for testing our understanding of processes that shape galaxy formation and evolution (for detailed information about the galaxy see the review by [2]).

Recent studies, 'peering through the dust' with near-infrared spectrographs, investigated the presence of the SMBH and found that, in order to describe the kinematic properties of the nuclear region (both for ionised gas and stars), it is necessary to place a dark object in the nucleus with

B.S. Koribalski, H. Jerjen (eds.), *Galaxies in the Local Volume*,
doi: 10.1007/978-1-4020-6933-8_38,

a mass of $M_\bullet = (2^{+3.0}_{-1.4}) \times 10^8$ $M_\odot$ for inclination $i > 15°$ ([3] ground-based gas kinematics), $M_\bullet = (2.4^{+0.3}_{-0.2}) \times 10^8$ $M_\odot$ for an edge-on inclination, $M_\bullet = (1.8^{+0.4}_{-0.4}) \times 10^8$ $M_\odot$ for $i = 45°$ and $M_\bullet = (1.5^{+0.3}_{-0.2}) \times 10^8$ $M_\odot$ for $i = 20°$ ([4] ground-based stellar kinematics), $M_\bullet = (8.6 \pm 0.3) \times 10^7$ $M_\odot$ at $i = 45°$ ([5] ground-based adaptive optic assisted observations of gas kinematics) and $M_\bullet = (1.1 \pm 0.1) \times 10^8$ $M_\odot$ for $i = 25°$ and $M_\bullet = (5.5^{+0.7}_{-0.6}) \times 10^7$ $M_\odot$ for $i = 45°$ ([6] ground- and space-based observations of gas kinematics). The last study also constrained the size of the central massive object to r ~ 0.6 pc suggesting that it is indeed a black hole. The importance of a robust measurement of Cen A's $M_\bullet$ is highlighted by the fact that the above masses place the black hole in Cen A approximately between 2 times and an order of magnitude above the $M_\bullet - \sigma$ relation [7, 8, 9, 10]. Although the large scatter in the relation and the low number statistics might be misleading, it is also possible that Cen A, as a recent merger, is a special case [4].

Each of these studies brought an improvement in spatial and spectral resolution, but they were all based on observations with long-slits along a few position angles. For construction of dynamical models, whether stellar or gaseous, it is crucial to have sufficient information about the behaviour of the constraints. In the case of gaseous models the geometry of the gas disk can only be confirmed by two-dimensional mapping and only a well-ordered gas disk can be used to reliably determine the enclosed mass. This is specifically important in complex system such as Cen A, where the dust lane is known to warp [11, 12, 13, 14] and the emission lines could come from different layers of the disk, or be under the strong influence of the nucleus.

In this contribution we present the first observations with an integral-field spectrograph (IFS) of the nucleus of Cen A in the near-infrared, which we use to determine the geometry of the nuclear gas disk and calculate the mass of the SMBH. A more detailed description of the data reduction methods, the data themselves, the kinematics of the observed emission-lines and constructed dynamical models are given in [15].

2 Emission-line kinematics and dynamical model

We used CIRPASS IFS in its high-resolution mode obtaining a spatial scale of $0\farcs25$ with $9\farcs3 \times 3\farcs5$ field of view to study the central region of Cen A with the spectral resolution of ~ 2.2Å/pixel (FWHM) and a resolution element of 1.8 pixels, in the spectral range between $1.1 - 1.35\mu m$. Within $1''$ of the nucleus, we detect three emission-lines. They are, in order of their observed relative strengths: [Fe II] λ12567, Paschen β λ12818 and [P II] λ11882. The observation of the [P II] line is, to our knowledge, the second extragalactic measurement of this emission-line, the first being in NGC 1068 by [16]. This line is, however, confined to the central $0\farcs5$ and we extracted two-dimensional kinematic maps (mean velocity and velocity dispersion) from the first two lines only.

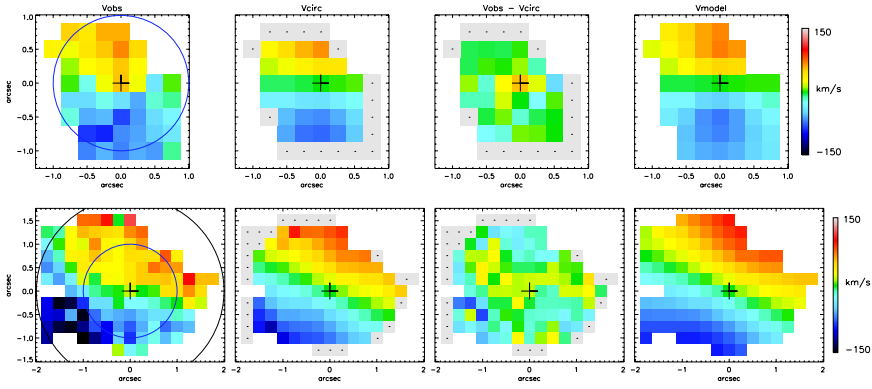

Fig. 1. Maps of the observed mean velocity *(far left)*, circular velocity *(middle left)*, residuals between the mean and circular velocity *(middle right)*, and the best fitting thin disk dynamical models *(far right)* using the derived orientation for Paβ *(top)* and [Fe II] *(bottom)* emission-line disks and the mass of SMBH, $M_\bullet = 8.25 \times 10^7$ $M_\odot$. Circles over-plotted on observed velocity maps have radii of $0\farcs9$ (inner circle on [Fe II] map and the only circle on Paβ map) and $1\farcs8$ (outer circle on [Fe II] map, not shown on Paβ map). Bins marked with black dots were not included when constructing circular velocity maps. The plus symbol denotes the origin of the map, assumed to be the position of the Cen A nucleus.

Both Paβ and [Fe II] emission-lines show ordered rotation (Fig. 1) and they are likely part of the nuclear disk structure discovered by [17]. Assuming that the emission originates in a thin disk we determined its geometry in a two step process. We first fit the position angle (PA) using the method described in the Appendix A of [18]. Later we fit a tilted ring model to the maps, but keeping PA fixed to the determined values (the kinematic models are shown in the second column of Fig. 1). With this method we determine the following geometric parameters of the gas disks: $PA = -3° \pm 10°$ and $i = 25° \pm 5°$ for Paβ and $PA = -23° \pm 3°$ and $i = 30° \pm 5°$ for [Fe II].

A confirmation that the emission originates in a disk comes also from the velocity dispersion maps (measured as the width of the emission-lines). The dispersion is generally low, but it rises towards the center. This effect is more noticeable in the case of [Fe II] line, which also show an extended region of high dispersion, with orientation of 120° with respect to the North. This is significant because the orientation of the central warp of the dust disk has a similar orientation. In addition, the [Fe II] line has smaller central velocity gradient and its kinematics are more disturbed (see residuals on Fig. 1). Based on these evidences and on the differences between Paβ and [Fe II] kinematics, we speculate that the excitation of the [Fe II] line happens also at larger radii from the central engine and the line-of-sight passes two times through the

warped disk, such that at the spatial resolution of our observations the data contain contributions of gas moving in two different directions (lowering the velocity, but increasing the velocity dispersion). Following this, we continue by considering only Paβ kinematics for determining the mass of SMBH.

The basic assumption of our simple dynamical models is that clouds of ionised gas move in circular orbits within a thin disk, under the gravitational influence of the SMBH and the surrounding stellar distribution, which we parameterise using ground- and space-based images. For the geometry of the disk independently determined above, we measure the mass of SMBH to be $M_\bullet = 8.25^{+2.25}_{-4.25} \times 10^7$ $M_\odot$. This value is consistent with previous measurements, while the predicted value of the SMBH mass from the $M_\bullet - \sigma$ relation is excluded at the 3σ level. This result is in good agreement with some of the previous measurements, suggesting that the post merger settling, visible in the galaxy on large scales, continues all the way to its nucleus and the lurking monster within.

References

1. Ferrarese, L., Mould, J. R., Stetson, P. B., Tonry, J. L., Blakeslee, J. P., & Ajhar, E. A. 2007, ApJ, 654, 186
2. Israel F. P., 1998, A&AR, 8, 237
3. Marconi A., Capetti A., Axon D. J., Koekemoer A., Macchetto D., Schreier E. J., 2001, ApJ, 549, 915
4. Silge J. D., Gebhardt K., Bergmann M., Richstone D., 2005, AJ, 130, 406
5. Häring-Neumayer N., Cappellari M., Rix H.-W., Hartung M., Prieto M. A., Meisenheimer K., Lenzen R., 2006, ApJ, 643, 226
6. Marconi A., Pastorini G., Pacini F., Axon D. J., Capetti A., Macchetto D., Koekemoer A. M., Schreier E. J., 2006, A&A, 448, 921
7. Gebhardt K., Bender R., Bower G., Dressler A., Faber S. M., Filippenko A. V., Green R., Grillmair C., Ho L. C., Kormendy J., Lauer T. R., Magorrian J., Pinkney J., Richstone D., Tremaine S., 2000, ApJL, 539, L13
8. Ferrarese L., Merritt D., 2000, ApJL, 539, L9
9. Tremaine S., Gebhardt K., Bender R., Bower G., Dressler A., Faber S. M., Filippenko A. V., Green R., Grillmair C., Ho L. C., Kormendy J., Lauer T. R., Magorrian J., Pinkney J., Richstone D., 2002, ApJ, 574, 740
10. Ferrarese L., Ford H., 2005, Space Science Reviews, 116, 523
11. Quillen A. C., de Zeeuw T., Phinney S., Phillips T. G., 1992, ApJ, 391, 121
12. Nicholson R. A., Bland-Hawthorn J., Taylor K., 1992, ApJ, 387, 503
13. Quillen A. C., Graham J. R., Frogel J. A., 1993, ApJ, 412, 550
14. Quillen, A. C., Brookes, M. H., Keene, J., Stern, D., Lawrence, C. R., & Werner, M. W. 2006, ApJ, 645, 1092
15. Krajnović, D., Sharp, R., & Thatte, N. 2007, MNRAS, 374, 385
16. Oliva E., Marconi A., Maiolino R., Testi L., Mannucci F., Ghinassi F., Licandro J., Origlia L., et al. 2001, A&A, 369, L5
17. Schreier E. J., Marconi A., Axon D. J., Caon N., Macchetto D., Capetti A., Hough J. H., Young S., Packham C., 1998, ApJL, 499, L143
18. Krajnović D., Cappellari M., de Zeeuw P. T., Copin Y., 2006, MNRAS, 366, 787

Visualising the Local Volume

David G. Barnes and Christopher J. Fluke

Centre for Astrophysics and Supercomputing, Swinburne University of Technology, PO Box 218, Hawthorn 3122, Australia dbarnes@swin.edu.au

Abstract

Over the last decade, multiwavelength, wide-field surveys have dramatically enhanced our knowledge of the Local Volume (LV). For this part of the Universe (closer than $\sim$ 10 Mpc), we now have large catalogues of bulk galaxy properties and, for more than half of the population, high resolution images at multiple wavelengths. We present new approaches to visualising the LV, with a view to improving qualitative *and* quantitative comprehension of the data at hand. Specifically we will demonstrate 3-dimensional, interactive models of the LV that blend data from multiple sources to (hopefully) reveal new structures and correlations. Our models enable *in situ* inspection of individual galaxies, statistical analysis of groups of galaxies, and (eventually) selection and discovery of "like me" galaxies.

1 Motivation

Rich datasets now exist for the $\sim$ 500 known galaxies in the LV, which by convention is that part of the Universe closer than 10 Mpc. For most of the galaxies catalogued in [4], broadband colours, radio and X-ray data, kinematics, internal dynamics, chemical abundances, metalliticites, and sometimes several independent distance measures are available in the literature.

Building our understanding of the LV depends substantially on our capacity to integrate the available data and generate and test new hyptheses regarding the formation and evolution of members of the LV. The inspection of graphical and pictorial representations of scientific data — *visualisation* — is a well-known technique for exploring and comprehending data, as well as for conveying ideas and scientific models.

B.S. Koribalski, H. Jerjen (eds.), *Galaxies in the Local Volume*,
doi: 10.1007/978-1-4020-6933-8_39,

2 Approach

Our focus is primarily on 3-dimensional (3-d) visualisation. All modern workstations and laptop computers contain graphics cards with hardware that is dedicated to the projection of 3-d scenes onto the standard flat (2-d) screen. For discrete data (eg. sparse samples, irregular grids), a simple 3-d visualisation can easily represent five parameters — three position ordinates plus point colour and size — and six or more by using vectors, symbols and/or movement. For continuous data (eg. images, regularly sampled density fields), techniques such as isosurfacing and volume rendering [3, 2] can be applied in combination to study the relationship between multiple scalar properties across a 3-d domain.

We have developed the S2PLOT programming library [1] to enable straightforward 3-d programming for science. S2PLOT[1] has an interface inspired by PGPLOT[2], and supports workstation screens, stereoscopic projection devices and curved projection surfaces. The examples in the following section are all S2PLOT programs that have been written specifically to explore LV-related science.

3 Visualising the Local Volume

3.1 Inside the Local Volume: the Milky Way satellites

With our collaborators (Forbes, Kroupa, Metz, et al.) we have constructed a visualisation of the globular clusters (GCs) and satellite galaxies (SGs) of the Milky Way. The motivation is generally to refine our understanding of the 3-d structure of the nearest neighbours to the Milky Way, and specifically to search for alignments and/or anti-alignments within and between the GCs and SGs. Fig. 1 shows a 2-d projection of the system with the classical SGs labelled, and includes the Magellanic Stream H I data [7]. We are presently adding models of the remnant Sagittarius and Orphan stellar streams (M. Fellhauer, *priv. comm.*) to the visualisation.

3.2 The Local Volume

With our collaborators (Koribalski, Kilborn, et al.) we are developing an experiment in "integrated data analysis". This is an interactive, 3-d visualisation of the 'Local Volume H I Survey" (LVHIS) sample [5] and the reference LV catalogue [4], which can display optical and H I images on-screen for galaxies selected in the visualisation. An example is presented in Fig. 2, where

[1] S2PLOT is available from `http://astronomy.swin.edu.au/s2plot`

[2] PGPLOT is written by Tim Pearson and available from `http://www.astro.caltech.edu/tjp/pgplot`

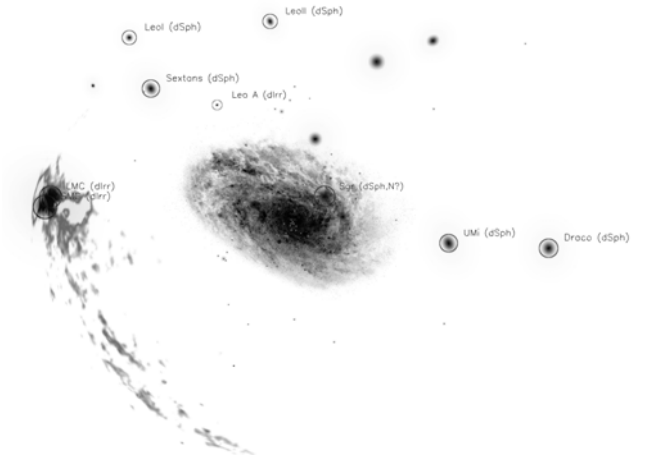

Fig. 1. Still frame from an interactive visualisation of the Milky Way and its satellite globular clusters and galaxies.

the galaxy ESO115-G021 has been chosen and the H I data from the LVHIS project[3] is displayed on the left of the screen.

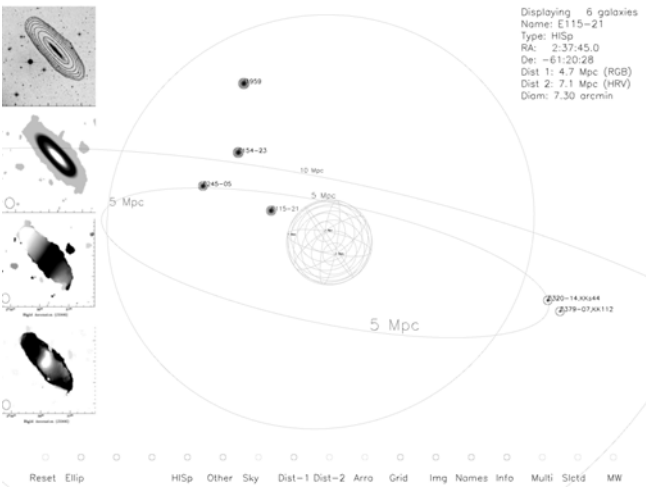

Fig. 2. Still frame from an interactive visualisation of the Local Volume galaxy sample, showing optical and H I data for the galaxy ESO115-G021 [5]. The panels are (from the top-left): H I integrated flux contours and *B*-band image; H I integrated flux; H I flux-weighted velocity; and H I velocity dispersion.

[3] LVHIS project webpage at `http://www.atnf.csiro.au/research/LVHIS`

3.3 Beyond the Local Volume: the HI Parkes All Sky Survey Catalogue

The H I Parkes All Sky Survey catalogue (HICAT [6] and HICAT-N [8]) is the largest, predominantly all-sky survey of neutral hydrogen to date. It extends beyond the LV, but serves as an interesting candidate for 3-d visualisation due to its unambiguous demonstration of large scale structure in the nearby Universe. Figure 3 shows a single frame from an interactive visualisation of HICAT. Structure is clearly visible, although the effect is markedly improved with the motion that is possible in the interactive display.

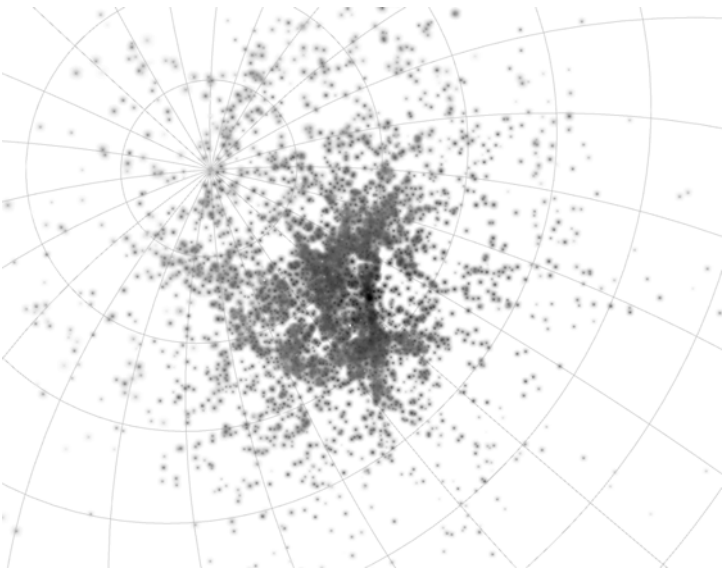

Fig. 3. Still frame from an interactive visualisation of the HIPASS catalogue.

References

1. D.G. Barnes, C.J. Fluke, P.D. Bourke, et al.: PASA **23**, 82 (2006)
2. B. Beeson, D.G. Barnes, P.D. Bourke: PASA **20**, 300 (2003)
3. R.A. Drebin, L. Carpenter, P. Hanrahan: Comp. Graphics **22**, 65 (1988)
4. I.D. Karachentsev, V.E. Karachentseva, W.K. Huchtmeier, et al.: AJ **127**, 2031 (2004)
5. B.S. Koribalski, this volume.
6. M.J. Meyer, M.A. Zwaan, R.L. Webster, et al: MNRAS **350**, 1195 (2004)
7. M.E. Putman, L. Staveley-Smith, K.C. Freeman, et al.: ApJ **586**, 170 (2003)
8. O.I. Wong, E.V. Ryan-Weber, D.A. Garcia-Appadoo, D.A., et al.: MNRAS **371**, 1855 (2006)

The Stromlo Missing Satellites Survey

Helmut Jerjen

Research School of Astronomy & Astrophysics, Mt. Stromlo Observatory,
Australian National University, jerjen@mso.anu.edu.au

1 Scientific Motivation

According to cosmological theory, density fluctuations of Cold Dark Matter (CDM) form the first structures in the Universe. The gravitational potential wells of these dark matter halos suck in primordial gas and provide the seeds for the formation of stars via energy dissipation and cooling, a billion years after the Big Bang. The observational Universe today is filled with these galaxies, the prime repositories of shining baryonic matter. For obvious reasons, most of the detected and catalogued galaxies are intrinsically the largest and the brightest, those that can be seen from the greatest distance and are most easily studied against the night sky. Ironically, a major limitation on our ability to develop a consistent model that describes how galaxies emerged out of dark matter comes from the incompleteness of our picture of the nearby universe, in particular from the lack of a detailed understanding of the phenomenon *dwarf galaxies*.

Dwarf galaxies are stellar systems composed almost entirely of dark matter with a minimum mass of the order of 10^6 solar masses. Examples have been discovered orbiting the Milky Way and Andromeda galaxies. Extreme low star densities make them transparent and hard to find, but they seem to dominate by numbers any volume in space and were more numerous in the cosmological past. CDM theory tells us that the dark matter mini halos and their optical manifestations, the dwarf galaxies, are the building blocks of larger galaxies like our Milky Way. Hence, if we want to shed light on the nature of dark matter and understand the driving mechanisms of galaxy formation/evolution we have to spend a disproportionate amount of effort on finding and physically characterising the faintest, most elusive galaxies that exist in the Universe.

B.S. Koribalski, H. Jerjen (eds.), *Galaxies in the Local Volume*,
doi: 10.1007/978-1-4020-6933-8_40,

2 Cold Dark Matter Theory on Galactic Scales

A generic prediction of the standard CDM galaxy formation paradigm (e.g. Moore et al. 1999; Klypin et al. 1999; Governato et al. 2004) is that primary dark matter halos around massive galaxies contain hundreds of smaller clumps of dark matter. It is thought that the majority of these mini halos will gravitationally collect sufficient primordial hydrogen gas and turn it into stars to form a dwarf satellite galaxy than can be observed today. However, in our best-studied case, the Milky Way, the predicted number of dark matter clumps exceeds that of the observed dwarf satellites by a factor of ≈20 (see Fig. 1). This current inconsistency between CDM cosmology and dwarf galaxy frequency is heavily debated in the literature and known as the *missing satellites* or *substructure problem* (Klypin et al. 1999; D'Onghia & Lake 2004).

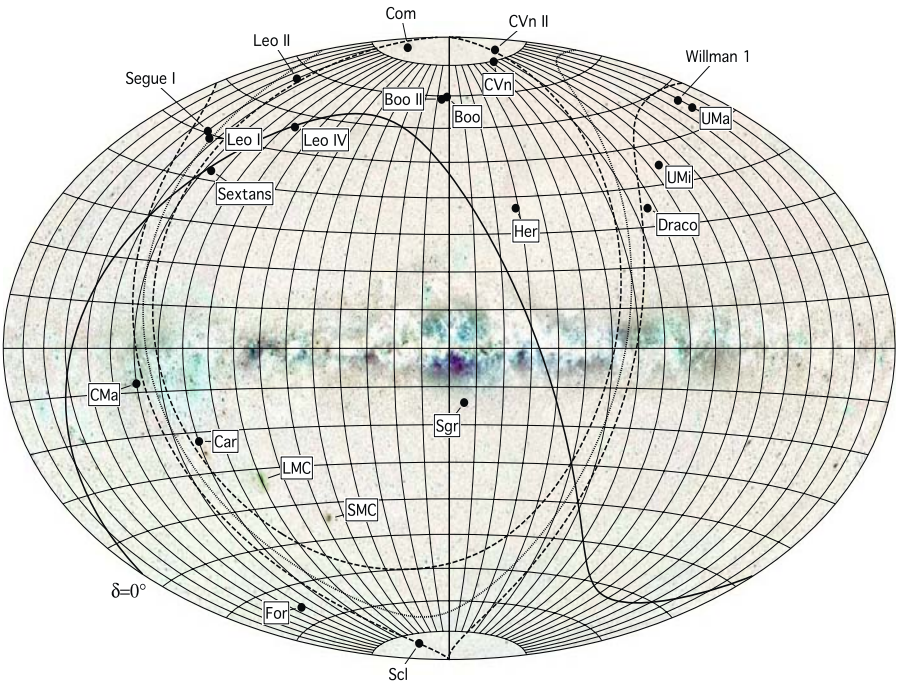

Fig. 1. Distribution of the known Milky Way satellites out to the Galactic virial radius $r_{vir} = 250\,\mathrm{kpc}$. Eleven dwarfs have been discovered in SDSS and 2MASS data in the last three years. The significance of the dwarfs being arranged in a plane (dotted line with the $\pm 15^\circ$ edges as dashed lines) has been discussed by Kroupa et al. (2005) and Metz, Kroupa & Jerjen (2007). Half of the entire sky (south of $\delta = 0^\circ$) will be surveyed by the Stromlo Missing Satellites program.

More recently the focus has shifted to whether the observed 3D-distribution of Milky Way satellites could actually be drawn from a population of dark

matter subhalos. The concern was raised when Kroupa et al. (2005) and Metz, Kroupa & Jerjen (2007) reported that the Milky Way satellites are statistically arranged in a disk, apparently inconsistent with a cosmological substructure population at the 99.5% confidence level. Although Kang et al. (2005) argued that finding a dozen dwarf galaxies in a planar distribution is not improbable, debating this issue is futile as the incompleteness of the census of Milky Way satellites remains the ultimate uncertainty.

Because incompleteness hinders any serious testing and possible refinement of the current cosmological model, progress can only be expected if observers can provide theoreticians with the full picture, including a robust dwarf satellite number and accurate estimates of their baryonic and dark matter contents, sizes, and galactocentric distances. The starting point of such a task is a deep and systematic photometric inventory of all the stars in the halo of the Milky Way, a technical challenge that has become feasible just recently.

3 Previous Work

Northern Hemisphere: Willman et al. (2005) conducted a first systematic blind search for Milky Way satellites using the Sloan Digital Sky Survey (SDSS; York et al. 2000) covering 25% of the sky. Careful analyses of resolved stars in both the SDSS and the Two Micron All Sky Survey (2MASS) revealed a first new Milky Way satellite, Ursa Major (UMa). Since then, nine more satellites have been reported (Zucker et al. 2006; Berlokurov et al. 2007; Walsh, Jerjen & Willman 2007).
Southern Hemisphere: due to the lack of any digital imaging data until recently, the search for dwarf galaxies in the vicinity of the Milky Way generally had to rely on photographic plates (e.g. Côté et al. 1998; Jerjen et al. 1998, 2000; Karachentsev et al. 2004). For example, Whiting et al. (1999) detected the Cetus dwarf in the outskirts of the Local Group (at 780 kpc) that was faintly visible on UK Schmidt plates. Five years later, the great potential of finding new Milky Way satellites with modern technology was demonstrated when Martin et al. (2004) discovered the Canis Major (CMa) dwarf in 2MASS.

4 The Stromlo Missing Satellites Survey

The ANU 1.35 m SkyMapper telescope at Siding Spring Observatory represents investment in Australian frontier technologies of A$13 million. It is among the first of a new breed of specialised telescopes which are capable of scanning the sky more quickly and sensitively than ever before using a 16k $\times$ 16k CCD mosaic camera with a 5.7 sq degree FOV (Keller et al. 2007; Tisserand et al., this volume). Over the next five years, that telescope is dedicated to carry out the multi-colour, multi-epoch Stromlo Southern Sky (S3) Survey generating 150 Terabytes of CCD data. The final product will be a

catalogue with positions and photometry for ≈ 1 billion objects in six bands: SDSS u, g, r, i, and z plus an extra, Strömgren-like v filter. The survey will cover all 20,000 square degrees south of the equator ($\delta < 0°$, see Fig. 1) and has photometric limits $0.5 - 1.0$ mag fainter than SDSS.

The various releases of the S3 catalogue will be systematically analysed by the Stromlo Missing Satellites (SMS) team employing sophisticated data mining algorithms that have been developed and extensively tested with the publicly available Sloan DR4. Among others, we have announced the detection of Boötes II (Walsh, Jerjen & Willman 2007; see also Walsh et al., this volume), a Milky Way satellite candidate with size-luminosity properties close to SEGUE 1 (Belokurov et al. 2007), the second faintest of the currently known Milky Way companions.

Studies of such satellite candidates with a typical baryonic content of a few thousand stars or less require comprehensive imaging and spectroscopic follow-up programs to separate the wheat from the chaff. If the SMS project and the SDSS survey, probing 75% of the Milky Way's entire sphere of influence, will find significant numbers of true dwarf satellites that populate the same parameter space as model galaxies from high resolution simulations, these experiments would corroborate the standard model of cosmology in a remarkable way. Whatever the results, they will provide an unprecedented set of observational constraints that will show how tightly baryons and dark matter are bound on galactic scales and will energise the debate about new physics.

References

1. Belokurov, V., Zucker, D.B., Evans, N.W. et al. 2007, ApJ, 654, 897
2. Côté, S., Freeman, K.C. Carignan, C. et al. 1997, AJ, 114, 1313
3. D'Onghia, E. & Lake, G. 2004, ApJ, 612, 628
4. Governato, F., Mayer, L., Wadsley, J. et al. 2004, ApJ, 607, 688
5. Jerjen, H., Freeman, K.C. & Binggeli, B. 1998, AJ, 116, 2873
6. Jerjen, H., Freeman, K.C. & Binggeli, B. 2000, AJ, 119, 166
7. Kang, X., Jing, Y.P., Mo, H.J. et al. 2005, ApJ, 631, 21
8. Karachentsev, I.D., Karachentseva, V.E., Huchtmeier, W.K. et al. 2004, AJ, 127, 2031
9. Keller, S.C., Schmidt, B.P., Bessell, M.S. et al. 2007, PASA, 24, 1
10. Klypin, A., Kravtsov, A.V., Valenzuela, O. et al. 1999, ApJ, 522, 82
11. Kroupa, P., Theis, C., Boily, C.M. 2005, A&A, 431, 517
12. Martin, N.F., Ibata, R.A., Bellazzini, M. et al. 2004, MNRAS, 348, 12
13. Metz, M., Kroupa, P. & Jerjen, H. 2007, MNRAS, 374, 1125
14. Moore, B., Ghigna, S., Governato, F., et al. 1999, ApJ, 524, L19
15. Walsh, S., Jerjen, H., & Willman, B., 2007, ApJ, 662, L83
16. Whiting, A.B., Hau, G.K.T. & Irwin, M, 1999, AJ, 118, 2767
17. Willman, B., Dalcanton, J.J., Martinez-Delgado, D. et al. 2005, ApJ, 626, L85
18. York, D.G., Adelman, J., Anderson, J.E., Jr. et al. 2000, AJ, 120, 1579
19. Zucker, D.B., Belokurov, V., Evans, N.W. et al. 2006, ApJ, 650, L41

Boötes II: A Retrospective

Shane Walsh[1], Helmut Jerjen[1], and Beth Willman[2]

[1] Research School of Astronomy and Astrophysics, Mount Stromlo Observatory, Cotter Road, Weston ACT 2611, Australia swalsh@mso.anu.edu.au,
[2] Clay Fellow, Harvard-Smithsonian Center for Astrophysics, Cambridge MA, USA

Summary. During the course of a systematic search for low surface brightness Milky Way satellite galaxies we have discovered a previously unidentified stellar overdensity in the Sloan Digital Sky Survey. This overdensity has all the hallmarks of an extremely faint Dwarf Spheroidal companion which we designate Boötes II. The object is consistent with an old (~ 12 Gyr) metal-poor ([Fe/H] $\simeq -2.0$) population at a distance modulus $(m - M) = 18.9 \pm 0.5$ mag. We estimate a total magnitude for Boötes II of $M_V \sim -3.1 \pm 1.1$ mag and a half-light radius of $r_h \sim 72 \pm 28$ pc.

1 Introduction

The Sloan Digital Sky Survey (SDSS) has revealed a wealth of Milky Way halo substructure, not least of which are twelve new dwarf spheroidal satellites. While preparing for a search of the southern sky using the ANU Skymapper telescope we discovered one such object in the SDSS Data Release 5 (DR5) by analyzing the distributions of resolved stars.

2 Data and Discovery

DR5 includes a five color photometric catalogue covering 8000 square degrees around the north Galactic pole [1]. Using a method similar to that described in [4, 5], and described in full in Walsh et al. (in preparation), we use a set of cuts to identify all stellar sources in fields of 3° height in Declination and of arbitrary width in Right Ascension that are consistent in $(g - r, r)$ parameter space with that of a dSph at a desired distance (Red Giant Branch, Blue Horizontal Branch and Main-Sequence Turnoff). We then convolve the binned spatial positions of these sources with a Plummer surface brightness profile and subtract the $0.9° \times 0.9°$ running mean from each $0.02° \times 0.02°$ pixel. Two thresholds are defined; a high density threshold or a lower density plus minimum area threshold. Boötes II passes both although only one is necessary to be classed as a detection.

B.S. Koribalski, H. Jerjen (eds.), *Galaxies in the Local Volume*,
doi: 10.1007/978-1-4020-6933-8_41,

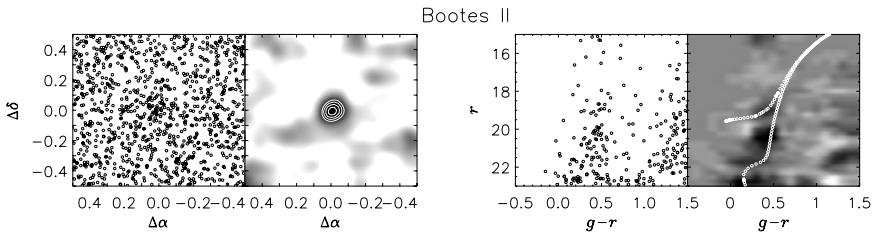

Fig. 1. Boötes II detection. *(Left:)* positions of SDSS stars passing the photometric selection criteria. *(Middle Left:)* Smoothed positions with contours at 0.5, 0.75, 1.0 (thick line), 1.2, 1.4, 1.6 and 1.8 multiples of threshold density. *(Middle Right:)* CMD of region within the 1.0 contour. *(Right:)* field subtracted Hess diagram of same region with overlaid stellar isochrone.

3 Object Properties

The best fit surface brightness profile consists of a 5.3 arcmin scalelength Plummer profile plus a constant field contribution. At a distance modulus of $m - M = 18.9$ this translates to a physical half-light radius of 72 pc. Integrating the Plummer component and comparing to the same fit of Boötes I (Belokurov et al. 2006) gives the flux ratio of the two objects, giving an estimated magnitude for Boötes II of $M_V \simeq 3.1$. The extremely faint nature of this object means quantitative analysis of the CMD is difficult, but it appears consistent with the old, metal-poor population expected of a dSph.

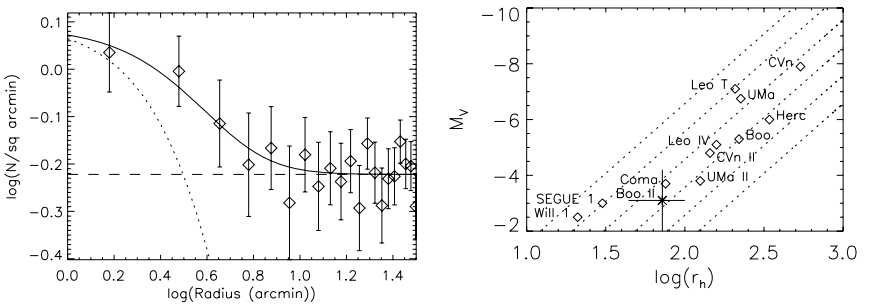

Fig. 2. *(Left:)* Surface brightness profile of Boötes II. The solid line is the combined Plummer profile (dotted) plus a constant field (dashed). *(Right:)* Size-Luminosity relationship of the recently discovered satellites.

4 Discussion and Conclusion

We present a new Galactic satellite called Boötes II. This object was discovered as a resolved stellar overdensity in an automated search of SDSS DR5. The combined evidences from CMD, surface brightness profile and the good agreement with the size-luminosity relationship of other MW satellites leads us to conclude this object is a previously undiscovered companion to the Milky Way at a tentative distance of 60 kpc. Full results are presented in Walsh et al. [3].

Table 1. Propeties of Boötes II

Parameter	Value
RA	$13^{\rm h}\,58^{\rm m}\,00^{\rm s}$
Dec	$+12^\circ\,51'\,00''$
Galactic l,b	353.7°, 68.9°
Age (Gyr)	12
[Fe/H]	-2.0
$(m-M)$	18.9 ± 0.5
r_h (Plummer)	$4'.1 \pm 1'.6$
$\mu_{0,\rm V}$ (Plummer)	29.8 ± 0.8
Distance (kpc)	60 ± 10
M_V (mag)	-3.1 ± 1.1

References

1. Adelman-McCarthy, J. K., et al. 2006, ApJS, 162, 38
2. Belokurov, V. et al. 2006b, ApJ, 647, L111
3. Walsh, S., Jerjen, H., Willman, B. 2007, ApJ, 662, L83
4. Willman, B., et al. 2002, AJ, 123, 848
5. Willman, B. 2003, PhD Thesis, University of Washington

Yasuo Fukui and Ron Ekers

Observational Constraints on the "Missing Satellite" Problem from SDSS

Sergey Koposov[1,2] and Vasily Belokurov[2]

[1] Max Planck Institute for Astronomy, Königstuhl 17, 69117 Heidelberg, Germany
koposov@mpia.de
[2] Institute of Astronomy, Madingley Road, Cambridge CB3 0HA, U.K.
vasily@ast.cam.ac.uk

1 Abstract

We quantify the algorithmic detectability of stellar Milky Way satellites in data release 5 (DR5) of the Sloan Digital Sky Survey (SDSS), and use this to estimate the luminosity function of faint satellite galaxies in our halo. We develop a satellite detection algorithm based on the convolution of the DR5 star catalog with a kernel of zero net flux that is the difference of a narrow positive Gaussian and a much wider negative Gaussian, which removes the background star-count level. This permits us to assess the significance of any (positive) detection in terms of deviations of this map. The efficiency of this algorithm is tested by computing the recovery rate of a large set of mock objects added to SDSS DR5 as a function of their luminosity, size and distance from the Sun. Most of the recent Milky Way satellite discoveries, made by SDSS, are shown to lie very close to the survey's detection limits. Calculating the maximum accessible volume V_{max} for all faint detected objects makes it possible for the first time to calculate the luminosity function for the Milky Way satellite galaxies, accounting consistently and algorithmically for their detection biases. The number density of satellite galaxies continues to rise towards low luminosities, but may flatten at $M_V \sim -5$. Within the uncertainties the luminosity function can be described by a simple power law $dN/dM_V = 10 \times 10^{0.1(M_V+5)}$, spanning luminosities from $M_V = -2.5$ all the way to the bright end. Comparing these results to several galaxy formation models, we find the predicted properties differ from the data.

2 Algorithmic Detection of Satellite Galaxies in SDSS

All the recent SDSS discoveries [1] of dSph around the Milky Way, bar Leo T, are not immediately visible in the images, but were detected as overdensities of resolved stars within certain magnitude and color ranges. This makes it

B.S. Koribalski, H. Jerjen (eds.), *Galaxies in the Local Volume*,
doi: 10.1007/978-1-4020-6933-8_42,

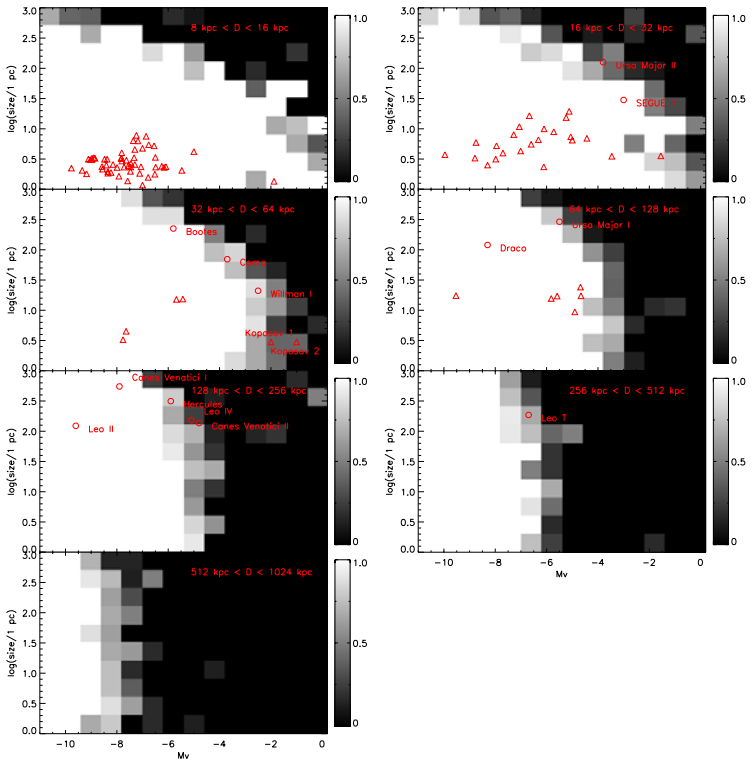

Fig. 1. Detection efficiency maps for Milky Way satellites, shown as a function of luminosity and size for different distance bins. White means 100% detection efficiency, black means 0%. Circles mark the locations of the known dwarf galaxies, triangles the known globular clusters. Notice that many of the very recent SDSS satellite galaxy discoveries occur near the detection boundary, where the efficiency is turning from unity to zero.

straightforward to automate a detection method and assess its efficiency. The essence of any detection algorithm is to count the number of stars in a certain (angular) region on the sky, color and magnitude range and compare it to the expected background value.

To identify the excess number of stars, a common approach is to convolve the spatial distribution of the data with window functions or filters. To estimate the star density on different scales, we use a Gaussian of width σ. This allows us to see the stellar density distribution at different spatial scales. The resulting "blobs", or overdensities, can be easily identified on the differential image maps. Such differential image maps are generally convolutions of the original distribution with the kernel, which is a difference of two Gaussians. When we convolve the map of sources with such a kernel, we get an estimate of the local density minus an estimate of the local background. To test our

detection algorithm, we carry out an extensive set of simulations where we add mock dwarf galaxy satellites and globular clusters to the SDSS DR5 catalog. In particular, we add to the catalog the g and r magnitudes of stars from the simulated objects, together with the right ascension and declination. These augmented catalogs are then fed through our automated pipeline, and the number of stellar overdensities with significance above the threshold is calculated as a function of distance, size and luminosity.

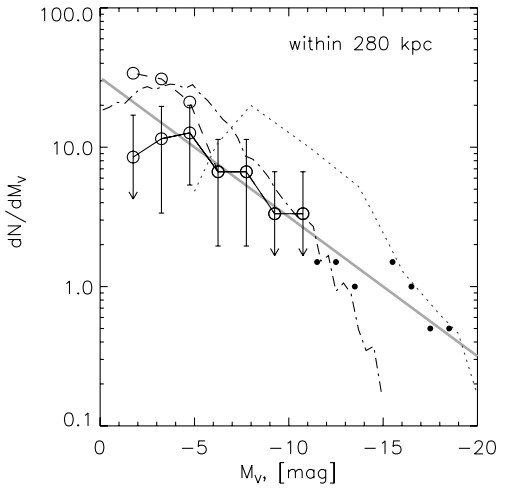

Fig. 2. The luminosity functions of objects within ∼280 kpc (virial radius) inferred from the satellite data under the assumption of two different radial distributions of satellites (isothermal and NFW-like). This uses the satellite list and the volume correction factor obtained with the pipeline using the cuts $r < 22.5$ and $S_{\rm star} > 5.95$. The theoretical prediction of Fig. 1 of [2] is shown in a dot-dashed line, and the prediction of [4] for $z_{\rm reion} = 10$ is shown as a dotted line. Additionally the luminosity function for the bright $M_V < -11$ satellites of the Milky Way sampled over the whole sky together with the bright M 31 satellites within 280 kpc is plotted with filled small symbols. The function $dN/dM_V = 10 \times 10^{0.1\,(M_V+5)}$ is shown in grey.

Illustrating the results of these simulations, Fig. 1 shows two-dimensional efficiency maps as a function of luminosity and size in seven distance bins spanning the range 8 kpc to 1 Mpc. Black corresponds to zero detection efficiency, and white to unit efficiency. The locations of the known Milky Way globular clusters and dwarf galaxies in this parameter space are recorded as triangles and circles. It is reassuring to see that all the known objects lie within or on the efficiency boundary.

3 Luminosity function of MW satellites

The observed luminosity function corrected for the incompletness effects is constructed using all the well-established dwarf galaxies in DR5, namely Leo II, Draco, Leo I, CVn I, Boo, Willman 1, Hercules, UMa II, Com, CVn II, Leo T, UMa I and Leo IV (Fig. 2). To refer the observed luminosity function for the same volume for all luminosities requires an assumption as to the underlying radial distribution of satellite galaxies. The calculation is carried out for two such density laws. The dashed line shows the luminosity function assuming the satellites are distributed in an isothermal sphere (namely, $n(r) \propto 1/r^2$). The solid line shows the luminosity function if the density fall-off is steeper at large radii (namely, $n(r) \propto r^{-2}(r+r_c)^{-1}$ with the core radius $r_c = 10$ kpc) – analogous to the NFW profile. On Fig. 2, we show the luminosity function determined for satellites within 280 kpc (a proxy for a Milky Way virial radius). To give an idea about the bright end of the luminosity function we have also included in Fig. 2 the estimate of the luminosity function (filled points) for the bright satellites of the Milky Way sampled over the full sky together with the bright M 31 satellites within 280 kpc. In Fig. 2, we also overplot the power-law function $dN/dM_V = 10 \times 10^{0.1\,(M_V+5)}$, which reasonably well approximates the datapoints in the range of $-19 < M_V < -3$ (with probably some flattening at $M_V \sim -4$).

There are a number of theoretical predictions of the luminosity function of the Local Group in the literature. For example, [4] shows the results of semianalytic galaxy formation calculations, including the effects of supernova feedback and photoionization. The luminosity function from [4] for $z_{\rm reion} = 10$ is plotted as a dotted line in Fig. 2. Although the numbers of luminous satellites are in reasonable agreement with the data, the shape of the luminosity function is not. All Somerville's (2002) luminosity functions turn over at $M_v \approx -9$ or brighter, depending on the epoch of reionization, whereas the luminosity function derived in Fig. 2 turns over at fainter than $M_V \approx -5$, if at all. [2] also provide calculations of the luminosity function of the Milky Way satellites, including the effects of tidal disruption as well as photoionization. At first glance, the fit seems reasonable, especially given the size of the error bars on the datapoints. The turn-over in Benson et al.'s luminosity function is at $M_V \approx -3$ and the numbers of predicted satellites are also consistent given the uncertainties. However, Benson et al.'s satellites have a much higher central surface brightness – our SDSS survey corresponds to a surface brightness cut of 30 mag arcsec^{-2}. A more detailed discussion of the results is given in [3].

References

1. Belokurov, V., et al. 2007, ApJ, 654, 897
2. Benson, A. J., et al. 2002, MNRAS, 333, 177
3. Koposov, S., et al. 2007, ArXiv e-prints, arXiv:0706.2687, submitted to ApJ
4. Somerville, R. S. 2002, ApJ, 572, L23

Space Motions of the Draco, Fornax, and Sagittarius Dwarf Spheroidal Galaxies

Slawomir Piatek[1], Carlton Pryor[2], and Edward Olszewski[3]

[1] Dept. of Physics, New Jersey Institute of Technology, Newark, NJ 07102, USA
piatek@physics.rutgers.edu
[2] Dept. of Physics and Astronomy, Rutgers, the State University of New Jersey, 136 Frelinghuysen Rd., Piscataway, NJ 08854–8019, USA
pryor@physics.rutgers.edu
[3] Steward Observatory, University of Arizona, Tucson, AZ 85721, USA
eolszewski@as.arizona.edu

Summary. Because of the diffraction-limited resolution of the Hubble Space Telescope (HST), it became possible to measure proper motions of the nearby dwarf spheroidal (dSph) galaxies using imaging with time baselines of only several years. This contribution discusses the motivation for measuring proper motions; describes highlights of the observational and data-reduction techniques; and reports the proper motions and their implications for the Draco, Fornax, and Sagittarius galaxies.

1 Introduction

The proper motion of a celestial object, $\boldsymbol{\mu} = (\mu_\alpha, \mu_\delta)$, is the change of its location on the sky over time. It is a difficult quantity to measure because multi-epoch imaging of fields containing the target object is required. The fields must also contain a standard of rest: an object that is distant enough so that its $\boldsymbol{\mu}$ is effectively zero over the time baseline. Compact-core galaxies and quasi-stellar objects (QSOs) are used for this purpose. Since the size of $\boldsymbol{\mu}$ decreases with distance when all else is equal, measuring $\boldsymbol{\mu}$ for even the nearest dSphs using ground-based telescopes requires time baselines of several tens of years. The challenges that make these ground-based measurements very difficult, albeit not impossible, are very long time baselines, multi-epoch imaging with different telescopes having different pointings and imagers, and the refraction of the Earth's atmosphere. For example, measurements exist for the dSphs Fornax [1] and Sculptor [6]. Most of these measurements have significant uncertainties which can only be reduced by extending the time baselines — meaning additional decades of waiting. With the launch of the HST, quickly improving the existing measurements and obtaining new ones became feasible.

B.S. Koribalski, H. Jerjen (eds.), *Galaxies in the Local Volume*,
doi: 10.1007/978-1-4020-6933-8_43,

Freed of the blurring caused by the Earth's atmosphere, the resolution of HST allows measuring $\boldsymbol{\mu}$s of dSphs using time baselines of only several years (e.g., [5] and the references therein). Doubling or even tripling the time baseline is possible even as part of the same observing program. However, there is a price to pay: the small field of view of HST requires that the target field contains a sufficiently bright QSO to serve as a standard of rest or that the exposure time is long enough so that faint compact-core galaxies can be used instead. Notwithstanding these difficulties, HST is the instrument of choice for precision astrometry. Why should we measure the $\boldsymbol{\mu}$s of dSphs, though?

2 Why Measure Proper Motions for dSphs?

Given the distance to a dSph, its $\boldsymbol{\mu}$ together with the heliocentric radial velocity gives the instantaneous space velocity of the galaxy. This velocity is a necessary initial condition in deriving the orbit of the dSph for a given Galactic potential. With the known orbit, it becomes possible to ascertain the degree of tidal interaction between the Milky Way and the dSph, and, thus, to impose realistic limits on the dark-matter content of the dSph. Due to the increasing number of known dSph satellites of the Milky Way increases resulting from all-sky surveys such as the Sloan Digital Sky Survey (SDSS), the probability that some of them have had encounters is not negligible. As more dSphs have their orbits determined, such investigations become possible. For example, the LMC and SMC most likely had a close encounter about 150 Myrs ago. Encounters of dSphs with other dSphs or with the Milky Way could affect star formation in these galaxies through ram pressure or tidal compression, possibly explaining why dSphs such as Carina and Ursa Minor have dissimilar stellar populations despite having comparable luminosities and structural properties. Several authors have proposed the existence of "large-scale" structure among the dSphs such as streams, where some dSphs and globular clusters move on similar orbits, or planes, where the majority of dSphs have orbits in a common plane. If they are real, these structures contain clues about the formation of the local volume. However, $\boldsymbol{\mu}$s are essential to test their reality.

Proper motions can also be used to constrain the form of the Galactic potential. Sagittarius is an example of a dSph that is undergoing a strong tidal interaction with the Milky Way. Its tidal debris has been traced all around the sky, as unequivocally demonstrated by [4] using data from the Two Micron All Sky Survey (2MASS). The debris traces out the orbit to first order. Then, given an accurate current space velocity, the form of the Galactic potential can be found by matching the integrated orbit with the debris.

3 How to Measure Proper Motions with HST?

Up to now, most of the successful HST measurements of $\boldsymbol{\mu}$s employed similar observational techniques. Multiple fields in a dSph are observed, each containing at least one bright QSO serving as a standard of rest. Because the point-spread function (PSF) of a point source is smaller than the pixels of the CCD cameras, the images are dithered. Other observing techniques are also possible. If a bright QSO is not available, faint compact galaxies can be used as a standard of rest, but here, long exposure times are needed (see [2]). Another example is the discussion below of the $\boldsymbol{\mu}$ for Sagittarius using Galactic bulge stars as the reference.

The method of deriving a $\boldsymbol{\mu}$ consists of these four steps. (1) Construct an effective PSF using bright stars and a QSO if it is available. (2) Measure accurate positions of stars and the QSO at all epochs by fitting the PSF. (3) Transform these positions to a common coordinate system that is comoving with the stars of the galaxy. (4) Determine the $\boldsymbol{\mu}$ of the dSph from the reflex motion of the QSO in the common coordinate system.

4 Results

In the sections below, we report $\boldsymbol{\mu}$s and some of their implications for three dSphs: Draco, Fornax, and Sagittarius. The measurements for Draco and Sagittarius are highly preliminary and therefore should be interpreted with a great deal of caution. In fact, we recommend that they not be used at all until they are published in a peer-reviewed journal.

4.1 Draco

The program to measure the $\boldsymbol{\mu}$ for Draco with HST is ongoing. Out of three fields, only one has two-epoch imaging using the Advanced Camera for Surveys. With a time baseline of 1.99 years, the measured $\boldsymbol{\mu} = (\mu_\alpha, \mu_\delta) = (19 \pm 13, -3 \pm 12)$ mas century^{-1}. This $\boldsymbol{\mu}$ is "as is" on the sky and, thus, includes contributions due to the motions of the LSR and Sun. Removing the contributions from these two motions gives the galactic rest frame $\boldsymbol{\mu}$, $\boldsymbol{\mu}^{\rm GRF} = (\mu_\alpha^{\rm GRF}, \mu_\delta^{\rm GRF}) = (55 \pm 12, 0 \pm 11)$ mas century^{-1}. Together with the heliocentric distance of 71 kpc and radial velocity of -293.8 ± 2.7 km s^{-1}, the radial and tangential velocities with respect to a stationary observer at the Galactic center are $V_r = -105 \pm 26$ km s^{-1} and $V_t = 185 \pm 30$ km s^{-1}, respectively. The resulting orbit, integrated in an NFW potential similar to that of [3], is almost polar with an inclination angle of 87° (65°, 108°), with peri- and apocenter of 49 (22, 61) kpc and 120 (89, 233) kpc, respectively, and period of 2.4 (1.4, 4.7) Gyrs. The quantities in parentheses represent the 95% confidence interval.

4.2 Fornax

We refer the reader to [5], which gives the details of how the $\boldsymbol{\mu}$ for this galaxy was measured, presents the result, and discusses its implications.

4.3 Sagittarius

The data for Sagittarius consist of imaging at three epochs for each of three fields using the Wide Field Planetary Camera 2. The first-epoch data are in two bands. There are no bright QSOs in the fields that could act as standards of rest and the images are not deep enough for faint compact galaxies to play this role. Instead, we measure the motion of Sagittarius with respect to Galactic bulge stars and then use the published $\boldsymbol{\mu}$ of the bulge stars to determine the $\boldsymbol{\mu}$ for the galaxy. At the time of writing this contribution, we are still in the process of analyzing the data and, thus, discourage the reader from using the following quoted results for detailed studies of the motion of Sagittarius.

Sagittarius has a measured $(\mu_\alpha, \mu_\delta) = (-312\pm13, -187\pm14)\,\mathrm{mas\,century}^{-1}$ and a $(\mu_\alpha^{\mathrm{GRF}}, \mu_\delta^{\mathrm{GRF}}) = (-251 \pm 13, -18 \pm 14)$ mas century^{-1}. The heliocentric distance of 26.3 kpc and radial velocity of 142.1 ± 0.7 km s^{-1} yield $V_r = 132 \pm 2\,\mathrm{km\,s}^{-1}$ and $V_t = 333 \pm 17\,\mathrm{km\,s}^{-1}$. The resulting orbit has a fairly high inclination of $63°(58°, 70°)$, a peri- and apocenter of 16 (15, 17) kpc and 85 (60, 125) kpc, respectively, and a period of 1.3 (0.93, 2.0) Gyr.

5 Future Prospects

We plan to continue measuring proper motions of dSphs being convinced that complete space motions are important in understanding the origin of the local volume. We are undertaking a search for QSOs behind the newly-discovered dSphs so that their $\boldsymbol{\mu}$s can be eventually measured with HST or a next-generation space telescope.

References

1. D. I. Dinescu, B. A. Keeney, S. R. Majewski, & T. M. Girard: AJ, **128**, 687 (2004)
2. J. S. Kalirai, et al.: ApJ, **657**, L93 (2007)
3. A. Klypin, H. Zhao, & R. S. Somerville: ApJ, **573**, 597 (2002)
4. S. R. Majewski, M. F. Skrutskie, M. D. Weinberg, & J. C. Ostheimer: ApJ, **599**, 1082 (2003)
5. S. Piatek, et al.: AJ, **133**, 818 (2007)
6. A. E. Schweitzer, K. M. Cudworth, S. R. Majewski, & N. B. Suntzeff: AJ, **110**, 2747 (2007)

Extragalactic Stellar Astronomy

Miguel A. Urbaneja, Rolf-Peter Kudritzki, and Fabio Bresolin

University of Hawaii Institute for Astronomy, 2680 Woodlawn Drive, Honolulu HI 96822, USA
urbaneja@ifa.hawaii.edu, kud@ifa.hawaii.edu, bresolin@ifa.hawaii.edu

Despite their paucity, massive hot stars are real *cosmic engines* of fundamental importance in shaping our Universe, from its very early stages up to its current appearance. Understanding the physics of massive stars is then a key issue for many relevant astrophysical phenomena. Their spectra provide constraints required for stellar and galactic evolution calculations, such as mass-loss rates, degree of chemical evolution at different evolutionary stages, star formation history (through [α/Fe] ratios) and spatial distribution of different species. Probing the massive stellar population of nearby galaxies by means of quantitative spectroscopy allows us to unveil a wealth of information that will aid our current understanding of stellar and galaxy evolution. In addition, blue luminous stars can be used as standard candles for extragalactic distances up to 10 Mpc.

Two main factors have contributed in recent years to mature the field of extragalactic stellar astronomy. On the one hand, new observational facilities, in particular ground-based large aperture telescopes equiped with very efficient multi-object optical spectrographs, which make it possible to collect data for a sensible number of stars in different galaxies. On the other hand, enormous advances on model atmosphere techniques allow for the first time the analysis of these large datasets by means of highly sophisticated and detailed models. In this contribution, we present a brief overview of recent steps we have undertaken in this exciting research field.

1 Quantitative spectroscopy of blue supergiant stars

The information about the physical properties of extragalactic massive stars is obtained through the comparison of the observed spectra with synthetic model atmospheres. In contrast to cooler spectral types, the physical processes in the atmospheres of blue supergiant stars are basically dominated by non-LTE conditions, due to the huge radiation field and the low density environment. As previously quoted, the most recent generation of model atmospheres [7, 12, 10]

B.S. Koribalski, H. Jerjen (eds.), *Galaxies in the Local Volume*,
doi: 10.1007/978-1-4020-6933-8_44,

are able to cope with the tremendous challenge posed by these conditions in the presence of supersonic outflows (the stellar wind). The application of such models to the analysis of samples of extragalactic stars, generally observed at lower spectral resolutions, requires first a detailed study of stars in the Milky Way and nearby galaxies to characterize the models and to assess our ability of reproducing the observations [15, 11]. To illustrate the quality than can be achieved, we show in Fig. 1 selected parts of the observed spectrum (ESI/Keck) of an early A Sg in M 33 and the best fitting model.

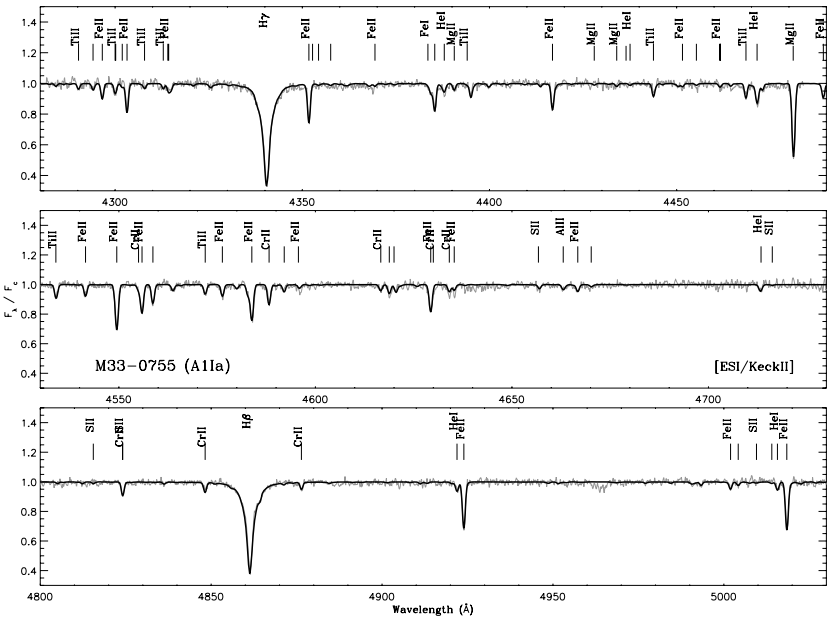

Fig. 1. Comparison of selected parts of the observed (ESI/KeckII, $R \sim 10000$) spectrum of the early A supergiant M33-0755 and the best model. Most prominet spectral features are identified.

Observation of stars in galaxies beyond the Local Group implies the use of low spectral resolution [1, 2]. However, as we have shown in recent years [13, 14, 4, 6], it is possible to get information from these objects even at these low resolutions, provided that the signal-to-noise is high enough (∼50). In the case of OB supergiants (∼O9I–B3I) it is possible to follow the classic techniques used with high-resolution data since the fundamental diagnostic lines are still available. In the case of BA supergiants (∼B4I–A3I), we have developed an alternative technique that enables the analysis of these spectral types even when it is impossible to use the classic methods [9].

2 Blue supergiants' applications

2.1 Chemical abundances in nearby galaxies

To date, studies of the spatial distribution of chemical species in galaxies have been mainly based on oxygen abundances in H II regions. As an alternative, and in some cases complementary, method, oxygen abundances can be determined from B- and A-type supergiant stars, by means of a solid and self-consistent methodology, based on detailed analyses of the atmospheres of such stars. The optical spectra of B- and A-type supergiants are rich in metal absorption lines from several elements (C, N, O, Mg, Al, S, Si, Ti, Fe, among others). As young objects they represent probes of the current composition of the inter-stellar medium (except for those species that are affected by the evolution of the star: C and N), hence these objects can be used to trace the present day abundance pattern in galaxies, with the ultimate goal of recovering its chemical and dynamical evolution history.

We would like to stress that not only oxygen abundances, but a large number of chemical species, in particular Fe-group elements (see Fig. 1), are available through stellar spectroscopy. In our recent work we have demonstrated how quantitative spectroscopy of blue supergiants can render accurate and relevant information about the spatial distribution of different species in several nearby galaxies: WLM [4], IC 1613 [5], NGC 3109 [6], M 33 [15] and NGC 300 [14]. For the Local Group galaxies studied so far, our results are consistent with nebular abundances obtained by the application of the direct method, while in the more distant NGC 300 ($\sim$2 Mpc), our results support some empirical calibrations, while ruling out some others.

2.2 The FGLR and distances in the local Universe

The best established stellar distance indicators, such as Cepheids, RR Lyrae and RGB stars, suffer from two major problems, extinction and metallicity dependence, both of which are difficult to determine for these objects with sufficient precision. In order to improve distance determinations in the local Universe and to assess the influence of systematic errors there is a need for alternative distance indicators, which are at least as accurate but are not affected by uncertainties arising from extinction or metallicity.

Blue supergiants are ideal objects for this purpose, because of their enormous intrinsic brightness, which makes them available for accurate quantitative spectroscopic studies even far beyond the Local Group. Quantitative spectroscopy allows us to determine stellar parameters and thus the intrinsic spectral energy distribution, which can be used to measure reddening and the extinction law. In addition, metallicity can be derived from the spectra.

Theoretical calculations predict that massive stars evolve from the Main Sequence, in their way to the red, at almost constant luminosity and mass [8]. During this brief transitionary period, the ratio of the effective temperature and the effective gravity remains constant. The relationship between the mass and luminosity of supergiants means that the luminosity of blue supergiants in this phase can be inferred from measurements of the effective temperature and effective gravity alone.

This means that spectroscopic observations of blue supergiants in other galaxies may be used, through the Flux-weighted Gravity – Luminosity Relationship, FGLR, to determine distances to these galaxies. This technique is robust, we have shown how observations of at least 10–15 blue supergiants may provide a distance modulus with an uncertainty of 0.1 mag [8]. We have also shown, from observations of blue supergiants in NGC 300, that the photometric variability has negligible effect on the distances determined through the FGLR [3]. The advantage of the FGLR-technique is the fact that individual metallicity, reddening and extinction can be determined for each star directly from spectroscopy combined with photometry.

References

1. F. Bresolin, R.-P. Kudritzki, R.H. Méndez et al: ApJ **548**, L159 (2001)
2. F. Bresolin, W. Gieren, R.-P. Kudritzki et al: ApJ **567**, 277 (2002)
3. F. Bresolin, G. Pietrzyński, W. Gieren et al: ApJ **600**, 182 (2004)
4. F. Bresolin, G. Pietrzyński, M.A. Urbaneja et al: ApJ **648**, 1007 (2006)
5. F. Bresolin, M.A. Urbaneja, G. Pietrzyński et al: ApJ, in press (2007)
6. C.J. Evans, F. Bresolin, M.A. Urbaneja et al: ApJ **659**, 1198 (2007)
7. D.J. Hillier & D.L. Miller: ApJ **496**, 407 (1998)
8. R.-P. Kudritzki, F. Bresolin & N. Przybilla: ApJ **582**, L83 (2003)
9. R.-P. Kudritzki, M.A. Urbaneja, F. Bresolin et al: ApJ, to be submitted
10. A.W.A Pauldrach, T.L. Hoffmann & M. Lennon: A&A **375**, 161 (2001)
11. N. Przybilla, K. Butler, S.R. Becker et al: A&A **445**, 1099 (2006)
12. J. Puls, M.A. Urbaneja, R. Venero et al: A&A **435**, 609 (2005)
13. M.A. Urbaneja, A. Herrero, F. Bresolin et al: ApJ **548**, L73 (2003)
14. M.A. Urbaneja, A. Herrero, R.-P. Kudritzki et al: ApJ **622**, 862 (2005a)
15. M.A. Urbaneja, A. Herrero, R.-P. Kudritzki et al: ApJ **635**, 311 (2005b)

First Results From the Large Binocular Telescope: Deep Photometry of New dSphs

Matthew G. Coleman, and Jelte de Jong

Max-Planck-Institut für Astronomie, Königstuhl 17, D-69117 Heidelberg, Germany
coleman@mpia-hd.mpg.de, dejong@mpia-hd.mpg.de

1 Introduction

At the end of last century, nine dwarf spheroidal (dSph) galaxies were known to orbit the Milky Way. This number has doubled in the past three years, with the majority of new discoveries achieved with the Sloan Digital Sky Survey. In this contribution we present the first deep photometry for two recently discovered Local Group dwarf galaxies. The Hercules dSph was one of five new Milky Way satellites announced last year [1], and Leo T (a transition dwarf) is the faintest known system with recent star formation [2]. Our aim was to derive (i) an accurate structural map of these systems, and (ii) star formation and chemical enrichment histories for both objects. Satellite systems are known to experience tidal disruption due to the Galactic gravitational field, however there are many factors (such as the influence of the satellite halo) whose influence on this processs are not understood. A structural map can reveal at what level the system has been distorted. These are the first scientific results obtained with the Large Binocular Telescope.

2 Photometry From the Large Binocular Telescope

The Large Binocular Telescope (LBT) is located on Mount Graham in Arizona, and consists of two 8.4 metre mirrors on a common mount [3]. Our data were obtained as part of the LBT Science Demonstration Time during which a single mirror of the LBT was fitted with the blue channel of the Large Binocular Camera (LBC; [4, 5]). The LBC is a wide-field imager which provides a $23' \times 23'$ field of view, sampled at 0.23 arcsec/pixel over four chips of 2048×4608 pixels. The observations of the Hercules system consisted of 30 min in B, 20 min in V and 25 min in r. We give an expanded description of the data reduction and photometry techniques in our associated publication [6]. In summary, we obtained photometry for approximately 5×10^4 sources over a $23' \times 23'$ field of view to a limiting magnitude of $V \sim 25.5$ (1.5 magnitudes

B.S. Koribalski, H. Jerjen (eds.), *Galaxies in the Local Volume*,
doi: 10.1007/978-1-4020-6933-8_45,

below the Hercules main sequence turnoff). Similarly, the Leo T observations consisted of 20 min in both the g and r filters, allowing a complete structural map of this system to a limiting magnitude of $g \sim 25.5$.

3 The Elongated Hercules dSph

The colour-magnitude diagram (CMD) of the Hercules system is shown in Fig. 1 (left panel). In this diagram, we are using the c_1 'colour', which is a combination of photometry in B, V and r designed specifically for the Hercules system. Essentially, if we plot a colour-colour-magnitude diagram in three dimensions (that is, $(B-V)$ vs $(V-r)$ vs V), the c_1 colour represents a compression of this dataset onto a two-dimensional plane which maximises the spread in colour of the Hercules stars. This enhances the contrast in the CMD between the Hercules stars and those of the field region, and therefore allows a CMD-selection which is more effective than a simple two-filter (for example, $(B-V)$ vs V space) CMD mask.

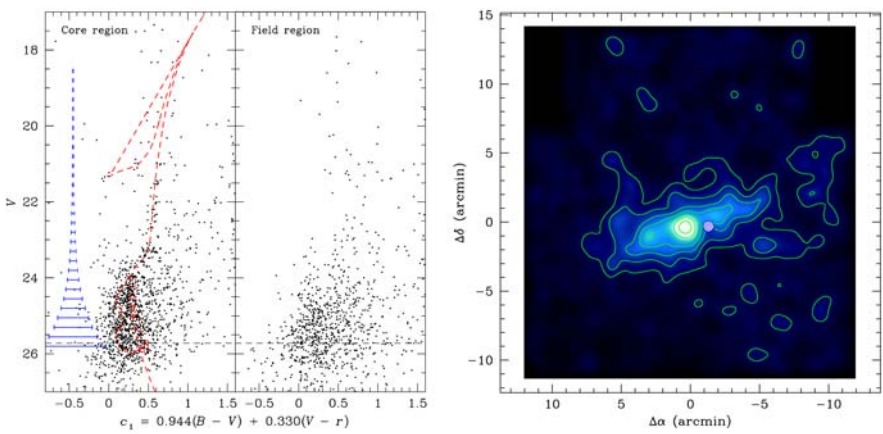

Fig. 1. *(Left:)* The Hercules and field CMDs, shown in the c_1 colour, combining the three-filter photometry. The dashed lines are isochrones representing the Hercules stellar population and the contour outlines our CMD selection region. *(Right:)* Structural contour diagram from the resulting CMD-cleaned dataset. The contours represent stellar densities $1.5\sigma, 3.0\sigma, \ldots, 10.5\sigma$ above the background. Both figures appear in our publication [6].

CMD selection was achieved using the method described by [7], in which a 'signal' map of Hercules stars compared to the field contamination is derived over the CMD. Stars were selected in the CMD region outlined by the red contour in Fig. 1, we convolved them with a Gaussian of radius $0.6'$ to

produce the stellar surface density contour diagram shown in Fig. 1 (right panel). We have found Hercules to be highly elongated. The ellipticity of this system ($e = 0.65$) gives a major-to-minor axis ratio of $3:1$, which is significantly greater than the $\leq 2:1$ values measured for other dSphs (excluding the highly disrupted Sagittarius system).

Three scenarios suggest themselves as explanations for this unusual structure. The first is that Hercules is cigar-shaped. This would make it, by some margin, the most flattened of the Milky Way dSphs known, and it is unclear what this would mean for the initial formation of this system. Also, every other system which has been observed with this level of flattening is a bright galaxy with a rotating disk. Thus, as a second secnario, Hercules may be rotating, however this is inconsistent with our understanding of dSphs, and is not seen in a recent kinematic survey of Hercules [8].

The third scenario is that Hercules has been tidally distorted by the gravitational field of the Milky Way, an effect seen in other systems. However, Hercules is relatively distant (132 ± 12 kpc; [6]), hence tidal distortion would require this system to be on an extreme orbit. We estimate [6] that a pericentric passage of $R_{\rm peri} \sim 8$ kpc is required to have induced tidal distortion. Hercules is not yet at apogalacticon ([8]: Hercules is moving at 144.6 $\mathrm{km\,s^{-1}}$ *away* from the Milky Way), hence our tidal distortion scenario requires an $e > 0.9$ orbit for Hercules. The dSphs with known proper motions all have orbital eccentricities less than 0.7 (see the contributions by Slawomir Piatek and Carlton Pryor). Therefore, although we favour the tidal distortion scenario, it does suggest that Hercules is on an extreme orbit.

4 The SFH of the Leo T Dwarf Galaxy

In the left panel of Fig. 2 we present the CMD of Leo T. Shown are all stars within a $1.4'$ radius from the centre of this very distant object ($\sim$420 kpc). The previously observed [2] very young ($<$1 Gyr) and a much older ($>$5 Gyr) stellar populations are confirmed by our deeper photometry. Several isochrones from [9] are overlayed: the green isochrones are 400 Myr, 650 Myr, and 1 Gyr isochrones with [Fe/H] $= -1.7$. These isochrones fit the young main-sequence stars bluewards of $g - r = 0.0$ and the helium-burning blue loop stars between $(g - r, g)$ of $(0.5, 23.5)$ and $(-0.3, 21)$. In blue and red the 5 Gyr and 12 Gyr for [Fe/H] $= -1.7$ are shown, respectively. Both follow the red giant branch and fit the short horizontal branch or red clump at $(g - r, g) = (0.4, 23.8)$.

To study the star formation history and metallicity evolution of Leo T in more detail, the CMD-fitting software MATCH [10] was used to fit the LBT photometry (see [11] for a description of this package as applied to SDSS-filter photometry). Stars at an appropriate distance from the centre of Leo T were

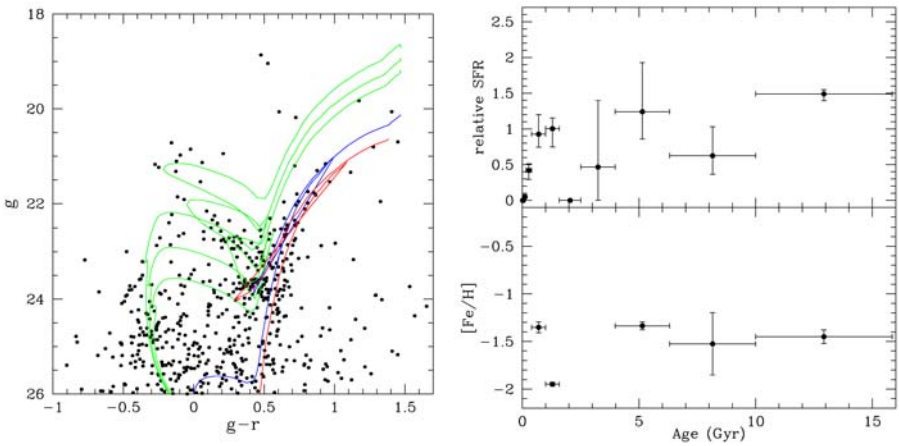

Fig. 2. *(Left:)* The Leo T CMD. *(Right:)* The star formation and [Fe/H] abundance histories of Leo T.

used to construct a control field CMD, which was used to fit the field star contamination. The resulting star formation rate and metallicity as function of time are plotted in the right panel of Fig. 2. As already implied by the overlayed isochrones, an exact age is not found for the older stars, but rather continuous star formation starting in the oldest age bin and continuing until roughly 5 Gyr ago. The young stars seem to have formed in a burst starting slightly more than 1 Gyr and ending a few hundred Myr ago. Remarkably, we find a uniform metallicity of [Fe/H] $\simeq -1.5$ during the early star forming phase. For the young stars we get a similar metallicity. Because of the sparseness of this system, care should be taken not to over-interpret these early results.

References

1. Belokurov, V., et al. 2007, ApJ, 654, 897
2. Irwin, M. J., et al. 2007, ApJ, 656, L13
3. Hill, J. M., Green, R. F., & Slagle, J. H. 2006, Proc. SPIE, 6267, 31
4. Ragazzoni, R., et al. 2006, Proc. SPIE, 6267, 33
5. Giallongo, E., Ragazzoni, R., Grazian, A. et al. 2007, in preparation
6. Coleman, M. G., et al. 2007, ApJL, in press, astro-ph/0706.1669
7. Grillmair, C. J., Freeman, K. C., Irwin, M., & Quinn, P. J. 1995, AJ, 109, 2553
8. Simon, S. D., Geha, M. 2007, ApJ, submitted, astro-ph/0706.0516
9. Girardi, L., Grebel, E. K., Odenkirchen, M., & Chiosi, C. 2004, A&A, 422, 205
10. Dolphin, A. E. 2002, MNRAS, 332, 91
11. de Jong, J. T. A., Butler, D. J., Rix, H.-W., Dolphin, A. E., & Martínez-Delgado, D. 2007, astro-ph/0701140

Proper Motions in the Andromeda Subgroup

Andreas Brunthaler[1], Mark J. Reid[2], Heino Falcke[3,4], Christian Henkel[1], and Karl M. Menten[1]

[1] Max-Planck-Institut für Radioastronomie, Auf dem Hügel 69, 53121 Bonn, Germany
[2] Harvard-Smithsonian Center for Astrophysics, 60 Garden Street, Cambridge, MA 02138, USA
[3] Department of Astrophysics, Radboud Universiteit Nijmegen, Postbus 9010, 6500 GL Nijmegen, The Netherlands
[4] ASTRON, Postbus 2, 7990 AA Dwingeloo, The Netherlands

Summary. This article presents results of VLBI observations of regions of H_2O maser activity in the Local Group galaxies M 33 and IC 10. Since all position measurements were made relative to extragalactic background sources, the proper motions of the two galaxies could be measured. For M 33, this provides this galaxy's three dimensional velocity, showing that this galaxy is moving with a velocity of 190 ± 59 km s^{-1} relative to the Milky Way. For IC 10, we obtain a motion of 215 ± 42 km s^{-1} relative to the Milky Way. These measurements promise a new handle on dynamical models for the Local Group and the mass and dark matter halo of Andromeda and the Milky Way.

1 Introduction

The problem when trying to derive the gravitational potential of the Local Group is that usually only radial velocities are known and hence statistical approaches have to be used. Kulessa and Lynden-Bell introduced a maximum likelihood method which requires only the line-of-sight velocities, but it is also based on some assumptions (eccentricities, equipartition) [1].

Clearly, the most reliable way of deriving masses is using orbits, which requires the knowledge of three-dimensional velocity vectors obtained from measurements of proper motions. However, measuring proper motions of members of the Local Group is difficult. In recent years, the proper motions of a number of Galactic satellites have been measured using the HST ([2] and references therein). These galaxies are all closer than 150 kpc and show motions between 0.2 and a few milliarcseconds (mas) per year. More distant galaxies, such as galaxies in the Andromeda subgroup at distances of ~ 800 kpc, have smaller angular motions, which are currently not measurable with optical telescopes.

B.S. Koribalski, H. Jerjen (eds.), *Galaxies in the Local Volume*,
doi: 10.1007/978-1-4020-6933-8_46,

2 Proper Motions of M 33 and IC 10

We observed H_2O maser emission from two star-forming regions in the disk of M 33 associated with the H II region complexes M 33/19 and IC 133 eight times with the NRAO[5] Very Long Baseline Array (VLBA) between March 2001 and June 2005 [3]. We observed the usually brightest maser in IC 10-SE with the VLBA thirteen times between February 2001 and June 2005 [4].

The motions of 4 components in M 33/19 and 6 components in IC 133 could be followed over all epochs. The component identification was based on the positions and radial velocities of the maser emission. A rectilinear motion was fit to each maser feature in each velocity channel separately. Then, the variance weighted average of all motions was calculated. This yields an average motion of the maser components in M 33/19 of 35.5 ± 2.7 μas yr^{-1} in right ascension and -12.5 ± 6.3 μas yr^{-1} in declination relative to the background source J0137+312. For IC 133 one gets an average motion of 4.7 ± 3.2 μas yr^{-1} in right ascension and -14.1 ± 6.4 μas yr^{-1} in declination.

The observed proper motion of a maser region in M 33 can be decomposed into the motion of the masers due to the internal galactic rotation in M 33, the apparent motion of M 33 caused by the rotation of the Sun around the Galactic Center, and the true proper motion of M 33 relative to the Galaxy. Since the motion of the Sun and the rotation of M 33 [5] are known, one can calculate the true proper motion of M 33: -101 ± 35 km s^{-1} in right ascension and 156 ± 47 km s^{-1} in declination, relative to the center of the Milky Way.

Finally, the systemic radial velocity of M 33 is -179 km s^{-1}. The radial component of the rotation of the Milky Way toward M 33 is -140 ± 9 km s^{-1}. Hence, M 33 is moving with -39 ± 9 km s^{-1} toward the Milky Way. Combining the proper motions and radial velocities, gives the three dimensional velocity vector of M 33. The total velocity of M 33 relative to the Milky Way is 190 ± 59 km s^{-1}.

In IC 10 only the strongest maser component was detected in all epochs. Rectilinear motion was fit to the data and yielded a value of 6 ± 5 μas yr^{-1} toward the East and 23 ± 5 μas yr^{-1} toward the North. Once again, the contributions of the known motion of the Sun and the known rotation of IC 10 [6] can be calculated. The true proper motion of IC 10 is -122 ± 31 km s^{-1} in right ascension and 97 ± 27 km s^{-1} in declination.

The measured systematic heliocentric velocity of IC 10 (-344 ± 3 km s^{-1}) is the sum of the radial motion of IC 10 toward the Sun and the component of the solar motion about the Galactic Center toward IC 10 which is -196 ± 10 km s^{-1}. Hence, IC 10 is moving with 148 ± 10 km s^{-1} toward the Sun. The

[5] The National Radio Astronomy Observatory is operated by Associated Universities, Inc., under a cooperative agreement with the National Science Foundation.

proper motion and the radial velocity combined give the three-dimensional space velocity of IC 10. The total velocity is 215 ± 42 km s^{-1} relative to the Milky Way.

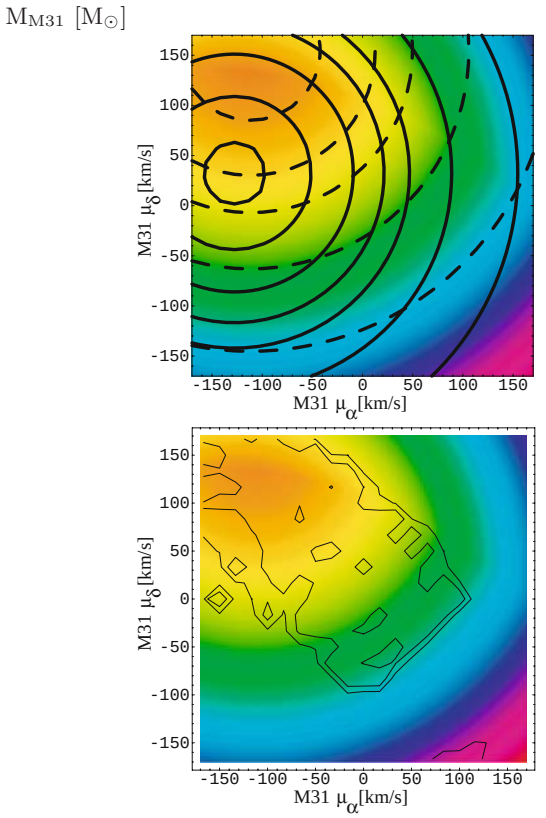

Fig. 1. *(Top:)* Lower limit on the mass of M 31 for different tangential motions of M 31 assuming that M 33 (dashed) or IC 10 (solid) are bound to M 31. The lower limits to the mass of M 31 are (4, 5, 7.5, 10, 15, 25) $\times 10^{11}$ $M_\odot$ for M 33, and (0.7, 1, 2.5, 5, 7.5, 10, 15, 25) $\times 10^{11}$ $M_\odot$ for IC 10, rising from inside. The colour scale indicates the maximum of both values. *(Bottom:)* The colour scale is the same as above and gives the lower limit on the mass of M 31. The contours show ranges of proper motions that would have led to a large amount of stars stripped from the disk of M 33 through interactions with M 31 or the Milky Way in the past. The contours delineate 20% and 50% of the total number of stars stripped [7]. These regions can be excluded, since the stellar disk of M 33 shows no signs of such interactions. Taken from [4].

3 Local Group Dynamics and Mass of M 31

If IC 10 or M 33 are bound to M 31, then the velocity of the two galaxies relative to M 31 must be smaller than the escape velocity and one can deduce a lower limit on the mass of M 31:

$$M_{M31} > \frac{v_{rel}^2 R}{2G}.$$

A relative velocity of 147 $\mathrm{km\,s^{-1}}$ – for a zero tangential motion of M 31 – and a distance of 262 kpc between IC 10 and M 31 gives a lower limit of 6.6×10^{11} $\mathrm{M_\odot}$. One can repeat this calculation for any tangential motion of M 31. The results are shown in Fig. 1 (top). The lowest value of 0.7×10^{11} $\mathrm{M_\odot}$ is found for a tangential motion of M 31 of –130 $\mathrm{km\,s^{-1}}$ toward the East and 35 $\mathrm{km\,s^{-1}}$ toward the North. For a relative motion of 230 $\mathrm{km\,s^{-1}}$ between M 33 and M 31 – again for a zero tangential motion of M 31 – and a distance of 202 kpc, one gets a lower limit of 1.2×10^{12} $\mathrm{M_\odot}$ [3]. Fig. 1 (top) shows also the lower limit of the mass of M 31 for different tangential motions of M 31 if M 33 is bound to M 31. The lowest value is 4×10^{11} $\mathrm{M_\odot}$ for a tangential motion of M 31 of –115 $\mathrm{km\,s^{-1}}$ toward the East and 160 $\mathrm{km\,s^{-1}}$ toward the North.

In [7] it was found that proper motions of M 31 in negative right ascension and positive declination would have lead to close interactions between M 31 and M 33 in the past. These proper motions of M 31 can be ruled out, since the stellar disk of M 33 does not show any signs of strong interactions.

Thus, we can rule out certain regions in Fig. 1. This results in a lower limit of 7.5×10^{11} $\mathrm{M_\odot}$ for M 31 and agrees with a recent estimate of $12.3^{+18}_{-6} \times 10^{11}$ $\mathrm{M_\odot}$ derived from the three-dimensional positions and radial velocities of its satellite galaxies [8].

Acknowledgements:

This research was supported by the DFG Priority Programme 1177.

References

1. Kulessa A. S., Lynden-Bell D., 1992, MNRAS, 255, 105
2. Piatek S., Pryor C., Bristow P., et al., 2006, AJ, 131, 1445
3. Brunthaler A., Reid M. J., Falcke H., Greenhill L. J., Henkel C., 2005, Science, 307, 1440
4. Brunthaler A., Reid M. J., Falcke H., Henkel C., Menten K. M., 2007, A&A, 462, 101
5. Corbelli E., Schneider S. E., 1997, ApJ, 479, 244
6. Wilcots E. M., Miller B. W., 1998, AJ, 116, 2363
7. Loeb A., Reid M. J., Brunthaler A., Falcke H., 2005, ApJ, 633, 894
8. Evans N. W., Wilkinson M. I., 2000, MNRAS, 316, 929

Contrasting the Milky Way and M 31 Satellite Galaxies

Alan W. McConnachie

Department of Physics and Astronomy, University of Victoria,
Victoria, B.C., V8P 1A1, Canada alan@uvic.ca

Recent observations of the Local Group dwarf galaxies are highlighting distinct and important differences between the different subgroups present, particular between the Milky Way and M 31 dSphs. These suggest environmentally-driven differences in the formation and/or evolution of these dwarf galaxies. In addition, new observations are causing us to revise our models of dwarf galaxies and their chemo-dynamical evolution. Here, we review some of these results and their implications for our understanding of these galaxies.

1 The size of dwarf galaxies

The top panel of Figure 1 shows the half-light radii of the most well-studied Milky Way and M 31 dSphs. There is a clear trend for the M 31 dSphs to be larger than their Milky Way counterparts of the same magnitude, by approximately a factor of two. This significant difference suggests that the M 31 environment in somehow conducive to either forming or evolving larger dwarfs than the Milky Way [4].

To investigate the origin of this difference between the populations, [7] and [8] investigate the observable properties of dwarf galaxies modelled as a stellar component described by a King profile embedded in a dominant, cosmologically-motivated, NFW dark halo. Crucially, the degree to which the light profile is embedded within the dark matter halo is a free parameter; [7] find that the velocity dispersion of a satellite is degenerate between this parameter and the mass of the halo (thus, for a given dark matter halo, the velocity dispersion is smaller for more embedded stellar components).

How does this apply to the Milky Way - M 31 satellite populations? Under the assumption that the sub-halo populations of the Milky Way and M 31 are similar, then the more extended light distribution of the M 31 dSphs requires that they possess larger velocity dispersions (bottom panel of Figure 1). In contrast, if future observations show that the velocity dispersions of the Milky

B.S. Koribalski, H. Jerjen (eds.), *Galaxies in the Local Volume*,
doi: 10.1007/978-1-4020-6933-8_47,

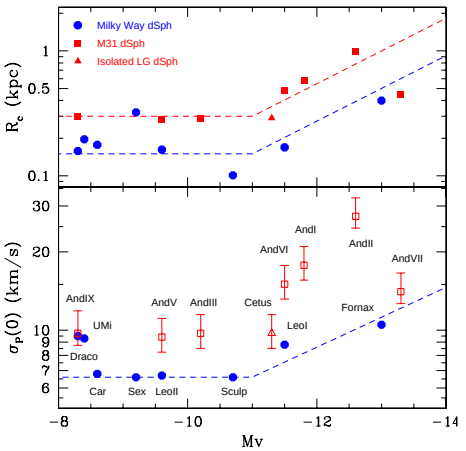

Fig. 1. *(Top panel:)* half-light radii of Milky Way (circles) and M 31 (squares) dSphs, as a function of magnitude. *(Bottom panel:)* **measured** velocity dispersions of the Milky Way dSphs and the **predicted** values for the M 31 dSphs assuming they both inhabit a statistically similar population of cosmological sub-halos.

Way and M 31 dSphs are similar, then this implies that the M 31 dSphs occupy *less massive* halos than their Milky Way counterparts.

Finally, [8] examine whether the differences between the populations of dSphs is because the populations have suffered different amounts of tidal stripping. They find that, although tidal effects can cause the reported difference in the scale sizes, tides would also affect other structural parameters in a way that is not observed. Thus tides do not appear to be sufficient to explain why M 31 and Milky Way have dSphs of different sizes.

2 Multiple dynamical components

McConnachie et al. [5, 3] obtained deep, multi-colour, wide field imaging of And I, II, III, V, VI, VII, Cetus and DDO 210 using Subaru/SuprimeCam. These data are of equivalent depth to previous HST/WFPC2 imaging (eg. [2]), but extend over an area 100 times larger than WFPC2. Figure 2 shows the V vs $(V - I)$ colour magnitude diagram and Hess diagram for And II, with various stellar populations indicated. Figure 3 shows the spatial distribution of these stellar populations.

Dwarf galaxies are traditionally considered as a single stellar component, described by an exponential or King radial profile. However, Figure 3 shows that the appearance of And II changes depending upon the stellar population used to trace its structure. In particular, the horizontal branch (ancient) has a spatially extended structure and the red clump (intermediate age) has a centrally concentrated distribution. McConnachie et al. [3] argue that And II

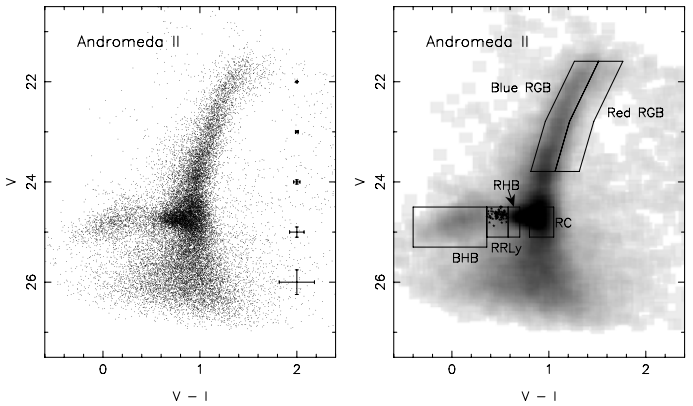

Fig. 2. V-band colour-magnitude *(left)* and Hess *(right)* diagrams for And II, taken with Subaru SuprimeCam. Various stellar populations are marked.

consists of at least two different structural components, one traced by the red clump and the other traced by the horizontal branch population. Recent discoveries for the Milky Way satellites [9, 1] suggest this may be a common structure.

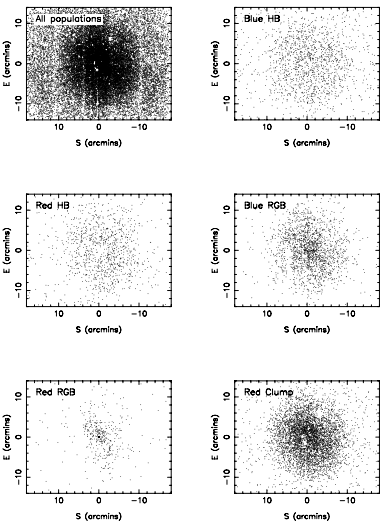

Fig. 3. Spatial distribution of various stellar populations in And II. The density profile of And II changes depending upon which stellar population is used as a tracer.

McConnachie et al. [6] calculate the dynamical structure of And II assuming a two component structure. Figure 4 shows the (normalised) radial profiles of the two proposed stellar components in And II, and the overall

profile. Each of these components must have different kinematic properties due to their vastly different density profiles; the top right panel of Figure 4

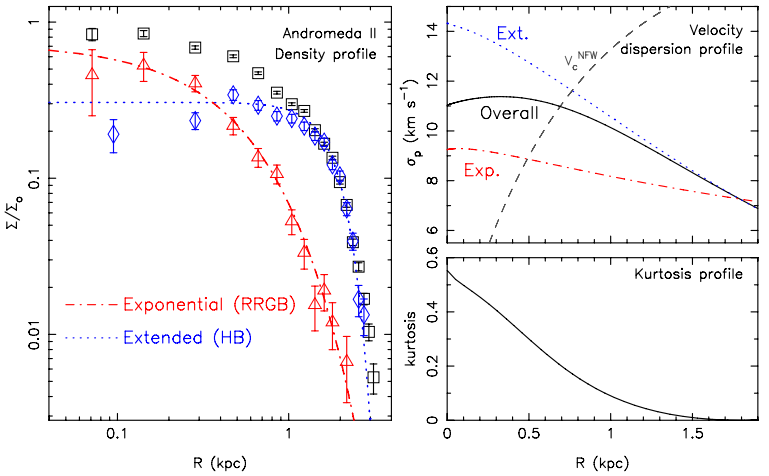

Fig. 4. *(Left panel:)* radial profiles of the two components of And II and the overall profile. *(Right top panel:)* predicted velocity dispersion profiles for the separate components and the overall profile. *(Right bottom panel:)* kurtosis profile for And II.

shows the expected velocity distributions of the two components and the overall profile. The velocity dispersion profile is flat (a common result for dwarf galaxies), but this is because it is the weighted sum of two very different dispersion profiles, one of which is steeply declining. Dynamically, this is a very distinct model of a dwarf galaxy to the standard one, and implies a chemodynamically complex formation process.

References

1. G. Battaglia et al.: A&A, 459, 423 (2006)
2. G. Da Costa, T. Armandroff, N. Caldwell, P. Seitzer: AJ, 119, 705 (2000)
3. A. McConnachie, N. Arimoto, M. Irwin: MNRAS, 379, 379 (2007)
4. A. McConnachie, N. Arimoto, M. Irwin, E. Tolstoy: MNRAS, 373, 715 (2006)
5. A. McConnachie, M. Irwin: MNRAS, 365, 1263 (2006)
6. A. McConnachie, J. Peñarrubia, J. Navarro: MNRAS, 380, L75 (2007)
7. J. Peñarrubia, A. McConnachie, J. Navarro: ApJ, in press (2007)
8. J. Peñarrubia, J. Navarro, A. McConnachie: ApJ, submitted (2007)
9. E. Tolstoy et al.: ApJ, 617, L119 (2004)

Strangers in the Night: Is AndXII Just Passing Through the Local Group?

Geraint F. Lewis[1], S. C. Chapman, J. Penarrubia, R. Ibata,
A. McConnachie, N. Martin, M. Irwin, A. Blain, B. Letarte,
K. Lo, A. Ludlow, and K. O'Neil

[1]Institute of Astronomy, School of Physics, University of Sydney, NSW 2006, Australia gfl@physics.usyd.edu.au

1 Introduction

In ΛCDM cosmologies, the formation and evolution of cosmological structure is an ongoing process, and we should expect a present day drizzle of dwarf galaxies into the Local Group from the nearby filaments. Such dwarfs would not have been shaken and stirred by the tidal fields of massive galaxies, and hence their populations may be more representative of the initial building blocks from which the Milky Way was formed (c.f. [7]). Clearly, the identification of such new members of the Local Group would provide an important test of our models of structure formation.

Newly accreted dwarfs should be identifiable through their kinematics, which should appear anomalous when compared to the overall dwarf population. Earlier this year, it was suggested that a newly discovered dwarf, AndXIV [4], is such a system, appearing close in projection to M 31 with a relative velocity of $\sim$200 km/s, making it potentially unbound. However, an analysis of its RGB properties indicates that AndXIV lies on the nearside of M 31, with respect to the Milky Way, and it has been suggested AndXIV used to be a tightly bound satellite and that its anomalously high velocity is due its ejection in a strong, three-body interaction [6].

The subject of this paper is another newly discovered dwarf galaxy, AndXII, whose location and kinematic properties make it an ideal candidate for being a newly accreted member of the Local Group. If it does not interact strongly with multiple members of the Local Group population, it will simply be passing by, like a stranger in the night.

2 Observations

AndXII was first identified in the CFHT extension of an INT survey of the halo of M 31 [5, 3]. Lying at a projected radius of $\sim$100 kpc, AndXII is quite

B.S. Koribalski, H. Jerjen (eds.), *Galaxies in the Local Volume*,
doi: 10.1007/978-1-4020-6933-8_48,

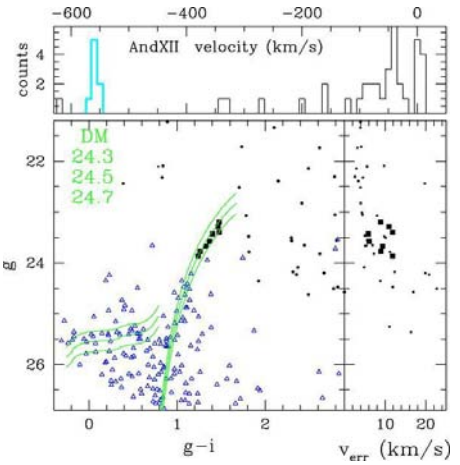

Fig. 1. The *upper panel* presents the velocity distribution of the stars in the AndXII survey. Those at redshift zero are Galactic contamination while those at ~ -300 km/s are M 31 halo stars. The peak at more than ~ -550 km/s is AndXII. The *lower panel* represents the colour-magnitude for the targeted stars, with the RGB of AndXII clearly visible. The *far-right panel* presents the velocity errors.

faint, with an estimated $M_v \sim -6.9$ and a poorly populated red giant branch whose properties indicate that it lies at approximately the same distance as M 31.

Two further sets of observations were obtained to elucidate the nature of AndXII. Firstly, deep imaging with Subaru SuprimeCam extended the CMD to substantially fainter magnitudes, revealing the presence of the horizontal branch (lower panel of Fig. 1). This was used to constrain the distance to AndXII through the fitting of theoretical isochrones drawn from Girardi et al. [2]; examples of these are overlaid on the lower panel of Fig. 1. The lower panel of Fig. 2 presents the distance probability distribution derived from the isochrone fitting. This is strongly skewed, demonstrating that AndXII most probably lies beyond M 31 (780 kpc), and is peaked at ∼850 kpc [1].

The second observations were obtained with the Deimos spectrograph on the Keck-II telescope. Utilizing the 600 line/mm grating, these targeted the spectral range from 5600Å to 9800Å at a resolution of ∼3.5Å. A total of 49 stars were observed and their velocities were determined via template matching of the prominent CaT lines at ∼8600Å. The resulting velocity accuracy proved to be ∼5–10 km/s, with a potential systematic error of ∼10 km/s.

The resulting velocity distribution is presented in the upper panel of Fig. 1; clearly present is local, Milky Way contamination at zero velocity, with additional contamination from the halo of M 31 at ~ -300 km/s. AndXII is clearly visible as a distinct kinematic feature with a velocity of ~ -556 km/s, corresponding to a velocity of ~ -281 km/s relative to M 31.

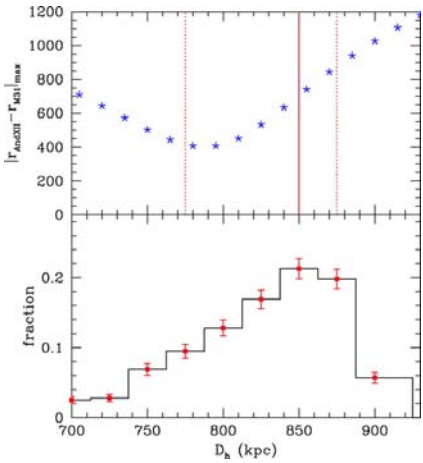

Fig. 2. *(Lower panel:)* the distance estimate to AndXII, peaking at 850 kpc. *(Upper panel:)* the initial distance behind M 31 from which AndXII has fallen to its present position, the most probable distance of ∼800 kpc beyond M 31.

3 Dynamics

The most measured velocity and distance to AndXII reveal that it is located beyond M 31 and is heading towards it. This situation rules out the possibility that AndXII was initially a bound satellite of M 31 which was ejected in a ménage á trois three-body interaction [6].

Is AndXII currently a bound member of the M 31 dwarf population? Fig. 3 presents the relative radial velocity of the members of the M 31 dwarf population, as a function of the separation from M 31. The dotted lines correspond to the rotational velocity of M 31, whereas the solid lines are the escape velocity. The majority of the population lie within the rotation velocity curves, indicating that they are truly bound members. Of the two outliers, AndXIV is close to being unbound, whereas AndXII is unbound, and hence is an ideal candidate for a dwarf galaxy entering the Local Group for the first time.

If AndXII is on its first passage through the Local Group, where did it begin its journey? This question can be addressed by integrating the orbit of AndXII for 10 Gyrs back though the potential of M 31. The results of this analysis are presented in the upper-panel of Fig. 2 which presents the starting distance of AndXII beyond M 31 as a function of its present distance. Given the most likely distance of ∼850 kpc (heliocentric), AndXII was ∼725 kpc beyond M 31 10 Gyrs ago, placing its birth beyond the Local Group. This analysis also confirms that the Hubble time is not long enough for AndXII to have been flung from the Local Group and to be currently on a return journey.

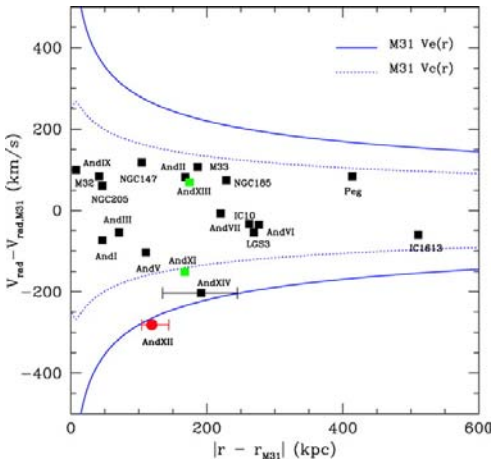

Fig. 3. The radial separation of the dwarf population of M 31, verses their radial velocity separation. The dotted line represents the circular velocity as a function of radius, while the solid line is the escape velocity. The only members of this population which are apparently unbound are AndXII and AndXIV.

4 Conclusions

Current theories of galaxy formation predict that there should be a steady drizzle of material falling into the Local Group from nearby filaments. Such material should include the accretion of dwarf galaxies which are falling into the Local Group for the first time. Such newly accreted dwarfs should be kinematic rogues with velocities distinct from the bound dwarf population.

One dwarf, AndXII, presents a clear candidate for being a newly accreted dwarf, with its position and kinematics revealing that it was most probably born outside the Local Group. Hence, it has not suffered the strong galactic tides that have shaken other members of the dwarf population, and so it may represent a pristine example of the building blocks from which our own stellar halo formed. Finally, if AndXII does not suffer any strong, three-body interactions during its passage, we can expect to sail past, like a stranger in the night, and eventually leave the Local Group.

References

1. S. C. Chapman et al. 2007, ApJ, **662**, L79
2. L. Girardi, E. K. Grebel, M. Odenkirchen & C. Chiosi 2004, A&A, **422**, 205
3. R. Ibata et al. 2007, astro-ph/0704.1318
4. S. R. Majewski et al. 2007, astro-ph/0702635
5. N. F. Martin et al. 2006, MNRAS, **371**, 1983
6. L. V. Sales, J. F. Navarro, M. G. Abadi & M. Steinmetz 2007, MNRAS, in press, astro-ph/0704.1773
7. E. Tolstoy 2003, AJ, **125**, 707

Substructure Along M 31's Southeast Minor Axis: The Forward Continuation of the Giant Southern Stream

Karoline M. Gilbert[1], M. Fardal[2], J. S. Kalirai[1,3], P. Guhathakurta[1], M. C. Geha[4], J. Isler[5], S. R. Majewski[6], J. C. Ostheimer[6], R. J. Patterson[6], D. B. Reitzel[7], E. Kirby[1], and M. C. Cooper[8]

[1] UCO/Lick Observatory, Univ. of California Santa Cruz, 1156 High Street, Santa Cruz, CA, 95064, USA kgilbert@ucolick.org, jkalirai@ucolick.org, raja@ucolick.org, ekirby@ucolick.org
[2] Dept. of Astronomy, Univ. of Massachusetts, Amherst, MA 01003, USA fardal@fcrao1.astro.umass.edu
[3] Hubble Fellow
[4] Plaskett Fellow, NRC Herzberg Institute of Astrophysics, 5701 West Saanich Road, Victoria, B. C., Canada V9E 2E7 marla.geha@nrc-cnrc.gc.ca
[5] Fisk Univ./Vanderbilt Univ., Nashville, Tennessee 37325, USA jcisler@ucolick.org
[6] Dept. of Astronomy, Univ. of Virginia, PO Box 400325, Charlottesville, VA 22904, USA srm4n@virginia.edu, jostheim@alumni.virginia.edu, rjp0i@virginia.edu
[7] Dept. of Physics & Astronomy, Knudsen Hall, Univ. of California, Los Angeles, CA 90095, USA reitzel@astro.ucla.edu
[8] Dept. of Astronomy, Campbell Hall, Univ. of California, Berkeley, CA 94720, USA cooper@astron.berkeley.edu

Summary. We present evidence of substructure along the southeastern minor axis of the Andromeda galaxy (M 31) that is likely the forward continuation of M 31's giant southern stream (GSS). M 31 red giant branch (RGB) stars are separated from foreground Milky Way (MW) dwarf stars using a likelihood method based on photometric and spectroscopic diagnostics. The separation is achieved *without* using the velocity of the stars, allowing an unbiased study of M 31's stellar kinematics in eight fields located 9 – 30 kpc from M 31's center (in projection). The line-of-sight velocity distribution of the 1013 M 31 RGB stars is composed of two components: a broad (hot) component ($\sigma_v^{\rm sph} = 129$ km s^{-1}) which presumably represents M 31's virialized spheroid, and a narrow (cold) component centered near M 31's systemic velocity with a velocity dispersion that decreases with increasing radial distance. The spatial and velocity distribution of the cold component is similar to that of the "Southeast shelf" predicted by the orbital model of the progenitor of the GSS presented in [1].

B.S. Koribalski, H. Jerjen (eds.), *Galaxies in the Local Volume*,
doi: 10.1007/978-1-4020-6933-8_49,

1 Motivation

In the hierarchical galaxy formation paradigm, a series of major and minor merger events results in the build-up of massive galaxies [2, 3]. As a consequence of hierarchical galaxy formation, tidal debris from past accretion events should be present in galactic stellar halos. Observations of tidal streams in the stellar halos of the Milky Way (MW) and M 31 are providing direct and detailed constraints on theories of stellar halo formation (e.g., [4, 5, 6]). In addition, if sufficient phase-space information is available, the observed properties of tidal streams can be used to constrain the galactic potential in which they are found (e.g., [7, 8]).

Detailed modeling of the interaction which produced M 31's GSS [9, 10, 11, 1] has been motivated by observations of its spatial and kinematical properties [12, 9, 13, 14]. The simulations of [1] indicate that several of the observed features in M 31 (the Northeast and Western shelves) may be the forward continuation of the GSS. Their model predicts the presence of a weak shelf on the eastern side of M 31 which would be most visible near the southeastern minor axis. We present evidence of substructure at the expected location of this shelf which has the distinct kinematic profile predicted by the orbital model of [1]. The substructure was discovered during an on-going spectroscopic survey of RGB stars in M 31's inner spheroid and outer halo using Keck/DEIMOS[9] [15]. A more detailed analysis of the data set and the origin of the observed substructure can be found in [16].

2 Observations

The data set is drawn from Keck/DEIMOS spectroscopy of several fields on/near the southeastern minor axis of M 31 which span a range of projected radial distances from M 31's center of $R_{\rm proj} \sim 9$–30 kpc. The largest source of contaminants in the data are foreground Milky Way (MW) dwarf stars. Since the radial velocity distribution of M 31 RGB stars and MW dwarf stars overlaps, we have developed an empirical method which uses several photometric and spectroscopic diagnostics to determine the probability that an individual star is an M 31 red giant or MW dwarf star [15]. These diagnostics include (i) radial velocity, (ii) DDO51 photometry to measure the strength of the (surface-gravity sensitive) MgH/Mg b absorption features, (3) strength of the Na I 8190 absorption line doublet, (4) location within an (I, $V - I$) color-magnitude diagram, and (5) comparison of photometric (color-magnitude diagram based) versus spectroscopic (Ca II 8500 triplet based) metallicity

[9] Data presented herein were obtained at the W. M. Keck Observatory, which is operated as a scientific partnership among the California Institute of Technology, the University of California and the National Aeronautics and Space Administration. The Observatory was made possible by the generous financial support of the W. M. Keck Foundation.

estimates. In the current work, all available diagnostics, with the exception of radial velocity, are used to determine whether an individual star is an M 31 RGB star or a MW dwarf star. This provides a kinematically unbiased sample of 1013 M 31 RGB stars.

Figure 1 (*left panel*) presents the (heliocentric) line-of-sight velocity distribution of the M 31 RGB stars. The distribution is best fit by a double Gaussian, composed of a relatively broad (hot, $\sigma_v^{\rm sph} = 129$ km s^{-1}) and narrow (cold, $\sigma_v^{\rm sub} = 42$ km s^{-1}, $N_{\rm sub}/N_{\rm tot} = 19\%$) component, both centered near the systemic velocity of M 31 ($v_{\rm sys} = -300$ km s^{-1}). The hot component represents the spheroid of M 31, while the cold component is evidence of substructure. Analysis of the individual fields shows that three of the eight fields (ranging from $R_{\rm proj} = 12 - 18$ kpc) are the primary contributors to the cold component; the cold component comprises $\approx 41\%$ of the stars in these three fields. The top right panel of Fig. 1 shows the M 31 RGB velocity distribution as a function of distance along the minor axis. The width of the cold component decreases with increasing distance from the center of M 31. The reader is referred to [16] for further details of the photometric and spectroscopic observations, spectroscopic data reduction, sample selection, and kinematical analysis.

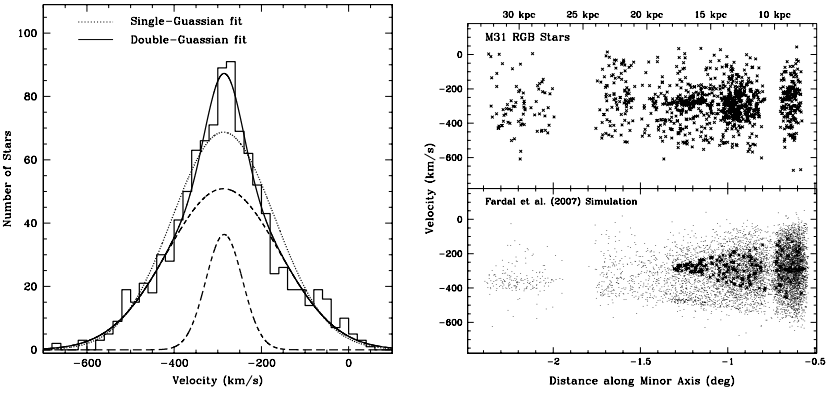

Fig. 1. (*Left:*) Line-of-sight velocity distribution of the M 31 RGB stars. The distribution is a poor fit to a single Gaussian ($\sigma = 117$ km s^{-1}, dotted line), but is well fit by a double Gaussian (solid line) consisting of a kinematically hot (broad) and cold (narrow) component ($\sigma_v^{\rm sph} = 129$ km s^{-1} and $\sigma_v^{\rm sub} = 42$ km s^{-1}, dashed lines), both centered near the systemic velocity of M 31. (*Right:*) Line-of-sight velocity vs. distance along M 31's minor axis for the data (*top*) and particles (M 31 plus substructure) from the simulations of [1] (*bottom*); the large points in the bottom panel represent particles associated with the predicted Southeast shelf.

3 Physical Origin of the Cold Component

The triangular shape of the observed cold component in the right panel of Fig. 1 (*top*) is characteristic of the velocity distribution of a shell formed by the tidal disruption of a satellite galaxy on a nearly radial orbit. Fardal et al. [1] present the hypothesis that the Northeast and Western "shelves" observed in M 31 (see Fig. 1 of [1]) are caused by the disruption of the progenitor of the GSS. Their best-fit orbit for the progenitor reproduces observations in the GSS, NE, and W shelves, and predicts a third shell which would be most easily visible along the SE minor-axis. This "Southeast" shelf is composed of leading debris which is between its third and and fourth pericentric passages. The bottom right panel of Fig. 1 shows the distribution of particles from the simulations presented in [1] (drawn from the same locations as our spectroscopic masks); the large points are particles associated with the predicted Southeast shelf. The predicted SE shelf particles have a very similar spread in velocities as a function of distance as the observed cold component, and the tip of the feature (i.e., the edge of the shell) is at the same projected radius in both the data and the simulations [16]. The remarkably good agreement between the predicted SE shelf and the observed substructure along the SE minor axis implies that the most likely explanation for the physical origin of the cold component is that it is the forward continuation of the GSS [16]. The discovery of the SE shelf will enable detailed modeling of M 31's mass distribution by adding significant observational constraints to those already existing from the GSS, Northeast shelf, and Western shelf [1].

References

1. M. Fardal, P. Guhathakurta, A. Babul et al.: MNRAS, in press, astro-ph/0609050 (2007)
2. L. Searle & R. Zinn: ApJ **225**, 357 (1978)
3. S. White & M. Rees: MNRAS **183**, 341 (1978)
4. K. Johnston: ApJ **495**, 297 (1998)
5. A. Helmi & T. de Zeeuw: MNRAS **319**, 657 (2000)
6. J. Bullock & K. Johnston: ApJ **635**, 931 (2005)
7. K. Johnston, D. Spergel & C. Haydn: ApJ **570**, 656 (2002)
8. J. Peñarrubia, A. Benson, D. Martínez-Delgado et al.: ApJ **645**, 240 (2006)
9. R. Ibata, S. Chapman, A. Ferguson et al.: MNRAS **351**, 117 (2004)
10. A. Font, K. Johnston, P. Guhathakurta et al.: AJ **131**, 1436 (2006)
11. M. Fardal, A. Babul, J. Geehan et al.: MNRAS **366**, 1012 (2006)
12. A. McConnachie, M. Irwin, R. Ibata et al.: MNRAS **343**, 1335 (2003)
13. P. Guhathakurta, R. Rich, D. Reitzel et al.: AJ **131**, 2497 (2006)
14. J. Kalirai, P. Guhathakurta, K. Gilbert et al.: ApJ **641**, 268 (2006)
15. K. Gilbert, P. Guhathakurta, J. Kalirai et al.: ApJ **652**, 1188 (2006)
16. K. Gilbert, M. Fardal, J. Kalirai et al.: ApJ, in press, astro-ph/0703029 (2007)

Young Star Clusters in M 31

Heather Morrison[1], Nelson Caldwell[2], Paul Harding[1], Jeff Kriessler[1], James A. Rose[3], and Ricardo Schiavon[4]

[1] Department of Astronomy, Case Western Reserve University, 10900 Euclid Ave, Cleveland OH 44106, USA
hlm5@case.edu,paul.harding@case.edu,jeffrey.kriessler@case.edu
[2] Smithsonian Astrophysical Observatory, Cambridge, MA 02138, USA
caldwell@cfa.harvard.edu
[3] Department of Physics and Astronomy, University of North Carolina, Chapel Hill, NC 27599, USA jim@physics.unc.edu
[4] Department of Astronomy, University of Virginia, Charlottesville, VA 22903-0818, USA ripisc@virginia.edu

Summary. In our study of M 31's globular cluster system with MMT/Hectospec, we have obtained high-quality spectra of 85 clusters with ages less than 1 Gyr. With the exception of Hubble V, the young cluster in NGC 205, we find that these young clusters have kinematics and spatial distribution consistent with membership in M 31's young disk. Preliminary estimates of the cluster masses and structural parameters, using spectroscopically derived ages and HST imaging, confirms earlier suggestions that M 31 has clusters similar to the LMC's young populous clusters.

1 Introduction

In the Milky Way, there is a clear separation between open clusters (which have diffuse structure, generally have low masses and ages, and belong to the disk) and globular clusters (which have a more concentrated structure, higher masses and ages, and where the majority belong to the halo). Other Local Group galaxies, however, have more complex cluster populations. For example, the LMC has "populous blue" clusters, which are young, structurally resemble the Milky Way globulars, and have masses which overlap the globular cluster range. It has been suggested [11] that these populous blue clusters are found in late-type galaxies only; more recently these populous blue clusters have also been compared to the "super star clusters" formed in galaxies with very high star formation rates [13]. Both are of interest in understanding globular cluster formation.

What of M 31's clusters? Remarkably, it is only recently that detailed constraints on the cluster populations have been obtained, particularly for clusters projected on the inner disk and bulge. HST imaging and multi-fiber

B.S. Koribalski, H. Jerjen (eds.), *Galaxies in the Local Volume*,
doi: 10.1007/978-1-4020-6933-8_50,

spectroscopy in particular have played an important role here. This paper describes 85 M 31 clusters, originally classified as globulars, which belong to the disk and have properties in common with both the Milky Way open clusters and the LMC populous blue clusters.

The existence of young clusters in M 31 was noted in work focused both on its globular clusters (eg [11, 1, 2, 3, 6]) and on its open clusters (eg [8, 9, 18]). In general, authors have associated these young clusters with M 31's disk, although [3] invoke an accretion of an LMC-sized galaxy by M 31. Observations are challenging for clusters projected on M 31's disk: many of the early velocities had large errors, there were issues with background subtraction. Here we discuss high-quality spectroscopic measurements of kinematics and ages for the young clusters, supplemented with HST imaging to delineate the structural, spatial and kinematical properties of these young clusters.

2 Observations and Discussion

We obtained data in observing runs on the MMT using Hectospec in 2004 to 2006. We now have high-quality spectral observations of over 350 confirmed clusters in M 31. We used the 270 gpm grating, which gave spectral coverage from 3650–9200Å with a resolution of ∼5Å. In order to sky subtract even in the bright central regions of M 31's disk and bulge, we obtained a number of offset sky exposures to supplement the normal sky fibers.

Using the models presented in [14] for Hδ/Fe4045 and Ca II indices to measure ages, we have identified 85 clusters with ages less than 1 Gyr. We have ACS imaging of a number of these clusters, and find that the ages obtained directly from the CMDs of the clusters agree quite well with the spectroscopic ages.

Inspection of a Spitzer/MIPS 24μm image of M 31 [7] showed that the spatial distribution of the young clusters is well correlated with the star-forming regions in M 31, with the majority associated with the 10 kpc "ring of fire". The kinematics of the young clusters bear out this disk association. The offset sky fibers provide us with an accurate map of the mean disk rotation throughout these inner regions, and the young cluster velocities follow the mean disk velocities closely.

Given the close similarity in spatial distribution and kinematics between the young clusters and other young disk objects, we now investigate both the structural properties and mass distribution of these young clusters.

Cohen et al. [5] highlighted the heterogeneous quality of the M 31 cluster catalogs when they found, using LGSAO on Keck II, that four of the six young clusters observed were in fact asterisms: accidental superpositions of stars which had appeared resolved on the original source material. High spatial resolution imaging can both check for asterisms and also explore the clusters' spatial structure: is their concentration low, like typical Milky Way

open clusters, or high, like globular clusters? There are ACS or WFPC2 images available for 19 of the young clusters. Two of these show no evidence of an underlying cluster, but the remaining 17 are clearly not asterisms. Interestingly, while 12 show the typical low-concentration structure typical of Milky Way open clusters, five of them are quite centrally concentrated, resembling the LMC populous clusters.

We have made rough estimates of the mass of these M 31 young disk clusters, as follows. We used the V-band images from the Local Group Survey [16] to derive new V magnitudes for all these clusters on a consistent and accurate system. We calculated M/L ratios from the spectroscopic age and Z measurements using the formalism in [14]. We have corrected for foreground reddening and a little reddening from M 31's disk (E(B–V) = 0.2 in total). We expect that it will be much higher in some cases (some clusters have E(B–V) as high as 1.3 [1], which will lead to a mass estimate which is too low by more than an order of magnitude). Thus our mass estimates are lower limits, and in some cases the true masses will be significantly higher. The mass histogram for the young clusters is shown in Fig. 1.

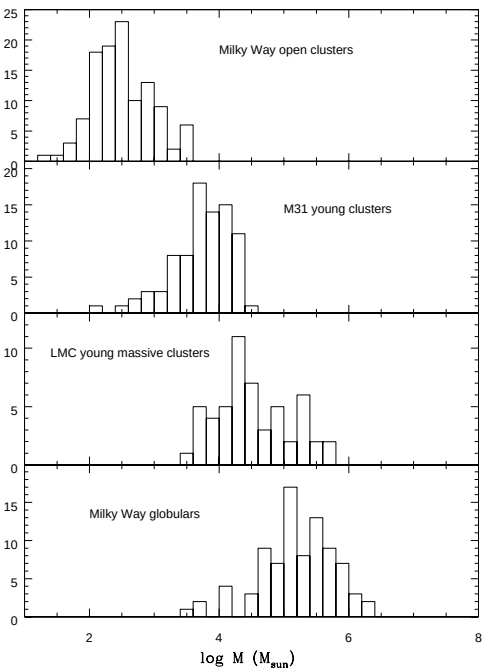

Fig. 1. *(From top to bottom:)* Mass histograms of Milky Way open clusters, M 31 young clusters, LMC massive clusters and Milky Way globular clusters.

We have also shown the mass distribution of Milky Way open clusters within 600 pc of the Sun, from [10], with mass calculations by [12]. This catalog will not include the most massive clusters in the Galaxy because of its relatively small sample size; for example, there have been recent discoveries of more distant young clusters which may have masses as high as 10^5 $M_\odot$ (eg [4]). The Milky Way globular and LMC young massive cluster histograms are shown in the bottom two panels (from [15]).

There is a trend in cluster mass, with the Milky Way open clusters having the lowest median mass, the Milky Way globulars the highest, and the LMC young massive clusters and the M 31 young clusters in between. Our work confirms earlier claims that young populous clusters exist in M 31 [18, 3, 6]: these are not restricted to late-type galaxies.

3 Summary

We have high-quality spectra taken with MMT/Hectospec for 85 star clusters in M 31 with ages less than 1 Gyr. The clusters have spatial and kinematical properties consistent with formation in the star-forming disk of M 31, and structural parameters (from HST imaging) ranging from the low concentrations typical of Milky Way open clusters to the higher concentrations of Milky Way globulars and LMC populous blue clusters. Initial estimates of their masses using spectroscopic ages and new photometry from the Local Group Survey show that some young clusters have masses similar to the populous blue clusters in the LMC: such clusters are not restricted only to late-type galaxies or to galaxies with a very high star formation rate.

References

1. Barmby, P. et al. 2000, AJ, 119, 727
2. Beasley, M. A. et al. 2004, AJ, 128, 1623
3. Burstein, D., et al. 2004, ApJ, 614, 158
4. Clark, J. S. et al 2005, A&A, 434, 949
5. Cohen, J. G., Matthews, K., & Cameron, P. B. 2005, ApJ, 634, L45
6. Fusi Pecci, F. et al. 2005, AJ, 130, 554
7. Gordon, K. D., et al. 2006, ApJ, 638, L87
8. Hodge, P. W. 1979, AJ, 84, 744
9. Hodge, P. W., Mateo, M., Lee, M. G., & Geisler, D. 1987, PASP, 99, 173
10. Kharchenko, N. et al. 2005, A&A, 438, 1163
11. Kennicutt, R. C., Jr., & Chu, Y.-H. 1988, AJ, 95, 720
12. Lamers, H. J. G. L. M. et al. 2005, A&A, 441, 117
13. Larsen, S. S. 2002, Extragalactic Star Clusters, IAUS 207, 421
14. Leonardi, A. J., & Rose, J. A. 2003, AJ, 126, 1811
15. McLaughlin, D. E., & van der Marel, R. P. 2005, ApJS, 161, 304
16. Massey, P. et al. 2006, AJ, 131, 2478
17. van den Bergh, S. 1969, ApJS, 19, 145
18. Williams, B. F., & Hodge, P. W. 2001, ApJ, 559, 851

A Spectroscopic Survey of M 31 Dwarf Spheroidal Galaxies

Jasonjot S. Kalirai[1,2], Puragra Guhathakurta[1], Marla C. Geha[3,4], Karoline M. Gilbert[1], Steven R. Majewski[5], and Rachael L. Beaton[5]

[1] University of California Observatories/Lick Observatory, University of California at Santa Cruz, Santa Cruz CA, 95060, USA jkalirai@ucolick.org
[2] Hubble Fellow
[3] National Research Council of Canada, Herzberg Institute of Astrophysics, Victoria BC, Canada, V9E 2E7
[4] Plaskett Fellow
[5] Department of Astronomy, University of Virginia, P. O. Box 3818, Charlottesville, Virginia 22903, USA

1 Introduction

Among all galaxies in the Universe, dwarf spheroidals (dSphs) may represent the most common morphological class. These low luminosity systems ($-6 < M_V < -13$) show no evidence of ongoing star formation and contain little or no interstellar matter. The distribution of dSphs on the sky indicates that these systems almost always orbit near massive galaxies, such as the Milky Way. Recent studies of the dozen or so dSph members of the Milky Way have demonstrated that this morphological class in fact contains galaxies with significant differences in their star formation histories and metallicities (e.g., Mateo 1998, Mighell & Burke 1999, Gallart et al. 1999). To what extent these differences result from in situ processes versus interactions of these dSphs with the Milky Way is still debated (e.g., Harbeck et al. 2001; Grebel 1997; van den Bergh 1994). Nonetheless, these seeds of galaxy formation likely play an important role in the processes that formed the halos of these massive systems (e.g., Bullock, Kravtsov, & Weinberg 2001).[6]

[6] Data presented herein were obtained at the W. M. Keck Observatory, which is operated as a scientific partnership among the California Institute of Technology, the University of California, and the National Aeronautics and Space Administration. The Observatory was made possible by the generous financial support of the W. M. Keck Foundation. — Based on observations obtained with the Kitt Peak National Observatory. Kitt Peak National Observatory of the National Optical Astronomy Observatories is Operated by the Association of Universities for Research in Astronomy, Inc., under cooperative agreement with the National Science Foundation.

B.S. Koribalski, H. Jerjen (eds.), *Galaxies in the Local Volume*,
doi: 10.1007/978-1-4020-6933-8_51,

Several recent observational campaigns have targeted the Andromeda spiral galaxy (M 31) with wide field imaging as well as spectroscopic instruments (Guhathakurta et al. 2005; Irwin et al. 2005; Gilbert et al. 2006; Kalirai et al. 2006a; Chapman et al. 2006; Ibata et al. 2007). These studies have now uncovered the stellar halo of M 31, and shown that it is in fact similar to the Milky Way in many respects. For example, M 31's halo contains abundant substructure, extends to beyond 100 kpc, and is dominated by stars that are metal-poor. Despite these similarities, the M 31 surface brightness profile differs strongly from the Milky Way in that the metal-poor, power law halo component only begins to dominate the metal-rich inner spheroid at $R > 20 - 30$ kpc, much further out than in the Milky Way (Guhathakurta et al. 2005). Galaxy formation models can reconcile this difference if the past accretion histories of the two galaxies were somewhat different; M 31 likely having experienced more early merger events (see also Hammer et al. 2007).

In just the past three years, the number of dwarf galaxies discovered in M 31 has increased by a factor of two, similar to the Milky Way. Yet, unlike for the Milky Way satellites, a detailed spectroscopic analysis of dozens to hundreds of stars in these dSphs does not yet exist. Such data is not only crucial to understand the detailed properties (e.g., masses, mass-to-light ratio, chemical abundances) of these galaxies, but also to allow a comparison of this sample to the Milky Way dSphs in order to understand whether a different accretion history may have imprinted a signature on the existing dSphs. In this short article, we present the first results from a large Keck/DEIMOS spectroscopic program aimed at measuring accurate radial velocities ($\sigma < 4$ km s^{-1}) for a large group of stars in five M 31 dSphs, And I, II, III, X, XIV.

2 Imaging and Spectroscopic Observations

The imaging data for And I, II, III, and XIV were collected with the wide-field Mosaic camera on the Kitt Peak National Observatory (KPNO) 4-m telescope (Ostheimer 2003; Majewski 2007, in preparation). This camera subtends an angular size of $36' \times 36'$, much larger than the tidal radii of the dSphs. For And X, which was discovered by the Sloan Digital Sky Survey, we use the photometry presented in Zucker et al. (2007).

Multiobject spectroscopic observations of the brightest red giants detected in the imaging studies were collected with the Keck/DEIMOS instrument. We targeted ∼100 stars in each of the five dSphs, using the 1200 lines mm^{-1} grating at a central wavelength of 7800Å. The spectral range of the data is therefore $\sim$ 6400 − 9100Å. The masks ($16' \times 4'$) were positioned in an orientation to include both stars near the centers of the galaxy as well as in the periphery of the galaxy. Further details on the setup of the observations as well as the reduction of the spectroscopic data are provided in several papers (e.g., Guhathakurta et al. 2005; Gilbert et al. 2006; Kalirai et al. 2006b).

Radial velocities are measured for all extracted one-dimensional spectra by cross-correlation with a series of high signal-to-noise stellar templates. The stellar templates were observed using the same DEIMOS setup described above and range in spectral type from G8III to M0III. Radial velocity histograms of those stars for each dSph with good cross-correlation peaks are presented in Figure 1.

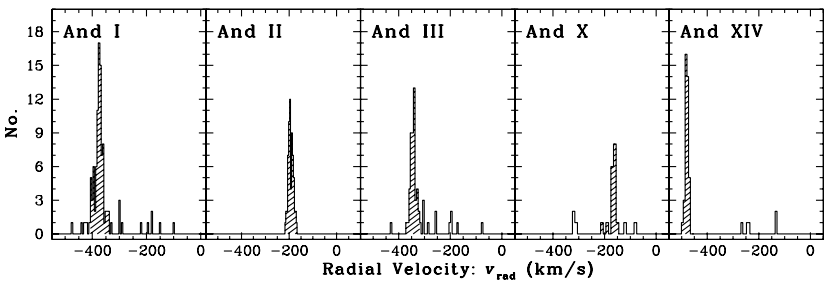

Fig. 1. Keck/DEIMOS radial velocity histograms in five fields centered on M 31's dSph galaxies, And I, II, III, X, and XIV. For each field, the data show a kinematically cold population of stars associated with the dSph (dashed histograms) at a mean radial velocity near M 31's systemic velocity of –300 km s^{-1}. Some residual foreground Milky Way dwarf stars at small negative velocities (most of which have been removed using the techniques in Gilbert et al. 2006) as well as potential M 31 halo stars are also seen.

3 Results

To date, approximately 100 radial velocities have been measured for stars in the entire sample of M 31 dSphs. These previous studies have successfully measured the mean velocities of the galaxies (Cote et al. 1999; Guhathakurta, Reitzel, & Grebel 2000; Chapman et al. 2005) and in the case of And II and IX, also an estimate of the central surface brightness based on ∼10 stars each. The radial velocity histograms in Figure 1 show that we have now measured accurate velocities for a few dozen to a hundred individual stars in each of And I, II, III, X, and XIV (the kinematically cold peaks).

These data will allow us to resolve the intrinsic velocity dispersions of these galaxies, and therefore to measure the total mass and mass-to-light ratios of each galaxy. A direct comparison of the velocity dispersion to that of the Milky Way satellites will help our understanding of the past accretion history of the Milky Way and M 31. For example, McConnachie & Irwin (2006) present a detailed analysis of the structural properties of six of the M 31 dSphs and find that their scale radii are approximately twice as large as the Milky Way dSphs, for the same luminosity. If these systems are of the same total mass, the

larger scale radii should imprint a signature on the kinematics. Penarrubia, McConnachie, & Navarro (2007) predict that the velocity dispersion of the M 31 satellites should be a factor of two larger than the Milky Way satellites. If it is found that in fact the velocity dispersions of the two sets of galaxies are in fact similar, then this suggests that the mass of the M 31 satellites is smaller than the Milky Way satellites, despite their similar luminosities. Such an effect could be explained if the dark matter in the M 31 satellites has been preferentially stripped due to a more violent accretion history.

References

1. Bullock, J., Kravtsov, A., & Weinberg, D. 2001, ApJ, 548, 33
2. Chapman, S. C., Ibata, R. A., Lewis, G. F., Ferguson, A. M. N., Irwin, M., McConnachie, A. W., & Tanvir, N. 2005, ApJ, 632, L87
3. Chapman, S. C., Ibata, R., Lewis, G. F., Ferguson, A. M. N., Irwin, M., McConnachie, A., & Tanvir, N. 2006, ApJ, 653, 255
4. Cote, P., Mateo, M., Olszewski, E. W., & Cook, K. H. 1999, ApJ, 526, 147
5. Gallart, C., Freedman, W. L., Aparicio, A., Bertelli, G., & Chiosi, C. 1999, AJ, 118, 2245
6. Gilbert, K. M., et al. 2006, ApJ, 652, 1188
7. Grebel, E. K. 1997, Rev. Mod. Astron., 10, 29
8. Guhathakurta, P., Reitzel, D. B., & Grebel, E. K. 2000, Proc. SPIE, 4005, 168
9. Guhathakurta, P., Ostheimer, J. C., Gilbert, K. M., Rich, R. M., Majewski, S. R., Kalirai, J. S., Reitzel, D. B., & Patterson, R. J. 2005, astro-ph/0502366
10. Hammer, F., Puech, M., Chemin, L., Flores, H., & Lehnert, M. 2007, ApJ, in press, astro-ph/0702585
11. Harbeck, D. et al. 2001, AJ, 122, 3092
12. Ibata, R., Martin, N. F., Irwin, M., Chapman, S., Ferguson, A. M. N., Lewis, G. F., & McConnachie, A. 2007, ApJ, submitted, astro-ph/0704.1318
13. rwin, M. J., Ferguson, A. M. N., Ibata, R. A., Lewis, G. F., & Tanvir, N. R. 2005, ApJ, 628, L105
14. Kalirai, J. S., Gilbert, K. M., Guhathakurta, P., Majewski, S. R., Ostheimer, J. C., Rich, R. M., Cooper, M. C., Reitzel, D. B., & Patterson, R. J. 2006a, ApJ, 648, 389
15. Kalirai, J. S., Guhathakurta, P., Gilbert, K. M., Reitzel, D. B., Rich, R. M., Majewski, S. R., & Cooper, M. C. 2006b, ApJ, 641, 268
16. Mateo, M. 1998, ARA&A, 36, 435
17. McConnachie, A. W., & Irwin, M. J. 2006, MNRAS, 365, 1263
18. Mighell, K. J., & Burke, C. J. 1999, AJ, 118, 366
19. Ostheimer, J. C. 2003, Ph.D. thesis, University of Virginia
20. Penarrubia, J., McConnachie, A., & Navarro, J. F. 2007, ApJ, submitted, astro-ph/0701780
21. van den Bergh, S. 1994, ApJ, 428, 617
22. Zucker, D. B. et al. 2007, ApJ, 659, L21

The Relics of Structure Formation: High-Velocity Clouds Around M 31

Tobias Westmeier[1,2], R. Braun[1], C. Brüns[2], J. Kerp[2], and D. A. Thilker[3]

[1] Australia Telescope National Facility, CSIRO, P.O. Box 76, Epping, NSW 1710, Australia Tobias.Westmeier@csiro.au
[2] Argelander-Institut für Astronomie, Universität Bonn, Germany
[3] Department of Physics & Astronomy, Johns Hopkins University, Baltimore, MD, USA

1 Introduction

One of the currently most favoured cosmological models is the so-called ΛCDM model which predicts a hierarchical formation of gravitationally bound structures in the universe. A major problem of the ΛCDM scenario is that the number of low-mass dark-matter satellites predicted around the Milky Way by structure formation simulations is more than one order of magnitude higher than the number of Milky Way satellite galaxies known to date. This discrepancy has been named the "missing satellites" problem.

A promising solution was suggested by [1] who proposed that the high-velocity clouds (HVCs) observed all over the sky in the 21-cm line of H I could be the gaseous counterparts of the "missing" dark-matter satellites. Unfortunately, the distances of most HVCs are only poorly constrained. This problem can be solved, however, by studying the HVC populations around other galaxies which would allow us to directly infer the radial distribution and mass spectrum of HVCs for comparison with ΛCDM simulations.

The first comprehensive search for HVCs around M 31, the nearest large spiral galaxy, was carried out by [8] with the 100-m Green Bank Telescope. They detected a population of about 20 HVCs in the 21-cm line of H I within about 50 kpc projected distance from M 31. We carried out a deep, complementary H I blind survey with the Effelsberg 100-m radio telescope to search for HVCs out to much larger projected distances from M 31 in excess of 100 kpc. In addition, follow-up synthesis observations were carried out with the Westerbork Synthesis Radio Telescope (WSRT) to learn more about the internal structure and evolution of the HVCs around M 31 [9].

B.S. Koribalski, H. Jerjen (eds.), *Galaxies in the Local Volume*,
doi: 10.1007/978-1-4020-6933-8_52,

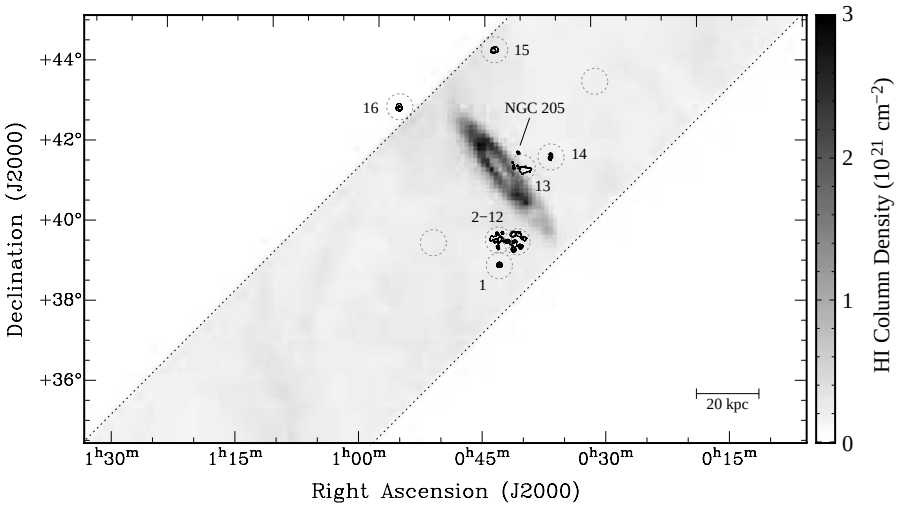

Fig. 1. Integrated H I column density map of our Effelsberg survey of M 31 (within the dotted black lines). The diffuse, faint emission all over the map is foreground emission from the Milky Way. The dotted circles adumbrate the nine fields observed with the WSRT. H I column density maps of the 16 HVCs detected with the WSRT and of NGC 205 are overlaid as black contour lines.

2 Observations and Data Reduction

The observations for the H I blind survey were accomplished between July 2003 and August 2004 with the 100-m radio telescope at Effelsberg. The covered region has a trapezoidal shape with a size of about $15° \times 5°$ (Fig. 1). It reaches out to a maximum projected distance from the centre of M 31 of about 140 kpc in the south-eastern direction, hence extending significantly beyond the region mapped by [8], although the azimuthal coverage at larger projected distances is limited. Our 3σ column density detection limit for the warm neutral medium is $2.2 \times 10^{18}\,\mathrm{cm}^{-2}$ for emission filling the $9'$ HPBW of the telescope, assuming a line width of 25 $\mathrm{km\,s}^{-1}$ FWHM and a velocity resolution of 20 $\mathrm{km\,s}^{-1}$. This translates into a 3σ mass detection limit of 8×10^4 $\mathrm{M}_\odot$ at a distance towards M 31 of 780 kpc [6].

In our follow-up observations with the WSRT, nine pointings were placed on the most conspicuous HVCs seen in the M 31 survey of [8]. The locations of the individual pointings are shown in Fig. 1. The data reduction procedure is described in detail in [9]. The resulting synthesised beam has a FWHM of about $2'$, corresponding to a spatial resolution of about 450 pc at the distance of M 31. The final rms sensitivity towards the centre of each field is about 40 mK. This implies a 3σ H I column density sensitivity of $2.6 \times 10^{18}\,\mathrm{cm}^{-2}$ for emission filling the $2'$ beam.

3 Results

Our Effelsberg observations confirm that M 31 is surrounded by a population of about 15–20 HVCs with typical H I masses of a few times 10^5 $M_\odot$ and diameters of the order of 1 kpc. With these parameters the HVCs detected near M 31 resemble the large HVC complexes observed around the Milky Way. Although our Effelsberg survey reaches out to projected distances in excess of 100 kpc, we do not detect any HVCs beyond a projected distance of about 50 kpc from M 31. In particular, we do not find an extended population of hundreds of compact high-velocity clouds (CHVCs, see [2] and [4]) around M 31. Assuming that the Milky Way and M 31 have a similar CHVC population, we can derive an upper distance limit for CHVCs from their host galaxies of about 60 kpc from our non-detection. Consequently, the small angular diameters of CHVCs are not due to their large distances from the Galaxy but simply reflect their intrinsically small sizes.

One of the most remarkable structures resolved in our follow-up observations with the WSRT is the complex of several HVCs close to the south-eastern edge of the disk of M 31. The individual clouds in this complex are arranged in multiple intersecting filaments. A comparison with the distribution of RGB stars around M 31 [3] reveals that the HVC complex spatially and kinematically overlaps with the giant stellar stream, suggesting a tidal origin of the gas in connection with the stream. Another HVC close to NGC 205 could also have been formed by tidal or ram-pressure forces during the interaction between NGC 205 and M 31. The remaining three clouds studied with the WSRT are completely isolated from any known satellite galaxy or stellar structure of M 31. They are the most promising candidates for primordial dark-matter halos.

4 Discussion

In their numerical structure formation simulations of Galaxy-sized dark-matter halos, [5] made the attempt to include the effects of gas and star formation in the evolution of dark-matter satellites. They concluded that about 2–5 dark-matter satellites with total gas masses of $M_{\rm gas} > 10^6$ $M_\odot$ should exist within a distance of 50 kpc from M 31. This is less than the 15–20 HVCs detected in our Effelsberg survey. However, as indicated by our WSRT observations and suggested by [5], only some of the HVCs found near M 31 could be primordial dark-matter satellites, whereas others were most likely created during the tidal distortion of satellite galaxies of M 31.

Nonetheless, the simulations of [5] predict many more (about 50–100 with $M_{\rm gas} > 10^6$ $M_\odot$) dark-matter satellites at distances beyond 50 kpc from M 31 which have not been detected in our Effelsberg H I survey. Obviously, the direct identification of HVCs with dark-matter satellites fails, and the simulations still predict too many gaseous dark-matter halos. To solve this problem we

can look at the structure of the individual halos in more detail. Sternberg et al. [7] carried out hydrostatic simulations of spherical, dark-matter-dominated CHVCs at a distance of 150 kpc from the Milky Way and compared their results with the parameters of the CHVCs observed on the sky. The basic parameters of their model clouds (such as H I mass, H I peak column density, or diameter) are in excellent agreement with the parameters of the HVCs detected near M 31 with the WSRT. In their model, [7] had to introduce an external pressure of $P/\mathrm{k} \gtrsim 50\,\mathrm{K\,cm^{-3}}$. This pressure – exerted by the hot, ionised circumgalactic corona – is required to stabilise the clouds in addition to their own gravitational potential. Without this constraint, the clouds would become so diffuse that the gas would no longer be sufficiently shielded against the extragalactic radiation field. Consequently, the HVCs would become mainly ionised and undetectable in the 21-cm line emission of neutral hydrogen.

Therefore, we can construct a consistent picture in which part of the HVCs observed around M 31 are the remnants of tidal stripping (e.g., in connection with the giant stellar stream) whereas others could be the gaseous counterparts of primordial dark-matter halos with parameters similar to the CHVC model of [7]. Within 50 kpc radius of M 31, the number of potential primordial HVCs is in agreement with the predictions made by [5] based on their ΛCDM structure formation simulations. Beyond this radius we do not detect any HVCs, although many more dark-matter satellites with sufficiently high gas masses should exist according to [5]. These "missing" satellites, however, could be mainly ionised and therefore undetectable in the H I line if the pressure exerted by the circumgalactic corona decreases below the critical value of $P/\mathrm{k} \approx 50\,\mathrm{K\,cm^{-3}}$ at larger distances from M 31. Consequently, we would detect only those dark-matter satellites which are close enough to M 31 to be stabilised by the external pressure, but many more highly ionised or pure dark-matter halos could exist at larger distances from M 31.

References

1. L. Blitz, D.N. Spergel, P.J. Teuben et al.: ApJ **514**, 818 (1999)
2. R. Braun, W.B. Burton: A&A **341**, 437 (1999)
3. A.M.N. Ferguson, S. Chapman, R. Ibata et al.: A Keck/Deimos Survey of Red Giant Branch Stars in the Outskirts of M 31. In: *Planetary Nebulae Beyond the Milky Way*, ed by L. Stanghellini, J.R. Walsh, N.G. Douglas (Springer, Berlin/Heidelberg 2006) pp 286–291
4. V. de Heij, R. Braun, W.B. Burton: A&A **392**, 417 (2002)
5. A.V. Kravtsov, O.Y. Gnedin, A.A. Klypin: ApJ **609**, 482 (2004)
6. K.Z. Stanek, P.M. Garnavich: ApJ **503**, L131 (1998)
7. A. Sternberg, C.F. McKee, M.G. Wolfire: ApJS **143**, 419 (2002)
8. D.A. Thilker, R. Braun, R.A.M. Walterbos et al.: ApJ **601**, L39 (2004)
9. T. Westmeier, R. Braun, D.A. Thilker: A&A **436**, 101 (2005)

High-Velocity Clouds Merging with the Milky Way

Felix J. Lockman

National Radio Astronomy Observatory[†], P.O. Box 2, Green Bank, WV, 24944, USA jlockman@nrao.edu

Summary. H I observations with the Green Bank Telescope have now given us two clear examples of high-velocity H I clouds which are encountering the Milky Way disk and losing matter to it: Complex H, passing through the plane of the Milky Way in the far outer Galaxy, and Smith's Cloud, just entering the disk in the inner Galaxy. These clouds may give unique insights into the ongoing formation of the Milky Way, its chemical history, and the nature of the high-velocity cloud phenomenon.

1 Introduction

High-velocity H I clouds (HVCs) cover nearly 40% of the sky. Their most likely provenance is as the detrius of galaxy formation: satellites which have not yet made stars, material stripped from satellite galaxies, or remnants of the initial collapse just now arriving on the scene [3, 1, 5, 7, 9]. New H I observations with the Green Bank Telescope (GBT) have shown that two HVCs stand apart from the others in offering particular insight into these phenomena: Complex H and Smith's Cloud.

2 Complex H

This HVC is unusual in that it lies in the Galactic Plane, and thus its high velocity cannot result from purely vertical motions as would arise in a galactic fountain [2]. Figure 1 shows its separation from Galactic emission. Barely visible in this figure, though apparent in GBT H I images which highlight fainter emission [6], is H I at velocities between that of Complex H and the Galaxy, gas which appears to have been stripped from the Complex by its interaction with the Milky Way. Complex H is thus in the class of HVCs studied by Brüns, Mebold and others [4] – HVCs which are interacting with their environment. What makes Complex H especially exciting is its kinematic

[†] The NRAO is a facility of the National Science Foundation operated under cooperative agreement with Associated Universities, Inc.

B.S. Koribalski, H. Jerjen (eds.), *Galaxies in the Local Volume*,
doi: 10.1007/978-1-4020-6933-8_53,

structure, marked by the dashed line. A coherent velocity gradient of this type is most simply explained as a projection effect of vertical motion: at b=0°, $dV_{LSR}/db = V_z$. The observed gradient implies $V_z = -170$ km s^{-1} and the entire kinematics of Complex H can be understood if it is a satellite of the Milky Way in an inclined, circular, retrograde orbit with a total velocity of 220 km s^{-1} at a distance $R \approx 30$ kpc from the Galactic Center [6].

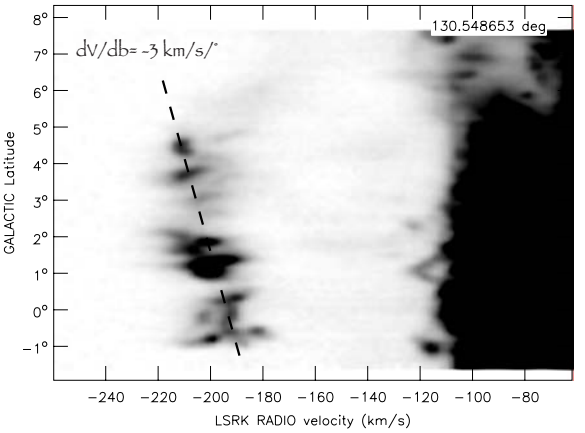

Fig. 1. A velocity-latitude cut through Complex H, which is the band of H I emission near −200 km s^{-1} in this image from GBT H I observations. There is faint H I emission connecting the cloud to the Galactic H I disk (the dark patch to the right at $V_{LSR} > -120$ km s^{-1}), most likely material stripped from the cloud by its encounter with the Milky Way. The cloud's velocity gradient (dashed line) implies a vertical motion of –170 km s^{-1}.

It is tempting to equate Complex H with the small gas-rich satellites found around many other galaxies, some of which have been presented at this meeting. Complex H, however, appears to be devoid of old stars, young stars, molecular clouds, and tracers of star formation [11]. Moreover, about half of its 6×10^6 M$_\odot$ of H I is in diffuse components which appear to have been stripped. Rather than a satellite, Complex H may have more in common with bits of tidal tails or the residual population of clouds expected in models of multiphase galaxy formation [9].

3 Smith's Cloud

This under-appreciated HVC was discovered more than 40 years ago [12] and could be the most important of all. There has been some speculation about its origin, but it has received little observational scrutiny, though it has been

detected in Hα [10]. It is unusual among HVCs in that it has a relatively low longitude and latitude, and has a velocity which is nearly permitted by Galactic rotation. New GBT H I observations show that the cloud has a stunning cometary structure confirming that it is plunging into the Milky Way at about a 45° angle to the plane, and is being shaped by the interaction. A full description of the Cloud will appear elsewhere [8]; here I concentrate on one aspect which makes Smith's Cloud especially important.

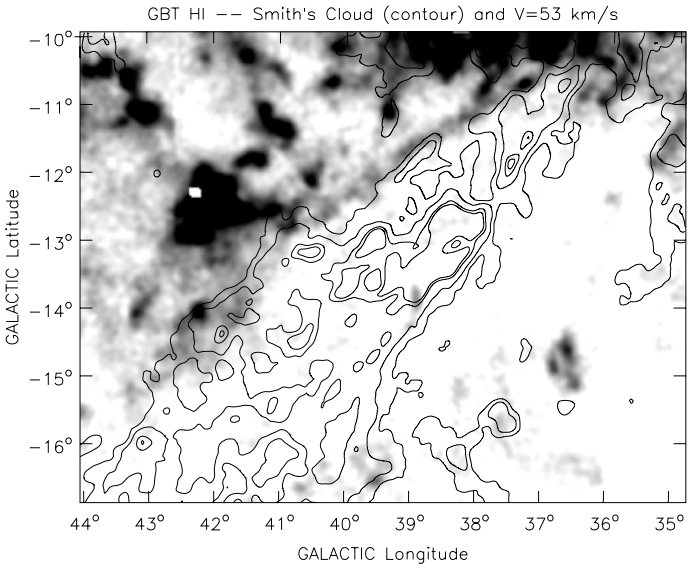

Fig. 2. GBT observations of a portion of Smith's Cloud (contours) and H I at a lower velocity (grey scale) showing a ridge of H I pushed up by the interaction of the cloud with the medium it is encountering. The velocity of the Galactic material which Smith's Cloud is hitting places limits on its distance [8].

Like Complex H, Smith's Cloud has a trail of H I from the high velocities of the cloud core to velocities allowed by Galactic rotation. Unlike Complex H, however, we see clear evidence of the interaction in the ambient medium (Fig. 2). We can estimate the "pre-encounter" velocity of the medium and thus a kinematic distance to the Cloud itself. Remarkably, the kinematic distance is essentially identical to the distance estimated from the Hα luminosity model [10] and a recent absorption-line study by B. Wakker. All place Smith's Cloud less than 8 kpc from the Galactic center, about 90 deg around the Galaxy from the Sun in the direction of galactic rotation, and about 3 kpc below the Galactic plane. It contains at least 10^6 $M_\odot$ of H I.

Smith's Cloud, like Complex H, has such a large angular extent that we can make use of projection effects to obtain information on its complete space

velocity. But unlike Complex H, Smith's Cloud appears to have been profoundly affected by drag and may be fragmenting, making a reconstruction of its initial trajectory more difficult. Early indications are that the cloud must have a total space velocity ≥ 250 km s^{-1} [8]. It is interesting that Smith's Cloud at a distance of 3 kpc from the Galactic plane shows evidence of strong interaction with the Galaxy's halo. Given its velocity relative to the local interstellar medium, it will be a useful probe of conditions in the hot halo.

4 HVCs and the Evolution of the Milky Way

We now have evidence that at least two HVCs are adding gas to the Milky Way. Complex H lies in the outer Galaxy [6], so its material will end up near the edge of the Galactic disk. Smith's Cloud is now plunging into the halo of the inner Galaxy, where its 10^6 $M_\odot$ of H I will encounter a region rich in interstellar gas with many molecular clouds [8]. Although little is known of the composition of the HVCs, their chemical histories are likely to be significantly different than that of the Galaxy. Their origins and the details of the trajectories which brought them to their fateful encounters with the Galaxy may yet be unraveled. After nearly 50 years of dispute and confusion, Galactic high-velocity H I clouds are now being seen as providing crucial elements for our understanding of the formation and evolution of large galaxies.

References

1. R.A. Benjamin: in *High Velocity Clouds*, ed. by H. van Woerden, B.P. Wakker, U.J. Schwarz, K.S. de Boer, Kluwer, Dordrecht, ASSL vol 312, p 371 (2004)
2. L. Blitz, D. Spergel, P. Teuben, D. Hartmann, W.B. Burton: ApJ, **514**, 818 (1999)
3. J.N. Bregman: in *High Velocity Clouds*, ed. by H. van Woerden, B.P. Wakker, U.J. Schwarz, K.S. de Boer, Kluwer, Dordrecht, ASSL vol 312, p 341 (2004)
4. C. Brüns, U. Mebold: in *High Velocity Clouds*, ed. by H. van Woerden, B.P. Wakker, U.J. Schwarz, K.S. de Boer, Kluwer, Dordrecht, ASSL vol 312, p 251 (2004)
5. T.W. Connors, K. Daisuke, J. Balin, J. Tumlinson, B.K. Gibson: ApJ, **646**, L53 (2006)
6. F.J. Lockman: ApJ, **591**, L33 (2003)
7. F.J. Lockman, E.M. Murphy, S. Petty-Powell, V.J. Urick: ApJS, **140**, 331 (2003)
8. F.J. Lockman, R.A. Benjamin, A.J. Heroux, G.I. Langston: ApJ, (in press)
9. A.H. Maller, J.S. Bullock: MNRAS, **355**, 694 (2004)
10. M.E. Putman, J. Bland-Hawthorn, S. Veilleux, B.K. Gibson, K.C. Freeman, P.R. Maloney: ApJ, **597**, 948 (2003)
11. J.D. Simon, L. Blitz, A.A. Cole, M.D. Weinberg, M. Cohen: ApJ, **640**, 270 (2006)
12. G.P. Smith: Bull. Astr. Inst. Netherlands, **17**, 203 (1963)

The Origin of the Magellanic Stream and its Leading Arm

David L. Nidever[1], Steven R. Majewski[1], and W. Butler Burton[2,3]

[1] Dept. of Astronomy, University of Virginia, Charlottesville, VA 22904-4325, USA dnidever@virginia.edu, srm4n@virginia.edu
[2] Sterrewacht Leiden, PO Box 9513, 2300 RA Leiden, The Netherlands
[3] National Radio Astronomy Observatory, 520 Edgemont Road, Charlottesville, Virginia 22903, USA bburton@nroa.edu

1 Introduction

Simulations using the currently favored concordance ΛCDM cosmology show that galaxies form through hierarchical accretion and merging of dark matter subhalos [20, 5, 15] even until late times [3]. Disruption and accretion of small galaxies gives rise to stellar and sometimes gaseous tidal streams that continue to orbit the accreting galaxy as fossil relics of the cannibalistic activity.

The most well-known gaseous stream around the Milky Way (MW) is the Magellanic Stream (MS). The MS has been extensively studied using 21cm observations, and there have also been many efforts to model the MS using two primary mechanisms: (1) tidal stripping, and (2) ram pressure stripping. In the recent past Putman et al. used the HIPASS data to discover a leading arm of the MS (which fits well with the predictions of the tidal model) and that the MS is spatially bifurcated into two filaments [18].

In recent modeling work Mastropietro et al. performed a large-scale ram pressure simulation of the MS [14] and were able to reproduce most features of the trailing MS, but could not create the Leading Arm. Connors et al. [4] carried out an extensive tidal simulation and were able to reproduce most of the characteristics of the MS and Leading Arm known so far, including the bent shape of the Leading Arm and the bifurcation of the MS.

However, there remain substantial challenges for each of these formation mechanisms of the MS. The tidal model reproduces most of the main characterstics of the MS and Leading Arm, but it also predicts that there should be stars in the MS which have not been observed. Ram pressure models naturally do not predict any stars in the MS, but can not reproduce the Leading Arm. A recent challenge to both mechanisms are the new orbits of the Magellanic Clouds (MCs) [2] (using the new HST proper motions [10, 11]) which indicate that the MCs were too far away from the MW around $\sim$1 Gyr (the approximate age of the MS) in order for these mechanisms to operate.

B.S. Koribalski, H. Jerjen (eds.), *Galaxies in the Local Volume*,
doi: 10.1007/978-1-4020-6933-8_54,

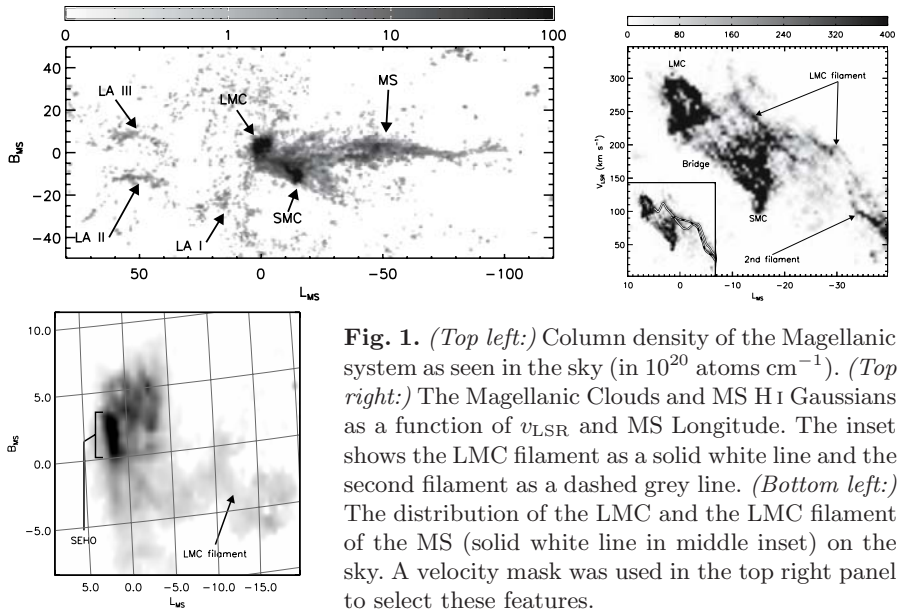

Fig. 1. *(Top left:)* Column density of the Magellanic system as seen in the sky (in 10^{20} atoms cm^{-1}). *(Top right:)* The Magellanic Clouds and MS H I Gaussians as a function of $v_{\rm LSR}$ and MS Longitude. The inset shows the LMC filament as a solid white line and the second filament as a dashed grey line. *(Bottom left:)* The distribution of the LMC and the LMC filament of the MS (solid white line in middle inset) on the sky. A velocity mask was used in the top right panel to select these features.

We undertook a detailed study of the H I structure of the MS and Leading Arm with the Leiden-Argentine-Bonn (LAB) H I all-sky survey [9] to understand their site of origin and formation mechanism.

2 The Origin of the Magellanic Stream

We wrote a Gaussian decomposition program, similar to that used by Haud [8], and ran it on the entire LAB datacube. This yields a map of identified H I structures, and allows us to (1) disentangle structures overlapping in velocity, (2) reduce our data by a factor of ∼30, and (3) track and enhance features in the H I datacube by plotting only their Gaussian centers.

Figure 1 shows the results of the Gaussian decomposition. The two filaments that Putman et al. found to be spatially bifurcated are also distinct in velocity (*top right panel*), and can be traced farther back to the MCs than Putman et al. were able to do. Most previous studies [18, 4] have assumed that the MS originates in the SMC/Bridge region, however, our analysis shows that one of the filaments (solid white line in inset) can be tracked back to the Large Magellanic Cloud (LMC). The second filament can be tracked back to a region near the SMC/Bridge, but it is not clear where it originates. We have used a velocity mask to isolate the gas of the first filament and the LMC in order to ascertain where in the LMC it originates. The results of the masking are shown in the *right panel* of Figure 1 and indicate that the filament originates from the southeastern region of the LMC. This region is very dense in

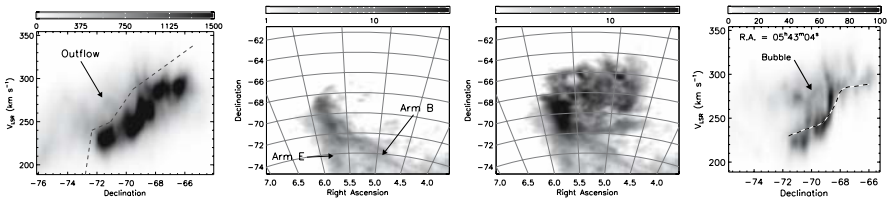

Fig. 2. *(Left:)* Position-velocity plot of the Parkes LMC H I datacube [19] (integrated in R.A.) showing the high-velocity outflow. *(Middle-Left:)* The column density of the high-velocity gas (in units of 10^{20} atoms cm^{-1}) after applying the velocity boundary shown in the left panel (*dashed line*). The high-velocity gas is coming from the SEHO region and is the beginning of the Leading Arm (Arm E) and the LMC filament of the MS (Arm B). *(Middle-Right:)* The column density of the LMC for all velocities for comparison with the middle panel (in units of 10^{20} atoms cm^{-1}). *(Right:)* Position-velocity plot of the Parkes LMC H I datacube [19] in the SEHO region of the LMC at R.A. = $05^{\rm h}\,45^{\rm m}\,04^{\rm s}$. The LMC rotation curve is overplotted in a dashed line. A bubble feature is visible near the positions of SGS 19 and 20, as well as a blob of gas "attached" to the edge of the bubble

H I, rich in CO [21], Hα emission [12], giant molecular clouds [21], and young star clusters [2]. There are also several supergiant shells [12] and two CO filaments [21] in this region. We call this region the Southeastern H I Overdensity (SEHO). The LMC filament connects to Arm B identified by [19].

An analysis of the first complex of the Leading Arm Feature, LA I, shows that it also originates in the SEHO region (see [16] for figures) and connects to Arm E as identified by [19]. Therefore both the Leading Arm and at least one-half of the MS originate in the SEHO region of the LMC, and *not* in the SMC/Bridge as previously assumed.

3 The Blowout Formation Mechanism

What is causing the H I gas to escape from the SEHO region of the LMC? It has been known since [13] that the gas in the southeastern region of the LMC is highly disturbed and has two velocity components. We have taken a closer look at the Parkes LMC H I datacube [19]. The position-velocity plot shows that the southeastern part of the LMC has two velocity components, and there is high-velocity gas escaping from the LMC (Fig. 2 *left panel*). After applying a velocity mask filter, we can derive the distribution of the high-velocity gas on the sky (Fig. 2 *middle-left panel*), which reveals that the high-velocity gas is escaping from the SEHO region and is the beginning of the LMC filament of the MS and the Leading Arm.

Kim et al. [12] discovered many giant and supergiant shells (SGS) in the LMC using high-resolution ATCA data. Three of the supergiant shells are in the SEHO region. Single position-velocity slices through the SEHO region

show evidence of a large bubble or cavity near the position of SGS 19 and 20, as well as a large "blob" of gas escaping from that region (Fig. 2, *right*). We believe that SGSs are responsible for blowing out the gas that eventually becomes the MS and Leading Arm. In this way, the *stripping* of the gas from the LMC is not performed by the "traditionally" discussed mechanisms (i.e. tidal and ram pressure), but by SGS blowout. Once the gas is sufficiently far from the LMC and its gravitational pull, tidal and ram pressure forces can act upon the gas and pull/push it to form the MS and Leading Arm. This explains the lack of stars, yet why it has a leading arm, as obtained in tidal models.

This new formation mechanism is viable even with the newly derived, hyperbolic orbits of the Magellanic Clouds [2] since the blowout of the gas from the LMC is independent of the LMC's orbit.[4] Once the gas is blown out the tidal and ram pressure forces should be sufficiently large (even with the new orbits) to shape the gas into the MS and Leading Arm. Self-propagating star formation (which Kim et al. [12] claim is ongoing in the SEHO region) or bow-shock induced star formation [6] might be necessary to sustain an approximately constant amount of SGS blowout from the SEHO region for $\sim$1 Gyr in order to create the $\sim$100° long MS.

References

1. Besla, G., et al. 2007, ApJ, submitted (astro-ph/0703196)
2. Bica, E.L.D., et al. 1999, A&A, 117, 238
3. Bullock, J. S., & Johnston, K. V. 2005, ApJ, 635, 931
4. Connors, T. W., Kawata, D., & Gibson, B. K. 2006, MNRAS, 371, 108
5. Davis, M., Efstathiou, G., Frenk, C. S., & White, S. D. M. 1985, ApJ, 292, 371
6. de Boer, K. S., Braun, J. M., Vallenari, A., & Mebold, U. 1998, A&A, 329, L49
7. Grillmair, C. J. 2006b, ApJ, 651, L29
8. Haud, U. 2000, A&A, 364, 83
9. Kalberla, P. M. W., et al. 2005, A&A, 440, 775
10. Kallivayalil, N., et al. 2006, ApJ, 638, 772
11. Kallivayalil, N., van der Marel, R. P., & Alcock, C. 2006, ApJ, 652, 1213
12. Kim, S., et al. 1999, A&A, 118, 2797
13. Luks, T., & Rohlfs, K. 1992, A&A, 263, 41
14. Mastropietro, C., et al. 2005, MNRAS, 363, 509
15. Navarro, J. F., Frenk, C. S., & White S. D. M. 1996, ApJ, 462, 563
16. Nidever, D.L, et al. 2007, ApJ, submitted (astro-ph/0706.1578)
17. Putman, M. E., et al. 1998, Nature, 394, 752
18. Putman, M. E., et al. 2003, ApJ, 586, 170 (P03)
19. Staveley-Smith, L., et al. 2003, MNRAS, 339, 87 (S03)
20. White, S. D. M., & Rees, M. J. 1978, MNRAS, 183, 341
21. Yamaguchi, R., et al. 2001, PASJ, 53, 985

[4] Although the orbit will influence the interaction history of the LMC with the SMC and other satellites, which might in turn affect the LMC star formation history and SGS blowout.

Evolution of the Small Magellanic Cloud

Kenji Bekki

School of Physics, University of New South Wales, Sydney 2052, Australia
bekki@phys.unsw.edu.au

1 Numerical simulations of the SMC evolution

We investigate (1) the origin of the bifurcation of the Magellanic stream (MS), (2) the formation of distinctively metal-poor stellar populations in the Large Magellanic Cloud (LMC) due to sporadic gas transfer from the SMC, and (3) the collision between the leading arms (LAs) of the MS and the outer part of the Galactic H I disk based on numerical simulations of LMC-SMC-Galaxy interaction for the last 2.5 Gyr (e.g., Bekki & Chiba [2]). We adopt numerical methods and techniques of the simulations on the evolution of the MCs used in our previous papers (Bekki & Chiba [1]): we first determine the most plausible and realistic orbits of the MCs by using "the backward integration scheme" (for orbital evolution of the MCs) by Murai & Fujimoto [5] for the last 2.5 Gyr and then investigate the evolution of the MCs using GRAPE systems (Sugimoto et al. [7]). The total masses of the LMC and the SMC are set to be 2.0×10^{10} $M_{\odot}$ and 3.0×10^{9} $M_{\odot}$, respectively, in all models. The SMC is represented by a fully self-consistent dynamical model whereas the LMC is represented by a point mass. We adopt the initial locations and velocities of the MCs with respect to the Galaxy that are similar to those adopted by [2].

2 The Magellanic impact

Although the bifurcation of the MS (i.e., two streams running parallel with each other in the MS) can be reproduced by the present tidal interaction model of the MS formation as well as by the previous ones (e.g., Connors et al. [3]), it has been unclear whether the tidal models can also reproduce the location of the kink of the LAs in the MS. We here propose that the observed location of the kink can be reproduced by the tidal model if the hydrodynamical interaction between the LAs and the outer part of the H I disk of the Galaxy is modeled in a reasonable and realistic way. Fig. 1 clearly shows that the LAs, which are composed of two main streams, can pass through the

B.S. Koribalski, H. Jerjen (eds.), *Galaxies in the Local Volume*,
doi: 10.1007/978-1-4020-6933-8_55,

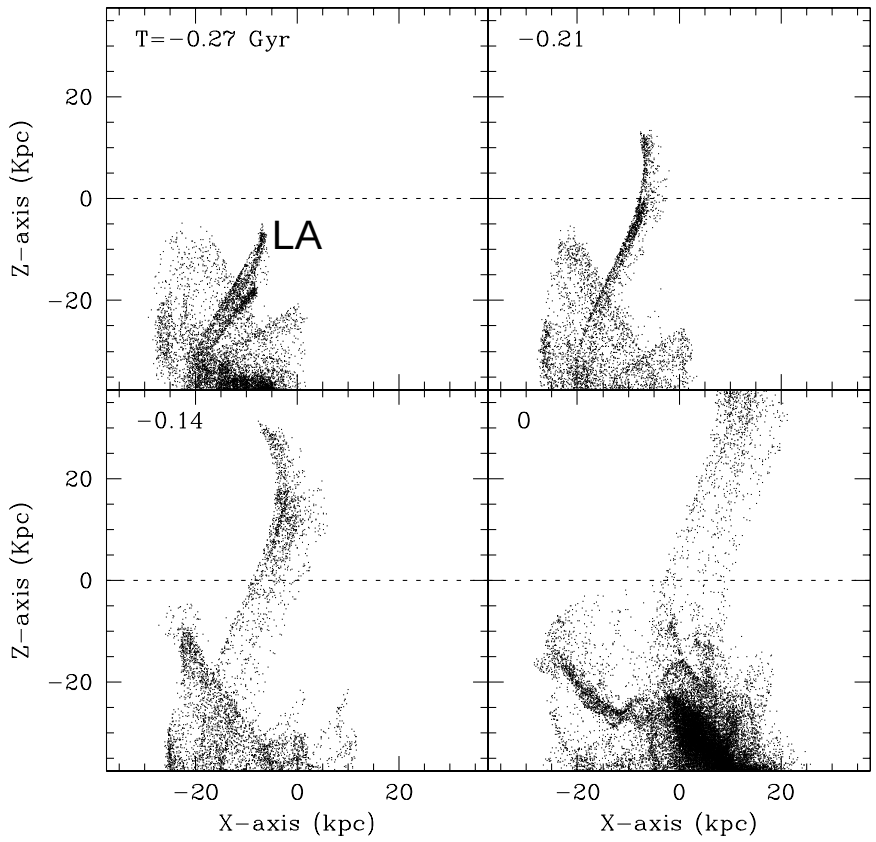

Fig. 1. Time evolution of the LAs of the MS for the last 0.27 Gyr. Only particles within 70 kpc from the center of the Galaxy are shown so that only the particles in the LAs can be more clearly seen. The time $T = 0$ Gyr means the present whereas $T = -0.27$ Gyr means 0.27 Gyr ago. The dotted line represents the disk plane of the Galaxy. Note that the LAs are composed of two streams passing through the Galactic disk about 0.2 Gyr ago.

outer part of the Galactic H I disk about 0.2 Gyr. This collision between the LAs and the H I disk is referred to as "the Magellanic impact" from now on for convenience. Fig. 2 shows that there are two peaks in the time evolution of the total mass ($m_{\rm SMC,g}$) of the SMC's gas particles that were initially within the SMC and later stripped to be *temporarily* within the central 35 kpc of the Galaxy (note that particles within the central 35 kpc are counted or not at each time step, regardless of whether they are already counted prior to the time step). About 1% of the initial gas mass of the SMC (which corresponds to an order of 10^7 $M_\odot$) can pass through the H I disk of the Galaxy within the last 0.2 Gyr during the Magellanic impact.

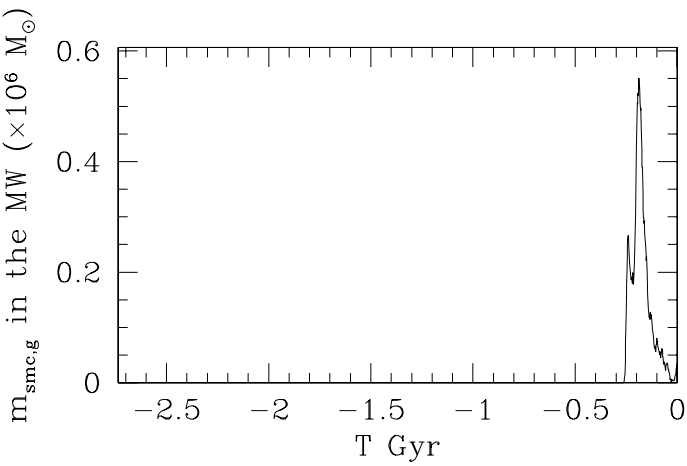

Fig. 2. Time evolution of the total mass of the SMC's gas particles that are within the central 35 kpc of the Galaxy ($m_{\mathrm{SMC,g}}$). The locations of the peaks correspond to the epochs when the LAs pass through the Galactic disk.

Fig. 3 shows the results of our hydrodynamical simulations on the collision between the LA and the outer part of the H I disk of the Galaxy. The final snapshot of the simulation shown in Fig. 3 demonstrates that the Magellanic impact can push out some fraction of the H I gas of the Galaxy so that a giant (kpc-scale) H I hole can be created about 0.2 Gyr after the Magellanic impact. A chimney-like bridge connecting between the LA and the Galactic H I disk can be also created by the Magellanic impact. The H I velocity field close to the giant hole is significantly disturbed so that ongoing and future observations on kinematics of the Galactic H I disk can detect such a disturbance. Furthermore, the high-density ridge along the giant hole is one of the predicted properties that can be tested against observations. Owing to the hydrodynamical interaction between the Galactic H I disk and the LA, the orbit of the LA can be significantly changed after the Magellanic impact at $l = 0$. This means that the location of the simulated kink of the LA should be around $l = 0$, which is consistent with the observed location of the kink.

3 The Magellanic squall

Another important result of the present simulations is that a significant amount of metal-poor gas is stripped from the SMC and has fallen into the LMC during the LMC-SMC-Galaxy interaction over the last 2 Gyrs. We find that the LMC can temporarily replenish gas supplies through the sporadic accretion and infall of metal-poor gas from the SMC. We also find that about 0.7% and 18% of the SMC's gas can pass through the central region of the LMC about 1.3 Gyr ago and 0.2 Gyr ago, respectively. The possible mean

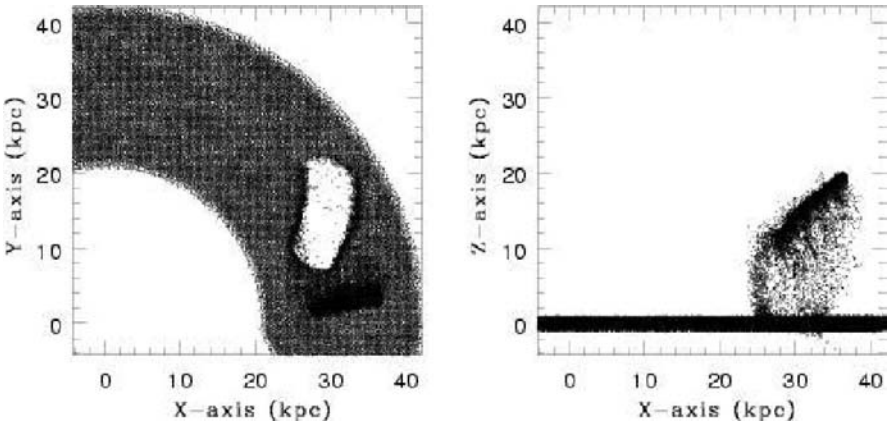

Fig. 3. The final gaseous distributions projected onto the x-y plane *(left)* and the x-z plane *(right)* for the Galactic H I disk about 0.2 Gyr after the Magellanic impact. Note that as a result of the Magellanic impact, a giant H I hole can be created in the Galactic H I disk.

metallicity of the replenished gas from the SMC to LMC is about [Fe/H] = –0.9 to –1.0 for the two interacting phases for an adopted steep initial metallicity gradient of the SMC's gas disk [2]. We thus propose that this metal-poor gas can closely be associated with the origin of the observed LMC's young and intermediate-age stars and star clusters with distinctively low-metallicities with [Fe/H] < -0.6 (e.g., Grocholski et al. [4]; Santos & Piatti [6]). We also suggest that if this gas from the SMC can collide with gas in the LMC to form new stars in the LMC, the metallicities of the stars can be significantly lower than those of stars formed from gas initially within the LMC. Accordingly this "Magellanic squall", which means gas-transfer from the SMC to the LMC, can be very important for the recent star formation history of the LMC: The evolution of the LMC is influenced not only by tidal effects of the SMC and the Galaxy but also by the mass-transfer from the SMC, if the MCs have been interacting with each other for the last 2 Gyrs.

References

1. K. Bekki, M. Chiba: MNRAS, **356**, 680 (2005)
2. K. Bekki, M. Chiba: MNRAS, in press (2007)
3. T. W. Connors, D. Kawata, B. K. Gibson: MNRAS, **371**, 108 (2006)
4. A. J. Grocholski, A. A. Cole, A. Sarajedini, D. Geisler, V. V. Smith: AJ, **132**, 1630 (2006)
5. T. Murai, M. Fujimoto: PASJ, **32**, 581 (1980)
6. J. F. C. Santos Jr., A. E. Piatti: A&A, **428**, 79 (2004)
7. D. Sugimoto, Y. Chikada, J. Makino, T. Ito, T. Ebisuzaki, M. Umemura: Nature, **345**, 33 (1990)

Spitzer Survey of the Large Magellanic Cloud: Surveying the Agents of a Galaxy's Evolution (SAGE): Initial Results

Margaret Meixner[1], K. Gordon[1,2], R. Indebetouw[3], B. Whitney[4], M. Meade[5], B. Babler[5], J. Hora[6], U. Vijh[1], S. Srinivasan[7], C. Leitherer[1], M. Sewilo[1], C. Engelbracht[2], M. Block[2], B. For[8], R. Blum[9], W. Reach[10], J-P. Bernard[11], and the SAGE Team

[1] Space Telescope Science Institute, 3700 San Martin Dr., Baltimore, MD 21218, USA meixner@email.address
[2] University of Arizona, Tucson, AZ, USA
[3] University of Virgina, Charlottesville, VA, USA
[4] Space Sciences Institute, Boulder, CO, USA
[5] University of Wisconsin, Madison, WI, USA
[6] Harvard/CfA, Cambridge, MA, USA
[7] Johns Hopkins University, Baltimore, MD, USA
[8] University of Texas, Austin, TX, USA
[9] NOAO, Tucson, AZ, USA
[10] Spitzer Science Center, Pasadena, CA, USA
[11] Centre d'Etude Spatiale des Rayonnements, Toulouse, France

We have performed a uniform and unbiased imaging survey of the Large Magellanic Cloud (LMC), using the IRAC and MIPS instruments on board the Spitzer Space Telescope (*Spitzer*). Meixner et al. (2006) provide an overview of the project and initial results; their Table 1 (repeated here) outlines the survey's salient characteristics. In this project, we are surveying the agents of a galaxy's evolution (SAGE), i.e. the interstellar medium (ISM) and stars, and their interaction on the galaxy wide scale of the LMC. Spitzer IRAC and MIPS images provide key insights into the life cycle of matter in a galaxy because the infrared emission from dust grains is an effective tracer of the ISM, star formation, and stellar mass-loss. Three key science goals determined the coverage and depth of the survey. The detection of diffuse ISM with column densities $> 1.2 \times 10^{21}$ H cm^{-2} permits detailed studies of dust processes in the ISM. SAGE's point source sensitivity enables a complete census of newly formed stars with masses >3 $M_\odot$ that will determine the current star formation rate in the LMC. SAGE's detection of evolved stars with mass loss rates $> 10^{-8}$ $M_\odot\,yr^{-1}$ will quantify the rate at which evolved stars inject mass into the ISM of the LMC (Blum et al. 2006). The SAGE data are non-proprietary. The preliminary SAGE catalog of epoch 1 photometry, prepared

B.S. Koribalski, H. Jerjen (eds.), *Galaxies in the Local Volume*,
doi: 10.1007/978-1-4020-6933-8_56,

by the SAGE Team and released to the public on January 3, 2006, contains over 4 million IRAC sources, band-merged with 2MASS photometry and over 60,000 MIPS 24 micron sources. Preliminary estimates indicate that foreground Milky Way stars and background galaxies may comprise as much as 18% and 12%, respectively, of these catalogs. To learn more about the SAGE project: `http://sage.stsci.edu/` .

Table 1. Principal Characteristics for SAGE Survey (Meixner et al. 2006)

Characteristic	IRAC Value	MIPS Value
Nominal Center point		
RA(2000)	$5^{\rm h}\,18^{\rm m}\,48^{\rm s}$	$5^{\rm h}\,18^{\rm m}\,48^{\rm s}$
Dec(2000)	$-68^\circ 34' 12''$	$-68^\circ 34' 12''$
survey area	$7\overset{\circ}{.}1 \times 7\overset{\circ}{.}1$	$7\overset{\circ}{.}8 \times 7\overset{\circ}{.}8$
AOR size, grid size	$1\overset{\circ}{.}1 \times 1\overset{\circ}{.}1$, 7×7	$25' \times 4^\circ$, 19×2
Total time (hrs)	290.65	216.84
λ (μm)	3.6, 4.5, 5.8 and 8	24, 70 and 160
pixel size at λ	$1\overset{''}{.}2$, $1\overset{''}{.}2$, $1\overset{''}{.}2$, $1\overset{''}{.}2$	$1\overset{''}{.}2$, $4\overset{''}{.}8$, $15\overset{''}{.}6$
angular resolution at λ	$1\overset{''}{.}7$, $1\overset{''}{.}7$, $1\overset{''}{.}9$, $2''$	$5\overset{''}{.}8$, $17''$, $38''$
Exposure time/ pixel at λ (s)	48, 48, 48, 48	60, 30, 9
Predicted point source sensitivity, 5 σ at λ (mJy)	0.0051, 0.0072, 0.041, 0.044	0.31, 10, 60
Predicted point source sensitivity, 5 σ at λ (mag.)	19.3, 18.5, 16.1, 15.4	10.9, 3.5 , -0.6
Saturation limits (Jy) at λ	1.1, 1.1, 7.4, 4.0	4.1, 23, 3
Saturation limits (mag) at λ	6, 5.5, 3.0, 3.0	0.61, -3.7 , -3.2
Surface brightness limits (MJy/sr) at λ	... , ... , 0.5, 1	1, 5, 10
Epoch 1	July 15 – 26, 2005	July 27 – Aug. 3, 2005
Epoch 2	Oct. 26 – Nov. 2, 2005	Nov. 2–9, 2005

1 Initial Results SAGE

Using color magnitude diagrams such as shown in Figure 1, Blum et al. (2006) identified the various evolved star populations finding ∼18,000 oxygen rich asymptotic giant branch (AGB) stars, ∼7000 carbon rich AGB stars, ∼1200 extreme AGB stars, ∼1200 red supergiants which inhabit the top left cluster of sources in Figure 1. Known and well studied AGB stars in the LMC are marked by crosses. Srinivasan et al. (this volume) finds a trend of increasing infrared

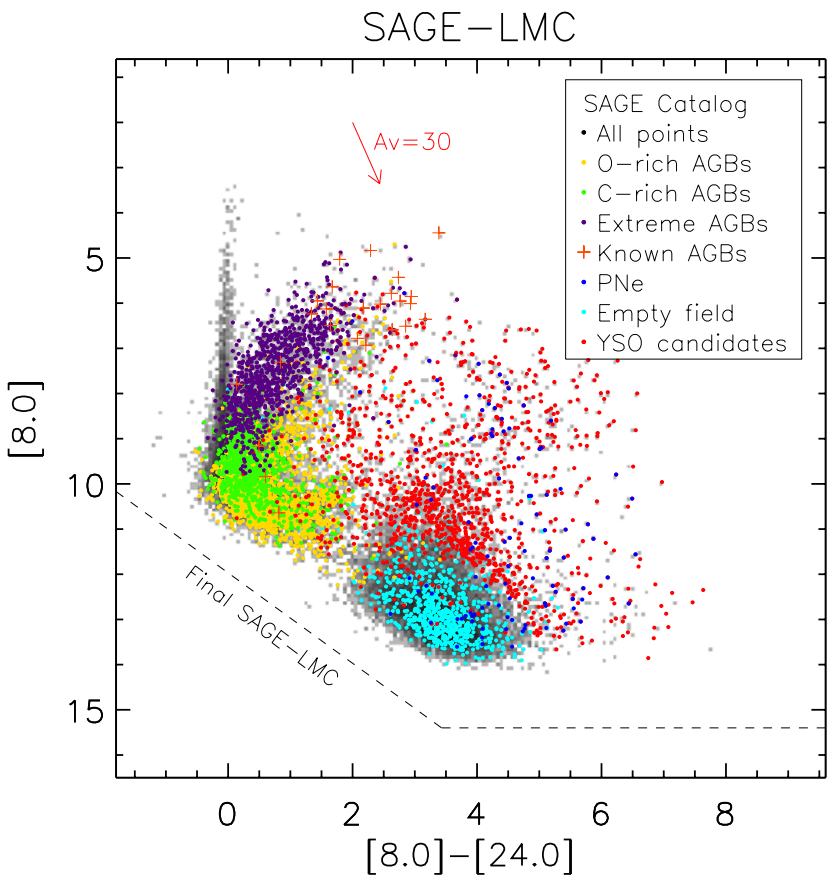

Fig. 1. This IRAC 8 vs IRAC 8 – MIPS 24 micron color-magnitude diagram shows all the SAGE EPOCH 1 catalog point sources in grey. Overplotted are SAGE sources classified by their infrared colors by various SAGE team members. The dashed line shows the final expected sensitivity limit when both epochs will be combined.

excess emission with increasing luminosity of the star. Hora et al. (2007) used known lists of planetary nebulae in the LMC to extract SAGE photometry and find them scattered thinly at all luminosities in the right red (black) cluster of sources in Figure 1. Whitney et al. (2007) discovered over 1000 new young stellar objects (YSOs) in the SAGE catalogs based on color cuts that are guided by the model calculations of Robitaille et al. (2006) but purposely avoiding regions of confusion with the evolved star population and background galaxies. These new YSO candidates are found on the redward edge of the evolved star population and extend to the redward clump of sources on the right of Figure 1. Most of the new YSO candidates tend to be luminous and

massive because the lower mass YSO candidates are confused with background galaxies which reside in large numbers in the faint red clump of point sources in Figure 1.

The types of infrared point sources we observe in SAGE can be detected at the larger distances of the galaxies in the local volume. The distance of the LMC is ∼50 kpc (Feast 1999). If we simply move the SAGE sensitivity with distance modulus, we can estimate which types of sources will be detectable at which distances. At a distance of 1 Mpc, the more luminous YSO candidates, AGB stars and planetary nebulae are detectable. At a distance of 10 Mpc, the outer perimeter defined as the local volume of galaxies by this conference, only the most luminous YSO candidates and red supergiants are visible. Thus we encourage our colleagues with Spitzer data on other galaxies in the local volume to pursue infrared population studies with their data.

Bernard et al. (2007, in preparation) have been analyzing the extended IRAC and MIPS emission from the ISM in the LMC and comparing it to the gas distribution of neutral atomic and molecular hydrogen as traced by the H I 21 cm emission and CO rotational transitions. The amount of dust per unit mass in gas is ∼3.3 times smaller than found in the Milky Way. The dust to gas ratio appears to vary in the galaxy. If we assume an XCO factor derived by virial analysis in the LMC, we find that the amount of dust per hydrogen atom is ∼3.7 times less in the CO traced molecular gas compared to the atomic hydrogen gas. If we use a Milky Way XCO factor, we find no difference. We conclude that the XCO factor is probably more like the Milky Way, but we cannot completely rule out the presence of undetectable molecular hydrogen.

In summary, galactic nature is a cycle of ISM, star formation consuming the ISM and locking it up into stars, and the evolved stars returning dust enriched matter to the ISM. As a field, the work on the local volume has been focused too much on the star formation and not enough on the whole cycle. Be green, think recycling not just consumption.

References

1. R. D. Blum, et al.: AJ, **132**, 2034 (2006)
2. M. Feast: The Distance to the Large Magellanic Cloud; A Critical Review. In: *New Views of the Magellanic Clouds*, vol 190, eds by Y.-H. Chu, N. Suntzeff, J. Hesser, D. Bohlender, p. 542 (1999)
3. J.L. Hora, M. Cohen, R.G. Ellis, M. Meixner, et al.: AJ, submitted (2007)
4. M. Meixner, et al.: AJ, **132**, 2268 (2006)
5. T. P. Robitaille, B. A. Whitney, R. Indebetouw, K. Wood, & P. Denzmore: ApJS, **167**, 256 (2006)
6. B. A. Whitney, M. Sewilo, R. Indebetouw, T. P. Robitaille, M. Meixner, et al.: AJ, submitted (2007)

Metallicity and Mean Age Across M 33

Maria-Rosa L. Cioni[1,3], M. Irwin[2], A. M. N Ferguson[3], A. McConnachie[4], B. C. Conn[5], A. Huxor[6], R. Ibata[7], G. Lewis[8], and N. Tanvir[9]

[1] Centre for Astrophysics Research, University of Hertfordshire, Hatfield, AL10 9AB, UK, M.Cioni@herts.ac.uk
[2] Institute for Astronomy, University of Cambridge, Madingley Road, Cambridge CB3 0HA, UK, mike@ast.cam.ac.uk
[3] SUPA, School of Physics, University of Edinburgh, IfA, Blackford Hill, Edinburgh EH9 3HJ, UK, ferguson@roe.ac.uk
[4] Department of Physics & Astronomy, University fo Victoria, PO Box, 3055, STN CSC, Victoria BC, V8W 3P6 Canada, alan@uvic.ca
[5] European Southern Observatory, Alonso de Cordova 3107, Vitacura, Santiago, Chile, bconn@eso.org
[6] Department of Physics, University of Bristol, Tyndall Avenue, Bristol BS8 1TL, UK, Avon.Huxor@bristol.ac.uk
[7] Observatorie de Strasbourg, 11 rue de l'Université, F-67000 Strasbourg, France, ibata@astro.u-strasbg.fr
[8] Institute of Astronomy, School of Physics, A29, University of Sydney, NSW 2006, Australia, gfl@physics.usyd.edu.au
[9] Department of Physics and Astronomy, University of Leicester, Leicester LE1 7RH, UK, nrt3@star.le.ac.uk

New wide-field near-infrared (NIR) imaging observations of M 33 were obtained from UKIRT. These show a large population of intermediate-age stars considerably improving on previous NIR data. The spatial distribution of super giant stars. C-rich (or C stars) and O-rich (or M stars) AGB stars distinguished from the NIR colour-magnitude diagram (CMD) have been studied as well as the C/M ratio distribution. The K_s magnitude distribution has been interpreted using theoretical models to derive the mean age and the mean metallicity across M 33.

1 Introduction

M 33 is the third brightest Local Group (LG) member. It is of Sc II-III type, thus intermediate between large spirals and dwarf irregular galaxies. It has a nucleus, a disk and a halo and its stellar population exhibits both a metallicity and age gradient [11].

NIR observations of the stellar content of M 33 began with [8]. While looking for a signature of a bulge component, which was not found, they

B.S. Koribalski, H. Jerjen (eds.), *Galaxies in the Local Volume*,
doi: 10.1007/978-1-4020-6933-8_57,

observed numerous intermediate-age stars in the central 7.′6 of the galaxy down to $K \sim 17 - 18$. Several years later [10] reaching $K \sim 22$ detected young, intermediate-age and old stars in the central 22″. Wide-field, relatively shallow observations ($K_s \sim 16$) by [2] claimed the existence of arcs of metal poor C stars in the outer parts of M 33.

2 Observations, analysis & results

New NIR observations of M 33 have been obtained from UKIRT as part of a programme to survey luminous red stars in LG galaxies (PI Irwin). UKIRT data combine wide-field and good sensitivity improving considerably on former studies. A mosaic of 4 WFCAM tiles covering ~ 3 deg^2 was observed with an average seeing of $1.''07 \pm 0.''$. This allowed to reach sources as faint as $K_s = 18.32$ with S/N = 10 including most intermediate-age asymptotic giant branch (AGB) stars. The data was dereddened assuming $E(B-V) = 0.07$ and using the reddening law [5] such that the absorption in each wave band is $A_J = 0.06$, $A_H = 0.04$ and $A_{K_s} = 0.02$.

The tip of the red giant branch (TRGB) is found at $K_s = 18.15$. The distribution of stars in the CMD ($J - K_s$, K_s) shows that foreground stars, oxygen-rich and carbon-rich AGB stars occupy clearly distinct regions. Figure 1 shows confirmed long-period-variables (LPVs), AGB stars from the cross-identification with the variability study by [6] as well as obscured sources observed by Spitzer.

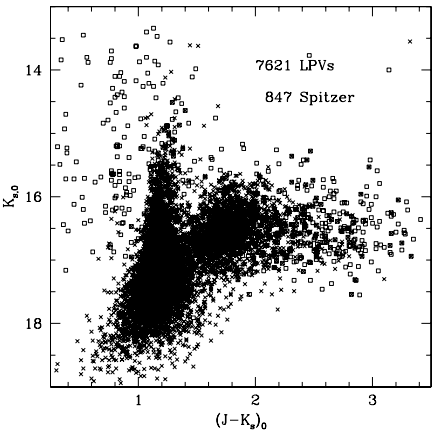

Fig. 1. CMD of NIR sources matched with LPVs candidates from Hartman et al. [6] (crosses) and Spitzer detections (squares). The TRGB is at $K_s = 18.5$. C-rich AGB stars are redder than $J - K_s \sim 1.5$ while O-rich stars are bluer. Stars observed by Spitzer with $J - K_s < 1$ are likely supergiants.

The spatial distribution of supergiant stars is clumpy and extends asymmetrically to the NE while AGB stars trace a smoother distribution with hints of the major galaxy spiral arms. The ratio between C- and O-rich AGB stars (the C/M ratio) also outlines a ring-like feature and suggests a metallicity spread of [Fe/H] = 0.6 dex across the galaxy, using the Battinelli & Demers [1] calibration, in agreement with the results by [9].

2.1 Structure & Extinction

By subdividing the galaxy disk into 4 concentric ellipses and 8 sectors we investigated the orientation as well as the contribution by differential extinction within the galaxy, if any. The peak of the magnitude and colour differences from the mean, for C stars, describe a sinusoidal pattern which indicates that stars in the NW of the galaxy are fainter than stars in the SE of it. This sinusoid is consistent with the distance moduli distribution derived by [7] in 10 different regions scattered within M 33 suggesting that it is almost entirely a structure rather then an extinction effect.

2.2 Mean age and metallicity

The K_s magnitude distribution of stars within each sector of each ellipse has been fitted with theoretical distributions spanning a range of mean ages ($2 - 10.6$ Gyr) and mean metallicities (Z = 0.0005–0.016). The theoretical models used to create the distributions are those by [4]. This method was first used by [3] to investigate the stellar population of the Large Magellanic Cloud.

Maps of the best fit mean metallicity versus mean-age and combined maps of best fit mean-age and metallicity have been created separately for C-rich and O-rich AGB stars. These show an inhomogeneous distribution of age and metallicity. Note that relative values are much more significant than absolute values which can be model dependent.

The very central region of the galaxy or regions around it appear metal rich compared to the overall disk. In particular, C stars trace a disk/halo population which is metal poor ([Fe/H] ≤ -1.6 dex while the nucleus and other regions around it are as metal rich as [Fe/H] ~ -1.2 dex. There is an outer thick ring of stars on average 6 Gyr old or older. O-rich AGB stars also suggest an old ($6 - 8.5$ Gyr) and metal poor ([Fe/H] ≤ 0.5 dex) outer ring while the centre of the galaxy is young ($1 - 5$ Gyr) and metal rich ([Fe/H] ≥ 0.3 dex). Although trends are the same for both C-rich and O-rich AGB stars, the latter show higher metallicity values but very similar ages.

3 Conclusions & Future studies

The K_s method is an efficient way to constrain the parameters of a galaxy stellar population using bright IR targets like AGB stars. The existence of a

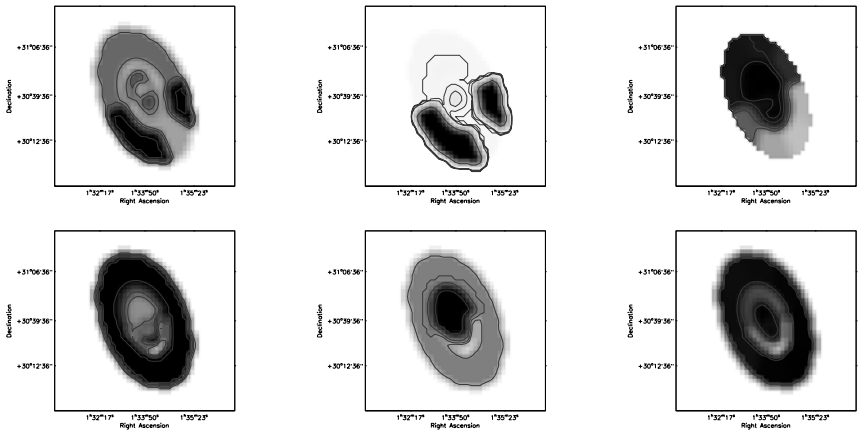

Fig. 2. Spatial distribution of the mean-age of the stellar population of M 33 *(left)*, of the metallicity *(middle)* and of the statistical probability that expresses the confidence level of the previous distributions *(right)*. These distributions have been constructed from the comparison between the observed K_s magnitude distribution of C-rich *(top)* and O-rich *(bottom)* AGB stars selected from the CMD. Darker regions correspond to higher numbers. North is up and East is left.

metallicity and age gradient throughout M 33 is confirmed. The C/M ratio, mean-age and metallicity show much more structure/substructures. The SE of the galaxy is closer to us; the position angle of bright/faint stars is in the direction of the galaxy warp. Many of the detected AGB stars are LPVs.

More galaxies have been observed within the same programme and will be soon analysed. Theoretical models are already good enough to fit entirely CMDs instead of just magnitude distributions. The study of galaxies well beyond the LG has to wait next generation facilities like JWST and E-ELT.

References

1. P. Battinelli, S. Demers: A&A **434**, 657 (2005)
2. D.L. Block, K.C. Freeman, T.H. Jarret, et al.: A&A **425**, L437 (2004)
3. M.-R.L. Cioni, L. Girardi, P. Marigo, H.J. Habing: A&A, **448**, 77 (2006a)
4. L. Girardi, A. Bressan, G. Bertelli, C. Chiosi: A&AS, **141**, 371 (2000)
5. I. Glass, M. Schultheis: MNRAS **345**, 39 (2003)
6. J.D. Hartman, D. Bersier, K.Z. Stanek, et al.: MNRAS **371**, 1405 (2006)
7. M. Kim, E. Kim, M.G. Lee, et al.: AJ **123**, 244 (2002)
8. I.S. McLean, T. Liu: ApJ **456**, 499 (1996)
9. J.F. Rowe, H.B. Richer, J.P. Brewer, et al.: AJ **129**, 729 (2005)
10. A.W. Stephens, J.A. Frogel: AJ **124**, 2023 (2002)
11. S. van den Berg: *The Galaxies of the Local Group*, Cambridge Astrophysics Series 35

How does Gas Get into Galaxies?

Joss Bland-Hawthorn

Institute of Astronomy, School of Physics, University of Sydney, NSW 2006, Australia j.bland-hawthorn@physics.usyd.edu.au

Summary. Most stars reside within disk galaxies. We are far from understanding just why this should be. The conventional picture of baryon accretion invokes shock processes during cold dark matter (CDM) collapse followed by a cooling phase in the hot medium. Some have even suggested that we must search for evidence of the "missing link" − disk galaxies with relic hot halos − as proof of the conventional paradigm. But on the scale of individual disk galaxies, accretion through the hot phase cannot be the dominant process. So how do baryons find their way into disk galaxies? We review recent advances from multiwavelength observations. Interestingly, a diffuse hot halo can assist in the formation of disks by slowing down and disrupting the orbitting gas. A complete baryon inventory of disk galaxies may require much deeper observations of all gas phases at sub-virial temperatures, and only then can we properly account for the required accretion rate consistent with the stellar record.[1]

1 New developments on disk galaxies

Disk galaxies continue to surprise us. We used to believe that the majority of stars were locked up in spheroidal systems (e.g. Fukugita & Peebles 2004). But with better disk-bulge separations now possible in large imaging surveys, it appears that disk stars dominate over spheroids (Benson et al. 2007; Driver et al. 2007). Just recently, it was thought that essentially all stellar disks declined exponentially with a well defined cut-off close to the Holmberg radius. In late-type spirals, the H I disk was commonly observed to extend about a factor of two further in radius. This already posed a problem in the conventional picture of a disk that acquires its angular momentum from a collapsing protocloud (Fall 1983). Does the specific angular momentum of the outermost gas or stars relate to the collapsing protocloud (van der Kruit & Searle 1981)? If the latter, does the warped H I envelope reflect a later phase of accretion (Binney 1992)?

[1] A detailed synopsis is to appear in the Proceedings for the 2007 Saas Fee Lectures.

B.S. Koribalski, H. Jerjen (eds.), *Galaxies in the Local Volume*,
doi: 10.1007/978-1-4020-6933-8_58,

The relationship between the H I and the stars is not as simple as it first appeared. Low star formation rate densities can often be detected over much of the H I envelope (Bland-Hawthorn et al. 1997; Ferguson et al. 1998; Thilker et al. 2005). Moreover, it no longer appears that the stellar disk truncates rapidly in all cases, although there are now well established examples that are independent of surface photometry (e.g. Ferguson et al. 2006).

In a few spectacular cases, the disk remains exponential out to ∼10 optical scale lengths and far into the H I (Irwin et al. 2005; Bland-Hawthorn et al. 2005). Even more surprising, the stellar disk appears to flatten off at large radius in some cases (Pohlen & Trujillo 2006). The statistics on the different classes is unknown at the present time, but Pohlen & Trujillo suggest the following breakdown:

- sub-exponential (exponential + break at large radius): 60%
- exponential (exponential to the limits of the data): 10%
- super-exponential (exponential + flattening at large radius): 30%

More extensive H I surveys reveal that gas disks do not always extend far beyond the stellar disk even in isolated environments (Hogg et al. 2007). To the other extreme, there are now several dwarf galaxies known where the H I extends 30–40 optical scale lengths (e.g. Begum et al. 2005).

The well-established thick stellar disk of the Galaxy was thought to be relatively unusual, but the opposite now appears to be true (Seth et al. 2005). Just how the thick disk relates to the presence of the thin disk remains unclear. Do these even share a similar radial extent? Observations in the far field appear to suggest that disks grow with cosmic time (Bouwens et al. 2004) but this may contradict the age distribution of open clusters in the Galaxy (Friel 1995). Another interesting development is the recent claim that the declining abundance gradient in the Galaxy appears to flatten off at large radius (e.g., Yong et al. 2006). This latter finding emphasizes the importance of measuring abundance gradients for the different classes of exponential decline. In particular, does the Yong result hint at a flattening of the disk at large radius? Would we expect to see a different signature in the thick disk component assuming that it extends this far?

2 What is the required rate of baryon accretion in the Galaxy?

The stellar record of the Galaxy tells us something quite remarkable. The star formation rate has been fairly constant for the past 11 Gyr, i.e. back to $z = 2.5$ and within 2.7 Gyr of the Big Bang (Binney et al. 2000; Rocha-Pinto et al. 2000). What is particularly striking is how this conflicts with the rapid variation in the universal star formation rate over the same time frame (Drozdovsky, this conference).

There are numerous independent lines of evidence to indicate that the accretion of fresh gas (as distinct from other sources of baryons, e.g. stars) onto the Galaxy must have been maintained over most of the lifetime of the disk (Tinsley 1980; Pagel 1987), at least as far as we can determine from the Solar Neighbourhood.

As I review in the Saas Fee proceedings, a wide literature shows us that the total mass of disk stars is 1.8×10^{11} $M_\odot$ with a total mass in gas of 4.5×10^9 $M_\odot$, which are accurate to 20%. The required rate of gas accretion must have been ≈ 2 $M_\odot\,yr^{-1}$ for most of this time. Such a large value is quite difficult to reconcile with observations of late-type spirals. The rate of gas *recycling* in stellar evolution may be as high as 3 $M_\odot\,yr^{-1}$ (or higher for short periods). This process can manifest itself as a strong disk-halo interaction (Norman & Ikeuchi 1989) which can complicate our attempts to quantify the accretion processes from direct observation (see below).

3 Accretion processes

Many numerical simulators hold onto the idea that the initial CDM collapse shock-heats the infalling baryons to form a relic hot halo. This gas then cools to supply the galaxy with a reservoir of cold gas. Recent simulations even attempt to account for the nearby halo clouds with such a picture (Maller & Bullock 2004; Kaufmann et al. 2006). There are many criticisms that can be raised with such a scenario concerning the non-linear growth of instabilities, and from direct observation. Simply put, the hot halo is unlikely to be a major source of star-forming gas. A detailed discussion of this point is left to the upcoming review.

Indeed, much of the groundwork has already been laid out by Binney (1977; 2004). This seminal work preceded several studies (Keres et al. 2005; Dekel & Birnboim 2006) that demonstrate how a large fraction of the infalling baryons could not have been heated to the virial temperature, and would therefore lead to a flow of cool gas. Binney's finding should not come as too much of a surprise; bulk gas processes are rarely efficient in any astrophysical arena. But I would extend this by saying that much of the gas could even be ionized (i.e. sub-virial temperatures), as we discuss below, and may therefore be missing from the accretion budget.

A great deal of gas can exist in the outer disk, and this provides a ready source of baryons. Bars or oval distortions may exist in most disk galaxies (Pohlen 2002) and their benefits in funnelling gas inwards, even to the required accretion rates, are well known (Combes 2007). But in the presence of gas, it is not at all clear that this action can be sustained for very long (Friedli & Benz 1993). Accretion rates through spiral arms are substantially lower (Visser 1980). In any event, this beautiful phenomenon is the dynamical equivalent of waves crashing on a beach, and is therefore not sustained for more than a few rotation periods (Sellwood 1999).

H I clouds and streams in orbit about galaxies are all too frequently taken as bona fide evidence of accretion without any reference to a physical mechanism. A cloud is quite happy to orbit a galaxy since the dynamical timescales are long for a diffuse, extended object. However, Bland-Hawthorn et al. (2007) have now shown that the Magellanic Stream is likely to be infalling through a process of disruption. They show that the observed source of Hα emission along the Stream can be explained by a "shock cascade," i.e. upstream clouds (immediately trailing the Magellanic Clouds) disrupting through their interaction with the halo gas, being subsequently crushed by the following Stream clouds. The disrupting material must accrete onto the Galactic halo. Our new work shows how this process can assist in the disk accretion process.

In searching for direct evidence of baryon accretion, the disk-halo interaction may obscure much of the behaviour. An interesting development is the detection of lagging H I and H^+ halos in the best observed late-type disks (Fraternali et al. 2001, 2004; Barbieri et al. 2005; Heald et al. 2006). The prospect for some sort of cool gaseous infall at levels of 0.1–0.3 $M_\odot\,yr^{-1}$ seems good, but does this estimate correctly account for the disk-halo interaction driven by disk star formation? Extensive hot halos are almost always the result of a large-scale wind, disk-halo circulation, and the activity can survive long after the starburst has subsided. This may argue against the "missing link" idea proposed by Pedersen et al. (2006) for one particular spiral with a bright X-ray halo. Most of the X-ray emission lies within the typical scale height of disk-halo recycling.

The lagging H I halos may be related to the infalling high-velocity and intermediate-velocity clouds observed in the Galaxy (Wakker et al. 2003). The new Hα distances (Bland-Hawthorn et al. 1998; Putman et al. 2003) place the HVC gas within the distance of the Stream which lowers their total mass content but also decreases the overall infall time. When we include the Stream, the total infall rate is unlikely to exceed 0.2 $M_\odot\,yr^{-1}$ (Peek et al. 2007) although an ionized component could more than double this figure (Bland-Hawthorn et al. 2007).

On the (dynamically hot) accretion of stars and gas through mergers, Wyse (2001) points out that there have been no major mergers during the past 11 Gyr. We do see evidence, however, of stellar streams across the Galaxy, but the total baryon accretion rate is quite small and these may be more significant for the halo (Purcell et al. 2007). Even if each of the infalling dwarfs brought in an equivalent fraction of H I, this would not explain the observed shortfall.

4 Missing baryons: towards a full inventory

We conclude that it is difficult to fully account for the Galactic accretion requirement at the present time. But have we correctly accounted for all possible phases of the ISM? Maloney & Bland-Hawthorn (1999) show that a great deal of warm gas existing below the virial temperature of the Galactic halo

($\sim 1.8 \times 10^6$K at the Stream distance) could be concealed within the limits set by the microwave background. There are few accurate measurements at the present time on the true mass of ionized gas and, therefore, potential accretion rates of warm gas onto the disk.

One way to see this is to compare the particle column density between H I and Hα from imaged observations. The limiting H I column density is about $N_H \approx \langle n_H \rangle L \approx 10^{18}$ cm^{-2} where $\langle n_H \rangle$ is the mean atomic hydrogen density, and L is the depth through the slab. By comparison, the Hα surface brightness can be expressed as an equivalent emission measure, $E_m = \langle n_e^2 \rangle L = \langle n_e \rangle N_e$. Here n_e and N_e are the local and column electron density. The limiting value of E_m in Hα observations is about 0.3 cm^{-6} pc, and therefore $N_e \approx 10^{18}/\langle n_e \rangle$ cm^{-2}.

Whether the ionized and neutral gas are mixed or distinct, we can hide a lot more ionized gas below the imaging threshold for a fixed L, particularly if the gas is at low density ($\langle n_e \rangle \ll 0.1$ cm^{-3}). A small or variable volume filling factor can complicate this picture but, in general, the ionized gas still wins out because of ionization of low density H I by the cosmic UV background (Maloney 1993). In summary, a large fraction of the gas can be missed if it occupies a large volume in the form of a low density plasma.

A critical problem in studies involving dynamical processes is that we need to compare *time-averaged* properties of galaxies with the requirements demanded by the evidence of the stellar record. It may not be sufficient to attempt to explain what we observe in a "snapshot" of a given phase in the Galaxy. Clearly, we need more extensive and much deeper observations across all phases of the ISM. Detailed disk models that include all phases of the disk and halo ISM will be crucial to future progress. This is to be a major focus for several international groups over the next decade.

References

1. Barbieri, C. V., Fraternali, F., Oosterloo, T., Bertin, G., Boomsma, R., & Sancisi, R. 2005, A&A, 439, 947
2. Begum, A., Chengalur, J. N., & Karachentsev, I. D. 2005, A&A, 433, L1
3. Benson, A. J., Džanović, D., Frenk, C. S., & Sharples, R. 2007, MNRAS, 379, 841
4. Binney, J., Dehnen, W., & Bertelli, G. 2000, MNRAS, 318, 658
5. Binney, J. 1977, MNRAS, 181, 735
6. Binney, J. 1992, ARA&A, 30, 51
7. Binney, J. 2004, MNRAS, 350, 939
8. Bland-Hawthorn, J., & Maloney, P. R. 1999, ApJ, 510, L33
9. Bland-Hawthorn, J., Freeman, K. C., & Quinn, P. J. 1997, ApJ, 490, 143
10. Bland-Hawthorn, J., Veilleux, S., Cecil, G. N., Putman, M. E., Gibson, B. K., & Maloney, P. R. 1998, MNRAS, 299, 611
11. Bland-Hawthorn, J., Vlajić, M., Freeman, K. C., & Draine, B. T. 2005, ApJ, 629, 239

12. Bland-Hawthorn, J., Sutherland, R., Agertz, O. & Moore, B. 2007, ApJL, in press
13. Bouwens, R. J., Illingworth, G. D., Blakeslee, J. P., Broadhurst, T. J., & Franx, M. 2004, ApJ, 611, L1
14. Combes, F. 2007, ArXiv e-prints, 709, arXiv:0709.0091
15. Dekel, A., & Birnboim, Y. 2006, MNRAS, 368, 2
16. Driver, S. P., Allen, P. D., Liske, J., & Graham, A. W. 2007, ApJ, 657, L85
17. Fall, S. M. 1983, Internal Kinematics and Dynamics of Galaxies, 100, 391
18. Ferguson, A. M. N., Wyse, R. F. G., Gallagher, J. S., & Hunter, D. A. 1998, ApJ, 506, L19
19. Ferguson, A. M. N. et al. 2006, Planetary Nebulae Beyond the Milky Way, 286
20. Fraternali, F., Oosterloo, T., Sancisi, R., & van Moorsel, G. 2001, ApJ, 562, L47
21. Fraternali, F., Oosterloo, T., & Sancisi, R. 2004, A&A, 424, 485
22. Friedli, D., & Benz, W. 1993, A&A, 268, 65
23. Friel, E. D. 1995, ARA&A, 33, 381
24. Fukugita, M., & Peebles, P. J. E. 2004, ApJ, 616, 643
25. Heald, G. H., Rand, R. J., Benjamin, R. A., Collins, J. A., & Bland-Hawthorn, J. 2006, ApJ, 636, 181
26. Hogg, D. E., Roberts, M. S., Haynes, M. P., & Maddalena, R. J. 2007, AJ, 134, 1046
27. Irwin, M. J., Ferguson, A. M. N., Ibata, R. A., Lewis, G. F., & Tanvir, N. R. 2005, ApJ, 628, L105
28. Kaufmann, T., Mayer, L., Wadsley, J., Stadel, J., & Moore, B. 2006, MNRAS, 370, 1612
29. Kereš, D., Katz, N., Weinberg, D. H., & Davé, R. 2005, MNRAS, 363, 2
30. Maller, A. H., & Bullock, J. S. 2004, MNRAS, 355, 694
31. Maloney, P. R., & Bland-Hawthorn, J. 1999, ApJ, 522, L81
32. Maloney, P. 1993, ApJ, 414, 41
33. Norman, C. A., & Ikeuchi, S. 1989, ApJ, 345, 372
34. Pagel, B. E. J. 1987, NATO ASIC Proc. 207: The Galaxy, 341
35. Pedersen, K., Rasmussen, J., Sommer-Larsen, J., Toft, S., Benson, A. J., & Bower, R. G. 2006, New Astronomy, 11, 465
36. Peek, J. E. G., Putman, M. E., McKee, C. F., Heiles, C., & Stanimirović, S. 2007, ApJ, 656, 907
37. Pohlen, M., & Trujillo, I. 2006, Island Universes, Ed. R. S. de Jong, Dordrecht, The Netherlands, p. 253
38. Pohlen, M. 2002, Ph.D. Thesis, Bochum, Germany
39. Purcell, C. W., Bullock, J. S., & Zentner, A. R. 2007, ApJ, 666, 20
40. Putman, M. E., Bland-Hawthorn, J., Veilleux, S., Gibson, B. K., Freeman, K. C., & Maloney, P. R. 2003, ApJ, 597, 948
41. Rocha-Pinto, H. J., Scalo, J., Maciel, W. J., & Flynn, C. 2000, A&A, 358, 869
42. Sellwood, J. A. 1999, Galaxy Dynamics - A Rutgers Symposium, 182, 351
43. Seth, A. C., Dalcanton, J. J., & de Jong, R. S. 2005, AJ, 130, 1574
44. Tinsley, B. M. 1980, Fundamentals of Cosmic Physics, 5, 287
45. van der Kruit, P. C., & Searle, L. 1981, A&A, 95, 116
46. Visser, H. C. D. 1980, A&A, 88, 159
47. Wakker, B. P., et al. 2003, ApJS, 146, 1
48. Wyse, R. F. G. 2001, Galaxy Disks and Disk Galaxies, 230, 71
49. Yong, D., Carney, B. W., Teixera de Almeida, M. L., & Pohl, B. L. 2006, AJ, 131, 2256

Part II

Poster Contributions

(Left side:) Yoji Mizuno, Cath Fleming, Akiko Kawamura, Margaret Meixner.
(Right side:) Hiroyuki Nakanishi, Erik Muller, and Adam Ruzicka.

New HST/ACS Data of the Starburst Irregular Galaxy NGC 4449

Francesca Annibali[1], A. Aloisi[1,2], J. Mack[1], M. Tosi[3], R. P. van der Marel[1], L. Angeretti[3], C. Leitherer[1], and M. Sirianni[1,2]

[1] Space Telescope Science Institute, 3700 San Martin Drive, Baltimore, MD 21218, USA, annibali@stsci.edu
[2] On assignment from the Space Telescope Division of the European Space Agency
[3] INAF-Osservatorio Astronomico di Bologna, Via Ranzani 1, Bologna, Italy

Summary. We present B, V and I photometry with HST/ACS of the resolved stellar populations in the Magellanic starburst galaxy NGC 4449. Our photometry provides $\approx$ 300,000 objects in the (B, V) color-magnitude diagrams (CMDs) and $\approx$ 400,000 objects in the (V, I) CMDs. The features observed in the CMDs imply a variety of stellar ages up to at least 1 Gyr, and possibly as old as a Hubble time. Our data clearly indicate the presence of an age gradient, with young and intermediate-age stars concentrated toward the galactic center, and old stars present everywhere. We derive the distance of NGC 4449 with an accuracy of 5% from the tip of the red giant branch: $D = 3.82 \pm 0.18$ Mpc.

1 Introduction

Starbursts are short and intense episodes of star formation that usually occur in the central regions of galaxies and dominate their integrated light. The associated star formation rates are so high that the existing gas supply can sustain the stellar production only on timescales much shorter than $\sim$1 Gyr. The Magellanic irregular galaxy NGC 4449 is a global starburst with a widespread star formation activity that could have been triggered by interaction or accretion. It closely resembles Lyman Break galaxies at high redshift in some aspects [2], and is a perfect laboratory where to characterize those processes, like merging and accretion, related to the formation and evolution of galaxies in the early Universe.

2 Color-magnitude diagrams

We have acquired HST/ACS imaging of NGC 4449 in the F435W (B), F555W (V), F814W (I) and F658N (Hα) filters. Details on the observations and data reduction can be found in [1]. The left panel of Figure 1 shows the V, B-V color-magnitude diagram (CMD) of the 299,014 stars simultaneously

B.S. Koribalski, H. Jerjen (eds.), *Galaxies in the Local Volume*,
doi: 10.1007/978-1-4020-6933-8_59,

photometred in B and V, while the right panel shows the I, $V-I$ CMD of the 402,045 stars photometred in V and I. The CMDs refer to the total field of view of NGC 4449. We can recognize the following evolutionary phases: the blue lume at $V-I \approx 0$ (main sequence stars and blue supergiants), the red plume at $V-I \approx 1.5$ (red supergiants and Asymptotic Giant Branch (AGB) stars), the Red Giant Branch (RGB) and the red horizontal finger populated by carbon (TP-AGB) stars. The discontinuity of the RGB tip (TRGB) is detected at $I = 24.00 \pm 0.02$, which implies a distance modulus $(m - M) = 27.91 \pm 0.10$, i.e. $D = 3.82 \pm 0.18$ Mpc.

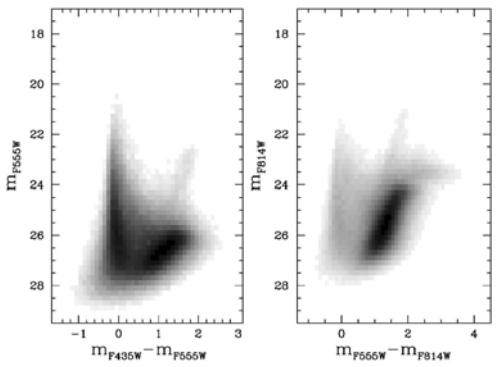

Fig. 1. *(Left:)* V, $B-V$ color-magnitude diagram (CMD) in the total field of view of NGC 4449. *(Right:)* I, $V-I$ CMD. The CMDs are represented through Hess diagrams.

3 Gradients

We performed a spatial analysis of the CMD morphology, of the carbon star luminosity and of the RGB color, in order to investigate the presence of age and/or metallicity gradients. The spatial variation of the CMD morphology shows that the youngest massive stars are mainly located towards the center, while low-mass old RGB stars are detected over the whole galaxy. We find that the carbon stars are brighter in the central regions of NGC 4449. Also, the RGB is bluer in the center than in the periphery of the galaxy. More luminous carbon stars and bluer RGB colors can be due to both metal poorer and younger stellar populations. However, since studies of abundance gradients in galaxies show that metallicity tends to decrease from the center outwards or to remain constant, we are inclined to interpret the observed trends as due to a younger stellar population in the center of NGC 4449.

References

1. Annibali, F., Aloisi, A., Mack, J., Tosi, M., van der Marel, R. P., Angeretti, L., Leitherer, C., & Sirianni, M.: AJ, submitted, arXiv:0708.0852 (2007)
2. Steidel, C. C., Giavalisco, M., Pettini, M., Dickinson, M., & Adelberger, K. L.: ApJ, **462**, L17 (1996)

H I Deficiency in X-ray Bright Groups

Ramesh Balasubramanyam, Chandreyee Sengupta, and K.S. Dwarakanath

Raman Research Institute, Sadashivanagar, Bangalore 560080, India
ramesh@rri.res.in

Denser environments do influence the evolution of neutral gas in galaxies as demonstrated by the studies of galaxies in clusters. In them, ram-pressure stripping seems the important mechanism responsible for the gas evolution. However, not all the gas evolution in cluster galaxies may be due to their present environment. Redshift surveys indicate that a large fraction of galaxies occur in small groups [2, 4, 5]. These groups possibly merge to form subclusters which in turn may combine to form clusters. Various evidences suggest that the gas evolution in such "sub-clusters" may be important.

Lower velocity dispersion among galaxies in groups enhance tidal interactions, which can affect their gas content, morphology and possibly star formation rate. However, the cold gas evolution in groups is an idea relatively unexplored. Therefore, we carried out two observational studies of H I content of galaxies in groups, with the view to study the effect of the hot IGM, on the H I content of the spiral galaxies.

Here, we summarise the results of these studies: (a) comparative study of the H I content of galaxies in groups with and without hot intra-group medium (IGM), (b) H I imaging of some of the galaxies from X-ray bright groups.

1 A Statistical Study

In this study, we looked for statistical evidence to establish that the galaxies in X-ray bright groups are on average deficient in H I content compared to galaxies in groups, not detected in X-rays. We had chosen 74 galaxies from 10 X-ray bright groups and 96 galaxies from 17 non-X-ray groups for this purpose. We obtained their H I data from HIPASS and other sources in the literature and contructed their H I deficiencies and compared them using various statistical tests.

We [3] found that the galaxies from X-ray bright groups have an average H I deficiency of $\sim 0.28 \pm 0.04$, whereas those from non-X-ray groups have $\sim 0.09 \pm 0.03$. A Kolomogorov-Smirnov test on the H I surface density of

B.S. Koribalski, H. Jerjen (eds.), *Galaxies in the Local Volume*,
doi: 10.1007/978-1-4020-6933-8_60,

galaxies shows only an 8% chance that the galaxies in these two categories are drawn from the same parent population.

2 GMRT H I imaging of galaxies

Having found from the above study that there is gas evolution in galaxies in X-ray bright groups possibly caused by their IGM, we undertook H I imaging of some galaxies from X-ray bright groups to detect signatures of IGM assisted gas stripping in these galaxies, as is often found in clusters. Simple estimates suggest that under favorable circumstances the IGM ram pressure is capable of stripping ∼50% of H I in some galaxies in X-ray bright groups.

We imaged 13 galaxies from four groups: 6 galaxies from NGC 5044, 2 from NGC 720, 4 from NGC 1550 and one from IC 1459. On source integration time on each source was ∼3.5 hrs and we achieved an rms sensitivity of ∼1 mJy/beam at a resolution of $\sim 20'' \times 20''$.

In most cases H I morphologies are found disturbed and H I disks appear truncated. Average D_H/D_{25} of the sample is 1.1 ± 0.12 compared to 1.7 ± 0.05 for galaxies in the field and in non X-ray groups.

3 Conclusion

X-ray bright groups with their relatively higher IGM density and dispersion than non-X-ray groups, present an intermediate environment between clusters and normal groups (without hot IGM). In this environment ram pressure (a process otherwise considered inefficient in groups) and/or tidal aided ram pressure can remove gas from the galaxies rendering them H I deficient [1].

References

1. Sengupta C., Balasubramanyam R., Dwarakanath K. S., 2007, MNRAS, 378, 137
2. Crook A. C., Huchra J. P., Martimbeau N., Masters K. L., Jarrett T., Macri L. M., 2007, ApJ, 655, 790
3. Sengupta C., Balasubramanyam R., 2006, MNRAS, 369, 360
4. Huchra J. P., Geller M. J., 1982, ApJ, 257, 423
5. Holmberg E., 1950, MeLu2, 128, 1

Ca II and Na I Absorption Signatures from the Circumgalactic Gas of the Milky Way

Nadya Ben Bekhti[1], M. Murphy[2], P. Richter[3], and T. Westmeier[4]

[1] Argelander-Institut für Astronomie, Auf dem Hügel 71, 53121 Bonn, Germany
nbekhti@astro.uni-bonn.de
[2] Faculty of Information & Communication Technologies, Swinburne University of Technology, Victoria 3122, Australia
[3] Institut für Physik, Am Neuen Palais 10, 14469 Potsdam, Germany
[4] Australia Telescope National Facility, Epping NSW 1710, Australia

Spiral galaxies are surrounded by large gaseous halos that represent the interface between the condensed galactic discs and the surrounding circumgalactic medium. A powerful method for studying the properties and nature of these circumgalactic gaseous structures is the analysis of absorption-line systems in the spectra of distant quasars (e.g., [3, 4]). Here we concentrate on the study of metal-line absorption systems in the halo of our own galaxy and link them with the distribution of neutral gaseous structures in the Milky Way as seen in H I 21-cm emission.

Our sample contains in total 106 sight lines towards quasars observed in the optical with VLT/UVES. Along 43 of them we detect halo Ca II and/or Na I absorption lines at intermediate or high velocities. For these we have additional H I emission spectra obtained with the 100-m telescope at Effelsberg. The absorption profiles of Ca II and Na I for one of the sight lines are plotted in the left panel of Fig. 1 on an LSR velocity scale together with the corresponding 21-cm emission spectrum. In many cases the Ca II/Na I absorption is connected with H I gas at column densities in the range of a few times $10^{18}\,\mathrm{cm}^{-2}$ to $10^{20}\,\mathrm{cm}^{-2}$. Our 3σ H I column density detection limit is about $2 \times 10^{18}\,\mathrm{cm}^{-2}$ for the warm neutral medium. In a few cases the detected H I signals are below the detection limit of large H I surveys (e.g. LAB survey, [2]). The measured H I line widths imply that for most of the sight lines the gas is relatively cold with temperatures below 1000 K. The directions and velocities of several of the clouds suggest a possible association with known HVC or IVC complexes. Most Ca II/Na I absorbers show multiple intermediate- and high-velocity components, indicating the presence of filamentary or clumpy structures.

The right panel of Fig. 1 shows the logarithm of the number of sight lines observed with UVES versus $\log(N_{\mathrm{CaII}}/\mathrm{cm}^{-2})$. The distribution of the column density follows a power law with slope $\beta = -1.6 \pm 0.3$. The vertical

B.S. Koribalski, H. Jerjen (eds.), *Galaxies in the Local Volume*,
doi: 10.1007/978-1-4020-6933-8_61,

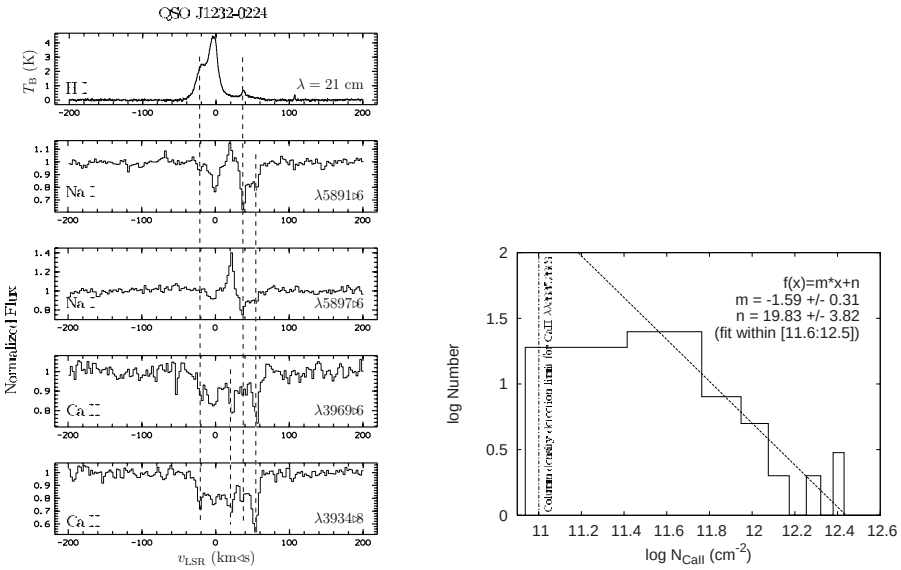

Fig. 1. *(Left:)* Ca II and Na I absorption and the corresponding H I emission spectra of QSO J1232–0224 obtained with UVES and the Effelsberg 100-m telescope. *(Right:)* Logarithm of the number of intermediate- or high-velocity absorption lines versus the logarithm of the Ca II column density with a linear binning of $\log N_{\rm HI}$. The dashed line represent a power law fit with $N^{-1.6}$ defined over the range of column densities from $\log(N_{\rm CaII}/{\rm cm}^{-2}) = 11.6$ to $\log(N_{\rm CaII}/{\rm cm}^{-2}) = 12.5$.

dashed-dotted line indicates the UVES 4σ detection limit of $\log(N_{\rm CaII}/{\rm cm}^{-2}) = 11$. Therefore, the lower column density cut-off is only a selection effect determined by the detection limit of the instrument. As a consequence we are not able to make conclusions about a typical column density of the Ca II absorbers.

The fact that among 106 random lines of sight through the halo we observe 43 absorption systems with at least one intermediate- or high-velocity component suggests that the Milky Way halo is filled with low column density gas clouds. Their investigation with synthesis telescopes will allow us to determine their metallicities and, thus, to learn more about their origin. Studying the clouds will also allow us to draw conclusions about the absorption line systems commonly observed in the halos of other galaxies (e.g., [1]) and the physical state of this gas.

References

1. N. Bouché, M.T. Murphy, C. Péroux et al.: MNRAS **371**, 495 (2006)
2. P.M.W. Kalberla, W.B. Burton, D. Hartmann et al.: A&A **440**, 775 (2005)
3. P. Richter, K.R. Sembach, B.P. Wakker et al.: ApJ **562**, L181 (2001)
4. P. Richter, T. Westmeier, C. Brüns: A&A **442**, L49 (2005)

The Orbital History of the LMC

Gurtina Besla[1], Nitya Kallivayalil[1], Lars Hernquist[1], Brant Robertson[2], T. J. Cox[1], Roeland P. van der Marel[3], and Charles Alcock[1]

[1] Harvard Smithsonian Center for Astrophysics, USA gbesla@cfa.harvard.edu
[2] Kavli Institute for Cosmological Physics, USA
[3] Space Telescope Science Institute, USA

The recent proper motion (PM) measurement of the Large Magellanic Cloud (LMC) by Kallivayalil et al. [3] (hereafter K1) implies that its 3D velocity is substantially higher ($\sim$100 km/s) than previously estimated and now approaches the escape velocity of the Milky Way (MW). Previous studies have also assumed that the MW can be adequately modeled as an isothermal sphere to large distances. We have re-examined the orbital history of the LMC using the new PMs and a λCDM-motivated MW model and find that the L/SMC are either on their first passage about the MW, or, if the MW is substantially more massive ($> 2 \times 10^{10}$ $M_\odot$ than currently believed, that their orbital period and apogalacticon distance must be a factor of two larger than previously estimated [2]. All phenomenological studies pertaining to the Clouds have implicitly assumed that they have been bound to the MW for a Hubble time, that is, their orbits have been described as quasi-periodic and thought to be slowly decaying due to dynamical friction. This assumption is inconsistent with the new PMs. As such, all theories concerning the origin of the Magellanic Stream (MS), a stream of H I gas trailing the L/SMC that extends $\sim$100° across the sky, need to be revisited. In light of the controversial nature of these results we have chosen to elaborate here on the reliability of the new PMs.

Kallivayalil et al. [3] used ACS on *HST* to track the LMC's motion relative to 21 background QSOs discovered from their optical variability in the MACHO database. The PM of the LMC was thus determined to better than 5% accuracy: $\mu_W = -2.03 \pm 0.08$ mas/yr, $\mu_N = 0.44 \pm 0.05$ mas/yr. The corresponding mean 3D velocity is 378 ± 18 km/s. We note here that even using the weighted average of all pre-2002 PM measurements as given by [4] (v = 300 km/s) does not change the conclusions of [2] that the past orbit of the Clouds is not co-located with the MS. Furthermore, these old velocities also yield drastically different orbital histories if the MW is described using a cosmologically motivated model rather than an isothermal sphere.

The significant improvement in the accuracy of K1's PM measurement over that of previous works owes largely to three factors: 1) ACS has high

B.S. Koribalski, H. Jerjen (eds.), *Galaxies in the Local Volume*,
doi: 10.1007/978-1-4020-6933-8_62,

resolution (plate scale of 28 mas/pixel) and is well-calibrated and very stable for astrometry [1]; 2) 21 QSOs, distributed reasonably uniformly behind the LMC, were used as an inertial frame of reference; 3) space-borne telescopes such as *HST*, are capable of imaging targets (here meaning fields centered on each QSO) at random orientations on the detector. As such, possible systematic PM errors tied to the CCD frame average out and each of the 21 fields can thus be treated as independent measurements.

There was a great deal of debate at this conference over the extent to which the assumptions used to model the LMC's internal kinematics affected the PM determination. We address those concerns here by pointing out that even taking the straight unweighted average of the *observed* PM for all 21 QSO fields yields: $\mu_W = -1.97 \pm 0.09$ mas/yr and $\mu_N = 0.46 \pm 0.1$ mas/yr (see Figure 11a of K1). This result is independent of any model assumptions and is remarkably consistent with the final values, illustrating that the K1 results do not depend sensitively on the details of either the modeling of the field dependence of the PMs or the actual statistic applied to obtain the average. The errors were, however, significantly reduced by modeling the internal kinematics of the LMC using parameters from [4]. K1 varied these parameters within realistic uncertainties, i.e. by: 5 km/s in the line of sight velocity, 10° in inclination, $120° - 155°$ for the line-of-nodes position angle, $0.^{\circ}5$ in the LMC's center position and 0.1 magnitudes in the distance modulus. None of these changes affected the final estimate of the LMC's PM by more than 0.02 mas/yr: i.e. by a quarter of the 1σ errors (see K1 section 4.1).

Although K1 did not account for the degrading charge transfer efficiency of the ACS HRC CCD and also chose to use a single PSF for all data, rather than to craft it specifically for each field, Piatek et al. (2007, in prep.) recently re-analysed the *HST* data taking those factors into account an yet obtained the *same* result as K1 for the PM of the LMC.

Thus, any reasonable modification of the assumptions made in the analysis of the *HST* data by K1 *cannot* change the 3D velocity such that it approaches the old values of ∼300 km/s. The conclusion that the Clouds are on their first passage about the MW is therefore similarly robust. The remaining issue is the limited time baseline: the K1 PMs were based on a two year baseline. We have obtained time on *HST* cycle 16 using WFPC2 to verify the K1 PMs with a new epoch of data.

References

1. Anderson, J. & King, I. R. 2003, PASP, **115**, 113
2. Besla, G, Kallivayalil, N., Hernquist, L., Robertson, B., Cox, T. J., van der Marel, R. P., & Alcock, C. 2007, astro-ph 0703196
3. Kallivayalil, N., van der Marel, R. P., Alcock, C., Axelrod, T., Cook, K. H., Drake, A. J., & Geha, M. 2006a, ApJ, **638**, 772 [K1]
4. van der Marel, R. P., Alves, D. R., Hardy, E., & Suntzeff, N. B. 2002, AJ, **124**, 2639

Star Formation in the SMC Young Cluster NGC 602: Spatial and Temporal Distribution

Lynn Redding Carlson[1], E. Sabbi, M. Sirianni, J. L. Hora, A. Nota, M. Meixner, J. S. Gallagher III, M. S. Oey, A. Pasquali, L. J. Smith, M. Tosi, and R. Walterbos

[1]Johns Hopkins University, Baltimore, MD, USA carlson@stsci.edu

NGC 602 is a young stellar cluster located in the wing of SMC. We present the spatially and temporally resolved stellar and proto-stellar populations as viewed in the optical with HST/ACS and in the near IR with Spitzer/IRAC. Color-Magnitude Diagrams over a range of wavelengths in comparison with theoretical models and isochrones reveal a distinct spatial distribution of

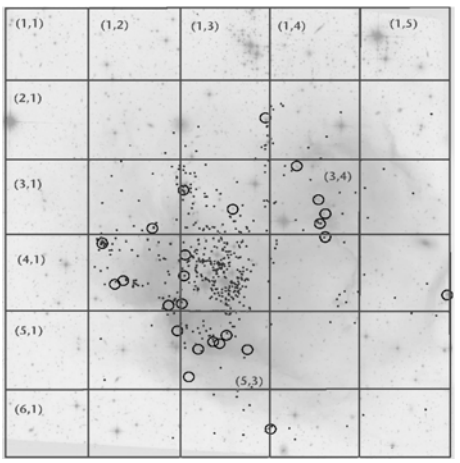

Fig. 1. HST/ACS image of NGC 602 with North up and East to the left, $\approx 200'' \times 200''$ or 58 pc × 58 pc. Black circles mark the locations of YSO candidates as identified from Spitzer/IRAC photometry. Dark dots mark the positions of probable pre-Main Sequence stars. Note that the spatial distributions are distinct. The pre-MS stars are highly concentrated at the cluster center, surrounding the brightest blue stars in the cluster. The YSOs are systematically farther from cluster center and occupy the dustier regions.

bright Main Sequence (MS), newly-discovered pre-MS stars, and IR-bright Young Stellar Objects (YSOs), still embedded in nebular material.

Details of the population identifications are available in [2]. In Fig. 1, we begin to explore the spatial distribution of these young objects by overlaying a grid and considering the sections. Pre-MS stars (dots) are ∼4 Myrs old and are heavily concentrated near cluster center, near the brightest MS stars. YSOs, identified via infrared photometry, are only ∼1 Myr old and are located in the dusty ridges.

B.S. Koribalski, H. Jerjen (eds.), *Galaxies in the Local Volume*,
doi: 10.1007/978-1-4020-6933-8_63,

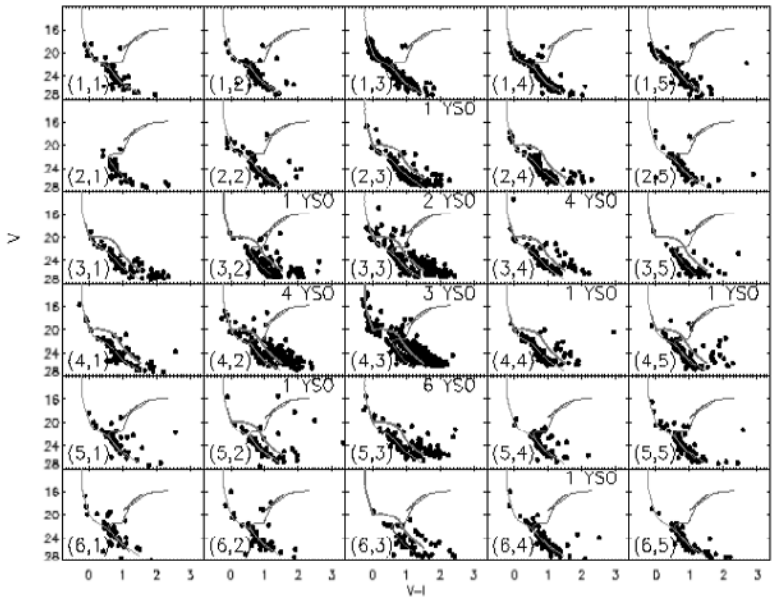

Fig. 2. Optical Color-Magnitude Diagram for each of the grid sections. The darkest isochrone delineates the oldest with an age of 6 Gyr. Lighter isochrones show the younger Main and pre-MS populations with an age of ∼4 Myr. The pre-MS lies within the color region between ∼1 and 2 and runs almost parallel to the faint Main Sequence. (Note: We have used V and I to represent the ACS filters F555W and F814W, respectively. Isochrones come from [1] and [3].)

The optical color-magnitude diagrams for each grid-section, shown in Fig. 2, give a more quantitative picture. Many of the edge regions contain only Main Sequence and old Turn-Off stars, consistent with nearby field star populations. This is notably true of the entire top row. The concentration of pre-MS stars is striking. 38% of all of the candidate pre-MS stars lie within grid-section (4,3), and more than 61% lie within regions (4,3), (3,5), and (4,2). The concentration of YSO candidates lies a little farther out. Grid-section (5,3) contains 6 of the 25 YSO candidates along its dusty ridge but contains less than 7% of the pre-MS stars. We infer that star formation began near the center of this region ∼4 Myrs ago and has continued propagating outward, with the youngest observed sources a mere 1 Myr in age.

References

1. Bertelli et al.: A&AS **106**, 275 (1994)
2. Carlson et al.: ApJ **665**, L109 (2007)
3. Siess, L., Dufour, E., and Forestini, M.: A&A **358**, 593 (2000)

Supernova Remnant Populations in Nearby Star-Forming Galaxies

Laura Chomiuk and Eric Wilcots

University of Wisconsin–Madison, 475 N. Charter St. Madison, WI 53706, USA
chomiuk@astro.wisc.edu, ewilcots@astro.wisc.edu

We present a study of the supernova remnant (SNR) populations in several nearby galaxies, using some of the deepest radio continuum maps to date. We compare the radio SNR luminosity functions (LFs) of these galaxies, and attempt to explain any differences in terms of the properties of the parent galaxies. This is a crucial step in understanding how the efficiency of cosmic ray production and synchrotron radiation vary across galaxies.

1 Observation and Selection of SNRs

We obtained radio maps with the Very Large Array at 6 and 20 cm for three nearby spiral galaxies: NGC 628, NGC 3184, and NGC 3631. The maps have $\sim 4''$ resolution, and are some of the deepest ever observed, with rms noise levels of $\sim$0.015 mJy/beam. We consider SNRs to be discrete radio sources which satisfy the following three criteria, as set out by Pannuti et al. [5]:

- Integrated 20 cm flux density greater than 3 times the local noise.
- Nonthermal spectral index ($\alpha = \frac{-ln\ (S_{20cm}/S_{6cm})}{ln\ (\nu_{20cm}/\nu_{6cm})} > 0.2$). This allows us to separate SNRs from H II regions.
- Spatially coincident with Hα emission in a narrow-band image. This is required to distinguish SNRs from background sources.

We find that 25 sources meet these criteria in NGC 3184, 19 in NGC 3631, and 31 in NGC 628.

2 Radio Luminosity Functions

Figure 1 presents the cumulative luminosity functions of SNRs in these three spiral galaxies, and also includes SNR data for six galaxies from the literature (NGC 6946 [3], M 33 [2], LMC [1], SMC [1], NGC 7793 [4], and NGC 300 [5]).

B.S. Koribalski, H. Jerjen (eds.), *Galaxies in the Local Volume*,
doi: 10.1007/978-1-4020-6933-8_64,

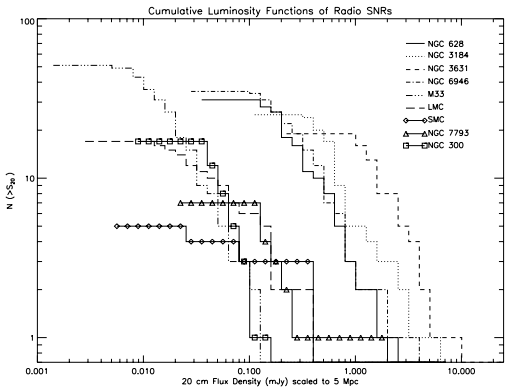

Fig. 1. Cumulative luminosity functions for SNRs in nine galaxies, as measured by their 20 cm radio continuum flux.

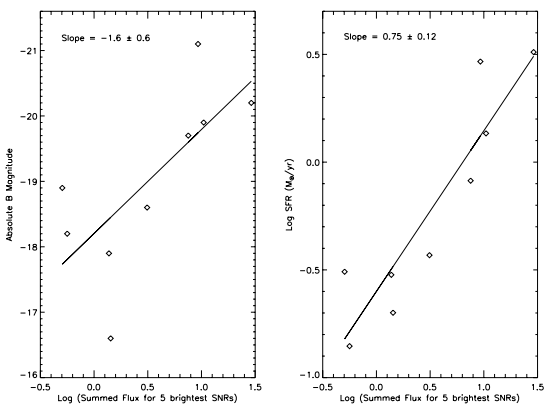

Fig. 2. For each galaxy, its five brightest SNRs are summed together, and plotted against the absolute B-band magnitude of the galaxy (left) and the star formation rate of the galaxy (right).

The SNR "luminosities" plotted here are 20 cm flux densities, scaled so that all SNRs appear at a distance of 5 Mpc.

Clearly, some galaxies contain much more luminous SNRs than others. It appears that the brightest SNRs in lower luminosity galaxies (M_B fainter than –19.0) are ∼10 times fainter than the most luminous SNRs in galaxies with $M_B < -19.5$. Figure 2 shows that the luminosity of the brightest SNRs correlates with the luminosity of the parent galaxy, and correlates even more strongly with the global star formation rate of the parent galaxy.

References

1. M. D. Filipovic, W. Pietsch, R. F. Haynes et al: A&AS **127**, 119 (1998)
2. S. M. Gordon, N. Duric, R. P. Kirshner et al: ApJS **120**, 247 (1999)
3. C. K. Lacey & N. Duric: ApJ **560**, 719 (2001)
4. T. G. Pannuti, N. Duric, C. K. Lacey et al: ApJ **565**, 966 (2002)
5. T. G. Pannuti, N. Duric, C. K. Lacey et al: ApJ **544**, 780 (2000)

Simulations of Dynamical Evolution of Galaxy Groups

Yaroslav Chumak and Oleg Chumak

Sternberg Astronomical Institute, 119992, Universitetski pr., 13 Moscow University, Moscow, Russia chyo@mail.ru, chumak@sai.msu.ru

It is known [1, 2] that observations of the Local Volume (LV) show a specific feature – 'cold' Hubble flow on relatively small scale, often called the Hubble-Sandage paradox. A possible solution of the paradox has been suggested by [3] soon after the discovery of the cosmic vacuum (dark energy or the cosmological constant) in observations of distant type Ia supernovae [4, 5]. It has been recognized [6, 7] that the cosmic vacuum with its perfectly uniform density makes the Universe effectively uniform at various spatial scales, both large and relatively small, where cosmic vacuum dominates by density over dark matter and baryons. As a result the Hubble's flux should be cooled down on the relatively short scales and this fact opens possibilities to solve the Hubble-Sandage paradox. We have made attempt to check these possibilities by simulations.

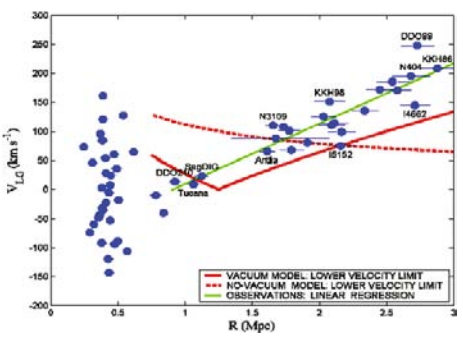

Fig. 1. Hubble diagram for LV galaxies within $R = 3$ Mpc, based on 'A Catalog of Neighboring Galaxies'. The galaxies of the Local Group are located within 1 Mpc. The flow of divergent galaxies in the outskirts of the group reveals the linear velocity-distance relation (the Hubble flow) at $R \geq 2$ Mpc (according to [9]).

We have made simulations for a few galaxy groups and were ascertained in relevance of this idea. Here we show some results of simulations for the Local galaxy group only as an example. The numerical simulation is based on Aarseth's NBODY2 code [8], which has been upgraded in order to include antigravity effects of vacuum.

B.S. Koribalski, H. Jerjen (eds.), *Galaxies in the Local Volume*,
doi: 10.1007/978-1-4020-6933-8_65,

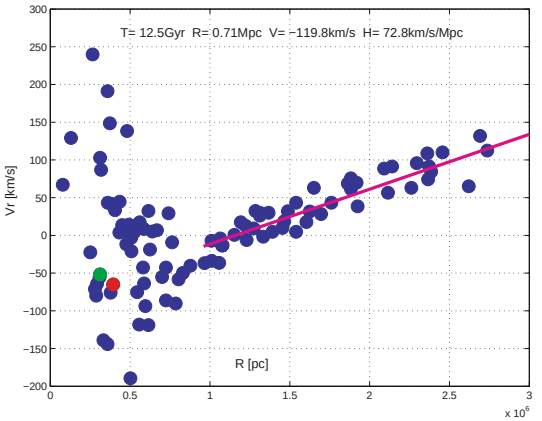

Fig. 2. Hubble diagram of the Local Volume (distance $R < 3$ Mpc) based on the results of our simulations including antigravity. The simulation results have been obtained under the following conditions: initial total mass of the Local Volume is 2.7×10^{12} $M_{\odot}$, initial distance between the Milky Way and M 31 is 1.4 Mpc, initial relative velocity of these two galaxies is –9 km/s, module of average velocity of dwarf galaxies is 40 km/s. The results of the calculations are given on the top of the figure.

Fig. 1 shows the Hubble diagram for the Local Volume, according to [9]. On Fig. 2 one of our result is shown — the Hubble diagram for the Local Volume is based on simulations with reliable initial conditions. One can see a good correspondence between these two diagrams.

Acknowledgements: The authors would like to thank Proff. A.D. Chernin for fruitful discussions and care, Proff. S. Aarseth for his kind assistance with the NBODY2 code, Proff. A.S. Rastorguev for permanent attention, help and support. This study is supported by Russian Fundamental Research Foundation: Grants 7-02-00961-a, 06-02-16366-a, and 07-02-08333-z.

References

1. A. Sandage: ApJ, **527**, 47, 9, (1999)
2. A. Chernin, I. Karachentsev, M. Valtonen, V. Dolgachev, L. Domozhilova, D. Makarov: A&A, **415**, 19 (2004)
3. A. Chernin, P. Teerikorpi, Yu. Baryshev: astro-ph/0012021 (2000); Adv. Space Res. **31** 459 (2003)
4. A. Riess, A. Filippenko, P. Challis, et al.: AJ **116**, 1009, (1998)
5. S. Perlmutter, G. Aldering, G. Goldhaber, et al.: ApJ, **517**, 565, (1999)
6. A. Chernin: Physics-Uspekhi, **44**, 1099, (2001)
7. Yu. Baryshev, A. Chernin, P. Teerikorpi: A&A, **378**, 729, (2001)
8. S. J. Aarseth: *Gravitational N-Body Simulations*, (Cambridge University Press 2003)
9. A. Chernin, I. Karachentsev, et. al.: astro-ph/0706.4068v1, (2007)

Surveying the Monoceros Ring: Locations, Velocities and a Contentious Dwarf

Blair Conn[1], G. Lewis[2], R. Lane[2], R. Ibata[3], N. Martin[4], and M. Irwin[5]

[1] European Southern Observatory, Chile bconn@eso.org
[2] The University of Sydney, Australia gfl@physics.usyd.edu.au
[3] Observatoire de Strasbourg, France
[4] Max Planck Institute for Astronomy Heidelberg, Germany
[5] Institute of Astronomy Cambridge, U.K.

In 2002, Newberg et al. [7], using the Sloan Digital Sky Survey (DSS), found an overdensity of stars in the outer reaches of the Milky Way. At 11 kpc from the Sun and covering a wide range of longitudes, this structure was dubbed the Monoceros Ring (MRi). Ibata et al. [5] and Conn et al. [1, 2, 3, 4] have shown that this structure is found around the Galactic Plane and on both sides of the Galactic Disc. Several interpretations have been suggested for this structure ranging from perturbations of the outer Disc to the tidal stream of an accreting dwarf galaxy. To investigate these scenarios, a deep imaging survey around the Galactic plane has been performed with both the INT/WFC and AAT/WFI instruments. The Colour-Magnitude diagrams (CMDs) of these regions are compared with the Besançon synthetic galaxy model, see Figure 1.

Importantly, the Monoceros Ring can be seen as a distinct main sequence away from the bulk Milky Way components. A main sequence fiducial has been placed on the detection to estimate the distance. This method is used, as isolating the Red Giant Branch from Milky Way stars is difficult in high stellar density regions of the CMD.

Radial velocities of MRi stars have been observed in several fields. Conn et al. [1, 2] show the detection of the stream behind the CMa overdensity. In general, the MRi velocity profile is not well known around the Galactic Plane but importantly though, each detection of the MRi does report a cold population of stars, typically with a velocity dispersion of $\sim$20 km/s. This is combined with a tight correlation in distance. Together these suggest a tidal stream scenario, however more MRi stars need to be observed to better illustrate this correlation.

If the MRi is an in-plane accretion event then searching for its progenitor is an important step in understanding its evolution and impact on the Milky Way. Two independent simulations have placed such a progenitor in the Canis Major region, (Martin et al. [6], Peñarrubia et al. [8]). The Galactic Disc warps significantly in Canis Major and this needs to be accounted for when

B.S. Koribalski, H. Jerjen (eds.), *Galaxies in the Local Volume*,
doi: 10.1007/978-1-4020-6933-8_66,

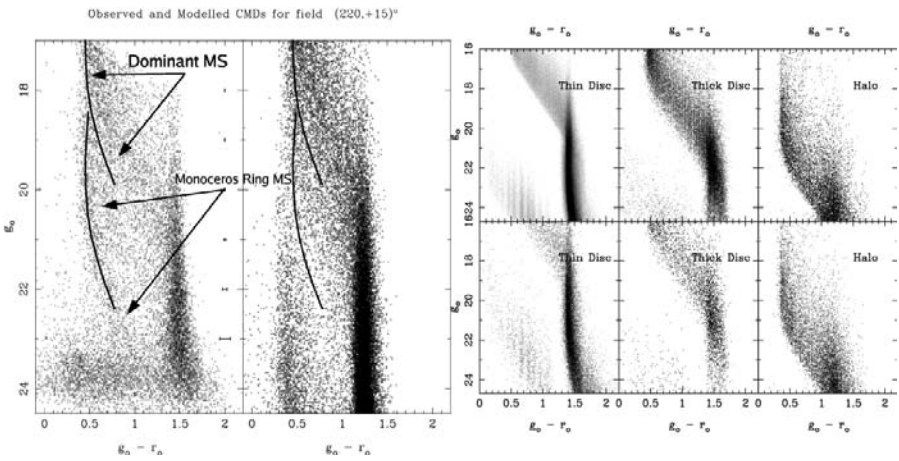

Fig. 1. *(Left:)* Colour-Magnitude Diagram showing the location of the Monoceros Ring with respect to the dominant Main sequence of the Milky Way. *(Right:)* The Besançon Synthetic Galaxy model showing the location of the bulk Milky Way components in the Colour-Magnitude Diagram.

interpreting the data. Observations of this region have not been well matched by synthetic Galaxy models with warps and determining whether a dwarf galaxy progenitor of the MRi resides here is still under debate.

Finally, the MRi and Canis Major overdensity stars have been associated with an outer spiral arm of the Milky Way. While an outer spiral arm has been detected in gas in this direction, attributing a strong stellar component to this structure is difficult and preliminary. With all these possibilities, the MRi is certainly an interesting new structure of our Milky Way.

References

1. B. C. Conn, G. F. Lewis, M. J. Irwin, R. A. Ibata, A. M. N. Ferguson, N. Tanvir, J. M. Irwin, MNRAS, **362**, 475 (2005a)
2. B. C. Conn, N. F. Martin, G. F. Lewis, R. A. Ibata, M. Bellazzini, M. J. Irwin, MNRAS, **364**, L13 (2005b)
3. B. C. Conn et al., MNRAS, **376**, 939 (2007a)
4. B. C. Conn et al., MNRAS, in prep (2007b)
5. R. A. Ibata, M. J. Irwin, G. F. Lewis, A. M. N. Ferguson, N. Tanvir, MNRAS, **340**, L21 (2003)
6. N. F. Martin, R. A. Ibata, M. Bellazzini, M. J. Irwin, G. F. Lewis, W. Dehnen, MNRAS, **348**, 12 (2004)
7. H. J. Newberg et al., ApJ, **569**, 245 (2002)
8. J. Peñarrubia et al., ApJ, **626**, 128 (2005)

The Stellar Structures Around Disk Galaxies

Igor Drozdovsky[1,2], N. Tikhonov[3], A. Aparicio[1], C. Gallart[1], M. Monelli[1], S. Hidalgo[1], E. J. Bernard[1], O. Galazutdinova[3], G. Bono[4], N. Sanna[4], and the LCID team[5]

[1] Instituto de Astrofísica de Canarias, Tenerife, Spain dio@iac.es
[2] Astronomical Institute of St.Petersburg State University, Russia
[3] Special Astrophysical Observatory, Russia
[4] INAF - Osservatorio Astronomico di Roma, Italy
[5] http://www.iac.es/project/LCID

We present a brief summary of current results on the stellar distribution and population gradients of the resolved stars in the surroundings of ~ 50 nearby disk spiral and irregular galaxies, observed with space- (Hubble & Spitzer) and ground-based telescopes (Subaru, VLT, BTA, Palomar, CFHT, & INT). We examine the radial (in-plane) and vertical (extraplanar) distributions of resolved stars as a function of stellar age and metallicity by tracking changes in the color-magnitude diagram of face-on and edge-on galaxies. Our data show that the scale length and height of a stellar population increases with age, with the oldest detected stellar populations identified at a large galactocentric radius or extraplanar height, out to typically a few kpc. In the most massive of the studied galaxies there is evidence for a break in number density and color gradients of evolved stars, which plausibly correspond to the thick disk and halo components of the galaxies. The ratio of intermediate-age to old stars in the outermost fields correlates with the gas fraction, while relative sizes of the thick-to-thin disks anticorrelate with galactic circular velocity.

Extended faint stellar structures have been detected around many nearby disk galaxies of different morphological types over the past decade, but their nature has been a matter of some debate. Sometimes referred either as a 'sheet'-like (thick disk), or a spherical 'halo' structure, these stellar formations together with streams are now recognized as an important probe of galaxy formation and evolution (e.g., [1]). Using the multiband photometry of resolved stars, we know that the scale length and height of a stellar population in the disk galaxies increase with age, with the oldest detected stellar populations identified at large galactocentric radii or extraplanar height, out to typically a few kpc (e.g., [2, 3, 4]). The extraplanar height of the thick disk in low mass disk galaxies is systematically larger than the young thin disk of giant spirals (see Fig. 1), suggesting that stars in low-mass galaxies form in a thicker disk. In the most massive of the studied galaxies (highest circular

B.S. Koribalski, H. Jerjen (eds.), *Galaxies in the Local Volume*,
doi: 10.1007/978-1-4020-6933-8_67,

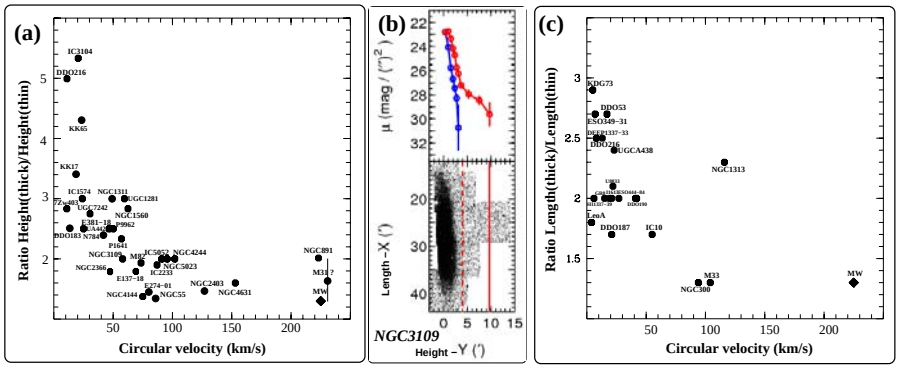

Fig. 1. *(Left:)* Ratio of thick- to thin-disk height as a function of the rotational velocity for the high-inclination galaxies, based on the distribution of resolved young and evolved stars. *(Middle:)* An example of such a study for the edge-on galaxy. *(Right:)* A similar plot for the radial length ratio in the face-on sub-sample.

velocity), there is evidence for a break in number density and color gradients of evolved Red Giant Branch (RGB) and Red Clump (RC) stars, which plausibly correspond to the transition from the thick disk to the evasive stellar spheroid, the halo.

As a next step in our study we selected four prominent Local Group disk galaxies – NGC 6822, NGC 3109, IC 1613, and IC 10 – to analyze in-depth the radial (in-plane) and vertical (extraplanar) gradients as a function of stellar age in a wide range of galactocentric distances. Our data include wide-field imaging with ground-based telescopes aimed at reaching the old (∼10 Gyr) stellar population, such as horizontal branch (HB) stars – signposts of an ancient stellar population – and deep pencil beam fields with HST/ACS & WFPC2 reaching the old main-sequence turnoffs (based in part on the LCID team data). We are working on the modeling of the star formation history and chemical evolution of the different stellar sub-structures in these galaxies.

When complemented with detailed chemical abundances and kinematic information from the spectra of the individual stars, our optical/near-IR photometric data will allow us to shed light on fundamental questions about the evolution of disk galaxies, such as disk heating versus merger scenarios and the role of these mechanisms in forming the stellar disks and halos.

References

1. Abadi, M. G., Navarro, J. F., & Steinmetz, M.: MNRAS, **365**, 747 (2006)
2. Drozdovsky, I., Tikhonov, N., & Schulte-Ladbeck, R.: in "The Local Group as an Astrophysical Laboratory", 25 (2003)
3. Tikhonov, N., Galazutdinova, O., Drozdovsky I.: A&A, **431**, 127 (2005)
4. Tikhonov, N. A.: AstrRep, **49**, 501 (2005); AstrRep, **50**, 517 (2006)

A Long Overdue Synthesis Image of Centaurus A

Ilana J. Feain[1], T. J. Cornwell, R. D. Ekers, R. Norris, B. M. Gaensler, J. Ott, M. Johnston-Hollitt, T. Murphy, E. Middelberg, and J. Bland-Hawthorn

Australia Telescope National Facility, CSIRO, PO Box 76, Epping, NSW 1710, Australia Ilana.Feain@csiro.au

Centaurus A (NGC 5128) is by far the closest active supermassive black hole in the Universe. But until now only about 1% of its radio morphology has been imaged at high resolution with aperture synthesis. Why? Because its large angular size ($9^\circ \times 5^\circ$) and low surface brightness outer lobes made imaging this radio galaxy daunting and expensive in time. Only now are image processing algorithms sophisticated enough to deal with the high dynamic range (10^5) and large field-of-view to properly image Centaurus A. The mosaic that we are making will have a spatial resolution of 600 pc over a radio source 600 kpc in size. It will be the most detailed image ever of a radio galaxy!

The left image of Figure 1 shows the full extent of the radio emission at 1.4 GHz, mapped with the Parkes telescope well over a decade ago (courtesy Norbert Junkes). The right image shows the DSS optical image of NGC 5128 overlaid with VLA 1.4 GHz radio continuum contours of the inner jets [1]. The position and scale of the right image with respect to the full radio emission of Centuarus A is indicated by the white rectangle. Thus, the inner VLA jets amount to less than 1% of the entire radio structure.

Commencing on 2006 December 20, we began the first set of observations with the Australia Telescope Compact Array (ATCA) at 1.4 GHz to mosaic the full radio structure of Centaurus A. We cover the field with about 400 pointings, in mosaic imaging mode. The complicated structure associated with this source means that *uv*-coverage is of paramount importance, and we therefore require observations with all four 750 metre array configurations.

A first look at the data shows promising results. The large-scale polarised emission seen in the Parkes images is already evident, although a much more densely sampled *uv*-plane is crucial to successfully image these diffuse, complicated lobe structures. In addition, there are several hundred background point sources in the field that are strong enough to probe the Faraday rotation in the radio lobes and the intergalactic medium into which the lobes are expanding. The science goals of this experiment are to:

B.S. Koribalski, H. Jerjen (eds.), *Galaxies in the Local Volume*,
doi: 10.1007/978-1-4020-6933-8_68,

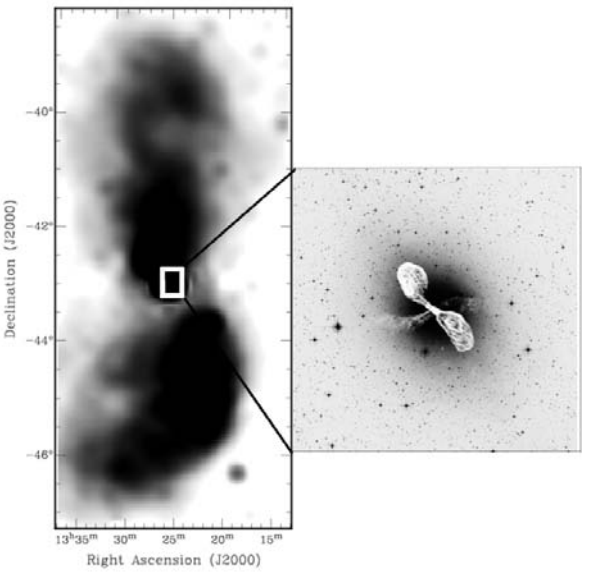

Fig. 1. *Left:* Parkes 1.4 GHz image of Centaurus A (courtesy Norbert Junkes). The white rectangle indicates the position and scale of the right image. *Right:* DSS optical image of NGC 5128 overlaid with VLA 1.4 GHz radio continuum contours of the inner jets [1].

- Explore feedback between the polarised radio jets/lobes and the environment of the Centaurus group of galaxies to look for jet-cloud interactions and jet-induced star-formation.
- Exploit Centaurus A as a background polarised screen to probe the magnetic fields of HVCs and galaxies residing in front of the radio lobes.
- Derive Faraday rotation measures for the polarised radio sources behind the lobes to probe the magnetic field structure of Centaurus A itself.
- Investigate the Galactic magnetic field via Faraday rotation measures of both the polarised background sources and the diffuse lobes of Centaurus A.

Aperture synthesis mosaicing of Centaurus A will be hugely significant because its angular size and close proximity allows us to study its lobe structures in a detail not possible for other radio galaxies [2].

References

1. J. O. Burns, E. D. Feigelson, E. J. Schreier: ApJ **273**, 128 (1983)
2. F. P. Israel: A&ARv **8**, 237 (1998)

The SAGE View of Star Formation in the Large Magellanic Cloud

Jason Harris[1], B. Whitney[2], K. Gordon[3], M. Meixner[3], M. Meade[4], B. Babler[4], R. Indebetouw[5], J. Hora[6], C. Engelbracht[1], B.-Q. For[1], M. Block[1], K. Misselt[1], U. Vijh[3], C. Leitherer[3], and T. Robitaille[7]

[1] Steward Observatory, Tucson, Arizona, USA jharris@as.arizona.edu
[2] Space Science Institute, USA
[3] Space Telescope Science Institute, USA
[4] Department of Astronomy, University of Wisconsin, Madison, USA
[5] Department of Astronomy, University of Virginia, USA
[6] Harvard-Smithsonian Center for Astrophysics, USA
[7] School of Physics and Astronomy, University of St. Andrews, U.K.

SAGE (Surveying the Agents of a Galaxy's Evolution) is a Legacy program of the *Spitzer Space Telescope* [1], providing imaging of the central $7^\circ \times 7^\circ$ of the Large Magellanic Cloud (LMC) in all seven of *Spitzer*'s mid-infrared bands (IRAC 3.6μm, 4.5μm, 5.8μm and 8.0μm; and MIPS 24μm, 70μm and 160μm). We have used color selections to isolate a sample of more than 1000 high-probability young stellar object (YSO) candidates from the SAGE point-source catalog, and have fit protostellar models [2] to their photometry to determine their physical characteristics [3]. The YSO candidates are spatially correlated with high-density regions of the LMC's interstellar medium.

We use separate IRAC and MIPS data-reduction pipelines to perform optimal point-source extraction and photometry on the SAGE images, resulting in a catalog of approximately 6 million mid-infrared point sources. The SAGE catalog is expected to include thousands of YSOs in the LMC, but photometric degeneracies with other types of mid-infrared sources make it difficult to unambiguously identify all of the YSOs on the basis of photometry alone.

We have developed a set of photometric criteria that allow us to select a subset of YSOs with a high degree of confidence, by excluding regions of the photometric parameter space that are known to be occupied by non-YSO objects (see Fig. 1). We construct photometric criteria like those shown in Fig. 1 for several color-magnitude and color-color projections of our multi-dimensional photometric space, and adopt the set of objects that pass all of these criteria as our final list of high-confidence YSO candidates [3].

There are over 1000 high-confidence YSOs in the SAGE catalog, and while this sample is not complete, it represents the best view of a galaxy's

B.S. Koribalski, H. Jerjen (eds.), *Galaxies in the Local Volume*,
doi: 10.1007/978-1-4020-6933-8_69,

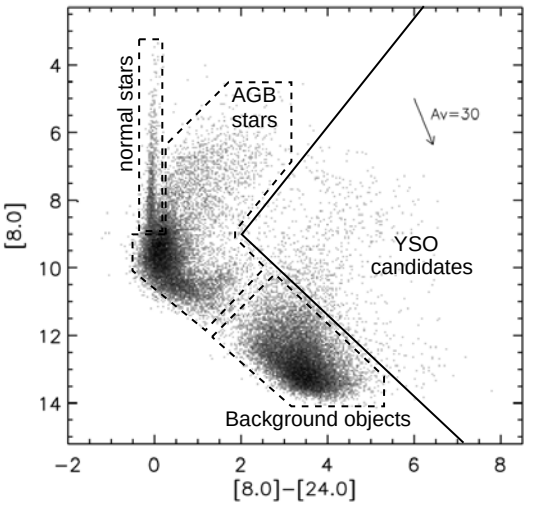

Fig. 1. One of many projections of the SAGE point-source photometry: a color-magnitude diagram showing the [8.0]-[24] color vs. the [8.0] magnitude. The regions occupied by several non-YSO object types are indicated with dashed lines, and we adopt the heavy line as one of the photometric selection criteria for YSO candidates (i.e., everything to the right of the heavy line is considered a YSO candidate).

protostellar population ever obtained. In Fig. 2, we show the frequency distribution of the YSO candidates as a function of the local H I and CO column density, and it is clear that YSO candidates tend to be found in regions where the density of the interstellar medium is high.

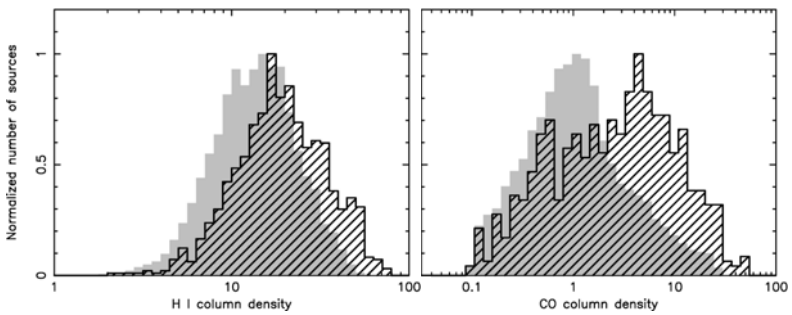

Fig. 2. The frequency distribution of the high-confidence YSO candidates as a function of the local H I and CO column density is shown as the hashed histogram in the *left* and *right panels*, respectively. For comparison, the frequency histograms for all SAGE sources are shown as the grey histogram in each panel.

References

1. M. Meixner et al.: AJ **132**, 2268 (2006)
2. T.P. Robitaille, B.A. Whitney, R. Indebetouw, K. Wood, & P. Denzmore: ApJS **167**, 256 (2006)
3. B.A. Whitney et al.: submitted to AJ (2007)

CO 4–3 and [C I] 1–0 in Circinus and NGC 4945

Carsten Kramer[1], Marc Hitschfeld[1], Manuel Aravena[2], Frank Bertoldi[2], Jürgen Stutzki[1], Yasuo Fukui[3], and the NANTEN2 team

[1] I. Physikalisches Institut, Universität zu Köln, Germany
kramer@ph1.uni-koeln.de, hitschfeld@ph1.uni-koeln, stutzki@ph1.uni-koeln.de
[2] Argelander-Institut für Astronomie, Universität Bonn, Germany
maraven@astro.uni-bonn.de, bertoldi@astro.uni-bonn.de
[3] Department of Astrophysics, Nagoya University, Japan
fukui_c@a.phys.nagoya-u.ac.jp

Studying molecular gas in the central regions of the starburst galaxies Circinus and NGC 4945 enables us to characterize the physical conditions and compare to previous local and high-z studies (Hitschfeld et al. 2007). We estimate temperature, molecular density and column densities of CO and atomic carbon. Using model predictions we give a range of estimated CO/C abundances.

Using the new NANTEN2 4m sub-millimeter telescope in Pampa La Bola, Chile, we observed for the first time CO 4–3 and [C I] 1–0 in the centers of both galaxies at linear scale of 732 pc and 682 pc, respectively. We compute the cooling curves of ^{12}CO and ^{13}CO using radiative transfer models and estimate the physical conditions of CO and [C I].

The centers of Circinus and NGC 4945 are very [C I] bright objects, exhibiting [C I] 1–0 luminosities of 67 and 91 K km s^{-1} kpc^2, respectively. The [C I] 1–0/CO 4–3 ratio of integrated intensities are large at 3.1 in Circinus and 1.23 in NGC 4945. Combining previous CO J= 1–0 , 2–1 and 3–2 and ^{13}CO J= 1–0 , 2–1 studies with our new observations, the radiative transfer calculations give a density $n = 10^3 - 3 \times 10^4$ cm^{-3} and a wide range for the kinetic temperature $T_{\rm kin} = 20 - 100$ K depending on the density. To discuss the degeneracy in density and temperature we study two representative solutions. In both galaxies the estimated total [C I] cooling intensity is stronger by factors up to ∼1–3 compared to the CO cooling intensity. The CO/C abundances are $0.2 - 2$, similar to values found in Galactic translucent clouds.

Our new observations enable us to further constrain the excitation conditions and estimate the line emission of higher-J CO- and the upper [C I]-lines.

B.S. Koribalski, H. Jerjen (eds.), *Galaxies in the Local Volume*,
doi: 10.1007/978-1-4020-6933-8_70,

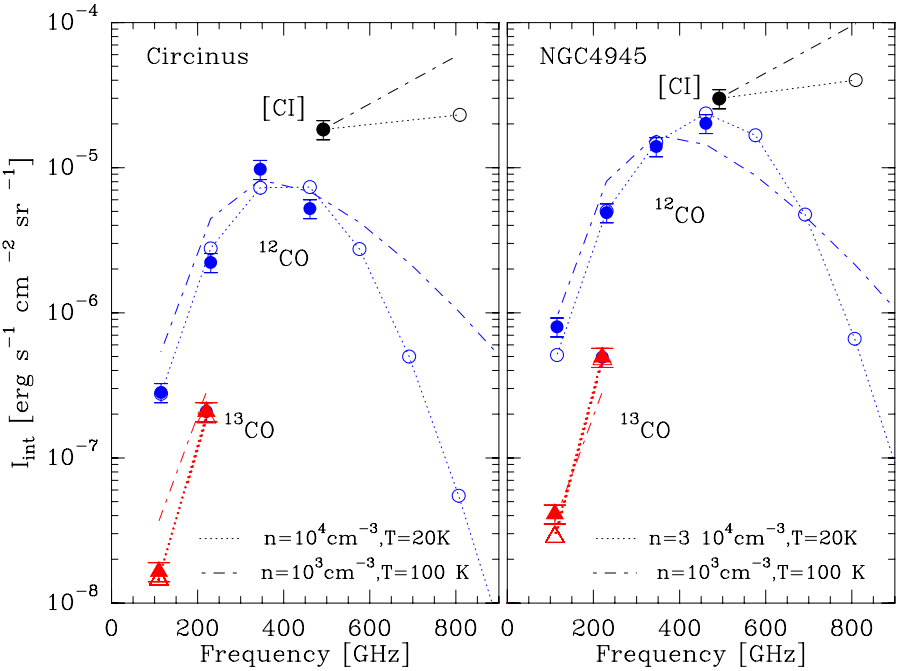

Fig. 1. Filled symbols show the observed [C I] 1–0, CO 1–0, 2–1, 3–2, 4–3, and ^{13}CO 1–0, 2–1 data. Dashed lines show two solutions of the radiative transfer analysis. The [C I] 1–0 and CO 4–3 data are new detections with NANTEN2. Low-J ^{12}CO and ^{13}CO data were obtained by Curran et al. (1998, 2001) and Mauersberger et al. (1996).

For the first time we give estimates for the CO/C abundance in the center regions of these galaxies. Future CO J= 7–6 and [C I] 2–1 observations will be important to resolve the ambiguity in the physical conditions and confirm the model predictions.

References

1. S.J. Curran et al.: A&A **338**, 683 (1998)
2. S.J. Curran et al.: A&A **367**, 457 (2001)
3. M. Hitschfeld, M. Aravena, C. Kramer et al.: A&A, submitted (2007)
4. R. Mauersberger et al.: A&A **309**, 705 (1996)

Atomic Gas Associated with GMCs in the LMC

Annie Hughes[1], T. Wong[2], J. Ott[3], E. Muller[4], J. L. Pineda[5], and Y. Mizuno[6]

[1] Centre for Astrophysics and Supercomputing, Swinburne University of Technology, Hawthorn VIC 3122, Australia ahughes@astro.swin.edu.au
[2] Department of Astronomy, University of Illinois at Urbana-Champaign, 1002 W. Green Street, Urbana IL 61801, USA
[3] NRAO, 520 Edgemont Road, Charlottesville VA 22903-2475, USA
[4] Australia Telescope National Facility, PO Box 176, Epping NSW 1710, Australia
[5] Argelander Institut für Astronomie, Auf dem Hügel 71, D-53121 Bonn, Germany
[6] Department of Physics and Astrophysics, Nagoya University, Chikusa-Ku Nagoya 464-8602, Japan

1 Introduction

We are using the ATCA+Parkes H I survey of the Large Magellanic Cloud (LMC) [1] and our ongoing Mopra survey of the ^{12}CO J=(1-0) emission in the LMC to study the properties of the atomic gas associated with a large sample of giant molecular clouds (GMCs). The overall aim of the project is to search for observational signatures of molecular cloud formation in the interstellar gas. A statistical analysis of this kind is not feasible in the Milky Way due to the large angular size of nearby GMCs and confusion along Galactic sightlines.

2 Results

In Figure 1, we plot the mass of atomic gas within the CO-emitting region of each GMC as a function of molecular mass. The molecular mass is determined using a CO-to-H_2 conversion ratio of 5×10^{20} cm^{-2} (K km s^{-1})$^{-1}$. The mass fraction of atomic gas within GMCs is $\sim$10% across the range of GMC masses in our sample. This fraction does not vary with GMC mass or star formation activity, where we have used the average 24μm flux within the 1 K km s^{-1} contour of each GMC as an indicator of star formation [2].

We also measured the mass of the atomic gas surrounding each of the GMCs in our sample. Here we use the FWHM of the H I line profile at the centre of each GMC to define the extent of the H I envelope along the velocity axis. We find that the mass of atomic gas surrounding each GMC is comparable to the molecular mass when the radius of the H I envelope is $\sim$1.6 times the GMC radius (Figure 2). The GMC-to-envelope size ratio does not vary

B.S. Koribalski, H. Jerjen (eds.), *Galaxies in the Local Volume*,
doi: 10.1007/978-1-4020-6933-8_71,

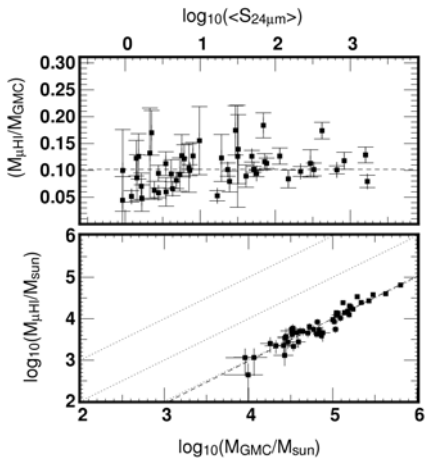

Fig. 1. *(Top:)* The atomic mass fraction plotted as a function of the average 24 μm flux within each GMC. *(Bottom:)* GMC mass vs mass of atomic gas within the CO-emitting volume. The dotted lines indicate atomic masses of 0.1, 1.0 and 10.0 times the GMC mass. The dashed line is a simple least-squares fit to the data.

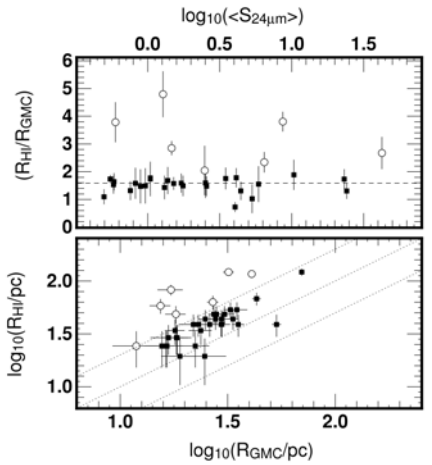

Fig. 2. *(Top:)* The GMC-to-envelope size ratio as a function of the average 24 μm flux within each GMC. *(Bottom:)* GMC radius vs the envelope radius where the contained atomic mass is equivalent to the GMC mass. The dotted lines indicate GMC-to-envelope size ratios of 0.5, 1.0 and 2.0. In both panels, the open circles indicate GMCs where the GMC-to-envelope size ratio is greater than 2.

with GMC mass or star formation activity. The seven GMCs with GMC-to-envelope size ratios greater than 2 are all spatially coincident with the LMC's stellar bar. A possible explanation is that higher interstellar pressures in the bar region favour the conversion of atomic gas to molecular gas.

References

1. S. Kim, L. Staveley-Smith, M.A. Dopita, R.J. Sault, K.C. Freeman, Y. Lee and Y.-H. Chu: ApJS **148**, 473 (2003)
2. M. Meixner and the SAGE Survey team: AJ **132**, 2268 (2006)

Molecular Clouds and Star Formation in the Magellanic System by NANTEN

Akiko Kawamura[1], Y. Mizuno[1], T. Minamidani[2], N. Mizuno[1], T. Onishi[1], A. Mizuno[3], and Y. Fukui[1]

[1] Department of Astrophysics, Nagoya University, Nagoya 464-8602, Japan
kawamura@a.phys.nagoya-u.ac.jp
[2] Department of Cosmosciences, Hokkaido University, Chikusa-ku, Nagoya 464-8602, Japan
[3] Solar-terrestrial Environment Lab., Nagoya University, Nagoya 464-8601, Japan

1 Introduction

The Magellanic system is an ideal laboratory to study star formation and cloud evolution because of its proximity to the Sun. Studies of the distribution and the properties of the young massive stars and clusters have been carried out by optical, infrared and radio continuum observations for decades. More than 300 H II regions are identified (e.g., Davies et al. 1976). Stellar clusters called "populous clusters" with masses $\sim 10^4 - 10^5$ $M_\odot$, were found by photometric studies (e.g., Hodge 1961). There are populous clusters significantly younger, i.e., a few Myr to 10 Gyr, than the Galactic globular clusters and some populous clusters are still being formed at present (e.g., Brandl et al. 1996). Recent infrared satellites like Spitzer (e.g., Meixner et al. 2006, Meixner et al. in these proceedings) and AKARI (e.g., Doi et al. 2007) have started to reveal the distribution and properties of the young stars with intermediate mass. In this paper, we focus on the result from comparisons of the molecular clouds with H II regions and young clusters in the LMC.

2 Molecular Clouds and Star Formation in the Large Magellanic Cloud (LMC)

The LMC offers the best site because of its unrivaled closeness and of the nearly face-on view to us. We carried out CO(1–0) observations toward the LMC with NANTEN, a 4 m telescope of Nagoya University at Las Campanas Observatory, Chile, from 1998 April to 2003 August. The resolution is ∼40 pc at the distance of the LMC. The 3 σ noise level of the velocity-integrated intensity is ∼1.2 K km s^{-1}. This corresponds to $N(H_2) \sim 8 \times 10^{20}$ cm^{-2}, by assuming a conversion factor from CO intensity to the hydrogen column

B.S. Koribalski, H. Jerjen (eds.), *Galaxies in the Local Volume*,
doi: 10.1007/978-1-4020-6933-8_72,

density, $X = 7 \times 10^{20}$ cm^{-2} (K km s^{-1})$^{-1}$. We identified 272 molecular clouds by using the *fitstoprops* method (Rosolowsky & Leroy 2006), 230 out of which are detected at more than 2 observed positions (for the details, see Fukui et al. 2007).

We made comparisons of the 230 Giant Molecular Clouds (GMCs) with H II regions (e.g., Davies et al. 1976, Filipovic et al. 1998) and young clusters (e.g., Bica et al. 1996). Bica et al. (1996) studied the colors of the clusters and classified them into an age sequence from SWB 0 to SWB VII. The datasets of H II regions have a detection limit in Hα flux of $\sim 10^{-12}$ ergs cm^{-2} s^{-1} (Kennicutt & Hodge 1986). In order to examine any optically obscured H II regions we have also used the Parkes/ATNF radio continuum survey (e.g., Dickel et al. 2005, Filipovic et al. 2007). The typical sensitivity of the new datasets is good enough to reach the flux limit equivalent to that of Hα. We note that the detection limit of H II regions is quite high, corresponding to one-fourth the luminosity of the Orion Nebula.

A study of the distance of H II regions and clusters measured from the nearest GMCs shows that a large number of the young clusters ($\tau < 10$ Myr) and H II regions are found within 100 pc of the GMCs. On the other hand, older clusters show almost no correlation with the GMCs. We have examined the association between the individual GMCs and the H II regions and young clusters and found that about a half of the H II regions and young clusters are associated with the GMCs. The GMCs are classified into three types; *Type I.* starless GMCs (no early O stars), *Type II.* GMCs with H II regions only, and *Type III.* GMCs with H II regions and stellar clusters. It is found that ∼24% of the GMCs are starless (*Type I*), while 52% (*Type II*) and 24% (*Type III*) are associated with H II regions and young clusters, respectively. It is shown that the number ratio of massive GMCs is higher in Type III than those in the other two, and the mass of Type I GMCs tends to be smaller than the rest. This may suggest that Type I, and possibly Type II GMCs, are still growing in mass via mass accretion from their surrounding lower density atomic gas.

The completeness of the present GMC sample covering the whole LMC enables us to infer the evolutionary timescales of the GMCs. We assume a steady state evolution and therefore the time spent in each phase is proportional to the number of the GMCs at each class. The absolute time scale is based on the age of young clusters, which is taken to be 10 Myr. The total lifetime of a GMC is then estimated to be ∼30 Myr.

References

1. M. Doi et al.: PASJ, submitted (2007)
2. Y. Fukui et al.: ApJS, submitted (2007)
3. M. Meixner et al.: AJ, **132**, 2268 (2006)

Wide-Field Imaging Survey of Leo II Dwarf Spheroidal Galaxy: Stellar Content and Distribution

Yutaka Komiyama

National Astronomical Observatory of Japan, komiyama@subaru.naoj.org

We carried out a wide-field V & I-band imaging survey of the Local Group dwarf spheroidal galaxy Leo II using Subaru Prime Focus Camera (Suprime-Cam) on the 8.2m Subaru Telescope. We find that (1) the radial number density profiles of bright and faint RGB stars are extended beyond the tidal radius. This is well explained by the existence of an extra-tidal substructure which is as large as globular clusters in luminosity. (2) The HB morphology index shows a radial gradient in the sense that red HB stars are more concentrated than blue HB stars; (3) there are a mixture of stellar populations at the center and a more homogeneous population in the outskirt, and (4) there is a considerable contribution of stellar populations younger than 8 Gyr at the center.

1 Observation

The observations were carried out using Suprime-Cam [1] which covers an area of $34' \times 27'$ with $0\farcs2$ per pixel sampling. The conditions were good and the seeing was fair ($\sim 0\farcs8$) during the observations. The integration times in the V and I bands were 3900 sec and 2700 sec, respectively, and the 50% complete magnitudes were $V = 25.9$ and $I = 24.7$, respectively. In total, 82252 stars are detected in the $26\farcm67 \times 26\farcm67$ area centered on Leo II. Details of the data analysis are found in [2].

2 Results

Based on the color-magnitude diagram (Fig. 1, left), the number density profiles of each stellar component are investigated (Fig. 1, right). The profiles for RGB stars are well fitted by a King profile ($r_t \sim 8-9$ arcmin), but changes of the slopes occur near the tidal radius, suggesting the existence of extra-tidal substructure around Leo II. A Smoothed surface brightness map reveals a diffuse ($\sim 31\,\mathrm{mag\,arcsec^{-2}}$) but 99.92% significant knotty substructure outside

B.S. Koribalski, H. Jerjen (eds.), *Galaxies in the Local Volume*,
doi: 10.1007/978-1-4020-6933-8_73,

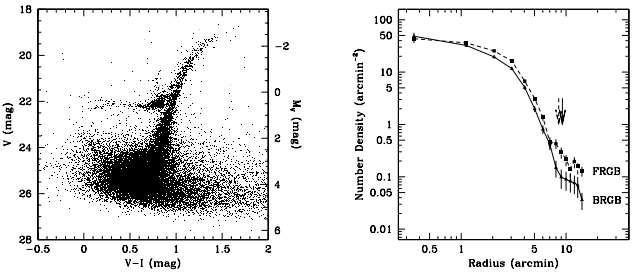

Fig. 1. *(Left:)* Color-magnitude diagram of stars in the central $6'.67 \times 6'.67$ field. *(Right:)* The number density profiles for bright ($V < 22.18$) and faint ($22.18 < V < 23.5$) RGB stars.

the tidal radius. The field-subtracted HESS diagram for the knot shows concentrations of stars at red clump and the MSTO, suggesting an old and metal poor population similar to that dominating in the main body of Leo II. The origin of the knot is possibly a disrupted globular cluster of Leo II that has survived until the recent past, but it is unlikely that the knot is comprised of stars which were stripped from Leo II by tidal force.

The HB morphology shows a radial gradient in the sense that red HB stars are more concentrated than blue HB stars. Such a trend is also observed in several Local Group dSphr [3]. The color distribution around the mean RGB sequence shows a broader distribution at the center ($r < 3'$) than in the outskirts, suggesting a variety of stellar populations for the center and a more homogeneous population for the outskirts.

The age distribution is investigated using sub-giant branch (SGB) stars whose magnitudes are sensitive indicators of age [4]. Comparing the observed number ratios of SGB stars to faint RGB stars (N_{SGB}/N_{FRGB}) with the calculated ratio N_{SGB}/N_{FRGB} for a simple stellar population, the significance of the input simple stellar population can be estimated [2]. From the analysis of bright SGB stars ($23.5 < V < 24.0$, corresponding to a $\sim 2.5 - 4$ Gyr population), it is found that a population younger than 4 Gyr is not a dominant population, although it certainly resides in the center. An intermediate-age population ($\sim 4 - 8$ Gyr), which is represented by intermediate SGB stars ($24.0 < V < 24.5$), is found to be significant at the galaxy center, while most of the stars in the outskirts are found to be older than 8 Gyr.

References

1. S. Miyazaki, et al.: Publ. Astron. Soc. Japan. **54**, 833 (2002)
2. Y. Komiyama, et al.: AJ **134**, 835 (2007)
3. D. Harbeck, et al.: AJ **122**, 3092 (2001)
4. K. J. Mighell & R. M. Rich: AJ **111**, 777 (1996)

Interactions and Star Formation Activity in Wolf-Rayet Galaxies

Ángel R. López-Sánchez[1] and César Esteban[2]

[1] Australia Telescope National Facility, CSIRO, Australia
[2] Instituto de Astrofísica de Canarias, Spain, cel@iac.es

We present some global results of the PhD Thesis carried out by López-Sánchez (2006), in which a detailed morphological, photometrical and spectroscopical analysis of a sample of 20 Wolf-Rayet (WR) galaxies was realized. The main aims are the study of the star formation and O and WR stellar populations in these galaxies and the role that interactions between low surface companion objects have in the triggering of the bursts. We analyze the morphology, stellar populations, physical conditions, chemical abundances and kinematics of the ionized gas, and star-formation activity of each system.

1 Introduction

WR galaxies are a subtype of H II galaxies whose integrated spectra show broad emission lines attributed to WR stars, indicating the presence of an important population of massive stars and the youth of the burst. Studying a sample of WR galaxies, [3] and [4] suggested that interactions with or between dwarf objects could be the main star formation triggering mechanism in dwarf galaxies and noted that the nature of WR galaxies can only be detected when deep and high-resolution images and spectra are available. Subsequent works also found a relation between massive star formation and the presence of interaction signatures. Thus, we have performed a detailed analysis of a sample of 20 WR galaxies combining deep optical and near-infrared (NIR) broad band and Hα imaging together with optical spectroscopy (long slit and echelle) data. Additional X-ray, far-infrared and radio data were compiled from literature.

2 Global properties

The global analysis of our sample of 20 Wolf-Rayet galaxies is the most complete and exhaustive data set of this kind of galaxies, involving multiwavelength results and every system being analyzed following the same procedures (see [3] and references within). Our main global results are:

B.S. Koribalski, H. Jerjen (eds.), *Galaxies in the Local Volume*,
doi: 10.1007/978-1-4020-6933-8_74,

1. The analysis of WR features in our sample suggests that aperture effects and localization of the bursts with WR stars seem to play a fundamental role in the detection of this sort of massive stars in starburst galaxies.
2. Photometric data have been corrected for both extinction and nebular emission using our spectroscopic values. A good agreement between our optical and NIR colors and theoretical models is found; small discrepancies are explained by the existence of several stellar populations.
3. Physical and chemical properties are in agreement with both previous observations and models of chemical evolution of galaxies. We have compared abundances obtained by the direct method with those obtained for several empirical calibrations: [6, 7] seem to give similar results whereas calibrations based in photoionization models such as [2] and [1] give abundances higher (∼0.20 dex) than expected.
4. The comparison of the SFR derived from our Hα data (corrected by *both* extinction and [N II] emission using our spectroscopic data) is in good agreement with the SFR obtained using multiwavelength relations. We have also derived an X-ray based SFR for this kind of starburst galaxies.
5. We determined the ionized gas mass ($M_{\rm HII}$), the neutral gas mass ($M_{\rm HI}$), the mass of the ionizing stellar cluster ($M_\star$), the warm dust mass (M_{dust}), and the dynamical mass (M_{dyn}) both from the rotation curves of the ionised gas and the H I gas. As expected, all mass values increase with the luminosity of the galaxy. Furthermore, we find a good correlation between $M_{\rm dyn}$ and the luminosity of the galaxy, as well as a clear relation between the reddening coefficient derived from the Balmer decrement, $C(\rm H\beta)$, and $M_{\rm dust}$. This fact suggests that extinction is mainly produced within the starburst.
6. However, our main conclusion is that **the majority of studied galaxies** (16 up to 20, ∼80% of the objects) **show clear interaction features** such as plumes, tails, tidal dwarf galaxies (TDGs), regions with very different chemical abundances inside galaxies, perturbed kinematics of the ionized gas or lack of neutral hydrogen gas, **confirming the hypothesis that interaction with or between dwarf objects triggers the star formation activity in Wolf-Rayet galaxies**.

References

1. Kewley, L.J. & Dopita, M.A. 2002, ApJS, **142**, 35
2. McGaugh, S.S. 1994, ApJ, **426**, 135
3. Méndez, D.I. 1999, *Gas ionizado y formación estelar en galaxias Wolf-Rayet*, PhD Thesis, La Laguna University, Tenerife, Spain
4. Méndez, D.I. & Esteban, C., 2000, A&A, **359**, 493
5. López-Sánchez, Á.R. 2006, *Massive star formation in dwarf Wolf-Rayet galaxies*. PhD Thesis, La Laguna University, Tenerife, Spain
6. Pilyugin, L.S. 2001a, A&A, **369**, 594
7. Pilyugin, L.S. 2001b, A&A, **374**, 412

Interactions and Starburst Activity in Galaxy Groups: The Case of Tol 9 in Klemola 13 Group

Ángel López-Sánchez[1], B. S. Koribalski[1], C. Esteban[2], and J. Hibbard[3]

[1] Australia Telescope National Facility, CSIRO, Australia
[2] Instituto de Astrofísica de Canarias, Spain
[3] NRAO, Charlottesville, VA, USA

We are performing a multiwavelength analysis of galaxy groups hosting starburst galaxies in order to understand their general properties, environment, star formation history and the importance of the interactions and mergers between galaxies in their evolution. Some important results concerning the galaxy groups HCG 31 [1] and Mkn 1087 [2] have already been published. Here we present our new ATCA H I map of the starburst galaxy Tol 9 within the Klemola 13 group.

1 The starburst Tol 9 within the Klemola 13 group

The Klemola 13 group (HIPASS J1034–28), located at 43.3 Mpc, contains at least 7 galaxies with different morphological types including an intense starburst galaxy, Tol 9 (ESO 436-42). This galaxy seems to host an important population of Wolf-Rayet stars indicating both the youth and the strength of the starburst [3]. Several independent objects are found in the neighbourhood of Tol 9, in particular the nearby spiral galaxy ESO 436-46 (at 20.2 kpc).

The analysis of the optical, NIR and Hα images and the optical spectroscopy of Tol 9 is presented in [3]. An old stellar population bridge from Tol 9 towards a dwarf companion located 5.9 kpc (28") at SW indicates probable interaction phenomena. The continuum-subtracted Hα emission map and the kinematics of the ionized gas suggest that an outflow of material or a galactic wind exists in Tol 9. The estimated oxygen abundance in Tol 9 is 12+log(O/H) = 8.57 and the nitrogen to oxygen ratio is log(N/O) = –0.81.

The HIPASS spectrum reveals a considerable amount of atomic gas. ATCA H I observations show (see Fig. 1) that the neutral gas is mainly found in two regions: one located around the spiral galaxy ESO 436-46 and the other embedding Tol 9 and two nearby objects (W cloud). We also detect H I emission in the far object ESO 437-04 (not shown). Although we should expect that the neutral gas is mostly associated with ESO 436-46, the maximum H I column density is actually found in Tol 9. Our H I map also reveals a long H I

B.S. Koribalski, H. Jerjen (eds.), *Galaxies in the Local Volume*,
doi: 10.1007/978-1-4020-6933-8_75,

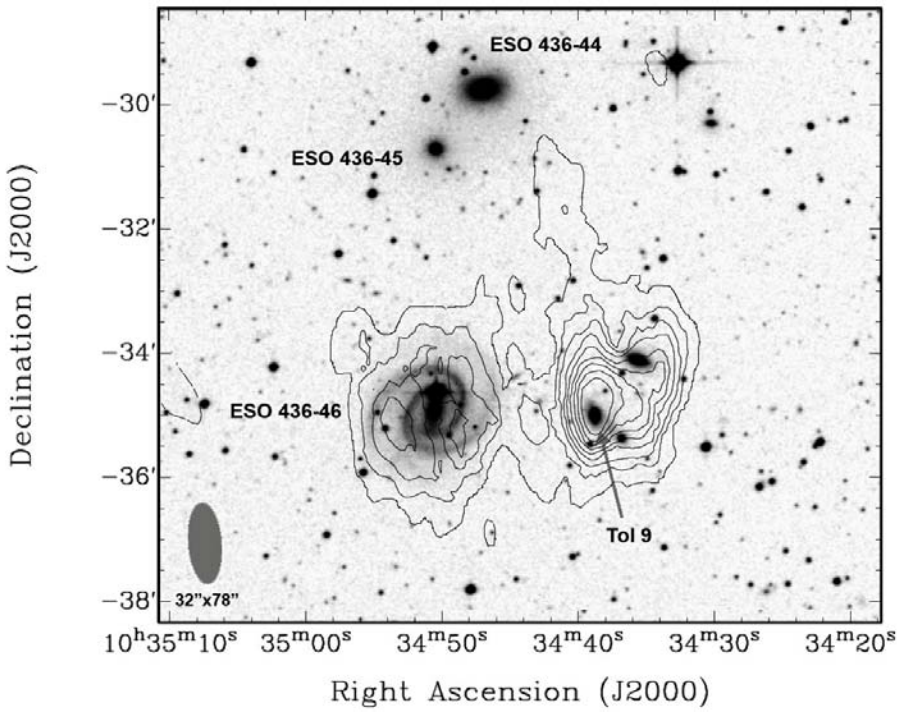

Fig. 1. Contours of the H I distribution in the Klemola 13 group overlaid onto a DSS *R*-band image. The most important objects are labeled.

structure at the north of the W cloud in direction to ESO 436-44 and ESO 436-45. These two galaxies, composed by an old stellar population, do not show H I emission.

The H I kinematics are very intriguing. The H I cloud around ESO 436-46 reveals the rotation pattern expected for a spiral galaxy. But this characteristic is also found in the H I cloud embedding Tol 9 and its surrounding dwarf galaxies. From the H I velocity field alone it seems that they constitute one single object. The kinematics of the long tail at the north of the W cloud suggest that it is of tidal origin formed from material from this cloud.

References

1. López-Sánchez, Á.R., Esteban, C. & Rodríguez, M. 2004a, ApJS, **153**, 243
2. López-Sánchez, Á.R., Esteban, C. & Rodríguez, M. 2004b, A&A, **428**, 445
3. López-Sánchez, Á.R. 2006, *Massive star formation in dwarf Wolf-Rayet galaxies*. PhD Thesis, La Laguna University, Tenerife, Spain, *see astro-ph/0704.2846 for a 16 pages English summary with figures.*

The Complex H I Structure of IC 10

Eva Manthey and Tom Oosterloo

ASTRON, 7990AA Dwingeloo, Netherlands manthey@astron.nl

1 Cold Accretion

One of the major questions in galaxy research is still unanswered: How do (spiral) galaxies acquire their gas? Two possible accretion modes are discussed:

- *Hot phase:* Gas which is falling into a dark potential well is shock-heated to the halo virial temperature of $\sim 10^6$ K [3, 4]. In the dense, inner region the gas radiates its thermal energy and settles into a rotation disk.
- *Cold phase:* Recent high resolution hydrodynamical simulations, e.g., [6, 5] show, that gas can be accreted without being shock-heated, thus at lower temperatures of 10^5 K or even less. This 'cold accretion mode' occurs mainly along the filamentary structure of the cosmic web.

Cold accretion may dominate in small DM halos, hot accretion in high mass halos. Hence, cold accretion may dominate at high redshift, where most potential wells are still small.

So far, only a few observations of possible local cold accretion are known: the extended halo of NGC 891 [8], H I complexes in nearby galaxies (e.g., [7]), and maybe some Galactic compact HVCs. But other origins are possible in these cases, e.g. H I blown out by star formation driven outflows (galactic fountains) or merging of a small companion.

2 IC 10 – The Nearest Starburst Galaxy

IC 10 is a nearby dwarf irregular galaxy (distance = 820 kpc) undergoing a phase of enhanced star formation. Based on the large number of Wolf-Rayet stars and a deficiency of red supergiants, the starburst must have occured a few 10^6 yr ago [1]. Previous H I studies found a small central rotation disk embedded in a very extended filamentary distribution with chaotic kinematics [2]. Since the extended H I filaments do not have any optical counterparts, it was suggested that IC 10 might be interacting with an intergalactic (primordial) gas cloud, fuelling the starburst [2].

B.S. Koribalski, H. Jerjen (eds.), *Galaxies in the Local Volume*,
doi: 10.1007/978-1-4020-6933-8_76,

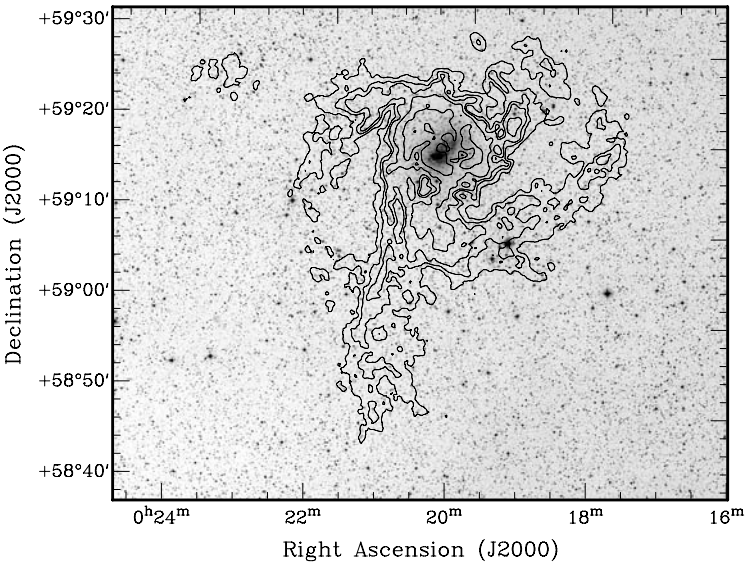

Fig. 1. H I contours overlaid onto an optical image (DSS). We observed a mosaic of 7×12 h of IC 10, using the Westerbork Radio Synthesis Telescope (WSRT). After Hanning smoothing, we gained a velocity resolution of 2 km/s, reaching an rms of 0.8 mJy/beam in the robust weighted maps.

Figure 1 shows our total intensity map of the H I distribution. We identified at least four gaseous 'tails' with a complex kinematic structure even in the outer regions. If the chaotic structure appeared due to interaction/merging with a companion galaxy, a rather regular velocity structure would be expected in the outer parts. Therefore, the observations seem to favour the scenario of cold accretion of H I, however the analysis is still ongoing.

References

1. P. Massey et al: AJ **133**, 2393 (2007)
2. E.M. Wilcots, B.W. Miller: AJ **116**, 2363 (1998)
3. S.D.M. White, M.J. Rees: MNRAS **183**, 341 (1978)
4. S.M. Fall, G. Efstathiou: MNRAS **193**, 189 (1980)
5. T. Kaufmann et al.: MNRAS **370**, 1612 (2006)
6. D. Keres et al.: MNRAS **363**, 2 (2005)
7. F. Fraternali et al.: AJ **123**, 3124 (2002)
8. T. Oosterloo et al.: AJ **134**, 1019 (2007)

Constrained Simulations of the Local Universe

Luis A. Martinez-Vaquero[1], Gustavo Yepes[1], Yaniv Dover[2], Yehuda Hoffman[2], Anatoly Klypin[3], and Stefan Gottlöber[4]

[1] Universidad Autónoma de Madrid, Spain
l.martinez@uam.es, gustavo.yepes@uam.es
[2] Racah Institute of Physics, Israel
yanivd@phys.huji.ac.il, hoffman@huji.ac.il
[3] New Mexico State University, USA aklypin@nmsu.edu
[4] Astrophysikalisches Institut Potsdam, Germany sgottloeber@aip.de

1 Simulating the Local Universe

This project is part of an international collaboration between different institutions around the world with the aim of generating the most accurate simulations of the formation of the Local Universe from cosmological initial conditions. In these kind of simulations, the smaller Fourier modes of a random realization of the power spectrum of density fluctuations are substituted by observational constrains in order to recover our real environment. These observational data come from MARK III [1], SBF [2], nearby X-ray clusters of galaxies [3] and the Karachentsev catalogues [4].

Different N-body simulations, with different resolutions, box sizes, codes and goals, have been performed up to now. Our higest resolution run consists of a resimulated region of 2 h^{-1} Mpc radius around the Local Group candidate found in a computational box of $L_{box} = 64\ h^{-1}$ Mpc for the ΛCDM model with WMAP3 parameters. Initial conditions were generated with 4096^3 particles. The particle mass in the high resolution area correspond to $M_p = 2.54 \times 10^5 h^{-1}\ \mathrm{M}_\odot$. It lets us make an unprecedented detailed analysis of the dynamics and substructures of the Local Group members.

2 The numerical Local Group

Our Local Group candidate is formed by three members: M 31 ($M_{vir} = 5.69 \times 10^{11}\ h^{-1} M_\odot$ and $R_{vir} = 173.5\ h^{-1}$ kpc), Milky Way ($M_{vir} = 4.63 \times 10^{11}\ h^{-1}$ $\mathrm{M}_\odot$ and $R_{vir} = 162.0\ h^{-1}$ kpc) and M 33 ($M_{vir} = 2.24 \times 10^{11}\ h^{-1}\ \mathrm{M}_\odot$ and $R_{vir} = 127.2\ h^{-1}$ kpc). Some properties of the members of the Local Group were studied and compared with the higher resolution *"Via Lactea"* simulation [5], where the particle mass is $5.64 \times 10^5\ h^{-1}\ \mathrm{M}_\odot$. In Figure 1, the

B.S. Koribalski, H. Jerjen (eds.), *Galaxies in the Local Volume*,
doi: 10.1007/978-1-4020-6933-8_77,

subhalo mass functions and the fractions of dark matter mass in substructures are shown for each LG member. Radial density profiles for the members of the Local Group were fitted using different analytical models. The best fits correspond to those models with at least two free parameters ([6] and [7]).

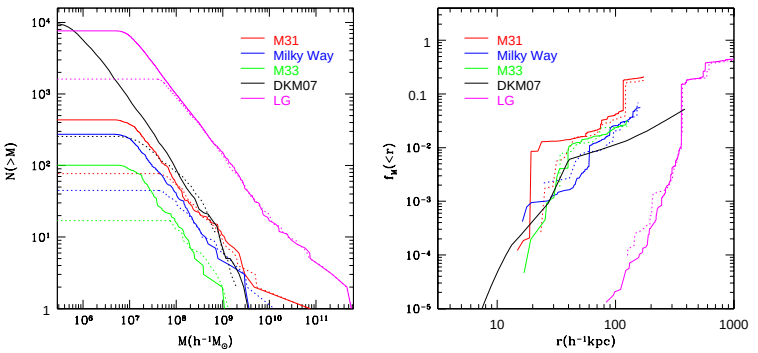

Fig. 1. Subhalo mass function *(left)*, and fraction of mass in substructures as a function of the distance to the halo center *(right)* for the three main halos and the whole LG. Solid lines are for high resolution runs and dashed for lower resolution (2048^3 effective particles).

3 Mass and Motion in the Local Volume

From a set of lower resolution constrained, and unconstrained simulations (256^3 particles), we have also studied the dynamics of the Local Volume as a function of environment and cosmology [8]. We have checked the hypothesis of modeling the gravitational field inside the observed Local Volume by computing the pairwise Newtonian forces between galaxies [9]. According to our simulation results it does not seem to be a valid approximation. This is mainly due to two main effects: the non-negligible contribution of matter in substructures and in the diffuse filaments linking the main halos, and the tidal field caused by the external mass distribution.

References

1. J. A. Willick et al.: ApJ, 109, 333 (1997)
2. J. L. Tonry et al.: ApJ, 546, 681 (2001)
3. T. H. Reiprich, H. Böhringer: ApJ, 567, 716 (2002)
4. I. D. Karachentsev: AJ, 129, 178 (2005)
5. J. Diemand, M. Kuhlen, P. Madau: ApJ, 657, 262 (2007)
6. J. F. Navarro et al.: MNRAS, 349, 1039 (2004)
7. Y. P. Jing, Y. Suto: ApJ, 529, L69 (2000)
8. L.A. Martinez-Vaquero, G. Yepes, Y. Hoffman: MNRAS, 378, 1601, (2007)
9. A. B. Whiting: ApJ, 622, 217 (2005)

The Outer Stellar Populations in the LMC

Ingrid Meschin[1], C. Gallart[1], A. Aparicio[1,2], R. Carrera[1,3], M. Monelli[1], and P. B. Stetson[4]

[1] Instituto de Astrofísica de Canarias, Tenerife, Spain imeschin@iac.es
[2] Departamento de Astrofísica, Universidad de La Laguna, Tenerife, Spain
[3] Centro de Investigaciones de Astronomía, Mérida, Venezuela
[4] Dominion Astrophysical Observatory, Herzberg Institute of Astrophysics, National Research Council, Victoria, Canada

In the context of a major project aimed at obtaining detailed star formation histories across the Large Magellanic Cloud (LMC) disk, we present here the first results for the outermost fields in the northern direction.

1 The Project

We are undertaking a major project aimed at obtaining detailed star formation histories across the LMC disk, in order to characterize its stellar population gradients and to delimit the total extent of its stellar population. To this end, we have imaged 12 fields, 6 approximately toward the North of the bar at $3°, 5°, 6°, 8°, 9°$ and $10°$ from the LMC center, and 6 fields in the East-West directions at $5°, 7°, 9°$ on both sides of the bar. This will allow us to find its actual outer edge and to fully characterize the differences in the SFH at each side of the bar.

B-, V- and I-images were taken in 3 campaigns using the Mosaic II CCD Imager on the CTIO Blanco 4m telescope and the WFI camera at the 2.2 m ESO/MPI telescope at La Silla Observatory. These wide field imagers provide a total field of $36' \times 36'$ and $34' \times 33'$, respectively. Several Landolt standards were also observed in photometric nights for calibration purposes. The mosaic frames were pre-reduced in a standard way, using the MSCRED package within IRAF. Photometry of North LMC fields was obtained using the DAOPHOT/ ALLFRAME suite of programs [3, 4].

2 First Results: The LMC Outer Populations

In Fig. 1 we show the $[(V - I), I]$ CMDs of the 3 North-fields located at $8°, 9°$ and $10°$ from the LMC center. The CMD of the field at $8°$ distance is deeper (it reaches 2 magnitudes below the old MS turnoff) than the other two (1.2/1.5) mag for the fields at $9°$ / $10°$). This is due to the different diameters

B.S. Koribalski, H. Jerjen (eds.), *Galaxies in the Local Volume*,
doi: 10.1007/978-1-4020-6933-8_78,

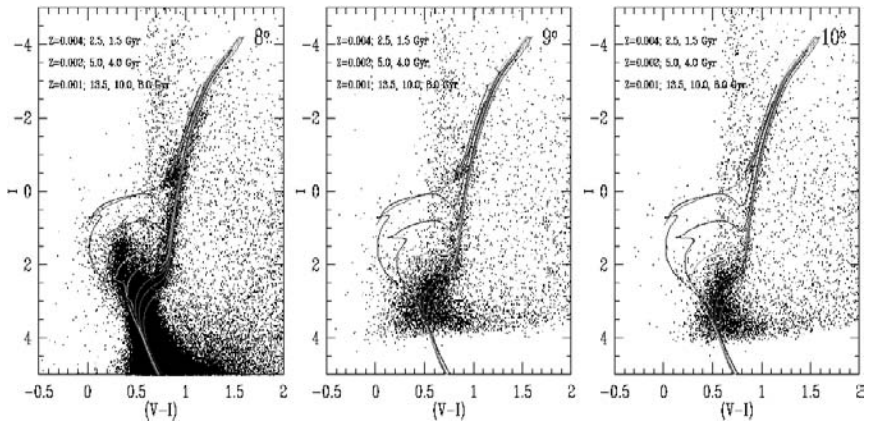

Fig. 1. Observed $[(V-I), I]$ CMDs in order of increasing distance from the LMC center (8°, 9° and 10°, from left to right). BaSTI isochrones have been superposed.

of the telescopes used and to the different integration times, which are both greater for the field at 8° offset. BaSTI isochrones [2] have been superposed.

Each of these CMDs show, for the first time, the details of the age structure of the stellar population in these outer parts of the LMC. The field at 8° offset was studied and presented in [1]. They showed the presence of a substantial intermediate-age stellar population in this field, with a relatively strong gradient in the number of 2.5–4 Gyr old stars. The surface brightness profile of the LMC remains exponential and shows no evidence of disk truncation out to this radius. CMDs of the fields at 9° and 10° offset disclose the same behavior, i.e. the presence of an intermediate-age population with a relatively strong gradient in the density of stars with age in the ≈4–5 Gyr range. A group of stars brighter and bluer than the main population is well matched by a 1.5 Gyr isochrone. Its number shows a genuine gradient, decreasing outwards, which would indicate that a small burst of star formation 1.5 Gyr ago (or merged event) was more intense in the inner regions of the LMC. The fainter stars in the subgiant branch are well matched by the 13.5 Gyr ($Z = 0.001$) isochrone, but no blue extended horizontal branch can be seen in the CMDs.

References

1. C. Gallart, P. B. Stetson, E. Hardy, F. Pont & R. Zinn: ApJ **614**, L109 (2004)
2. A. Pietrinferni, S. Cassisi, M. Salaris & F. Castelli: ApJ **612**, 168 (2004)
3. P. B. Stetson: PASP **99**, 191 (1987)
4. P. B. Stetson: PASP **106**, 250 (1994)

Characterising Magellanic Stream Turbulent H I

Deanna Matthews[1,2], Lister Staveley-Smith[3], Peter Dyson[1], Naomi McClure-Griffiths[2], and Erik Muller[2]

[1] School of Physics, La Trobe University, Bundoora, VIC 3086, Australia
d.matthews@latrobe.edu.au
[2] Australia Telescope National Facility, CSIRO, PO Box 76, Epping, NSW 1710
[3] School of Physics, University of Western Australia, Crawley, WA 6009, Australia

1 Introduction

The injection and transport of energy in the interstellar medium (ISM) directly affects structure and motions. In both netural and ionised gas, a hierarchy of structure is present down to very small scales [1, 2]. Two-dimensional spatial power spectrum (SPS) analyses can be used to investigate the hierarchical nature of turbulent ISM gas by showing the power distributed as a function of spatial scale. Furthermore, important three-dimensional statistical properties can be inferred from the two-dimensional spatial power spectra [4]. We present some results of a statistical analysis applied to a higher resolution ($\sim$7 arcmin) ATCA and Parkes[4] H I data set of the Magellanic Stream, which shows a damped range of velocity fluctuations with a steep velocity index. This analysis suggests the presence of some process which acts on the Stream ISM to restrict the normal range of velocity fluctuations.

2 Observations

The compact H75 configuration of the Australia Telescope Compact Array was used to construct a mosaic of the Magellanic Stream from about -73° -0° declination in July–August 2005 and September 2006. A bandwidth of 4 MHz with 1024 channels per baseline was used, producing a Hanning smoothed velocity resolution of 1.65 $\mathrm{km\,s^{-1}}$. The rms sensitivity is 0.1 K and the angular resolution is $7\farcm4 \times 6\farcm2$. Stray-radiation corrected Galactic All Sky Survey (GASS) data [5] were regridded to the same spatial and velocity dimensions at the ATCA data and the two sets combined in the Fourier plane.

[4] The Australia Telescope Compact Array and the Parkes telescope are part of the Australia Telescope, which is funded by the Commonwealth of Australia for the operation as a National Facility managed by CSIRO.

B.S. Koribalski, H. Jerjen (eds.), *Galaxies in the Local Volume*,
doi: 10.1007/978-1-4020-6933-8_79,

3 Results and Discussion

A summary of the SPS analysis technique used on the Magellanic Stream can be found in [7]. Two dimensional spatial power indices (γ, $P(k) \propto k^{\gamma}$) were calculated for each channel and also over a range of integrated velocity widths, permitting the calculation of the 2-D power index for "thick" and "thin" regime [7]. These indices were then used to determine the three-dimensional velocity power index (Fig. 1). Many of the 31 fields show 3-D velocity indices of $-4 > \gamma > -5$, but there is no evidence of a pattern with length along the Stream. The indices are quite steep compared with previous SMC, LMC and Magellanic Bridge investigations [7, 3, 6] and significantly steeper than the case for a Kolmogorov turbulent flow. The steepness of the power spectra indicate the absence of structure on smaller scales and that the turbulence in the Stream is density dominated. A lack of high velocity gas and little mixing is also implied. This may be an indicator of the Galactic Halo confining the clouds and damping out any of the normal fast turbulent velocity motions.

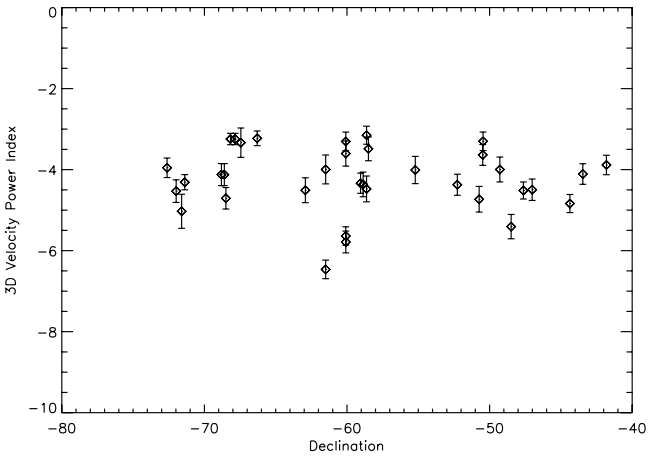

Fig. 1. Three-dimensional Velocity Power Index vs Declination (in degrees) as calculated for 128^2 and 256^2 pixel fields between declinations $-73°$ and $-40°$. The Stream runs approximately parallel to lines of constant RA.

References

1. S. Crovisier, J. Dickey: A&A **122**, 282 (1983)
2. J. Dickey et al.: ApJ **561**, 264 (2001)
3. B. Elmegreen et al.: ApJ **548**, 749 (2001)
4. A. Lazarian and Pogosyan: ApJ **537**, 730 (2000)
5. N. McClure-Griffiths et al.: in preparation (2007)
6. E. Muller et al.: ApJ **616**, 845 (2004)
7. S.Stanimirovic and A. Lazarian: ApJ **551**, L53 (2001)

An Observational Study of the GMCs in the Magellanic Clouds in Millimeter and Submillimeter Wavelengths

T. Minamidani[1], N. Mizuno[2], Y. Mizuno[2], A. Kawamura[2], T. Onishi[2], T. Hasegawa[3], K. Tatematsu[3], M. Ikeda[4], Y. Moriguchi[2], N. Yamaguchi[3], J. Ott[5], T. Wong[6], E. Muller[7], J. L. Pineda[8], A. Hughes[9], L. Staveley-Smith[10], U. Klein[8] A. Mizuno[11], S. Nikolić[12], R. S. Booth[13], A. Heikkilä[14], L.-Å. Nyman[15], M. Lerner[15], G. Garay[12], S. Kim[16], M. Rubio[12], and Y. Fukui[2]

[1] Department of Physics, Faculty of Science, Hokkaido University, Japan
tetsu@astro1.sci.hokudai.ac.jp
[2] Department of Astrophysics, Nagoya University, Japan
[3] National Astronomical Observatory of Japan, Japan
[4] Research Center for the Early Universe and Department of Physics, University of Tokyo, Japan
[5] National Radio Astronomy Observatory, USA
[6] Department of Astronomy, MC 221, University of Illinois, USA
[7] Australia Telescope National Facility, CSIRO, Australia
[8] Radioastronomisches Institut der Universität Bonn, Germany
[9] Center for Supercomputing and Astrophysics, Swinburne University of Technology, Germany
[10] School of Physics, University of Western Australia, Australia
[11] Solar-Terrestrial Environment Laboratory, Nagoya University, Japan
[12] Departament de Astronomia, Universidad de Chile, Chile
[13] Hartebeesthoek Radio Astronomy Observatory, South Africa
[14] Onsala Space Observatory, Sweden
[15] European Southern Observatory
[16] Astronomy & Space Science Department, Sejong University, Korea

1 Giant Molecular Clouds in the Large Magellanic Cloud

It is of a particular interest to observe the dense molecular gas in the Magellanic Clouds, where populous clusters are still being formed. The observations of NANTEN 4m telescope in 2.6 mm ^{12}CO(J=1-0) emission reveal the distribution of GMCs in the whole LMC at 40 pc resolution [1]. These studies revealed that there are 3 types of GMCs in terms of star formation activities; Type I is starless, Type II is with H II regions only, and Type III is associated with both huge H II regions and young star clusters [2]. They suggest that these GMC types correspond to the evolutional stages of GMCs.

B.S. Koribalski, H. Jerjen (eds.), *Galaxies in the Local Volume*,
doi: 10.1007/978-1-4020-6933-8_80,

2 Observations and Results

We performed high resolution millimeter and submillimeter observations towards 6 GMCs (7 regions) in the LMC with ASTE, SEST, and Mopra telescopes [3]. The ^{12}CO($J = 3 - 2$) emissions accentuate the detailed structures, although the overall distribution of these 2 emissions are similar, because of the higher angular resolution and possible due to the more compact distribution of warmer and denser gas in $J = 3 - 2$ than in $J = 1 - 0$. We identified clumps based on ^{12}CO($J = 3 - 2$) integrated intensity. As a result, 32 clumps have been identified. The clump size, line width, and virial mass range 1.1 – 12.4 pc, 4.0 – 12.8 km s^{-1}, and $4.6 \times 10^3 - 2.2 \times 10^5$ M$_\odot$, respectively.

3 Physical Properties of Clumps

To estimate the physical properties of molecular gas, we performed an LVG analysis [4] of CO rotational transitions. Of the 32 clumps, 13 clumps are analized with 3 transitions of ^{12}CO($J = 3{-}2$), ^{12}CO($J = 1{-}0$), and ^{12}CO($J = 1 - 0$). We performed calculations with CO rotational levels J of 0 – 40. The results of our LVG analysis indicate that clumps are distributed from cool to warm in temperature and from less dense to dense in density. These differences of clump properties show good correspondence with the GMC Types based on the star formation activity. Clumps in Type III GMCs are warm ($T_{\rm kin} \sim 30 - 200$ K) and are either dense ($n(\rm H_2) \sim 10^{3.5-5}$ cm^{-3}) or less dense ($n(\rm H_2) \sim 10^3$ cm^{-3}). Clumps in Type II GMCs are either warm ($T_{\rm kin} \sim 30 - 200$ K) or cool ($T_{\rm kin} \sim 10 - 30$ K) and less dense ($n(\rm H_2) \sim 10^3$ cm^{-3}). Clumps in Type I GMCs are cool ($T_{\rm kin} \sim 10 - 30$ K) and less dense ($n(\rm H_2) \sim 10^3$ cm^{-3}).

4 Evolution of GMCs

These defferences of clump density and temperature represent an evolutionary sequence of GMCs in terms of density increase leading to star formation; Type I/II GMCs are at a young phase of star formation where density has not yet reached high enough values to cause active massive star formation, and Type III GMCs represent the later phase where the average density is higher, including both high and low density sub-types.

References

1. Fukui, Y., et al. 2007, ApJ, submitted
2. Fukui, Y. 2006, in IAU Symp. 237, Triggered Star Formation in a Turbulent ISM, eds. B. G. Elmegreen & J. Palous, in press
3. Minamidani, T. et al. 2007, ApJS, submitted
4. Goldreich, P. & Kwan, J. 1974, ApJ, 189, 441

The Results of Sub-mm Observations in the Large Magellanic Cloud with the NANTEN2 Telescope

Yoji Mizuno[1], N. Mizuno[1], A. Kawamura[1], T. Onishi[1], Y. Fukui[1], H. Ogawa[2], J. Stutzki[3], F. Bertoldi[4], B. C. Koo[5], M. Rubio[6], M. Burton[7], A. Benz[8], and the NANTEN2 Team

[1] Nagoya University, Japan y_mizuno@a.phys.nagoya-u.ac.jp
[2] Osaka Prefecture University, Japan
[3] University of Cologne, Germany
[4] University of Bonn, Germany
[5] Seoul National University, Japan
[6] University of Chile, Chile
[7] University of New South Wales, Australia
[8] Swiss Federal Institute of Technology in Zurich, Switzerland

The study of the Large Magellanic Cloud (LMC) is important to understand the formation process of massive stellar clusters. N159 is one of the most active cluster forming regions in the LMC. Bolatto et al. [2] observed sub-mm CO and C I lines in this region and found CO(J=4–3) the emission peak at N159 W. This observation didn't have enough resolution to reveal the high temperature molecular cloud structure. So we observe with the NANTEN2 telescope to improve the image resolution.

1 Observation

The NANTEN2 telescope is the 4-m radio telescope of Nagoya University equipped with SIS receivers at 490 GHz and 810 GHz. The beam size of both frequency bands is $38''$ and $26.5''$, respectively. In 2004, the NANTEN2 telescope was installed at Pampa la Bola observatory in Chile near the ALMA site. We observed N159 from September to December 2006. The system temperature is $\sim$1000 K at 460 GHz.

2 Results

Figure 1 (left panel) shows the CO(J=4–3) and CO(J=3–2) distributions. The CO(J=4–3) peak is located at the western peak. It is consistent with previous

B.S. Koribalski, H. Jerjen (eds.), *Galaxies in the Local Volume*,
doi: 10.1007/978-1-4020-6933-8_81,

work. We can see that the distribution of both lines is similar. Figure 1 (right panel) shows the spectra of both lines at the N159 W, E, and S peaks as well as the line ratio. At the nothern peak, the CO(J=4–3) intensity is stronger than the CO(J=3–2) and CO(J=4–3) excess at high velocity. Conversely, the southern peak shows flat line ratio.

3 Discussion

What is the high velocity CO(J=4–3) excess? Jones et al. [1] showed a great image of N159 with the Spitzer/IRAC camera. They suggested a star formation region located along a circle centered at the radio peak. There may be a wind-blown bubble triggering the star formation activity. We think the bubble affects the molecular cloud and possibly the CO(J=4–3) excess of that is evidence. Efremov & Elmegreen [3] studied the super shell LMC4 and mentioned that the super bubble plays an important role in the star formation in the LMC. We suppose N159 is a good site to study regarding triggered star formation in the LMC.

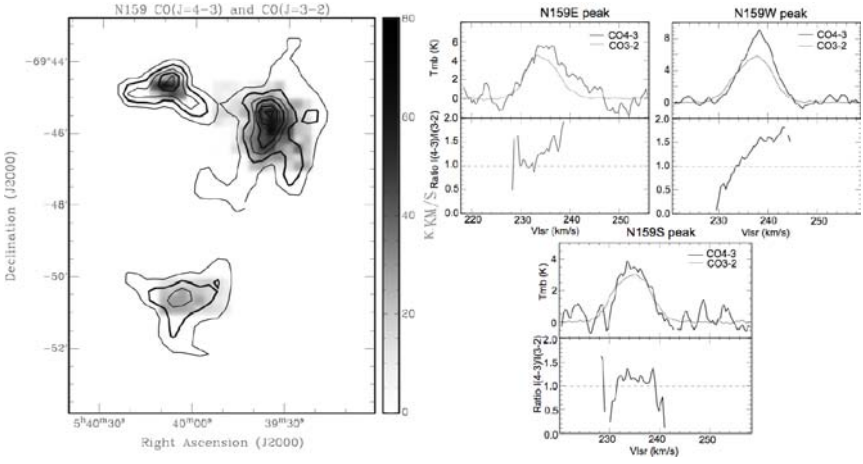

Fig. 1. *(Left:)* Integrated intensity of the CO(J=4–3) line (greyscale) and the CO(J=3–2) line (contours) as taken with ASTE telescope. *(Right:)* The top graph of each panel shows the intensity of both lines at the N159 W, E, and S peaks. The bottom graph shows the R(4–3)/(3–2) line ratio.

References

1. T. J. Jones, C. E. Woodward, M. L. Boyer, R. D. Gehrz, & E. Polomski: ApJ **620**, 731 (2005)
2. A. Bolatto, J. Jackson, F. Israel, X. Zhang, & S. Kim: ApJ **545**, 234 (2000)
3. Y. N. Efremov, & B. G. Elmegreen: MNRAS **299**, 643 (1998)

Kiso Outer Galaxy Survey: Stellar Radial Distribution of the Galaxy

Hiroyuki Nakanishi[1], H. Mito[2], F. Egusa[3], S. Komugi[3], Y. Nakada[2,3], N. Kobayashi[2,3], S. Onodera[2], T. Aoki[2,3], Y. Sofue[2], R. Kandori[4], and T. Miyata[2,3]

[1] Australia Telescope National Facility, CSIRO, PO Box 76, Epping NSW 1710, Australia Hiro.Nakanishi@csiro.au
[2] Kiso Observatory, The University of Tokyo, Japan
[3] Institute of Astronomy, The University of Tokyo, Japan
[4] National Astronomical Observatory of Japan

Summary. We carried out the 'Kiso Outer Galaxy Survey' (KOGS) project to measure the size of the Galactic stellar disk. $UBVI$-band images of the outer Galactic disk were obtained using the Kiso Schmidt telescope equipped with a 2k CCD camera. We found that the stellar density distribution is an exponential disk which appears extended beyond 20 kpc.

1 Introduction

The size of the stellar disk of a spiral galaxy is an essential parameter. Robin et al. [1] investigated that of the Milky Way and concluded that it was 14.0–14.5 kpc, based on their observation at the CFHT 3.6-m telescope. Despite the obvious need to confirm this result with follow-up observations, few have been done.

2 Observations and Data Reduction

We observed the plane of the outer Galaxy ($l = 161° - 213°$, $b = 0°$) in $UBVI$-bands using the 105-cm Schmidt telescope equipped with the 2k CCD camera at the Kiso Observatory from October 2004 to April 2006. The field of view was as large as $50' \times 50'$ and the pixel scale was $1''.5$.

We applied standard reduction procedures (bias subtraction and flat fielding) to the raw data. Photometry was calibrated using the catalogue published by Londolt [2]. Since there are many available standard stars in the field of $(l, b) = (213°, 0°)$ where we can do accurate photometric calibration, we here report a result obtained using only this field.

B.S. Koribalski, H. Jerjen (eds.), *Galaxies in the Local Volume*,
doi: 10.1007/978-1-4020-6933-8_82,

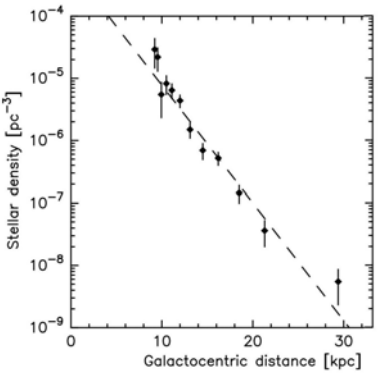

Fig. 1. Density profile of the Galactic stellar disk. The dahsed line denotes the fit which is $\rho = 6 \times 10^{-4} \exp(-R/2.3 \text{ kpc})$.

3 Method and Results

Assuming that the main-sequence stars are dominant and that the reddening law obeys $\Delta(U-B)/\Delta(V-I) = 0.4$, we can estimate the interstellar reddening, E_{V-I}, and the intrinsic color, $(V-I)_0$, of each star using the color-color diagram of $(V-I)$ vs $(U-B)$. The interstellar extinction, A_V, and the absolute magnitude, M_V, can be calculated from E_{V-I} and $(V-I)_0$. The distance of each star, d, can be calculated by solving $M = m - A_V + 5 - 5\log_{10} d$, where the apparent magnitude, m, is obtained by the observations. Finally, we count stars at each distance, and calculate the stellar density by dividing the stellar number by the volume of the field of view to obtain the stellar density profile. In this study, we chose only earlier type stars than B6 to avoid confusion with F stars.

Fig. 1 shows that the Galactic stellar disk is an exponential disk whose scale-length is 2.3 kpc and that the volume density at the solar neighbourhood is 2.1×10^{-5} pc^{-3}, as expected. It is interesting that the exponential stellar disk extends beyond 20 kpc. Because the Galactic stellar disk was believed to be truncated around 14.00–14.5 kpc, our result suggests that the Galactic stellar disk might be much larger than previously thought. Recent deep observations towards nearby spiral galaxies such as NGC 300 and M 31 show quite similar results, namely that these galaxies have quite extended stellar disks [3, 4]. To confirm this new picture of the Galaxy, follow-up spectroscopic observations are necessary.

References

1. Robin, A. C., Creze, M., & Mohan, V.: ApJ, **400**, L25 (1992)
2. Landolt, A. U.: AJ, **104**, 340 (1992)
3. Bland-Hawthorn, J., Vlajić, M., Freeman, K. C., & Draine, B. T.: ApJ, **629**, 239 (2005)
4. Ibata, R., Chapman, S., Ferguson, A. M. N., Lewis, G., Irwin, M., & Tanvir, N.: ApJ, **634**, 287 (2005)

Large Magellanic Cloud Distance from Cepheid Variables using Least Squares Solutions

Choong Ngeow[1] and S. M. Kanbur[2]

[1] University of Illinois, Urbana, IL 61801, USA cngeow@astro.uiuc.edu
[2] State University of New York at Oswego, Oswego, NY 13126, USA kanbur@oswego.edu

Summary. Distance to the Large Magellanic Cloud (LMC) is determined using the Cepheid variables in the LMC. We combine the individual LMC Cepheid distances obtained from the infrared surface brightness method and a dataset with a large number of LMC Cepheids. Using the standard least squares method, the LMC distance modulus can be found from the ZP offsets of these two samples. We have adopted both a linear P-L relation and a "broken" P-L relation in our calculations. The resulting LMC distance moduli are 18.48 ± 0.03 mag and 18.49 ± 0.04 mag (random error only), respectively, which are consistent to the adopted 18.50 mag in the literature.

1 Introduction

Recently, Gieren et al. [1] (hereafter G05) has used the infrared surface brightness method to obtain individual distances to 13 LMC Cepheids with an averaged LMC distance modulus of 18.56 ± 0.04 mag (random error only). However, the LMC hosts more than 600 Cepheids with data available from the Optical Gravitational Lensing Experiment (OGLE) [2]. A linear least squares solution (LSQ) will allow a simultaneous determination for *both* of the LMC distance and the P-L relation (see Figure 1).

2 Data, Method and Results

The data include the absolute magnitudes for the 13 Cepheids with individual distance measurements from G05 and the apparent magnitudes (after extinction correction) for ~ 630 LMC Cepheids from [3], which is based on the OGLE database. For both datasets, we fit the following regression using the LSQ: $x = \alpha\Delta\mu + a + b\log(P)$ where $\alpha = 0$ if $x = M$ (for G05 data) or $\alpha = 1$ if $x = m$ (for OGLE data). The results of the LSQ are: $M^V = -2.76 \pm 0.04\log(P) - 1.36 \pm 0.07$ with $\Delta\mu(V) = 18.47 \pm 0.06$, and

B.S. Koribalski, H. Jerjen (eds.), *Galaxies in the Local Volume*,
doi: 10.1007/978-1-4020-6933-8_83,

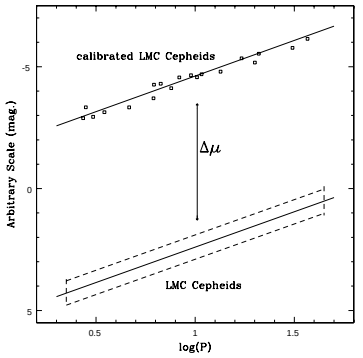

Fig. 1. Illustration of the LSQ. Introducing an offset, $\Delta\mu$, between the calibrated Cepheids and the other LMC Cepheids will allow us to simultaneously solve for the LMC distance modulus and the P-L relation with LSQ.

$M^I = -2.98 \pm 0.02 \log(P) - 1.86 \pm 0.05$ with $\Delta\mu(I) = 18.48 \pm 0.04$. The weighted average of these $\Delta\mu$ is 18.48 ± 0.03 mag (random error only).

Since the recent studies have strongly suggested the LMC P-L relation is not linear ([3, 4, 5, 6]), we also use the following "broken" regression to fit the data:

$$x = \alpha\Delta\mu + a_S + \beta b_S \log(P) + \gamma(a_L - a_S) + \epsilon b_L \log(P),\ \alpha = \begin{cases} 0 \text{ if } x = M \\ 1 \text{ if } x = m \end{cases} \quad (1)$$

where subscripts $_S$ and $_L$ refer to the short and long period Cepheids, respectively, and $\beta = 1,\ \gamma = 0,\ \epsilon = 0$, for $\log(P) < 1.0$; $\beta = 0,\ \gamma = 1,\ \epsilon = 1$, for $\log(P) \geq 1.0$. The results are: $M_L^V = -2.84 \pm 0.16 \log(P) - 1.23 \pm 0.21$; $M_S^V = -2.94 \pm 0.06 \log(P) - 1.28 \pm 0.07$ with $\Delta\mu(V) = 18.49 \pm 0.06$, and $M_L^I = -3.09 \pm 0.11 \log(P) - 1.69 \pm 0.14$; $M_S^I = -3.09 \pm 0.04 \log(P) - 1.80 \pm 0.05$ with $\Delta\mu(I) = 18.49 \pm 0.04$. The weighted average of the distance moduli in both bands is 18.49 ± 0.04 mag (random error only). F-test ([4, 5]) is also applied to examine if the data is more consistent with a single-line regression (the null hypothesis) or a two-lines regression (the alternate hypothesis). For our data, we obtain $F(V) = 7.3$ and $F(I) = 6.9$, where $F \sim 3$ at 95% confident level. This suggested the null hypothesis can be rejected and the data is more consistent with the broken P-L relation.

References

1. Gieren, W., et al., 2005, ApJ, **627**, 224 (G05)
2. Udaski, A., et al., 1999, Acta Astron., **49**, 223
3. Kanbur, S. & Ngeow, C., 2006, MNRAS, **369**, 705
4. Kanbur, S. & Ngeow, C., 2004, MNRAS, **350**, 962
5. Ngeow, C., et al., 2005, MNRAS, **363**, 831
6. Sandage, A., Tammann, G. A. & Reindl, B., 2004, A&A, **424**, 43

High-Resolution Dark Matter Density Profiles of Two THINGS Dwarf Galaxies

Se-Heon Oh[1], W. J. G. de Blok[1], Fabian Walter[2], and Elias Brinks[3]

[1] Research School of Astronomy & Astrophysics, Mt. Stromlo Observatory, The Australian National University, ACT 2611, Australia
seheon@mso.anu.edu.au, edeblok@circinus.ast.uct.ac.za
[2] Max Planck Institut für Astronomie, Königstuhl 17, 69117 Heidelberg, Germany
walter@mpia-hd.mpg.de
[3] Center for Astrophysics Research, Science & Technology Research Institute, University of Hertfordshire, Hatfield AL10 9AB, United Kingdom
ebrinks@star.herts.ac.uk

1 Rotation curves of IC 2574 and NGC 2366

We present high-resolution ($\sim 6''$) rotation curves of IC 2574 and NGC 2366 from 'The H I Nearby Galaxy Survey' (THINGS) [1] as shown in the top panels of Fig. 1. In order to minimize the effect of chaotic non-circular motions on the observed kinematics, we use the bulk velocity fields that contain only the circularly rotating components from H I data [3]. These high-resolution rotation curves from the bulk velocity fields suffer less from not only the systematic effects, such as beam smearing and pointing effects, but also the chaotic non-circular motions in galaxies.

2 Mass modeling

In order to separate the dynamical contribution of the stellar component from the total dynamics we use Spitzer Infrared Nearby Galaxies Survey (SINGS) [4] and ancillary optical data (B-, V-, and R-band) taken from the WIYN 2.1m telescope at Kitt Peak. We derive the stellar mass-to-light ratio based on the Bruzual and Charlot population synthesis models [2] for two Spitzer bands (3.6 μm and 4.5 μm) to construct the mass models for the stellar components (see [3] for a more detailed discussion). Mass models for the baryonic matter (i.e., stars and gas) of IC 2574 and NGC 2366 are shown in Fig. 1 (top panels).

B.S. Koribalski, H. Jerjen (eds.), *Galaxies in the Local Volume*,
doi: 10.1007/978-1-4020-6933-8_84,

3 Dark matter distribution

As shown in the lower panels of Fig. 1, we derive the mass density profiles of IC 2574 and NGC 2366 by converting their observed rotation velocities under a spherical dark halo assumption. This allows us to constrain the dark matter halo shape directly. We measure the inner slopes of the mass density profiles,

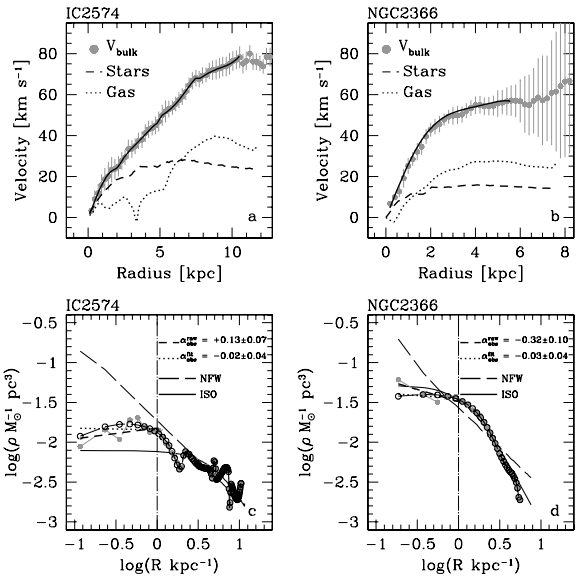

Fig. 1. *(Top:)* Rotation curves of IC 2574 and NGC 2366 from THINGS. *(Bottom:)* Mass density profiles of IC 2574 and NGC 2366. The filled grey and open black circles in the lower panels are derived from V_{bulk} and its smooth curve (solid line) in the upper panels, respectively. α_{obs}^{raw} and α_{obs}^{fit} are the inner-density slopes measured using the filled grey and open black circles in the lower panels.

and find that these are $\alpha_{raw}^{IC2574} = +0.13 \pm 0.07$ and $\alpha_{raw}^{NGC2366} = -0.32 \pm 0.10$. This shows that the dark matter distributions of IC 2574 and NGC 2366 are closer to the ISO model ($\alpha \sim 0.0$) with a sizeable constant-density core and are inconsistent with the NFW model which predicts $\alpha \sim -1.0$.

References

1. F. Walter, E. Brinks, W. J. G de Blok et al: in preparation (2007)
2. G. Bruzual & S. Charlot: MNRAS **344**, 1000 (2003)
3. S. H. Oh, W. J. G de Blok, F. Walter, & E. Brinks: in preparation (2007)
4. R. C. Kennicutt, L. Armus, L. Bendo et al: PASP **115**, 928 (2003)

VLA-ANGST: Star Formation History and ISM Feedback in Nearby Galaxies

Jürgen Ott[1], Evan Skillman[2], Julianne Dalcanton[3], Fabian Walter[4], Andrew West[5], Bärbel S. Koribalski[6], and Dan Weisz[2]

[1] National Radio Astronomy Observatory, 520 Edgemont Road, Charlottesville, VA 22903, USA; jott@nrao.edu
[2] Department of Astronomy, University of Minnesota, Minneapolis, MN 55455, USA; skillman@astro.umn.edu
[3] Department of Astronomy, University of Washington, Box 351580, Seattle, WA 98195, USA; jd@astro.washington.edu
[4] Max-Planck-Institut für Astronomie, Königstuhl 17, D-69117 Heidelberg, Germany; walter@mpia-hd.mpg.de
[5] Astronomy Department, 601 Campbell Hall, University of California, Berkeley, CA 94720, USA; awest@astro.berkeley.edu
[6] Australia Telescope National Facility, CSIRO, PO Box 76, Epping, NSW 1710, Australia; Baerbel.Koribalski@csiro.au

Star formation is driven by complex interactions between gas and stars. Because of this complexity, understanding star formation in galaxies remains one of the biggest challenges in current observational and theoretical astrophysics. Stars are thought to form in response to high gas densities, driven by turbulence, by interactions, or triggered stochastically (e.g., [4, 3]). The evolution of the stars in turn is believed to affect the surrounding gas, as supernovae and stellar winds deposit kinetic and thermal energy, as well as ionizing photons into the interstellar medium (ISM). Untangling the interplay between these different processes is difficult, because in most cases, the events that trigger star formation are not obvious, nor are the events that feed back into the dynamics and structure of the ISM.

Our approach to this problem are multi-wavelength observations that capture both the detailed history of star formation and the rich structure of the ISM. We gained $\sim$ 480 hours of VLA time in the context of a Large Project (start of the observations: September 2007) to produce the definitive sample for studying the interplay of gas and stars. Specifically, we are to perform high spatial resolution ($\sim 6''$), BCD array VLA H I observations of a volume-limited sample of galaxies that recently has been targeted with complete HST/ACS observations in the context of the ANGST project [1]. The ANGST dataset will deliver spatially resolved star formation histories for all galaxies within 4 Mpc distance, excluding the Local Group (see also [2]

B.S. Koribalski, H. Jerjen (eds.), *Galaxies in the Local Volume*,
doi: 10.1007/978-1-4020-6933-8_85,

for a demonstration of this technique). The follow-up VLA H I observations (identical in depth and resolution to the THINGS survey [5]) are to produce rich data cubes of the atomic neutral gas over a large range of morphologies, masses, and environments. This is needed to study the triggering of star formation and the impact of stellar feedback into the ISM (for an example, see Fig. 1). The 36 galaxies to be observed within VLA–ANGST include Antlia, BK 3 N, DDO 6, DDO 99, DDO 125, DDO 181, DDO 187, DDO 190, GR 8, HS 117, KDG 73, KK 230, KKH 37, KKH 86, KKH 98, KKR 25, NGC 247, NGC 253, NGC 3109, NGC 3741, NGC 4163, NGC 4190, Sex A, Sex B, UA 292, UGC 8508, UGC 4483, UGC 8833.

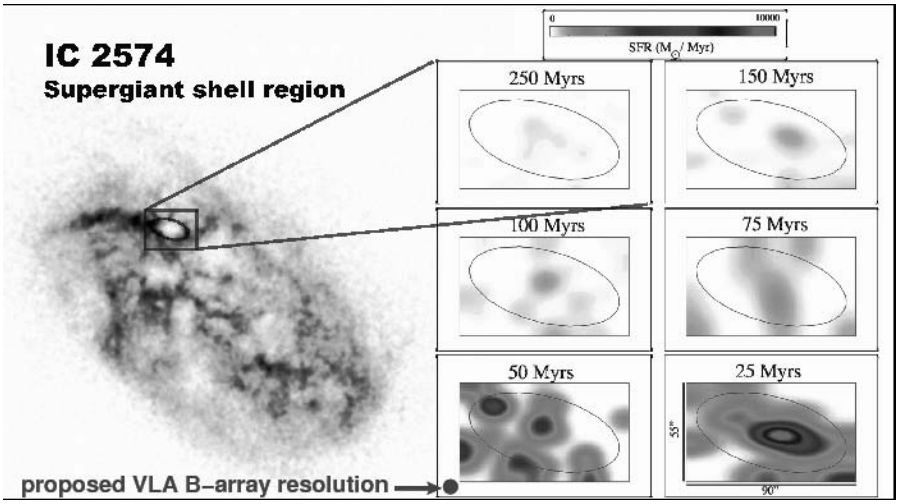

Fig. 1. An example of what we propose to analyze for the ANGST sample. The galaxy shown here is the nearby dwarf irregular IC 2574. *(Left:)* A VLA image of the H I column density in the M81 group dwarf galaxy IC 2574 taken at the VLA B-array resolution (image obtained from the THINGS survey [5]). *(Right:)* A mosaic of time frames from the reconstructed spatially resolved star formation history within a supergiant shell in IC 2574 derived from HST ACS imaging. The movie was convolved with a Gaussian kernel (80 pc and 30 Myr). The frames are not uniformly distributed in time; they were chosen to demonstrate the SF events that led to the formation and evolution of the supergiant shell in IC 2574. The beam size of the proposed VLA survey is marked as a filled circle close to the 50 Myr panel - it is a perfect match to the resolution of the reconstructed HST star formation history.

References

1. Dalcanton, J.: Bulletin of the American Astronomical Society, **38**, 1063 (2006)
2. Dohm-Palmer R. C., et al.: AJ **116**, 1127 (1998)
3. Kauffmann, G., et al.: MNRAS **367**, 1394 (2006)
4. Seiden, P. E. & Gerola, H.: ApJ **233**, 56 (1979)
5. Walter, F., et al.: ApJ **661**, 102 (2007)

Lessons from the Space Velocities of the Satellite Galaxies of the Milky Way

Carlton Pryor[1], Slawomir Piatek[2], and Edward Olszewski[3]

[1] Dept. of Physics & Astronomy, Rutgers, the State University of New Jersey, 136 Frelinghuysen Rd., Piscataway, NJ 08854-8019, USA
pryor@physics.rutgers.edu
[2] Dept. of Physics, New Jersey Insitute of Technology, Newark, NJ 07102, USA
piatek@physics.rutgers.edu
[3] Steward Observatory, The Univ. of Arizona, Tucson, AZ 85721, USA
eolszewski@as.arizona.edu

Proper motions have been measured using images from the Hubble Space Telescope for at least eight of the dwarf galaxy satellites of the Milky Way, and this sample is large enough to search for correlations between their kinematics and spatial distribution. We take proper motions from the literature for Carina, Fornax, Sculptor, and Ursa Minor ([5] and references therein). We use values for the LMC and SMC from [6] (a reanalysis of the data in [1] and [2]). Finally, proper motions for Draco and Sagittarius are from the contribution to this conference by Piatek, Pryor, & Olszewski. These two values are preliminary and may change.

We convert proper motions to space velocities in a frame at rest with respect to the Galactic center using the methods of [5]. Figure 1 plots Galactic-

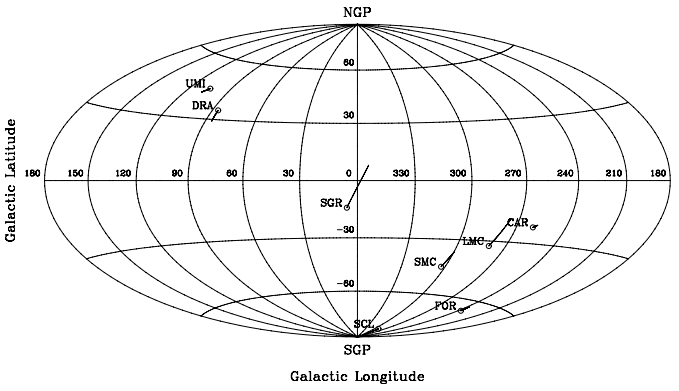

Fig. 1. Galactic-rest-frame proper motions plotted as vectors at the location of each satellite galaxy on the sky.

B.S. Koribalski, H. Jerjen (eds.), *Galaxies in the Local Volume*,
doi: 10.1007/978-1-4020-6933-8_86,

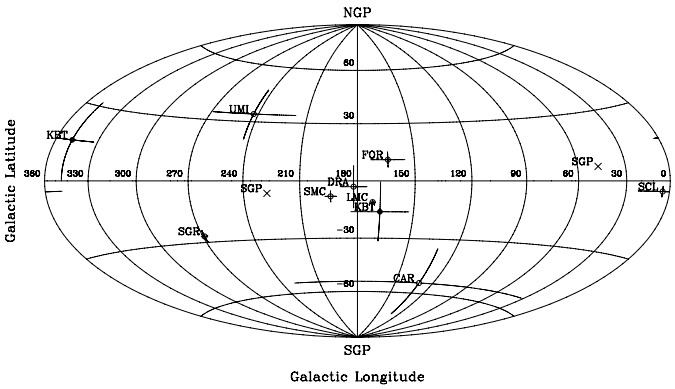

Fig. 2. Poles of the satellite orbits compared to those of the plane proposed by [4] (KBT) and to the poles of the supergalactic plane (SGP).

rest-frame proper motions as vectors at the location of each satellite galaxy on the sky. All of the galaxies except for Sgr lie approximately along a great circle that goes through the galactic poles and $\ell = 90°$ and 270°. The motions of the galaxies are approximately along the great circle and, except for Scl, indicate that they are orbiting in the same direction.

The adopted Galaxy model is approximately that of [3]: an NFW Halo with a virial radius of 258 kpc and a virial mass of 1.2×10^{12} solar masses, a Miyamoto & Nagai disk, and a bulge. The circular velocity is about 200, 175, and 150 $\mathrm{km\,s^{-1}}$ at radii of 50, 100, and 200 kpc, respectively.

Figure 2 compares the poles of the satellite orbits to those of the plane proposed by [4] (KBT) and to the poles of the supergalactic plane. The error bars for the orbit poles are the 1σ uncertainty in the direction of the orbital angular momentum vector. The error bars for poles of the KBT plane show the range of orbit inclinations that would produce the observed rms thickness of the plane, 26.4 kpc, for a circular orbit with a radius of 140 kpc (the current radius of Fornax). The orbits are approximately aligned with the KBT plane, but the range of orbital inclinations is too large to maintain a planar distribution as thin as that proposed by [4]. The orbital poles show some tendency to be aligned with the poles of the supergalactic plane.

References

1. N. Kallivayalil, R. P. van der Marel, C. Alcock, T. Axelrod, K. H. Cook, A. J. Drake, & M. Geha: ApJ, **638**, 772 (2006)
2. N. Kallivayalil, R. P. van der Marel, & C. Alcock: ApJ, **652**, 1213 (2006)
3. A. Klypin, H. Zhao, & R. S. Somerville: ApJ, **573**, 597 (2002)
4. P. Kroupa, C. Theis, & C. M. Boily: A&A, **431**, 517 (2005)
5. S. Piatek, C. Pryor, P. Bristow et al.: AJ, **133**, 818 (2007)
6. S. Piatek, C. Pryor, & E. W. Olszewski: AJ, submitted (2007)

Spectral Diagnostics, Kinematics and Abundances Based on a New Population of Planetary Nebulae Discovered in the LMC

Warren Reid[1] and Quentin Parker[1,2]

[1] Macquarie University, Sydney, Australia warren@ics.mq.edu.au
[2] Anglo-Australian Observatory, Australia qap@ics.mq.edu.au

We report our discovery of 460 planetary nebulae (PNe) in the central 25 deg^2 region of the Large Magellanic Cloud (LMC). Candidate emission sources were discovered using a deep, high resolution UKST stack of 6 Short Red (SR) and 12 Hα images which go respectively 1 and 1.5 magnitudes deeper than a single exposure. The two digitized stacks were then assigned false colours and merged to reveal emission sources. Confirmatory spectroscopy was largely performed using 2dF on the AAT, with low and high resolution gratings. Additional follow-up in selected regions was also performed using FLAMES on the ESO VLT2 and Gemini South [2]. Optical spectroscopy not only allowed us to identify PNe from our large sample but results are allowing physical conditions to be determined. The new PNe have implications for the LMC PN luminosity function, kinematics, abundance gradients, chemical evolution and the initial to final mass relation for low to intermediate mass stars via the AGB halos revealed on the Hα map [3].

All the previously known PNe in the survey area have also been spectroscopically observed, resulting in a sample of 629 PNe. These have now been used to produce nebula diagnostics including temperatures, electron densities and masses [4]. Together with newly derived excitation classes [5], these diagnostics and fluxes have led to the discovery of new evolutionary tracks for LMC PNe [4]. Luminosity gradients have been compared to masses and densities for different excitation classes. Newly derived dynamical ages have also been estimated. PN abundances have been determined, comprising the largest sample ever obtained in any galaxy beyond the Milky Way, allowing clear trends to be graphically displayed for the first time. A new luminosity function has been constructed, providing the first clues to the shape of the faint end. This is compared to a new luminosity function constructed from a very complete sample of local PNe. Radial velocities from the complete LMC sample have been used to compare PN kinematics to that of the H I disk. The resulting transverse velocity and angle of inclination for PNe in the central 25 deg^2 region of the LMC have been found [3].

B.S. Koribalski, H. Jerjen (eds.), *Galaxies in the Local Volume*,
doi: 10.1007/978-1-4020-6933-8_87,

The most accurate radial velocities measured for the largest sample of LMC PNe

Emission line and cross-correlation techniques have been employed to calculate the velocity of 587 PNe in the survey area where high resolution 2dF 1200R spectra have been obtained. Excellent agreement to 3.9 ± 6.6 km s^{-1} was found between the emission line and cross-correlation measurements. This work represents the largest number of radial velocities obtained thus far for LMC PNe. There are now >5 times as many PNe with accurate velocity measurements in the central 25 deg^2 region of the LMC. An overall mean difference of only 0.68 ± 11.2 km s^{-1} between radial velocities measured in this work and all other published works for a sample of 97 LMC PNe establishes a high degree of confidence in the measurements for the ∼500 newly discovered PNe.

A new kinematic study of PNe in the LMC

The high quality LMC PN velocities, were used to explore the kinematics of the LMC central bar region. We find that the PNe population occupies a warped disk with its own kinematic line of nodes which is also warped in a similar tangential direction but to a greater extent than the H I disk. The measurement and comparison of PNe and H I indicates that the innermost 2.6 deg bar region has solid-body rotation. We may therefore conclude that the LMC disk is warped and its line of nodes is twisted at the SW edge in agreement with [1]. The percentage of Type I (high nitrogen and helium) PNe to the total population increases in a clockwise direction from 7% in the NE to 19% in the SE, which may indicate a younger population in that region. The angle of inclination between the planes of the PN population and the H I gas disk is never greater than 7.9 deg with the centre of symmetry for the PN population at $\alpha, \delta(\mathrm{J2000}) = 05^{\mathrm{h}}\,19^{\mathrm{m}}\,12^{\mathrm{s}}$, $-69^\circ\,26'\,17''$. Here, the PNe and H I gas disk are also at their closest point of agreement. This position is roughly 1 degree south of the central optical counterpart and may be assumed to be the centre of the PN population.

References

1. Olsen K. A. G., Salyk, C. 2002, AJ. 124, 2045
2. Reid W., Parker Q. 2006a, MNRAS, 365, 401
3. Reid W., Parker Q. 2006b, MNRAS, 373, 521
4. Reid W., 2007, "A new population of PNe discovered in the LMC" (PhD thesis)
5. Reid W., Parker Q. 2006c, IAU. Symp. 234, *Planetary Nebulae in our Galaxy and Beyond*, eds. M. J. Barlow and R. H. Mendez, Cambridge, p. 487

Magellanic Clouds in Interaction: Evolutionary Search for Good Models

Adam Ruzicka[1], Jan Palous[1], and Christian Theis[2]

[1] Astronomical Institute, Academy of Sciences of the Czech Republic, v.v.i., Boční II 1401a, 141 31 Prague, Czech Republic adam.ruzicka@gmail.com, palous@ig.cas.cz

[2] Institut für Astronomie der Universität Wien, Türkenschanzstrasse 17, A-1180 Wien, Austria theis@astro.univie.ac.at

We performed an extended analysis of the parameter space for the interaction of the Magellanic System (MS) with the Milky Way (MW). The varied parameters cover the phase space parameters, the structure of both Magellanic Clouds, as well as the flattening of the dark matter (DM) halo of the

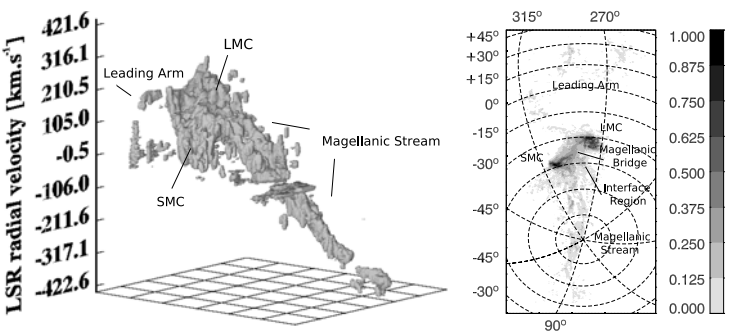

Fig. 1. *(Left:)* The figure depicts the original 3 D H I data cube of the MS by [1]; we offer 3 D visualization of the column density isosurface $\Sigma_{\rm HI} = 0.2 \times 10^{18}\,{\rm cm}^{-2}$ [2]. *(Right:)* Contour map of the observed H I integrated relative column density in the System. Data by [1] is projected on the plane of the sky.

MW. The analysis was done by a genetic algorithm (GA), together with a fast restricted N-body model of the interaction, searching for the best match between numerical models and the detailed H I map of the MS by [1]. By this, we were able to analyze more than 10^6 models. Here we focus on the flattening q of the axially symmetric MW DM halo potential, that is studied within the range $0.74 \leq q \leq 1.20$. We show that creation of the Magellanic Stream and the Leading Arm is quite a common feature of the MS-MW interaction, and

B.S. Koribalski, H. Jerjen (eds.), *Galaxies in the Local Volume*,
doi: 10.1007/978-1-4020-6933-8_88,

such structures were modeled across the entire range of halo flattening values. However, important differences exist between the models, concerning density distribution and kinematics of H I, and also the dynamical evolution of the MS. Detailed analysis shows that the models assuming aspherical DM halos of the MW allow for better satisfaction of H I observations than the models with a nearly spherical halo configuration.

The GA optimizer (for details on GA-based modeling of galactic interactions see e.g. [3] or [4]) was run repeatedly and over 100 high-fitness models were collected. To discuss the models with respect to the MW DM halo flattening q, three model groups were defined – A: $0.74 \leq q \leq 0.92$; B: $0.94 \leq q \leq 1.06$; C: $1.08 \leq q \leq 1.20$

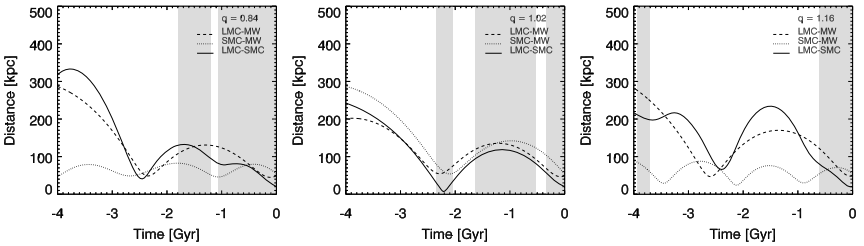

Fig. 2. Orbital evolution of the Magellanic Clouds for the model A *(left)*, B *(middle)* and C *(right)*. The plots correspond to logarithmic halos of the flattening q =0.84, 1.02 and 1.16, respectively. Plot areas with filling mark when the Clouds were gravitationally bound to each other.

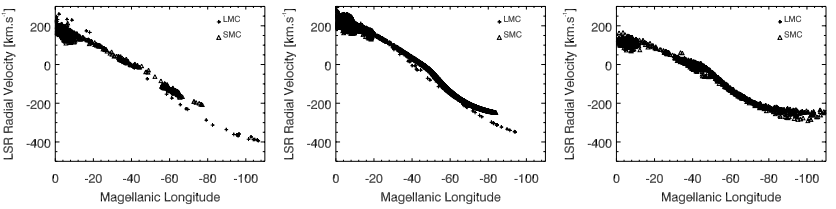

Fig. 3. LSR radial velocity profile of the Magellanic Stream for the model A *(left)*, B *(middle)* and C *(right)*.

References

1. Brüns, C., Kerp, J., Staveley-Smith, L., et al.: A&A, 432, 45 (2005)
2. Růžička, A., Palouš, J., Theis, Ch.: A&A, 461, 155 (2007)
3. Theis, Ch.: Rev. Mod. Astron., 12, 309 (1999)
4. Wahde, M.: A&A, 132, 417 (1998)

Compact and Isolated Groups of Galaxies in the Local Universe

Julio Saucedo-Morales[1], P. Loera-González[1], and A. Santillán-González[2]

[1] DIFUS, Universidad de Sonora, México jsaucedo@astro.uson.mx
[2] DGSCA, Universidad Nacional Autonoma de México
alfredo@astroscu.unam.mx

Summary. An algorithm that searches for groups of galaxies in redshift catalogues has been applied to data obtained from the Sloan Digital Sky Survey DR5, which includes over half a million galaxies. The program finds galaxy groups according to chosen isolation and compactness parameters within a certain redshift range. The results for the SDSS are then compared to those previously obtained by us for the 2dF redshift catalog. Using these results it is possible to learn about the properties of these type of groups. For instance, statistical properties of masses, sizes, velocity dispersions, as well as the population of these groups. Furthermore, due to the large number and redshift range of the galaxies involved, these properties can be studied as a function of redshift. Extrapolating this result to $z = 0$, it might be possible to extract these properties for compact and isolated groups in the local Universe.

1 Introduction

The importance of galaxy groups is widely recognized, for a review see Eke (2007), where he discusses group definitions and approaches that have been adopted to find them. For more specific details related to this work on compact and isolated groups of galaxies (CIGGs) see Saucedo & Loera (2007).

The Friends-of-Friends (FOF) group searching program was introduced by Huchra & Geller (1982). Since then, several investigators have implemented updated versions to find groups in redshift surveys. Some of the more recent searches include the final data release of the 2dF by Eke et al. (2004), and the groups in the 2MASS Resdshift Survey by Crook et al. (2007).

The approach adopted in this work is quite different from that of the FOF. For CIGGs the selection criteria is based on the compactness radius R_c, the isolation radius R_i, and a redshift range Δz. Given a set of parameters, the program finds CIGGs of any number of galaxies. For instance a CIGG of 3 galaxies contains them within R_c, and the next neighbor lies beyond R_i. The main objective of this work is to study the statistical properties of CIGGs, as well as those of the galaxies within them, in the hope that such information can be useful to study the evolution of galaxies in these groups.

B.S. Koribalski, H. Jerjen (eds.), *Galaxies in the Local Volume*,
doi: 10.1007/978-1-4020-6933-8_89,

2 Results and discussions

As an example of the results, Fig. 1 presents the normalized fraction of groups. For instance, the points on top represent the fraction of pairs (number of pairs divided by number of groups within each $\Delta z = 0.05$ bin). The results for the SDSS and 2dF are quite similar. Extrapolating to $z = 0$, one can argue that these provide information about the population of CIGGs in the local universe. With regard to the masses, virialized radius and velocity dispersions, no significant trend is found as a function of redshift. However, the masses and velocity dispersions strongly depend on the degree of compactness and isolation. The smaller the degree of compactness and isolation, the higher the masses and velocity dispersions.

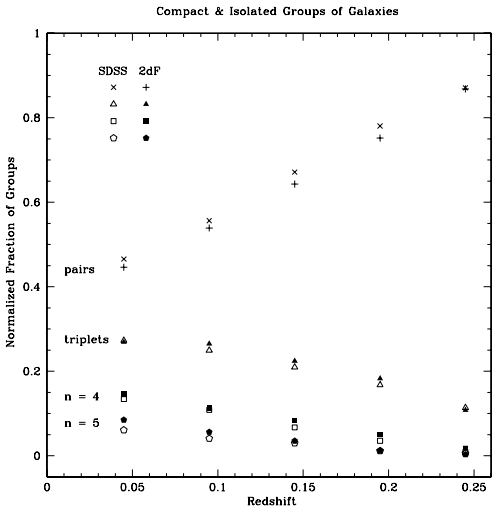

Fig. 1. Comparison of the fraction of groups found for the SDSS and the 2dF, for pairs, triplets, quadruplets and quintuplets. These results were obtained for $R_c = 1.1$ Mpc, $R_i = 2.0$ Mpc, and $\Delta z = 0.01$

References

1. Eke, V.R.: Galaxy Groups Searches and Surveys. In: *Groups of Galaxies in the Nearby Universe*, ed. by I. Saviane et al. (Springer, 2007) pp 53–66
2. Saucedo, J., & Loera, P.: Isolated Compact Groups of Galaxies in the 2dF. In: *Groups of Galaxies*, ed. by I. Saviane et al. (Springer, 2007) pp 73–77
3. Huchra, J.P., & Geller, M.J.: ApJ **257**, 423 (1982)
4. Eke, V.R., et al.: MNRAS **348**, 866 (2004)
5. Crook, A.C., et al.: ApJ **655**, 790 (2007)

Structure and Kinematics of CO ($J = 2 - 1$) Emission in the Central Region of NGC 4258

Satoko Sawada-Satoh[1,2], P. T. P. Ho[1], S. Muller[1], S. Matsushita[1], and J. Lim[1]

[1] ASIAA, Taipei, Taiwan 106
[2] Yamaguchi University, Yamaguchi, Japan 753-8512 sss@yamaguchi-u.ac.jp

We present ^{12}CO ($J = 2 - 1$) observations towards the central region of the nearby Seyfert 2 galaxy NGC 4258 with the Submillimeter Array (SMA; Ho et al. [3]). NGC 4258 is well known to exhibit a sub-pc-scale molecular disk as traced by H_2O maser emission (Miyoshi et al. [4], Herrnstein et al. [2]). The major axis of the molecular disk is along the east-west direction although the P.A. of the host galaxy is around $-30°$ (e.g. van Albada [6], Cox and Downes [1]), and the angle between the two rotation axes of the sub-pc-scale disk and the galactic disk is $\sim 120°$ [4]. This indicates a significant misalignment between the axes of rotation for the entire galaxy and for the nuclear

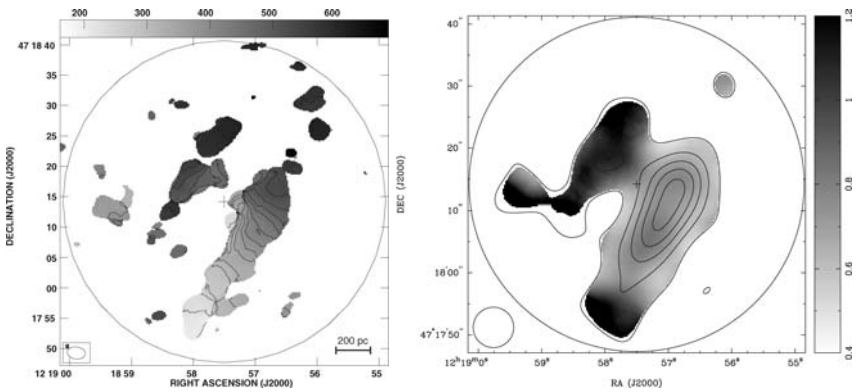

Fig. 1. *(Left:)* Isovelocity CO (2–1) map of NGC 4258. Contour levels are in 25 km s^{-1} intervals from 200 km s^{-1}. The synthesized beam size is shown at the lower left. Linear scale is shown at the lower right. *(Right:)* Line ratio map of CO(2–1)/CO(1–0) from the SMA CO (2–1) map and the BIMA CO (1–0) map with the SMA *uv*-coverage. The two maps have the same *uv*-sampling and were smoothed by a $6\farcs5 \times 6\farcs5$ beam. The smoothed beam size is shown at the lower left. Grey scale shows the line ratio of CO(2–1)/CO(1–0). Contours indicate the smoothed CO (2–1) intensity with levels of 3, 6, 9, 12 and 15σ before the primary beam correction.

B.S. Koribalski, H. Jerjen (eds.), *Galaxies in the Local Volume*,
doi: 10.1007/978-1-4020-6933-8_90,

disk. Until now, the morphological and kinematical connections between the host galaxy and the nuclear disk have not been elucidated.

Our interferometric CO (2–1) maps show two arm-like elongated components along the major axis of the galaxy, with no strong nuclear concentration. The CO (2–1) morphology and kinematics are similar to previous CO (1–0) results. The velocity field of the components agrees with the general galactic rotation, except for the east elongated component, which shows a significant velocity gradient along the east-west direction and deviate from the galactic rotation curve (Fig. 1). In order to account for the velocity field, we propose a kinematical model where the warped rotating disk is also expanding. The line ratio of CO(2–1)/CO(1–0) reveals that the eastern component with the anomalous velocity gradient appears to be warmer and denser (Fig. 2). This is consistent with the gas in this component being closer to the center, being heated by the central activities, and possibly interacted by expanding motions from the nuclear region. More detailed discussions of the modeling are described in Sawada-Satoh et al. [5].

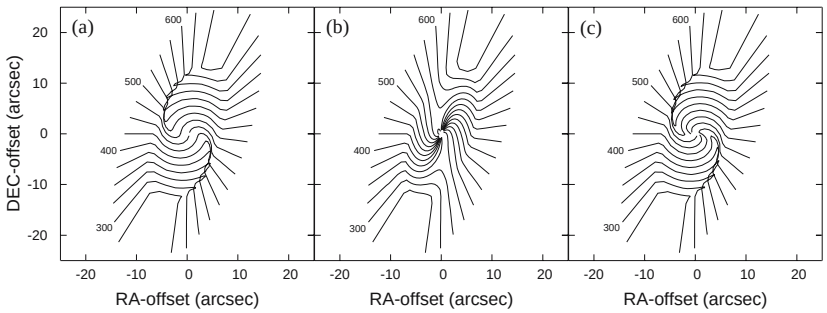

Fig. 2. Velocity fields of the rotation models featuring (a) a warped disk, (b) an expansion disk and (c) a warped expansion disk. The contour levels are in 25 km s^{-1} intervals from 200 km s^{-1}. We adopt the circular solid-body rotation with P.A. of $-20°$ for all models. The warped disk is tilted from P.A. of $90°$ to $-20°$.

References

1. Cox, P., Downes, D.: ApJ, **473**, 219 (1996)
2. Herrnstein, J.R., Moran, J. M., Greenhill, L.J., Diamond, P.J., Inoue, M., Nakai, N., Miyoshi, M., Henkel, C., Riess, A.: Nature, **400**, 539 (1999)
3. Ho, P. T. P., Moran, J. M., Lo, F.: ApJ, **616**, L1 (2004)
4. Miyoshi, M., Moran, J.M., Herrnstein J.R., Greenhill, L.J., Nakai, N., Diamond, P.J., Inoue, M.: Nature, **373**, 127 (1995)
5. Sawada-Satoh, S., Ho, P.T.P., Muller, S., Matsushita, S., Lim, J.: ApJ, **655**, 851 (2007)
6. van Albada, G. D.: A&A, **90**, 123 (1980)

Infrared Excess Emission From Asymptotic Giant Branch Stars in the Large Magellanic Cloud

Sundar Srinivasan[1], M. Meixner, U. Vijh, C. Leitherer, K. Volk, F. Markwick-Kemper, R. D. Blum, J. R. Mould, K. A. Olsen, S. Points, B. A. Whitney, M. Meade, R. Indebetouw, J. L. Hora, K. Gordon, C. Engelbracht, B. For, M. Block, and C. Misselt

[1]Johns Hopkins University, Baltimore, MD, USA, sundar@pha.jhu.edu

We present empirical relations for infrared (IR) excess emission from asymptotic giant branch (AGB) stars to the Large Magellanic Cloud (LMC) using data from the Spitzer Space Telescope SAGE (Surveying the Agents of a Galaxy's Evolution [1]) survey, combined with the 2MASS [2] survey and the optical Magellanic Cloud Photometric Survey (MCPS [4]) catalog.

The mass-loss rates of LMC extreme AGB stars correlate well with their mid-infrared excess fluxes, and with the luminosities, suggesting a corresponding relation between IR excess and luminosity in moderately obscured AGB stars. Please see [3] for more details regarding the source selection and method of calculation of excesses.

Figure 1 shows plots of excess versus luminosity for oxygen-rich, carbon-rich and extreme AGBs. The 8 μm excess in each case admits a power-law fit, as does the 24 μm plot for extreme AGBs. There is a large scatter to the relation, partly due to the fact that the variability has not been taken into account. These relations hint towards a similar rise of mass-loss rate with luminosity on the AGB.

Figure 2 shows the variation of the temperature and opacity of the circumstellar dust shells around these AGB stars. While there is no obvious trend in the O-rich and C-rich stars with excess, there is a power-law falloff for the extreme stars. The calculated optical depths for all three sources rise with excess. Both these results are consistent with increasing mass-loss rates resulting in progressively higher obscuration of the central source.

B.S. Koribalski, H. Jerjen (eds.), *Galaxies in the Local Volume*,
doi: 10.1007/978-1-4020-6933-8_91,

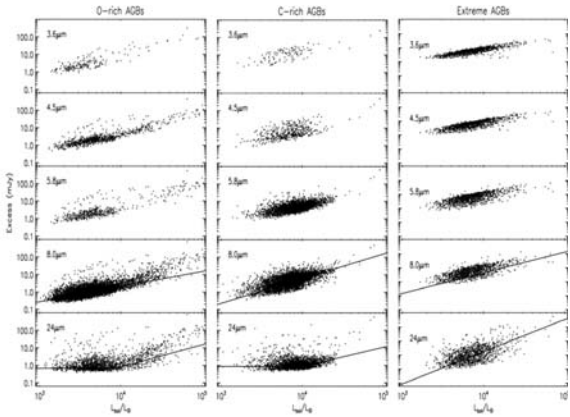

Fig. 1. The variation of excess with luminosity for O-rich, C-rich and extreme AGB stars in the LMC. See text and [3] for discussion.

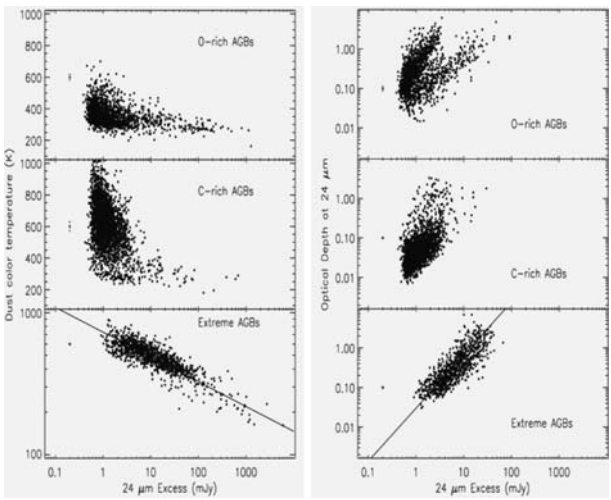

Fig. 2. Dust temperature and opacity versus excess for O-rich, C-rich and extreme AGB stars in the LMC. See text and [3] for discussion.

References

1. Meixner, M. et al.: AJ **132**, 2268 (2006)
2. Skrutskie, M. F. et al.: AJ **131**, 1163 (2006)
3. Srinivasan, S. et al.: in preparation
4. Zaritsky, D., Harris, J., & Thompson, I.: AJ **114**, 1002 (1997)

The Origin of the Giant Stellar Stream of M 31

Mikito Tanaka[1], M. Chiba, Y. Komiyama, M. Iye, and P. Guhathakurta

National Astronomical Observatory of Japan, 2-21-1 Osawa, Mitaka, Tokyo 181-8588, Japan miki@optik.mtk.nao.ac.jp

We have carried out wide-field imaging of the giant stream in the Andromeda galaxy using the Subaru/Suprime-Cam. Although it was with slightly higher seeing than $1''$, 50% completeness was reached at $V \geq 25.70$ and $I \geq 24.85$. We observed two stream fields located at $2.^\circ4$ ($\sim$34 kpc) from the M 31 center. Figure 1 shows the color-magnitude diagrams (CMDs) for the giant stream and for the control field. The stream's CMDs clearly present the broad red giant branch (RGB), suggesting that this feature is the wide spread of metal abundance and the existence of metal-rich populations [7, 4, 8]. Detecting the tip of the RGB from I-band luminosity functions using a Sobel filter algorithm, we have found that the distance to our observed stream fields is slightly larger ($\sim$850 kpc) than that of M 31's main body (770 kpc) [5].

We have estimated statistically significant metallicity distributions (MDs) of the giant stream, by comparing more than 6000 RGB stars in each field with the RGB templates of Galactic globular clusters [1]. Both MDs of the two fields have the same features which are the peak metallicity of $[\mathrm{Fe/H}]_{\mathrm{peak}} \sim -0.3$, the average metallicity of $[\mathrm{Fe/H}]_{\mathrm{ave}} = -0.54 \pm 0.48$ and the median metallicity of $[\mathrm{Fe/H}]_{\mathrm{med}} = -0.5 \pm 0.2$. The average metallicity is in excellent agreement with that of kinematically selected RGB stars in the same stream field [6].

As well as the stream's features based on the RGB morphology, we have also detected the AGB bump and RC features, which enable us to estimate. We convolved the MDs of the stream with the theoretical models for the AGB bump and RC magnitudes, which are dependent on both age and metallicity, to estimate a mean age of stellar population. And, we found it of $9.6^{+2.4}_{-5.5}$ Gyr for the stream's stars. The mean age derived from only the RC magnitude is consistent with one derived by Brown et al. [2], however, the AGB bump magnitude indicates slightly younger ages, although the age estimation based on the AGB bump is rather susceptive to both the accurate determination of the AGB bump magnitude and the assumption for $[\alpha/\mathrm{Fe}]$ ratios. We note that the presence of the AGB bump feature indicates the existence of young and metal-rich populations in the giant stream; Rejkuba et al. [9] notified that in the models with ages $\gtrsim 10$ Gyr there are hardly more AGB bump stars than the RC or horizontal-branch stars and that in metal-poor ($[\mathrm{M/H}] < -1$ dex)

B.S. Koribalski, H. Jerjen (eds.), *Galaxies in the Local Volume*,
doi: 10.1007/978-1-4020-6933-8_92,

and old (age > 9 Gyr) models the AGB bump is not subsistent at all. It's also noted that this detection of the AGB bump feature suggests the existence of young and metal-rich populations in the stream. This fact may be associated with the result of Brown et al. [2] (their Figure 17b), indicating a second major starburst event that may have happened ~ 5.5 Gyr ago. This age is basically consistent with the younge age indicated from the AGB bump magnitudes, although it is difficult to precisely determine the metallicity distribution of such young AGB populations from our present data.

The total mass of the stellar system predicted for the original galaxy of the giant stream can be assessed from the average metal abundance of stars in the stream ($[\mathrm{Fe/H}]_{\mathrm{ave}} = -0.54$) in combination with the metallicity-luminosity relation for Local Group dwarfs [3]. The relationship presents, on average, more metal-rich populations in more luminous galaxies, and we found $M_{\mathrm{stars}} \sim 10^8$ $\mathrm{M}_\odot$ for the original galaxy assuming that the mass-to-light ratio is $M/L \sim 4$. Such a dwarf galaxy may have been accreted to the Andromeda galactic halo at recent epochs, possibly within some billion years, considering it leaves yet a conspicuous giant stream like the Sgr stream in the Milky Way.

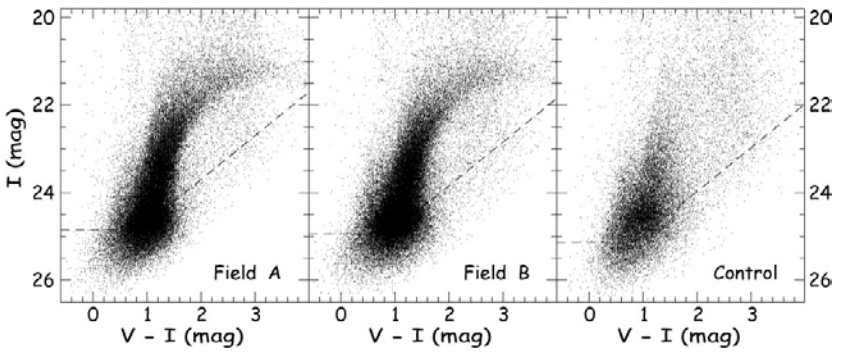

Fig. 1. CMDs for the giant stream (Field A and B) and for the control field. The dashed line in each diagram shows the 50% completeness limit.

References

1. Bellazzini, M., et al. 2003, A&A, 405, 867
2. Brown, T. M., et al. 2006, ApJ, 652, 323
3. Côté, P., et al. 2000, ApJ, 533, 869
4. Ferguson, A. M. N., et al. 2002, AJ, 124, 1452
5. Freedman, W. L., & Madore, B. F. 1990, ApJ, 365, 186
6. Guhathakurta, P., et al. 2006, AJ, 131, 2497
7. Ibata, R. A., et al. 2001, Nature, 412, 49
8. McConnachie, A. W., et al. 2003, MNRAS, 343, 1335
9. Rejkuba, M., et al. 2005, ApJ, 631, 262

SkyMapper and the Southern Sky Survey*

Patrick Tisserand, S. Keller, B. Schmidt, and M. Bessell

Research School of Astronomy and Astrophysics, Australian National University, Mt Stromlo Observatory, Cotter Road, Weston, ACT 2611, Australia
tisserand@mso.anu.edu.au

1 SkyMapper telescope

The SkyMapper telescope, currently under construction by RSAA (ANU), is a new wide-field survey facility in Australia. The 1.35m robotic telescope will be equipped with a Cassegrain Imager camera featuring a fast-readout, low-noise 268 million pixel mosaic (32 E2V CCD, 2048x4096 pixels) that provides a 5.7 square degree field of view. The CCDs have excellent quantum efficiency from 300nm-950nm, near perfect cosmetics, and low-read noise, making them well suited for an all-sky ultraviolet through near-IR Southern Sky Survey.

The construction work at Siding Spring Observatory has started in May 2007. The pier is currently set and the dome mounted (see Fig. 1). The first light of the telescope took place during the time of the conference (July 2007) in Arizona. Regular operation and the start of the Southern Sky Survey is expected at the beginning of 2008.

2 Southern Sky Survey

The main program of the SkyMapper telescope will be to survey the entire southern sky ($2\,\pi$ steradian), in 6 filters (uvgriz) and 6 epochs over the next five years (see [1] for more details). Stellar and galaxy photometry is expected to reach a global accuracy of 3% and astrometry will be better than 50 mas. With the combination of 6 epochs, each 110 sec integration time, the photometric catalog will be between 0.4 and 1 magnitude deeper that SDSS (see Table 1). The catalogue of $\approx$1 billion objects together with the CCD images will be made available to the astronomical community in two releases. The first is expected around 2010.

Seven key projects have been defined that will be carried out as part of the survey. Among others we will probe the epoch of reionization using bright,

* http://www.mso.anu.edu.au/skymapper

B.S. Koribalski, H. Jerjen (eds.), *Galaxies in the Local Volume*,
doi: 10.1007/978-1-4020-6933-8_93,

Table 1. Expected Survey Depth (1.5″ median seeing)

	u	Vs	g	r	i	z
1 epoch	21.5	21.3	21.9	21.6	21	20.6
6 epochs	22.9	22.7	22.9	22.6	22	21.5
SDSS	22.0	n/a	22.2	22.2	21.3	20.5

high redshift QSOs ($z > 5.8$), study the distribution of large solar system objects beyond Neptune's orbit, search for extremely metal poor stars and put constrains on the shape and size of the galactic dark matter halo. Other non-survey programs are planed to use the SkyMapper camera. Their main objectives are planet transits, nearby Supernovae, the faint end of the galaxy luminosity function. The Stromlo Missing Satellites Survey is another large program that will extensively use the Southern Sky Survey data. It has been designed to carry out the deepest, most extended search for the missing Milky Way satellites (see Jerjen, this volume).

Fig. 1. Image of the SkyMapper telescope and the recent work sites achieved, look at `http://www.mso.anu.edu.au/public/skymapcam.php` for a live view.

References

1. S. C. Keller, B. P. Schmidt, M. S. Bessell et al: PASA, 24, 1 (2007)

NIBLES: an HI Census of Local SDSS Galaxies

Wim van Driel[1], S. Schneider[2], M. Lehnert[1], and the NIBLES Consortium

[1] Observatoire de Paris, GEPI, 92195 Meudon, France wim.vandriel@obspm.fr
[2] Univ. of Massachusetts, Astronomy Program, Amherst, MA 01003, USA

NIBLES (Nançay Interstellar Baryons Legacy Extragalactic Survey) is a Key Project proposed for the 100m-class Nançay Radio Telescope (NRT) in France. Its aim is a census of the H I gas content and dynamics of 4,000 Sloan Digital Sky Survey galaxies in the Local Volume ($900 < cz < 12,000$ km/s). The galaxies were selected based on their total stellar mass (absolute z-band magnitude M_z), and are distributed evenly over the entire range of M_z covered by local SDSS galaxies (–10 to –24 mag, for $H_0 = 70$ km s^{-1} Mpc^{-1}). A related survey, TICLES, was proposed for CO(1–0) line observations at the IRAM 30m. An NRT pilot survey is being made of over 600 galaxies. NIBLES will be complementary to the ALFALFA and EBHIS blind H I surveys, which will detect a different ensemble of local galaxies, and which our pilot survey results indicate will detect ∼40–45% of the NIBLES sample. NIBLES is an open collaboration and anyone interested in the science and willing to contribute to the project is welcome to join the score of NIBLErS.

The science goals of this project are:

- Provide a complete and statistically robust analysis of the density of baryons in the local Universe, and determine the phase in which these baryons reside. That is, determine the co-moving space density of H_2, H I, stellar mass, and dynamical mass;
- Determine the H I mass function and the CO luminosity function and the joint probability distribution of H I mass/CO luminosity and other galaxy characteristics (i.e., infrared luminosity, morphological type, stellar mass, stellar age, etc.);
- Determine the H I/CO gas content and fraction as a function of total stellar mass (fit from the optical/near-infrared spectral energy distribution and M/L$_z$), dynamical mass (estimated from H I and CO line widths), morphological type, and average stellar density;

B.S. Koribalski, H. Jerjen (eds.), *Galaxies in the Local Volume*,
doi: 10.1007/978-1-4020-6933-8_94,

- Determine the systematic relationships and variability between dynamical, stellar, and gas masses (e.g., do the estimated dynamical masses change in proportion to total baryonic mass?);
- Compare galactic gas fractions and metallicity, to determine the effective yields of the largest sample of galaxies available and to allow for the most detailed comparison with theoretical models of the evolution of galaxies. This will enable us to determine the relative influence of outflows and infall on the evolution of galaxies. We will use metallicities determined from the SDSS data and compare them with the overall gas fractions to determine the effective yields as a function of galaxy type, dynamical and stellar masses, and stellar mass surface densities. Comparing these results with chemical evolution models will provide a robust test of our understanding of gas recycling yet performed.

The H I data that are presently available in the literature are largely insufficient for our proposed studies; of the 4000 galaxies in the NIBLES sample, only 13% have published H I data, half of which concern only the gas-rich spiral galaxies in the highest luminosity range ($-20.5 < M_z < -23.5$). Also the data that will ultimately be provided by the Arecibo ALFALFA and Effelsberg EBHIS blind surveys will not be sufficient; our ongoing NRT pilot survey indicates that they will detect 40–45% of the NIBLES sample.

NIBLES selection criteria are: (1) high quality SDSS magnitudes, and high quality SDSS optical spectra, (2) within the Local Volume (recession velocity of $900 < cz < 12,000$ km/s), (3) sampling of each 0.5 magnitude wide bin in M_z, with a maximum of 200 galaxies for the most populated bins, and of all galaxies (minimum 20) for the poorer bins, (4) focus on the most nearby objects in each M_z bin, as these will have the highest H I flux densities.

Pilot surveys: in 2007 we obtained 500 hours of telecope time at Nançay for NIBLES pilot surveys. To date, 340 galaxies have been observed for 30 minutes (half the intended average time per object in NIBLES). The data have a typical rms noise level of 3.5 mJy at a 10 km/s velocity resolution, comparable to the point source detection sensitivity of the blind ALFALFA and EBHIS surveys. The overall detection rate is 66%, and similar over the entire 12 magnitude range in M_z. We estimate that ∼40–45% of the NIBLES sample galaxies would be detectable by ALFALFA or EBHIS, based on the sensitivities of these surveys and our detected H I fluxes.

This shows that NIBLES, which will on average have a two times longer integration time than the NRT pilot surveys, will provide a unique H I census of optically selected Local Volume galaxies. NIBLES will be complementary to the ALFALFA and EBHIS blind H I surveys of galaxies in the Local Volume. In general, blind H I surveys provide a basis for determining whether there are classes of galaxies being missed in an optically selected sample, such as gas-rich Low Surface Brightness objects, but the NRT data will be better for detailed studies of the properties of the SDSS galaxies themselves.

Fabry-Pérot Interferometry of Nearby Irregular Dwarf Galaxies

Janine van Eymeren[1], Michel Marcelin[2], and Dominik J. Bomans[1]

[1] Astronomisches Institut der Ruhr-Universität Bochum, Universitätsstrasse 150, 44780 Bochum, Germany jeymeren@astro.rub.de
[2] Observatoire Astronomique de Marseille-Provence, 2, Place Le Verrier, 13248 Marseille Cedex 04, France michel.marcelin@oamp.fr

Summary. Fabry-Pérot (FP) interferometry centred on the Hα line was performed to analyse the kinematics of the most prominent ionised gas structures in a sample of nearby irregular dwarf galaxies. The complete spatial coverage of the galaxy in one exposure enables us to follow already known expanding gas structures further out than before. Additionally, we use these 3d images to determine the velocities of structures which could not be kinematically analysed, yet. We here present as an example our results of NGC 2366.

1 Introduction

Irregular dwarf galaxies can be the sites of giant star formation regions. Photoionisation and shocks that are produced by stellar winds and supernova explosions lead to numerous ionised structures in and around the galactic plane of these galaxies. Many of them have already been detected by e.g., [1]. However, ionised gas also exists at kpc distances away from any place of current star formation [3]. In this case, the excitation mechanisms are not obvious. Additionally, it is not clear whether these gaseous features stay gravitationally bound to their host galaxy or whether they can leave the gravitational potential into the intergalactic medium.

2 Observations and Data Reduction

FP interferometry centred on the Hα line was performed with the 1.93m telescope at the OHP, France. We used the Marseille's scanning FP and a photon counting camera with a field of view of $5.5' \times 5.5'$. The scanning was done in steps of 15 km/s, the spatial resolution is about $0.68''$. We reduced the data using the software ADHOCw by Jacques Boulesteix (CNRS, Marseille).

All velocities were measured manually, using a Gaussian fitting routine and only considering detections above a $3\,\sigma$ limit. At several places, the Hα emission is split into two to three components. The FP velocity map in Figure 1, right panel only contains the velocities of the strongest component.

B.S. Koribalski, H. Jerjen (eds.), *Galaxies in the Local Volume*,
doi: 10.1007/978-1-4020-6933-8_95,

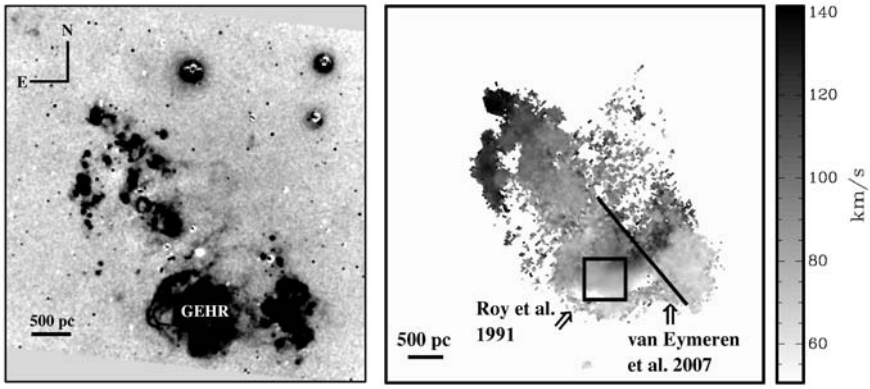

Fig. 1. *(Left:)* Continuum-subtracted Hα image of the dwarf galaxy NGC 2366. *(Right:)* FP velocity map. The observations of [2] and [4] are marked in black.

3 First Results

Figure 1 shows the continuum-subtracted Hα image (left panel) and the FP velocity map of NGC 2366 (right panel). The velocity gradient from the south-west to the north-east indicates the rotation of the galaxy. The most prominent feature is the huge outflow to the north-west of the Giant Extragalactic H II Region (GEHR), which has been detected before by [4] also using a FP and by [2] performing long-slit echelle spectroscopy. We estimate a total length of 1.4 kpc, which is two times larger than thought by [2] and even four times larger than measured by [4]. This length makes it one of the largest outflows ever detected in dwarf galaxies. The gas expands with a moderate velocity of 35 km/s in comparison to its surroundings, which is in good agreement with the detections of [2] and [4]. Additionally, we found several small H II regions at kpc-distance from the galactic disk, especially the one south of the GEHR. The large western H II region follows the overall velocity gradient, which means that it is not a satellite galaxy interacting with NGC 2366 as thought before.

References

1. Bomans, D. J. et al. 1997, AJ, **113**, 1678
2. van Eymeren, J. et al. 2007, A&A, in press
3. Hunter, D. A. et al. 1993, AJ, **106**, 1797
4. Roy, J. et al. 1991, ApJ, **367**, 141

Astronomers! Do You Know Where Your Galaxies are?

Matthew T. Whiting

Australia Telescope National Facility, PO Box 76, Epping NSW, 1710, Australia
Matthew.Whiting@csiro.au

We present the *Duchamp* source finding software package, designed to detect objects in spectral-line data cubes. It makes use of innovative searching and noise-reduction techniques. *Duchamp* is available for download from http://www.atnf.csiro.au/people/Matthew.Whiting/Duchamp.

1 Large-scale surveys: finding the sources

Large-scale spectral-line radio surveys, particularly those using the H I transition, are an effective means of studying the populations of galaxies in the local Universe. Surveying on a large scale allows one to both probe to the fainter flux levels and remain sensitive to the rare but interesting objects at the brightest fluxes.

Effective use of large-scale surveys is dictated by the efficiency of detection of the objects of interest. Finding the extreme bright objects is often the easy part – to find the more typical sources you need to push down to fainter fluxes close to the noise level. The complexity and volume of three-dimensional survey data also requires a large degree of automation and reliability to find the desired sources quickly and in a uniform way.

We present the *Duchamp* source finder as a solution to these problems. It is a stand-along software package, designed to detect objects in three-dimensional, specifically spectral-line, FITS data cubes, and produce source lists and graphical results showing the detected objects (see Fig. 1). It is optimised for the case of a large number of separated sources embedded in a cube dominated by noise: the typical situation expected for extra-galactic H I surveys.

2 Innovations in searching

A key aspect of source detection is the application of a threshold. This is calculated by using either a simple n-sigma cutoff, or derived through the use

B.S. Koribalski, H. Jerjen (eds.), *Galaxies in the Local Volume*,
doi: 10.1007/978-1-4020-6933-8_96,

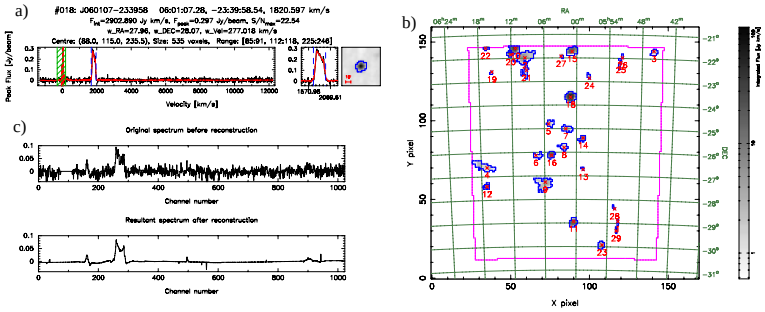

Fig. 1. a) The spectral output of a source detected by *Duchamp*. **b)** The 0th moment map showing all sources detected in a cube. **c)** An example of *à trous* reconstruction on a 1D spectrum.

of the False Discovery Rate method [1], which controls the number of false detections. The statistics for the threshold calculations are obtained through robust methods, and can be measured from the full cube or a specified subset.

Searching in 3D is in general a complex problem. *Duchamp* approaches this by searching in each 2D channel map separately, using the technique of [2], and comparing detections made in one channel with those in neighbouring channels. An efficient merging algorithm then merges the 2D detections to form 3D objects.

3 Beating the noise

The limiting factor in detecting faint objects is the background noise, and *Duchamp* provides ways to minimise its effects. Simple smoothing before searching is possible, either spectrally using a Hanning filter, or spatially using a 2D Gaussian kernel.

Alternatively, the cube can be reconstructed using the *à trous* wavelet technique [3]. This filters the cube at a range of scales, thresholding each scale and only keeping those pixels with significant signal. This very effectively removes noise from the cube, allowing searching to be done on much cleaner data (see Fig. 1). The reconstruction can be done either one-dimensionally (on each individual spectrum separately), or three-dimensionally, which gives a better reconstruction at the expense of greater computational overheads.

References

1. C. J. Miller et al: AJ **122**, 3492 (2001)
2. R. K. Lutz: The Computer Journal **23**, 262 (1980)
3. J. Starck, R. Siebenmorgen & R. Gredel: ApJ **482**, 1011 (1997)

The Effelsberg–Bonn H I Survey (EBHIS)

Benjamin Winkel[1,2], J. Kerp[2], P. Kalberla[2], and R. Keller[1]

[1] Max-Planck-Institut für Radioastronomie, International Max Planck Research School (IMPRS) for Radio and Infrared Astronomy at the Universities of Bonn and Cologne, Auf dem Hügel 69, 53121 Bonn, Germany
bwinkel@astro.uni-bonn.de
[2] Argelander-Institut für Astronomie, Auf dem Hügel 71, 53121 Bonn, Germany

The new L-band (20-cm) 7-feed-array at the 100-m telescope in Effelsberg will be used to perform an unbiased fully sampled H I survey of the entire northern hemisphere observing the galactic and extragalactic sky using simultaneously two different backends. The integration time per position will be 10 min towards the SDSS area and 2 min for the remaining sky, thereby achieving a sensitivity competitive with the Arecibo ALFALFA and GALFA surveys but covering a much larger area of the sky.

Both backends are FPGA-based digital fast fourier transform (DFFT) spectrometers, offering a superior dynamic range and temporal resolution. The latter is crucial for a sophisticated RFI mitigation scheme (Winkel et al. [5]) but produces huge amounts of data over the projected five years of observing. Consequently, we put considerable effort into efficient data reduction. Table 1 compares the survey parameters with several recent H I surveys.

The data processing is organized making use of individual data reduction modules. Each module calculates correction factors/spectra that are stored in a database. A special merger module is used to apply all corrections to the data before the gridder produces a final data cube. The advantage of this approach is the flexibility to modify individual modules without having to recompute all corrections.

Most of the reduction modules are ready-for-use. Winkel et al. [5] describe a very sensitive RFI detection scheme, utilizing the high temporal resolution spectra from the DFFT spectrometers. The stray-radiation correction is performed using the method of Kalberla et al. [4] . Their approach enables stray radiation correction even within the regime of the high velocity clouds. We also implemented and improved (see Winkel & Kerp [6]) the recently proposed least-squares frequency switching (LSFS) method of Heiles [3]. Using more than two different intermediate frequency settings, one is able to calculate the baseline even for faintest H I emission with unprecedented quality. Finally, we developed a graphical user interface (GUI) optimized for the search and parametrization of galaxies in the H I data cubes. We implemented a very

B.S. Koribalski, H. Jerjen (eds.), *Galaxies in the Local Volume*,
doi: 10.1007/978-1-4020-6933-8_97,

Table 1. Parameters of several recent H I surveys in compared to EBHIS.

Survey	Telescope	Type	Status	Area (sq.deg.)	Beam size (arcmin)	$z_{\max}$	Δv (km/s)
LAB	Dwing/Arg	g	Completed	41 300	36		1.3
HIPASS	Parkes	e	Completed	29 300	14.1	0.05	18
GASS		g	Ongoing	20 600			0.8
ALFALFA	Arecibo	e	Ongoing	7 100	3.4	0.06	11
GALFA		g	Ongoing				0.7
EBHISe	Effelsberg	e	Planned	20 600 (8 500*)	9	0.07	7
EBHISg		g	Planned				1

Survey	RMS noise (mJy/Beam)	$N_{\rm HI}$ limit (10^{18} cm^{-2})	Mass limit (10^7 M$_\odot$)	Velocities (km/s)	Integr. time per beam (s)
LAB	620	3.3		− 450 . . . 400	
HIPASS	13		8.7	−1 280 . . . 12 700	450
GASS	95	2.6		− 400 . . . 450	90
ALFALFA	1.6		0.8	−2 000 . . . 18 000	28
GALFA	13.2	3.2		− 700 . . . 700	18
EBHISe	4.5 (2*)		1.9 (0.8*)	−2 000 . . . 18 000	120(600*)
EBHISg	12 (5.5*)	0.9 (0.4*)		− 500 . . . 500	

*Towards the SDSS area EBHIS has higher sensitivity.

promising finder algorithm based on the Gamma test (Boyce [1]). The GUI is designed to allow a fast working flow and is able to compute statistical errors using Markov chain Monte Carlo methods.

EBHIS will be extremely valuable for a broad range of research topics: study of the low-mass end of the H I mass function (HIMF) in the local volume, environmental and evolutionary effects (as seen in the HIMF), the search for galaxies near low-redshift Lyman-alpha absorbers, and analysis of multiphase and extraplanar gas, H I shells, and ultra-compact high velocity clouds (Brüns & Westmeier [2]).

References

1. P. Boyce: GammaFinder: a java application to find galaxies in astronomical spectral line data cubes. MA Thesis, Cardiff University, Cardiff (2003)
2. C. Brüns and T. Westmeier: A&A **426**, L9 (2004)
3. C. Heiles: to appear in PASP (2007)
4. P.M.W. Kalberla, W.B. Burton, D. Hartmann et al: A&A, **440**, 775 (2005)
5. B. Winkel, J. Kerp, and S. Stanko: Astronomische Nachrichten **328**, 68 (2007)
6. B. Winkel and J. Kerp: to appear in ApJ (2007)

Near-Infrared Properties of NOIRCAT

O. Ivy Wong[1,2], Rachel L. Webster[1], Meryl Waugh[1], Virginia A. Kilborn[3], and Lister Staveley-Smith[4]

[1] School of Physics, University of Melbourne, VIC 3010, Australia
iwong@ph.unimelb.edu.au
[2] Australia Telescope National Facility, CSIRO, PO Box 76, Epping, NSW 1710, Australia
[3] Swinburne University of Technology, PO Box 218, Hawthorn, VIC 3122, Australia
[4] School of Physics, University of Western Australia, 35 Stirling Hwy, Crawley, WA 6009, Australia

1 Introduction

The Northern HIPASS Optical/Infrared Catalogue (NOIRCAT) consists of optical/near-infrared identification of the sources found in the Northern HIPASS catalogue, NHICAT [1]. NHICAT and NOIRCAT have sampled the entire region of sky between the declinations of $+2°$ and $+25.5°$. Of the 1002 sources in NHICAT, 655 have previously-observed optical counterparts with matching optical velocities. Here, we present the optical/near-infrared properties of these matches.

2 Properties of NOIRCAT

Of the 655 NOIRCAT sources with optical counterpart matches, we examine the properties of the 414 matches which correspond to matches to single optical galaxies with 2MASS observations. In general, we found that galaxies with greater H I masses corresponded to redder $J - K$ magnitudes. The left panel in Figure 1 shows the relationship between the H I mass and the 2MASS $J - K$ colours of our sample. We attribute the scatter of this relation to the uncertainties related to the 2MASS automated processing pipeline.

The observed NIR colour-colour distribution of normal galaxies with nuclei dominated by older stellar population spans a very narrow window for optically-selected samples of galaxies. The NIR colour-colour distribution of our sample is plotted in grey in the right panel of Figure 1. The observed scatter in our data can be explained using a model by Geller et al. [2]. Their model explained that: i) dust extinction reddens the intrinsic colours of the galaxies, ii) emission from bursts of star formation shifts the NIR colour blueward,

B.S. Koribalski, H. Jerjen (eds.), *Galaxies in the Local Volume*,
doi: 10.1007/978-1-4020-6933-8_98,

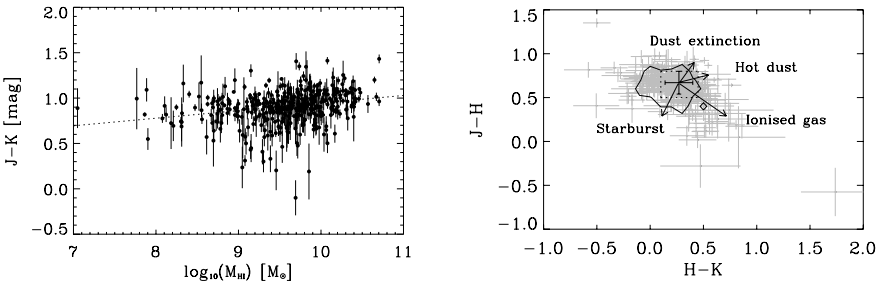

Fig. 1. *(Left:)* $J-K$ colour as a function of the H I mass. The dotted line shows the linear fit to the data. *(Right:)* $J-H$ versus $H-K$ colour-colour diagram. The black contour provides the 1-σ contour of the two-dimensional NIR colour distribution of our sample. The black cross marks the normal range of the NIR colours (indicated by the error bars) for galaxies with older stellar population dominated nuclei. The black arrows indicate the shift in direction of a galaxy's NIR colours due to factors such as starbursts, gaseous emission from ionised regions, thermal re-radiation of hot dust and dust reddening [2].

iii) re-radiation of hot dust reddens the NIR colours (particularly $H-K$), and iv) the emission from ionised gas regions shifts the $J-K$ colours blueward and the $H-K$ colours redward. These effects are summed up by the vector arrows shown in Figure 1 (right panel) extending away from the median NIR colour of normal field galaxies.

The general distribution of our sample is more widespread as 35% of our sample lies beyond the region bounded by the dotted lines in Figure 1 (right panel). We observe a significant number of galaxies exhibiting the effects of gaseous ionised regions which are under-sampled by previous optically-based surveys. Our 1-σ contour also suggests that a significant proportion (15%) of our sample is experiencing the effects of star formation.

3 Summary

A thorough description and analysis of NOIRCAT can be found in Wong et al. [3]. This catalogue will be submitted to the NASA/IPAC Extragalactic Database and will also be made publicly-available online at `http://hipass.aus-vo.org`.

References

1. O.I. Wong, E.V. Ryan-Weber et al: MNRAS **371**, 1855 (2006)
2. M.J. Geller, S.J. Kenyon, E.J. Barton et al.: AJ **132**, 2243 (2006)
3. O.I. Wong, R.L. Webster, M. Waugh et al.: *in preparation* (2007)

Galaxy Transformation in Action! The Spiral Galaxy WKK 6176

Patrick A. Woudt[1], Renée C. Kraan-Korteweg[1], Uta Fritze-von Alvensleben[2], and John Lucey[3]

[1] Department of Astronomy, University of Cape Town, Private Bag X3, Rondebosch 7700, South Africa Patrick.Woudt@uct.ac.za
[2] Centre for Astrophysics Research, University of Hertfordshire, College Lane, Hatfield AL10 9AB, UK
[3] Department of Physics, University of Durham, Durham DH1 3LE, UK

1 WKK 6176

Recently, the presence of a 70-kpc long X-ray tail and a 40-kpc Hα tail, respectively, was reported [5, 6] in WKK 6176, a spiral galaxy in the nearby ($cz = 4871 \pm 54$ km/s) and massive ($M_{R<2\,\mathrm{Mpc}} = 1 \times 10^{15}$ M$_\odot$) Norma cluster [7]. This galaxy is the low-redshift equivalent of the two recently detected spiral galaxies in massive rich clusters (Abell 2667 and Abell 1689) at $z \sim 0.2$ which show clear evidence for strong galaxy transformation [3].

The X-ray tail of WKK 6176 is aligned with the major axis of the galaxy-density profile of the cluster which is indicated by the diagonal line in the right panel of Fig. 1, which itself is aligned with the main large-scale structure of the Norma wall [7]. Figure 1 shows our deep R_C image of WKK 6176 before and after star-subtraction; it demonstrates the effectiveness of the star-subtraction. Numerous low-luminosity filaments and bright knots (not foreground stars) stand out, giving the galaxy its 'jelly-fish' appearance.

2 Galaxy transformation in dense environments

Given the proximity of the Norma cluster, WKK 6176 provides an excellent opportunity to study the interaction of a galaxy with the intracluster medium (ICM) at high resolution and sensitivity. Deep BVR_CJHK_s photometry of WKK 6176 (already obtained) will be used to generate pixel-by-pixel colour-magnitude diagrams and colour-colour diagrams [4] and to study the star formation history of WKK 6176 in detail in combination with GALEV [1].

The GALEV models now include an ever growing grid of refined models of undisturbed Sa, Sb, Sc and Sd galaxies falling into a cluster environment at a wide range of redshifts and experiencing various effects on their star formation

B.S. Koribalski, H. Jerjen (eds.), *Galaxies in the Local Volume*,
doi: 10.1007/978-1-4020-6933-8_99,

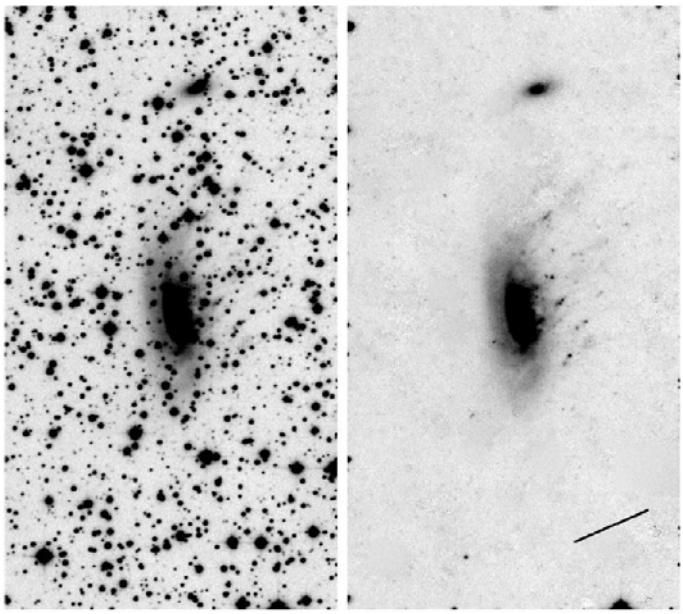

Fig. 1. A deep R_C image of WKK 6176 ($2.2' \times 4.0' = 43\text{kpc} \times 77$ kpc). The *left image* shows the original data, the *right image* shows WKK 6176 after star subtraction using the KILLALL routine [2]. Low surface brightness filaments and bright knots are clearly visible.

rates (e.g., starbursts at various strengths and with various time scales). For all those models, the evolution of the galaxies' spectra (ultraviolet, optical and near-infrared) and broad band spectral energy distribution is determined.

WKK 6176 is the nearest galaxy observed in a state of strong transformation through visible interactions with the ICM of a rich and massive cluster. Based on our multiwavelength observations and a comparison with galaxy evolution synthesis models, we aim to constrain the recent star formation history of this galaxy.

References

1. Bicker J., Fritze-v. Alvensleben U., Möller C.S., Fricke K.J.: A&A 413, 37 (2004)
2. Buta R., McCall M.: ApJS 124, 33 (1999)
3. Cortese L., Marcillac D., Richard J. et al.: MNRAS 367, 157 (2007)
4. de Grijs R., Lee J.T., Mora Herrera M. et al.: New Aastronomy 8, 155 (2003)
5. Sun M., Jones C., Forman W. et al.: ApJ 637, L81 (2006)
6. Sun M., Donahue M., Voit G.M.: arXiv:0706.1220 (2007)
7. Woudt P.A., Kraan-Korteweg R.C., Lucey J., Moore S.A.W.: MNRAS, submitted, arXiv:0706.2227 (2007)

Early-Type Galaxies at z < 0.2 Seen with GALEX

Suk-Jin Yoon, Hyun-Jin Bae, Kiyun Yun, Yumi Choi, Seok-Joo Joo, Hong-Gyun Woo, and Mihwa Han

Department of Astronomy, Yonsei University, Seoul 134, Korea
sjyoon@galaxy.yonsei.ac.kr

GALEX is performing the first massive survey of the UV properties of galaxies beyond the Local Group. New GALEX observations have revealed enhanced UV fluxes from an unexpectedly large fraction of SDSS early-type galaxies in the local ($0.05 < z < 0.2$) universe [1, 2]. This is taken as evidence for the presence of recent star formation (RSF) activities [3, 4]. Here we have identified two distinct types of RSF (i.e., UV-strong) galaxies. The first type (RSF I) is characterized by relatively strong Hα emission with no RSF signature in visual band. Analyses indicate that RSF I is a mode in which weak SF is present on an extended disk (i.e., increasing R_0 and μ_0). The second type (RSF II), on the other hand, show strong indications of the presence of an A-type population in UV and visual bands, but no emission lines. This type may have undergone weak, short-burst SF, and is first referred to "E+a" in comparison to "E+A" galaxies. [The color version of the article is available at http://csaweb.yonsei.ac.kr/∼sjyoon/LocalVolume/.]

Table 1. GALEX detections of different SF modes in early-type galaxies

RSF mode	Optical color	Emission lines	UV-opt color	Objects	Temporal & spatial type
Quiescent mode	Red	X (Hα<3 Å)	Red	QST	
Ongoing weak SF	Red	Weak	Blue	RSF I	Continuous / disk-like
Post weak SF	Blue or Red	X	Blue	RSF II "E+a"	Short / concentrated
Ongoing starburst	Very blue	Very strong	Very blue	Strong-Hα	
Post-starburst	Very blue	X	Very blue	"E+A"	Short / concentrated

B.S. Koribalski, H. Jerjen (eds.), *Galaxies in the Local Volume*,
doi: 10.1007/978-1-4020-6933-8_100,

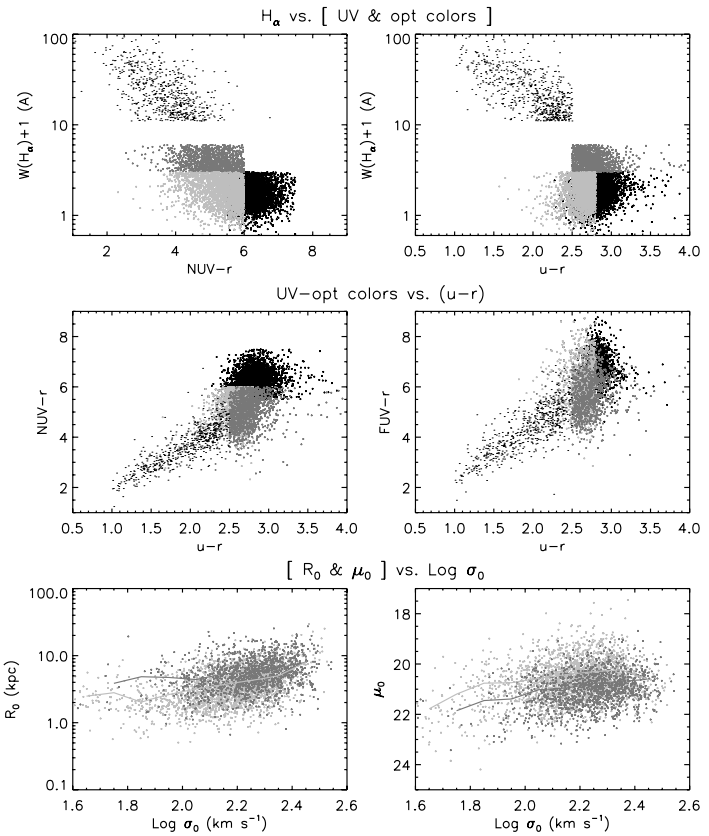

Fig. 1. *(Top:)* Selection of QST (black), RSF I (dark grey), RSF II (light grey), and SHa (small black) galaxies based on (NUV-r) and (u-r) colors and Hα emission strengths. *(Middle:)* Distribution of QST, RSF I & II, and SHa galaxies on the UV-optical colors vs. (u-r) planes. *(Bottom:)* Correlation of effective radius (R_0) and brightness (μ_0) of RSF I & II as functions of their central velocity dispersion (σ_0).

References

1. Yoon, S.-J., Yi, S., Kaviraj, S., Khochfar, S., et al. BAAS, **205**, 25.08 (2004)
2. Yi, S. K., Yoon, S.-J., Kaviraj, S., Deharveng, J.-M., Rich, R. M., et al. ApJ, **619**, L111 (2005)
3. Kaviraj, S., Schawinski, K., Devriendt, J. E. G., Khochfar, S., Yoon, S.-J., et al. ApJ Suppl., *in press* (arXiv:astro-ph/0601029)
4. Schawinski, K, Kaviraj, S., Khochfar, S., Yoon, S.-J., Yi, S. K., et al. ApJ Suppl., *in press* (arXiv:astro-ph/0601036)

A

List of Participants

Name	Institution and country	email
Aloisi, Alessandra	ESA / STScI, USA	*aloisi@stsci.edu*
Annibali, Francesca	STScI, USA	*annibali@stsci.edu*
Balasubramanyam, Ramesh	Raman Research Institute, India	*ramesh@rri.res.in*
Barnes, David	Swinburne University, Australia	*david.g.barnes@gmail.com*
Beaton, Rachael	University of Virginia, USA	*rlb9n@virginia.edu*
Begum, Ayesha	Institute of Astronomy, Cambridge, UK	*ayesha@ast.cam.ac.uk*
Ben Bekhti, Nadya	University of Bonn, Germany	*nbekhti@astro.uni-bonn.de*
Bekki, Kenji	University of NSW, Australia	*bekki@phys.unsw.edu.au*
Belokurov, Vasily	University of Cambridge, UK	*vasily@ast.cam.ac.uk*
Bernard, Jean-Philippe	CESR, France	*Jean-Philippe.Bernard@cesr.fr*
Besla, Gurtina	Harvard-Smithsonian CfA, USA	*gbesla@cfa.harvard.edu*
Bigiel, Frank	MPI für Astronomie, Germany	*bigiel@mpia-hd.mpg.de*
Bland-Hawthorn, Joss	AAO, Australia	*jbh@aao.gov.au*
Bolatto, Alberto	UCB, USA	*bolatto@berkeley.edu*
Bonne, Nicolas	ANU/ATNF, Australia	*nic42@mso.anu.edu.au*
Bot, Caroline	California Institute of Technology, USA	*bot@caltech.edu*
Braun, Robert	ATNF/CSIRO, Australia	*Robert.Braun@csiro.au*
Brunthaler, Andreas	MPI für Radioastronomie, Germany	*brunthal@mpifr-bonn.mpg.de*
Cannon, Russell	AAO, Australia	*rdc@aao.gov.au*
Carlson, Lynn R.	Johns Hopkins University, USA	*carlson@stsci.edu*
Chaname, Julio	STScI, USA	*jchaname@stsci.edu*
Chengalur, Jayaram	NCRA, India	*chengalu@ncra.tifr.res.in*
Chomiuk, Laura	University of Wisconsin-Madison, USA	*chomiuk@astro.wisc.edu*
Chumak, Yaroslav	Sternberg Astronomical Institute, Russia	*chyo@mail.ru*
Ciardullo, Robin	Penn State University, USA	*rbc@astro.psu.edu*
Cioni, Maria-Rosa	University of Edinburgh, UK	*mrc@roe.ac.uk*
Coleman, Matthew	MPI für Astronomie, Germany	*coleman@mpia-hd.mpg.de*
Colless, Matthew	AAO, Australia	*colless@aao.gov.au*
Conn, Blair	ESO Chile	*bconn@eso.org*
Da Costa, Gary	ANU, Australia	*gdc@mso.anu.edu.au*
Dalcanton, Julianne	University of Washington, USA	*jd@astro.washington.edu*
Dale, Danny	University of Wyoming, USA	*ddale@uwyo.edul*
Drozdovsky, Igor	IAC, Spain	*dio@iac.es*
Ekers, Ron	ATNF/CSIRO, Australia	*Ron.Ekers@csiro.au*
Feain, Ilana	ATNF/CSIRO, Australia	*Ilana.Feain@csiro.au*
Fraser, Vicki	ATNF/CSIRO, Australia	*Vicki.Fraser@csiro.au*
Fukui, Yasuo	Nagoya University, Japan	*fukui@a.phys.nagoya-u.ac.jp*
Gilbert, Karoline	University of California, USA	*kgilbert@ucolick.org*
Guhathakurta, Raja	USO/Lick Observatory, USA	*raja@ucolick.org*
Harding, Paul	Case Western Reserve University, USA	*harding@dropbear.cwru.edu*

Name	Institution and country	email
Harris, Jason	Steward Observatory, USA	*jharris@as.arizona.edu*
Hernández, Francisco J.	UNAM, Mexico	*f.hernandez@astrosmo.unam.mx*
Hitschfeld, Marc	Universität zu Köln, Germany	*kramer@ph1.uni-koeln.de*
Hughes, Annie	Swinburne University, Australia	*ahughes@astro.swin.edu.au*
Irwin, Mike	University of Cambridge, UK	*mike@ast.cam.ac.uk*
Ishiyama, Tomoaki	Tokyo University, Japan	*ishiyama@provence.c.u-tokyo.ac.jp*
Jarrett, Thomas	IPAC/SSC/Caltech, USA	*jarrett@ipac.caltech.edu*
Jerjen, Helmut	ANU, Australia	*jerjen@mso.anu.edu.au*
Kalirai, Jason	University of California, USA	*jkalirai@ucolick.org*
Karachentsev, Igor	SAO, Russia	*ikar@luna.sao.ru*
Kawamura, Akiko	Nagoya University, Japan	*kawamura@a.phys.nagoya-u.ac.jp*
Kepley, Amanda	University of Wisconsin-Madison, USA	*kepley@astro.wisc.edu*
Kim, Hak-Sub	Yonsei University, South Korea	*gapiel96@galaxy.yonsei.ac.kr*
Kirby, Emma	ANU/ATNF, Australia	*emma@mso.anu.edu.au*
Komiyama, Yutaka	NAOJ, Japan	*komiyama@subaru.naoj.org*
Koposov, Sergey	MPI für Astronomie, Germany	*koposov@mpia-hd.mpg.de*
Koribalski, Bärbel	ATNF/CSIRO, Australia	*Baerbel.Koribalski@csiro.au*
Kraan-Korteweg, Renée	University of Cape Town, South Africa	*kraan@circinus.ast.uct.ac.za*
Krajnovic, Davor	University of Oxford, UK	*dxk@astro.ox.ac.uk*
Kramer, Carsten	Universität zu Köln, Germany	*kramer@ph1.uni-koeln.de*
Lane, Richard	University of Sydney, Australia	*R.Lane@physics.usyd.edu.au*
Lavaux, Guilhem	IAP, France	*lavaux@iap.fr*
Lee, Henry	Gemini Observatory (South), Chile	*hlee@gemini.edu*
Lewis, Geraint	University of Sydney, Australia	*gfl@physics.usyd.edu.au*
Lockman, Felix J.	NRAO, USA	*jlockman@nrao.edu*
López-Sánchez, Ángel	ATNF/CSIRO, Australia	*Angel.Lopez-Sanchez@csiro.au*
Madsen, Greg	University of Sydney, Australia	*madsen@physics.usyd.edu.au*
Majewski, Steven	Virginia University, USA	*srm4n@mail.astro.virginia.edu*
Manthey, Eva	ASTRON, The Netherlands	*manthey@astron.nl*
Mao, Sui Ann	Harvard Smithsonian CfA, USA	*samao@cfa.harvard.edu*
Martínez, Luis Alberto	UAM, Spain	*l.martinez@uam.es*
Mastropietro, Chiara	USM, Germany	*chiara@usm.uni-muenchen.de*
Matthews, Deanna	La Trobe University, Australia	*D.Matthews@latrobe.edu.au*
McClure-Griffiths, Naomi	ATNF/CSIRO, Australia	*naomi.mcclure-griffiths@csiro.au*
McConnachie, Alan	University of Victoria, USA	*alan@uvic.ca*
Meixner, Margaret	STScI, USA	*meixner@stsci.edu*
Meschin, Ingrid	IAC, Spain	*imeschin@iac.es*
Minamidani, Tetsuhiro	Hokkaido University, Japan	*tetsu@astro1.sci.hokudai.ac.jp*
Mizuno, Yoji	Nagoya University, Japan	*y_mizuno@a.phys.nagoya-u.ac.jp*
Morrison, Heather	Case Western Reserve University, USA	*heather@vegemite.astr.cwru.edu*
Muller, Erik	ATNF/CSIRO, Australia	*Erik.Muller@csiro.au*
Murphy, Tara	University of Sydney, Australia	*tm@it.usyd.edu.au*
Nakanishi, Hiroyuki	ATNF/CSIRO, Australia	*Hiroyuki.Nakanishi@csiro.au*
Ngeow, Chow Choong	University of Illinous, USA	*cngeow@astro.uiuc.edu*
Nidever, David	University of Virginia, USA	*dln5q@mail.astro.virginia.edu*
Onishi, Toshikazu	Nagoya University, Japan	*ohnishi@a.phys.nagoya-u.ac.jp*
Oosterloo, Tom	ASTRON, The Netherlands	*oosterloo@astron.nl*
Ott, Jürgen	NRAO, USA	*jott@nrao.edu*
Paradis-Cami, Deborah	CESR Toulouse, France	*Deborah.Paradis@cesr.fr*
Piatek, Slawomir	New Jersey Institute of Technology & Rutgers University, USA	*piatek@physics.rutgers.edu*

Name	Institution and country	email
Pryor, Carlton	Rutgers University, USA	*pryor@physics.rutgers.edu*
Reid, Warren	Macquarie University, Australia	*warren@ics.mq.edu.au*
Roussel, Helene	MPI für Astronomie, Germany	*roussel@mpia-hd.mpg.de*
Ruzicka, Adam	Astronomical Institute, Czech Republic	*adam.ruzicka@gmail.com*
Ryder, Stuart	AAO, Australia	*sdr@aao.gov.au*
Saucedo, Julio	Universidad de Sonora, Mexico	*jsaucedo@cajeme.cifus.uson.mx*
Sawada-Satoh, Satoko	Academia Sinica Institute, Taiwan	*satoko@asiaa.sinica.edu.tw*
Seth, Anil	Harvard-Smithsonian CfA, USA	*aseth@cfa.harvard.edu*
Shafi, Nebiha	University of Cape Town, South Africa	*nshafi@circinus.ast.uct.ac.za*
Sim, Helen	ATNF/CSIRO, Australia	*Helen.Sim@csiro.au*
Skillman, Evan	University of Minnesota, USA	*skillman@astro.umn.edu*
Spekkens, Kristine	NRAO / Rutgers University, USA	*spekkens@physics.rutgers.edu*
Srinivasan, Sundar	Johns Hopkins University/STScI, USA	*sundar@pha.jhu.edu*
Staveley-Smith, Lister	UWA, Australia	*lister.staveley-smith@uwa.edu.au*
Tanaka, Mikito	NAOJ, Japan	*miki@optik.mtk.nao.ac.jp*
Tauber, Leigh	James Cook University, Australia	*leigh.tauber@jcu.edu.au*
Thilker, David	Johns Hopkins University, USA	*dthilker@pha.jhu.edu*
Tikhonov, Anton	Saint-Petersburg State University, Russia	*ti@hotbox.ru*
Tisserand, Patrick	ANU, Australia	*tisseran@mso.anu.edu.au*
Torii, Kazufumi	Nagoya University, Japan	*torii@a.phys.nagoya-u.ac.jp*
Tully, Brent	University of Hawaii, USA	*tully@willick.ifa.hawaii.edu*
Urbaneja, Miguel A.	University of Hawaii, USA	*urbaneja@ifa.hawaii.edu*
van der Hulst, Thijs	Kapteyn Astronomical Institute, The Netherlands	*vdhulst@astro.rug.nl*
van Driel, Wim	Paris Observatory, France	*Wim.vanDriel@obspm.fr*
van Eymeren, Janine	Ruhr-Universität Bochum, Germany	*jeymeren@astro.ruhr-uni-bochum.de*
Walsh, Shane	ANU, Australia	*swalsh@mso.anu.edu.au*
Walsh, Wilfred	University of NSW, Singapore	*wilfred.walsh@unsw.edu.au*
Walter, Fabian	MPIfA, Germany	*walter@mpia-hd.mpg.de*
Wehner, Elizabeth	McMaster University, Canada	*wehnere@physics.mcmaster.ca*
Westmeier, Tobias	ATNF/CSIRO, Australia	*Tobias.Westmeier@csiro.au*
Whiting, Matthew	ATNF/CSIRO, Australia	*Matthew.Whiting@csiro.au*
Wilcots, Eric	University of Wisconsin, USA	*ewilcots@astro.wisc.edu*
Winkel, Benjamin	MPIfR & AIfA, Germany	*bwinkel@astro.uni-bonn.de*
Wong, O. Ivy	University of Melbourne, Australia	*iwong@physics.unimelb.edu.au*
Woodley, Kristin	McMaster University, Canada	*woodleka@univmail.cis.mcmaster.ca*
Woudt, Patrick	University of Cape Town, South Africa	*pwoudt@circinus.ast.uct.ac.za*
Yoon, Suk-Jin	Yonsei University, South Korea	*sjyoon@galaxy.yonsei.ac.kr*

Index

H-band photometry, 51

AAT, 51
abundances, 87
accretion, 261, 305
Aloisi, 141, 271
Andromeda, 213, 217, 221, 225, 229, 233, 237, 337
AndXII, 221
And IV, 67
ANGST, 117, 133, 323
Annibali, 271
ASKAP, 79
ATCA, 43, 149, 289, 311

Balasubramanyam, 273
Barnes, 185
Beaton, 233
Begum, 63, 67
Bekki, 249
Belokurov, 197
Ben Bekhti, 275
Bernard, 253
Besla, 277
Bigiel, 99, 107
black hole, 181
Bland-Hawthorn, 261, 289
Boötes II, 193
Bolatto, 95
Bonne, 43, 47
Bot, 87
Braun, 237
Brunthaler, 213

Carlson, 279
Chengalur, 63, 67
Chomiuk, 281
Chumak, 283
Ciardullo, 157
Cioni, 257
Circinus, 293
Coleman, 209
Colless, 17
Complex H, 241
Conn, 257, 285

Dalcanton, 117, 323
Dale, 83
dark matter, 37, 47
dark matter halos, 31, 59, 189, 237
Da Costa, 125
distances, 21, 205, 319
Drozdovsky, 145, 287
Duchamp, 345
dust temperature, 83
dwarf galaxies, 59, 63, 67, 71, 95, 125, 141, 189, 201, 217, 233

EBHIS, 347
Effelsberg telescope, 237, 347
Ekers, 289
ESO540-032, 125

Feain, 289
feedback, 71
FIGGS, 63, 67
Fukui, 153, 293, 297, 313, 315

galaxy evolution, 95
galaxy finder, 345
galaxy groups, 21, 273, 283, 303, 331
GALEX, 83, 111, 353
Gemini, 181
GHOSTS, 129
Gilbert, 225, 233
globular clusters, 177, 229
GMRT, 63, 67, 273
Great Attractor, 3
Green Bank Telescope, 241
Guhathakurta, 225, 233, 337

Harding, 229
Harris, 291
Hercules dwarf, 209
HI, 99, 107, 273, 305, 311, 321, 323, 341, 345, 347, 349
HI distribution, 43
HI mass function, 59, 79
high velocity clouds, 237, 241, 275
HIPASS, 13, 43, 185, 349
Hitschfeld, 173, 293
HST, 117, 133, 141, 161, 201, 271, 279, 325
Hubble flow, 21
Hubble-Sandage paradox, 283
Hughes, 295, 313

IC 10, 71, 213, 305
IC 1613, 205
IC 2574, 321
IC 342, 157
irregular galaxies, 71, 75, 343
Irwin, 221, 257, 285
I Zw 18, 141

Jarrett, 165
Jerjen, 43, 51, 125, 189, 193

Kalirai, 225, 233
Karachentsev, 21, 43, 63, 67
Kawamura, 297, 313, 315
Kepley, 75
Kirby, 43, 51
KOGS, 317
Komiyama, 299, 337
Koposov, 197
Koribalski, 13, 43, 55, 303, 323
Kraan-Korteweg, 13, 351
Krajnovic, 181
Kramer, 293

Large Binocular Telescope, 209
large-scale structure, 3, 13, 17, 21
Lavaux, 37
Leo II, 299
Leo T, 59, 209
Lewis, 221, 257
Local Group, 145, 153, 201, 205, 209, 213, 217, 221, 287, 299
Local Velocity Anomaly, 3
Local Void, 3, 13, 31
Lockman, 241
Lopez-Sanchez, 43, 55, 301, 303
LVHIS, 43, 47, 55, 185

M 101, 157
M 31, 197
M 33, 157, 205, 213, 257
M 51, 173
M 74, 157
M 83, 55, 111
M 94, 157
Magellanic Clouds, 249, 253, 277, 279, 291, 295, 297, 309, 313, 315, 319, 327, 329, 335
Magellanic Stream, 245, 249, 311
magnetc fields, 75
Majewski, 225, 233, 245
Manthey, 305
Martinez-Vaquero, 307
mass-to-light ratios, 51, 157
Matthews, 311
McClure-Griffiths, 311
McConnachie, 217, 221, 257
Meixner, 253, 279, 291, 335
Meschin, 309
Milky Way satellites, 189, 193, 197, 209, 217, 241, 325
Minamidani, 313
Mizuno, 295, 313, 315
molecular gas, 95, 149, 153, 293, 297, 313, 315, 333
molecular hydrogen, 91
Monoceros Ring, 285
Morrison, 229
Muller, 295, 311, 313

Nakanishi, 317
NANTEN2, 153, 293, 313, 315
NGC 1365, 149
NGC 1569, 75
NGC 205, 237
NGC 2366, 321, 343
NGC 2403, 99
NGC 2976, 169
NGC 300, 205
NGC 3109, 205
NGC 3379, 161
NGC 3631, 71
NGC 3741, 63, 67
NGC 4214, 75
NGC 4244, 129
NGC 4258, 333
NGC 4449, 271
NGC 4945, 293
NGC 5128, 177, 181, 289
NGC 5253, 55
NGC 6946, 165
Ngeow, 319
NIBLES, 341
Nidever, 245
numerical simulations, 31, 37, 249, 307, 329

Oh, 321
Onishi, 153, 313, 315
Oosterloo, 59, 305
Ott, 43, 149, 289, 295, 313, 323

peculiar velocities, 3, 17, 21, 37
Piatek, 201, 325
planetary nebulae, 157, 177, 327
proper motions, 201, 213, 277, 325
Pryor, 201, 325

redshift surveys, 17
Reid, 327
rotation curves, 47, 169, 321
Roussel, 91
Ruzicka, 329
Ryder, 51

SAGE, 253, 291, 335
Saucedo-Morales, 331
Sawada-Satoh, 333
SBS 1415+437, 141
Sculptor group, 125
SDSS, 193, 197, 331, 341, 347
Seth, 129
Sextans A, 133
Shafi, 13
SINGS, 83, 87, 91, 99, 165
Skillman, 133, 323
SkyMapper, 189, 339
Smith's Cloud, 241
spectral energy distribution, 83
Spekkens, 169
Spitzer, 83, 87, 91, 165, 253, 279, 335
Srinivasan, 253, 335
star formation, 95, 107, 133
star formation histories, 117, 133, 145
star formation laws, 173
star formation rate, 149
star formation rates, 21, 353
Staveley-Smith, 13, 43, 79, 311, 313, 349
stellar populations, 117
Subaru Telescope, 299, 337
supernova remnants, 165, 281

Tanaka, 337
Thilker, 111, 237
THINGS, 99, 107, 321
Tikhonov, 31, 287
Tisserand, 339
Tully, 3, 37

Urbaneja, 205

van der Hulst, 59
van Driel, 341
van Eymeren, 43, 343
visualisation, 185
VLA, 281, 323
voids, 31

Walsh, 193
Walter, 95, 99, 107, 149, 321, 323
Wehner, 161
Westmeier, 237, 275
Whiting, 345
Wilcots, 71, 75, 281
Winkel, 347
WKK 6167, 351
WLM, 205
Wolf-Rayet galaxies, 301

Wolf-Rayet stars, 55
Wong, 349
Woodley, 177
Woudt, 351

XUV-disks, 111

Yoon, 353

ZOA Survey, 13
Zone of Avoidance, 13